

UNCLASSIFIED

AD NUMBER	
AD385084	
CLASSIFICATION CHANGES	
TO:	UNCLASSIFIED
FROM:	CONFIDENTIAL
LIMITATION CHANGES	
TO: Approved for public release; distribution is unlimited.	
FROM: Distribution authorized to U.S. Gov't. agencies and their contractors; Critical Technology; OCT 1967. Other requests shall be referred to Air Force Rocket Propulsion Lab., Research and Technology Div., Attn: RPPR-STINFO, Edwards AFB, CA 93523. This document contains export-controlled technical data.	
AUTHORITY	
AFRPL ltr dtd 3 Jan 1986 AFRPL ltr dtd 3 Jan 1986	

THIS PAGE IS UNCLASSIFIED

GENERAL DECLASSIFICATION SCHEDULE

IN ACCORDANCE WITH
DOD 5200.1-R & EXECUTIVE ORDER 11652

THIS DOCUMENT IS:

CLASSIFIED BY DDC

Subject to General Declassification Schedule of
Executive Order 11652-Automatically Downgraded at
2 Years Intervals-DECLASSIFIED ON DECEMBER 31, 73.

BY

Defense Documentation Center
Defense Supply Agency
Cameron Station
Alexandria, Virginia 22314

AD 385 084

AUTHORITY:

AFR PL Hr

Dec 85



THIS REPORT HAS BEEN DELIMITED
AND CLEARED FOR PUBLIC RELEASE
UNDER DOD DIRECTIVE 5200.20 AND
NO RESTRICTIONS ARE IMPOSED UPON
ITS USE AND DISCLOSURE.

DISTRIBUTION STATEMENT A

APPROVED FOR PUBLIC RELEASE;
DISTRIBUTION UNLIMITED.

SECURITY

MARKING

The classified or limited status of this report applies to each page, unless otherwise marked.

Separate page printouts MUST be marked accordingly.

THIS DOCUMENT CONTAINS INFORMATION AFFECTING THE NATIONAL DEFENSE OF THE UNITED STATES WITHIN THE MEANING OF THE ESPIONAGE LAWS, TITLE 18, U.S.C., SECTIONS 793 AND 794. THE TRANSMISSION OR THE REVELATION OF ITS CONTENTS IN ANY MANNER TO AN UNAUTHORIZED PERSON IS PROHIBITED BY LAW.

NOTICE: When government or other drawings, specifications or other data are used for any purpose other than in connection with a definitely related government procurement operation, the U. S. Government thereby incurs no responsibility, nor any obligation whatsoever; and the fact that the Government may have formulated, furnished, or in any way supplied the said drawings, specifications, or other data is not to be regarded by implication or otherwise as in any manner licensing the holder or any other person or corporation, or conveying any rights or permission to manufacture, use or sell any patented invention that may in any way be related thereto.

CONFIDENTIAL

19
AFRPL-TR-67-196

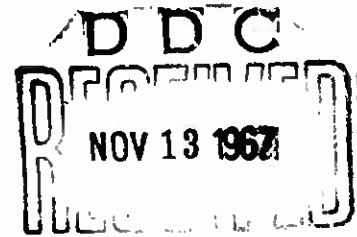
TE2-189-10-7
Copy No. [REDACTED]

AD 385084

FINAL REPORT
DEVELOPMENT AND DEMONSTRATION OF AN
OMNIAxIAL FLEXIBLE SEAL MOVABLE
NOZZLE FOR THRUST VECTOR CONTROL (U)

TECHNICAL REPORT AFRPL-TR-67-196

October 1967



DOWNGRADED AT 3 YEAR INTERVALS
DECLASSIFIED AFTER 12 YEARS
DOD DIR 5200.10

IN ADDITION TO SECURITY REQUIREMENTS WHICH MUST BE MET, THIS DOCUMENT IS SUBJECT TO SPECIAL EXPORT CONTROLS AND EACH TRANSMITTAL TO FOREIGN GOVERNMENTS OR FOREIGN NATIONALS MAY BE MADE ONLY WITH PRIOR APPROVAL OF AFRPL (RPPR/STINFO), EDWARDS, CALIFORNIA 93523.

THIS MATERIAL CONTAINS INFORMATION AFFECTING THE NATIONAL DEFENSE OF THE UNITED STATES WITHIN THE MEANING OF THE ESPIONAGE LAWS, TITLE 18, U.S.C., SECTIONS 793 AND 794, THE TRANSMISSION OR REVELATION OF WHICH IN ANY MANNER TO AN UNAUTHORIZED PERSON IS PROHIBITED BY LAW.

AIR FORCE
ROCKET PROPULSION LABORATORY
RESEARCH AND TECHNOLOGY DIVISION
AIR FORCE SYSTEMS COMMAND
Edwards, California

CONFIDENTIAL

SPECIAL NOTICES

Qualified users may obtain copies of this report from the Defense Documentation Center.

Do not return this copy. When not needed, destroy in accordance with pertinent security regulations.

When U. S. Government drawings, specifications, or other data are used for any purpose other than a definitely related Government procurement operation, the Government thereby incurs no responsibility nor any obligation whatsoever; and the fact that the Government may have formulated, furnished, or in anyway supplied the said drawings, specifications, or other data is not to be regarded by implication or otherwise, as in any manner licensing the holder or any other person or corporation, or conveying any rights or permission to manufacture, use, or sell any patented invention that may in anyway be related thereto.

CONFIDENTIAL

FINAL REPORT
DEVELOPMENT AND DEMONSTRATION OF AN
OMNIAXIAL FLEXIBLE SEAL MOVABLE
NOZZLE FOR THRUST VECTOR CONTROL (U)

Approved by



Thomas Walker
Program Manager

Approved by



Robert Ziegler
Project Engineer

DOWNGRADED AT 3 YEAR INTERVALS
DECLASSIFIED AFTER 12 YEARS
OOO OIR 5200.10

IN ADDITION TO SECURITY REQUIREMENTS WHICH MUST BE MET, THIS DOCUMENT IS
SUBJECT TO SPECIAL EXPORT CONTROLS AND EACH TRANSMITTAL TO FOREIGN GOV-
ERNMENTS OR FOREIGN NATIONALS MAY BE MADE ONLY WITH PRIOR APPROVAL OF
AFRPL (RPPR/STINFO), EDWARDS, CALIFORNIA 93523.

THIS MATERIAL CONTAINS INFORMATION AFFECTING THE NATIONAL OFFENSE OF THE
UNITED STATES WITHIN THE MEANING OF THE ESPIONAGE LAWS, TITLE 18, U.S.C.,
SECTIONS 793 AND 794, THE TRANSMISSION OR REVELATION OF WHICH IN ANY MANNER
TO AN UNAUTHORIZED PERSON IS PROHIBITED BY LAW.

AIR FORCE
ROCKET PROPULSION LABORATORY
RESEARCH AND TECHNOLOGY DIVISION
AIR FORCE SYSTEMS COMMAND
Edwards, California

Publications No. 1067-15435

CONFIDENTIAL

FOREWORD

This Final Technical Engineering Report covers the work performed during July 1966 thru June 1967 under Contract AF 04(611)-11643, "Development and Demonstration of an Omniaxial Flexible Seal Movable Nozzle for Thrust Vector Control."

The program motor, designated by the Air Force as the 156-9 rocket motor, was identified as the TU-562 rocket motor for Thiokol internal processing.

The contract with Thiokol Chemical Corporation, Wasatch Division, was performed under the overall direction of SAMSO with technical direction by Captain John Schmuck (RPMMS), Solid Rocket Division of the Air Force Rocket Propulsion Laboratory, Research and Technology Division, Air Force Systems Command, Edwards, California.

This manuscript was released for publication as an Air Force Rocket Propulsion Laboratory Technical Report in October 1967. This report contains no classified information extracted from other classified documents.

This Technical Report has been reviewed and is approved.

Charles R. Cooke
Chief Solid Rocket Division
AFRPL, Edwards, California

ABSTRACT

(U) The 156-9 Motor Program, Development and Demonstration of an Omniaxial Flexible Seal for Thrust Vector Control, was conducted by Wasatch Division, Thiokol Chemical Corporation for the Air Force Space and Missile Systems Organization. The program was under the technical direction of the Air Force Rocket Propulsion Laboratory. The primary objective of the program was to develop and successfully demonstrate an omniaxial flexible seal movable nozzle on a one million pound thrust class, 156 in. diameter motor. This objective was attained. The 156-9 motor was static test fired on 26 May 1967 and successfully demonstrated the flexible seal design and fabrication concept for movable nozzles. All motor and nozzle components were intact and in good condition at the completion of the test. The motor operated longer and at a lower chamber pressure than predicted, but with no adverse effect on the overall objective. Post-test inspection of the motor and components disclosed that the internal insulation, nozzle design, and flexible seal design were satisfactory and the nozzle performed as predicted. The torque required for thrust vector control was demonstrated to be reasonable with respect to actuation system power requirements.

TABLE OF CONTENTS

	<u>Page</u>
I INTRODUCTION AND SUMMARY	1
A. Introduction	1
B. Summary	3
1. Design Criteria	3
2. Motor Design and Processing	4
3. Static Test	8
II FLEXIBLE SEAL DESIGN, FABRICATION AND TEST	11
A. Flexible Seal Design	11
1. Related Experience	11
2. Design Criteria	13
3. Configuration	13
4. Design Analysis	21
5. Boot Redesign	38
B. Flexible Seal Fabrication	39
1. Component Breakdown	39
2. AF Seal No. 1 Fabrication	50
3. AF Seal No. 1 Verification Testing	56
4. AF Seal No. 2 Fabrication	57
5. AF Seal No. 2 Qualification Testing	59
6. Test Summary	64
III NOZZLE DESIGN AND FABRICATION	79
A. Nozzle Design	79
1. Component Configuration and Materials Selection	79
2. Flexible Seal Location	86
3. Aerodynamic Analysis	89
4. Thermal Analysis	107
5. Structural Analysis	121
6. Torque Analysis	125
7. Weight Analysis	144
8. Final Design	144
9. Predicted Performance	147

TABLE OF CONTENTS (Cont)

	<u>Page</u>
B. Nozzle Fabrication	151
1. Vender Selection	151
2. Component Fabrication	151
3. Final Assembly of Nozzle	152
4. Deviations from Design	159
IV GRAIN DESIGN	167
A. Ballistics Design	167
1. Predicted Performance	167
2. Pressure and Thrust vs Time	167
3. Gas Flow Characteristics	173
B. Structural Design	176
1. Grain Configuration	176
2. Structural Analysis	177
V CASE	189
A. Acceptance Inspection	189
B. Case Refurbishment	191
VI INSULATION AND LINER DESIGNS	193
A. Insulation Design	193
1. Design Criteria	193
2. Insulation Design, Formulation, and Predicted Performance	193
3. Previous Experience	196
4. Weight Analysis	196
B. Liner Design	196
1. Liner Design Criteria	196
2. Liner Design and Formulation	199
3. Previous Experience	199
4. Weight Analysis	199
C. Verification Testing	199
1. Types of Tests	199
2. Test Procedure	204

TABLE OF CONTENTS (Cont)

	<u>Page</u>
D. Insulation and Liner Installation	217
1. Insulation Application	217
2. Liner Application	224
 VII PROPELLANT DESIGN AND PROCESSING	 227
A. Propellant Design	227
1. Propellant Design Criteria	227
2. Formulation and Properties	227
3. Previous Experience	229
B. Propellant Standardization and Verification	229
1. Standardization	232
2. Verification	232
3. Production	236
4. Discussion	239
5. Summary	245
C. Propellant Processing	245
1. Mixing Procedure	245
2. Casting and Curing Procedure	248
3. Finishing	255
 VIII IGNITION SYSTEM DESIGN AND FABRICATION	 265
A. Ignition System Design	265
1. Safety and Arming (S & A) Device	265
2. Initiating System	269
3. Booster PYROGEN	270
4. Adapters	270
B. Igniter Ballistic Design and Motor Ignition Transient . .	272
C. Igniter Insulation Design	273
1. Case Internal Insulation	273
2. Case External Insulation	275
3. Igniter Cap Insulation	275
D. Igniter Weight Analysis	276
E. Ignition System Propellant	277
F. Ignition System Structural Analysis	278
G. Igniter Fabrication, Assembly and Installation	278
H. Ignition System Functional Verification (Bench Test) . .	282

TABLE OF CONTENTS (Cont)

	<u>Page</u>
IX ACTUATION SYSTEM	287
A. Actuation System Design	287
1. Actuator Design	287
2. Servovalve Design	291
3. Torque Analysis	295
B. Actuator Size and Force Output	299
1. Actuator Size	299
2. Actuation Geometry	299
C. Weight Analysis	301
D. Hydraulic System	301
E. Electrical System	305
F. 156-9 Duty Cycle	305
G. TVC Actuation System Fabrication	312
1. Bench Test	312
2. Compatibility Tests	314
X MASS PROPERTIES	315
XI TOOLING	319
A. Process Tooling	319
1. Process Handling Harness	319
2. Slot Former	319
3. Dispersion Cone Extension	323
4. Core Cap	323
5. Casting Dam Seating and Removal Tool	323
6. Casting Hopper Adapter Base	323
7. Hopper Funnel Adapter	324
8. Plaster Sweep Template	324
9. Vacuum Dome Adapter	324
10. Casting Dam	325
11. Dispersion Cone	325
12. Core Modification	325

TABLE OF CONTENTS (Cont)

	<u>Page</u>
B. Test Tooling	326
1. Flexible Seal Test Fixture	326
2. Nozzle Handling Arrangement	328
C. Flexible Seal and Protective Boot Fabrication Tooling	328
1. Flexible Seal Tooling	328
2. Boot Tooling	335
 XII STATIC TEST RESULTS	 337
A. Introduction	337
1. Test Objectives	338
2. Test Article Description	338
B. Motor Handling and Assembly	344
1. Motor Installation in Test Bay	344
2. Nozzle Installation and Checkout	346
3. Leak Test	351
4. Quench System	353
5. Antiflight	353
C. Instrumentation	355
D. Test Results Summary	367
1. General Results	367
2. Flexible Seal Performance	372
3. Nozzle Performance	402
4. Case Performance	429
5. Insulation Performance	432
6. Ballistic Performance	435
7. Ignition System Performance	443
8. Motor Quench	449
9. Instrumentation Performance	451
 XIII CONCLUSIONS AND RECOMMENDATIONS	 453
A. Conclusions	453
B. Recommendations	454

LIST OF ILLUSTRATIONS

<u>Figure</u>		<u>Page</u>
1	156-9 Rocket Motor	5
2	Flexible Seal Design	14
3	Forward End Ring	15
4	Aft End Ring	17
5	Spherical Shim	19
6	Flexible Seal Design	22
7	Flexible Seal Deflection	24
8	Determination of Moment Arm	26
9	Flexible Seal Spring Rate vs Chamber Pressure	28
10	Critical Pressure vs Buckling Constant	31
11	Buckling Constant as a Function of Spherical Radius to Shim Thickness Ratio	32
12	Flexible Seal Metal Shim Stress Distribution	34
13	Shim Hoop Stress vs Shear Angle	36
14	Flexible Seal Stress Distribution	37
15	Flexible Seal	40
16	Flexible Seal Assembly Fixture	41
17	Flexible Seal Fabrication Functional Flow Diagram	42

LIST OF ILLUSTRATIONS (Cont)

<u>Figure</u>		<u>Page</u>
18	Wedge Arrangement for Shim Layup	43
19	Shim Distortion Due to Internal Components	60
20	Seal Assembly Prior to Test	61
21	Seal Assembly with Boot Installed	62
22	AF Seal No. 2, Event No. 7, Torque vs Position	65
23	AF Seal No. 1 Duty Cycle Torque Data	67
24	AF Seal No. 1, Event No. 3, Torque vs Position	68
25	AF Seal No. 1, Event No. 7, Torque vs Position	70
26	AF Seal No. 1 Spring Rate Vector Angle	71
27	AF Seal No. 1 Prior to Test (OD)	73
28	AF Seal No. 1 Prior to Test (ID)	74
29	AF Seal No. 1 Actuator Location Area after Failure	75
30	AF Seal No. 1 Location of Shim Wrinkling after Failure	76
31	Shim Hoop Stress vs Shear Angle	77
32	156-9 Motor Nozzle Design	81
33	Comparison of Forward and Aft Pivoted Seals	90
34	156-9 Nozzle Nose Mach No. vs Axial Distance from Throat	94

LIST OF ILLUSTRATIONS (Cont)

<u>Figure</u>		<u>Page</u>
35	156-9 Nozzle Nose Convective Heat Transfer Coefficient vs Axial Distance from Throat	95
36	Description of Viscous and Skin Friction Drag Parameters . .	96
37	Aft Case Geometry and Grain Burnout	98
38	Backside of 156-9 Nozzle (Silica Cloth)	100
39	Backside of 156-9 Nozzle (Asbestos Filled NBR)	101
40	Backside of 156-9 Nozzle (TI-H7043 Mastic)	102
41	Motor Flow Near Splitline in Vectored Nozzle at Motor Ignition	104
42	Mode of Flow Near Splitline	105
43	Convective Heat Transfer Coefficient vs Erosion Rate, Carbon Cloth	112
44	44 Convective Heat Transfer Coefficient vs Erosion Rate, Silica Cloth	113
45	156-9 Nozzle Entrance Temperature Profile, $A/A^* = 3.88$ (Backside)	116
46	156-9 Nozzle Entrance Temperature Profile, $A/A^* = 2.52$ (Backside) Carbon Cloth	117
47	156-9 Nozzle Entrance Temperature Profile, $A/A^* = 1.17$ Carbon Cloth	118
48	156-9 Nozzle Temperature Profile, $A/A^* = 1.0$ Carbon Cloth Phenolic	119
49	156-9 Nozzle Exit Cone Temperature Profile, $A/A^* = 8.16$	120

LIST OF ILLUSTRATIONS (Cont)

<u>Figure</u>		<u>Page</u>
50	Summary of Materials and Minimum Ultimate Strengths . . .	122
51	Load Distribution Summary	126
52	Flexible Seal Deflection	129
53	Determination of Moment Arm	131
54	Seal Torque vs Vector Angle	133
55	Aerodynamic Spring Rate vs Pivot Location	136
56	Flexible Seal Transient Response, MRC-2A	140
57	Offset Torque vs Pivot Location Zero Second Grain	142
58	Maximum Predicted Erosion and Char for the 156-9 Nozzle. .	148
59	Predicted Seal Component of Torque in Yaw Plane	149
60	156-9 Motor Nozzle Component Fabrication	153
61	Lowering the Fixed Housing Assembly to Rest on the Exit Shell	157
62	Seal, Nose, and Barrier Assembly	158
63	Installation of Bolts between Fixed Housing and Seal	160
64	Completed Nozzle Assembly	161
65	Repair of Barrier Assembly	163
66	Loaded Rocket Motor Case Assembly	169
67	Chamber Pressure and Thrust vs Time at 80°F	172

LIST OF ILLUSTRATIONS (Cont)

<u>Figure</u>		<u>Page</u>
68	Flow Comparison Points in the 156-6 and 156-9 Plenums . . .	174
69	Propellant Stress Relaxation Modulus	180
70	Failure Boundary Selected for the 156-9 Study	182
71	156-9 Cure-Thermal Shrinkage Stress Analysis Grain Deformation	183
72	156-9 Ignition Pressure 682 psi Stress Analysis Grain Deformation	184
73	Dilatational Failure Boundary	186
74	Distortional Failure Boundary	187
75	Aft Dome Thickness Measurements in Area of Defect.	190
76	Insulation Configuration	197
77	Insulation Design Information.	198
78	180 Degree Peel Test Specimen	202
79	180 Degree Peel Test Specimen and Arrangement	203
80	Tensile Adhesion, Tenshear	205
81	Tenshear Test Apparatus	206
82	Adhesion Cup Test Specimen	207
83	Lap Shear Adhesion Test Specimen	208
84	Phase I Test Specimens	210
85	Phase II Test Specimens	213
86	Modified TI-H704B Mixing Bowl Mounted on Vacuum Deaeration Chamber	218

LIST OF ILLUSTRATIONS (Cont)

<u>Figure</u>		<u>Page</u>
87	Extruding TI-H704B Insulation for Ease in Handling.	219
88	Slot Former Support Ring after Plaster Mold Removal.	221
89	Insulating the 156-9 Motor Case	222
90	Applying Insulation at the Nozzle Mold Ring	223
91	Liner Application Arrangement	225
92	Burning Rate vs Special Fine Oxidizer, TP-H1115 Propellant Standardization.	233
93	Modulus vs HB Polymer, TP-H1115 Propellant Standardization.	234
94	Pressure Exponent (K_p) Curve (Burning Rate vs Chamber Pressure, TP-H1115 Propellant, 430 Gallon Verification Mix)	235
95	Strand Burning Rate vs Cumulative Mix Number, TP-H1115 Propellant Production	237
96	Modulus vs Cumulative Mix Number, TP-H1115 Propellant Production	238
97	Burning Rate vs Special Fine Oxidizer, TP-H1115 Propellant Production	241
98	Comparison of Regression Lines for Strand Burning Rate vs Percent Special Fine Oxidizer	243
99	Modulus vs HB Polymer, TP-H1115 Production Mix	244
100	Initial 156-9 Motor Propellant Casting and Deaeration Arrangement.	249

LIST OF ILLUSTRATIONS (Cont)

<u>Figure</u>		<u>Page</u>
101	Minuteman Program Propellant Casting and Deaeration Arrangement	251
102	Removing Broadcloth Which Secures the Aft Relief Flap	253
103	Discs Used to Remove Cured Propellant Blocks from the Motor	254
104	Removing Teflon Dividers	256
105	Unseating the Casting Dam	257
106	Removing Cured Propellant Blocks	258
107	Removing Slot Former Segment	259
108	Removing the Loaded Motor from the Casting Pit	261
109	Breaking the Loaded Motor Over to the Horizontal Position	262
110	Loading the 156-9 Motor on the Transporter	263
111	Transporting the 156-9 Motor to the Test Bay	264
112	156-9 Rocket Motor Ignition System	267
113	Igniter Pressure Time Trace	271
114	Predicted Igniter and Motor Pressure vs Time During Ignition Transient (Utah Conditions)	274
115	Summary of Structural Analysis, Condition 1	279
116	Summary of Structural Analysis, Condition 2	280
117	156-9 Igniter in Test Stand (Before Firing)	283
118	156-9 Igniter in Test Stand (After Firing)	284

LIST OF ILLUSTRATIONS (Cont)

<u>Figure</u>		<u>Page</u>
119	Actuator Cylinder	289
120	Servo valve	293
121	Servoactuator Assembly	297
122	Hydraulic System Schematic	303
123	Block Diagram of Actuation Control System	306
124	Frequency Response Actuator S/N 1	307
125	Frequency Response Actuator S/N 2	308
126	156-9 Motor Duty Cycle	309
127	156-9 Motor Center of Gravity Reference Sketch	317
128	Propellant Vacuum Casting Fixture	321
129	Flexible Seal Test Fixture	327
130	Nozzle Handling Operation Sequence	329
131	Flexible Seal Assembly Fixture	331
132	156-9 Motor Installed in the Test Bay	345
133	Leak Test Arrangement Showing Nozzle Plug	349
134	Nozzle Plug Installed	352
135	Instrumentation Drawing	363

LIST OF ILLUSTRATIONS (Cont)

<u>Figure</u>		<u>Page</u>
136	156-9 Duty Cycle Actual Nozzle Position Superimposed on Programed Input	369
137	Actuation System Installation	373
138	Yaw Servoamplifier Input and Position Feedback	375
139	Pitch Servoamplifier Input Position Feedback	376
140	Yaw Servoamplifier Input and Outer Loop Position Feedback, T + 43 to 50 Seconds	378
141	Yaw Servoamplifier Input and Outer Loop Position Feedback, T + 15.8 to 17.6 Seconds	379
142	Yaw Outer Loop Position Feedback, T + 32 to 39 Seconds . .	380
143	Hydraulic Supply and Manifold Pressure	381
144	Hydraulic Return Pressure and System Flow	382
145	Yaw Actuator Differential Torque	383
146	Pitch Actuator Differential Torque	384
147	Yaw Actuator Differential Torque, Events 10 and 12	385
148	Yaw Actuator Differential Torque, Events 14 and 16	386
149	Yaw Actuator Differential Torque, Events 18 and 20	387
150	Yaw Actuator Differential Torque, Event 28	388
151	Pitch Actuator Differential Torque, Events 8 and 12	389
152	Pitch Actuator Differential Torque, Event 18	390
153	Total Side Force vs Time	395

LIST OF ILLUSTRATIONS (Cont)

<u>Figure</u>		<u>Page</u>
154	Thrust Vector Angle vs Time	396
155	Thrust Vector Angle vs Nozzle Position, Events 10 and 12	397
156	Thrust Vector Angle vs Nozzle Position, Events 14 and 16	398
157	Thrust Vector Angle vs Nozzle Position, Events 18 and 20	399
158	Thrust Vector Angle vs Nozzle Position, Event 28	400
159	Cross Section of Flexible Seal	402
160	Postfired Nozzle Exit Cone	404
161	Postfired Nozzle Submerged Section	405
162	Nozzle Submerged Section	406
163	Nose Cap, Drilled and Non-Drilled Surfaces	407
164	Nose Cap, Drilled and Non-Drilled Surfaces	408
165	Crossover Ring	410
166	Movable Surface of Gap	411
167	Fixed Surface of Gap	412
168	Cross-Section of Repaired Barrier Assembly	413
169	Comparison of Nose Cross-sections	414
170	Comparison of Throat Erosion Sections	415
171	Submerged Section Erosion	417

LIST OF ILLUSTRATIONS (Cont)

<u>Figure</u>		<u>Page</u>
172	Nose Erosion	418
173	Throat Erosion	419
174	Exit Cone Erosion	420
175	Erosion and Char Measurements	421
176	Insulation Material Loss	433
177	Chamber Pressure vs Time, Predicted and Actual	437
178	Axial Thrust vs Time, Predicted and Actual	438
179	Special Fine Oxidizer Distribution	439
180	Depressurization Rate as a Function of Time (dp/dt) during Tailoff	441
181	Igniter and Motor Pressure vs Time Curves during Ignition Transient.	444
182	Postfired Ignition System	446
183	Sectioned Igniter Case Showing Insulation Thickness	447
184	Sectioned Igniter Case Showing Minimum Insulation Thickness.	448
185	Motor Quench	450

LIST OF TABLES

<u>Table</u>		<u>Page</u>
I	Flexible Seal Configurations	12
II	Material Properties	23
III	Shim Compressive Yield Strength, Tension and Hardness Data	48
IV	Comparison of Bench Test Torque Values	58
V	AF Seal No. 2 Yaw Plane Duty Cycle Data	63
VI	AF Seal No. 1 Yaw Plane Duty Cycle Data	66
VII	Material Use History	85
VIII	Material Thermal Properties	108
IX	Summary of Minimum Margins of Safety	123
X	156-9 Nozzle Torque Prediction, 4 Deg Event, Sinc Actuation	137
XI	Mass Properties Data for 156-9 Motor Nozzle	145
XII	Summary of Deviation from Original Design	165
XIII	156-9 Rocket Motor Predicted Performance at 80 and 100°F	171
XIV	Aft Plenum Initial Flow Characteristic Comparison	175
XV	Grain Design Parameters	177
XVI	156-9 Motor Propellant	178
XVII	Worst Stress-Strain Conditions and Failure Criteria Comparison	188
XVIII	TI-H704B Insulation	194

LIST OF TABLES (Cont)

<u>Table</u>		<u>Page</u>
XIX	Previous Usage of TL-H704B and TL-H714A Insulation Liner System	195
XX	TL-H714A Liner	200
XXI	Propellant Characteristics, TP-H1115	228
XXII	Physical Properties of TP-H1115 Propellant	228
XXIII	TP-H1115 Propellant Ballistic Properties	229
XXIV	Summary of Ballistic and Physical Properties, TP-H1115 Propellant, Evaluation 516	230
XXV	Ballistic Characteristics - 156-9 (TU-562) Igniter	285
XXVI	156-9 Nozzle Actuation Duty Cycle	310
XXVII	Mass Properties Data 156-9 Motor Summary	316
XXVIII	Instrumentation Coding System	356
XXIX	Torque at Various Events of Duty Cycle	391
XXX	Spring Rates for Various Actuation Events	393
XXXI	Erosion and Char Measurements	425
XXXII	Summary of Nozzle Stresses	427
XXXIII	Summary of Case Stresses	431
XXXIV	156-9 Motor Performance	436
XXXV	Igniter Performance	445

SECTION I

INTRODUCTION AND SUMMARY

A. INTRODUCTION

(U) On 30 June 1966, Thiokol Chemical Corporation received notification from the Air Force Space Systems Division of the award of Contract AF 04(611)-11643 for the Development and Demonstration of an Omniaxial Flexible Seal Movable Nozzle. As detailed in the Statement of Work, Exhibit "A" to the contract, the program objective was to successfully static test fire a one million pound thrust class, 156 inch diameter, monolithic solid propellant rocket motor with an omniaxial flexible seal movable nozzle (OFSMN) thrust vector control system.

(U) The scope of work required to accomplish the program objective is described in the following task breakdown:

- (U) 1. Task A. Motor Demonstration--This task encompassed the effort necessary to (1) design, fabricate, and static test the 156 inch diameter motor, (2) develop, design, and fabricate a flexible seal and nozzle, (3) design and fabricate the TVC actuation system, and (4) refurbish the GFP motor chamber.
- (U) 2. Task B. Special Tooling--The contractor was required by this task to furnish the special handling, processing, and test tooling necessary to accomplish the program, except for those items specifically detailed in the contract.

- (U) 3. Task C. System Support--Included in this task was the quality assurance effort required to accomplish the program objectives.
- (U) 4. Task D. Program Administration and Reporting--All effort necessary for technical and administrative direction of the program, including preparation of reports and documentation, was specified in Task D.

(U) The contractual period of performance for technical effort was from 11 July 1966 through 12 June 1967, with the final report rough draft submittal date being 26 July 1967. During this period two modifications to the basic contract were received. The first of these modifications affected the security requirements check list only and did not change program cost, scope, or schedule. Modification No. 2 (Supplemental Agreement) directed a nozzle material change, which increased the target cost by \$3,000.00, provided a change in the nozzle and seal fabrication and test subtask of the work statement (Exhibit "A" to the Contract), and extended the schedule. The scheduled completion of technical effort was changed to 21 July 1967 and the final report rough draft submittal date was changed to 15 September 1967.

- (U) The final report is contained in one volume and includes:
1. A program summary;
 2. Detailed discussions on the design and fabrication of all motor components, including the flexible seal, the nozzle, propellant and grain, insulation and liner, ignition system and TVC actuation system;
 3. Flexible seal bench test procedures and results;
 4. The static test report including test results and detailed post fire analysis of components; and
 5. Conclusions and recommendations.

CONFIDENTIAL

B. SUMMARY

(U) The 156-9 motor demonstration program performed under this contract encompassed the design, manufacture and testing of a 156 inch diameter monolithic steel case solid propellant rocket motor utilizing an omniaxial flexible seal movable nozzle (OFSMN) for thrust vector control. The motor design and fabrication was conservative in order that the primary objective of demonstrating the flexible seal concept for large motors would not be compromised.

1. DESIGN CRITERIA

(C) Design criteria specified in the contract statement of work included the following:

- (U) 1. The motor will be capable of successful operation after being subjected to either vertical or horizontal storage at any thermal environment for a period of time sufficient to provide a maximum temperature gradient through the grain.
- (U) 2. The nozzle shall be a submerged type, flightweight (except for the flexible seal portion and the nozzle support shell), capable of omniaxial movement, and shall have a minimum expansion ratio of 8.0.
- (C) 3. The TVC system shall attain a vector angle of ± 4 deg, a maximum thrust deflection rate of 20 deg per sec, a side impulse of 1.1 percent of axial impulse, four full deflections at 1-1/4 cps, and a cycling rate of 1-1/2 cps at a thrust deflection angle of 0.5 degree.
- (U) 4. Liner and insulation designs for the motor shall include, but not be limited to, proven materials compatible with the propellant.

CONFIDENTIAL

(THIS PAGE IS UNCLASSIFIED)

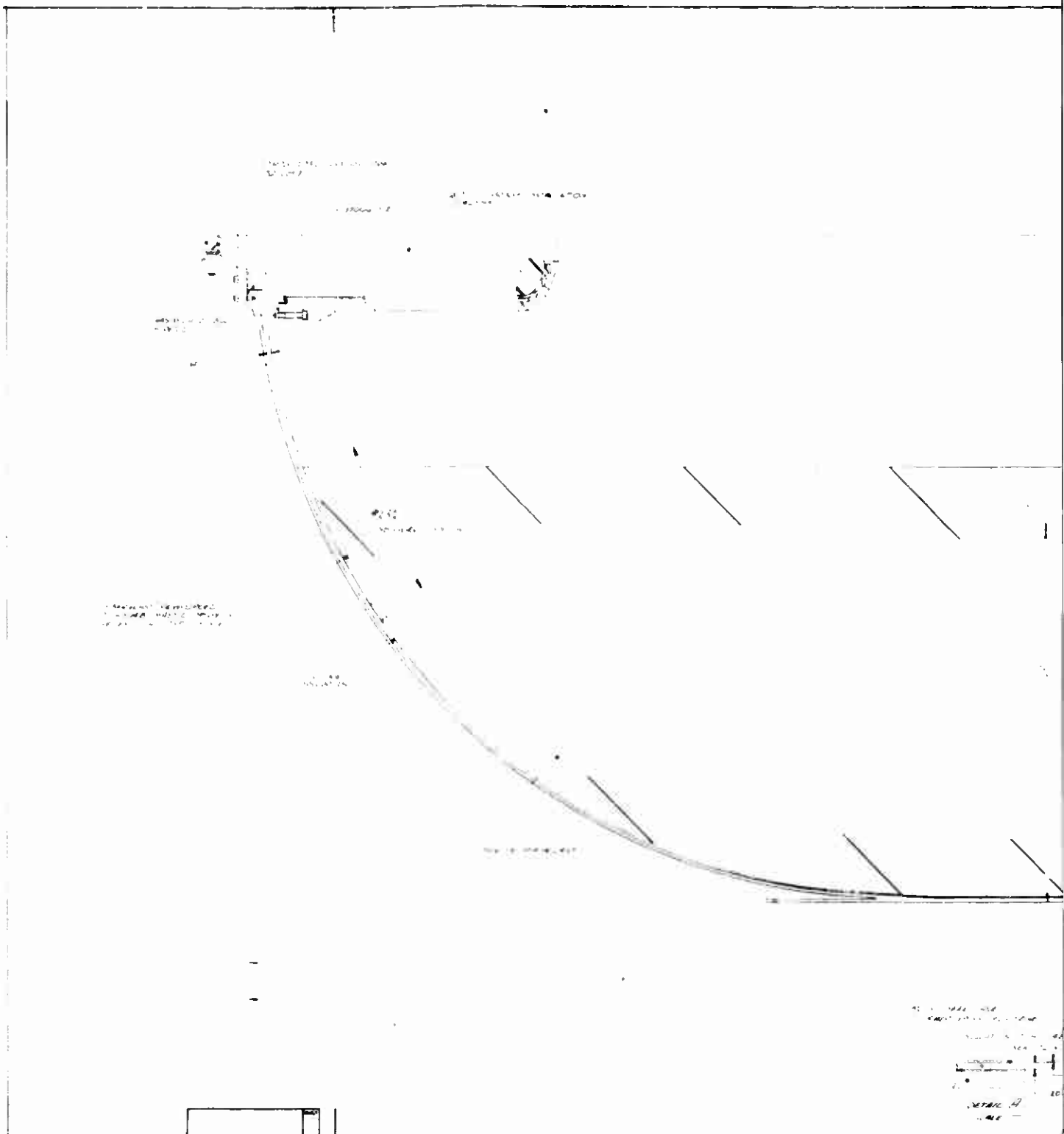
- (U) 5. The propellant shall be one of the polybutadiene/AP/Al family of propellants.
- (U) 6. A head end PYROGEN igniter shall be used.
- (U) 7. The motor will have a mass fraction design goal of 0.90.
- (U) 8. The motor should have a maximum action time of 70 seconds.
- (U) 9. The motor should produce a burn time average thrust of 1,000,000 pounds.

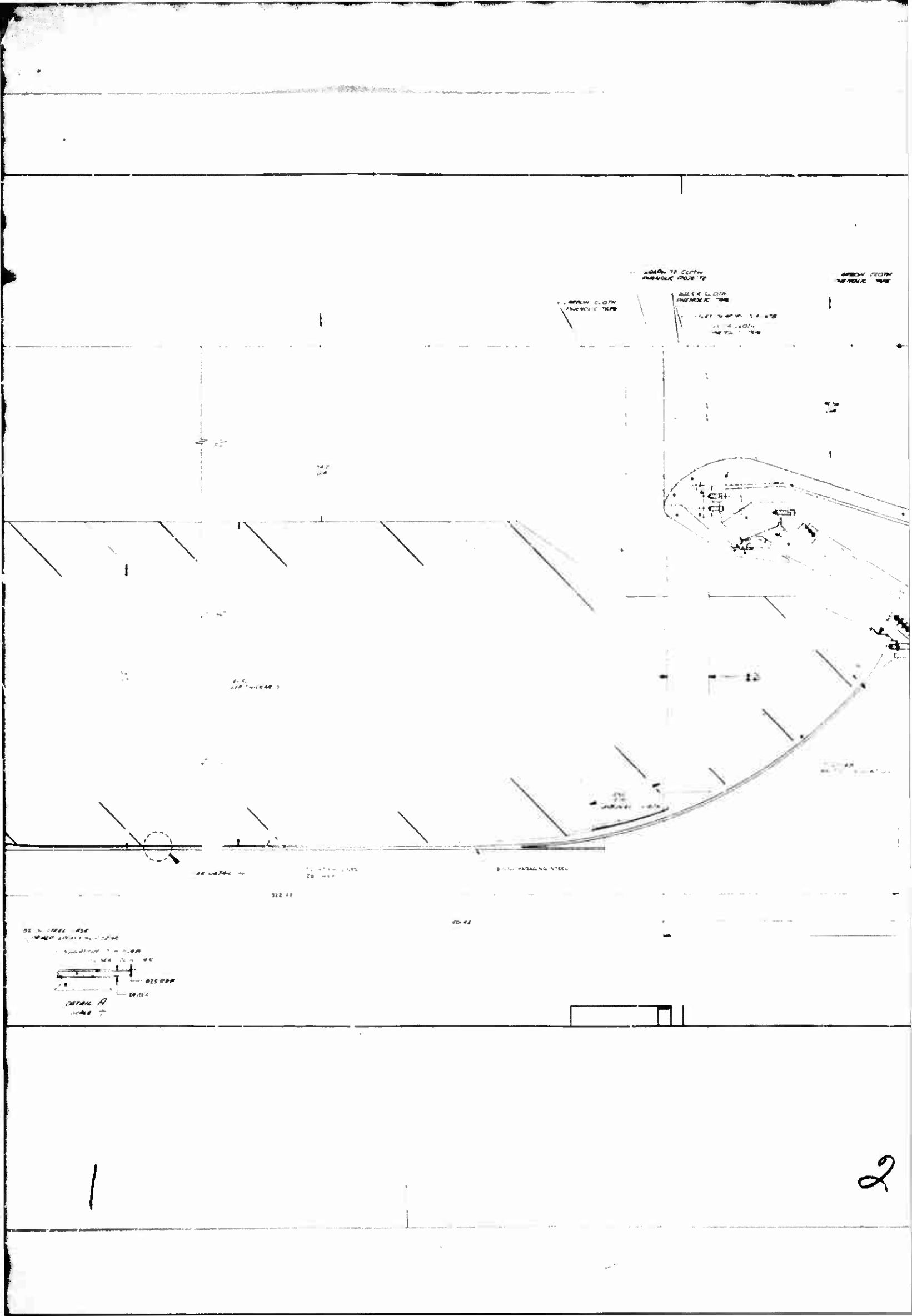
2. MOTOR DESIGN AND PROCESSING

- (U) The 156-9 motor design is shown in Figure 1 and detailed discussions are contained in following sections.
- (U) The motor chamber used in this program was the previously fired 156-6 motor chamber. Upon receipt at the Wasatch Division, the case was cleaned of all insulation and char and subjected to dye penetrant inspection in the weld areas. A Ketonon coating was applied to the interior of the chamber prior to installation of the insulation.
- (U) Mastic insulation, TI-H704B was used throughout for case insulation and fiberglass reinforced mastic, TI-H704B, was used for stress relief flap fabrication. The insulation thickness requirements were based primarily on design data from previous motor firings using the TI-H704B and thermal and erosion properties. A nominal 0.050 in. thickness of TL-H714A liner was applied to the surface of the insulation to provide good bonding between the insulation and propellant. Details of the insulation and liner design effort are contained in Section VI.
- (U) The propellant for this motor, designated TP-H1115, was a polybutadiene acrylonitrile/AP/Al type propellant utilizing 87 percent solids and had a Class 2 explosive classification. The motor had a slotted CP grain design in order to maintain a relatively neutral pressure trace. Vacuum casting techniques were employed during motor loading. Grain design details are in Section IV and propellant design and processing is in Section VII.

CONFIDENTIAL

(THIS PAGE IS UNCLASSIFIED)





SPRAY DECK
NO. 101.10 1988

WIND TOWER
NO. 101.10 1988

NO. 101.10

NO. 101.10

NO. 101.10

ST. CLAIR
COMBUSTION ENGINE

NO. 101.10

NO. 101.10

NO. 101.10

NO. 101.10

NO. 101.10

NO. 101.10

NO. 101.10

NO. 101.10

NO. 101.10

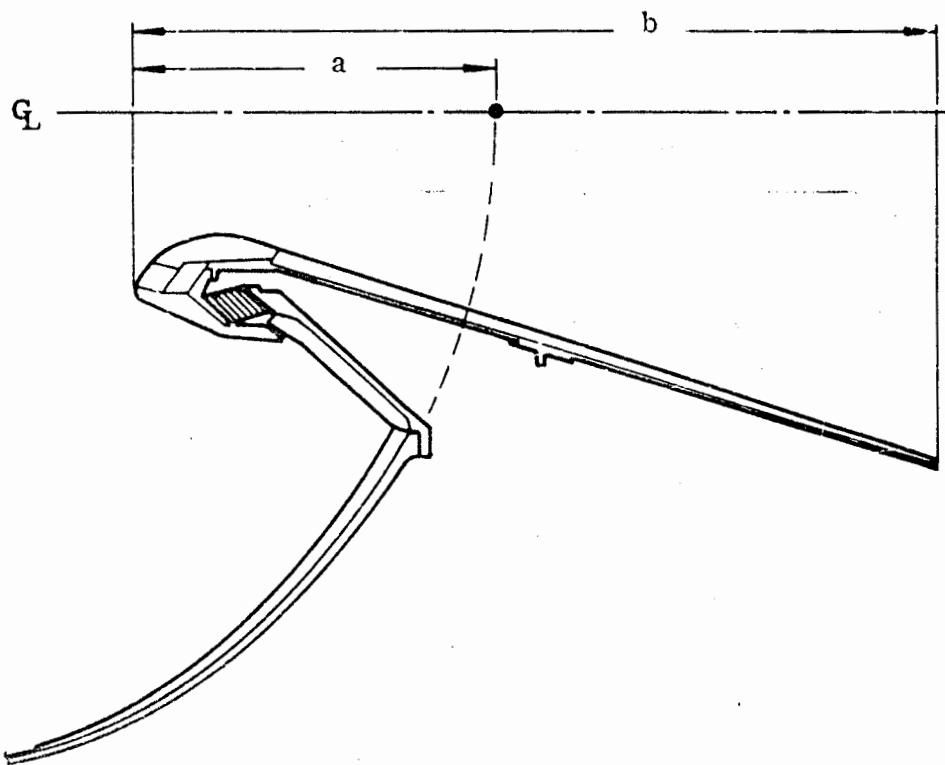
2

3

CONFIDENTIAL

(U) A conventional head end PYROGEN ignition system was utilized for motor ignition. This system employed a Minuteman type safety and arming device, an initiating PYROGEN igniter and the booster PYROGEN igniter. The booster PYROGEN metal case was externally insulated with V-45 rubber. The igniter cap was designed with ports for the injection of CO_2 gas for motor quench after static testing. Ignition System Design and Fabrication details are found in Section VIII.

(U) The nozzle design approach was conservative in that the aerodynamic configuration was identical to the 156-6 nozzle which performed satisfactorily. The design incorporated a 47 percent submergence, an 8.15 to 1 expansion ratio exit cone and a 34.5 in. throat diameter. Submergence (a) is defined as the percent of the overall length of the nozzle (b) which is forward of the theoretical intersection of the inner surface of the closed vessel with the motor centerline.



(C) The nozzle was capable of ± 4 deg omniaxial movement through a flexible seal joining the fixed and movable sections. The fixed housing and the movable housing were fabricated from 4130 steel. The plastic parts were fabricated from materials previously proven in nozzles tested on large motors. Section III presents a description of the detailed design, analyses, and fabrication effort.

CONFIDENTIAL

(THIS PAGE IS UNCLASSIFIED)

- (U) The flexible seal design, fabrication and bench testing are discussed in detail in Section II. The seal consisted of two forged 4140 steel end rings joined together with 0.040 in. thick stainless steel shims separated by 0.025 in. thick layers of polyisoprene rubber.
- (U) The TVC actuation system consisted of two linear servoactuators mounted between the fixed section and the movable section of the nozzle. The actuators were mounted 90 deg apart with one actuating pitch motion and the other actuating yaw motion. Intermediate angles of vectoring were accomplished by simultaneous movement of both actuators. The system was operated by a facility hydraulic power supply and an external electronic control system. TVC actuation system design and fabrication are described in detail in Section IX.

3. STATIC TEST

- (U) The loaded motor was transported to the test area and installed horizontally in the bay. The motor was aligned in the thrust stand by the use of hydrosets.
- (U) The nozzle was transported to the test bay and assembled on the motor using zinc chromate putty in the case-to-nozzle insulation joint. A foam plug was installed in the nozzle prior to assembly on the motor in order that a leak check could be performed. The case was pressurized to 50 ± 10 psi and Leak-tec was used to test for gas leakage. The nozzle plug was completely removed from the nozzle prior to static test firing. The TVC actuation system was installed and checked out prior to attachment of the actuator rods to the nozzle movable section. A dry run of the complete duty cycle was performed with the actuator rods attached to the nozzle. The case and nozzle were instrumented and the CO₂ quench system installed.
- (U) The motor was static fired on 26 May 1967. Motor ignition occurred normally and no abnormality in motor or component performance was observed during the firing. A review and analysis of the test data confirmed the successful operation.

CONFIDENTIAL

(THIS PAGE IS UNCLASSIFIED)

Nozzle actuation torques were slightly higher than predicted but were well within the capabilities of the system. The motor operated longer and at a lower pressure than predicted with no adverse effects on the test objective. All motor and component parts were in excellent condition at completion of the firing. Afterburning of the insulation and degradation of the nozzle plastic parts and flexible seal were prevented by the CO₂ quench system. This enabled post fire analysis of parts which were in a condition approximating end of burn time. Motor static test operations, test results and post fire analyses are presented in Section XII.

SECTION II

FLEXIBLE SEAL DESIGN, FABRICATION AND TEST

A. FLEXIBLE SEAL DESIGN

1. RELATED EXPERIENCE

(U) The flexible seal design for the TU-562 nozzle was based on elastic stability criteria established by Thiokol Chemical Corporation during a company funded development program. Original justification of this design was incorporated into the first quarterly technical report* with an action item to re-evaluate the design based on bench testing of the 100 in. motor program flexible seals under AF Contract No. AF 04(694)-774. Seal bench test results on the 100 in. motor program were as expected.

(U) Testing of seal configurations for a Hercules/Thiokol joint effort related to Poseidon resulted in failure pressures substantially lower than expected. These designs were cylindrical configurations and the analytical study provided a reason for their premature failure. Comparison of the test results between the conical designs of the 100 in. motor program and the cylindrical designs of the Hercules/Thiokol joint effort illustrates the superior stability qualities of the conical shape. Table I gives an overview of the total flexible seal work conducted by Thiokol.

* Development and Demonstration of an Omniaxial Flexible Seal Movable Nozzle for Thrust Vector Control - Quarterly Technical Report No. 1 TE2-237-11-6, November 1966.

TABLE I

FLEXIBLE SEAL CONFIGURATIONS

Program	Serial No. thru yr	Vendor Angle (deg)	Material and Method of Application	Elastomer No. of Pys and Thickness (in.)	Shear Modulus (psi)	Stem		Test Results		Remarks
						Material and Configuration	Stem Thickness (in.)	Spring Rate (in./lb./deg)	Pressure Test (psi)	
Flat Washer IR & D	MRC-1*	3	Styrene Screened	15 - 0.004	--	Styrene - Bress - Foil - Conduits	0.002	--	1,000 1,100	Buckling tests
			Screened	30 - 0.004	--	SS 302 Baffles	0.002	--	--	Not tested, unbonded
	MRC-2A	5	DC 86571/15 Screened	41 - 0.007	130	SS 302 Split Spherical	0.002	10,000 at 400 psi	1,500	Failed at 1,500 psi at 3 deg deflection
	MRC-2B	3	DC 86571/15 Spray	41 - 0.007	105	SS 302 Herringbone	0.002	--	--	Bond failure
	MRC-3	6	DC 86571/15 Screened	78 - 0.007	40	SS 302 Split Conical	0.002	--	--	In fabrication, seal 1 Nov
	MRC-4	2, 25	DC 86571/15 Screened	83 - 0.007	105	SS 302 Split Spherical	0.002	11,000 at 400 psi	400	Shipped stem
	MRC-5	2, 25	DC 86571/15 Spray	94 - 0.007	40	SS 302 Laboratory Formed Spherical	0.002	--	--	Stem fabricated 15 Nov
	MRC-2C	3	DC 86571/15 Spray	90 - 0.007	40	SS 302 Laboratory Formed Spherical	0.002	--	--	Stem fabricated 1 Dec
	TCC-1**	3	Goodyear 357-2 Polyisoprene Calendered	7 - 0.046	97	SS 304 Laboratory Formed Spherical	0.003	15,400 at 400 psi	400	Leaked at pressure
	TCC-2	3	Goodyear 357-2 Polyisoprene Calendered	7 - 0.046	97	SS 304 Laboratory Formed Spherical	0.003	15,400 at 400 psi	400	Did not fail at 2,000 psi at 3 deg deflection
BSD 100 in.	TCC-3	3	Shell Modified Polyisoprene Calendered	7 - 0.046	38	SS 304 Laboratory Formed Spherical	0.003	15,400 at 400 psi	400	Exceeded stem at 500 psi
	TCC-4	2, 25	Goodyear 357-2 Polyisoprene Calendered	7 - 0.046	87	SS 304 Laboratory Formed Spherical	0.005	15,400 at 400 psi	400	Did not fail at 2,000 psi at 3 deg deflection
	TCC-5	3	Goodyear 357-2 Polyisoprene Calendered	3 - 0.130	97	SS 304 Laboratory Formed Spherical	0.003	--	2,000	To be tested on motor
	TCC-6	2, 25	Goodyear 357-2 Polyisoprene Calendered	7 - 0.046	97	SS 304 Laboratory Formed Spherical	0.003	15,400 at 400 psi	400	To be tested on motor
	TCC-1	5	Goodyear 357-11 Polyisoprene Calendered	34 - 0.056	50	SS 304 Laboratory Formed Spherical	0.003	--	--	In fabrication, seal 15 Feb
	TCC-2	3	Goodyear 357-11 Polyisoprene Calendered	34 - 0.046	50	SS 304 Laboratory Formed Spherical	0.004	--	--	To be tested on motor
	TCC-3	5	Goodyear 357-11 Polyisoprene Calendered	34 - 0.046	50	SS 304 Laboratory Formed Spherical	0.004	--	--	To be tested on motor
	MRC-1	5	DC 86571/15 Silastic - Spray	38 - 0.017	50	SS 302 Lysol-form Spherical	0.001	--	--	In fabrication, seal 7 Nov
	FCC-1	4	Goodyear 357-11 Polyisoprene Calendered	40 - 0.025	70	SS 301	0.001	--	--	IR & D design has seal materials prepared
	FCC-2	3	Goodyear 357-11 Polyisoprene Calendered	40 - 0.025	70	SS 201	0.001	--	--	First program seal
TCC-3		4	Goodyear 357-11 Polyisoprene Calendered	40 - 0.025	70	SS 301	0.001	--	--	Tested on 1 Jan

* MRC - Mar in Buckwell Corp.
 ** TCC - TCC in Chemical Co.
 *** With Bond.

CONFIDENTIAL

2. DESIGN CRITERIA

- (C) Most of the design criteria for the flexible seal was contained in the work statement. It included a vector angle of ± 4 deg, a maximum thrust vector rate of 20 deg/sec, a minimum side impulse over action time of 1.1 percent of the total axial impulse, four full deflections at 1-1/4 cps, and a cycle rate of 1-1/2 cps at a thrust deflection angle of 0.5 degrec.
- (U) The design also considered a high factor of safety for the initial designs. Shims were designed in accordance with shear spinning techniques presently available. Pre-calendcred rubber was evaluated, and end rings, which may be easily fabricated from ring rolled forgings with normal machining techniques, also were used.
- (U) Other design criteria were reasonable costs and cost reduction potential. To minimize technical risks the flexible seal design was not flightweight. However, it does have weight reduction potential.

3. CONFIGURATION

- (U) The seal design for the 156-9 motor utilizes alternate layers of polyisoprene rubber (UF-4001) and 304 stainless steel vulcanized as an assembly with steel end rings that interface with the nozzle movable and fixed housings.
- (U) The stainless steel shims were shear formed into spherical segments from welded conical sections that are 0.040 in. thick. There are a total of 82 metal shims in the composite. The rubber layers between the shims are 0.025 in. thick. Figures 2 thru 5 show the assembly and detailed parts of the seal design.
- (U) The pivot center of the seal is located 19.1 in. aft of the aft end ring and the average spherical radius is 36.8 inches. The angle between the motor axis and

CONFIDENTIAL
(THIS PAGE IS UNCLASSIFIED)

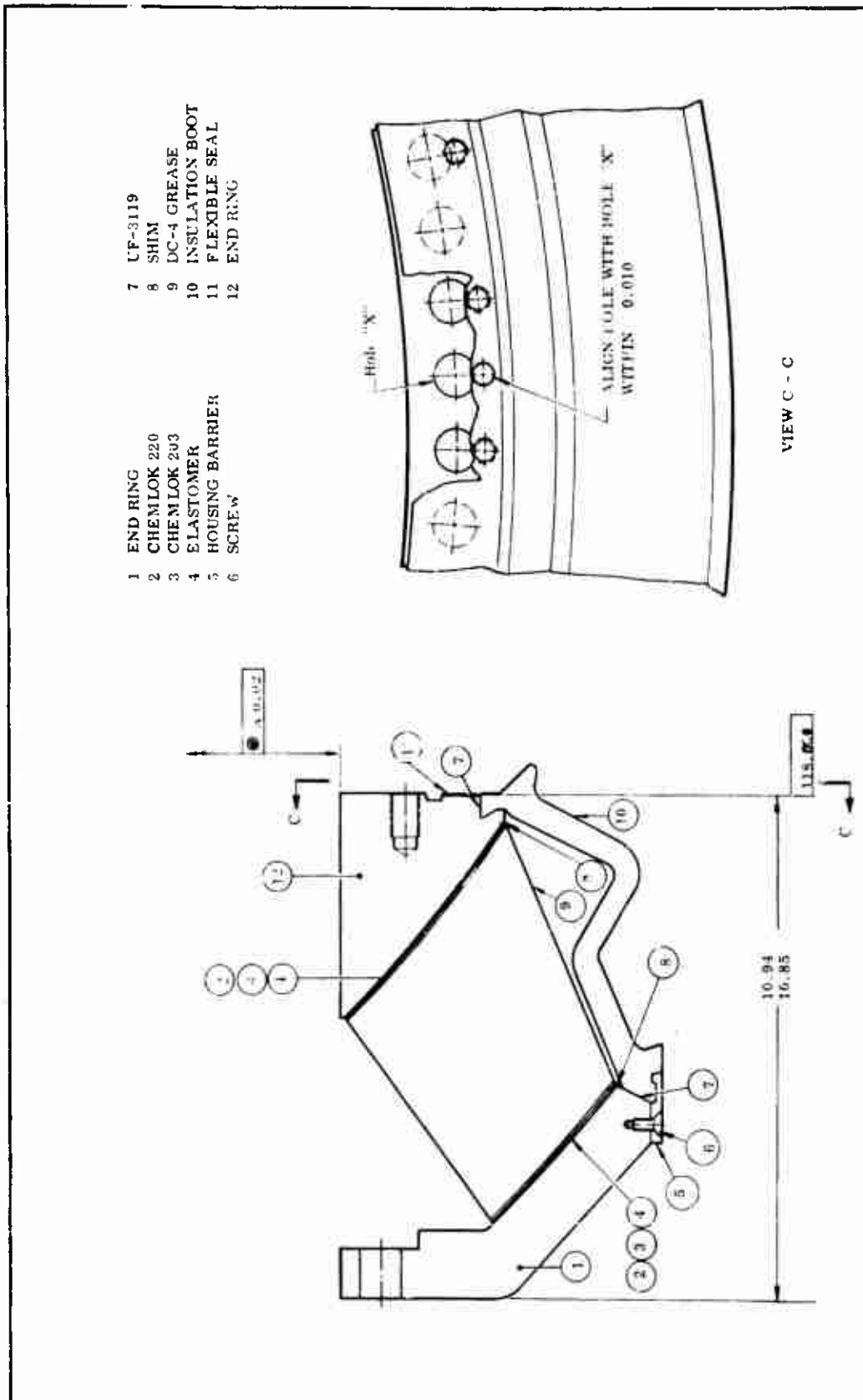
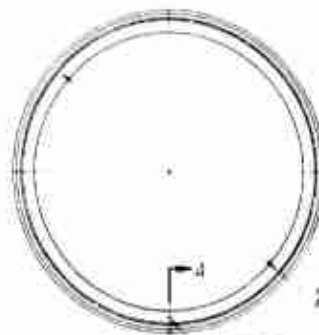


Figure 2. Flexible Seal Design

CONFIDENTIAL
(THIS PAGE IS UNCLASSIFIED)

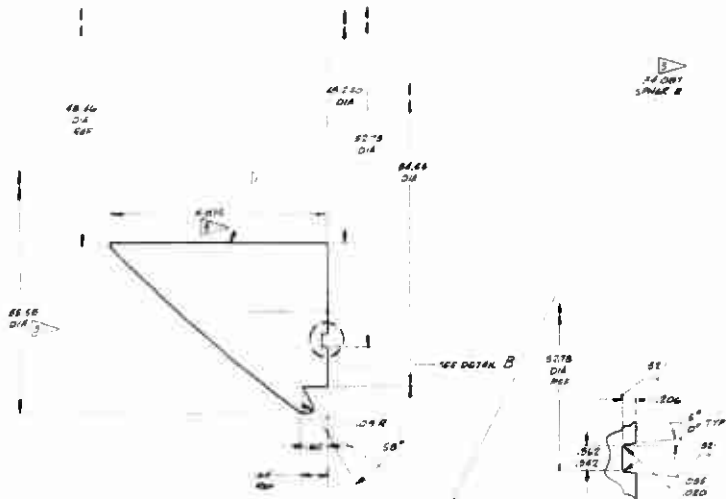
[illegible]



1.100 ± .005
 2.000 ± .005
 3.000 ± .005
 4.000 ± .005
 5.000 ± .005
 6.000 ± .005
 7.000 ± .005
 8.000 ± .005
 9.000 ± .005
 10.000 ± .005
 11.000 ± .005
 12.000 ± .005
 13.000 ± .005
 14.000 ± .005
 15.000 ± .005
 16.000 ± .005
 17.000 ± .005
 18.000 ± .005
 19.000 ± .005
 20.000 ± .005
 21.000 ± .005
 22.000 ± .005
 23.000 ± .005
 24.000 ± .005
 25.000 ± .005
 26.000 ± .005
 27.000 ± .005
 28.000 ± .005
 29.000 ± .005
 30.000 ± .005
 31.000 ± .005
 32.000 ± .005
 33.000 ± .005
 34.000 ± .005
 35.000 ± .005
 36.000 ± .005
 37.000 ± .005
 38.000 ± .005
 39.000 ± .005
 40.000 ± .005
 41.000 ± .005
 42.000 ± .005
 43.000 ± .005
 44.000 ± .005
 45.000 ± .005
 46.000 ± .005
 47.000 ± .005
 48.000 ± .005
 49.000 ± .005
 50.000 ± .005
 51.000 ± .005
 52.000 ± .005
 53.000 ± .005
 54.000 ± .005
 55.000 ± .005
 56.000 ± .005
 57.000 ± .005
 58.000 ± .005
 59.000 ± .005
 60.000 ± .005
 61.000 ± .005
 62.000 ± .005
 63.000 ± .005
 64.000 ± .005
 65.000 ± .005
 66.000 ± .005
 67.000 ± .005
 68.000 ± .005
 69.000 ± .005
 70.000 ± .005
 71.000 ± .005
 72.000 ± .005
 73.000 ± .005
 74.000 ± .005
 75.000 ± .005
 76.000 ± .005
 77.000 ± .005
 78.000 ± .005
 79.000 ± .005
 80.000 ± .005
 81.000 ± .005
 82.000 ± .005
 83.000 ± .005
 84.000 ± .005
 85.000 ± .005
 86.000 ± .005
 87.000 ± .005
 88.000 ± .005
 89.000 ± .005
 90.000 ± .005
 91.000 ± .005
 92.000 ± .005
 93.000 ± .005
 94.000 ± .005
 95.000 ± .005
 96.000 ± .005
 97.000 ± .005
 98.000 ± .005
 99.000 ± .005
 100.000 ± .005

910

1.100 ± .005



SECTION A-A
 SCALE: 1/1

DETAIL B
 SCALE: NONE

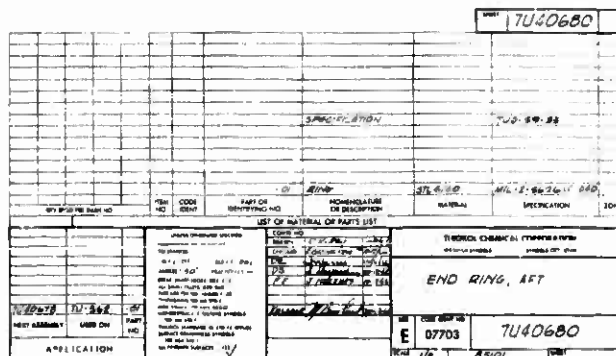


Figure 4. Aft End Ring

2

站名	站址	站址	站址
1. 100	100	100	100
2. 100	100	100	100
3. 100	100	100	100
4. 100	100	100	100
5. 100	100	100	100
6. 100	100	100	100
7. 100	100	100	100
8. 100	100	100	100
9. 100	100	100	100
10. 100	100	100	100
11. 100	100	100	100
12. 100	100	100	100
13. 100	100	100	100
14. 100	100	100	100
15. 100	100	100	100
16. 100	100	100	100
17. 100	100	100	100
18. 100	100	100	100
19. 100	100	100	100
20. 100	100	100	100
21. 100	100	100	100
22. 100	100	100	100
23. 100	100	100	100
24. 100	100	100	100
25. 100	100	100	100
26. 100	100	100	100
27. 100	100	100	100
28. 100	100	100	100
29. 100	100	100	100
30. 100	100	100	100
31. 100	100	100	100
32. 100	100	100	100
33. 100	100	100	100
34. 100	100	100	100
35. 100	100	100	100
36. 100	100	100	100
37. 100	100	100	100
38. 100	100	100	100
39. 100	100	100	100
40. 100	100	100	100
41. 100	100	100	100
42. 100	100	100	100
43. 100	100	100	100
44. 100	100	100	100
45. 100	100	100	100
46. 100	100	100	100
47. 100	100	100	100
48. 100	100	100	100
49. 100	100	100	100
50. 100	100	100	100
51. 100	100	100	100
52. 100	100	100	100
53. 100	100	100	100
54. 100	100	100	100
55. 100	100	100	100
56. 100	100	100	100
57. 100	100	100	100
58. 100	100	100	100
59. 100	100	100	100
60. 100	100	100	100
61. 100	100	100	100
62. 100	100	100	100
63. 100	100	100	100
64. 100	100	100	100
65. 100	100	100	100
66. 100	100	100	100
67. 100	100	100	100
68. 100	100	100	100
69. 100	100	100	100
70. 100	100	100	100
71. 100	100	100	100
72. 100	100	100	100
73. 100	100	100	100
74. 100	100	100	100
75. 100	100	100	100
76. 100	100	100	100
77. 100	100	100	100
78. 100	100	100	100
79. 100	100	100	100
80. 100	100	100	100
81. 100	100	100	100
82. 100	100	100	100
83. 100	100	100	100
84. 100	100	100	100
85. 100	100	100	100
86. 100	100	100	100
87.			

- NOTES
1. HAZARDOUS WASTE NUMBER FOR T-1000 IS 10000
 2. HAZARDOUS WASTE NUMBER FOR T-1000 IS 10000
 3. HAZARDOUS WASTE NUMBER FOR T-1000 IS 10000
 4. HAZARDOUS WASTE NUMBER FOR T-1000 IS 10000
 5. HAZARDOUS WASTE NUMBER FOR T-1000 IS 10000
 6. HAZARDOUS WASTE NUMBER FOR T-1000 IS 10000
 7. HAZARDOUS WASTE NUMBER FOR T-1000 IS 10000
 8. HAZARDOUS WASTE NUMBER FOR T-1000 IS 10000
 9. HAZARDOUS WASTE NUMBER FOR T-1000 IS 10000
 10. HAZARDOUS WASTE NUMBER FOR T-1000 IS 10000

B.1

C.1

Answer

71340082

1

2

[illegible]

19

2

3

the center of the seal ($\bar{\beta}$) is 48 deg 30 minutes. Figure 6 is a schematic picture of the seal with all the important design data summarized. The angle between the seal load path and the normal to the center of the center shim, which is referred to as the shear angle, is 18 deg 5 minutes. The angle is an important design parameter in the seal configuration.

- (U) Table II is a summary of the material mechanical properties for the 304 stainless steel and polyisoprene rubber. Stainless steel has been used as the reinforcement material in most of the Thiokol seal assemblies fabricated to date because of its formability. A deficiency of this material is its low compressive yield strength. Alternate shim materials, such as 17-7 PH stainless steel which have increased strength properties, were investigated. The polyisoprene rubber selected for the 156-in. seal, UF-4001, was used in all of the other seal programs at Thiokol because of its high tensile and shear strength and excellent processing properties. Other polyisoprene compounds, UF-4002 and UF-4005, having lower values of shear modulus were tested in smaller size seals for performance evaluation. Direct substitution of the UF-4002 compound into the design would reduce the 156-in. seal spring torque 40 percent and have little effect on the structural integrity of the design.

4. DESIGN ANALYSIS

- (U) a. Torque--The torque produced by the flexible seal can be established by summing the incremental forces around the periphery of the seal multiplied by the moment arms of these forces about the pivot axis.

- (U) As illustrated in Figure 7, the force acts in the plane of the seal at point A and acts normal to the seal plane at point B. The deflection in the seal as well as the length of the moment arm also vary from point A to point B. It was necessary to define these variables so the summation of the incremental torques around the seal could be accomplished.

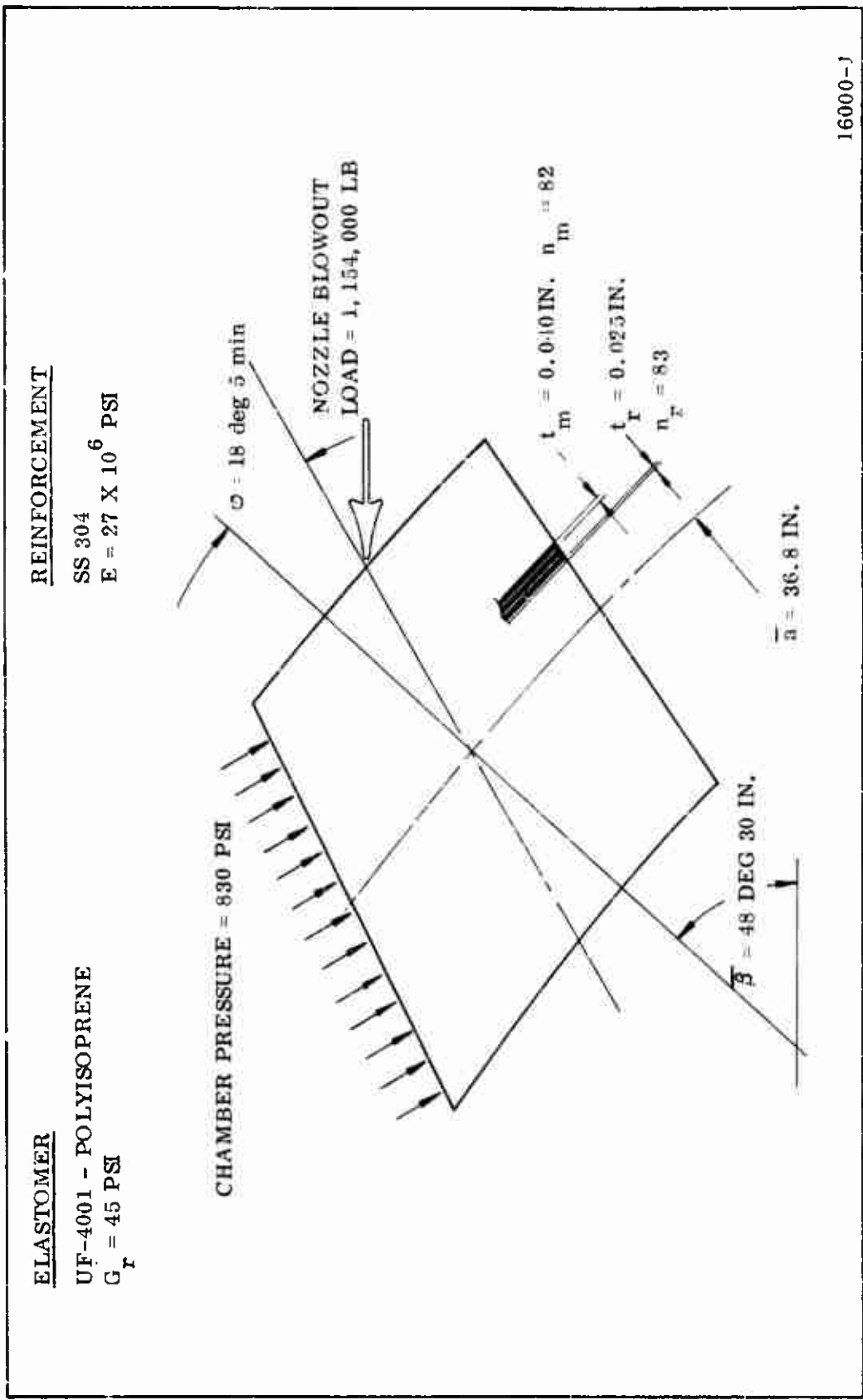


Figure 6. Flexible Seal Design

TABLE II

MATERIAL PROPERTIES

Elastomer Polyisoprene UF 4001		Reinforcement Shims S. S. 304	
Shear Strength, psi	685	Yield Tensile Strength, psi	74,200*
Tensile Strength, psi	2,890	Young's Modulus, psi	27×10^6
Maximum Elongation, percent	730	Poisson's Ratio	0.125
Shear Modulus, psi (100 percent strain)	45.5	Compressive Yield Strength, psi	73,263**
Poisson's Ratio	0.4998		

*Test data for "as spun" condition of shims

**Average from actual compressive tests of six longitudinal specimens
taken from "as spun" shims

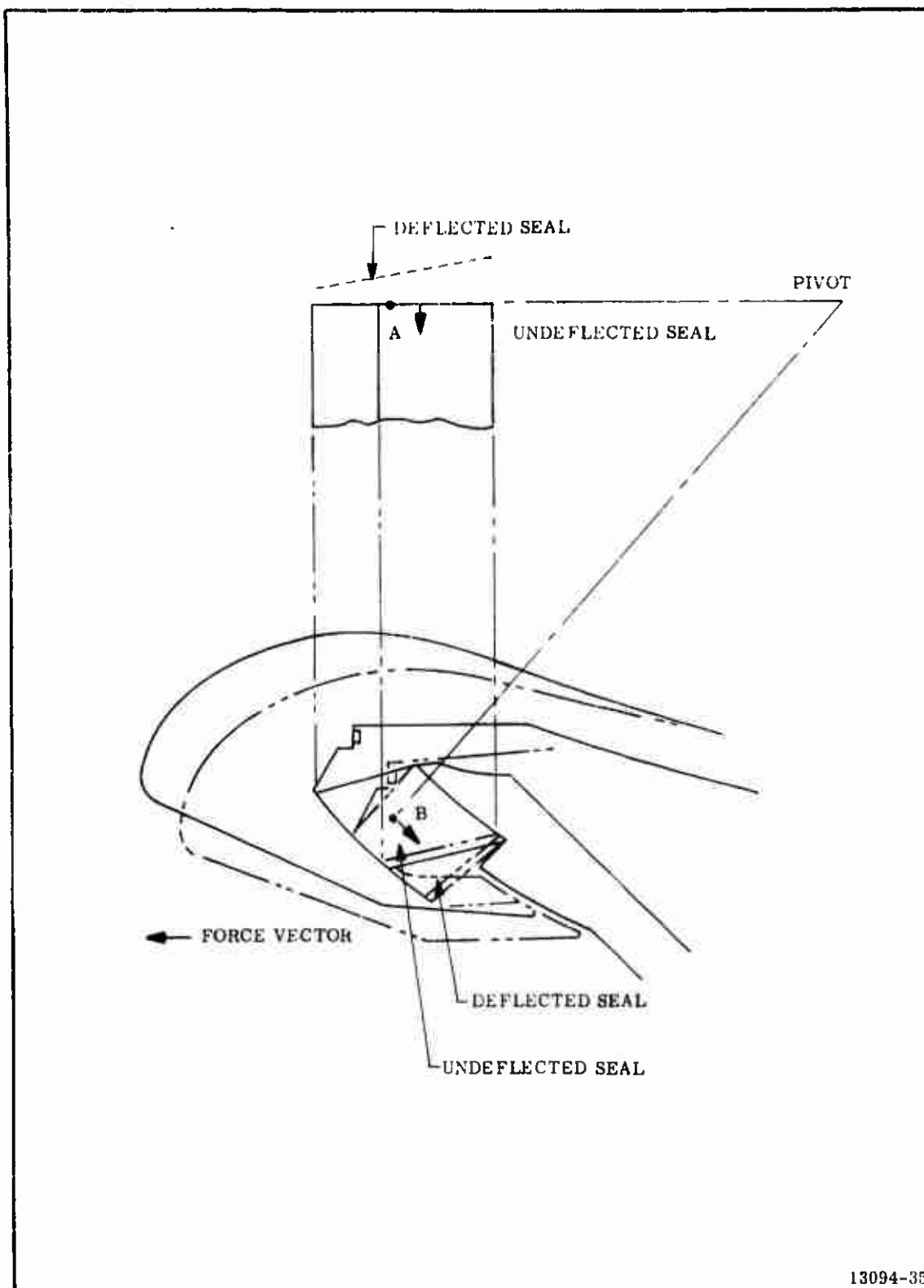


Figure 7. Flexible Seal Deflection

(U) The following paragraphs present the derivation of the seal torque expression. Since the seal deflects in the same manner in all four quadrants, this derivation will consider only a single quadrant of the seal.

(U) The general expression for seal torque is:

$$T = \sum_0^{\pi/2} F_i \bar{l}_i$$

where: F = force
 \bar{l} = moment arm

(U) The incremental force in the seal then can be expressed in terms of seal deflection, shear modulus of the rubber, and seal geometry.

$$F_i = \frac{\delta_i G dA}{nt_r}$$

where: δ_i = seal deflection
 G = shear modulus
 dA = incremental cross-sectional area
 n = number of rubber laminates
 t_r = thickness per laminate

The seal deflection is simply \bar{l}_θ where \bar{l} is the moment arm and θ is the nozzle deflection angle (Figure 8). The general expression for the moment arm length is:

$$\bar{l} = \bar{a} (\sin^2 \beta \sin^2 \Phi + \cos^2 \beta)^{1/2}$$

where: \bar{a} = radius of curvature
 β = angle between seal axis and the mean radius of the seal

(U) The incremental area also is

$$dA = (\bar{a} \sin \beta d\Phi) W.$$

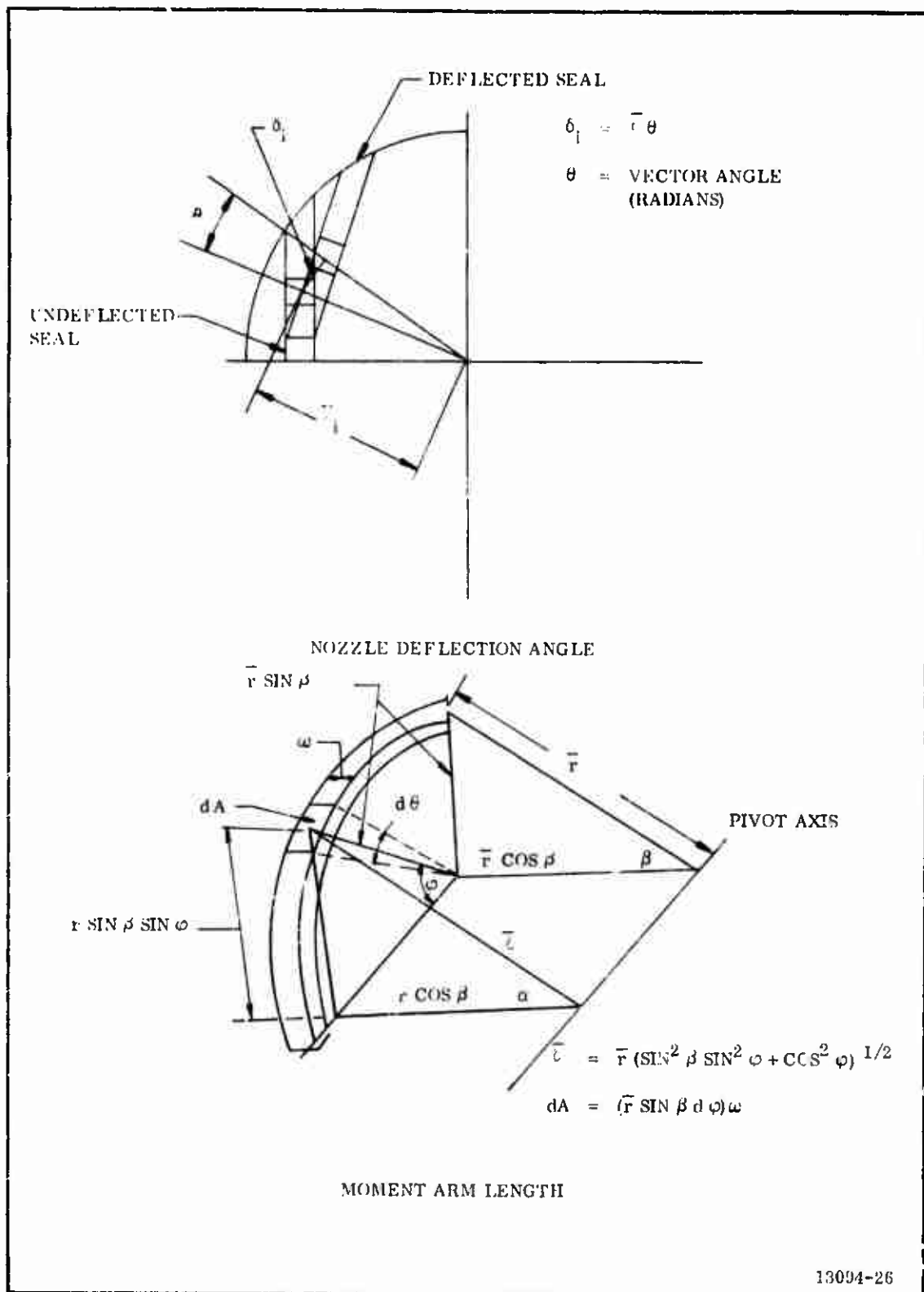


Figure 8. Determination of Moment Arm

- (U) The width (W) can now be expressed in terms of β_1 and β_2 , the angles measured between the seal centerline, and the inside and outside radii of the seal, respectively, so that

$$w = \bar{a} (\beta_2 - \beta_1),$$

β_2 and β_1 expressed in radians.

- (U) The force in the seal thus becomes

$$F_i = \frac{G}{nt_r} a^3 \sin \beta (\sin^2 \beta \sin^2 \Phi + \cos^2 \beta)^{1/2} (\beta_2 - \beta_1) d\Phi$$

The torque for the entire seal can then be determined from the integral

$$T = 4 \int_0^{\pi/2} \bar{I} F_i = 4 \int_0^{\pi/2} \frac{G}{nt_r} a^4 \sin \beta (\sin^2 \beta \sin^2 \Phi + \cos^2 \beta) (\beta_2 - \beta_1) d\Phi$$

Performing the integration and converting all angles from radians to degrees:

$$T = \frac{\theta G a^3}{3.24 \times 10^4 nt_r} \bar{a}^4 \sin (1 + \cos^2 \beta) (\beta_2 - \beta_1).$$

Since the seal torque is linear with deflection angle, expression of this component is more convenient as torque per degree of vector. Hence,

$$\frac{T}{\theta} = \frac{G \pi a^{3-4} \sin \beta}{3.24 \times 10^4 nt_r} (1 + \cos^2 \beta) (\beta_2 - \beta_1)$$

- (U) In Figure 9 the theory is compared with test data. The theory predicts torque slightly lower than data recorded at the low pressures and slightly higher than the data from the high pressure testing. The predicted curve was calculated using the shear modulus quoted for the zero pressure condition.

- (U) It has been determined experimentally that the change in seal torque with chamber pressure is also a function of the shear angle of the seal. That is, the larger shear angle results in a greater percentage change in seal torque as a

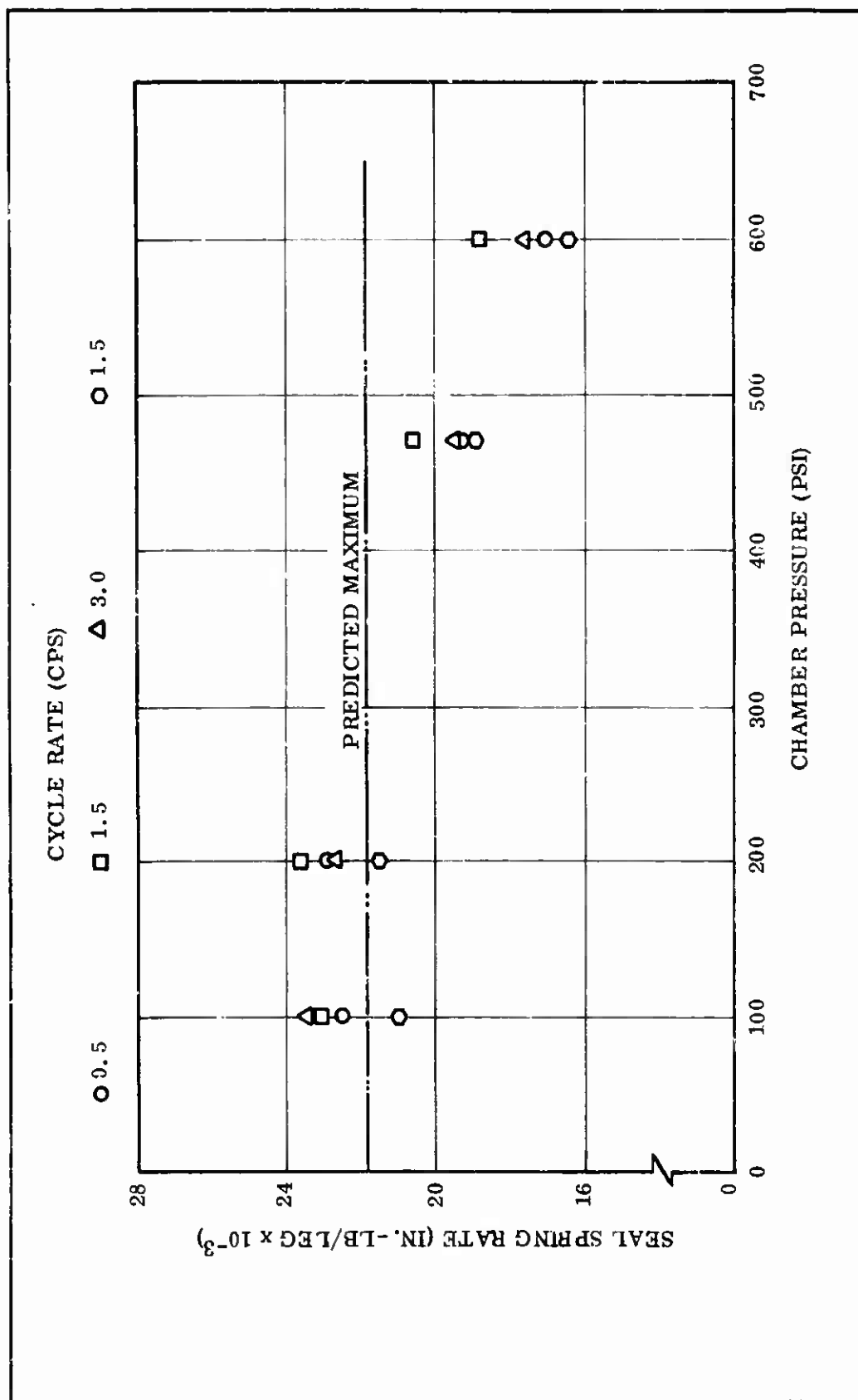


Figure 9. Flexible Seal Spring Rate vs Chamber Pressure

function of pressure. The data shown in Figure 9 are for a seal having a shear angle of 25 degrees. The TU-562 seal has an 18 deg shear angle, which should result in a somewhat less pronounced torque reduction due to pressurization.

(U) The predicted torque values for the unpressurized TU-562 seal are as follows:

Maximum	374,700 in. -lb/deg
Minimum	341,400 in. -lb/deg

(U) b. Structural--The design of the flexible seal is based upon elastic stability criteria that was developed by Thiokol during a company-sponsored development program. The equation for critical pressure was empirically derived from test data from washer specimens having very thin metal shims and rubber layers. Bench testing of 11-in. and 24-in. flexible seals indicated that the predicted values of critical pressure were well within the accuracy expected for a stability equation. All of these test specimens were conical in shape and had fairly low shear angles. Thiokol tested 22-in. seals under another contract that had cylindrical shapes and very high shear angles. Failures occurred at pressures well below the values predicted based on the stability equation. An extensive analysis of the bench test seal that failed prematurely and a parametric study of the effect of seal shape on shim and rubber stresses and axial deflection was conducted.

(U) The study indicated that the stress level in the shims of the cylindrical seals at the low failure pressures were of the same order of magnitude as the stresses in the conical seals at failure pressures four to five times higher. Further study and testing led to the following conclusions.

1. Shim hoop compressive stresses and elastomer shear stresses decrease rapidly as the seal configuration approaches a conical shape.
2. Axial deflection also decreases as the conical shape is approached, despite an increase in axial load due to the larger projected area.

(U) All of these results were investigated and included in the analysis of the 156-in. seal before fabrication of the first seal was begun. The results indicated that the design was adequate.

(U) Originally the equation for critical pressure due to material yield strength was based upon the thick walled cylinder equation for stresses due to radial pressure. This equation was changed to incorporate a factor based on the seal configuration as follows:

$$\max = K \frac{2 P_o^2}{(R_o^2 - R_i^2)} (1 + t_r/t_m) P_c$$

where K is a function of shear angle. The 156-in. seal has an 18 deg 5 min shear angle which increases to 39 deg when the seal is vectored 4 degrees. Using the design equation the maximum compressive stress levels predicted for the null and 4 deg position are, respectively, 23,730 psi and 38,985 psi. Comparison of these values to available test data from designs having the same shim thickness indicated that the 156-in. design was structurally sound.

(U) The critical pressure for the 156-in. design was calculated as a function of the buckling constant and is plotted in Figure 10. Based on this curve the maximum acceptable value of the buckling constant is 0.60. Figure 11 shows the curves of the buckling constant as a function of the radius to thickness ratio that was used to design the 156-in. seal. Additional test data indicated that the buckling constant for the 156-in. design should be less than 0.60 because of the conical shape and low shear angle.

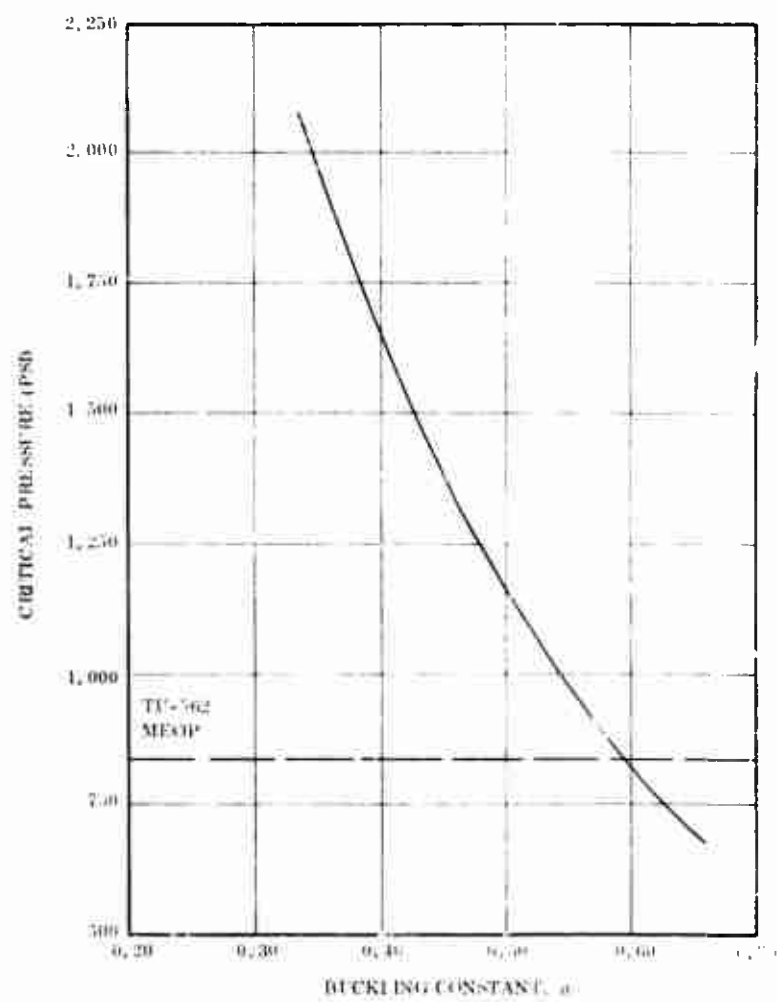


Figure 10. Critical Pressure vs Buckling Constant

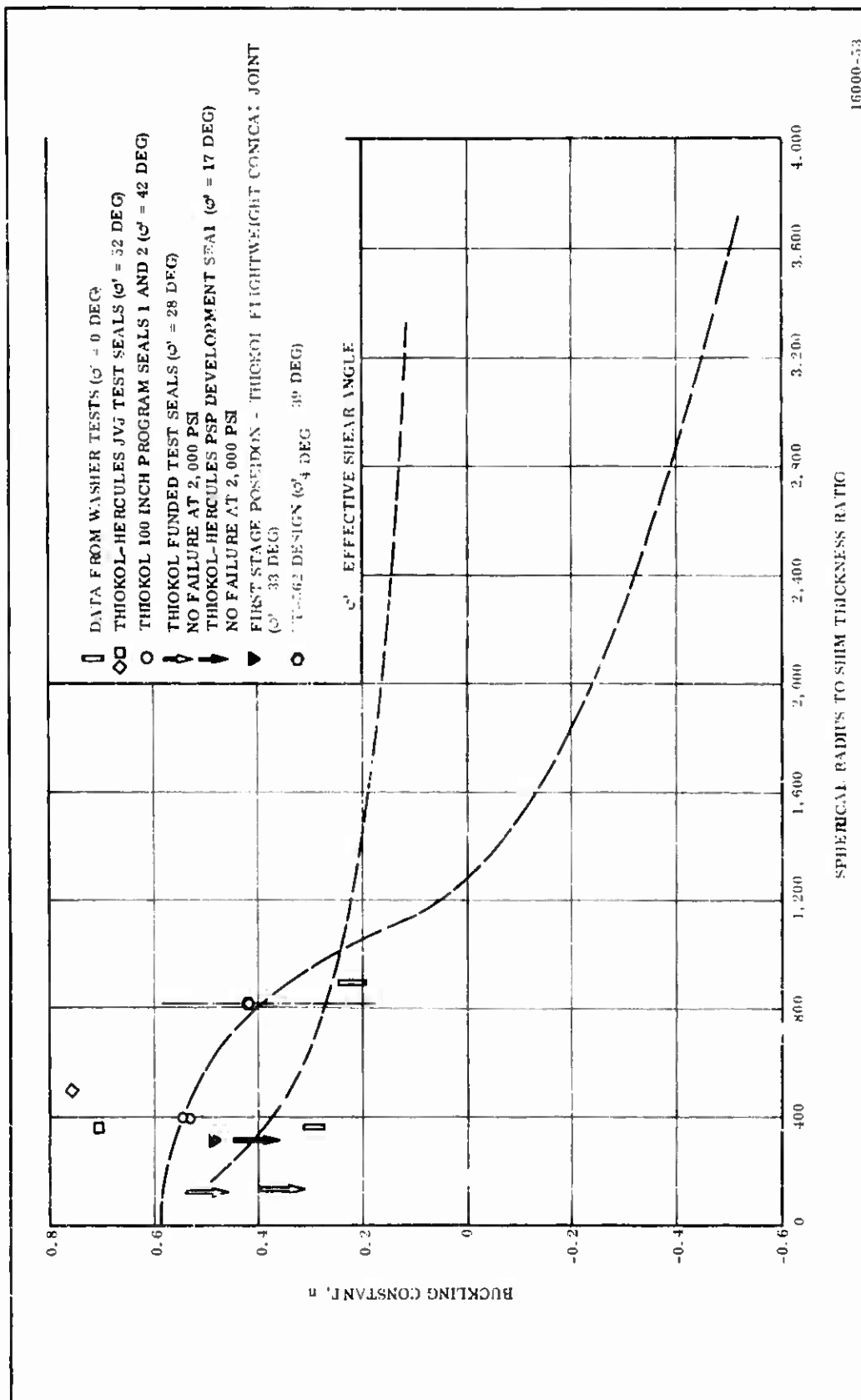


Figure 11. Buckling Constant as a Function of Spherical Radius to Shim Thickness Ratio

- (U) Elastic stability considerations are dominant in the determination of the initial flexible seal geometry. A detailed stress investigation is necessary to predict the overall adequacy of the design. To completely evaluate the flexible seal installation, it is necessary to develop a technique by which the state-of-stress may be predicted. This capability has been developed by Thiokol through the application of an existing procedure for the evaluation of an axisymmetric, composite, two-dimensional body by a finite element solution.
- (U) The technique involved was programmed for the electronic computer. The input data consisted of a description of the geometry, material properties, boundary conditions and loadings. The output consisted of displacements, stresses and strains at various points throughout the body, and an optional graphic presentation of the solutions.
- (U) The program available is limited to 59 metal and 60 rubber layers. Since the design of the TU-562 seal incorporated 82 metal shims, 0.040 in. thick and 83 rubber shims, 0.025 in. thick, analysis was not within the program capability.
- (U) Analysis of the seal was therefore performed in the following manner:
1. Analyze the seal in a slightly abbreviated envelope (58 metal, 59 rubber shims) with the correct shim thicknesses.
 2. Analyze the seal with the proper envelope, but with slightly increased shim thicknesses (0.056 metal and 0.035 rubber) holding the ratio of metal to rubber constant.
- (U) Figure 12 is a graphical presentation of the hoop stress in the metal shims along the ID and OD surface of the shims. This is the critical stress in the seal which induces buckling of the shims above a critical level. Although the critical stress level may not be accurately predicted on a theoretical basis, experience in test hardware indicates that it is at least 45,000 psi for the combination of metal and rubber used. Figure 12 shows that the maximum predicted stress in the null position is 18,000 psi compression. These numbers predict a factor of safety of

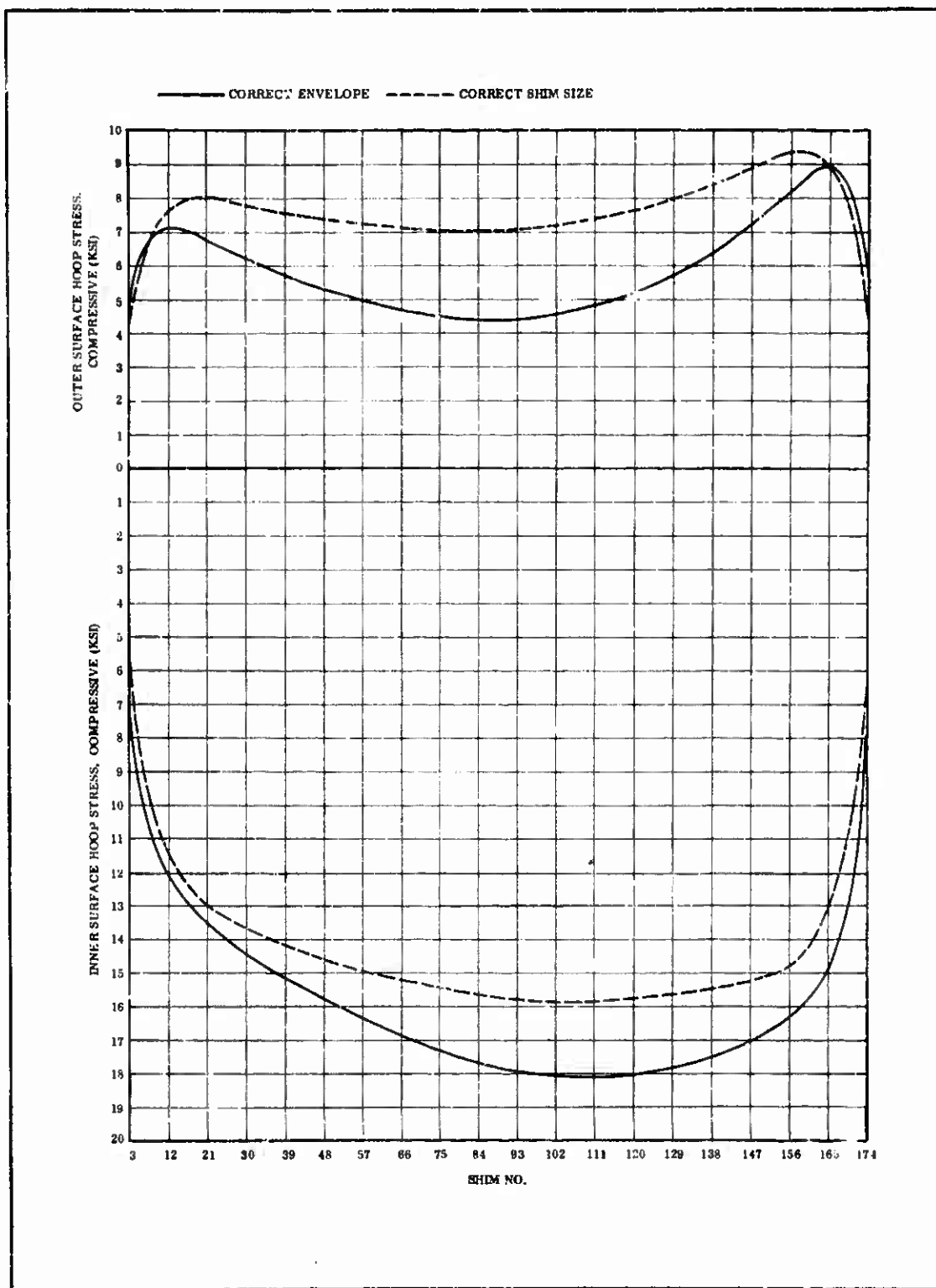


Figure 12. Flexible Seal Metal Shim Stress Distribution

2.5, suggesting a very conservative design. However, the critical stress level occurs when the seal is in a fully vectored position. Figure 13 indicates how the maximum stress value for the vectored position was derived. The maximum stress level in the vectored position is 26,000 psi compression, which reduces the factor of safety to 1.6.

(U) Figure 14 is a presentation of the loading experienced by a typical metal shim in the central section of the seal. The load center of the axial compressive load is slightly on the ID side of the shim center but almost perfectly balanced across the shim, inducing no bending in the shim.

(U) The shear distribution on both sides of the shim also is shown in Figure 14. The maximum elastomer shear stress of approximately 72 psi occurs close to the end rings. This shear stress is increased when the seal is vectored plus or minus 4 degrees. This component of the stress is determined as follows:

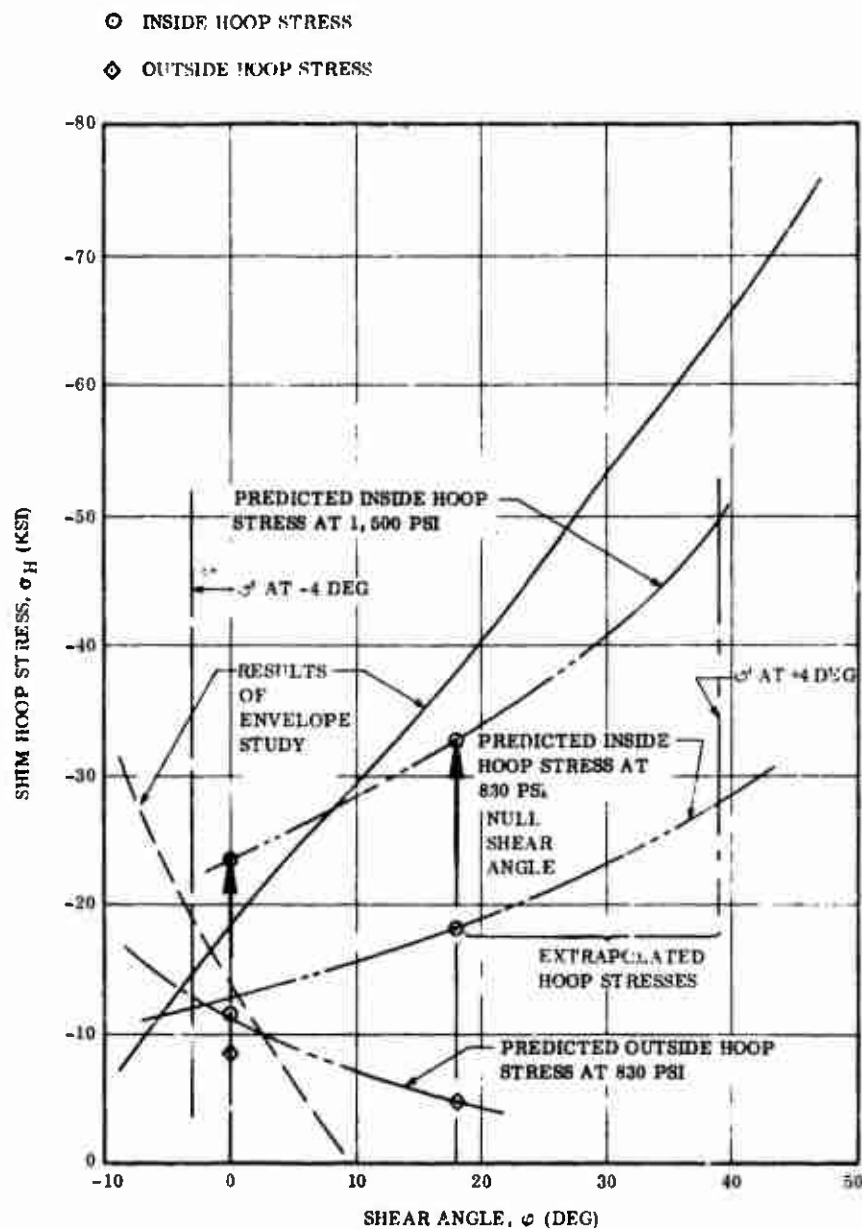
$$\tau = \frac{G_R a_o \theta_{\max}}{n t_r}$$

where: G_R = Rubber Shear Modulus, psi
 a_o = Outer Spherical Radius, in.
 θ_{\max} = Maximum Vector Angle, radians
 n = Number of Rubber Layers
 t_r = Rubber Layer Thickness, in.

$$\tau = \frac{(55.1) (39.48)}{83 (0.025)} \frac{4\pi}{180} = 73.1 \text{ psi}$$

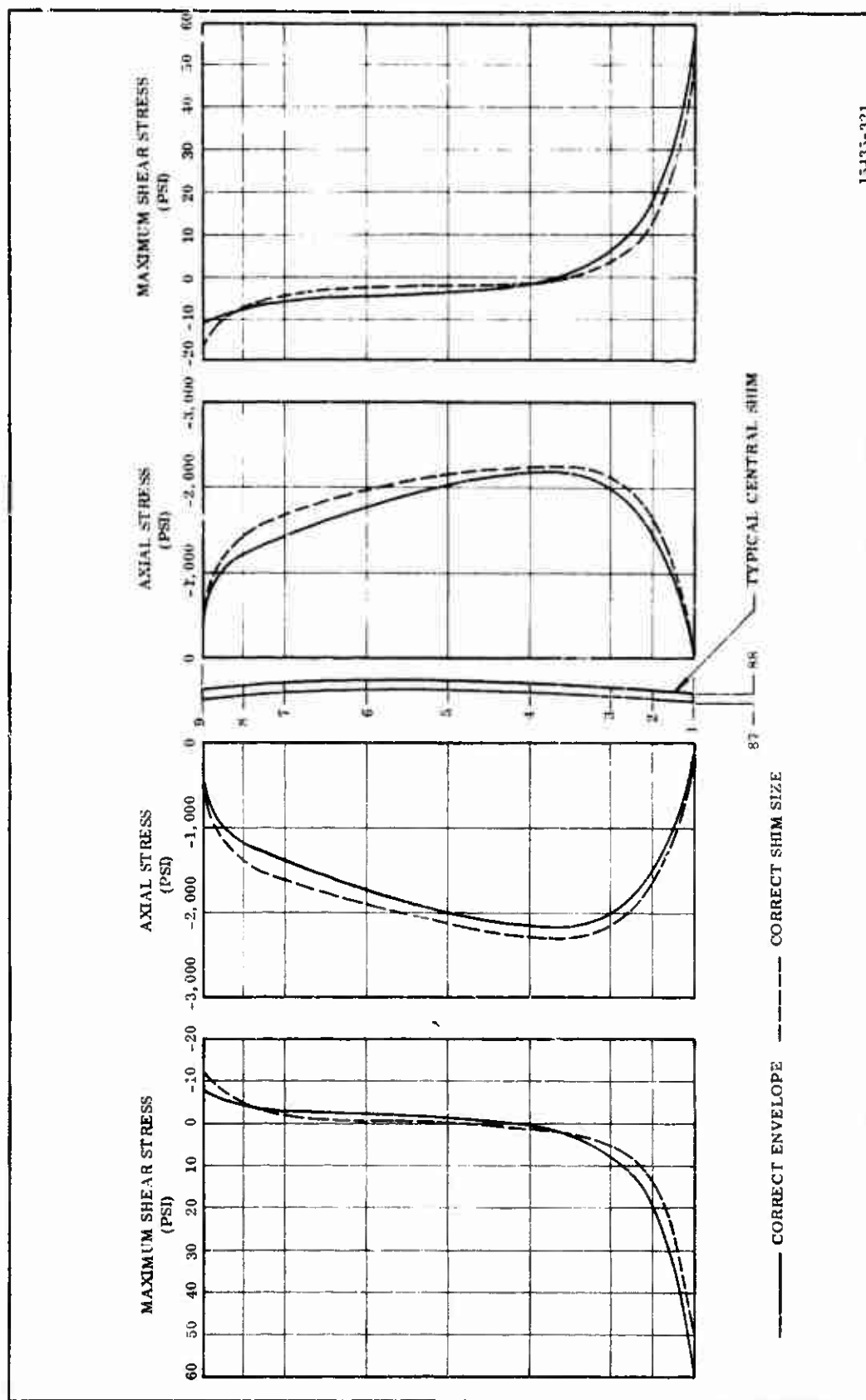
The total shear stress of 145 psi is well below the average shear strength of the rubber.

(U) The axial deflection of the seal also was determined during this analysis. The analysis was based on the correct rubber layer thickness but with an abbreviated envelope. The analysis showed an axial deflection of 0.039 in. which was scaled to 0.055 in. based on the correct number of shims.



15495-324

Figure 13. Shim Hoop Stress vs Shear Angle



13435-321

Figure 14. Flexible Seal Stress Distribution

5. BOOT REDESIGN

- (U) The design of the protective boot surrounding the flexible seal was changed subsequent to the original design. The material was changed from silicone rubber (K1255) to silica filled NBR (V-45) and the thickness increased from 0.3 to 0.55 inch. The change was made in order to increase the margin of safety.
- (U) No measurements of the erosion or char of either material under identical conditions were available. Pressure, temperature, and Mach number of the gas in a cavity separated from the chamber by a narrow gap (of varying length in the vectored position) had not been measured during actual motor firings. Mach number had been measured in several similar cavities during cold flow tests.
- (U) Tests also have been performed by Thiokol in which the erosion rates of these two materials were measured in the inlets of the nozzles of small test motors. Curves of erosion rate as a function of one-dimensional Mach number were prepared. The Mach numbers predicted in the boot cavity by cold flow tests were then converted to erosion rates with the curves prepared from these tests.
- (U) The environment in the nozzle inlets was more severe than the environment in the cavity because of two factors:
1. Direct radiation to the boot in the cavity is prevented by the presence of the barrier.
 2. The energy of the gas is somewhat attenuated in passing through the gap.
- (U) As discussed above, the exact amount of conservatism in the erosion prediction based on the inlet firings and the cold flow Mach numbers was unknown. To insure a conservative design, the product of predicted erosion rate and predicted web time was used to calculate the thickness of the boot. The erosion rate of V-45 was less at the Mach number predicted from cold flow testing than the K1255 erosion rate. Therefore, V-45 was selected to minimize the boot thickness, thus minimizing the changes necessary in the mating parts.

B. FLEXIBLE SEAL FABRICATION

1. COMPONENT BREAKDOWN

- (U) Fabrication of the 156 in. flexible seal was originally started with a sub-contract to Marlin-Rockwell Co (MRC), in Jamestown, New York. This effort was later cancelled and a redesigned seal was fabricated by Thiokol with assistance from other vendors.
- (U) The seal is comprised of five principal parts: end rings, shims, elastomer, spacers, and boot (Figures 15 thru 18). Materials, components and most of the tooling used in the manufacture of this flexible seal were supplied by subcontractors as listed below.

<u>Components and Materials</u>	<u>Part No.</u>	<u>Subcontractor</u>
Forward and Aft End Rings (machined)	7U40679-01 7U40680-01	Supreme Tool and Engineering Co, Santa Fe Springs, California (Supreme)
Shear Spun Shims	7U40682-01 thru -82	Precision Sheet Metal Co Los Angeles, California (PSM)
Polyisoprene Elastomer (calendered)	TCC Spec STW4-488	Rubber Engineering Co Salt Lake City, Utah
Seal Assembly Fixture	SK40748	Supreme

- (U) a. End Rings--Both forward and aft end rings were machined from ring rolled forgings of 4140 steel. Six forgings were originally procured by MRC from Ajax Steel and Forge in Detroit, Michigan. They were shipped in the "as rolled" condition to Supreme where they were machined to the specified configuration (Figures 3 and 4). All operations performed by Supreme were straightforward machining operations. The rings were rough machined on a large vertical mill, heat treated by an outside source, and final turntable machined. All required holes were drilled, or

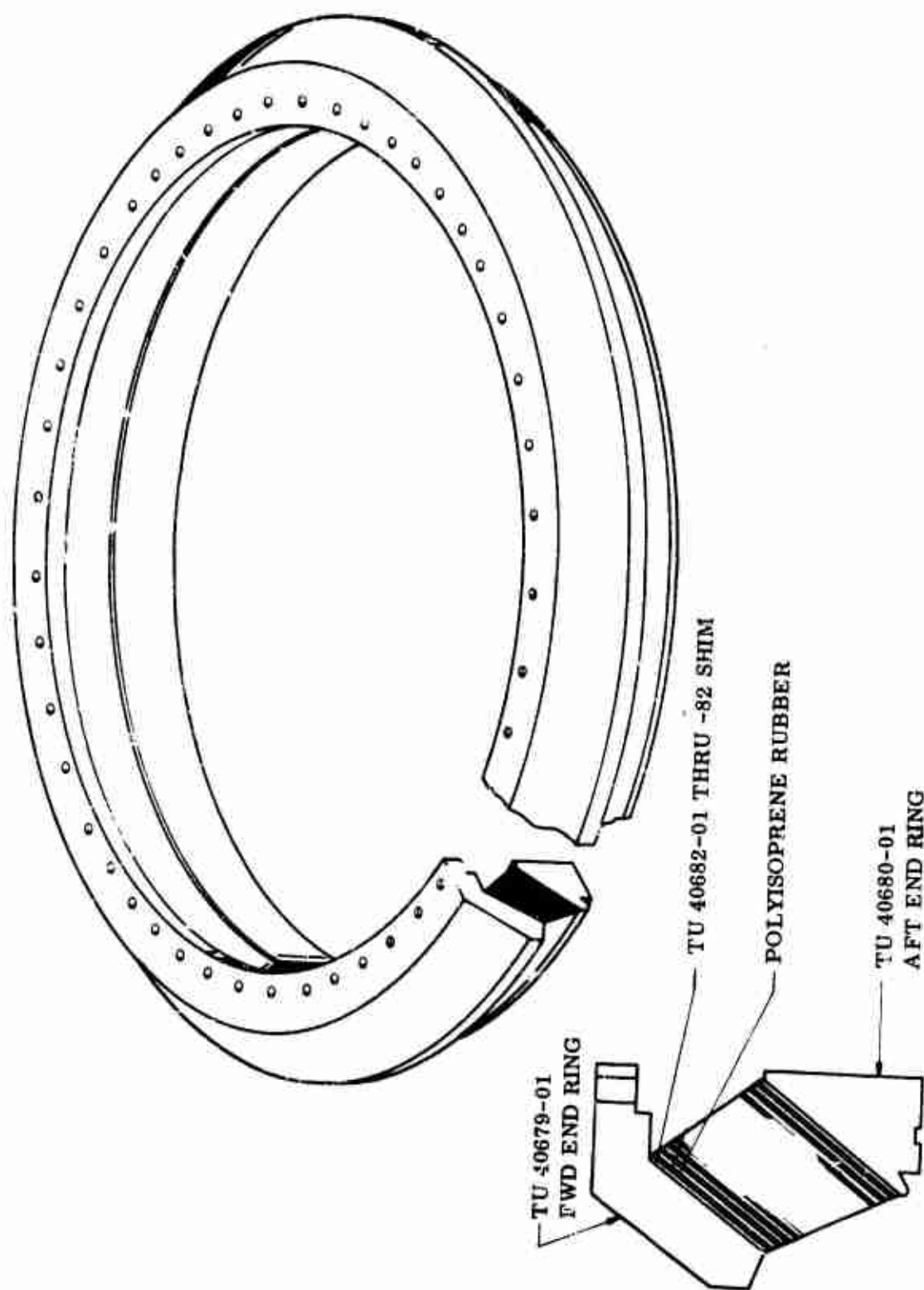


Figure 15. Flexible Seal

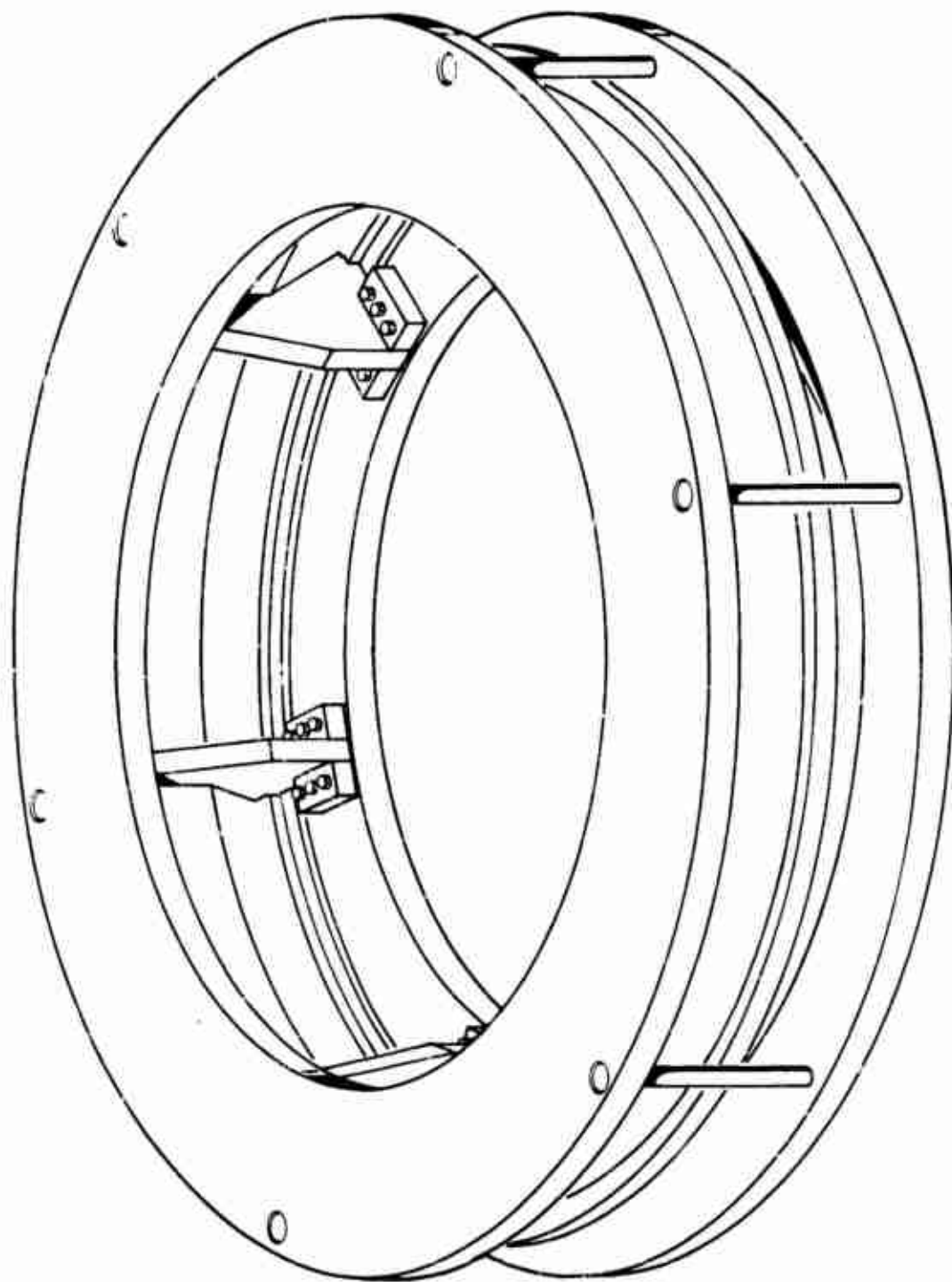


Figure 16. Flexible Seal Assembly Fixture

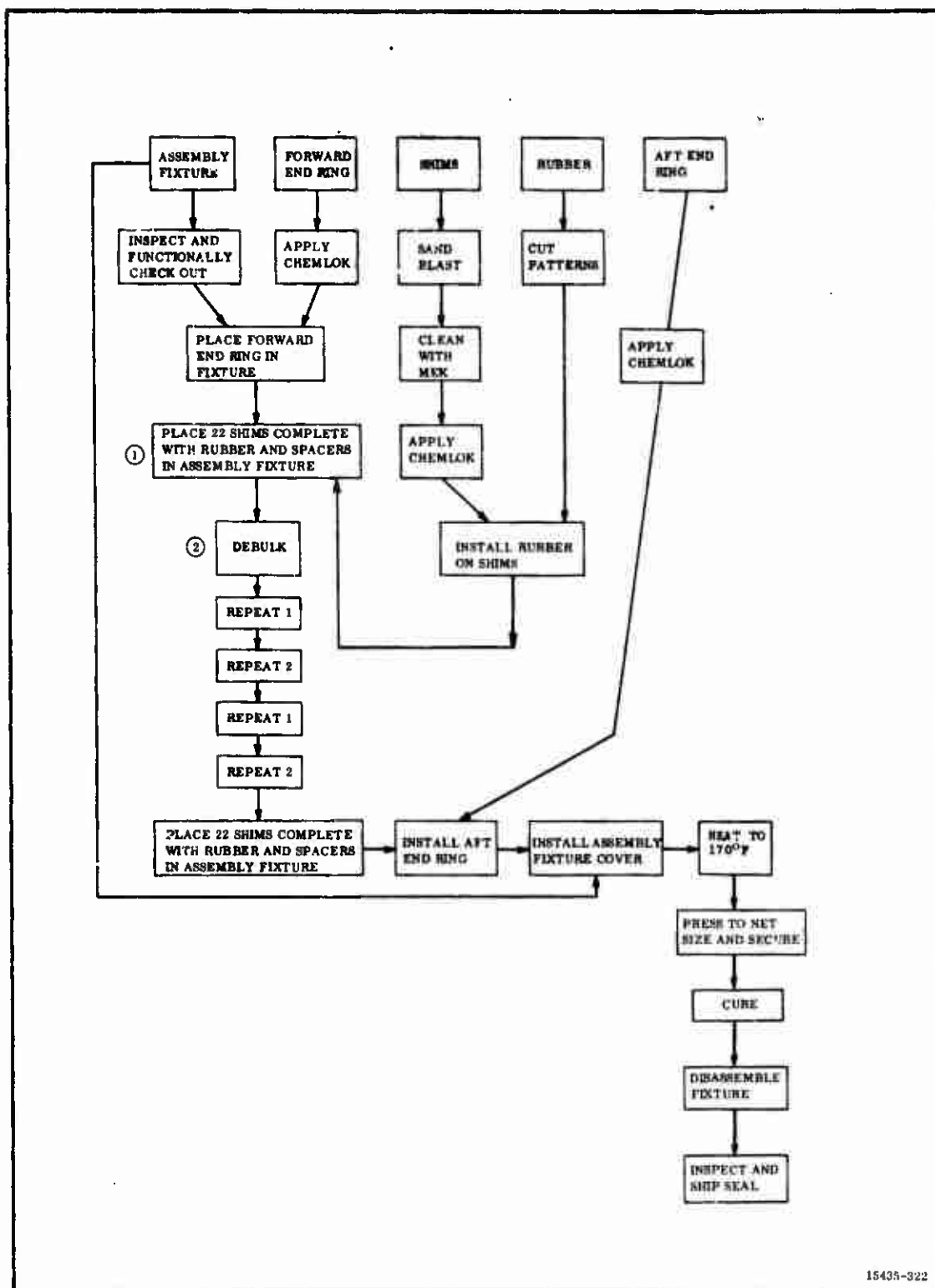


Figure 17. Flexible Seal Fabrication Functional Flow Diagram

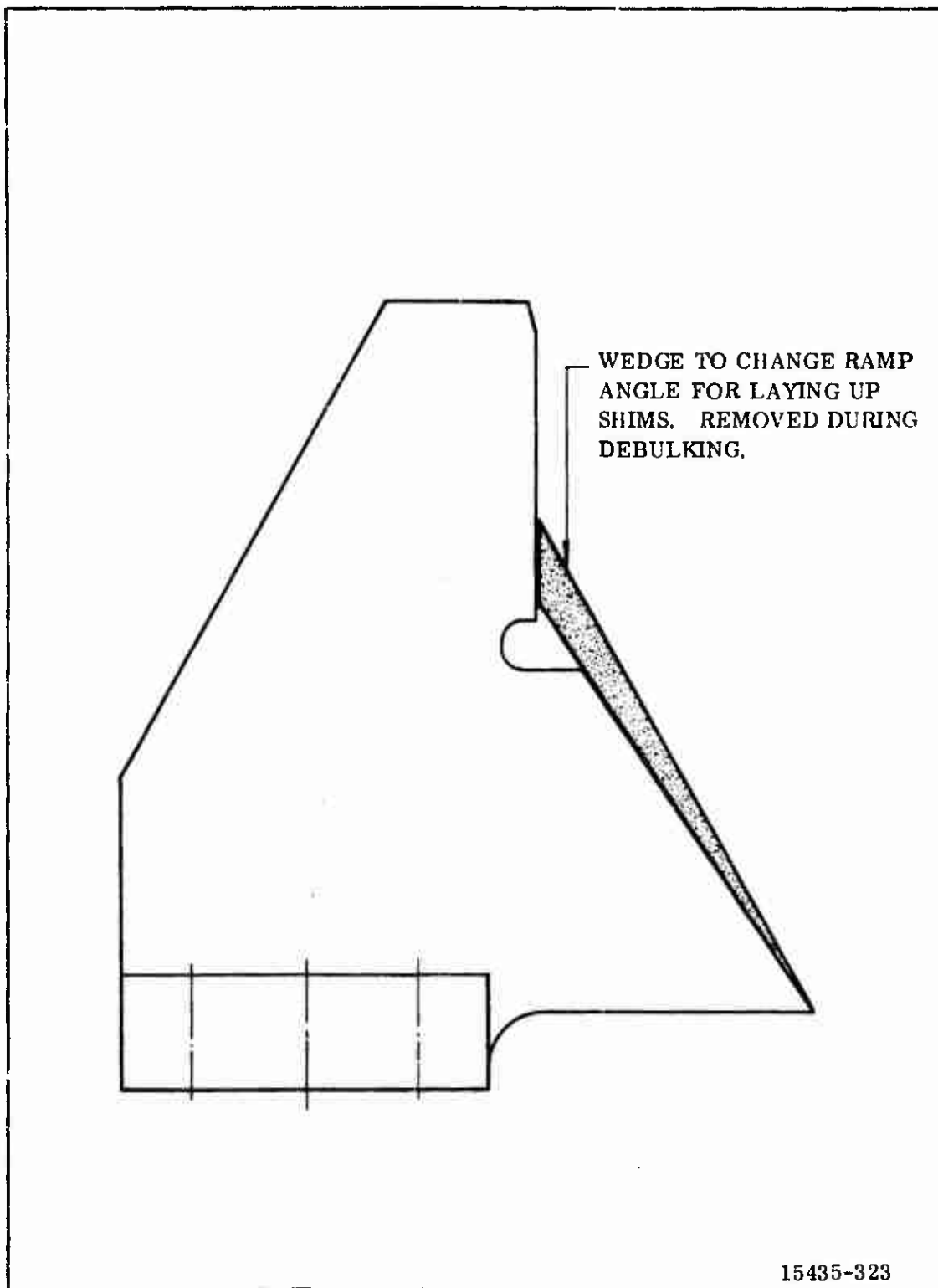


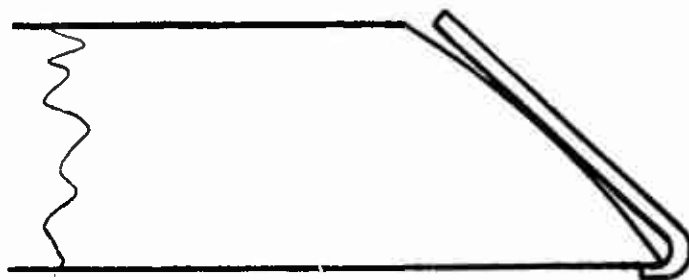
Figure 18. Wedge Arrangement for Shim Layup

drilled and tapped on a large radial drill. Drill ring templates were used to assure precise hole location and to assure proper fitting of nozzle metal parts. The finished end rings were delivered to Reinhold.

(U) b. Shims--Precision Sheet Metal procured one coil of 20 gage, Type 304 stainless steel, 36 in. wide by 0.041 in. thick by 682 ft long. Shim thickness is extremely critical since an increase of 0.001 in. could result in a seal 0.082 in. longer than desired. Steel rolling mill thicknesses vary 0.005 in. but the thickness variance within a given coil, from one melt, through one set of rollers, not adjusted during the run is extremely small (0.001 in.). To obtain the tight thickness tolerances desired and to assure uniform shim thickness between and within sets, three complete sets of shims (82 per set) were fabricated from the single coil. Three complete sets were fabricated at one time because the shear spinning mandrel must be machined smaller and smaller as the various dash numbered shims are produced. The mandrel would be destroyed in the process whether one set or three sets were produced.

(U) Individual shim fabrication started with the cutting of arc patterns. Three each of these patterns were welded into a conical preform.

(U) For reasons of economy all shims were made from one standard conical preform, welded from three standard patterns which were cut from only one standard template. Thus, all conical preforms were wide enough to form any dash numbered shim. After welding, the conical preforms were stress relieved and then pressed onto a mandrel in a large horizontal shear spinning machine. Each preform was locked on the mandrel by spinning the periphery over a lip on the mandrel. The preform contacted the mandrel as shown below.



- (U) Each spherical shim was formed by spinning in each direction from the shim center. The center of the shim got the least amount of cold working and remained the thickest part of the shim. Shims tapered approximately 0.0005 in. from the center to the edges. After each shim was formed, the ID was marked by touching a single point tool to the spinning shim in the same manner as on a lathe. This marking by the single point tool was always started at an ID less than desired. The outside of this line formed represented the shim ID and was accurately measured with a caliper. The difference between this and the print requirement was determined and the single point tool repositioned the precise amount. The shim was then cut off, and the ID verified. The OD was then marked and measured in the same manner. When certain of tool position, the last cut was made freeing the shim from the mandrel. Each shim was then tied to a wooden cross for handling. All sharp edges were smoothed by hand filing and the weld areas dressed by hand sanding.
- (U) In their free state, the shims were not round and, therefore, accurate diameter measurements were impossible. Thus, PSM quality control department measured and recorded shim ID, OD, and spherical radius while the shim was on the mandrel. PSM manufacturing personnel could not part the shim from the mandrel until directed by PSM quality control.
- (U) Shim thickness was controlled by measuring the thickness of the conical preform prior to installing it on the mandrel. Preforms were intentionally on the high side of their thickness tolerance. The amount of thinning required was estimated in advance. Thinning was accomplished by belt sanding a predetermined length of time after the shim had been formed. This method assured that each shim got the same amount of cold working (by shear spinning). This, in turn, assured a uniform strength level between shims. Shim thickness was finally measured and recorded after the shim was released from the mandrel and tied to a wooden cross. PSM provided Thiokol with a certified record of all shim measurements (ID, OD, spherical radius, and thickness) as well as basic material certifications at the time of shipment.

(U) Testing--With Type 304 stainless steel, the relationship of compressive strength to tensile strength is not accurately predictable from tensile data only. Compressive testing was accomplished on samples taken from shims that had been spun (and thus cold worked) but had been rejected for dimensional considerations. Additional compressive testing was also performed on samples taken from the "as received" coil (not cold worked). The data thus obtained was used in the design analysis of the seal discussed in previous chapters. Test specimens were prepared from the above samples to the following precise configurations.

Length	3.000 ± 0.001
Width	0.500 ± 0.001
Thickness	$0.035 - 0.036$
End Parallelism	0.0005 TIR
Squareness	0.001 TIR

(U) These specimens were deburred by hand lapping on a surface plate to maintain sharp edges.

(U) All specimens, except those cut from the stainless coil, were flattened mechanically and subjected to $700 \pm 10^\circ\text{F}$ for one hour while compressed in a fixture. The compressive yield specimens required two flattening and two thermal operations. (Temperature of 725°F is used for stress relief of type 304 stainless steel springs without loss of mechanical properties.)

(U) The tension tests were conducted on standard 2 in. gage length specimens, machined and hand finished on the edges in accordance with MIL-STD-151. Yield strength was determined by 0.2 percent offset method from a stress-strain diagram.

(U) Microhardness tests were conducted on metallographically prepared sections cut from the 1 in. by 0.036 in. dimension of annealed, longitudinally spun, and transversely spun sections. These were converted to the Rockwell Hardness, B scale as were the hardness tests conducted on the 1 in. by 3 in. surfaces of the compression specimens.

- (U) Compressive yield sections, after having been flattened and thermally treated as described previously (within 0.004 TIR), were wet ground to the final thickness.
- (U) Compressive yield specimens were tested in a guided fixture such that no buckling occurred prior to yield. An extensometer measured the strain, which was recorded on a standard stress-strain recorder. The yield strength was determined by the 0.2 percent offset method.
- (U) Test results are shown in Table III.
- (U) c. Elastomer--The elastomer used was a polyisoprene formulated by Thiokol from basic Goodyear 357-11 stock. This polyisoprene rubber was mixed to Thiokol formulation by Rubber Engineering Co and the actual weights of each ingredient were certified. The rubber was then calendered to 0.029 in. (0.004 in. thicker than the final desired thickness). The extra thickness was to preclude voids or air gaps between shims of the finished seal. The calendered rubber was delivered to Thiokol in rolls 36 in. wide.
- (U) Physical property tests were conducted on the calendered rubber by Rubber Engineering Co prior to shipping it to Thiokol. Additional tests at Thiokol were conducted by the materials laboratory on samples taken from the "as received" rolls.
- (U) d. Boot--The protective boots were fabricated by Thiokol personnel at Wasatch Division. V-45 rubber was laid up by hand over a male mandrel. The boot was then shipped to HITCO where it was vacuum bagged and cured at 300°F and 300 psi in an autoclave. It was then returned to Wasatch Division and machined using a single point tool while the boot was still on the mandrel. The ends of the boot (to be retained by nozzle plastic parts and flexible seal metal parts) were molded net (no machining required) by use of sectioned OD rings bolted to the mandrel.

TABLE III
SHIM COMPRESSIVE YIELD STRENGTH, TENSION,
AND HARDNESS DATA

(U) 1. COMPRESSIVE YIELD STRENGTH:

<u>Specimen</u>	<u>Width (in.)</u>	<u>Thickness (in.)</u>	<u>Area (sq in.)</u>	<u>Yield (lb)</u>	<u>Yield (psi)</u>
Annealed					
1L	0.999	0.035	0.0350	1,550	44,285
2L	0.999	0.035	0.0350	1,620	46,285
3T	0.999	0.035	0.0350	1,720	49,142
4T	0.999	0.035	0.0350	1,695	48,428
Longitudinal					
5	0.999	0.036	0.0360	2,680	74,444
6	0.999	0.036	0.0360	2,730	75,833
7	1.000	0.036	0.0360	2,590	71,944
8	1.000	0.036	0.0360	2,665	74,027
9	0.999	0.036	0.0360	2,500	69,444
10	0.999	0.036	0.0360	2,660	73,888
Transverse					
11	0.999	0.035	0.0350	2,650	75,714
12	0.999	0.036	0.0360	2,660	73,888
13	1.000	0.036	0.0360	2,665	74,027
14	0.999	0.036	0.0360	2,670	74,166
15	0.999	0.036	0.0360	2,680	74,444
16	0.999	0.035	0.0350	2,610	74,571

(U) 2. TENSION DATA:

<u>Specimen No.</u>	<u>Yield Strength (psi)</u>	<u>Ultimate Tensile Strength (psi)</u>	<u>Elongation (percent)</u>
1L	73,750	97,450	40
2L	74,150	99,200	41
3L	73,450	99,200	41.5
4T	74,250	100,300	41.5
5T	75,800	100,300	41.5
6T	73,900	98,050	44

TABLE III (Cont)

SHIM COMPRESSIVE YIELD STRENGTH, TENSION,
AND HARDNESS DATA

(U) 3. HARDNESS DATA:

<u>Specimen No.</u>	<u>Knoop Hardness (K500)</u>	<u>Rockwell Hardness, B</u>
1A	193	88
2A	200	90
3A	196	89
4L	249	100
5L	247	99
6L	258	102
7T	258	102
8T	255	101
9T	250	100

A - Annealed

L - Longitudinal

T - Transverse

- (U) e. Assembly Fixture--The assembly fixture was fabricated by Supreme using conventional machine shop practices. Details were welded and rough machined. The fixture was then bolted together for final machine cuts. After inspection at Supreme, the assembly fixture was shipped directly to Reinhold.

2. AF SEAL NO. 1 FABRICATION

- (U) This flexible seal was assembled by Thiokol and Reinhold personnel working together as a team. Thiokol had cognizance over all operations and was responsible for the delivered article. Reinhold provided facilities, equipment, material, manufacturing and inspection personnel, and engineering consultant services on an "as required" basis under subcontract to Thiokol.
- (U) During previous programs Thiokol had developed a flexible seal manufacturing technology, but did not have facilities or equipment large enough to apply the same techniques to a 156 in. motor nozzle size seal. Reinhold was selected to assist in the fabrication because their facilities were ideally suited to the work and were in close proximity to other vendors.
- (U) A sketch of the flexible seal is shown in Figure 15 and the flexible seal assembly fixture is shown in Figure 16.
- (U) The end rings, shims, and flexible seal assembly fixture were shipped directly to Reinhold by Supreme and PSM. The polyisoprene rubber was delivered to Thiokol and transported by Thiokol personnel to Reinhold. The required cleaning solvent (MEK) and metal primer/adhesive (Chemlok 203 and 220) were also delivered to Reinhold by Thiokol.
- (U) A functional flow diagram outlining the major manufacturing steps is shown in Figure 17. The following paragraphs expand this diagram and explain each process.

- (U) a. Rubber Preparation--The first operation was the cutting of rubber patterns. Patterns were cut from metal templates in arc sections, six sections per shim. Four templates were made, one each representing the -20, -40, -60, and -82 shims, respectively. The templates were made by applying masking tape over a 60 deg arc of the proper shims, trimming the tape to the shim width, placing it on a flat aluminum sheet, and sawing the aluminum sheet along the tape edges. Using the patterns thus formed, all polyisoprene rubber required for the seal was cut and stored in a 40°F refrigerator.
- (U) b. Shim Preparation--Shim delivery was in groups. The first delivery consisted of shims Serial No. 1 and 2, Part no. -01 thru -50 respectively. The second and third deliveries were Serial no. 1, Part no.- 51 thru -60 and Serial no. 2, Part no. -51 thru -60, respectively. The next delivery included Serial no. 1, Part no. -61 thru -82 and the final delivery included Serial no. 2, Part no. -61 thru -82 as well as all Serial no. 3 shims.
- (U) Shims, as received from PSM, were grit blasted on both surfaces at Reinhold. Shims were identified by a part number and serial number rubber stamped on the metal. Since grit blasting would have destroyed this marking each shim was identified with a Thiokol provided brass tag wired to the individual shim prior to grit blasting.
- (U) After grit blasting, the shims were transferred to a clean room and stacked in numerical order. After the tag was removed each shim was wiped clean with a lintfree rag soaked in MEK, and visually inspected for cleanliness, process damage or other imperfections. One brush coat of Chemlok 203 gray primer was applied to each surface and allowed to dry for at least 15 minutes. Following application of the primer a brush coat of Chemlok 220 black adhesive was applied and allowed to dry. Then the shim was placed in its numerical slot on a rack for future use.
- (U) While the shims were being prepared as above, non-grit blasted shims were stacked on the assembly fixture using thin strips of rubber. This shim pack thus duplicated what the seal shim pack would be. The shims were debulked at the

-20, -40, and -60 intervals, thus checking out the assembly fixture and its debulking rings as well as the shim/rubber stackup.

- (U) After the fixture checkout, the forward end ring was placed on the assembly fixture and centered by shimming between the fixture and the ID of the ring. The bonding surface was wiped clean with MEK and Chemlok applied to it.
- (U) Previously cut patterns were placed on the surface by removing one side of the polyethylene protecting the rubber. When six rubber sections had been installed and trimmed to make clean butt joints, the upper layer of protective polyethylene was removed. Rubber was placed on the -01 shim in the same manner. After the rubber was trimmed, the shim was placed on the assembly fixture and the upper polyethylene film removed. This process was repeated through the -20 shim. At this point the fixture was transferred to a press and debulked. No rubber was extruded during this operation. The shim/rubber pack was squeezed to a dimension of 1.40 inches. The protective film was left on the rubber installed on shim No. 20. It should be noted that the shim/rubber pack in the debulked position did not contact the six fixture post ramps.
- (U) After debulking, the fixture was returned to the clean room and an additional 20 shims laid up and installed. At -40, the assembly was again debulked to a dimension of 2.80 inches. The next 20 shims were laid up in the same manner. After debulking the -60 shim to 4.20 in., the aft end ring was installed and centered on the fixture. It rested on six lands provided on the fixture posts and was easily movable in a radial direction. Then the top cover of the assembly fixture was lifted and aligned with two dowels indexing the cover to the posts at two positions 180 deg apart. While lowering the cover after these index pins were started, the aft end ring was moved radially until its index pin mated the index pin in the cover ring. Thus the top fixture cover was indexed to the lower fixture cover and the aft end ring indexed to the top fixture cover. In this position, scribe marks were placed on the aft end ring at the six fixture post edges. This procedure was necessary since the aft end ring

cannot be moved radially while resting on the rubber. After removing the top cover and end ring, the remaining 22 shims were laid up and installed in the same manner as before. Chemlok was applied to the bonding surface of the aft end ring and the ring was installed over the fixture in alignment with the previously made scribe marks and with its upper surface one inch above the fixture post tops. The fixture cover was placed over the end ring and properly indexed. In this position, the fixture was ready to be pressed to its closed position. The entire fixture seal assembly then was placed in a 170°F furnace and heated for five hours. When heated, the entire assembly was forklifted to a press and slowly compressed until the top cover rested on the six fixture posts. Rubber extruded during this process in a very uniform manner. The shims, however, did not shift or self align themselves on the ramp to the degree anticipated. When in the compressed position, nuts were placed on the 12 tie bolts of the assembly fixture and torqued to 600 inch-pounds. The bottom cover to top cover distance was measured in an attempt to verify seal length. This was not accomplished, however, since the bottom cover deflected over the supporting "I" beams, thus distorting any readings. Positive seating of the cover against the posts was assured, however, by the rapid rise in press ram pressure. The fixture and seal then were removed from the press and placed in a 315°F furnace for six hours to cure the rubber.

(U) Prior to fabricating AF Seal no. 1, Thiokol fabricated an IR & D funded seal. During the fabrication of this seal, fabrication techniques were developed and acceptance criteria established. Also during this process five events of significance were noted which influenced the fabrication of AF Seal no. 1 as discussed below.

- (U)
1. Shims -01 thru -10 on the IR & D seal distorted somewhat during the grit blasting. This was caused by the relieving of stresses within the shim from shot peening. Since these shims could be restrained in their proper shape, it was felt they would have no adverse effect on quality and they were used in the IR & D seal.

Extreme care was taken in the handling of shims for AF Seal no. 1 during grit blasting and in maintaining a uniform grit blasting pressure and distance of gun to shim. The shims did not distort.

(U)

2. Upon removal of the fixture and the IR & D seal from the curing oven the fixture was chilled with cold water to avoid overcuring the rubber. This sudden chilling caused the tie bolts and nuts to fail. The heads on two of the tie bolts were broken in the weld and on others the nut threads were stripped. This, however, did not affect the condition of the seal as rubber cure had been effected. The assembly was allowed to cool, the seal removed from the fixture and shipped to the Wasatch Division. The fixture was refurbished by cleaning with steel wool and MEK. The tie bolts were repaired by replacing the nuts and by chasing the bolt threads which were not damaged (bolt strength of 180,000 psi versus nut strength of 140,000 psi resulted in only the nuts being damaged). The two bolts with broken heads were rewelded.

(U)

Upon bringing the fixture and AF Seal no. 1 out of the furnace, it was noted that five of the tie bolts or nuts had failed and the top cover had lifted somewhat on one side. The two tie bolts, which had been weld repaired earlier, each failed at the head. The other three failures in the same area were nuts with stripped threads. It is assumed that the weld repairs were poor and the failure of these two tie bolts transferred loads to the other tie bolts sufficient to strip the nuts. The seal was cooled at room temperature.

After removal from the fixture, the parallelism between end rings was measured and was found to be discrepant by 0.072 inch. It is interesting to note that this lack of parallelism showed up in later seal tests as an offset torque.

- (U) 3. Thiokol inspection of the IR & D seal after cooldown revealed that the seal had shrunk from a total length of 10.938 in. while in the fixture prior to cure to a free length of 10.860 in., thus indicating considerable shrinkage in the rubber.

(U) To compensate for rubber shrinkage in AF Seal no. 1, a 0.060 in. shim was placed on top of each post of the assembly fixture, thus separating the end rings an additional 0.060 in. during cure. Since the average height of the nonparallel seal was within blueprint specifications, it appeared that the shims compensated for rubber shrinkage. An accurate evaluation was impossible due to the tie bolt failure during cure. Separating the end rings created less compaction in the shim/rubber pack and was the basis for choosing this particular seal for tests to destruction.

- (U) 4. During debulking of the IR & D seal the shims did not shift in the rubber and self center over the six tapered posts of the assembly fixture. The clamping force between rubber/shim laminate was greater than any self centering force that could be created against the thin (0.040 in. thick) shims. It was concluded, therefore, that the concentricity of the shims was a function of the accuracy with which they were placed during assembly. A number of tapered wedges were built to

adjust the post ramp angle to that defined by the rubber/shim pack in the as-laid-up-and-debulked configuration, i. e., rubber thickness of approximately 0.030 in. (Figure 18). These wedges were used during assembly of AF Seal no. 1 with a marked improvement in shim concentricity.

- (U) 5. The curing time temperature requirements used on AF Seal no. 1 were established during fabrication of the IR & D seal. Thermocouples were placed in the center of the rubber between shims -40 and -41 and between -41 and -42. Data obtained from these thermocouples during IR & D seal cure provided the necessary time/temperature information.

3. AF SEAL NO. 1 VERIFICATION TESTING

- (U) Qualification of the seal design for the 156-9 nozzle was achieved through a series of tests on the AF Seal no. 1 assembly. Axial deflection at 400 psi ($P = 1,148,000$ lb) was 0.083 in. which was greater than the predicted value but acceptable to the nozzle design. The seal assembly was subjected to a twang test, i. e., the seal was deflected 4 deg and then instantly released to return to null. The tests indicated a damping ratio of 0.2 and a natural frequency of 7 to 7.5 cps. The damping appeared to be a viscous type damping with little or no coulomb friction apparent. The nature of the oscillations indicated that the viscous damping was somewhat nonlinear. However, the scope of the test did not allow a detailed analysis of the damping. The inertia of the complete movable nozzle section was not simulated on the seal tests. Consequently, the results given apply to the seal only.

- (U) The torque and structural stability test was done in two steps. The torque evaluation test was completed with the thrust pin removed from the test rig in order to eliminate any friction components. For this test the maximum pressure was

400 psi, which is equivalent to an axial load of 1,148,000 pounds. The slow response of the industrial actuator negated use of a sinusoidal wave form and also contributed a continuous drift in actuator pressures which made it difficult to interpret the force data accurately. Table IV shows the average torque values for this test along with the values from the structural test, which was run with the thrust pin installed.

- (U) Visual inspection of the seal at 400 psi in the vectored and unvectored position did not reveal any deviations or shim wrinkles.

4. AF SEAL NO. 2 FABRICATION

- (U) Assembly of AF Seal no. 2 was started after the previously described verification testing of AF Seal no. 1 had been completed. Because of high confidence in the end rings and the economy of fabricating three sets of shims on one mandrel, these items were on dock at Reinhold prior to starting assembly of AF Seal no. 2. The twelve tie bolts on the assembly fixture had been replaced with studs using longer 160,000 psi nuts at each end.
- (U) Material property tests conducted on rubber calendered with that used in AF Seal no. 1 revealed a modulus on the high side of the specifications. New rubber of lower modulus was ordered and delivered to Reinhold. The change of rubber resulted in lower seal torques for seal no. 2 as opposed to seal no. 1.
- (U) An engineering change to increase the length of the aft end ring by 0.060 in. was accomplished during seal no. 1 tests. This allowed the same rubber/shim compaction and also hedged the seal length against rubber shrinkage.
- (U) Following incorporation of changes and Air Force approval, the seal no. 2 was assembled without incident in the same manner as seal no. 1. The seal was shipped to Wasatch Division in the assembly fixture. This was done to speed up seal qualification testing and subsequent delivery to the nozzle vendor.

TABLE IV
COMPARISON OF BENCH TEST TORQUE VALUES

Event	Pressure (psi)	Average Total Torque (in. lb)	
		AF Seal No. 1	AF Seal No. 2
<u>+</u> 4 deg pitch plane*	200	1,682,700	--
<u>+</u> 4 deg pitch plane*	340	1,572,000	--
<u>+</u> 4 deg pitch plane	200	1,802,000	1,634,700
<u>+</u> 4 deg pitch plane	340	1,857,400	--
<u>+</u> 4 deg pitch plane	500	1,895,700	--
<u>+</u> 4 deg pitch plane	700	1,951,100	1,709,000
<u>+</u> 4 deg pitch plane	830	2,062,500	1,796,450
<u>+</u> 4 deg yaw plane*	50	1,797,800	1,539,700
<u>+</u> 4 deg yaw plane*	200	1,742,400	--
<u>+</u> 4 deg yaw plane*	340	1,682,700	1,439,850
<u>+</u> 4 deg yaw plane*	400	1,614,600	--
<u>+</u> 4 deg yaw plane	200	1,900,000	1,652,800
<u>+</u> 4 deg yaw plane	340	1,883,000	--
<u>+</u> 4 deg yaw plane	500	1,917,000	--
<u>+</u> 4 deg yaw plane	700	2,040,600	1,780,150
<u>+</u> 4 deg yaw plane	830	1,959,600	1,765,350

*These events were without the thrust pin installed.

- (U) Receiving inspection was performed at Thiokol and, in spite of the measures taken to allow for rubber shrinkage, the overall seal length was short of blueprint tolerances. Appropriate engineering changes were processed on the affected, but yet to be machined, nozzle parts and the seal was accepted for use as fabricated.

5. AF SEAL NO. 2 QUALIFICATION TESTING

- (U) AF Seal no. 2 assembly was subjected to a series of qualification tests prior to shipment to the nozzle vendor. This included axial deflection, a limited torque study without the boot, structural verification, and torque studies with the boot using the program tape yaw plane duty cycle.
- (U) Visual inspection of the seal prior to testing revealed six areas on the ID surface where the shims were distorted. This condition shown in Figure 19 was caused by interference with the internal components of the assembly fixture. Figure 20 is an overall picture of the seal assembly prior to testing.
- (U) The axial deflection at maximum axial load ($P = 1,148,000$ lb) was 0.077 in., which was almost 8 percent less than the deflection of the AF Seal no. 1. Because of the lower shear modulus rubber in this seal, an increase in axial deflection was expected. However, the rubber/shim laminate in seal no. 2 had better compaction which contributed to the axial deflection decrease.
- (U) The torque values during the unbooted torque and structural integrity test were 8 to 14 percent lower than for the AF Seal no. 1. This was expected because of the lower shear modulus. Table IV shows a comparison of the torque values for the two seal assemblies for similar events with the industrial actuator.
- (U) The first insulation boot fabricated was defective because of voids. Temporary repairs were made and the boot was installed on the seal assembly for torque evaluation. A second boot was fabricated while initial torque testing was in process to replace the defective boot. This second boot was installed on the seal assembly (Figure 21) and the testing was completed. The last test subjected the seal assembly to the yaw plane duty cycle at 830 psi. Table V is a summary of torque values for certain events in the duty cycle.

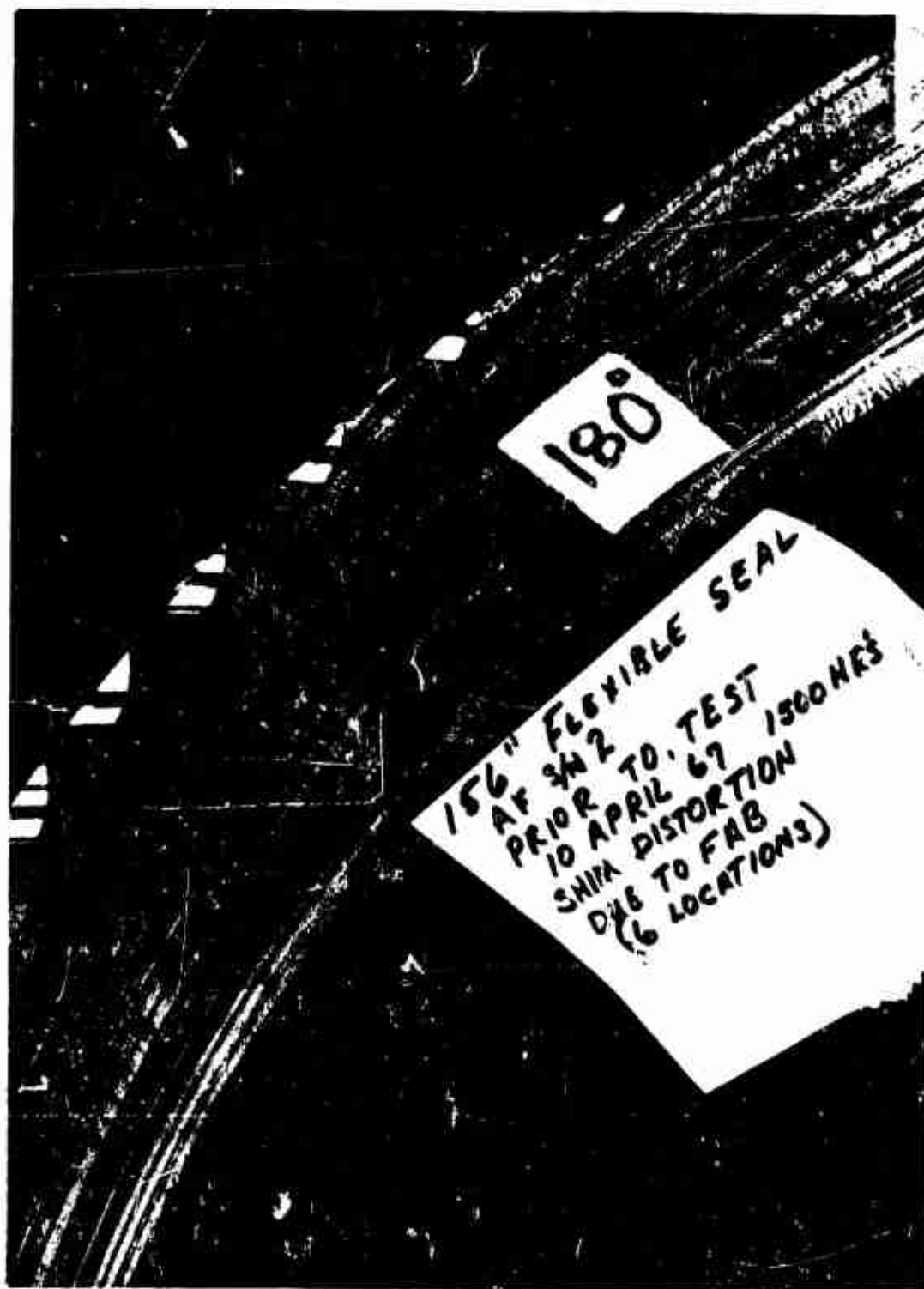


Figure 19. Shim Distortion Due to Internal Components

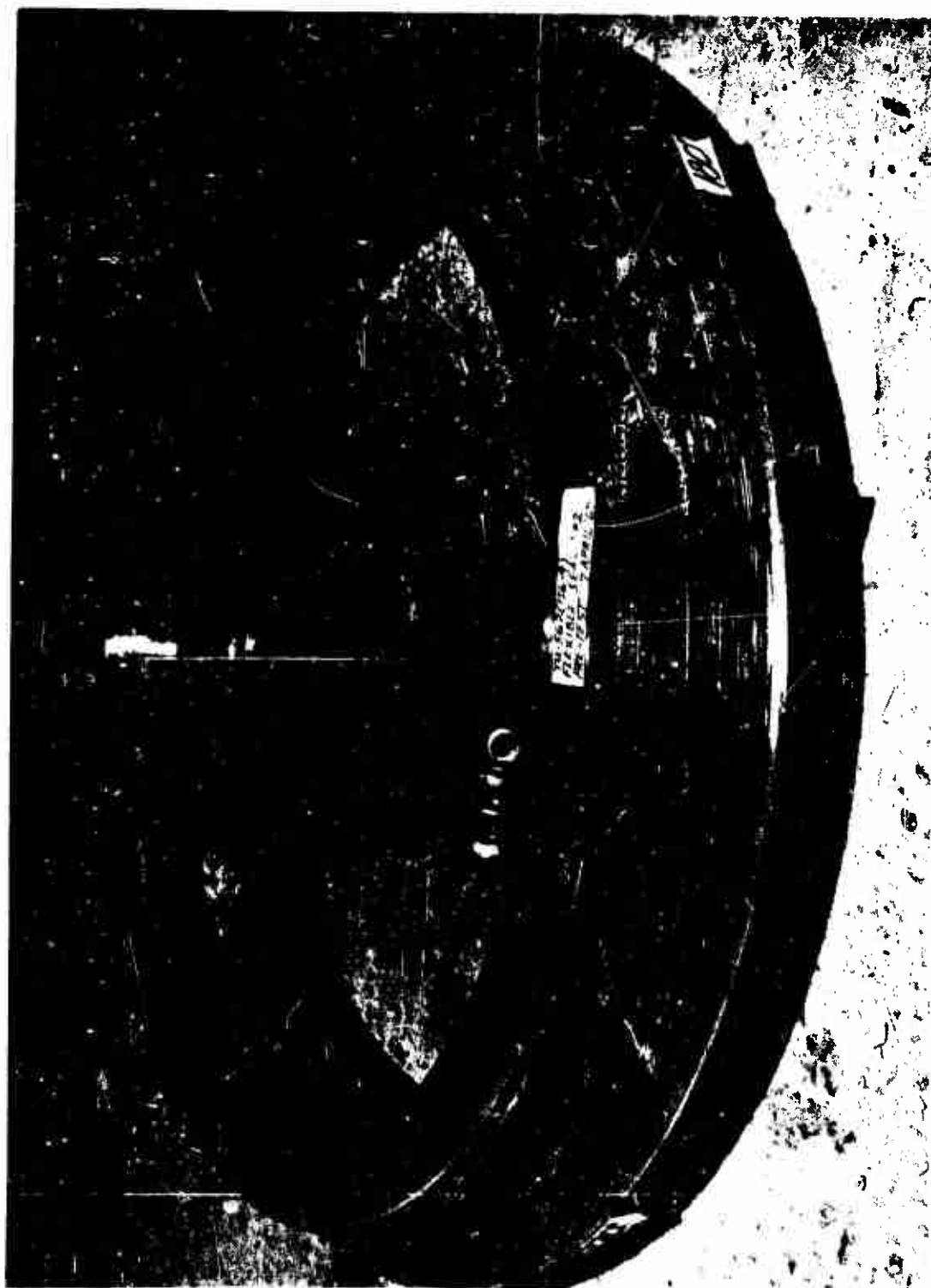


Figure 20. Seal Assembly Prior to Test



Figure 21. Seal Assembly with Boot Installed

TABLE V

AF SEAL NO. 2 YAW PLANE DUTY CYCLE DATA

<u>Event</u>	<u>Pressure (psi)</u>	<u>Average Torque (in. -lb)</u>
+ 3.3 deg triangular*	50	1,373,450
+ 3.3 deg triangular*	340	1,345,670
+ 3.7 deg sinusoidal*	50	1,544,220
+ 3.7 deg sinusoidal*	340	1,430,800
+ 3.7 deg sinusoidal	700	1,903,300
+ 3.7 deg sinusoidal	830	1,947,000

*These events were run without the thrust pin installed.

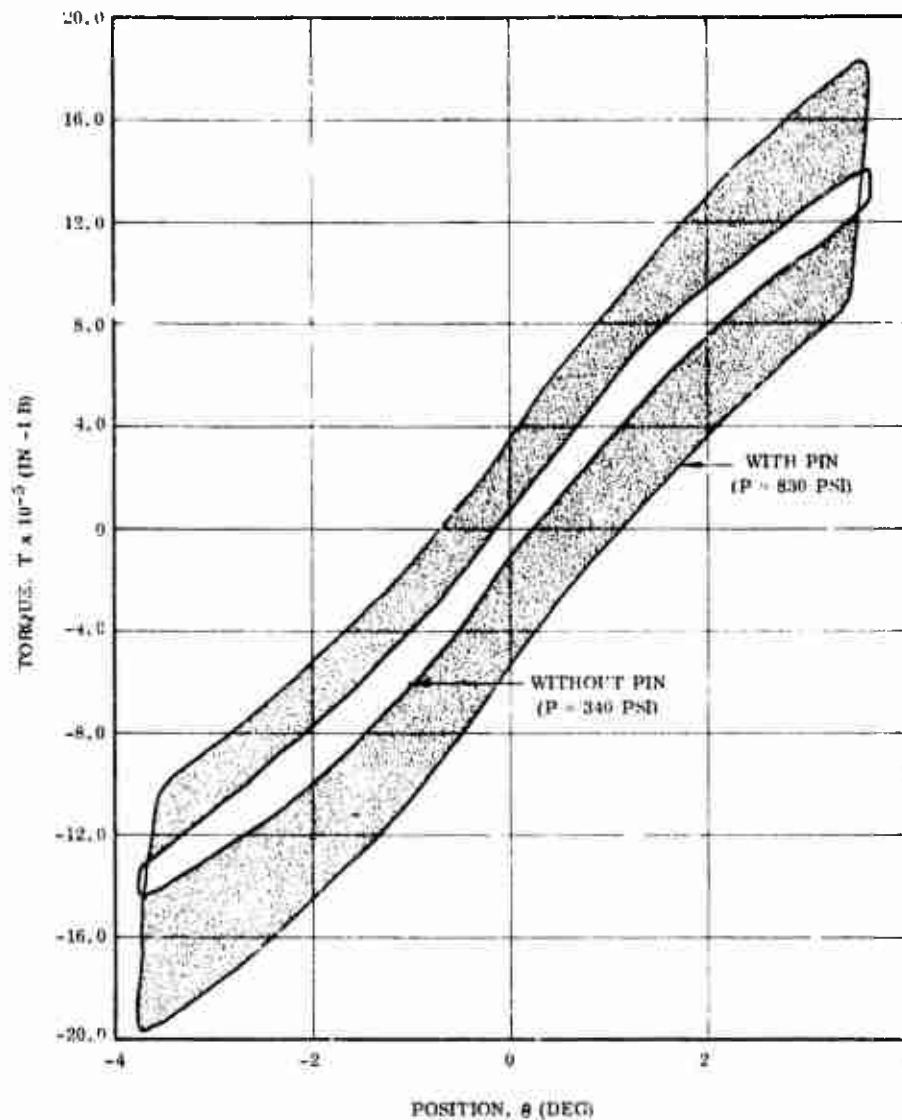
- (U) Visual observation of the seal during and after each test did not reveal any anomalies in the laminate structure.
- (U) Figure 22 is the torque vs position loop for Event 7 of the duty cycle showing the difference between the torques in the pinned and unpinned condition. The shaded area represents the torque contribution of the test rig when the axial load relieving pin is installed.

6. TEST SUMMARY

- (U) Testing of the first flexible seal (AF Seal no. 1) for the 156-9 motor program was completed in two steps. The first series of tests were completed 27 March and included an axial deflection test, torque and structural verification test, and a twang test. The results were first reported to the project office at AFRPL on 30 March when approval to fabricate the second seal assembly was requested. These results also are presented in this report.
- (U) Upon completion of acceptance testing of the second flexible seal (AF Seal no. 2) and shipment to the nozzle vendor, the first seal assembly was installed in the test fixture and a series of tests completed. Two major areas of performance were investigated.
1. Behavior of the seal under duty cycle vector requirements at 0 and 340 psi, and
 2. Structural response to chamber pressure greater than MEOP.
- (U) The seal was subjected to the yaw plane duty cycle (Table VI) at 0 and 340 psig. Figure 23 shows the torque traces for the two pressure levels. Because of dimensional deviations in the flight actuator, the seal could only be vectored plus or minus 3.7 deg with the flight actuator. In general, the torque levels at 0 psig were higher than those at 340 psig. A small amount of offset torque was measured during both tests. This can be attributed to a small amount of angulation that existed between the two end rings. The value of the offset torque was

CONFIDENTIAL

(THIS PAGE IS UNCLASSIFIED)



15435-101

Figure 22. AF Seal No. 2, Event No. 7, Torque vs Position

CONFIDENTIAL

(THIS PAGE IS UNCLASSIFIED)

CONFIDENTIAL

TABLE VI
AF SEAL NO. 1 YAW PLANE DUTY CYCLE DATA

Event No.	Duration (sec)	Function	Yaw Angle (deg)	Rate (deg/sec)	Position	Remarks
1	0.2	Ramp	--	5.0	Ramp from 0 to +1	
	1.0	Hold	--	--	+1	
	0.2	Ramp	--	5.0	Ramp from +1 to +2	
	1.2	Hold	--	--	+2	
	0.4	Ramp	--	5.0	Ramp from +2 to 0	
2	1.6	Triangular	3 deg, 42 min (max angle obtainable)	(1.25 Hz)	--	Plus direction first; 2 cycles
3	4.0	Sine	+2	(0.5 Hz)	--	Plus direction first; 2 cycles
4	2.0	Triangular	+0.5	(1.5 Hz)	--	Plus direction first; 3 cycles
5	4.0	Square	+1	(0.5 Hz)	--	Plus direction first; 2 cycles
6	4.0	Sine	+2	(0.5 Hz)	--	Plus direction first; 2 cycles
7	4.0	Sine	3 deg, 42 min (max angle obtainable)	(0.5 Hz)	--	Plus direction first; 2 cycles
8	0.4	Ramp	--	5.0	Ramp from 0 to +2	
	1.2	Hold	--	--	+2	
	0.2	Ramp	--	5.0	Ramp from +2 to +1	
	1.0	Hold	--	--	+1	
	0.2	Ramp	--	5.0	Ramp from +1 to 0	
9	4.0	Sine	+2	(0.5 Hz)	--	Plus direction first; 2 cycles

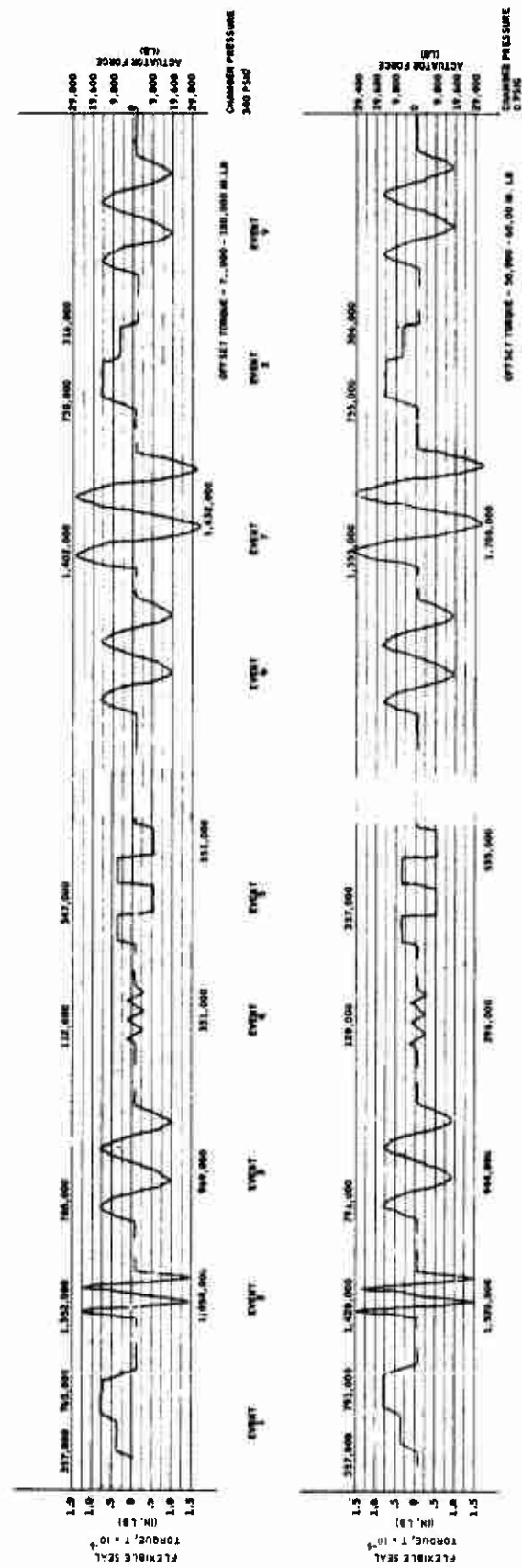


Figure 23. AF Seal No. 1 Duty Cycle Torque Data

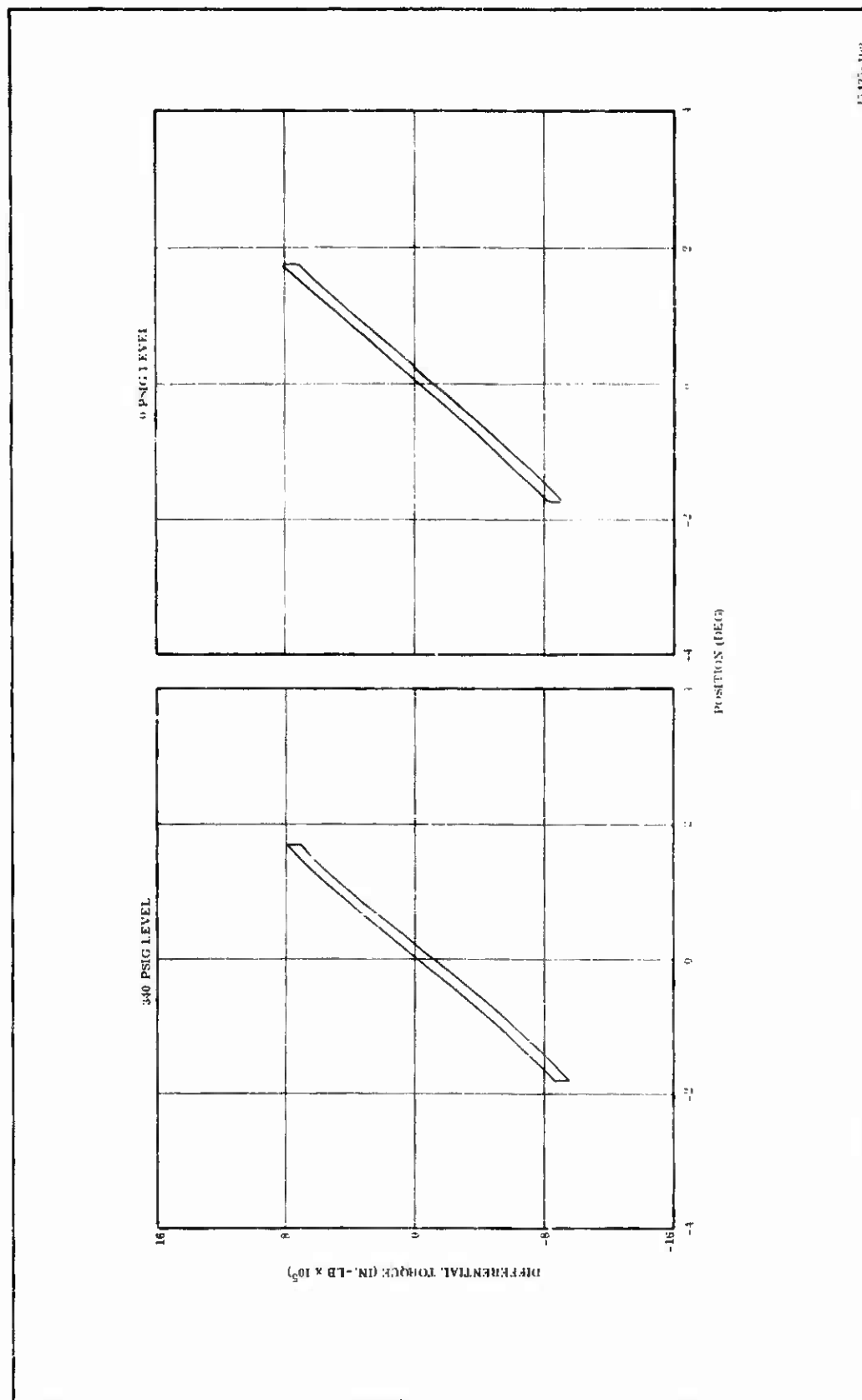
greater for the higher pressure indicating a tendency for the seal to rotate in the direction of angulation under pressurization.

- (U) Torque vs position plots are presented in Figures 24 and 25 for Events no. 3 and no. 7, respectively. A standard loop analysis was utilized to evaluate the torque components. The seal spring rates determined for these events are presented below.

<u>Event</u>	<u>Pressure (psig)</u>	<u>Spring Rate (in. -lb/deg)</u>
3	0	470,000
	340	465,000
7	0	430,000
	340	400,000

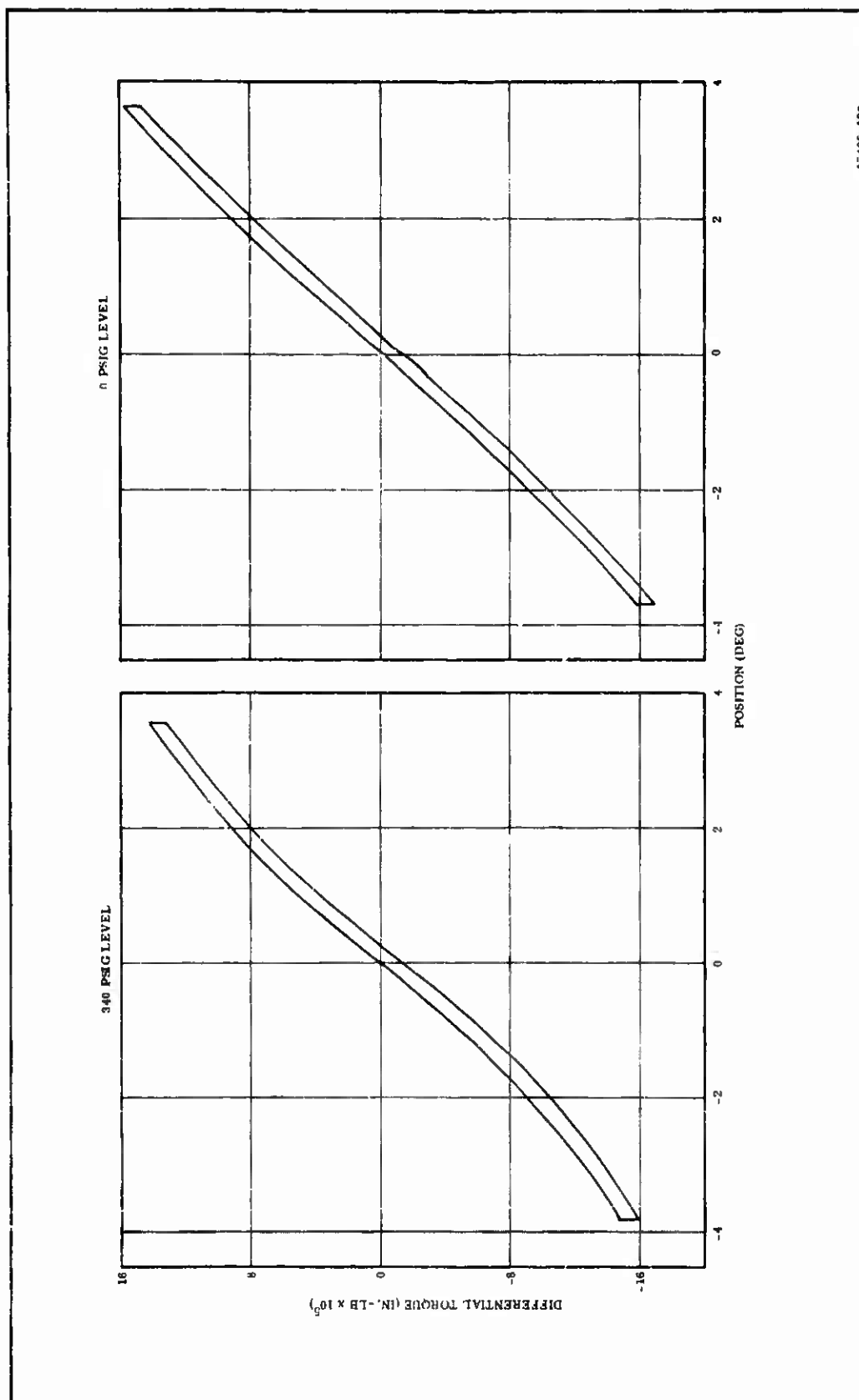
- (U) These spring rates were evaluated at the maximum vector angle, which is 1.75 deg for Event 3 and 3.7 deg for Event 7. This results in considerable difference in the spring rates measured for the two events and can be attributed to a nonlinear spring torque. The fact that the shear stress-strain relationship is nonlinear produces a varying shear modulus which accounts for the nonlinearity in the spring torque. In Figure 26, the spring rate as a function of vector angle has been plotted based on Events 3 and 7. The rate is constant up to two degrees and then starts to drop. The envelopes of predicted spring rate based on the shear modulus at 100 percent strain ($\theta = 3.45$ deg) and at 50 percent strain ($\theta = 1.72$ deg) are shown on the graph for comparison. Below 50 percent strain the shear modulus is constant and no change in spring rate is predicted. The curve indicates that the use of the elastomer shear modulus at 100 percent strain is acceptable when predicting maximum torque values, i.e., torque at maximum vector angle. In order to accurately predict torque values for small vector angles, the effect of varying shear modulus will have to be incorporated.

- (U) Also apparent in the "loop" plots is the existence of coulomb friction torque as evidenced by the difference in recorded torque while extending and retracting the actuator. This friction component is most likely produced in the actuator attachments and is approximately 3 percent of the total torque for a 3.7 deg vector angle.



15433-102

Figure 24. AF Seal No. 1, Event No. 3, Torque vs Position



13495-103

Figure 25. AF Seal No. 1, Event No. 7, Torque vs Position

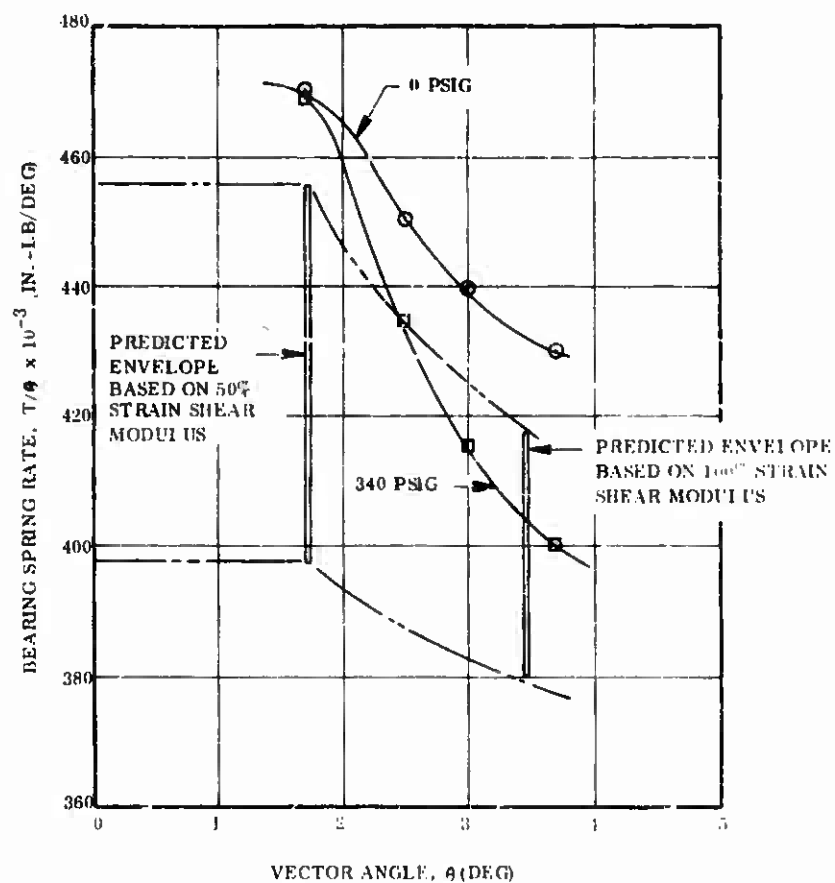


Figure 26. AF Seal No. 1 Spring Rate Vector Angle

(U) For the structural stability test, the thrust relieving pin was installed in the test rig and the industrial actuator used for moving the seal assembly. At each pressure the seal was cycled plus or minus 4 deg for five cycles. The seal was visually inspected following the vectoring at each pressure level up to 1,200 psi. Above that level the pressure was reduced to 1,200 for the inspection. Shim wrinkling was first noticed following the cycling of the seal at the 1,500 psig level. The buckled area occurred in the plane of actuation opposite the actuator location. The buckling was typical of those in other flexible seals tested by Thiokol under the 100-inch program (AFBSD) and the Hercules-Thiokol JVJ program. Testing was continued at 1,600 psig but a failure in the pressurization line, after 1 cycle, caused a loss of pressure. Before a repair could be made an extraneous signal caused a hardover movement of the actuator and the seal assembly separated into two rings. Figures 27 and 28 show the seal assembly prior to testing and Figures 29 and 30 show the seal assembly after failure still in the rig. Figure 30 shows the area where wrinkling first occurred. The surface condition of the shim and rubber at the failure plane indicates that an adhesive failure of the elastomer caused the separation.

(U) Torque was measured during the stability test. The high friction component due to the thrust pin and use of the industrial actuator made analysis of the results difficult.

(U) Other test results, on flexible seals that contained shims of similar material and thickness as the 156-inch flexible seal, indicated that the critical stress level for shim wrinkling was between -47,000 and -53,000 psi. Figure 31 is a plot of the predicted shim hoop stress for the 156-inch seal as a function of shear angle, which appeared in the design report. The extrapolated stress level for the plus 4 deg position at MEOP (830 psi) was -28,000 psi. This curve has been scaled to 1,500 psi, where shim wrinkling took place. It indicates that the stress level in the 4 deg vector position was -50,000 psi. This is an excellent correlation with the other test work and indicates that critical shim stress is unaffected by flexible seal size.



re 27. AF Seal No. 1 Prior to Test (OD)

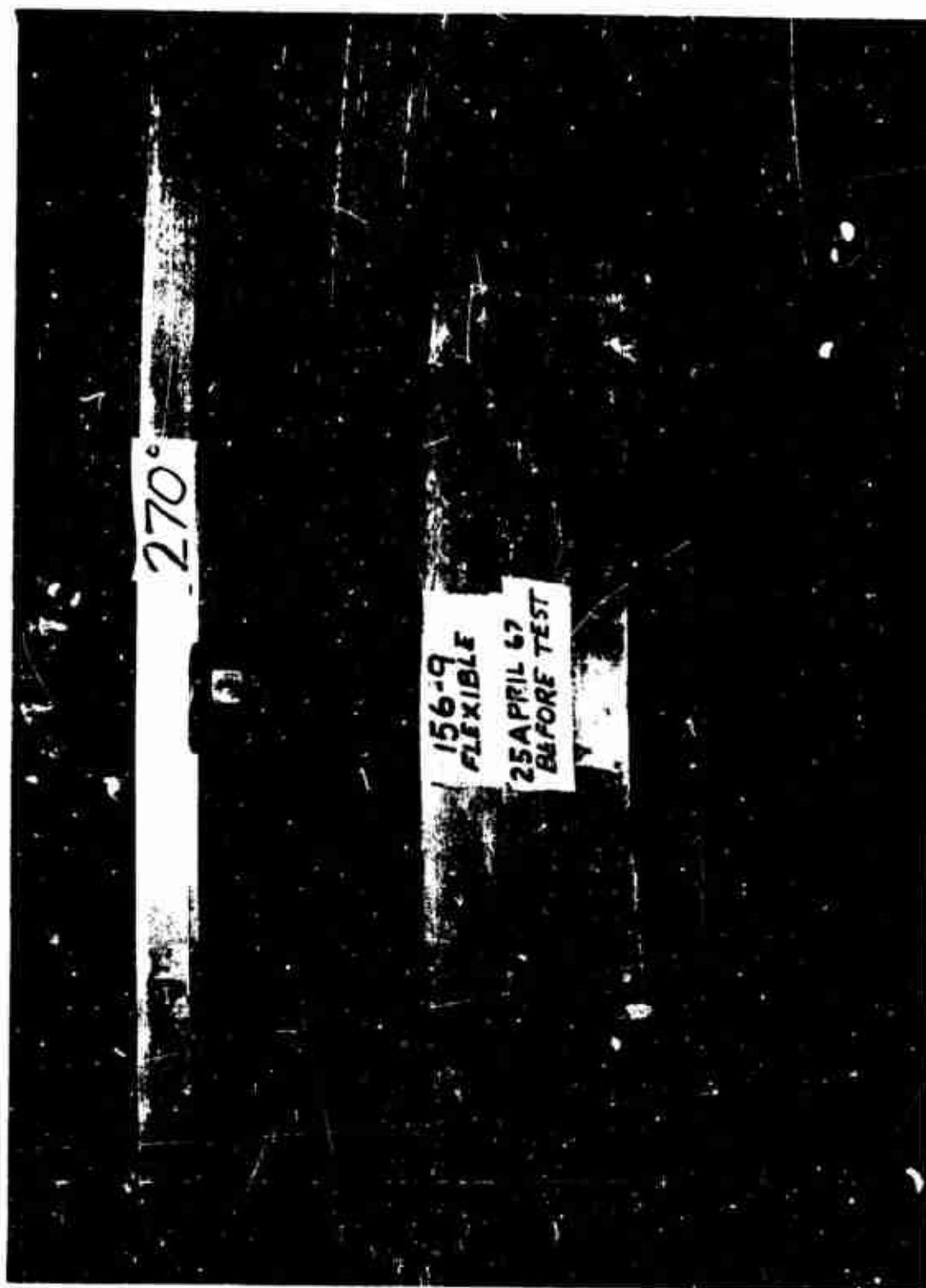


Figure 28. AF Seal No. 1 Prior to Test (ID)



Figure 29. AF Seal No. 1 Actuator Location Area after Failure

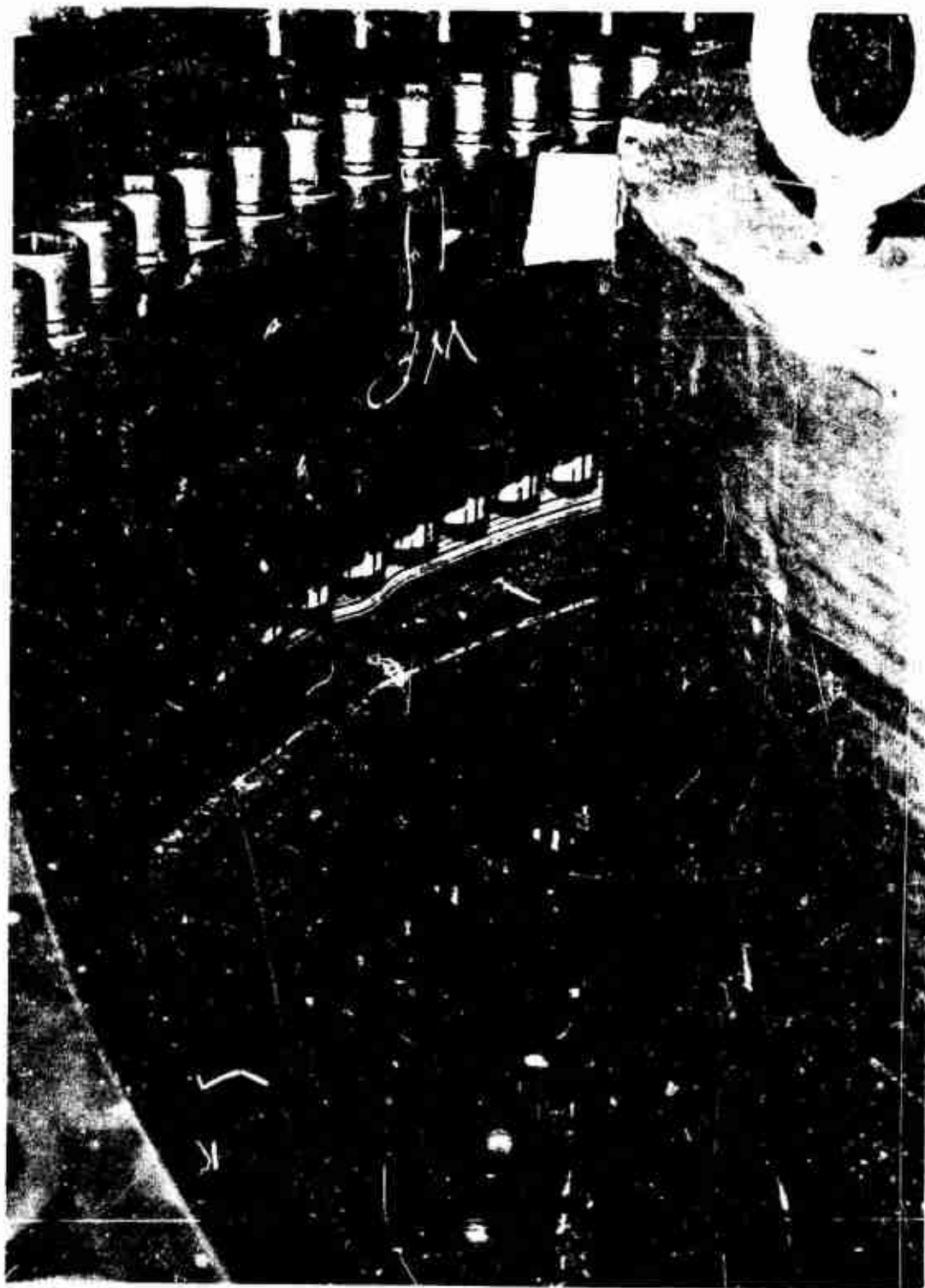
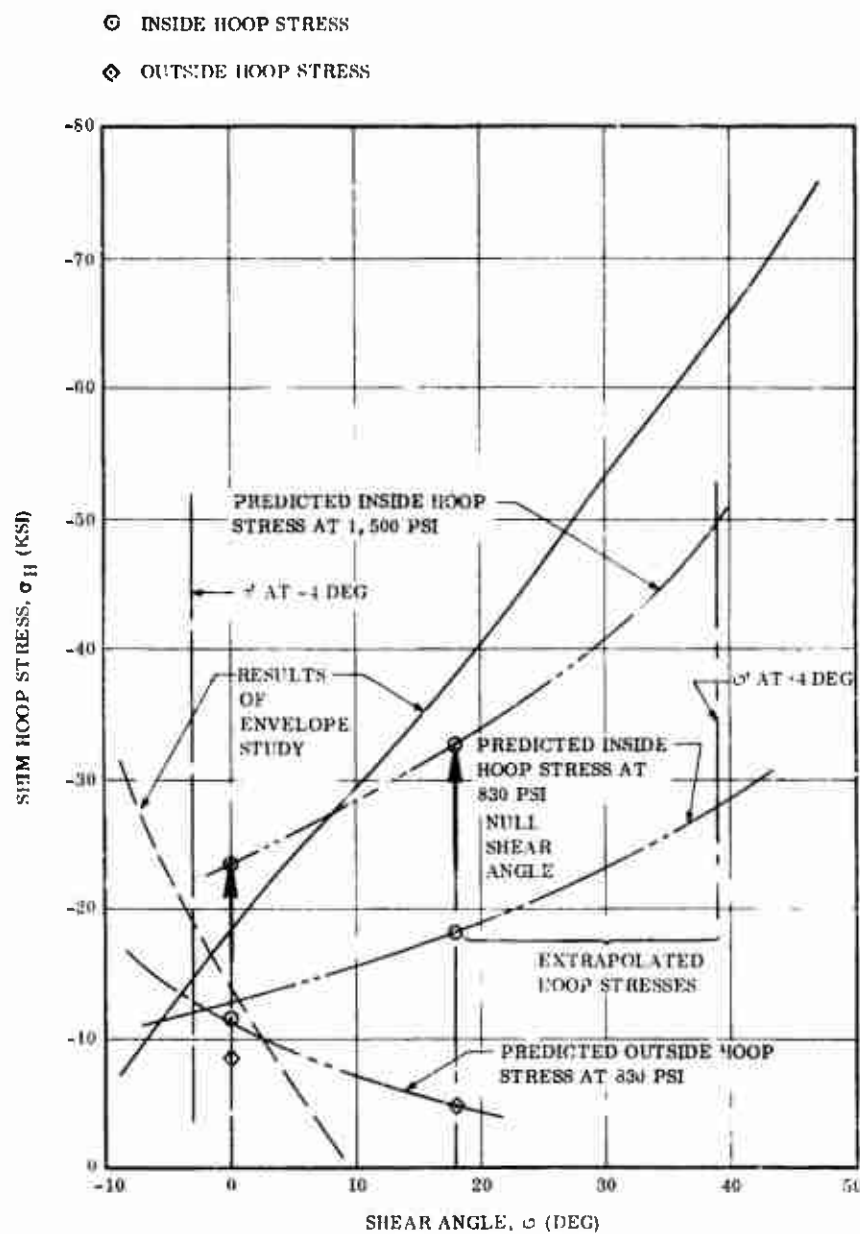


Figure 30. AF Seal No. 1 Location of Shim Wrinkling after Failure



15435-324

Figure 31. Shim Hoop Stress vs Shear Angle

(U) If a lower shear modulus elastomer were substituted in the design the predicted stress level would increase. For a shear modulus of 30 psi the stress level would increase about 20 percent, reducing the critical pressure to approximately 1,200 psi. This would still be structurally acceptable for the 156-inch program. The seal spring rate would be reduced 40 percent due to the lower shear modulus, substantially reducing the total nozzle torque.

SECTION III

NOZZLE DESIGN AND FABRICATION

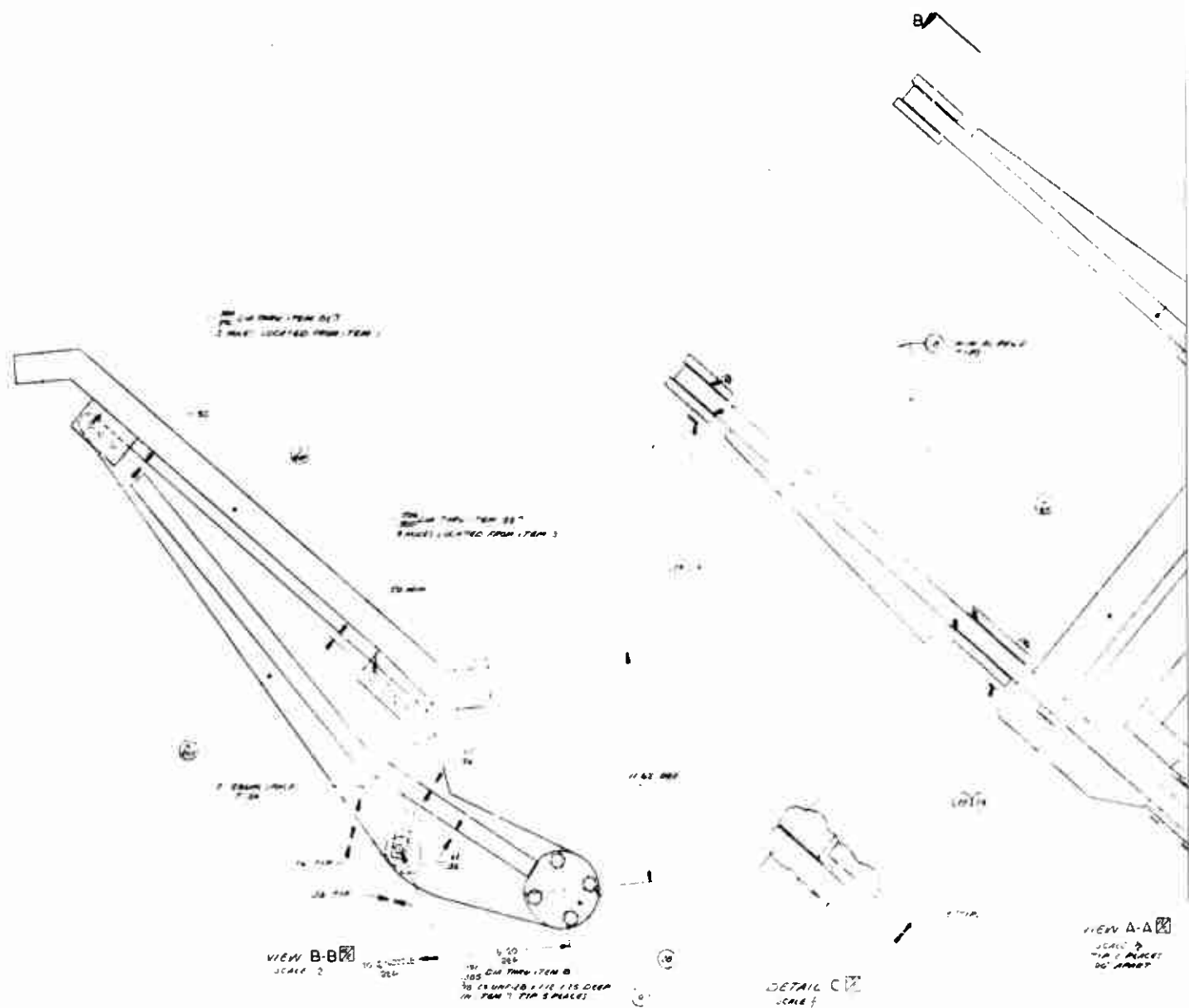
A. NOZZLE DESIGN

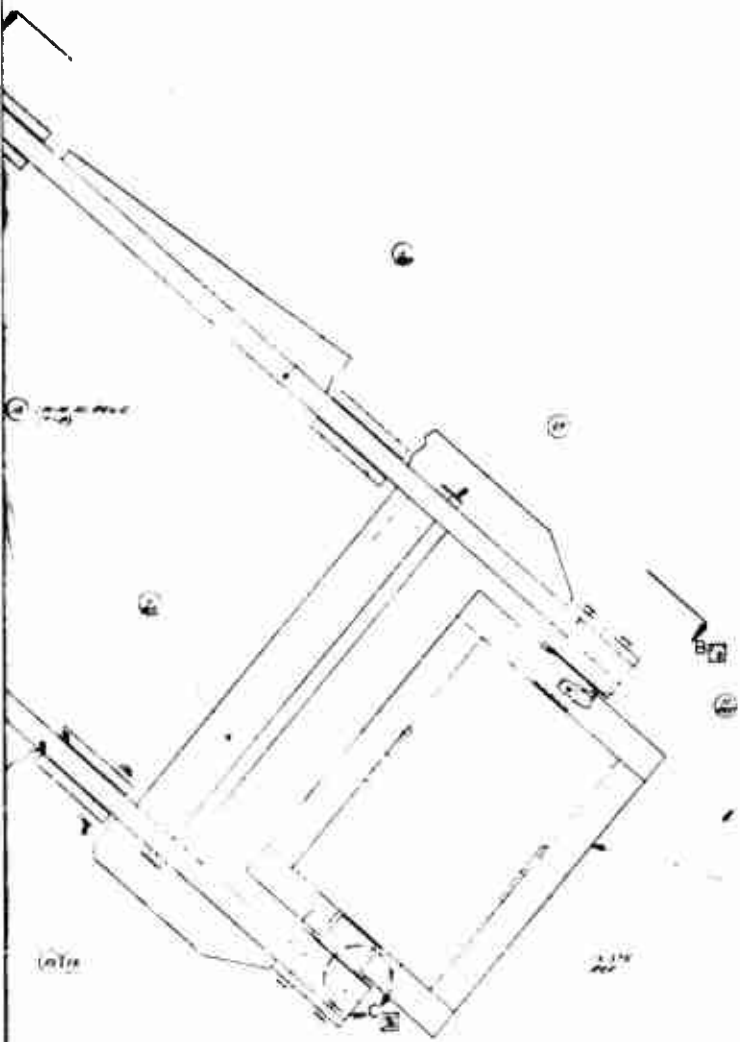
- (U) Detailed design analyses were conducted on the nozzle for the 156-9 demonstration motor. Design criteria included maximum utilization of 156-6 nozzle tooling, providing an envelope for the flexible seal installation, and insuring structural and thermal reliability.
- (U) Maximum use was made of recent developments in analytical techniques and test results from recent firings, especially the 156-6 motor nozzle. The results of these design analyses are presented here and show that program design objectives could be achieved and that the 156-9 nozzle design would perform successfully.

1. COMPONENT CONFIGURATION AND MATERIALS SELECTION

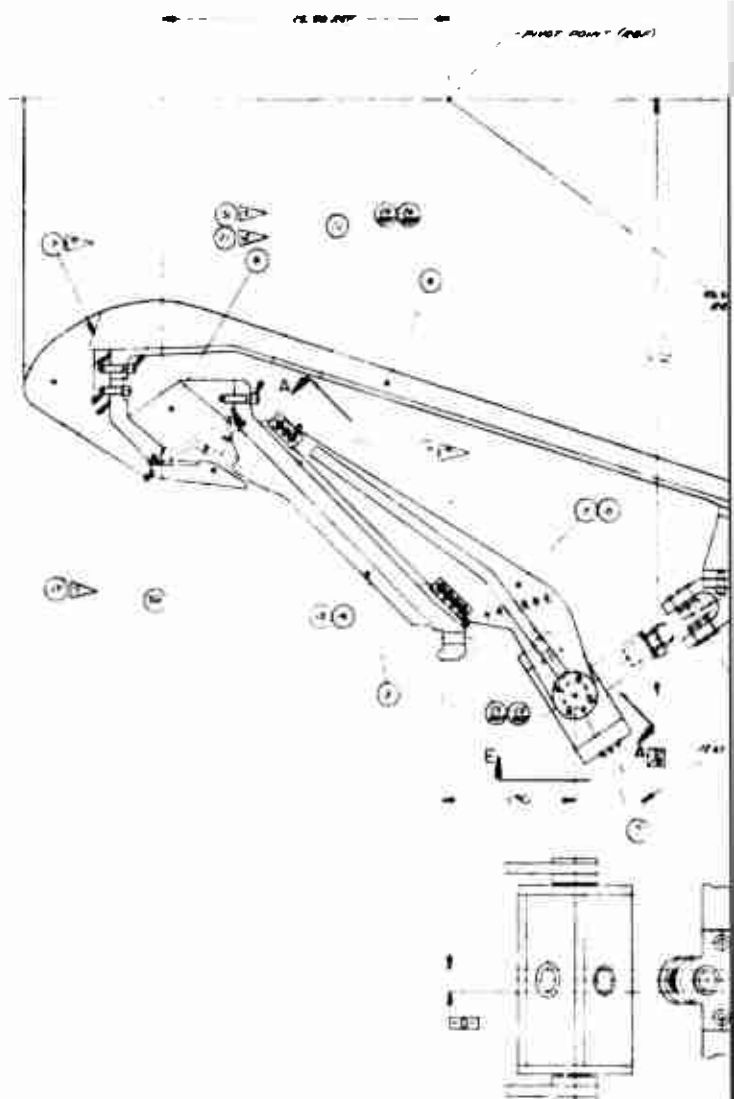
- (U) a. Component Configuration--The nozzle concept design for the 156-9 rocket motor was a submerged omniaxis movable flexible seal. The concept appeared particularly attractive in reducing the weight of nozzles capable of producing omniaxial movement. The philosophy behind the design of the 156-9 nozzle was to provide a minimum risk test vehicle for the flexible seal at a minimum cost. For this reason the 156-9 nozzle design was based primarily on the successfully tested 156-6 nozzle design. The aerodynamic configuration from the nosetip to the exit plane was identical to the 156-6 nozzle, and permitted the reuse of existing tooling. Modifications were made to the 156-6 nozzle design where necessary to incorporate the flexible seal and to provide for the resulting different flow conditions.

- (U) The 156-9 nozzle final design is shown in Figure 32. The submerged movable nozzle was capable of a plus or minus 4 deg omniaxial vectoring motion through the flexible seal joining the fixed and movable sections of the nozzle. The nozzle was actuated by two linear servoactuators mounted between the nozzle fixed housing and exit housing 90 deg apart; one actuated pitch motion and the other yaw motion. Intermediate angles of vector were accomplished by simultaneous combination motions.
- (U) The throat and exit diameters of the nozzle were 34.54 in. and 98.64 in., respectively, corresponding to an initial expansion ratio of 8.15. The overall length of the nozzle assembly was 116.1 inches. Forty-seven percent of the nozzle was submerged. The aerodynamic design of the internal nozzle surface from the nosetip to the exit plane was identical to the 156-6 nozzle. The nosetip was defined by a radius of 1.62 inches. An 8.00 in. radius joined the tip radius to a 15.00 in. radius into the throat. The throat and the 17.5 deg exit cone were joined by a radius of 13.859 inches.
- (U) Structural integrity and maintenance of the aerodynamic contour were provided by a mechanical design consisting of steel structural components, reinforced plastic erosion liners, and thermal insulators. Nozzle structural and insulation subassemblies were fabricated independently and bolted or bonded to form the complete nozzle assembly.
- (U) The nozzle fixed housing assembly consisted of a steel structure protected by silica cloth phenolic insulation. The steel consisted of two forged flanges welded to a conical section of roll and weld construction. The silica at the small end of the housing had an outer surface which, in the pressurized condition, became spherical about the flexible seal pivot point. This surface formed the fixed part of the secondary barrier gap which protected the flexible seal from direct radiant heating and sharply reduced convective flow. Ply orientation of the silica tape was parallel to the nozzle centerline to provide a direct vent path between plies.
- (U) The two actuator support brackets were bolted to clips on the fixed housing.

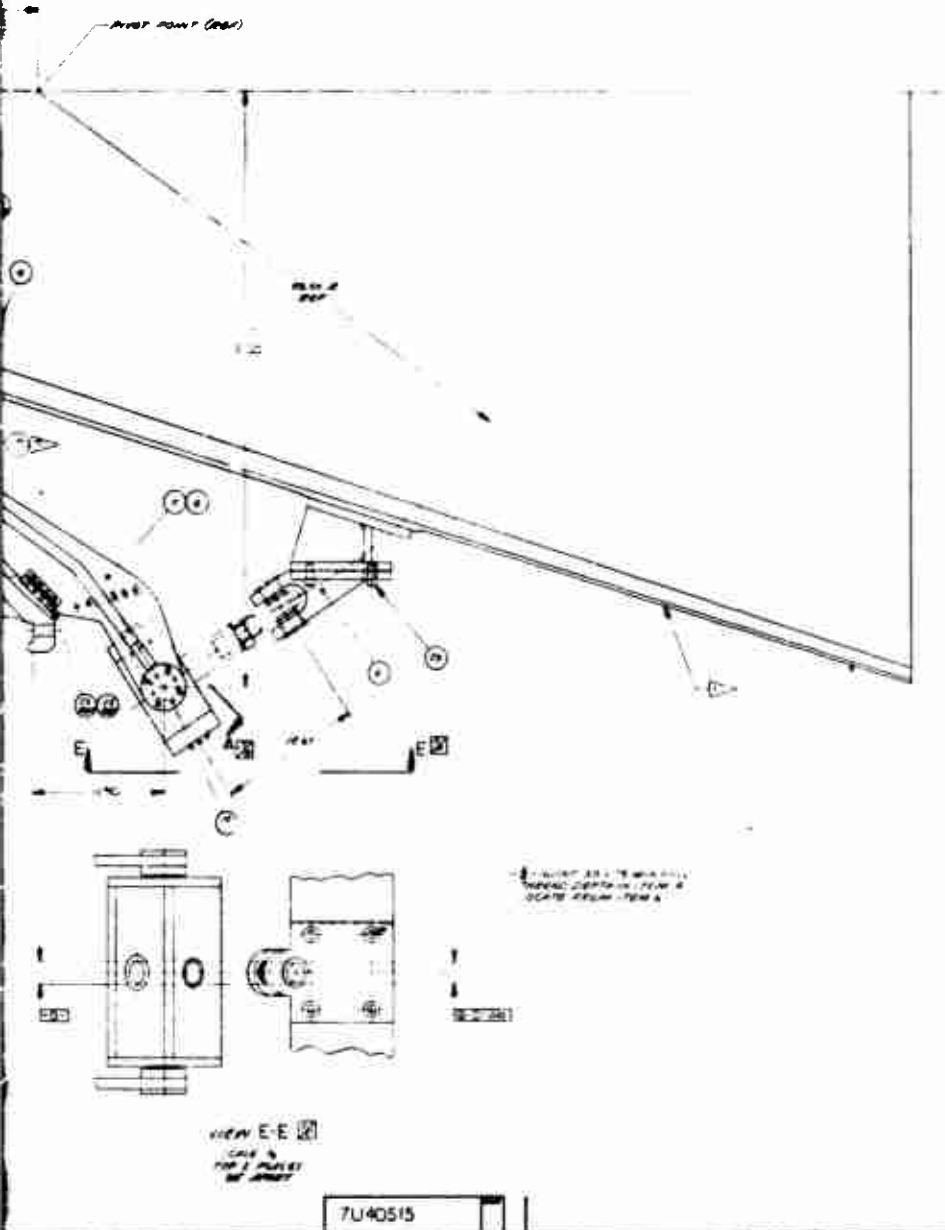




VIEW A-A
 SCALE 1/4" = 1'-0"
 10' 0" 10' 0"



VIEW E-E
 SCALE 1/4" = 1'-0"
 10' 0" 10' 0"



[illegible][illegible][illegible]

1. Name of the person or organization 2. Address 3. City 4. State 5. Zip 6. Telephone 7. Fax 8. E-mail 9. Other		10. Name of the person or organization 11. Address 12. City 13. State 14. Zip 15. Telephone 16. Fax 17. E-mail 18. Other	
19. Name of the person or organization 20. Address 21. City 22. State 23. Zip 24. Telephone 25. Fax 26. E-mail 27. Other		28. Name of the person or organization 29. Address 30. City 31. State 32. Zip 33. Telephone 34. Fax 35. E-mail 36. Other	

Figure 32. 106-1 Motor Nozzle Design

- (U) The movable part of the secondary barrier consisted of a silica cloth phenolic ring which remained separate until nozzle assembly. The ring was a tape layup (rosette) with ply orientation parallel to the centerline.
- (U) The nose assembly consisted of an entrance housing, two carbon cloth phenolic liners, a graphite cloth crossover ring, and two silica cloth phenolic insulators. The steel entrance housing was of roll and weld construction. The nose liner (backside or chamber side of the nose) was carbon cloth phenolic tape wrapped parallel to the centerline. Vent holes drilled in the nose liner were helpful in the 156-7 and Thiokol TU-455.02 and TU-465 motor nozzle designs. The liner ply layers in these three nozzles were at a small angle to the surface (0 to 12 deg). In the 156-9 nozzle, the angle of the ply layers was much higher (32 deg) providing the gas a more direct (shorter) escape path between the layers. To evaluate the need for additional vent paths (holes) at the higher (32 deg) angle, two quadrants of the surface were drilled with a hole pattern and the other two were left without holes.
- (U) The entrance liner was carbon cloth phenolic with ply orientation parallel to the centerline. The crossover ring was graphite cloth rosette with ply orientation 90 deg to the centerline. The silica cloth insulator behind the nose liner was a rosette layup with ply orientation parallel to the aft surface. The insulator behind the entrance liner was a rosette layup with two different ply orientations to facilitate the use of existing tooling.
- (U) The exit assembly consisted of a steel shell, three liners, and two insulators. The forward ring of the shell was a ring forging; the remainder was of roll and weld fabrication. A reinforcing I-beam type structure girdled the aft exit cone to limit distortion during vectoring and distribute the actuator loads. The throat liner was a single piece carbon cloth tape wrap with ply orientation 70 deg to the centerline. This is similar to the throats successfully tested on the 156-5, 156-7 and Thiokol TU-455.02 as well as the 260 in. diameter motor nozzles. An overwrap of silica phenolic tape was provided as an insulator behind the throat liner.

(U) The upper exit cone liner was carbon cloth phenolic tape wrapped parallel to centerline. This extended to an expansion ratio of 2.44 as in the 156-6 nozzle design. From this point to the exit the liner was silica phenolic tape, also wrapped parallel to centerline. Both liners were overwrapped with glass phenolic tape prior to final cure of the three components as an assembly. A row of retaining pins through the shell into the insulation was provided at an expansion ratio of 2.5 as a backup against bond failure.

(U) b. Materials Configuration--The aerodynamic configuration of the 156-6 nozzle was selected for the 156-9 nozzle to provide a configuration proven reliable by test in an almost identical environment. Materials to provide the aerodynamic contour, however, were not matched since a large number of materials have been qualified in large booster firings and similar environments. Therefore, selection was made from among all materials considered qualified in previous large booster firings.

(U) Every material selected for use in the 156-9 nozzle had been qualified by previous successful static test in nozzles for motors having diameters of 120 in. or larger. Each material had been successfully tested with similar exhaust gas environment. Table VII lists the materials selected for each nozzle component and the previous applicable experience.

(U) All steel components were 4130 steel. This material was selected for its high strength, machinability, excellent welding properties, and heat treatment response.

(U) Silica cloth phenolic was selected as the liner material for the fixed housing, the surfaces of the gap in the barrier, and the projecting radiation barrier because silica provides adequate erosion resistance in regions of moderate thermal severity and excellent insulation properties at a relatively low cost. Orientation parallel to centerline was selected for the silica on both sides of the barrier gap to provide a large angle between the plies and the respective surfaces providing a natural outgassing path to reduce blistering and delamination of the surface to a minimum. The orientation of the silica on the remainder of the fixed housing was also tape wrapped parallel to centerline.

TABLE VII

MATERIAL USE HISTORY

<u>Material</u>	<u>Vendor Designation</u>	<u>Use in 156-9</u>	<u>Previous Successful Experience</u>
Carbon Cloth Phenolic	FM-5055	Upper exit liner Entrance liner	156-7, Thiokol TU-465
	MXC-175	Nose liner, throat liner	156-5, 156-6
Graphite Cloth Phenolic	FM-5014	Crossover ring	156-1, TU-465
Silica Cloth Phenolic	MX-2646	Fixed housing insulator Barrier insulator Nose insulator Entrance insulator Throat insulator Lower exit cone liner Exit insulator	TITAN IIC Strap-on 156-6
Glass Cloth Phenolic	MX-4600		

- (U) Rubber insulators and mastic insulators were analyzed for this latter application, but were found unsatisfactory due to high erosion rate predictions. Flow conditions in this region are more severe in the 156-9 nozzle design than the 156-6 because of the differing geometry which controls the flow patterns. The details of this tradeoff are contained in the aerodynamic analysis portion of Section II.
- (U) Fiberite Corporation MX-2646 silica cloth phenolic was selected for the fixed housing and barrier plastic components. This material was extensively tested in the Titan IIC Program (Table VII) and it has performed successfully in all applications for which it was specified in the 156-9 motor nozzle.
- (U) The relatively severe flow conditions on the chamber side of the nozzle dictated the use of carbon cloth phenolic as the liner between the barrier and the tip of the nose. The thickness increased toward the nosetip where the flow velocities and resulting heat transfer increased. Carbon cloth provides excellent erosion resistance at moderate cost. Ply orientation was parallel to the centerline.
- (U) The entrance liner was of similar construction: carbon cloth phenolic oriented parallel to the centerline.
- (U) Fiberite MXC-175 was selected for the nose liner; U. S. Polymeric FM-5055 was selected for the upper exit cone liner. Both have substantial successful firing histories as given by Table VII.
- (U) The crossover ring which joins the entrance liner to the throat is graphite cloth phenolic, U. S. Polymeric FM-5014, fabricated in a rosette layup. This orientation, successfully tested in the 156-5, 156-6, 156-7, and the Thiokol TU-455 and TU-465 motor nozzles, provides desirable edge-orientation of plies to the gas stream along the entire exposed surface.
- (U) A rosette layup of carbon cloth phenolic was evaluated for use in the crossover ring. Graphite cloth phenolic was selected, however, because of the relatively poor performance of the carbon cloth rosette rings in the 156-5 and 156-6 motor programs. Graphite cloth rosette rings, by comparison, have performed well on the 156-1, 156-7, Thiokol TU-465 and TU-455 motor firings.

- (U) Fiberite MX-2646, a silica cloth phenolic material combining excellent insulation properties with exceptionally high strength, was selected for the insulators behind the nose and throat liners.
- (U) A single piece tape wrapped throat was selected for the 156-9 nozzle after evaluating a throat consisting of a series of rosette rings. The selected design was tested on the 156-5, 156-7, and the Thiokol TU-455.01. The rosette ring design was used on the 156-6 and the Thiokol TU-455.02 and TU-465. The TU-465 throat performance was excellent and exhibited uniform, smooth, relatively low erosion. The other two rosette throats, however, exhibited gouging; high non-uniform erosion, and delamination. In contrast all three tape wrapped throats performed as well or better than the TU-465 rosette throat. The tape wrapped throat was, therefore, determined to be a more reliable design. The 70 deg to centerline angle used in the three listed firings was again selected. MXC-175 carbon cloth phenolic was selected for the throat based upon demonstrated successful performance in previous 156 Inch programs. MX-2646 silica cloth phenolic was selected as the insulator behind the throat.
- (U) The exit cone was identical to the 156-6 except for the increased thickness of liner adjacent to the throat. This increase, and the increase in thickness at the throat, resulted from higher erosion rates observed in the throat and upper exit cone of movable nozzles as compared to fixed nozzles. The transition from carbon cloth liner to silica cloth liner, both parallel to centerline, occurred at the same expansion ratio, 2.44. Glass cloth phenolic was also used as the insulator for the exit cone and was parallel to centerline.
- (U) The materials selected for each component were U. S. Polymeric FM-5055 for the carbon cloth liner, Fiberite MX-2646 for the silica cloth liner, and Fiberite MX-4600 for the glass cloth insulator. Table VII indicates the qualification of each material.

2. FLEXIBLE SEAL LOCATION

(U) The location of the flexible seal within the nozzle was significant. A thorough study of the optimum axial and radial location was conducted by Thiokol as part of the design studies for Project 3246 (100 in. diameter motor) under Contract AF 04(694)-334. Various seal locations were investigated for a nozzle submerged 50 percent. The tradeoff study was among seal weight, seal torque, and fixed housing weight.

(U) As the seal was moved closer to the throat, the seal torque and weight reduced and the fixed housing weight increased. Results of the 100 in. motor study for three locations are:

<u>Seal Location</u>	<u>*Seal Torque (Percent)</u>	<u>*Total Nozzle Weight (Percent)</u>
Throat	100	100
Midway (flange to throat)	454	115
Case Flange	1,255	195

(*Seal torque and nozzle weight are given as percents of the value at the throat location.)

(U) These comparisons and a study of the equations governing seal design and torque indicated that minimization of the seal diameter was desirable.

(U) The study indicated that the seal should be located immediately outside the nozzle throat at a point compatible with throat insulation and structural requirements and nozzle vectoring motions. The seal should be as far upstream as is possible without increasing the size of the nose beyond that required for aerodynamic considerations.

(U) Selection of the pivot location was the next step in design selection. The dynamics of a flexible seal require that an angle of 45 to 55 deg exist between the nozzle axis and the center of the seal cross section. In order to keep seal torque at a minimum, the angle between the nozzle axis and the center of the seal cross section should be maximum. However, test experience at Thiokol was limited to angles

within a range of 45 to 55 degrees. This requirement forces the pivot to be either forward or aft of the throat on the nozzle axis. The choice must be made for each individual application based on vector angle requirements, depth of submergence, and case polar opening. Pivoting of the movable portion of the 156-9 nozzle was selected to be a point on the nozzle axis 25.50 in. aft of the throat. Location of the pivot in the exit cone aft of the throat presented the following advantages with a deeply submerged nozzle over the alternate location forward of the throat.

1. A smaller case polar opening was required for the same vector angle.
2. The aerodynamic forces always oppose the seal torque forces.
(In the 156-9 design, elimination of aerodynamic torque reduced the maximum total torque by 500,000 in. lb)
3. The radiation barrier gap (Figure 33) was located in a less severe environment.
4. A higher system steering angle was obtained from a given nozzle vector angle, since the moment arm about the system center-of-gravity was greater with an aft pivot.
5. A highly reliable radiation barrier was obtained with a smaller maximum nose outside diameter.
6. Cross-talk between the pitch and yaw actuators was minimized.

3. AERODYNAMIC ANALYSIS

(U) An aerodynamic study was conducted on the 156-9 motor to determine the nozzle and aft motor case wall heating environment and the eroded configuration of insulation materials. The aerodynamic nozzle geometry from the tip of the nose to the exit plane was identical to the 156-6 design. The aft part of the insulated case differed from the 156-6 configuration only in the thickness of the case internal insulation which alters the flow geometry only slightly. The backside of the nozzle nose, however, was modified to accommodate the flexible seal. The larger diameter of the nozzle backside changed flow conditions and thus affects the nozzle nose and aft case erosion.

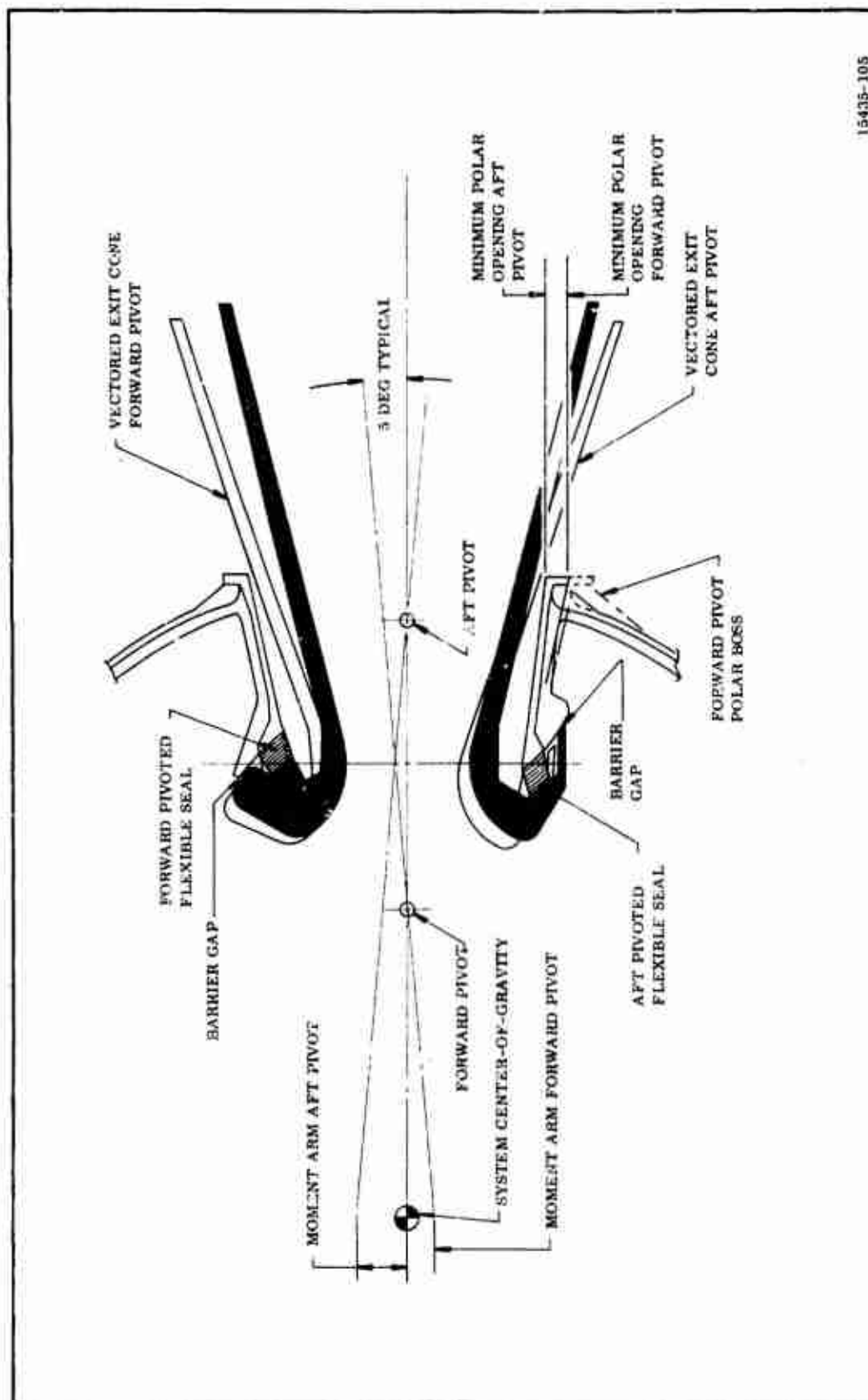


Figure 33. Comparison of Forward and Aft Pivoted Seals

- (U) A detailed flow analysis was conducted using a potential flow analogy programed on the IBM 7040 computer. This program calculated flow streamlines, Mach numbers, static temperatures, and static pressures in an axisymmetric, subsonic, compressible, potential flow field.
- (U) The potential flow properties were used to determine the boundary layer and the associated convective heat transfer coefficient on the entry. The heat transfer coefficient variation was then used to determine the erosion rate variation along the entry.
- (U) The erosion of graphite and graphite reinforced plastics in a solid propellant rocket motor primarily results from a diffusion limited chemical reaction occurring at the surface.* This erosion can be expressed as a function of the reacting species in the propellant combustion products (H_2O , CO_2 , O_2 , O and OH), the convective heat transfer coefficient, and the density of the carbonaceous material in the following manner:

$$\text{Erosion Rate } \left(\frac{\text{mils}}{\text{sec}} \right) = \frac{\beta (H/C_p)}{\rho} (12 \times 10^3)$$

where β = blowing rate determined from the species in the propellant combustion products (dimensionless).

$$H/C_p = \frac{\text{Convective heat transfer coefficient}}{(C_p)_{\text{gas}}} \left(\frac{\text{lbm}}{\text{sq ft} - \text{sec}} \right)$$

ρ = density of carbonaceous material (lbm/sq ft)

Measured erosion data are used to correlate with the theoretical parameter.

- (U) The analysis of silica base or asbestos base materials assumes they erode by melting. This heat of fusion is supplied by convection and radiation. Since the materials are not pure and the binder materials outgas and form a char layer,

*Erosion of Graphite in Solid Propellant Combustion Gases and Effects on Heat Transfer, A. M. McDonald, P. O. Hedman; AIAA Journal, Vol. 3, No. 7, July 1965.

the calculation is not exact and test data are used to relate erosion rate to total heat flux. The heat flux equation is:

$$Q_t = h (T_{aw} - T_w) + K \epsilon (T^4 - T_w^4)$$

where

- Q = total heat flux, Btu/sq ft sec
- h = convective heat transfer coefficient, Btu/sq ft sec °R
- T_{aw} = adiabatic wall temperature, °R
- T_w = wall temperature, °R
- K = Boltzmann's constant
- ε = emissivity
- T = free stream static temperature, °R

The parameters h, T_{aw}, and T are calculated assuming no erosion and outgassing, the wall temperature is near the melt temperature of the primary material, the emissivity of each material represents the best correlation of erosion in motor headend stagnant flow (all radiation), subsonic flow, and supersonic flow (nearly all convective). All materials in the design have been tested in similar application and the erosion data correlated to predicted heat flux.

(U) a. Nose--The final eroded nose configuration was determined using the above described techniques in the following manner.

1. The flow properties and heat transfer coefficient variations through the initial uneroded configuration were determined.
2. The erosion rates at the various locations on the nozzle entry were determined for the uneroded nozzle heating conditions and extrapolated over 15 sec motor burning time to determine this intermediate configuration.
3. The flow properties and heat transfer coefficient for the 15 sec configuration were calculated and compared with the initial calculations to determine

the error in extrapolation of the initially determined erosion rates. Because no large erosion rate changes occurred during the first 15 sec of burning time, the stepwise procedure was assumed adequate and no smaller increments of burning time were evaluated.

4. The process described in (3) was then repeated going to 38 sec, then 64.3 sec (web time).

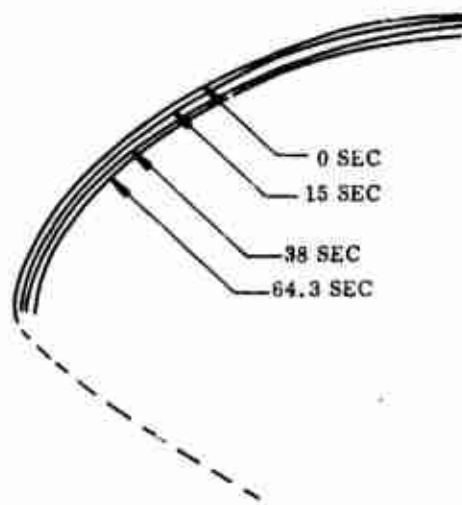
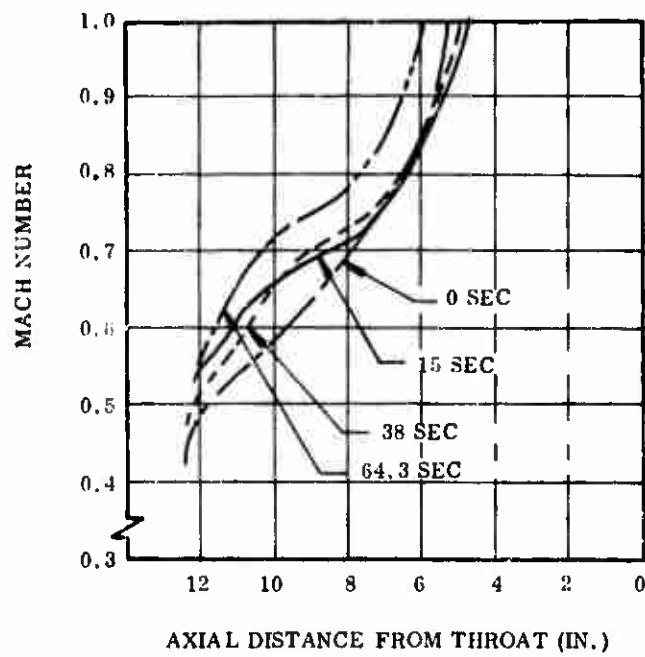
(U) The results of this erosion prediction are shown in Figure 34. The erosion along the nose is fairly uniform, about 0.60 inch. The heat transfer coefficient for the thermal analysis is shown in Figure 35.

(U) b. Aft Case--The flow in the aft case area was divided into two flow regions. For the first 30 percent of the web time a potential flow analysis was used, assuming the gas did not separate from the wall. After 30 percent of web time it was assumed the gas flow separates from the case wall at an axial station near the nose tip of the nozzle and leaves a separated area in the aft case. Analytical and cold flow studies verified this assumption.* The separated type of flow was not amenable to analytical techniques which describe the flow properties, heating rates and material erosion rates in a potential flow region. Therefore, prediction of these parameters depends on a different technique.

(U) Prediction of the erosion rates which will occur in the aft case area was achieved by equating the drag force driving the secondary flow and the wall drag length as shown in Figure 36. This relationship defines the velocities which occur on the backside of the nozzle nose and in the aft case. Using the velocities calculated in this manner, the boundary layer and heat transfer coefficients were determined.

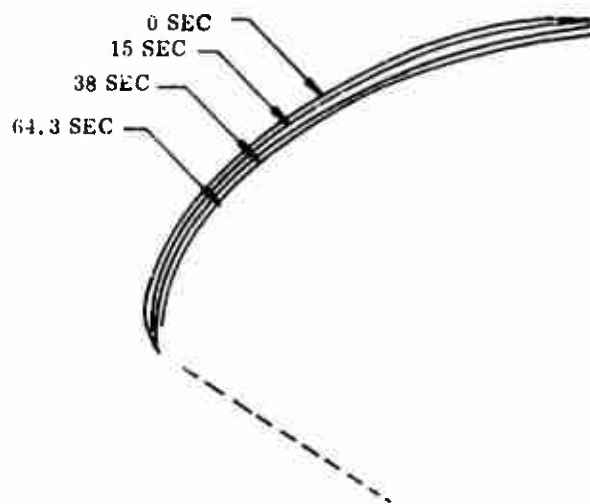
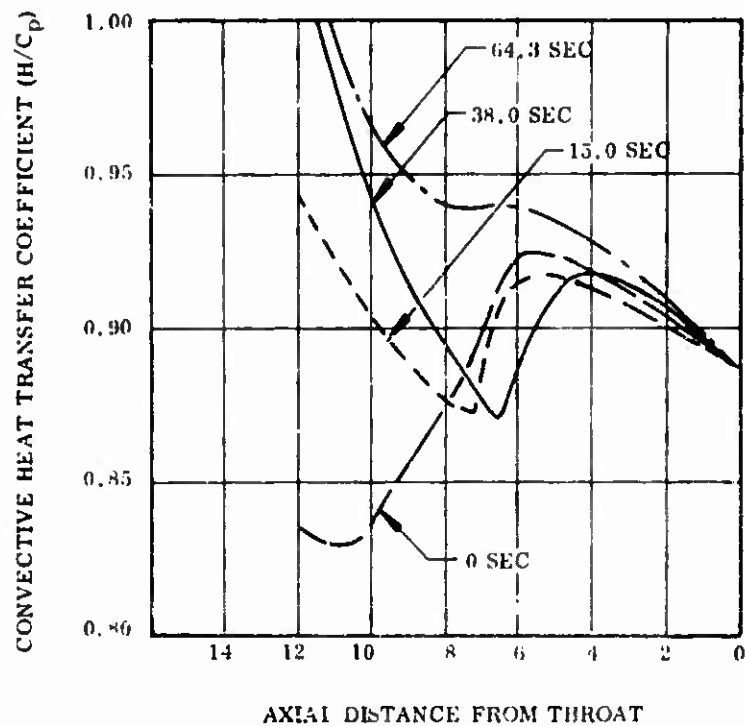
*Investigation of Flow in the Aft Case of Motors with Submerged Nozzles, Thiokol Chemical Corporation, Wasatch Division, TWR-1380; 22 Sep 1965.

Determination of Flow Properties in the Aft Chamber Region of the Poseidon C-3 First Stage Motor, Thiokol Chemical Corporation, Wasatch Division, TWR-1705; 24 Feb 1966.



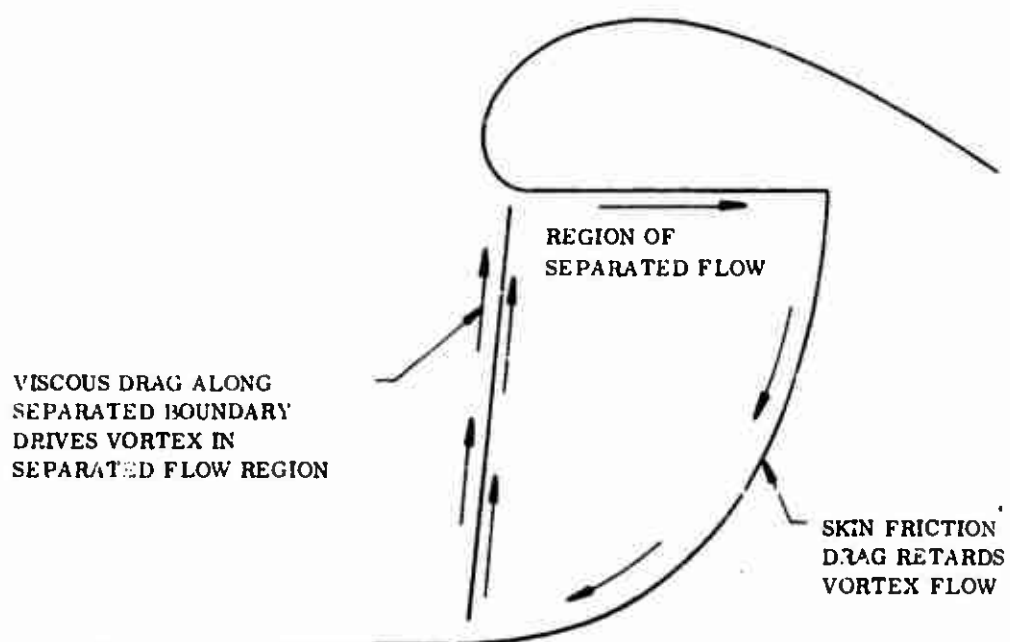
13094-28

Figure 34. 156-9 Nozzle Nose Mach No. vs Axial Distance from Throat



13094-27

Figure 35. 156-9 Nozzle Nose Convective Heat Transfer Coefficient vs Axial Distance from Throat



VISCOUS DRAG FORCE = SKIN FRICTION DRAG FORCE

13094-24

Figure 36. Description of Viscous and Skin Friction Drag Parameters

(U) Existing correlations between heat transfer coefficients and material loss rates were used to determine the erosion profiles.

(U) Aft case analysis differed somewhat from analysis of the nozzle backside because the propellant cover prevented erosion during this time.

(U) Nozzle backside analysis assumed a potential flow moving forward along the surface as follows.

1. The same flow net for the 0 sec nose analysis defines the flow properties on the backside of the nozzle. The boundary layer was calculated from the nozzle case joint forward to the nozzle splitline, then reinitiated (started with a smaller momentum thickness) and continued to the nose tip.
2. The erosion rates for the nozzle backside were determined from the boundary layer results and the erosion predicted at 12.86 seconds.
3. The flow analysis was repeated at 12.86 sec and the heat transfer coefficients and heat fluxes were averaged between 0 sec and 12.86 sec to predict 19.3 sec erosion.
4. The flow net was used to determine the flow conditions along the assumed separated boundary in Figure 37. These flow Mach numbers define the viscous mixing drag forces and the flow conditions along the backside of the nozzle and aft case. This flow condition was analyzed at the 32 sec configuration and the erosion from 19.3 to 64.3 sec calculated on the nozzle backside and erosion rate calculated for the aft case. The exact erosion in the aft case is a function of the exposure time.

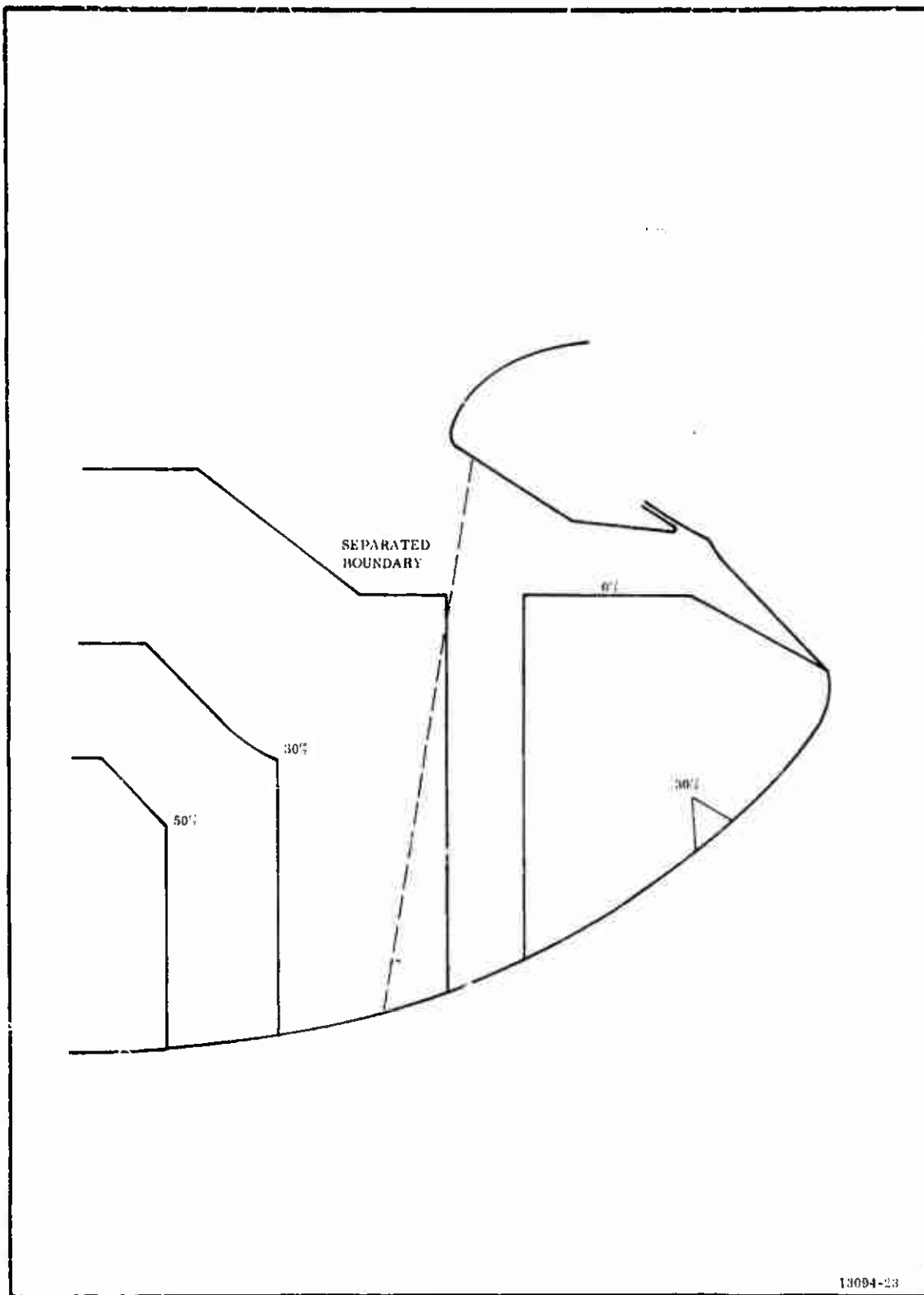


Figure 37. Aft Case Geometry and Grain Burnout

- (U) The final design of the nozzle backside is shown in Figure 38. The heat transfer coefficient is given along the carbon cloth and heat flux is given along the silica cloth because these parameters control erosion of the materials.
- (U) Other candidate materials, flow conditions and predicted erosion depths are shown in Figures 39 and 40.
- (U) c. Seal Region--The seal region of any movable nozzle must be designed to produce minimal gas velocities with resulting minimal convective heating for maximum reliability. The amount of radiant heating on the seal protective boot was minimized in the 156-9 nozzle by covering the boot with a projecting insulation harrier, which prevented direct radiation to the boot. Nozzle movement was allowed by providing a gap between the fixed and movable portions of the nozzle. An unprotected rubber boot would erode at a rapid rate due to radiation.
- (U) A rubber boot directly exposed to chamber environment would be subject to direct convective heating, and would require prohibitive boot thickness to insure seal survivability. *
- (U) Convective heating as well as radiation was adequately reduced, however, by using a projecting barrier and gap design concept. With this design concept, the following mode of flow in the boot region occurs.
- (U) At motor ignition, the flow from the aft surfaces is forward along the backside of the nozzle nose. When the nozzle is unvectored, the flow along the backside of the nozzle diffuses near the seal gap, separates across the gap, and reattaches on the forward side. This phenomenon occurs symmetrically producing equal pressure in the gap around the periphery of the nozzle.

*Lockheed Propulsion Company: Development of an Elastomeric Seal for Omniaxial Movable Nozzles (Lockseal), Progress Report No. 3, Technical Report No. AFRPL-TR-65-243, November 1965.

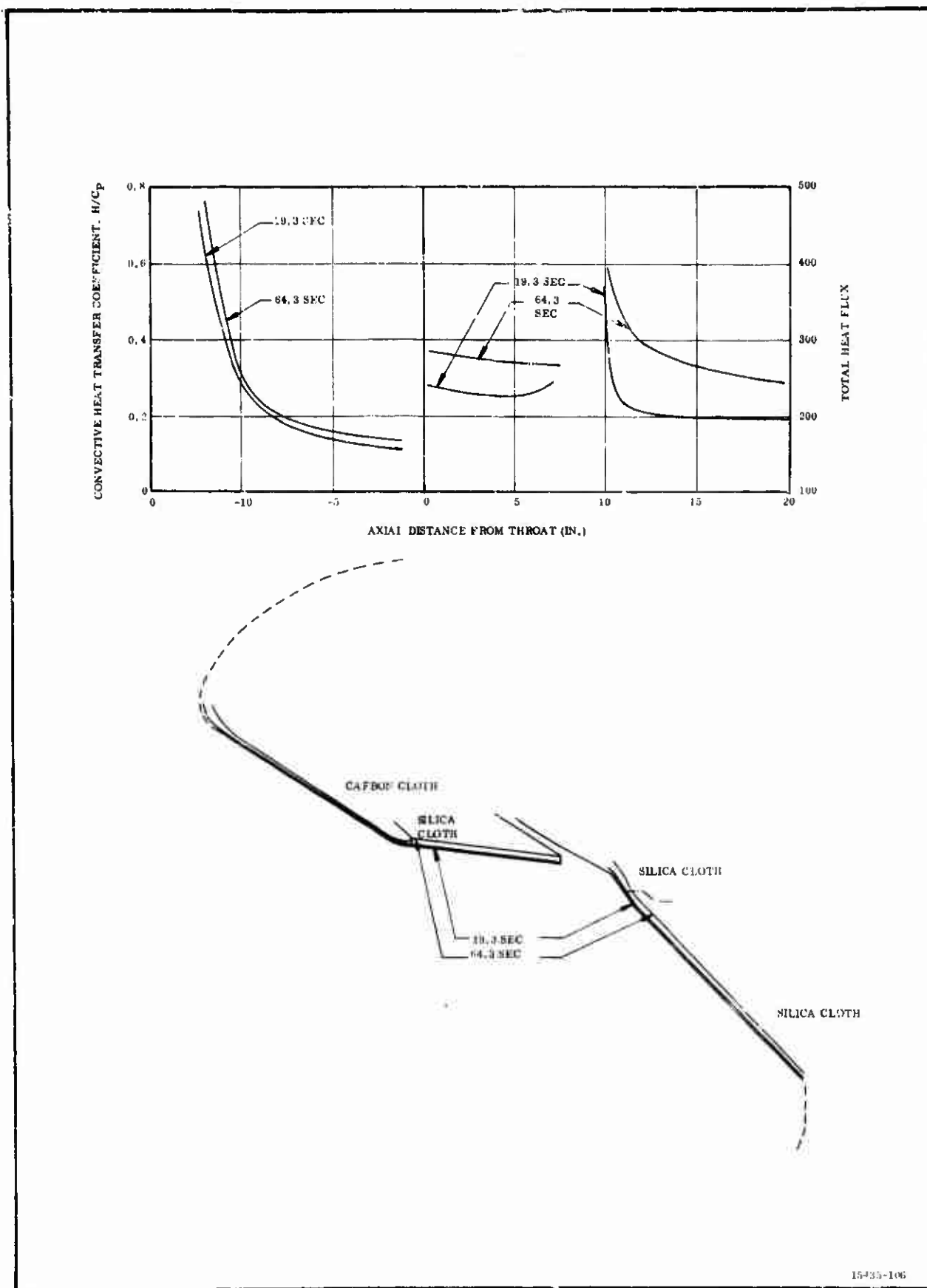


Figure 38. Backside of 156-9 Nozzle (Silica Cloth)

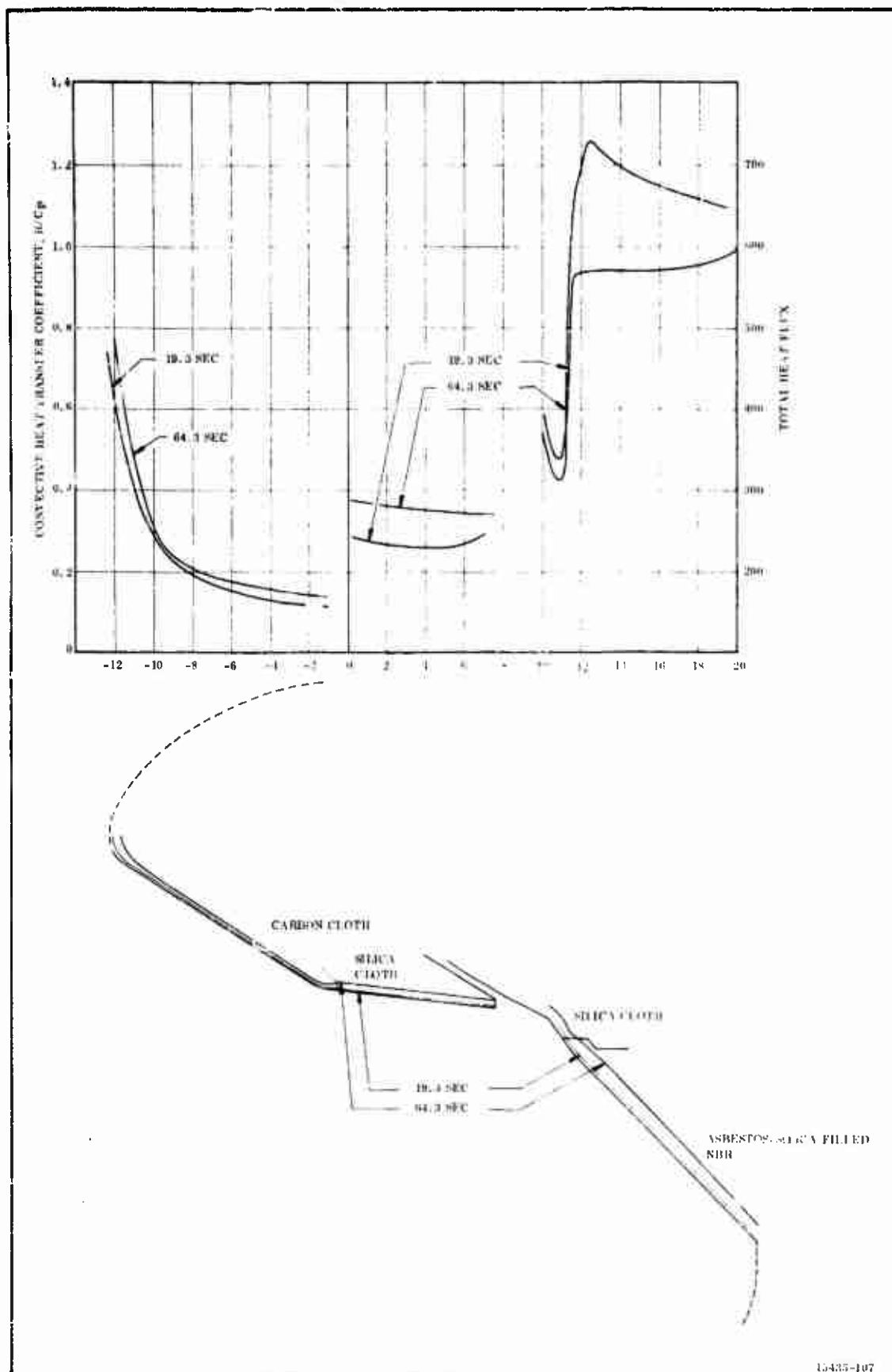


Figure 39. Backside of 156-9 Nozzle (Asbestos Filled NBR)

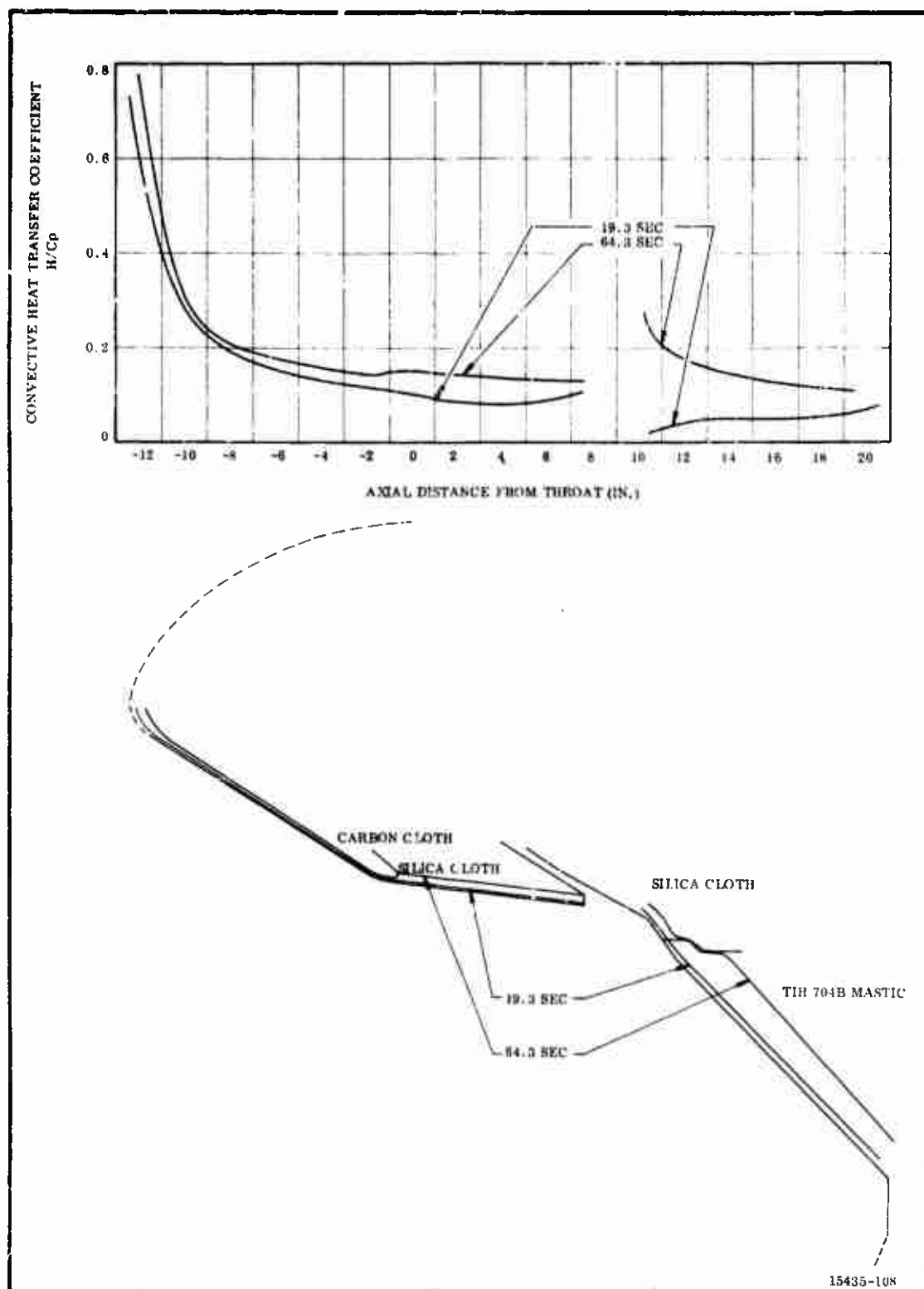
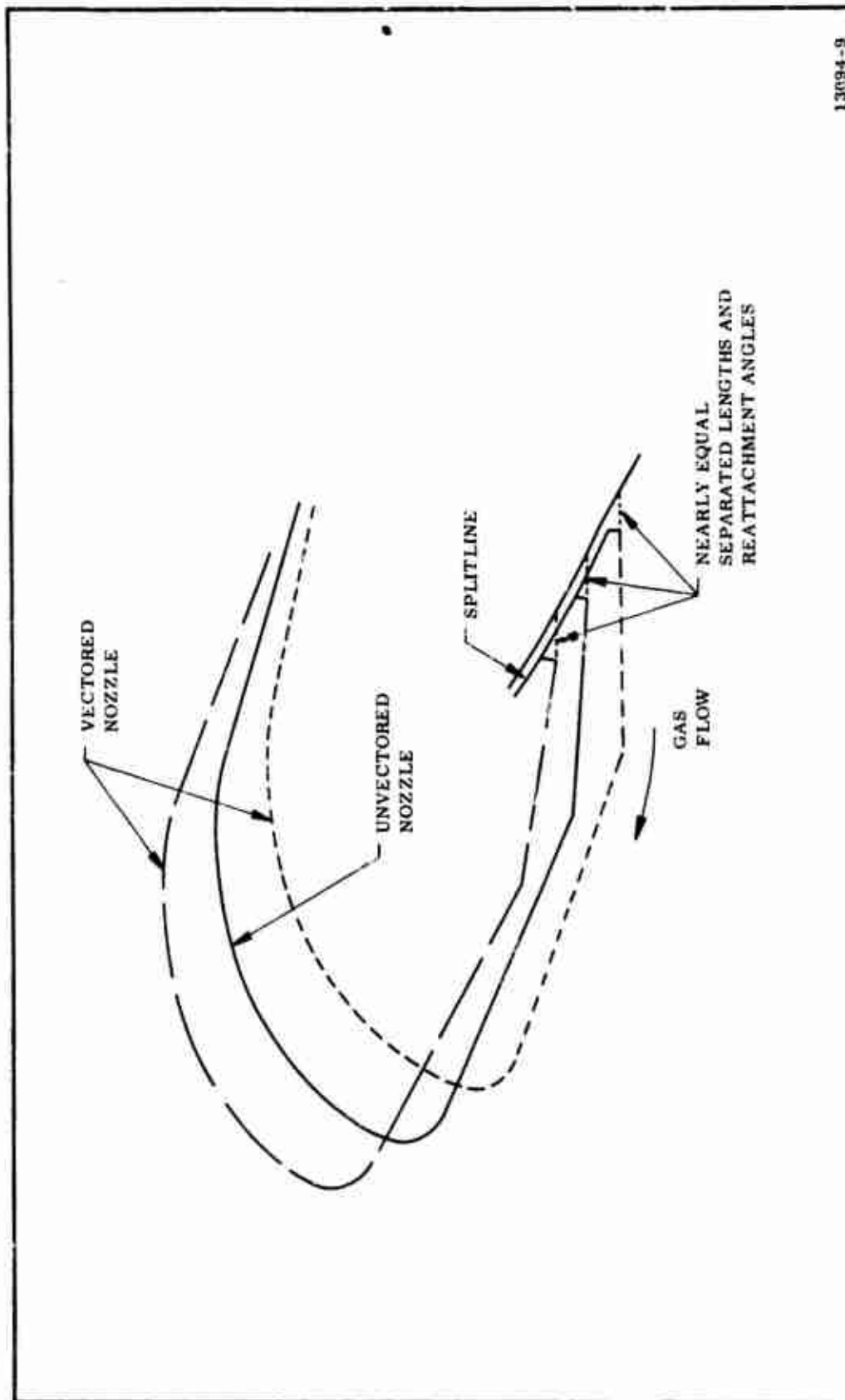


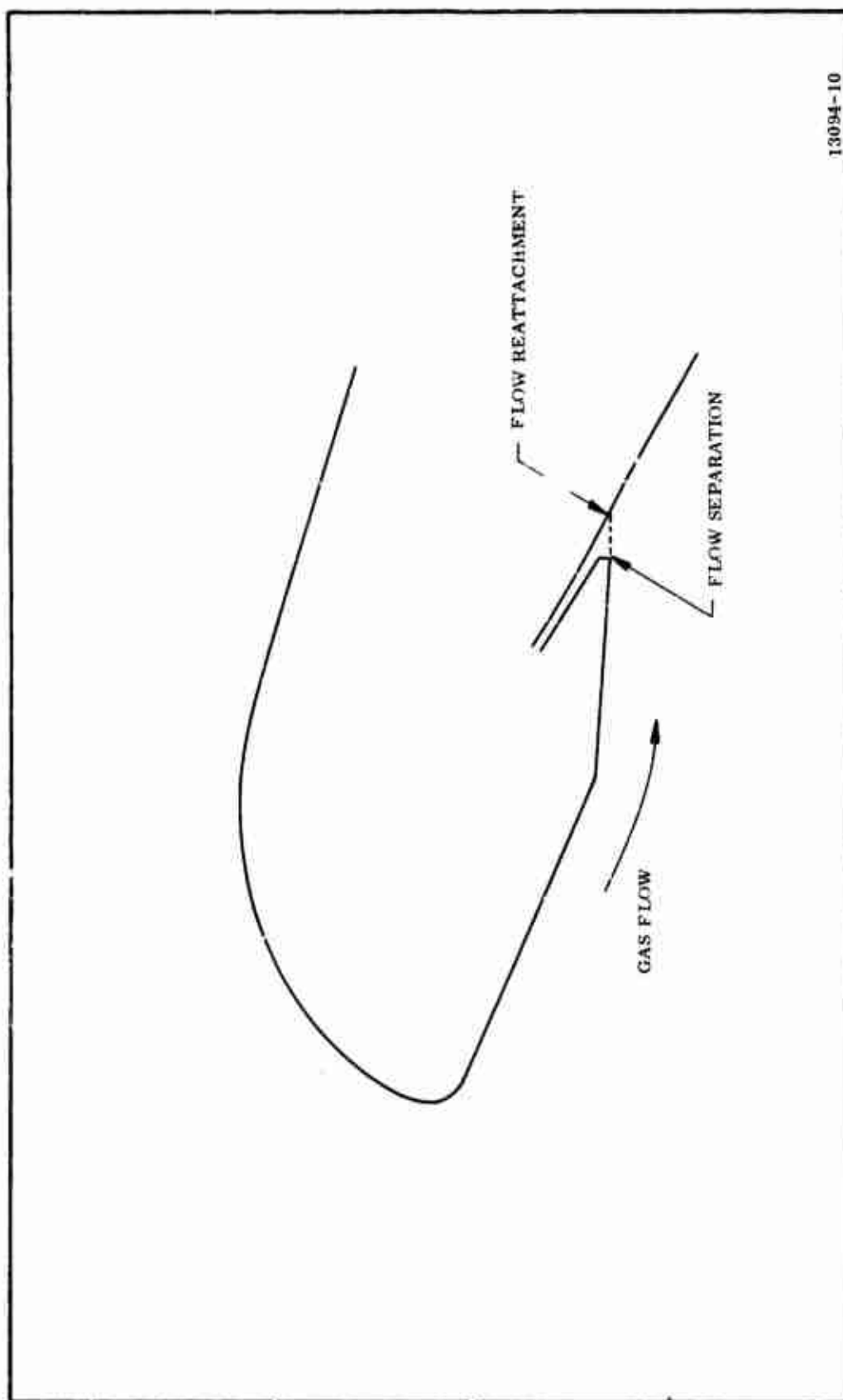
Figure 40. Backside of 156-9 Nozzle (TI-H704B Mastic)

- (U) When the nozzle is vectored, the equality of pressure about the periphery of the seal gap is still maintained. Equal pressures are produced because the distance from flow separation to reattachment and the angle of reattachment are maintained at a nearly constant value about the nozzle periphery by the spherical ball surface (Figure 41). Therefore, with this flow mode no driving potential is produced to cause peripheral flow and large heating rates near the seal.
- (U) As burning time progresses, however, the basic mode of flow in the aft case near the backside of the nozzle is modified. Cold flow studies and static test firings of motors with submerged nozzles have indicated the flow pattern shown in Figure 36. With this type of flow the gas separates from the aft case wall just aft of the propellant surface. A separated flow is formed in the aft case region. The flow moves along with the separated boundary and reattaches to the nozzle near the tip of the nozzle entrance section. At the reattachment point, the flow divides with a portion of the flow moving aft along the backside of nozzle.
- (U) The flow moving aft along the backside of the nozzle nose thus approaches the seal region in a direction opposite to that which occurs at motor ignition. With this basic flow mode and the nozzle unvectored, the flow in the seal region occurs as shown in Figure 42. The flow separates from the nozzle wall, flows across above the seal gap, and reattaches to the downstream wall. Again in this case, the flow separation and reattachment occur symmetrically about the nozzle periphery. No driving force for circumferential flow under the separated boundary about the periphery of the seal exists, and seal survivability is assured. Nozzle vectoring does not change the symmetrical separation and reattachment because of the spherical downstream surface.
- (U) A series of cold flow tests in which the flow velocities were measured in the cavity near a flexible seal indicated that the flow Mach numbers near the boot protecting the flexible seal were less than 0.03 for both a null and a 5 deg vector position. The seal region will then be exposed to nearly stagnant flow and convective heating of the boot will be constant throughout motor operation.



13094-9

Figure 41. Motor Flow Near Splitline in Vectored Nozzle at Motor Ignition



13094-10

Figure 42. Mode of Flow Near Splitline

(U) The gap between spherical surfaces was made as small as possible without risk of contact between the surfaces. After thorough consideration of the possible adverse tolerance buildup and of the relative deflection of the parts, a gap dimension of 0.200 in. was specified in the final design.

4. THERMAL ANALYSIS

(U) A thermal analysis was conducted to insure that adequate material had been provided to allow for the anticipated losses (erosion-corrosion) and to adequately insulate the structural parts during firing.

(U) The computer program determined the transient temperature response and surface-recession rates of a slab characterized by two receding surfaces.

The transient temperature response of the insulation and nozzle parts is a function of the thermal properties of the material and the internal environment to which the parts are subjected. The thermal properties are usually published values obtained from vendors and lab tests (Table VIII).

(U) The internal thermal environment of the motor is dependent on the composition of the propellant and the pressure at which combustion occurs. With these two parameters fixed, the combustion temperature, the enthalpy, the equilibrium composition of the combustion products, and the motor performance were calculated using an IBM 7040 computer. The computer program used simulated the isotropic gas expansion through the nozzle and calculated the static enthalpy of the gas at prescribed locations in the nozzle. From this information and a suitable recovery factor (a function of the Prandtl number), the recovery enthalpy is determined from the following relationship.

$$i_r = N_{rf} (i_T - i_s) + i_s$$

where:

i_r = recovery enthalpy (Btu/lb)

N_{rf} = recovery factor (dimensionless, the cube root of the Prandtl number)

i_T = total (stagnation) enthalpy (Btu/lb)

i_s = static enthalpy (Btu/lb)

(U) The recovery enthalpy represents the potential heat available for transmission across the boundary layer to the wall.

TABLE VIII
MATERIAL THERMAL PROPERTIES

Carbon Cloth Phenolic

<u>Temperature (° F)</u>	<u>Density (lb/cu ft)</u>	<u>Thermal Conductivity (Btu/ft-hr-° F)</u>	<u>Specific Heat (Btu/lb-° F)</u>
400	81	0.50	0.30
1,200	74	0.50	0.47
1,500	73	0.58	0.48
2,500	73	1.6	0.48
4,000	73	3.3	0.5
6,000	73	5.9	0.5

Silica Cloth Phenolic

<u>Temperature (° F)</u>	<u>Density (lb/cu ft)</u>	<u>Thermal Conductivity (Btu/ft-hr-° F)</u>	<u>Specific Heat (Btu/lb-° F)</u>
400	110	0.18	0.24
1,000	102	0.28	0.24
2,000	96	0.50	0.28
4,000	96	1.27	0.28
6,000	96	2.25	0.28

(U) To determine the amount of heat actually transmitted across the boundary layer by convection, the enthalpy on the wall side of the boundary layer must also be known. This was obtained by a second computer program which was used to calculate gas equilibrium composition and enthalpy as a function of temperature and pressure. From these data and the recovery enthalpy, the difference across the boundary layer at any instantaneous set of conditions can be determined by the computer. This information, as well as the convective heat transfer coefficient, was needed to evaluate convective heat flux.

(U) The simplified Bartz equation was used to calculate the convective heat transfer coefficients.

$$C_H = \frac{0.026}{(D_t)^{0.2} (A/A^*)^{0.9}} \left(\frac{\mu}{(P_r)^{0.6}} \right)^{0.2} \left(\frac{(P_c)}{C^*} \right)^{0.8} \left(\frac{(D_t)}{r_c} \right)^{0.1} \psi$$

where:

- C_H = heat transfer coefficient based on enthalpy difference (lb/sq ft/sec)
- 0.026 = a correlation constant derived by Bartz from turbulent boundary layer analyses
- D_t = nozzle throat diameter (ft)
- (A/A^*) = expansion ratio at the nozzle location under consideration
- μ = viscosity at stagnation conditions (lb/ft-sec)
- P_r = Prandtl number (c_p/k) (dimensionless)
- P_c = chamber pressure (psia)
- g = acceleration due to gravity (ft/sec²)
- C^* = characteristic gas velocity (ft/sec)
- r_c = throat radius of curvature (ft)
- ψ = dimensionless factor accounting for variation of ρ (gas density) and μ (gas viscosity) across the boundary layer

(U) Transport properties appearing in the Bartz equation were calculated with a computer program based on the kinetic theory of gases. The latest thermochemical data were used in this program and its predictions compared well with available experimental data.

(U) Heat transfer coefficients were determined as a function of wall temperature and nozzle expansion ratio.

(U) Having obtained the foregoing information, the convective heat flux was calculated according to the following equation.

$$Q_{\text{conv}} = C_H (i_r - i_w)$$

where:

C_H = convective heat transfer coefficient (lb/ft²-sec)

i_r = recovery enthalpy of the combustion gases (Btu/lb)

i_w = static enthalpy of the gases on the wall side of the boundary layer (Btu/lb)

(U) Conventional techniques were used to determine the net radiant heat flux to the wall. The net radiant heat flux may be expressed as:

$$Q_{\text{rad}} = \epsilon_w \sigma \left[\epsilon_g T_g^4 - \alpha_g T_w^4 \right]$$

where:

ϵ_w = effective wall emissivity

ϵ_g = gas emissivity

α_g = gas absorptivity

T_g = temperature of the gas (°K)

T_w = temperature of the wall (°K)

σ = Boltzmann's constant

(U) The emissivity (absorptivity of a particle laden gas at any particular temperature) may be expressed as:

$$\epsilon_g = 1 - (e)^{-NAL}$$

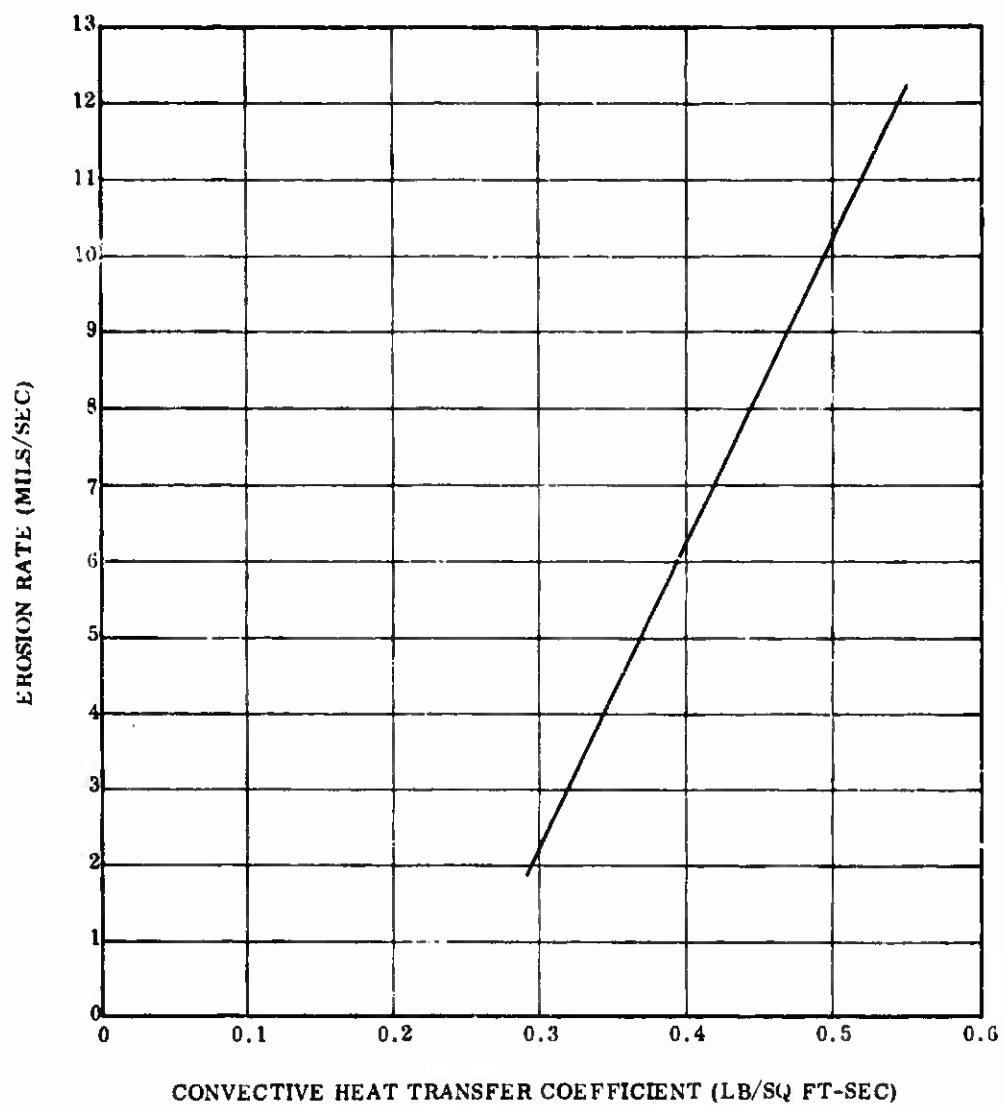
where:

N = particle number density (number/cu cm)

A = condensed particle cross-sectional area (cu cm)

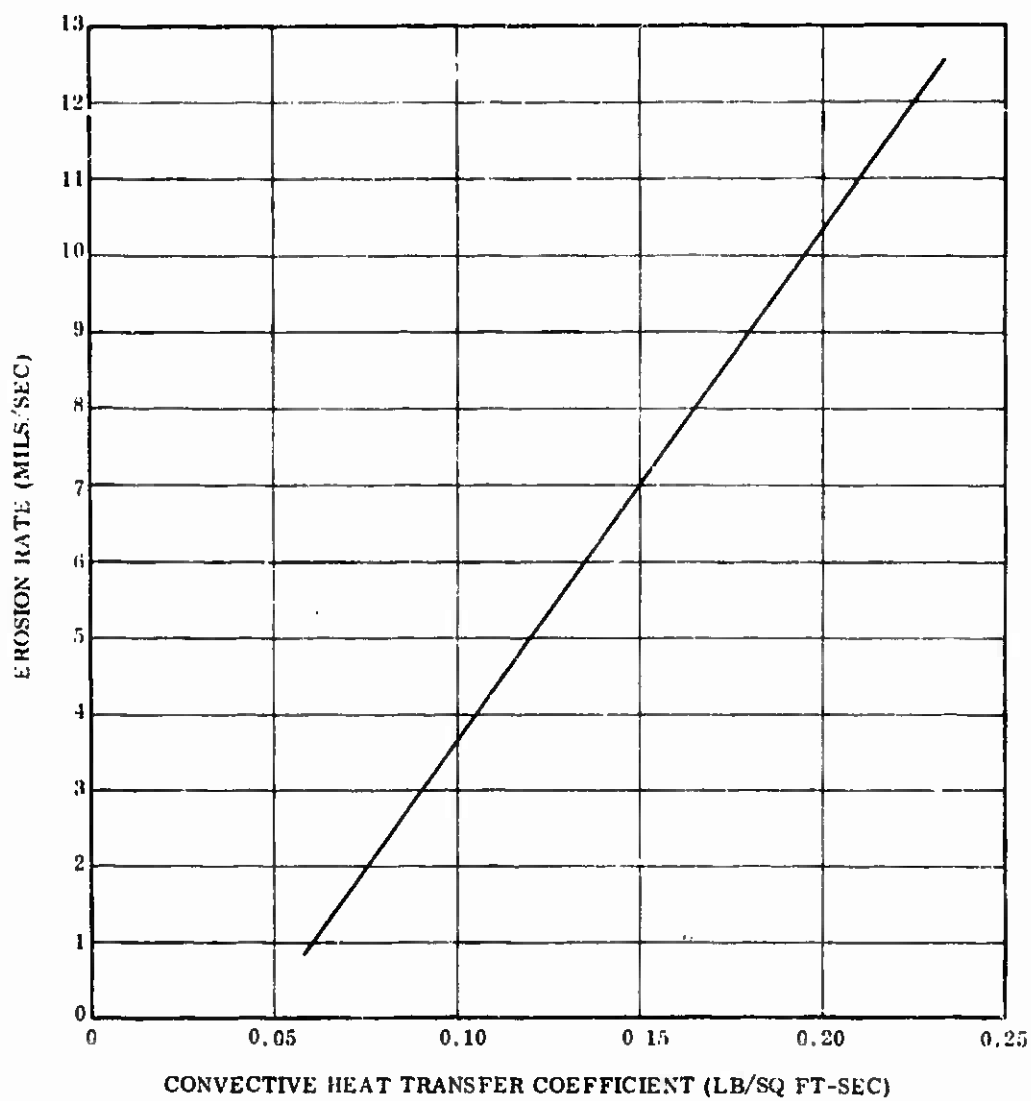
L = mean radiation beam length (cm)

- (U) The computerized thermal analysis requires an input erosion rate as a function of time. The predicted erosion rates for the nozzle exit cone were obtained using an empirical procedure which was developed as a result of analyzing static test data. This procedure consists of correlating nozzle exit cone erosion rates with convective heat transfer coefficients. Erosion data obtained in numerous firings with propellant formulation very similar to that proposed for the 156-9 motor have shown good correlation with convective heat transfer coefficients.
- (U) The relationships between the exit cone erosion rate and convective heat transfer coefficient are shown in Figures 43 and 44 for carbon cloth phenolic and silica cloth phenolic. These data are for the conditions of the test, i. e., the chamber pressure, nozzle configuration, and the exhaust gases predicted for the 156-9 motor.
- (U) The assumption implicit in the use of the correlation is that erosion is primarily a reaction of certain chemical species in the combustion gases with the nozzle material. Furthermore, it is assumed that the material is at a sufficiently high temperature so that the reaction rate of the reacting species and the wall material is infinite and that the overall rate of erosion (corrosion) is determined by boundary conditions which control the transport rate of reactants and the reaction products. These controlling boundary conditions were satisfactorily defined by the convective heat transfer coefficient.
- (U) It is recognized that this approach was somewhat specious with silica cloth since physical changes (melting, vaporization) controlled by environmental temperature play a more prominent role here than do chemical reactions. The correlation has, however, been found to yield dependable design data in applications and under conditions similar to those under which the reference test data were obtained.



13094-43

Figure 43. Convective Heat Transfer Coefficient vs Erosion Rate, Carbon Cloth



13094-42

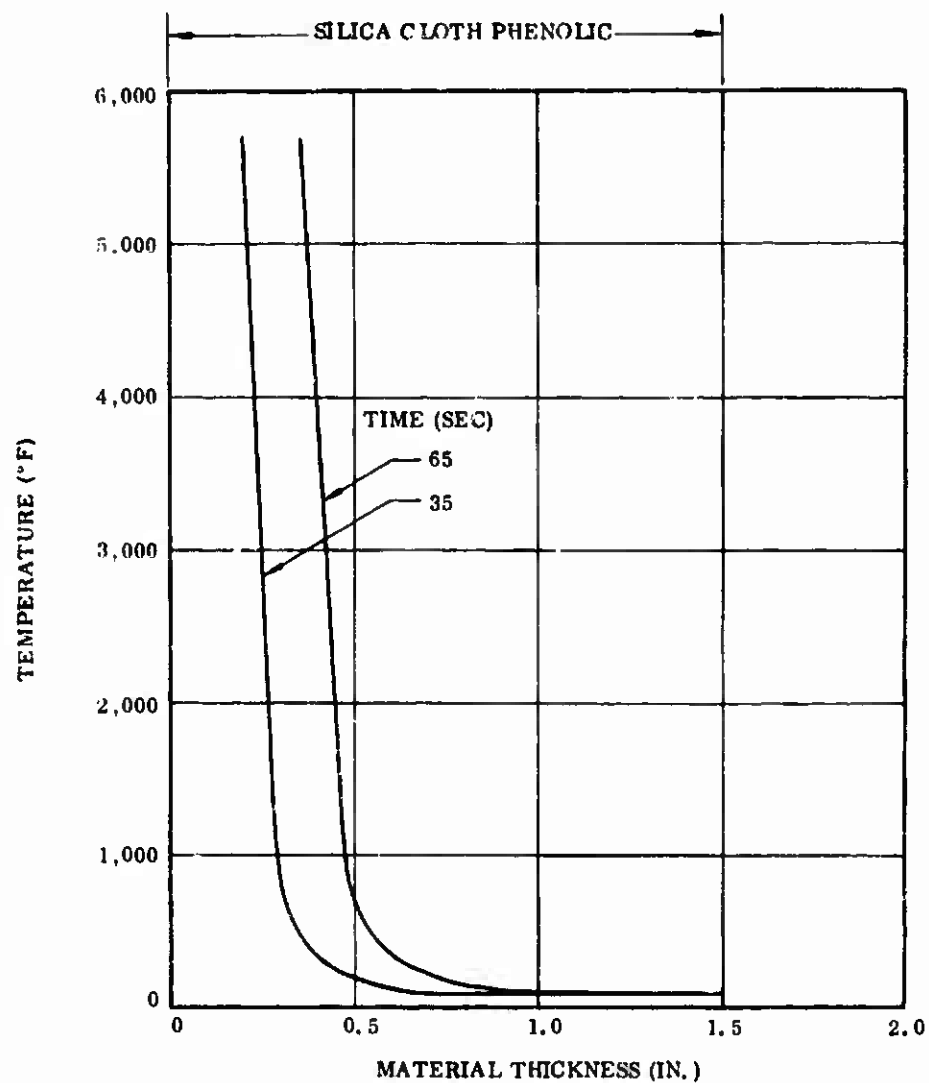
Figure 44. Convective Heat Transfer Coefficient vs Erosion Rate, Silica Cloth

- (U) This empirical technique somewhat circumvents uncertainties in the heat transfer coefficient calculation. The same method for computing this coefficient is used both to set up the correlation and to read values out of it. Uncertainty in the heat transfer coefficient is thus cancelled out.
- (U) It has been shown that the erosion of a graphite containing material is primarily the result of a chemical reaction occurring at the material surface.* The magnitude of this effect is dependent upon the quantity of oxygen containing species in the propellant combustion gas and is defined by a parameter called the blowing coefficient (β). Since different propellant formulations have different blowing coefficients, the resulting erosion of a carbon containing material will depend on the propellant formulation selected.
- (U) This blowing coefficient analysis is not applicable to plastic materials with siliceous reinforcement because corrosion is not the primary cause of material loss in this case. The char formed with this material is lost primarily by vaporization.
- (U) Separate correlations were used for the nose region and the nozzle exit because the convective heat transfer coefficients are calculated by different methods in the two cases.
- (U) The predicted erosion rates for the nozzle entrance or nose section were not as easily obtained as those for the exit cone. The nozzle inlet configuration may cause nonuniform acceleration of the gases into the throat resulting in high local velocities in the supersonic range. Subsequent deceleration to subsonic velocities will set up a shock pattern making a reliable estimate of convective heat transfer coefficients impossible. Hence, to predict erosion rates for the inlet section where the flow is supersonic, predicted convective heat transfer coefficients were extrapolated between the points of known flow conditions.

*McDonald, A. J., and Hedman, P. O., "The Determination of the Mechanism of Erosion of Graphite in Solid Propellant Combustion Gases and Resulting Effects on Heat Transfer Phenomena," January 1964.

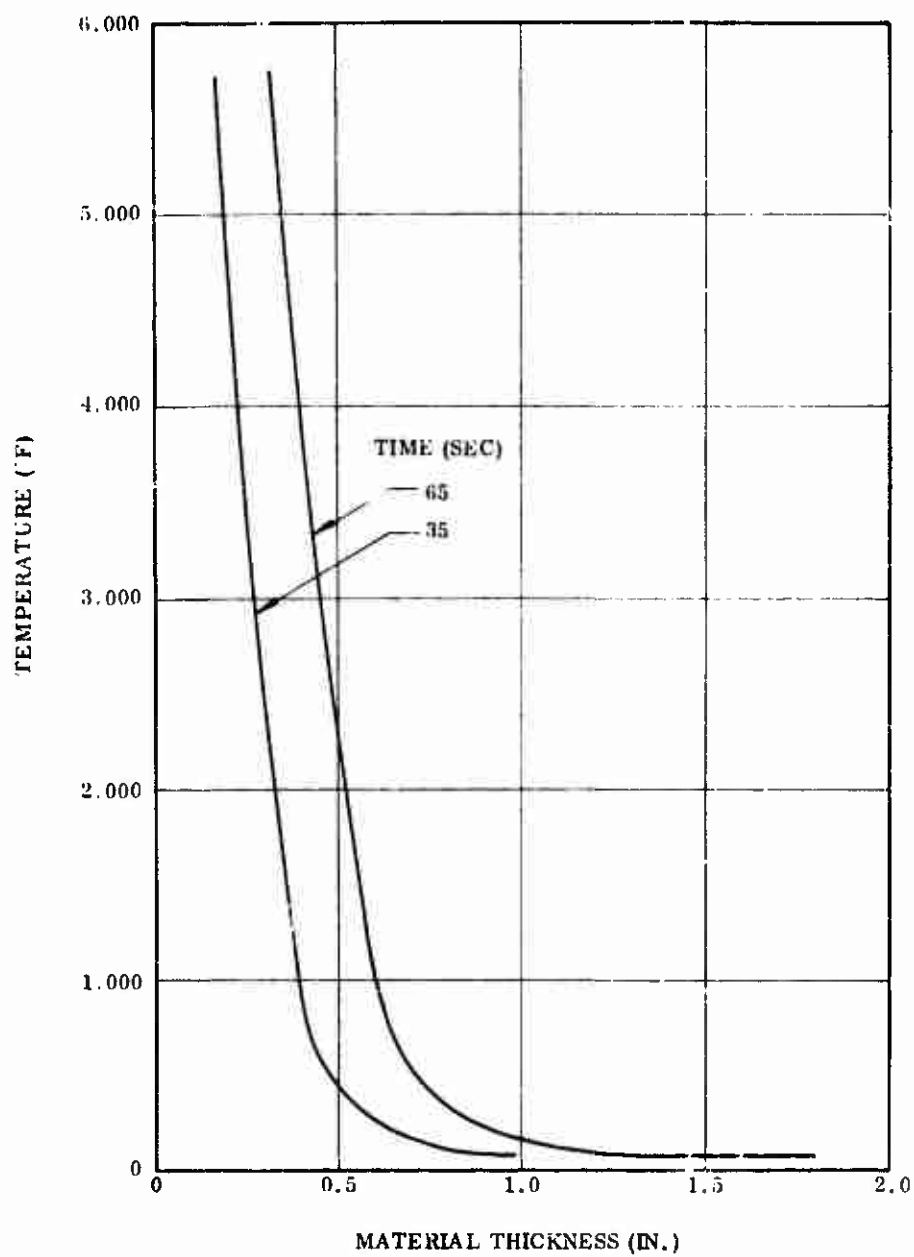
(U) The convective heat transfer coefficients were obtained by determining the Mach number profile around the inlet section of the nozzle up to the point of sonic flow. Output from this computer program included predicted material erosion rates which are dependent upon flow conditions and the composition of the combustion gases. The Mach numbers were converted to effective area ratios using one-dimensional flow assumptions. The resulting area ratios and corresponding gas dynamic properties of the combustion products were used as input to the Bartz equation to calculate the convective heat transfer coefficient.

(U) The erosion rates at various locations throughout the nozzle as determined by the methods previously discussed were used as input to the thermal program. The computer program handles the erosion as a function of the convective heat transfer coefficient with the nodal thickness being reduced with time. The predicted nozzle erosion and char profiles are presented later in this section under Predicted Performance. The predicted temperature profiles for the locations indicated are presented in Figures 45 thru 49.



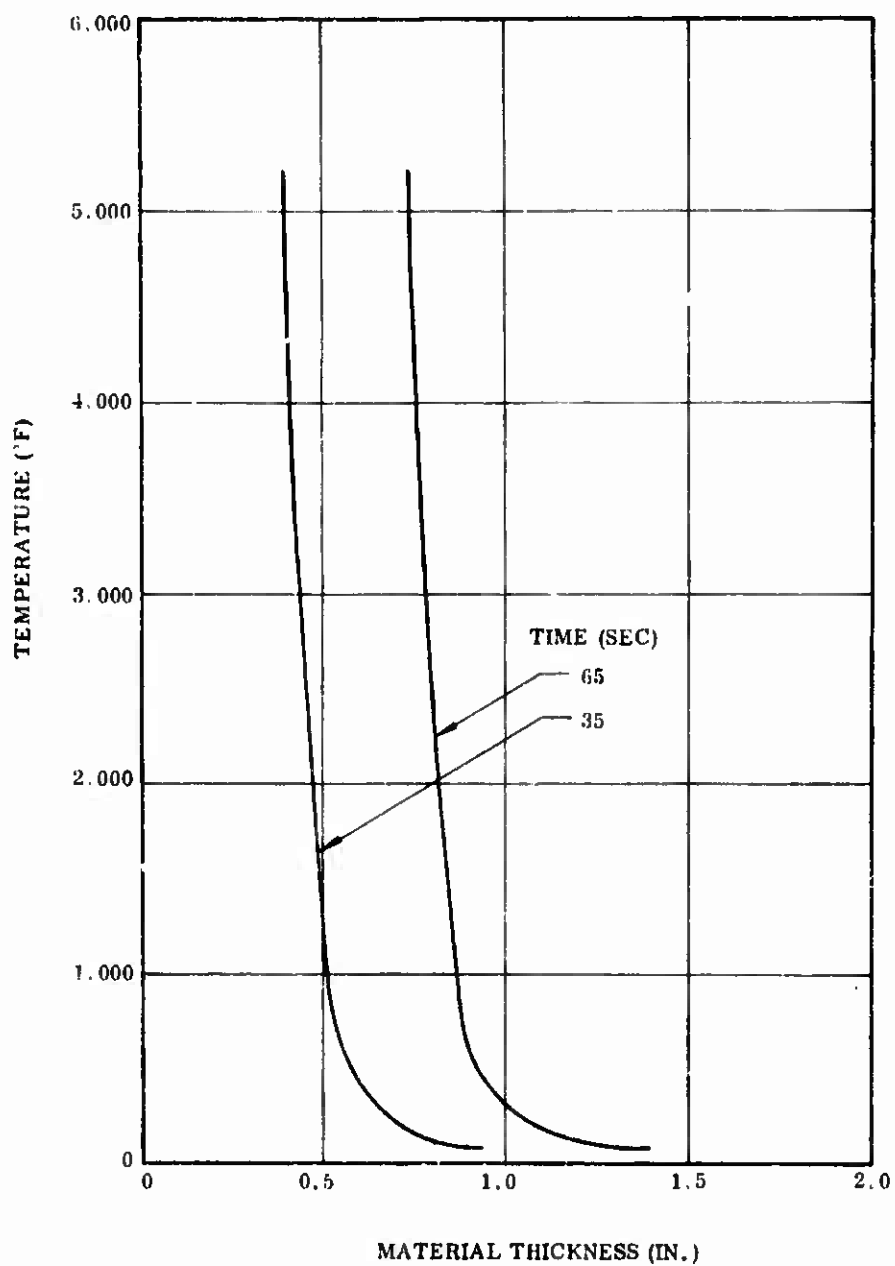
13094-32

Figure 45. 156-9 Nozzle Entrance Temperature Profile,
A/A* = 3.88 (Back Side)



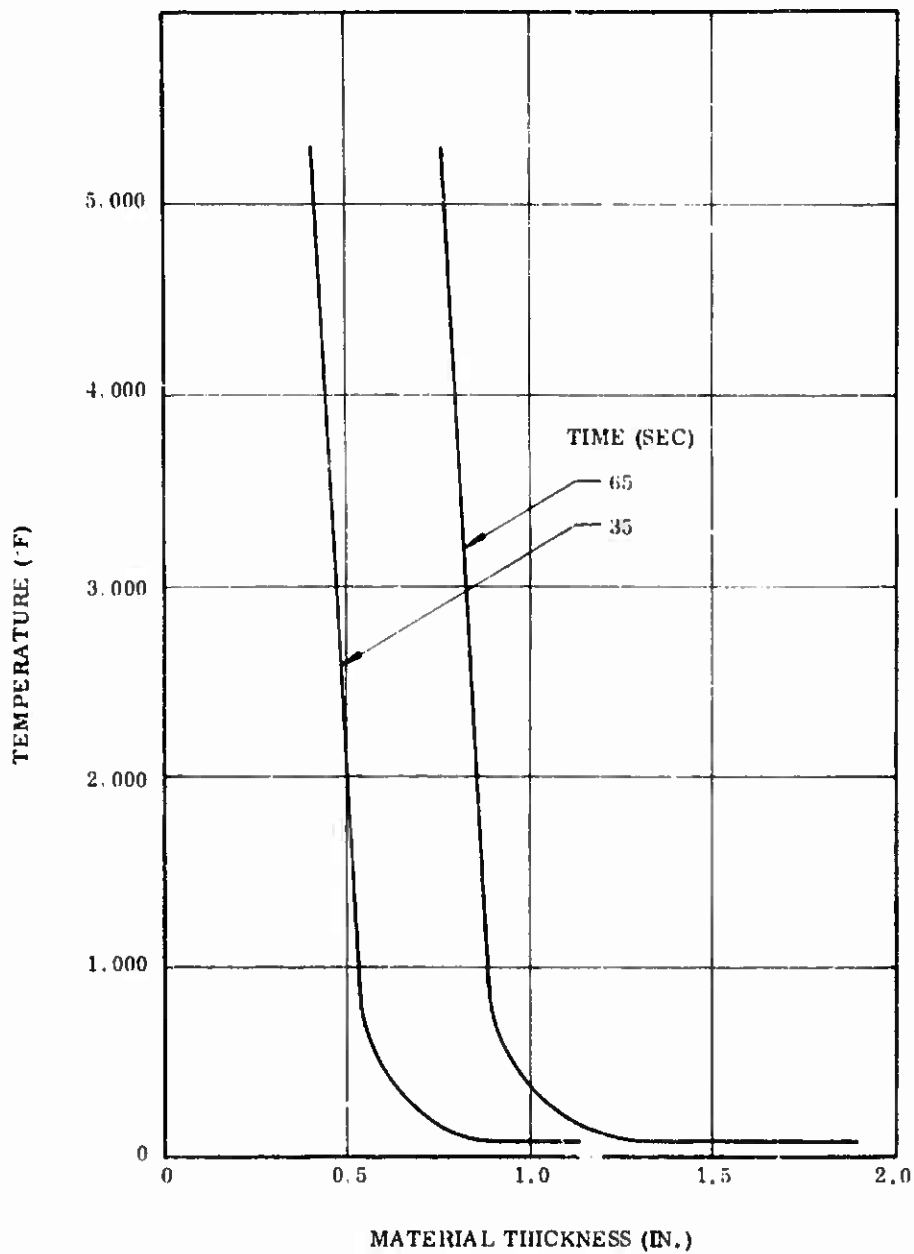
13094-31

Figure 46. 156-9 Nozzle Entrance Temperature Profile,
 $A/A^* = 2.52$ (Back Side) Carbon Cloth



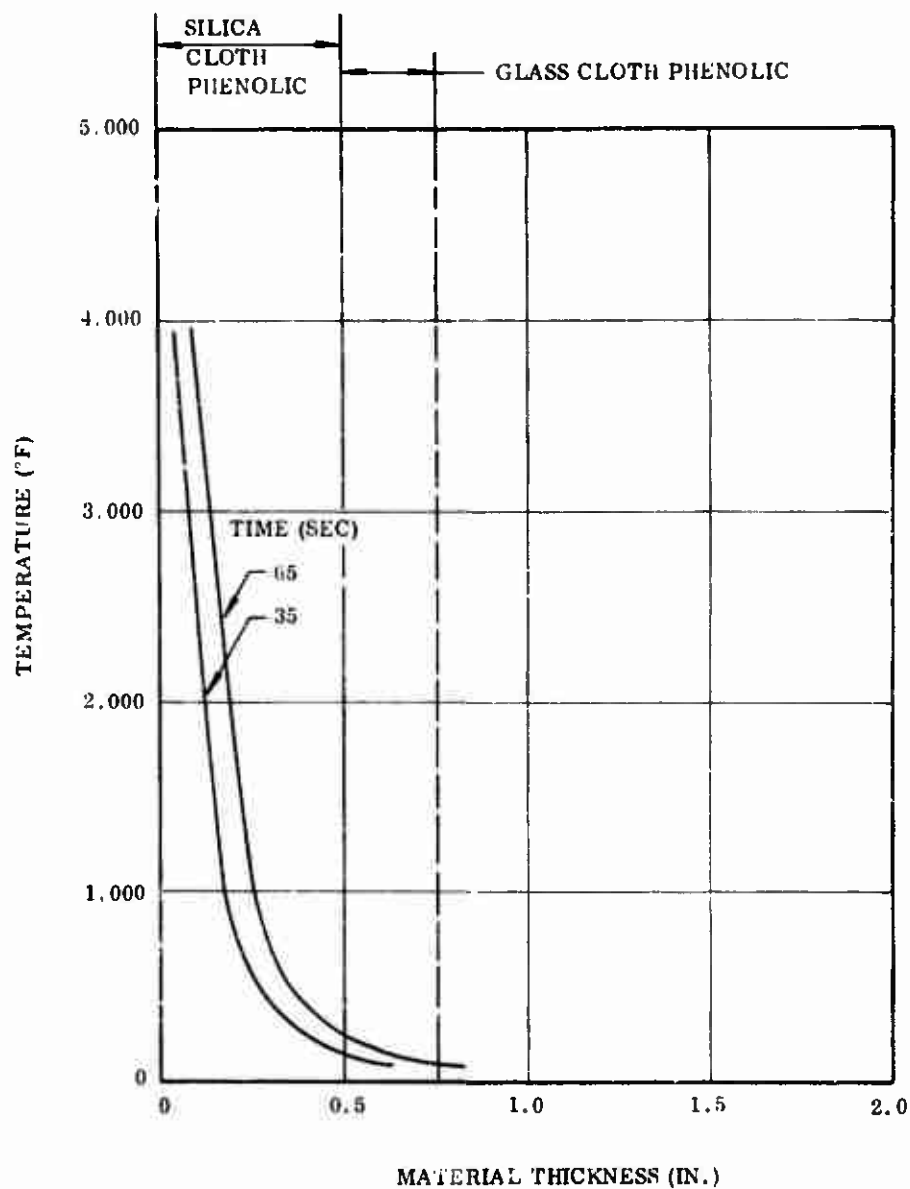
13094-30

Figure 47. 156-9 Nozzle Entrance Temperature Profile,
 $A/A^* = 1.17$ Carbon Cloth



13094-29

Figure 48. 156-9 Nozzle Temperature Profile
A/A* = 1.0 Carbon Cloth Phenolic



13094-1

Figure 49. 156-9 Nozzle Exit Cone Temperature Profile,
 $A/A^* = 8.16$

5. STRUCTURAL ANALYSIS

- (U) An analysis was conducted to verify the structural integrity of the fixed housing and nozzle at a maximum expected operating pressure (MEOP) of 830 psig, and to analyze the nozzle actuator brackets to determine structural integrity at an actuator stall load of 70,097 pounds.
- (U) The minimum ultimate tensile strength of the materials for the various components is shown in Figure 50. Ultimate bolt strengths were selected to insure a 0.25 minimum margin of safety.
- (U) The structural analysis was conducted at a case MEOP of 830 psig. The stresses that result from MEOP case pressure, or the stresses in the various components which result from actual predicted applied loads, are defined as limit stresses (σ).
- (U) The margins of safety presented here exist between limit stresses and ultimate strength capability or between limit stresses and critical buckling capability.
- (U) Basic design criteria for the various components indicated that a margin of safety of 0.25 be maintained in all areas during the most severe loading condition to be encountered during static firing. However analysis of the aft dome area of the GFP case showed a 0.185 margin of safety (Table IX). Since propellant loading could be controlled accurately to eliminate the possibility of any over-pressure condition, this margin of safety was considered adequate.

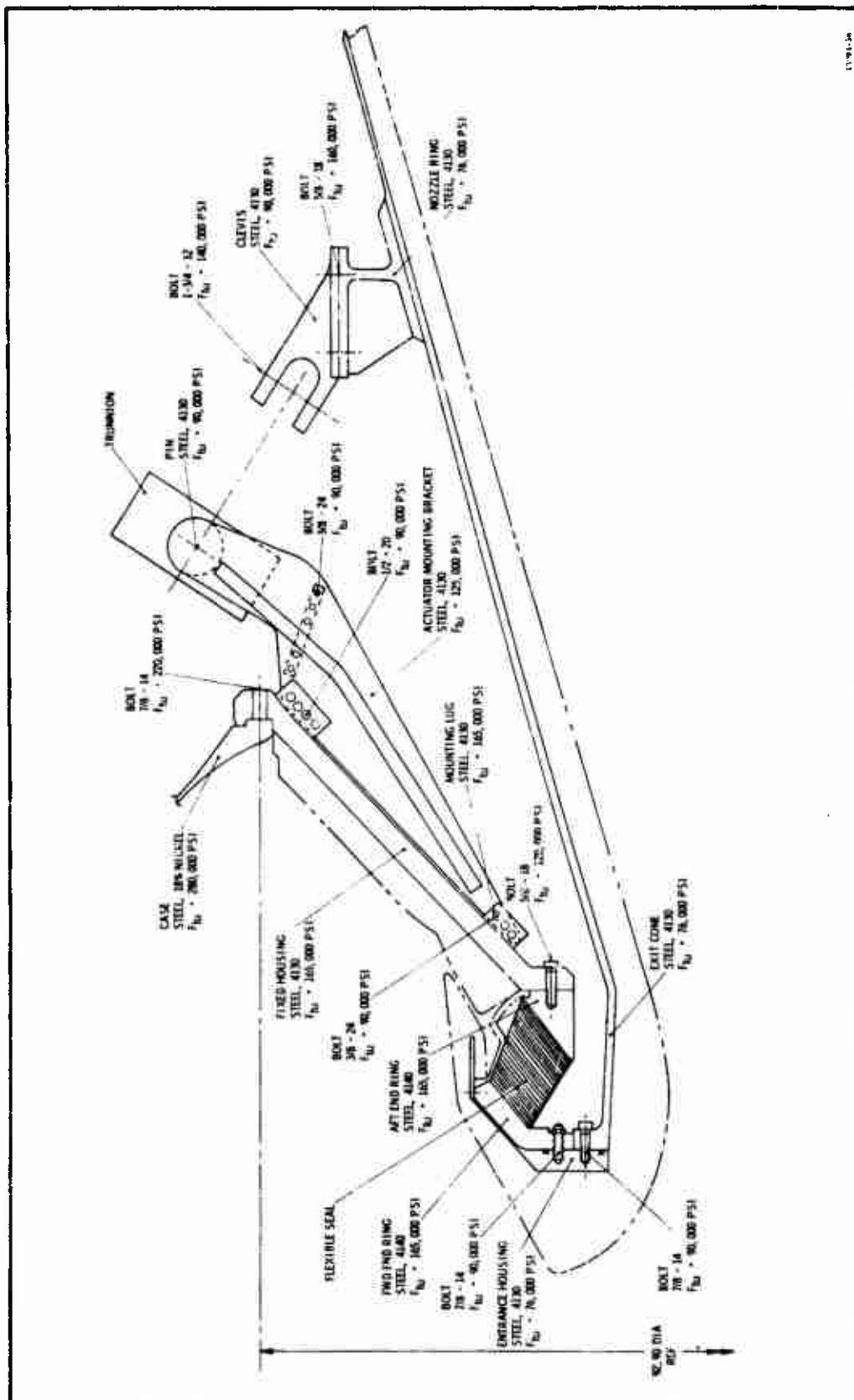


Figure 50. Summary of Materials and Minimum Ultimate Strengths

TABLE IX
SUMMARY OF MINIMUM MARGINS OF SAFETY

<u>Number</u>	<u>Component</u>	<u>Minimum M. S.</u>
1	Case	0.185
2	Bolt (Case to fixed housing)	0.28
3	Fixed Housing	1.10
4	Bolt (Fixed housing to flex seal)	0.54
5	Flex Seal, Forward end ring	10.45
6	Bolt (Flex seal to entrance housing)	2.32
7	Bolt (Entrance housing to exit cone)	2.18
8	Exit Cone	2.04
9	Nozzle Ring	1.31
10	Bolt (Nozzle ring to clevis)	0.31
11	Clevis	0.58
12	Actuator Bracket	0.47
13	Bolts (Actuator bracket to fixed housing lugs)	0.46

- (U) The area with the next lowest margin of safety was the bolts which attach the fixed housing to the case. The margin of safety for the bolt tension was 0.28 which was above the minimum requirements. Margins of safety for various areas are listed in Table IX.
- (U) Computer runs used in the analysis are included in Section V. The free body sketches of the geometrical shapes shown on the computer runs reflect the positive direction for the moment, shear, and axial loads.
- (U) The four basic components of the 156-9 nozzle considered here were the fixed housing, nozzle body, actuator mounting bracket, and nozzle ring and actuator attach bracket.
- (U) a. Fixed Housing--The fixed housing was a heavyweight design, 1.55 in. thick, which is considerably thicker than required to withstand the internal case pressure. The extra thickness was included to facilitate fabrication of the unit. The maximum stress is located at a radius of approximately 45 in. from the centerline of the part. This area is adjacent to the housing-to-case attachment ring and has a stress level of 78,599 psi and a margin of safety of 1.1.
- (U) b. Nozzle Body--The nozzle body analysis included the flexible seal end rings, the entrance housing ring, and the nozzle exit cone attachment ring. This analysis assumed that the flexible seal would transfer axial loads only and would not add significantly to the rigidity of the end rings or induce appreciable moments or shear into the rings. The maximum stress induced in the flexible seal end rings occurred in the forward ring and is only 14,403 psi with a margin of safety of 10.45.
- (U) c. Actuator Mounting Bracket--The actuator mounting bracket, trunnion, and mounting bracket to fixed housing lugs, were designed to sustain an actuator axial stall load of 70,097 pounds. The maximum stress in these three components occurs in the actuator mounting bracket and is 84,517 psi and results in a margin of safety of 0.47. This area is approximately midway down the bracket arm and is in the area directly over the mounting lugs closest to the actuator.

- (U) d. Nozzle Ring and Actuator Attach Clevis--The nozzle ring is used to distribute the actuation loads into the nozzle exit cone and reduce the deflection and stresses in the cone as a result of the point actuation loads. The ring was assumed to be loaded radially at two locations, 0 and 90 degrees. One load is applied toward the center of the ring and the other outward from the center of the ring. This load pattern is used to simulate the most severe anticipated actuation condition. The maximum deflection was 0.96 in. outward from the centerline. The maximum shear load was 25,338 lb at the 90 deg station and the maximum tensile stress was 32,846 psi at the 90 deg station. The minimum margin of safety was 1.31 at the 90 deg station. This analysis assumed that the total actuator loads are reacted by the ring only and does not include the rigidity or stiffness of the exit cone which in actual application complements the ring structure. The load distribution summary is shown in Figure 51.

6. TORQUE ANALYSIS

- (U) To move the nozzle mechanically in accordance with the specified dynamic requirements, the loads resisting nozzle deflection must be accurately defined. For convenience, these loads are normally expressed in terms of the torque produced about the pivot axis. The application of the results of the torque analysis and their effect on other motor components is shown in the discussion of the particular component.

- (U) Total torque is a summation of all contributing factors and is a direct function of the mechanics of the design and internal and external aerodynamics. For the 156-9 nozzle, the following major torque components were considered.

1. Dynamic spring torque.
 - (1) Flexible seal spring torque.
 - (2) Internal aerodynamic torque.
2. Frictional torque.
3. Offset torque.
4. Inertial torque.
5. Gravitational torque.

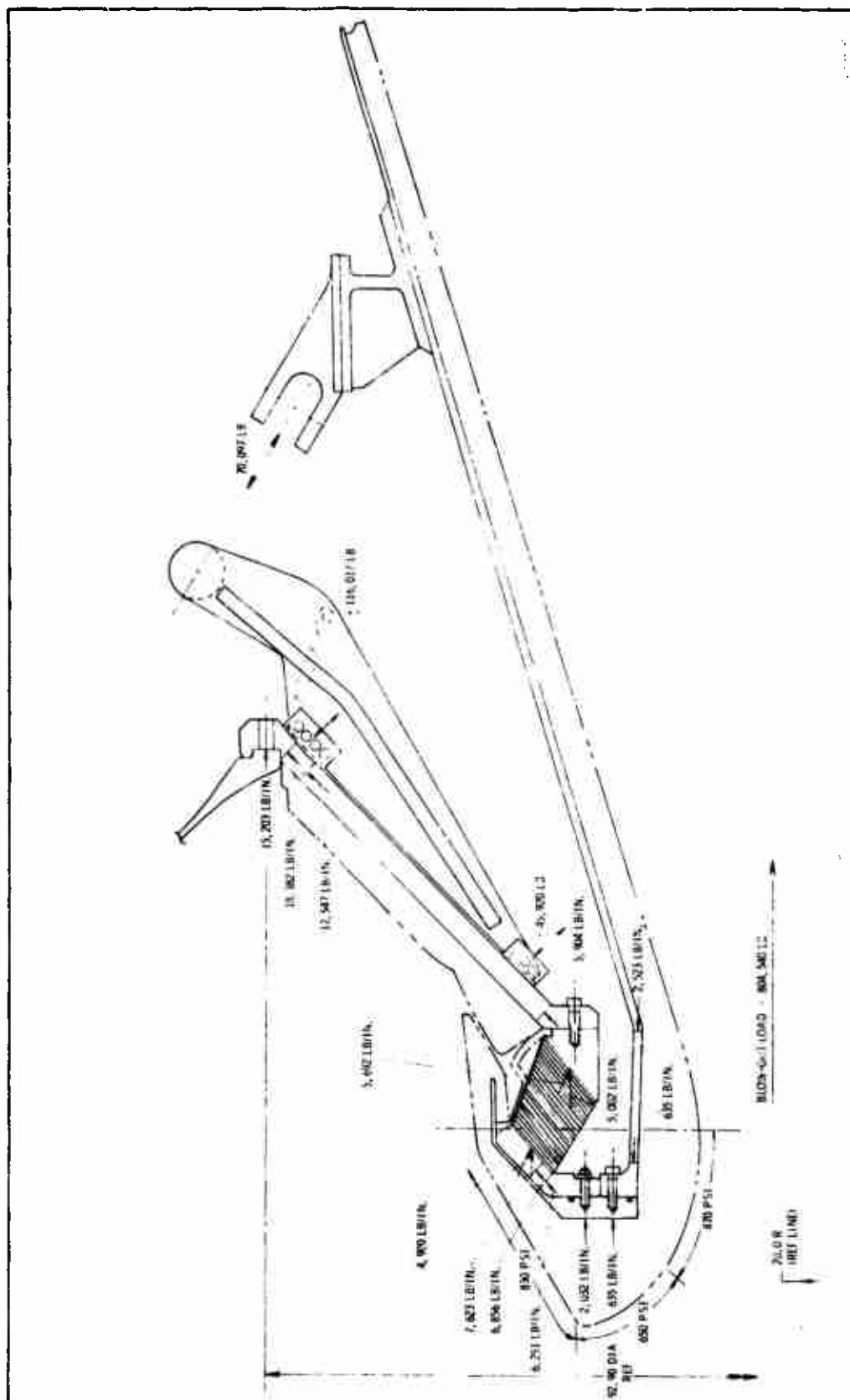


Figure 51. Load Distribution Summary

- (U) External aerodynamic torque is essentially nonexistent in static test applications. Coriolis torque (effect of earth's rotation on nozzle motion) also is of a very small magnitude and was not considered in this analysis.
- (U) Flexible seal torque and aerodynamic torque vary almost linearly with nozzle position and is expressed as a spring rate in units of in. -lb/degrees. These components are otherwise unrelated and are analyzed individually.
- (U) Gravity torque is maximum for a static firing condition when the motor is in the horizontal position.
- (U) The inertial torque is maximum during flight where the angular and lateral acceleration contribute appreciably to this component. However, missile accelerations produce inertial loads that are in the opposite direction to the spring torque, thus reducing the total torque. Static firing conditions will, therefore, produce a larger total torque than flight conditions. Hence, in the torque analysis static test conditions were assumed for each torque component, and the torque prediction is, therefore, conservative for flight conditions.
- (U) Individual analysis of each torque component provides a convenient method for establishing the design level torque. Definition of each component also is necessary to evaluate the performance characteristics of the TVC system.
- (U) The spring torque in the nozzle affects the response of the actuation system. An increase in spring torque produces a decrease in the damping ratio and, for large vector angles, results in a reduction in the system response. The steady state error as measured in vector angle will increase with increased spring rate.
- (U) The damping or viscous friction torque in the nozzle tends to stabilize the system. If the amount of damping is increased, the system becomes less oscillatory and if increased sufficiently the system will become overdamped, hence exhibiting zero overshoot.

- (U) The effect of increased inertia in the nozzle causes the system to become more oscillatory. This requires increased damping to stabilize the system. Offset and gravity torque will not affect the system stability but will contribute to the steady state error.
- (U) The following paragraphs present a brief discussion of the methods used in defining the torque characteristics of the 156-9 nozzle.
- (U) a. Flexible Seal Spring--The torque produced by the flexible seal can be established by summing the incremental forces around the periphery of the seal multiplied by the moment arms of these forces about the pivot axis.
- (U) As illustrated in Figure 52, the force acts in the plane of the seal at point A and acts normal to the plane of the seal at point B. The deflection in the seal as well as the length of the moment arm varies from point A to point B. It was, therefore, necessary to define these variables so the summation of the incremental torques around the seal could be accomplished.
- (U) The following paragraphs present the derivation of the seal torque expression. Since the seal deflects in the same manner in all four quadrants, this derivation will consider only a single quadrant of the seal.
- (U) The general expression for seal torque is:

$$T = \sum_0^{\pi/2} F_i \bar{l}_i$$

where: F = force,

\bar{l} = moment arm.

The incremental force in the seal then can be expressed in terms of seal deflection, shear modulus of the rubber, and seal geometry.

$$F_i = \frac{\delta_i G dA}{n t_r}$$

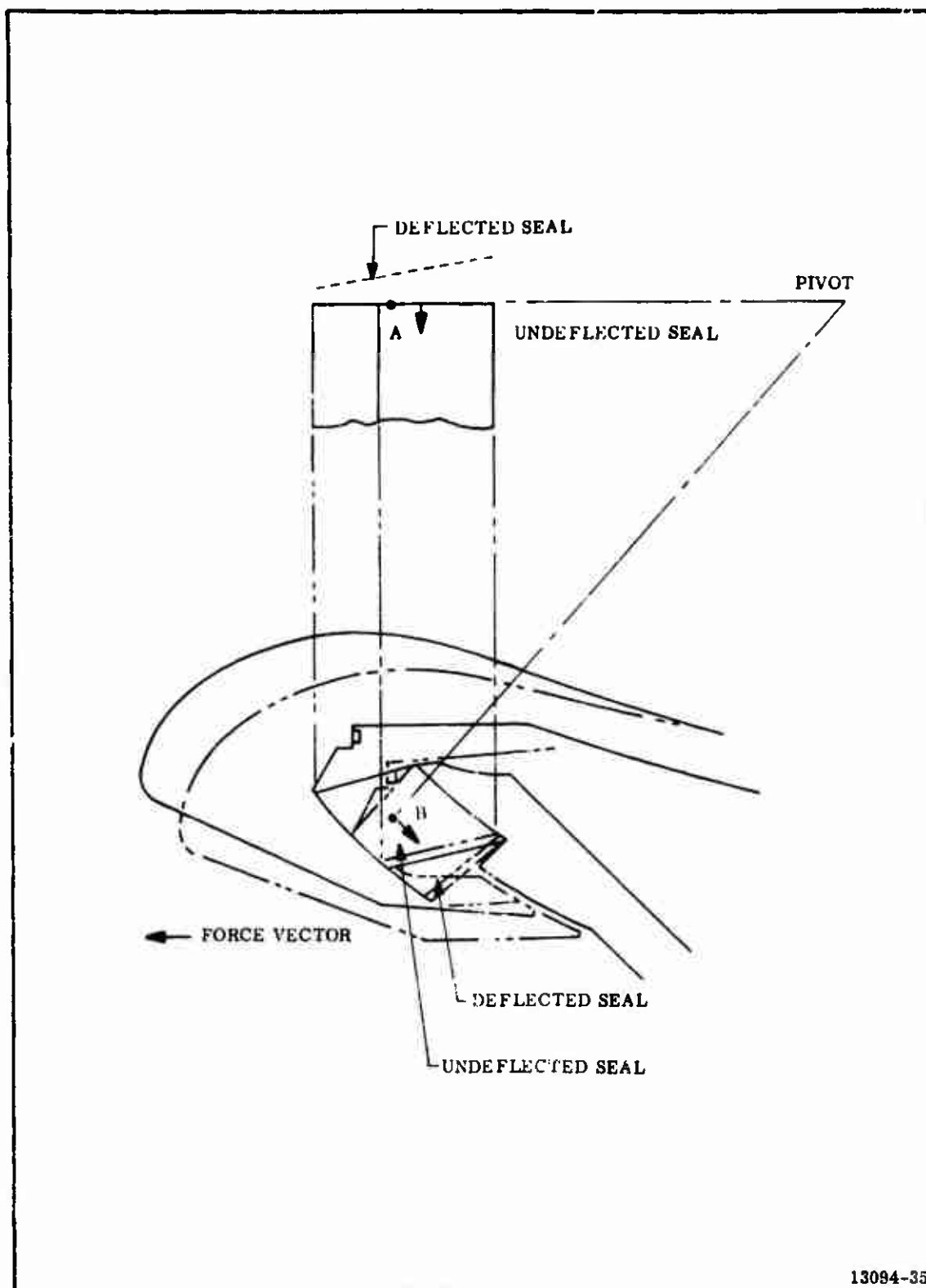


Figure 52. Flexible Seal Deflection

where: δ_i = seal deflection,
 G = shear modulus,
 dA = incremental cross-sectional area,
 n = number of rubber laminates,
 t_r = thickness per laminate

The seal deflection is simply \bar{l}_θ where \bar{l} is the moment arm and θ is the nozzle deflection angle (Figure 53). The general expression for the moment arm length is:

$$\bar{l} = \bar{r} (\sin^2 \beta \sin^2 \Phi + \cos^2 \beta)^{1/2}$$

where: \bar{r} = radius of curvature,

β = angle between seal axis and the mean radius of the seal.

The incremental area also is:

$$dA = (r \sin \beta d\Phi) w.$$

(U) The width (w) can now be expressed in terms of β_1 and β_2 , the angles measured between the seal centerline, and the inside and outside radii of the seal, respectively, so that

$$w = \bar{r} (\beta_2 - \beta_1),$$

β_2 and β_1 expressed in radians.

(U) The force in the seal thus becomes

$$F_i = \frac{G}{nt_r} r^3 \sin \beta (\sin^2 \beta \sin^2 \Phi + \cos^2 \beta)^{1/2} (\beta_2 - \beta_1) d\Phi$$

The torque for the entire seal can then be determined from the integral

$$T = 4 \int_0^{\pi/2} \bar{l} F_i = 4 \int_0^{\pi/2} \frac{G}{nt_r} r^4 \sin \beta (\sin^2 \beta \sin^2 \Phi + \cos^2 \beta)^{1/2} (\beta_2 - \beta_1) d\Phi$$

Performing the integration and converting all angles from radians to degrees:

$$T = \frac{G \pi^3}{3.24 \times 10^4 nt_r} \bar{r}^4 \sin \beta (1 + \cos^2 \beta) (\beta_2 - \beta_1).$$

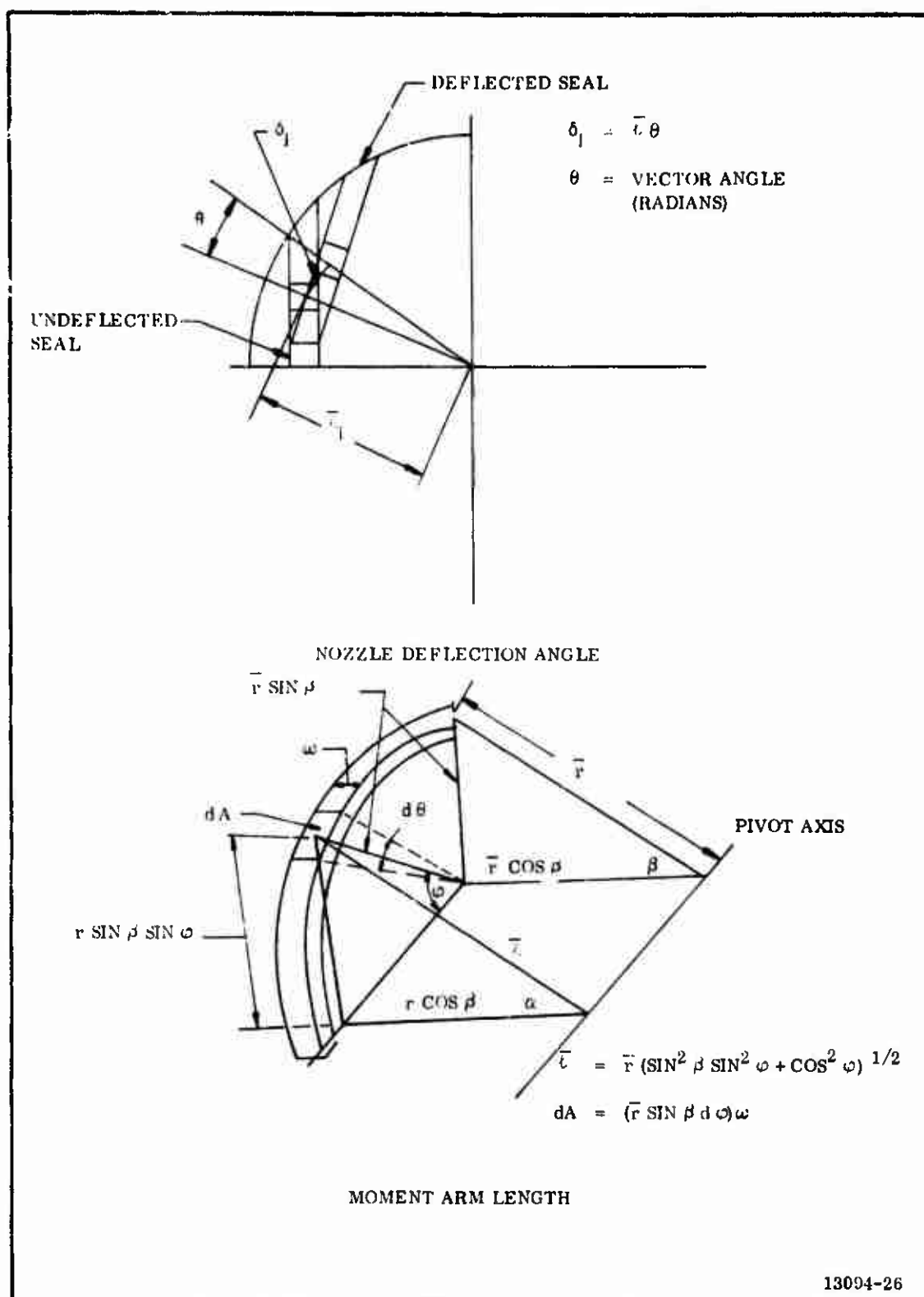


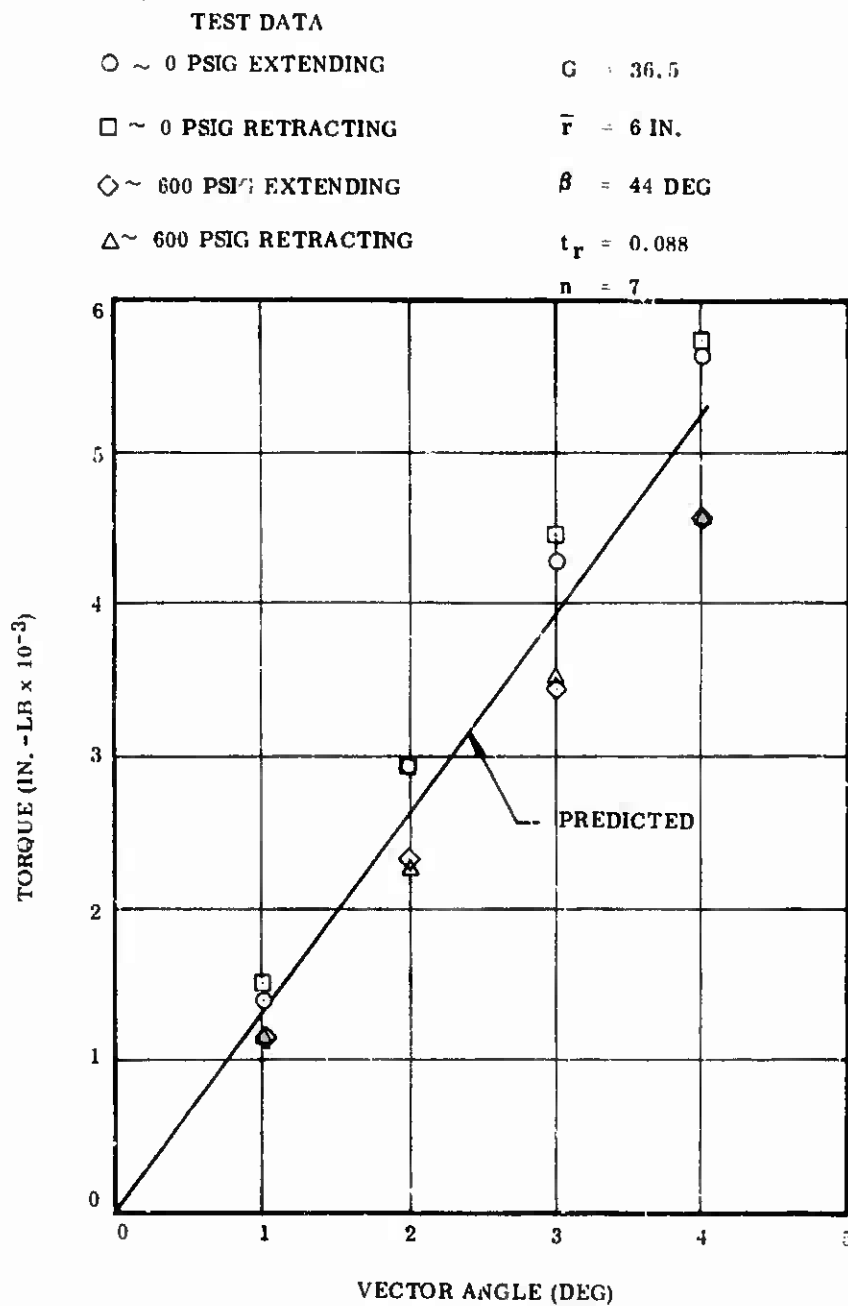
Figure 53. Determination of Moment Arm

Since the seal torque is linear with deflection angle, expression of this component is more convenient as torque per degree of vector. Hence,

$$\frac{T}{\theta} = \frac{G \pi r^{3-4} \sin}{3.24 \times 10^4 n t_r} (1 + \cos^2 \beta) (\beta_2 - \beta_1).$$

- (U) In Figure 54, the theory is compared with Lockheed test data.* The theory predicts torque slightly lower than data recorded at zero chamber pressure and slightly higher than the data from 600 psi testing. The predicted curve was calculated using the shear modulus quoted for the zero pressure condition. There is less than 10 percent error in the data and the error appears to be linear with position. The shear modulus appears as a linear function in the torque equation, leading to the conclusion that the shear modulus was in error.

*Lockheed Propulsion Co, Development of an Elastomeric Seal for Omniaxial Movable Nozzles (Lockseal), Progress Report No. 2, Technical Report No. AFRPL-TR-65-173. August 1965.



13094-36

Figure 54. Seal Torque vs Vector Angle

- (U) b. Internal Aerodynamic Spring--The internal aerodynamic torque acting on a submerged movable nozzle is the result of unsymmetrical flow in the vectored nozzle, thus producing a pressure differential in the actuation plane. Aerodynamic torque is normally linear with deflection angle and reacts as spring torque.

- (U) The aerodynamic torque can be calculated by summing the components of force produced by pressure acting on the nozzle wall multiplied by the perpendicular distance from the force to the nozzle pivot. The general equation describing the aerodynamic torque may be written as:

$$T_a = \int_{X_1}^{X_2} \int_0^{2\pi} p \sin \theta (rX + r^2 \tan \alpha) d\theta dx$$

where: θ = azimuthal angle (radians),

T_a = total aerodynamic torque about the pivot axis
(in. -lb),

r = nozzle radius at point of force application,

x = axial distance from pivot to point of calculation
in the nozzle (in.),

p = static pressure,

α = nozzle wall slope.

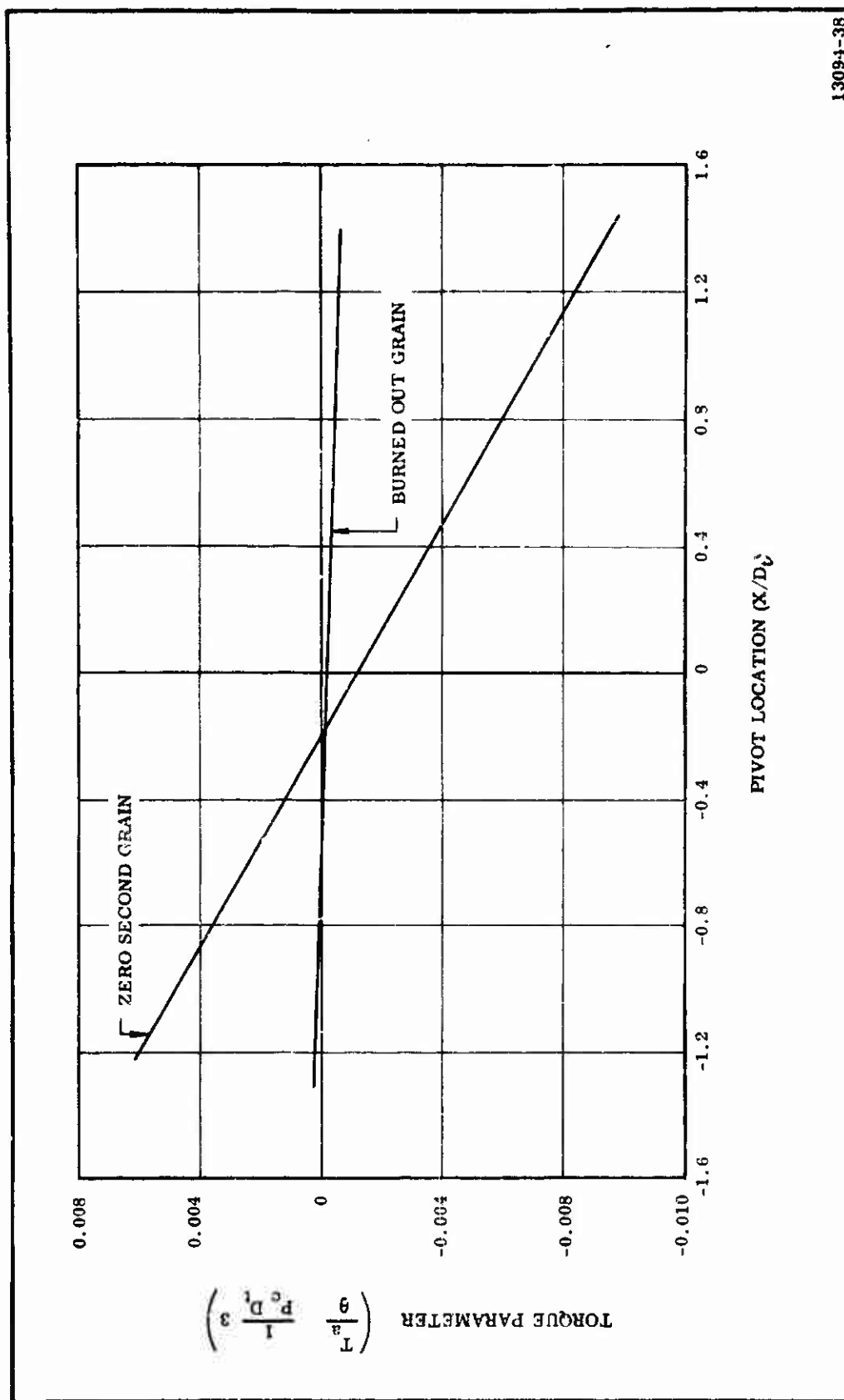
This equation requires knowledge of the wall static pressure and the pressure differentials which exist in the nozzle. Two procedures are available for developing internal wall pressure in a vectored nozzle. They are air flow simulation tests (cold flow) and a two dimensional method of characteristics solution.

- (U) The axial location (x) may be expressed as a function of the throat radius and the aerodynamic torque may be expressed as a function of chamber pressure and the cube of the throat diameter. This relationship may be used for scaling of geometrically similar nozzles.

- (U) The effect of nose design and propellant configuration on submerged movable nozzle torque was determined by cold flow testing. These data were used to predict the aerodynamic torque. The grain configuration has a major influence on aerodynamic

torque. In the 0 sec web time configuration, the gas has a relatively high velocity at the aft end of the grain and turning of the gas through the nozzle results in a nozzle wall pressure differential in the plane of actuation. However, as the propellant burns out a large plenum of low velocity gas is created. Therefore, vectoring the nozzle does not significantly alter the nozzle pressure distribution late in the firing. For this reason the aerodynamic torque for submerged nozzles decreases significantly with firing time.

- (U) Since the pivot location may vary considerably on submerged nozzles, it was necessary to investigate this effect of varying the pivot location. This was accomplished by analytically varying the pivot in the preceding equation. This technique assumes that pressure distribution in the nozzle is not altered when the pivot location is moved relative to the nozzle throat. Figure 55 presents the aerodynamic spring rate divided by chamber pressure and the cube of the throat diameter versus pivot location. Curves are shown for the 0 sec grain and burned out grain configuration.
- (U) As indicated in Figure 55 the present configuration produces nonrestoring aerodynamic torque which opposes the torque of the seal, thus reducing the total torque during the early portion of the firing.
- (U) Placing the pivot forward of the throat would produce a restoring torque which increases total torque. A forward pivot increases the moment arm through which the asymmetric forces act, thus the magnitude of the torque increases. Placing the pivot of the 156-9 nozzle an equal distance forward of the throat would increase the maximum total torque prediction by 500,000 inch pounds. The results of the aerotorque prediction are given in Table X.
- (U) Aerodynamic torque, however, becomes less significant as the firing progresses. Although total torque is reduced early in firing by the aerotorque, it was assumed to be zero throughout firing since it approaches zero late in the firing. This imparts further conservatism to the actuation system design since the



13094-38

Figure 55. Aerodynamic Spring Rate vs Pivot Location

TABLE X
156-9 NOZZLE TORQUE PREDICTION
4 DEG EVENT
SINE ACTUATION

<u>Torque Component</u>	<u>Predicted Spring Constant (in. -lb/deg)</u>		<u>Predicted Torque (in. -lb)</u>	
	<u>Nominal</u>	<u>Maximum</u>	<u>Nominal</u>	<u>Maximum (Worst-on-Worst)</u>
Dynamic Spring	--	--	872,000	1,560,000
Seal Component	356,500	389,800	--	--
Aerodynamic Component	-128,500	0	--	--
Seal Viscous	--	--	12,500	25,000
Offset	--	--	144,000	171,000
Gravitational	--	--	221,000	221,000
Inertia	--	--	<u>-117,300</u>	<u>-117,300</u>
			1,132,200	1,858,700

maximum vector angle on a flight version of the 156-9 motor will probably be required early in the firing when the aerotorque is diminishing the total predicted torque value.

- (U) c. Frictional--Frictional torque in conventional movable nozzles is the result of sliding surfaces such as bearings, O-rings, etc. Since there are no sliding surfaces in the flexible seal nozzle, the coulomb friction torque normally associated with movable nozzles does not exist.

- (U) Elimination of friction torque is one of the outstanding advantages of the flexible seal. Friction torque has two major disadvantages.

1. Friction torque is notoriously variable and therefore unpredictable with the desired accuracy.
2. Friction torque is the major source of steady state error in the servocontrol system.

- (U) Friction torque varies widely since it depends on surface conditions, lubricant condition, gap width, and applied load. There is also a variation from static friction to sliding friction which produces a "breakaway" peak in torque.

- (U) On Stage I MINUTEMAN motors, friction torque variations of 100 percent among the four nozzles on the same motor have been observed, and as high as 400 percent variations from motor to motor. Friction torque on these nozzles tends to increase with motor age. An average friction torque increase of 50 percent occurs in a three year storage period, probably resulting from lubricant and O-ring aging.

- (U) Elimination of the unpredictable friction torque thus reduces actuation system weight by reducing the statistical upper design limit.

- (U) Reducing steady state error simplifies the control system and improves the accuracy of the guidance. By reducing flight time spent off the flight path (by improving accuracy), the range is increased. Thus, eliminating friction torque improves the range and accuracy of a missile system while reducing cost.

- (U) The viscoelastic properties of the rubber produce a torque which is a function of the nozzle actuation rate. This torque is defined as viscous friction torque, which can be expressed as:

$$T_V = C \frac{d}{dt}$$

where:

C = damping coefficient of the seal

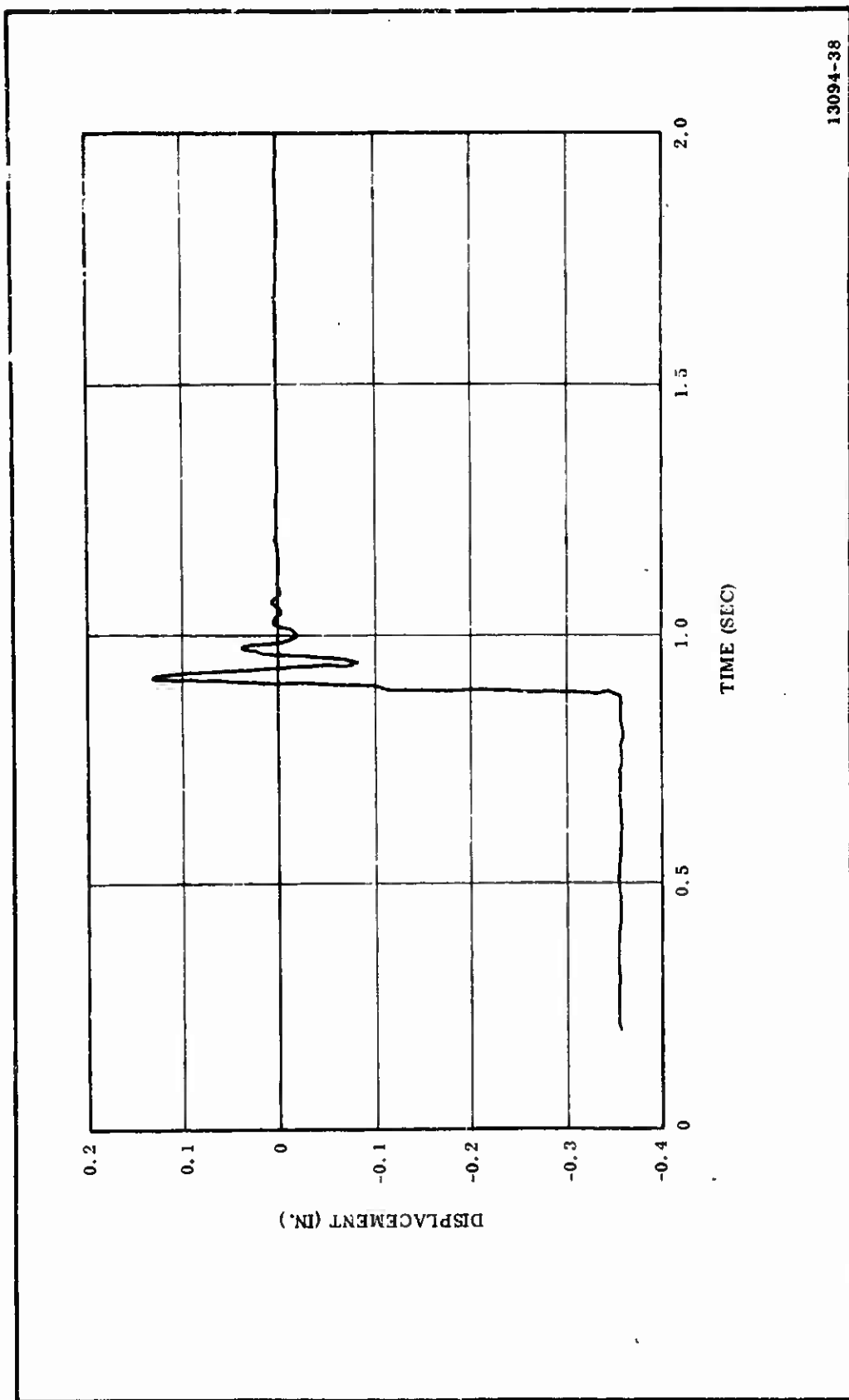
It is apparent that for the normal sinusoidal action this component does not contribute to the maximum total torque since this term is a maximum when the nozzle is at zero position and zero when the nozzle is fully vectored. This component, however, contributes to the stability of the TVC system and, therefore, must be thoroughly analyzed.

- (U) Amplitude decay tests were performed on a spherical shim bearing to determine the damping characteristics of the proposed seal. This seal has a radius of curvature of 7.6 in., 81 shims and a total rubber thickness of 0.567 inch. The shear modulus of the rubber was determined to be approximately 120 psi. Figure 56 shows a typical transient response curve obtained from this test program. This system appears to have a damping ratio of approximately 0.2. This value was used to determine the nominal viscous torque for the 156-9 nozzle seal. Viscous torque values are presented in Table X.

- (U) Viscous damping is also an important consideration in determining stability characteristics of the TVC system. An analog simulation study was performed and the damping requirement of the 156-9 TVC system was determined from this study.

- (U) d. Offset--Offset torque is considered to be the zero position aerodynamic torque resulting from asymmetrical flow in the unvectored nozzle. Therefore, it can be scaled in the same manner as aerodynamic torque.

- (U) Comparisons were made of cold flow data and hot firing data from four Thiokol submerged nozzle firings. It was determined that for all firings, scaling



13094-38

Figure 56. Flexible Seal Transient Response, MRC-2A

of the cold flow data resulted in overprediction of the offset torque. Therefore, to insure a conservative maximum offset torque prediction, the cold flow data were scaled directly. Offset torque is presented in dimensionless form as a function of pivot location in Figure 57. The predicted offset torque for the design configuration is presented in Table X.

- (U) e. Inertial--The inertial torque imposed on the nozzle during static firing is simply that torque resulting from accelerations produced by the actuator. Assuming a sinusoidal actuation, the maximum acceleration and the maximum inertial torque can be determined as:

$$\dot{\theta} = \dot{\theta} \times 2\pi f$$

$$T_{\text{inertial}} = \frac{\pi J}{180} \dot{\theta} \text{ Max}$$

where:

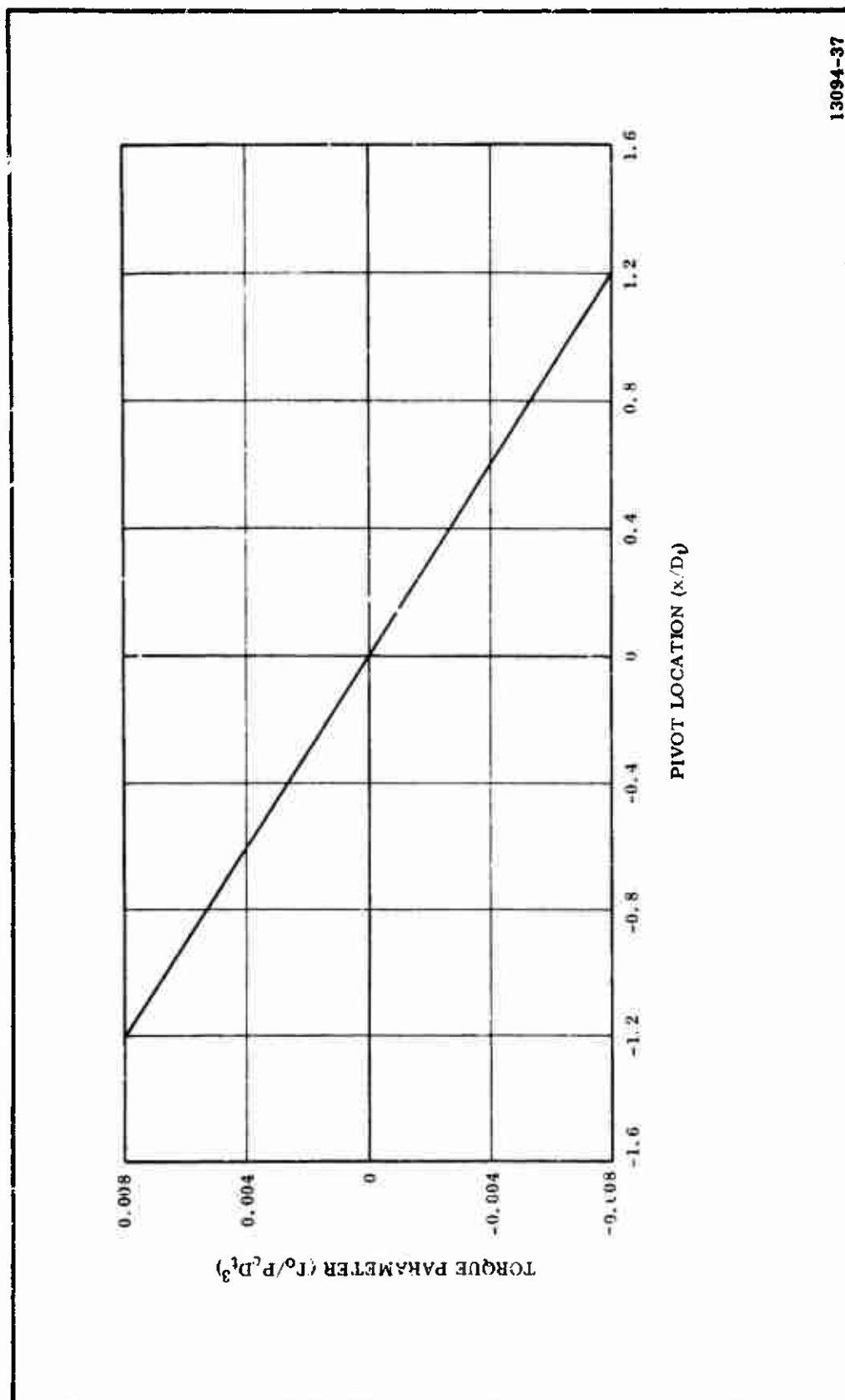
$$J = \text{max moment of inertial (in. lb-sec}^2\text{)}$$

$$\dot{\theta} \text{ Max} = \text{maximum angular acceleration (deg/sec}^2\text{)}.$$

Table 3-IV shows the predicted maximum inertial torque.

- (U) f. Gravitational--The moment produced by gravity is simply the nozzle weight multiplied by the distance from pivot to the center of gravity. The maximum gravity torque that will be experienced by the nozzle will occur when the nozzle is in the horizontal position. This distance will vary slightly with nozzle deflection. However, the maximum torque will occur with the nozzle in the zero position. Therefore a zero position nozzle was assumed for this prediction.

- (U) Missile attitude also affects the magnitude of the gravity torque component. For design purposes the missile was assumed to be in the horizontal position. This results in a conservative prediction since the minimum angle between the missile centerline and the horizontal axis is approximately 20 deg for normal flight conditions.



13094-37

Figure 57. Offset Torque vs Pivot Location Zero Second Grain

- (U) g. Total--Total torque can be expressed with the following general expression.

$$T_t = J \ddot{\theta} + C \dot{\theta} + K \theta + T_o + T_G$$

where:

J = mass moment of inertia,

C = damping coefficient,

K = combined seal plus aerodynamic spring rate,

T_o = offset torque,

T_G = gravity torque,

θ = nozzle vector angle for sinusoidal motion,

$\dot{\theta} = \theta_{\max} \sin 2\pi f t$,

$\ddot{\theta} = 2\pi f \theta_{\max} \cos 2\pi f t$,

$\ddot{\theta} = (2\pi f)^2 \theta_{\max} \sin 2\pi f t$.

Since

$$t = \frac{1}{2\pi f} \left(\sin^{-1} \frac{\theta}{\theta_{\max}} \right),$$

the following expression is readily obtained.

$$T_t = -J (2\pi f)^2 \theta + C (2\pi f) (\theta_{\max}^2 - \theta^2)^{1/2} \frac{\dot{\theta}}{\theta} + K \theta + T_o + T_G$$

- (U) For the sine wave actuation at the maximum required rate, the total torque has been calculated as a function of nozzle position using the equation above.
- (U) The predicted total torque as well as the various components are presented in Table 3-IV.
- (U) This number represents the maximum expected total torque for a sinusoidal actuation. To determine the worst condition value, the conservative upper limit predicted values for each component occur simultaneously in the same direction. This is a hypothetical condition since the maximum spring torque, inertial torque, and viscous torque cannot occur physically simultaneously in the same direction.

7. WEIGHT ANALYSIS

- (U) Total weight of the 156-9 nozzle assembly is 18,247 lb of which 11,849 lb is contained in the movable portion, 4,432 lb in the fixed portion, and 1,966 lb in the flexible seal.
- (U) In the weight analysis (Table XI) the nozzle is divided into movable, fixed, and bearing or seal portions. Each component is identified by drawing and item number. A format of title indentations is followed in the subtotals. The weights of items whose titles are indented are summed in the weight column for the title preceding the indentation. This format is continued up through the subassemblies to the complete nozzle assembly.
- (U) The plastic components of the nozzle are flightweight. The structural shells, however, were not required to be flightweight so relatively low cost fabrication methods were used in noncritical areas. These shells were not machined to flightweight thicknesses in order to reduce fabrication time and expense. As a result, the nozzle weight is approximately 5,000 lb heavier than it would be had the structural shells been made flightweight.

156-9 nozzle weight (lb)	18,247
Excess in structural shells (lb)	5,000
<hr/>	
Approximate weight of a similar flightweight nozzle (lb)	13,247

8. FINAL DESIGN

- (U) The final design of the 156-9 nozzle is shown in Figure 32.
- (U) One significant change was made to the original design of the nozzle. The barrier gap area was redesigned to accommodate a larger boot. A contour cut was taken on the small end of the fixed silica insulator (7U40519-02) which formed the convex surface of the gap. This cut provided a better anchor for the aft end of the thicker redesigned boot as well as providing space for boot movement during vector.

TABLE XI

MASS PROPERTIES DATA FOR 156-9 MOTOR NOZZLE

TOTAL NOZZLE ASSEMBLY		WEIGHT (LBS)	LONG.	CENTER OF GRAVITY LAT.	VERT.	PITCH	MOMENT OF INERTIA ROLL	YAW
MOVABLE PORTION		18247.000	633.837	99.007	99.007	6627.114	5455.427	6623.057
MUSE ASSEMBLY 7040516		13814.694	439.666	99.293	99.293	5455.113	4348.796	5457.188
BUSSING 7040521		957.202	391.747	100.000	100.000	69.124	136.136	54.124
SHELL		422.986	392.937	100.000	100.000	24.199	54.219	24.199
PLATE		36.982	395.639	100.000	100.000	3.620	2.233	3.520
ITEM 2-CARBON CLOTH		386.004	392.676	100.000	100.000	25.514	50.986	25.514
ITEM 3-CARBON CLOTH		167.757	391.483	100.000	100.000	15.147	25.843	15.147
ITEM 4-GRAPHITE CLOTH		105.842	388.109	100.000	100.000	6.247	12.421	6.247
ITEM 5-SILICA CLOTH		45.539	390.354	100.000	100.000	2.037	4.052	2.037
ITEM 6-SILICA CLOTH		108.153	392.720	100.000	100.000	9.109	18.069	9.109
ITEM 7-GLASS CLOTH		106.925	390.661	100.000	100.000	6.882	13.731	6.882
BARRIER ASSEMBLY 7041353		132.884	400.377	100.000	100.000	14.664	29.137	14.664
ITEM 1-SILICA CLOTH		9.400	399.874	100.000	100.000	1.958	1.511	1.758
BARRIER 7040523		123.484	400.415	100.000	100.000	13.706	27.226	13.706
MOVABLE ASSEMBLY 7040520		10368.380	452.632	100.000	100.000	3466.203	3329.504	3455.233
BUSSING 7040522		7945.682	454.023	100.000	100.000	2618.664	2585.251	2618.564
ITEMS 2+4-CARBON CLOTH		506.425	407.184	100.000	100.000	36.426	51.697	36.426
ITEM 3-SILICA CLOTH		432.925	452.461	100.000	100.000	142.657	124.659	142.657
ITEM 6-SILICA CLOTH		1416.973	463.559	100.000	100.000	359.479	450.122	359.479
ITEM 7-GLASS CLOTH		60.341	357.948	100.000	100.000	3.051	5.730	3.051
ITEM 8-SET SCREWS (90)		5.316	431.404	100.000	100.000	.488	.975	.488
ITEM 9-0-RINGS (2)		.719	406.726	100.000	100.000	.037	.070	.037
CLEVIS -AT 90 DEG 7040524		40.715	443.561	100.000	100.000	.083	.048	.105
ITEM 1-CLEVIS		40.306	443.704	100.000	100.000	.081	.047	.104
ITEM 2-BUSHING		.410	439.454	100.000	100.000	.000	.000	.000
CLEVIS -AT 0 DEG 7040524		40.715	443.661	100.000	100.000	.083	.048	.105
ITEM 1-CLEVIS		40.306	443.704	100.000	100.000	.081	.047	.104
ITEM 2-BUSHING		.410	439.454	100.000	100.000	.000	.000	.000
FLEXIBLE BEARING 7040678		1965.372	398.555	100.000	100.000	162.097	315.535	162.097
END RING 7040679		523.609	395.162	100.000	100.000	44.628	54.337	44.628
END RING 7040680		470.941	402.517	100.000	100.000	33.325	66.143	33.325
SHIMS 7040682		805.131	398.286	100.000	100.000	66.000	131.223	66.000
RUBBER + BOUNGING AGENT		83.668	398.286	100.000	100.000	6.858	13.636	6.858
BOOT 7041356		52.522	401.275	100.000	100.000	5.004	9.906	5.004
BARRIER MSO 7041347		29.411	396.869	100.000	100.000	3.036	5.154	3.036
PACKING 7040584		1.289	396.872	100.000	100.000	.091	.171	.091
TRIMMUM-AT 0 DEG 7040590		135.206	434.100	100.000	100.000	1.901	2.443	1.901
ITEMS 1-4 PLATES		133.625	434.100	100.000	100.000	1.351	1.631	1.351
ITEMS 5+6 BUSHINGS		.877	434.100	100.000	100.000	.000	.000	.000
PIMS-MS10555-60		.163	434.100	100.000	100.000	.000	.000	.000
SCREWS-MS1351-12-48		4.317	434.100	100.000	100.000	.001	.000	.001
WASHERS-AN935-1216L		.223	434.100	100.000	100.000	.000	.000	.000
TRIMMUM-AT 90 DEG 7040590		39.206	434.100	100.000	100.000	1.901	2.443	1.901
ITEMS 1-4 PLATES		133.625	434.100	100.000	100.000	1.351	1.631	1.351

TABLE XI (Cont)
MASS PROPERTIES DATA FOR 156-9 MOTOR NOZZLE

ITEMS 5-9 BUSHINGS	WEIGHT (LBS)	CENTER OF GRAVITY		PITCH	MOMENT OF INERTIA		YAN
		LUNG.	LAT.		ROLL	YAN	
PINS-NAS1555-60	.877	434.100	98.800	100.000	.000	.000	.000
SCREWS-NAS1351-12-48	.163	434.100	98.800	100.000	.000	.000	.000
WASHERS-AM935-1216L	6.317	434.100	98.800	100.000	.000	.000	.000
SCREWS-NAS1351-14-32	.223	434.100	98.800	100.000	.000	.000	.000
SCREWS-NAS1351-16-32	12.824	393.960	100.000	100.000	.873	1.744	.873
SCREWS-NAS1351-18-32	.854	393.960	100.000	100.000	.089	.177	.089
SCREWS-NAS1351-20-32	14.392	393.960	100.000	100.000	.845	1.637	.845
SCREWS-NAS1351-22-48	1.011	445.154	79.500	79.500	.146	.292	.146
SCREWS-NAS1351-24-48	.044	393.354	100.000	76.700	.000	.000	.000
SCREWS-NAS1351-26-48							
SCREWS-NAS1351-28-48							
SCREWS-NAS1351-30-48							
SCREWS-NAS1351-32-48							
SCREWS-NAS1351-34-48							
SCREWS-NAS1351-36-48							
SCREWS-NAS1351-38-48							
SCREWS-NAS1351-40-48							
SCREWS-NAS1351-42-48							
SCREWS-NAS1351-44-48							
SCREWS-NAS1351-46-48							
SCREWS-NAS1351-48-48							
SCREWS-NAS1351-50-48							
SCREWS-NAS1351-52-48							
SCREWS-NAS1351-54-48							
SCREWS-NAS1351-56-48							
SCREWS-NAS1351-58-48							
SCREWS-NAS1351-60-48							
SCREWS-NAS1351-62-48							
SCREWS-NAS1351-64-48							
SCREWS-NAS1351-66-48							
SCREWS-NAS1351-68-48							
SCREWS-NAS1351-70-48							
SCREWS-NAS1351-72-48							
SCREWS-NAS1351-74-48							
SCREWS-NAS1351-76-48							
SCREWS-NAS1351-78-48							
SCREWS-NAS1351-80-48							
SCREWS-NAS1351-82-48							
SCREWS-NAS1351-84-48							
SCREWS-NAS1351-86-48							
SCREWS-NAS1351-88-48							
SCREWS-NAS1351-90-48							
SCREWS-NAS1351-92-48							
SCREWS-NAS1351-94-48							
SCREWS-NAS1351-96-48							
SCREWS-NAS1351-98-48							
SCREWS-NAS1351-100-48							
SCREWS-NAS1351-102-48							
SCREWS-NAS1351-104-48							
SCREWS-NAS1351-106-48							
SCREWS-NAS1351-108-48							
SCREWS-NAS1351-110-48							
SCREWS-NAS1351-112-48							
SCREWS-NAS1351-114-48							
SCREWS-NAS1351-116-48							
SCREWS-NAS1351-118-48							
SCREWS-NAS1351-120-48							
SCREWS-NAS1351-122-48							
SCREWS-NAS1351-124-48							
SCREWS-NAS1351-126-48							
SCREWS-NAS1351-128-48							
SCREWS-NAS1351-130-48							
SCREWS-NAS1351-132-48							
SCREWS-NAS1351-134-48							
SCREWS-NAS1351-136-48							
SCREWS-NAS1351-138-48							
SCREWS-NAS1351-140-48							
SCREWS-NAS1351-142-48							
SCREWS-NAS1351-144-48							
SCREWS-NAS1351-146-48							
SCREWS-NAS1351-148-48							
SCREWS-NAS1351-150-48							
SCREWS-NAS1351-152-48							
SCREWS-NAS1351-154-48							
SCREWS-NAS1351-156-48							
SCREWS-NAS1351-158-48							
SCREWS-NAS1351-160-48							
SCREWS-NAS1351-162-48							
SCREWS-NAS1351-164-48							
SCREWS-NAS1351-166-48							
SCREWS-NAS1351-168-48							
SCREWS-NAS1351-170-48							
SCREWS-NAS1351-172-48							
SCREWS-NAS1351-174-48							
SCREWS-NAS1351-176-48							
SCREWS-NAS1351-178-48							
SCREWS-NAS1351-180-48							
SCREWS-NAS1351-182-48							
SCREWS-NAS1351-184-48							
SCREWS-NAS1351-186-48							
SCREWS-NAS1351-188-48							
SCREWS-NAS1351-190-48							
SCREWS-NAS1351-192-48							
SCREWS-NAS1351-194-48							
SCREWS-NAS1351-196-48							
SCREWS-NAS1351-198-48							
SCREWS-NAS1351-200-48							
SCREWS-NAS1351-202-48							
SCREWS-NAS1351-204-48							
SCREWS-NAS1351-206-48							
SCREWS-NAS1351-208-48							
SCREWS-NAS1351-210-48							
SCREWS-NAS1351-212-48							
SCREWS-NAS1351-214-48							
SCREWS-NAS1351-216-48							
SCREWS-NAS1351-218-48							
SCREWS-NAS1351-220-48							
SCREWS-NAS1351-222-48							
SCREWS-NAS1351-224-48							
SCREWS-NAS1351-226-48							
SCREWS-NAS1351-228-48							
SCREWS-NAS1351-230-48							
SCREWS-NAS1351-232-48							
SCREWS-NAS1351-234-48							
SCREWS-NAS1351-236-48							
SCREWS-NAS1351-238-48							
SCREWS-NAS1351-240-48							
SCREWS-NAS1351-242-48							
SCREWS-NAS1351-244-48							
SCREWS-NAS1351-246-48							
SCREWS-NAS1351-248-48							
SCREWS-NAS1351-250-48							
SCREWS-NAS1351-252-48							
SCREWS-NAS1351-254-48							
SCREWS-NAS1351-256-48							
SCREWS-NAS1351-258-48							
SCREWS-NAS1351-260-48							
SCREWS-NAS1351-262-48							
SCREWS-NAS1351-264-48							
SCREWS-NAS1351-266-48							
SCREWS-NAS1351-268-48							
SCREWS-NAS1351-270-48							
SCREWS-NAS1351-272-48							
SCREWS-NAS1351-274-48							
SCREWS-NAS1351-276-48							
SCREWS-NAS1351-278-48							
SCREWS-NAS1351-280-48							
SCREWS-NAS1351-282-48							
SCREWS-NAS1351-284-48							
SCREWS-NAS1351-286-48							
SCREWS-NAS1351-288-48							
SCREWS-NAS1351-290-48							
SCREWS-NAS1351-292-48							
SCREWS-NAS1351-294-48							
SCREWS-NAS1351-296-48							
SCREWS-NAS1351-298-48							
SCREWS-NAS1351-300-48							
SCREWS-NAS1351-302-48							
SCREWS-NAS1351-304-48							
SCREWS-NAS1351-306-48							
SCREWS-NAS1351-308-48							
SCREWS-NAS1351-310-48							
SCREWS-NAS1351-312-48							
SCREWS-NAS1351-314-48							
SCREWS-NAS1351-316-48							
SCREWS-NAS1351-318-48							
SCREWS-NAS1351-320-48							
SCREWS-NAS1351-322-48							
SCREWS-NAS1351-324-48							
SCREWS-NAS1351-326-48							
SCREWS-NAS1351-328-48							
SCREWS-NAS1351-330-48							
SCREWS-NAS1351-332-48							
SCREWS-NAS1351-334-48							
SCREWS-NAS1351-336-48							
SCREWS-NAS1351-338-48							
SCREWS-NAS1351-340-48							
SCREWS-NAS1351-342-48							
SCREWS-NAS1351-344-48							
SCREWS-NAS1351-346-48							
SCREWS-NAS1351-348-48							
SCREWS-NAS1351-350-48							
SCREWS-NAS1351-352-48							
SCREWS-NAS1351-354-48							
SCREWS-NAS1351-356-48							
SCREWS-NAS1351-358-48							
SCREWS-NAS1351-360-48							
SCREWS-NAS1351-362-48							
SCREWS-NAS1351-364-48							
SCREWS-NAS1351-366-48							
SCREWS-NAS1351-368-48							
SCREWS-NAS1351-370-48							
SCREWS-NAS1351-372-48							
SCREWS-NAS1351-374-48							
SCREWS-NAS1351-376-48							
SCREWS-NAS1351-378-48							
SCREWS-NAS1351-380-48							
SCREWS-NAS1351-382-48							
SCREWS-NAS1351-384-48							
SCREWS-NAS1351-386-48							
SCREWS-NAS1351-388-48							
SCREWS-NAS1351-390-48							
SCREWS-NAS1351-392-48							
SCREWS-NAS1351-394-48							
SCREWS-NAS1351-396-48							
SCREWS-NAS1351-398-48							
SCREWS-NAS1351-400-48							
SCREWS-NAS1351-402-48							
SCREWS-NAS1351-404-48							
SCREWS-NAS1351-406-48							
SCREWS-NAS1351-408-48							
SCREWS-NAS1351-410-48							
SCREWS-NAS1351-412-48							
SCREWS-NAS1351-414-48							
SCREWS-NAS1351-416-48							
SCREWS-NAS1351-418-48							
SCREWS-NAS1351-420-48							
SCREWS-NAS1351-422-48							
SCREWS-NAS1351-424-48							
SCREWS-NAS1351-426-48							
SCREWS-NAS1351-428-48							
SCREWS-NAS1351-430-48							
SCREWS-NAS1351-432-48							
SCREWS-NAS1351-434-48							

- (U) The housing (7U40526), on the movable part of the barrier, was modified per drawing 7U41347 and made part of the flexible bearing assembly (7U40678) where it serves the function of anchoring the forward end of the boot. The two silica parts of the barrier (7U40523 and 7U40518-02) were modified and combined into one assembly (7U41353).
- (U) The net effect of these changes was to reduce the gap between surfaces from 0.320 to 0.200 in. and allow the use of a thicker boot thereby sharply increasing the reliability of the only area of the nozzle not proven in previous large motor firings.

9. PREDICTED PERFORMANCE

- (U) a. Erosion and Char--The predicted postfire nozzle erosion and char profiles are depicted in Figure 58.
- (U) b. Flexible Seal Torque--The 156-9 flexible seal was bench tested in a test fixture which loaded the seal to the maximum load predicted during the static firing. While so loaded, the seal was actuated through the entire yaw plane duty cycle using the same yaw plane actuator that would be used during the static test. The actuator was controlled by the same control tape that would be used for control during the static firing. The torque trace from the bench test is presented in Figure 59.
- (U) The seal torque comprises roughly 90 percent of the total torque, thus the firing torque in the yaw plane is predicted to follow Figure 59 very closely. However, small deviations from this figure are predicted. These deviations will be produced by separate causes as follows.
- (U) (1) Aerodynamic Torque--The asymmetrical gas flow produced when the nozzle is vectored will result in an aerodynamic torque. In the 156-9 nozzle design, the pivot point of the nozzle is aft of the throat so the resulting aerodynamic torque will oppose the bearing torque and reduce total torque by as much as 100,000 in.-lb at 4 deg vector. As the grain burns the aerodynamic torque is reduced in magnitude

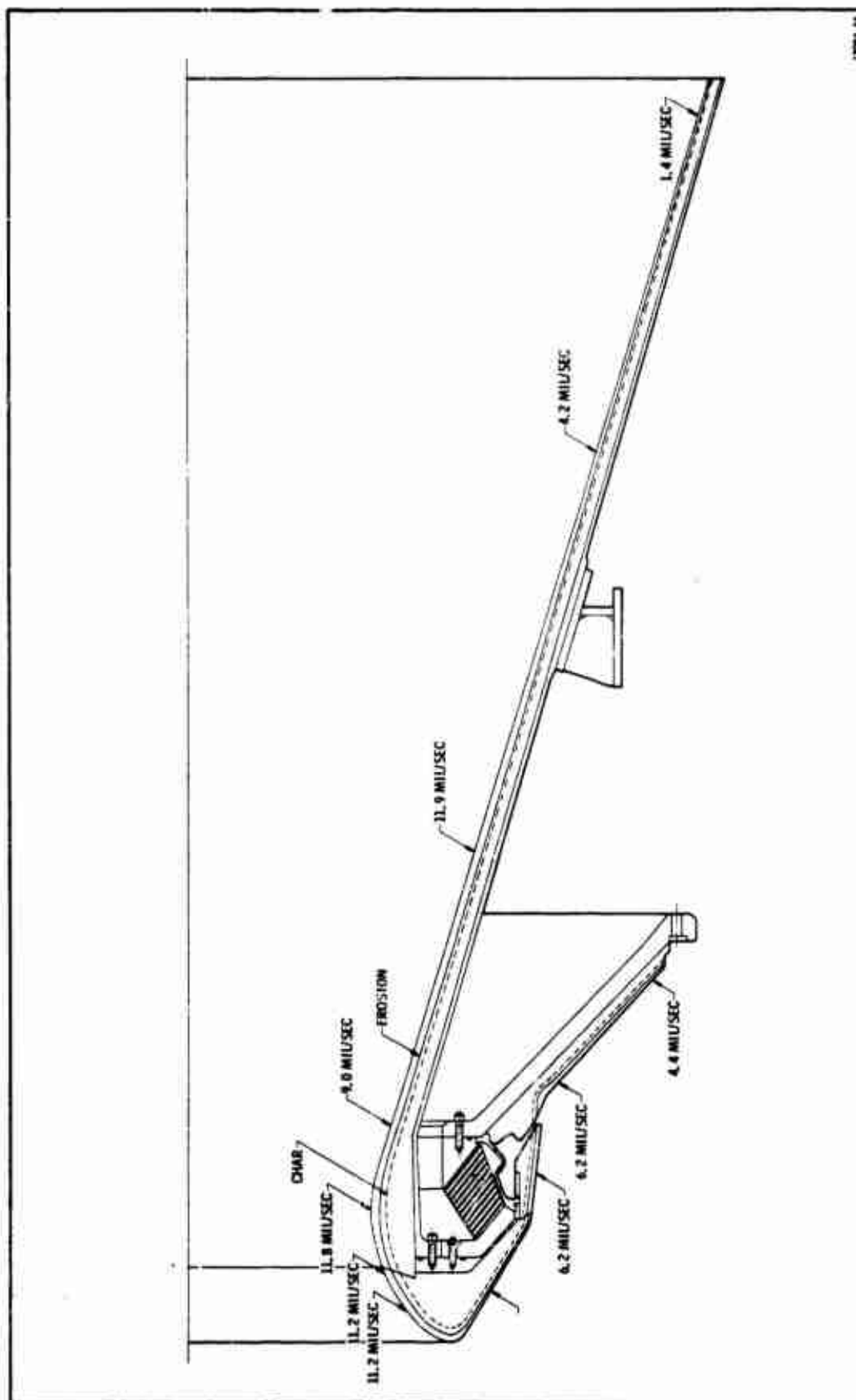


Figure 58. Maximum Predicted Erosion and Char for the 156-9 Nozzle

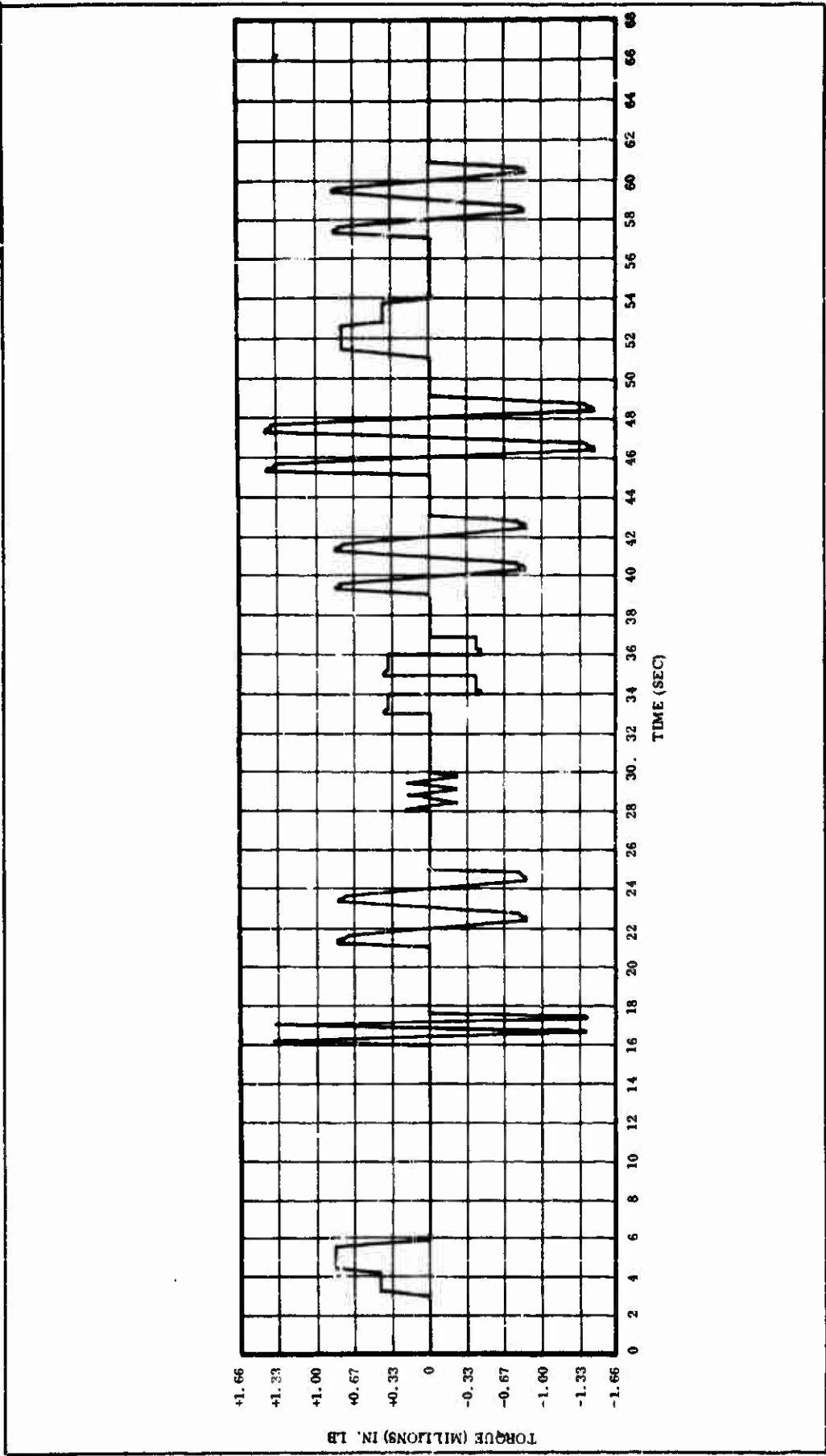


Figure 59. Predicted Seal Component of Torque in Yaw Plane

reaching zero about midway in the firing. The aerodynamic torque, in summary, is thus predicted to reduce the torque values of Figure 59 during the first part of the firing and to have no effect during the last part of the firing.

- (U) (2) Offset Torque--Offset torque results from asymmetrical gas flow in the null position, from asymmetry in the nozzle, and from misalignment of the nozzle and chamber. The direction of the offset torque is, therefore, unpredictable, but extrapolating from past firings, the magnitude is expected to be in the range of 140,000 to 170,000 in.-lb.

B. NOZZLE FABRICATION

1. VENDOR SELECTION

(U) The optimized nozzle design had a 34.5 in. throat, a 98.6 in. exit diameter and an overall length of 116 inches. The largest subassembly slightly over 110 in. long was the movable housing containing the throat and exit plane. The selection of candidate vendors, was therefore limited to those firms having hydroclave capacity to handle the large movable housing assembly. The only companies known to have adequate capacity and previous experience in fabricating solid rocket motor nozzles were HITCO, Rohr and TRW, Inc. All three companies had the technical capability and experience and each had previously built satisfactory large nozzles of the general type desired. Therefore, all three firms were invited to bid the 156-9 nozzle.

(U) Nozzle fabrication schedules were paced by Thiokol's ability to design, fabricate, test, and deliver a major nozzle component, the flexible seal. All three candidate vendors were rated equal in ability to meet the delivery schedule.

(U) TRW, Inc, declined to bid leaving only HITCO and Rohr competing. After lengthy negotiations with each firm, the final selection was made on the basis of sealed bid costs only. Each candidate knew these terms prior to making a sealed bid. The contract was awarded to HITCO.

2. COMPONENT FABRICATION

(U) The 156-9 nozzle was fabricated in five major component assemblies as follows:

1. Flexible seal assembly
2. Nose assembly
3. Barrier assembly

4. Fixed housing assembly
5. Movable housing assembly

(U) The flexible seal fabrication has been discussed in Section II. The fabrication of the actuator support brackets, trunnions, and clevises is straight forward as given on Figure 32 and need not be discussed further.

(U) The fabrication of the remaining four major components was accomplished as shown in Figure 60.

3. FINAL ASSEMBLY OF NOZZLE

(U) The final assembly of the nozzle was accomplished as follows.

1. The movable assembly was placed upright resting on the steel exit cone.
2. The actuator bracket and trunnion assemblies were bolted to the fixed housing assembly.
3. The fixed housing assembly was lifted and lowered past the exit cone flange to rest on the exit cone shell (Figure 61).
4. The flexible bearing assembly was bolted to the nose assembly.
5. The barrier assembly was dryfit and then bonded to the assembly consisting of the nose and bearing assemblies. Two views of this new assembly are shown in Figure 62.
6. The assembly resulting from Step 5 was lowered over the movable assembly, dryfit, and then bonded to the movable assembly. Bolts were installed between the flange of the movable assembly and the entrance housing and torqued to the prescribed value using a specially designed torque wrench.

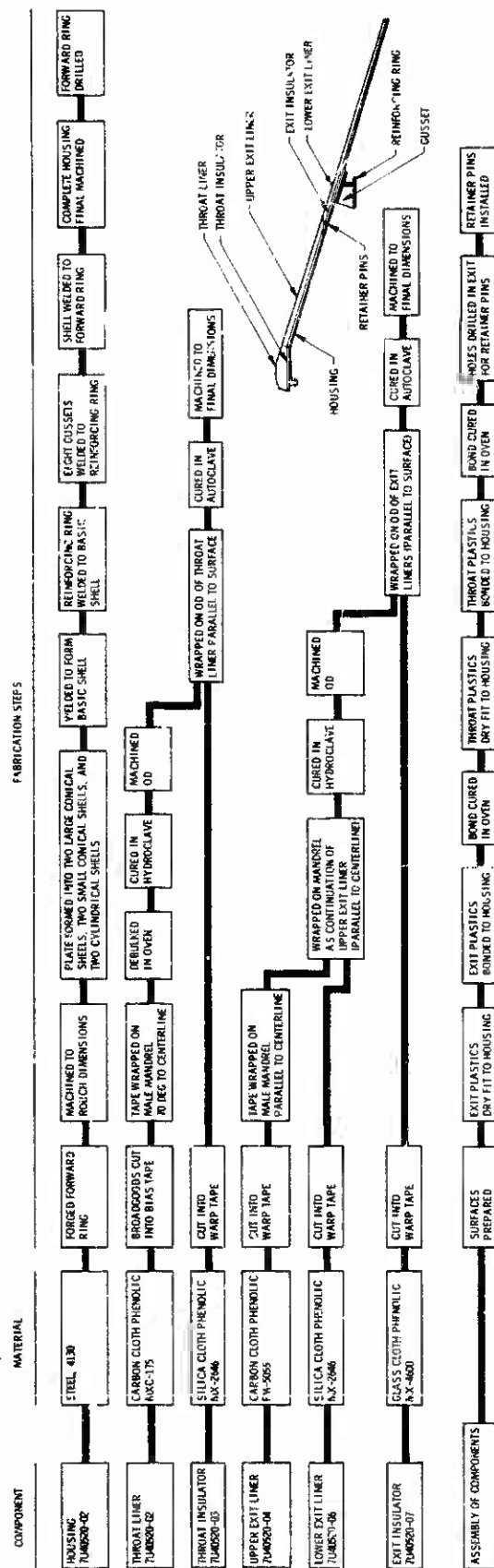


Figure 60. 159-9 Motor Nozzle Component Fabrication (Sheet 2 of 4)

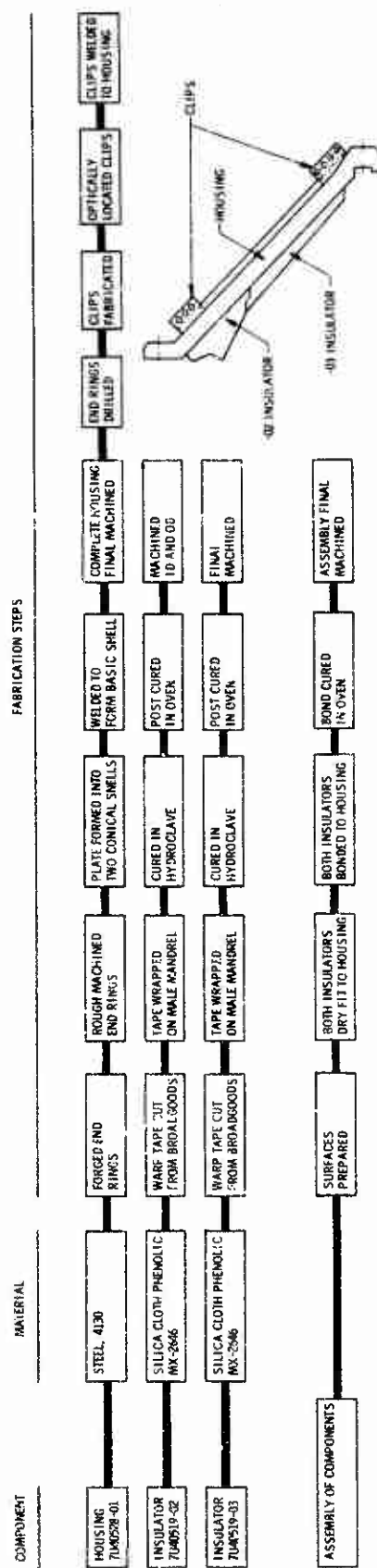


Figure 60. 159-9 Motor Nozzle Component Fabrication (Sheet 3 of 4)

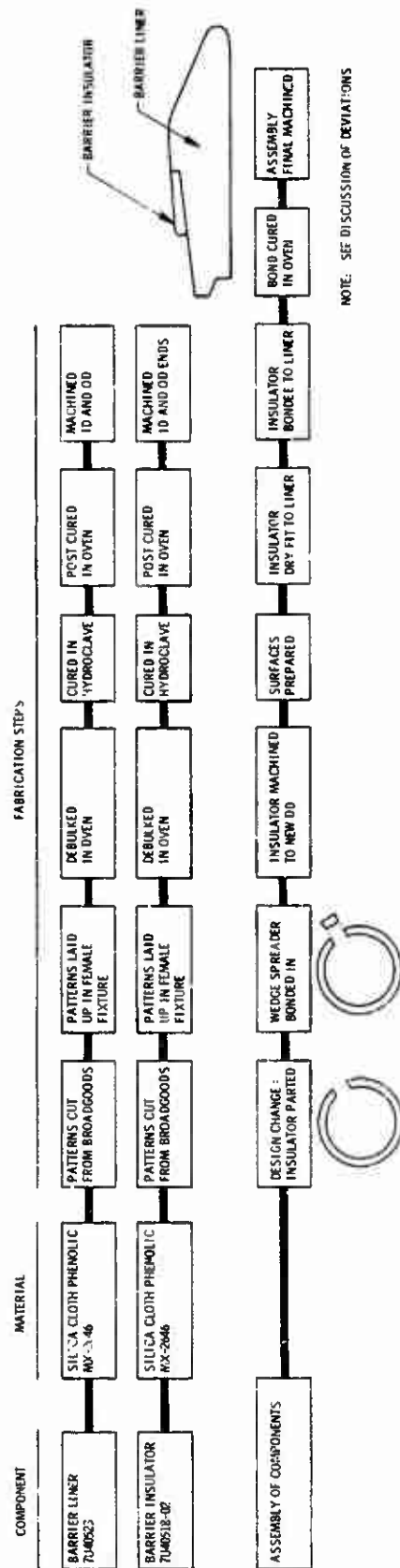


Figure 60. 159-9 Motor Nozzle Component Fabrication (Sheet 4 of 4)

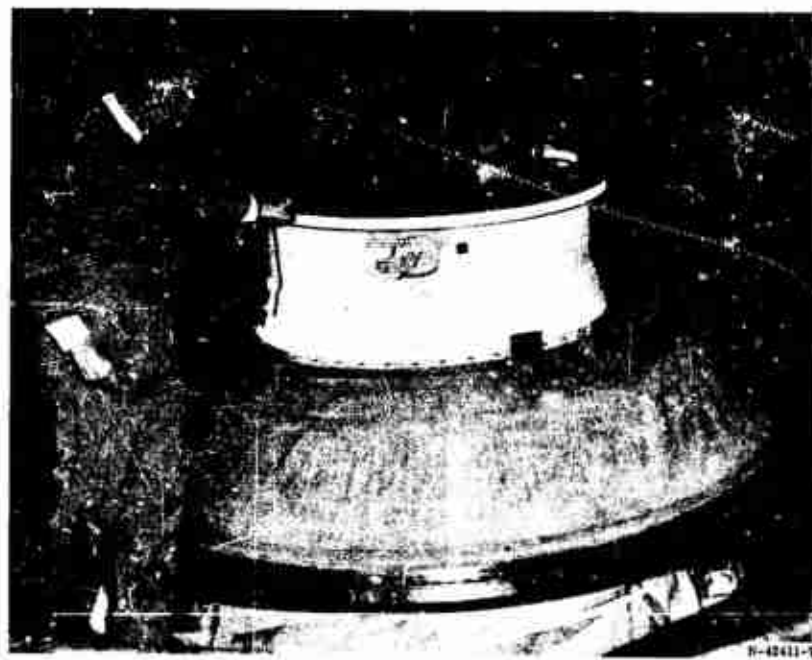
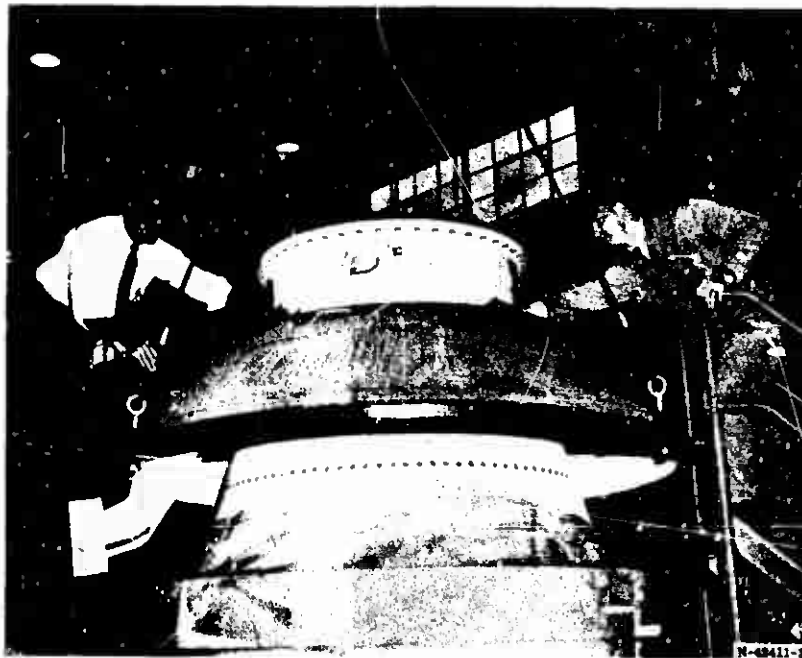


Figure 61. Lowering the Fixed Housing Assembly to Rest on the Exit Shell

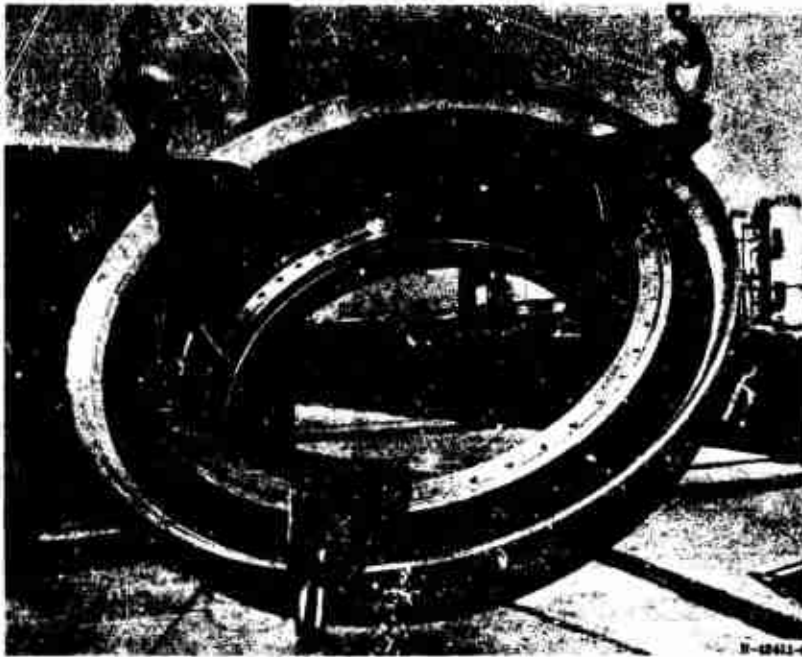


Figure 62. Seal, Nose, and Barrier Assembly

7. The fixed housing assembly was then raised and dryfit to the aft end of the bearing assembly. Adhesive was applied to the end of the boot and the surfaces mating with the end. The fixed housing was again raised into place and the bolts inserted between the small flange of the fixed housing and the aft end ring of the bearing (Figure 63).
8. Four shipping jacks (shown in Figure 64) were next installed between the reinforcing ring of the exit shell and the large flange of the fixed housing. These jacks were expanded to remove the weight of the fixed housing from the bearing and to hold the bearing in compression during shipping and handling. The jacks were removed prior to moving the nozzle at the test site.

(U) The completed nozzle assembly ready for installation in the shipping container is shown in Figure 64.

4. DEVIATIONS FROM DESIGN

(U) Fifteen design deviations were submitted by the nozzle vendor for disposition. One of these was considered a major deviation, the others were minor. Only the major deviation and four of the minor deviations required rework.

(U) The major deviation was a machining error of 0.46 in. in the length of the barrier liner and the location of the spherical surface machined into the aft end of this part. Use of the erroneously fabricated part would have produced the following unacceptable conditions:

1. The gap between the fixed and movable spherical surfaces would have doubled to 0.40 inch.

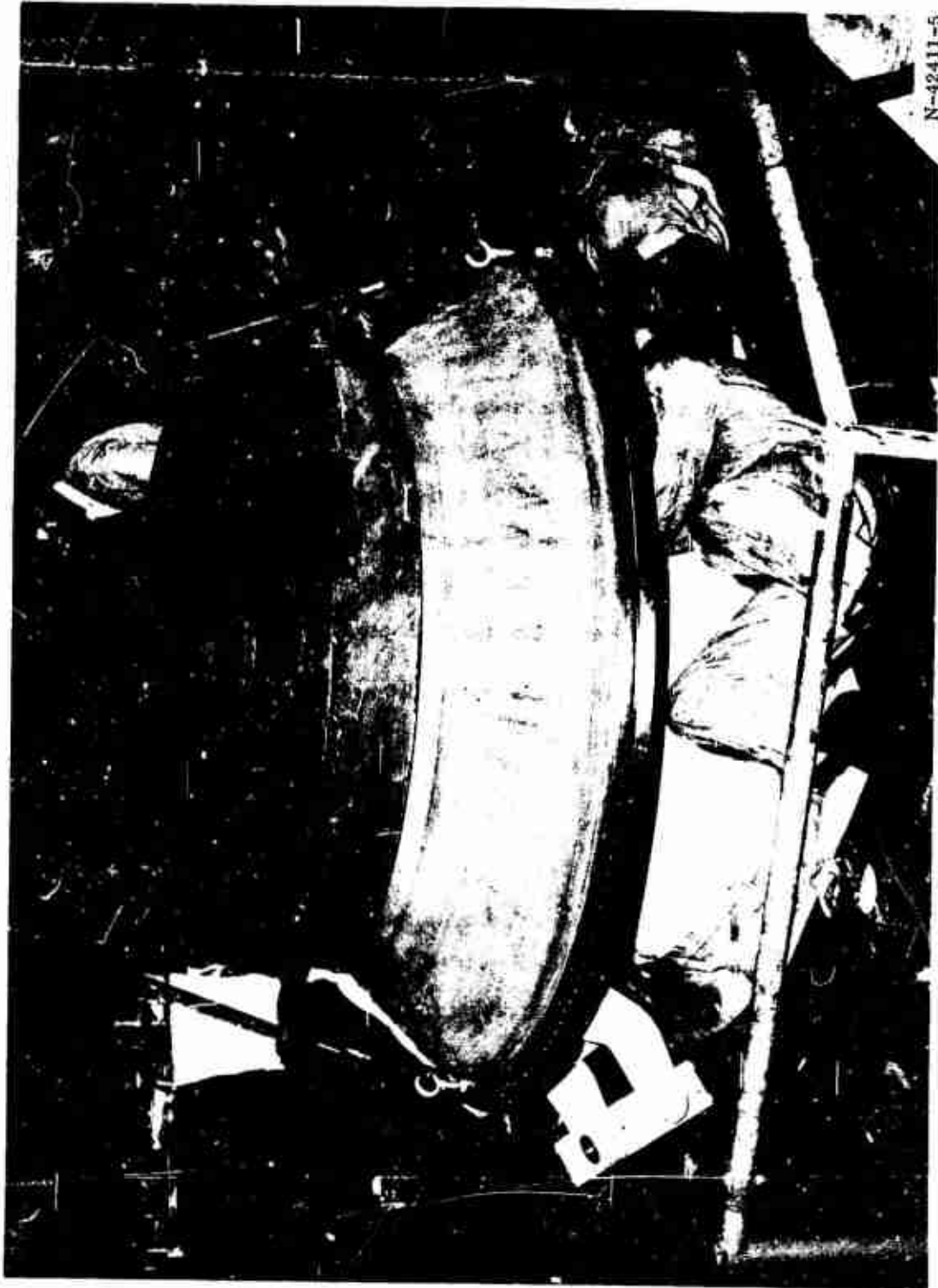


Figure 63. Installation of Bolts between Fixed Housing and Seal

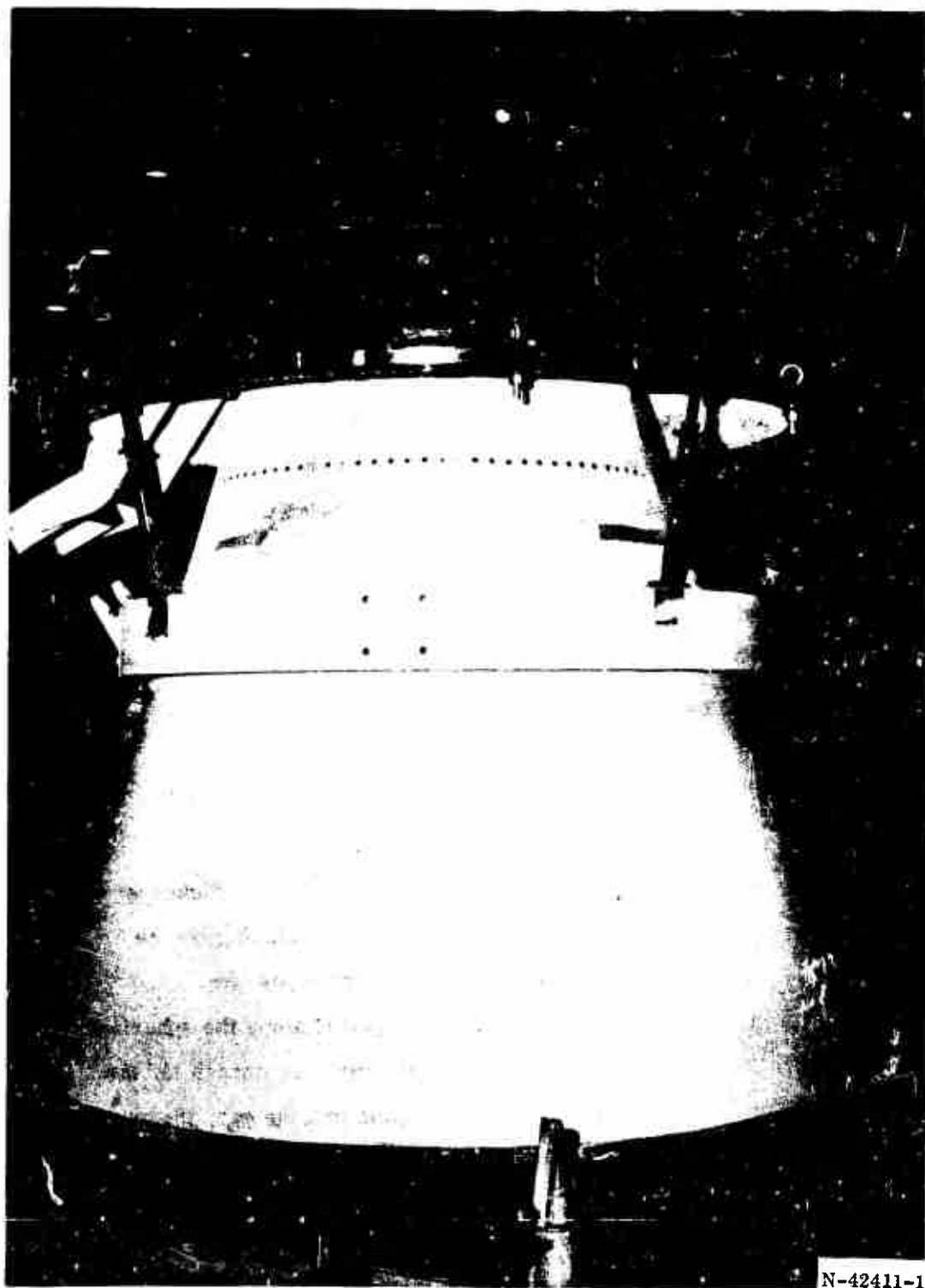


Figure 64. Completed Nozzle Assembly

2. The centers of the fixed and movable spherical surfaces would have been separated by 0.46 in. which would have caused the gap to vary around the periphery while vectored producing a driving potential for circumferential flow.

(U) Repair of the part as opposed to fabrication of a new part was considered. A repair of the part was designed which enabled attainment of the desired geometry without sacrifice of reliability.

(U) A further cut was taken in the part to provide a surface for laying up a repair part consisting of rosette plies of MX-2646 silica cloth phenolic. The entire part was then bagged and the repair area was autoclaved to cure and bond it to the basic part. The repair details are shown in Figure 65.

(U) The repair design had the following notable features.

1. The added material was mechanically locked to the basic part to hold it in place in the event of bond failure and because of the rosette construction, every ply was mechanically locked to the basic part.
2. Along the spherical surface the minimum thickness of the repair material was 0.50 in. which gave the repaired area structural integrity of its own.
3. Only superficial char was expected along the spherical surface, but should the part char deep enough for the charred rosette plies to expand into the gap, the narrowing of the gap would further restrict the flow moderating the environment. In order to close the gap and produce sliding friction, the rosette part would have to expand by 40 percent, which is highly improbable.

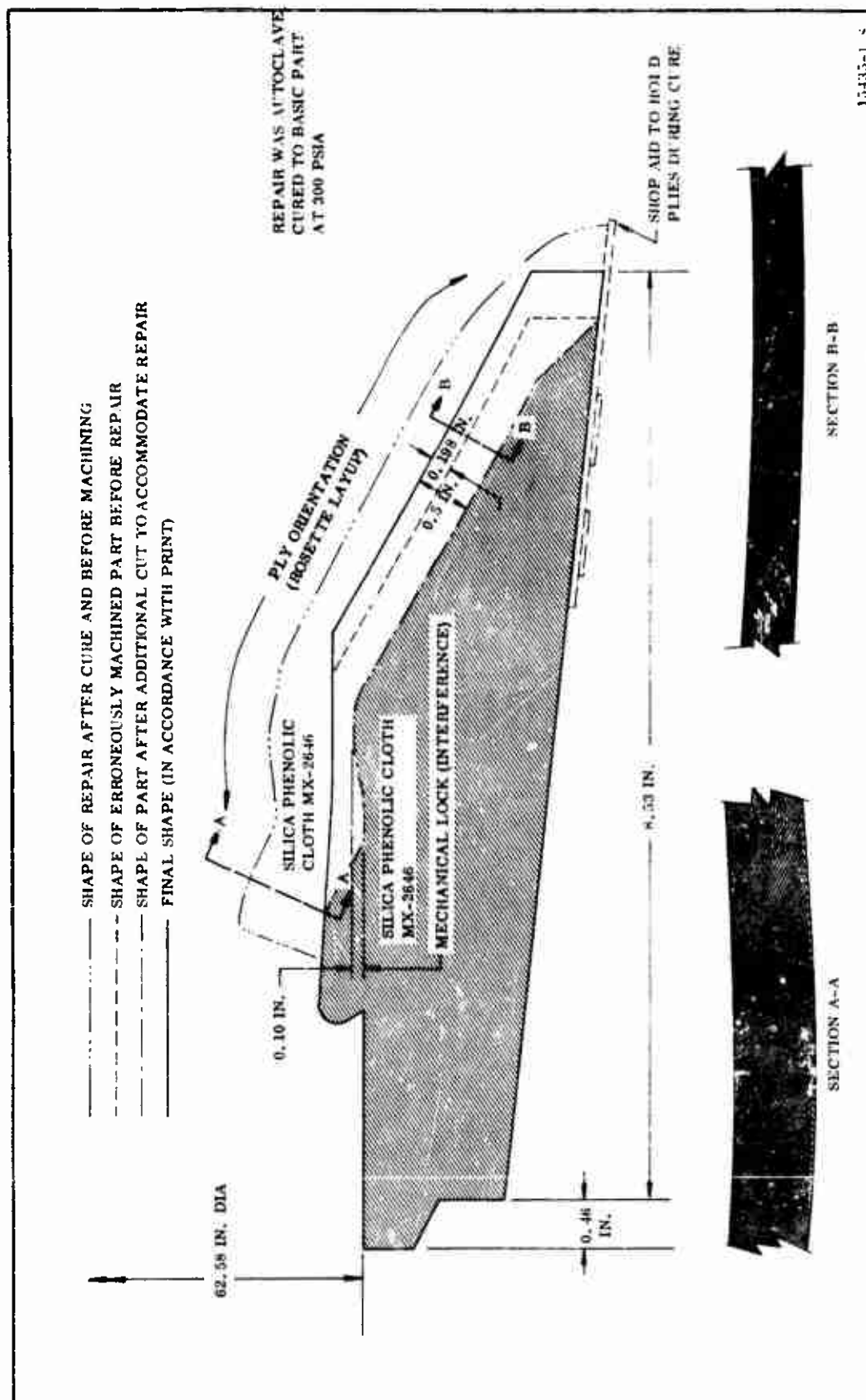


Figure 65. Repair of Barrier Assembly

(U) The reworked barrier assembly was, therefore, expected to perform as well as the originally designed part.

(U) The disposition of the remaining deviations are summarized in Table XII.

TABLE XII
SUMMARY OF DEVIATION FROM ORIGINAL DESIGN

Deviation	VRMA No.	Part	Deviation	Disposition
1	500-1	Fixed Housing 7U40528	Flange to flange length 0.28 in. less than design. Miscellaneous other surfaces not per design.	Areas under b. heads spot-faced to insure full seating. accepted.
2	500-1A	Entrance Housing 7U40521	Flange 0.050 in. thinner than design.	Accepted.
3	500-2	Entrance Housing 7U40521	Tapped holes not per print.	Threaded inserts installed in 17 holes. accepted.
4	500-3	Exit Housing 7U40522	Miscellaneous dimensions not per design.	Subjected to penetrant dye inspection, accepted.
5	500-4	Clevis 7U40524	0.015 in. thinner than design.	Accepted.
6	500-5	Entrance Housing 7U40521	Cone 0.020 in. thinner than design.	Accepted.
7	500-6	Exit Housing 7U40522	Superficial groove in reinforcing ring.	Accepted.
8	500-7	Fixed Housing 7U40528	Miscellaneous dimensions not per design.	Accepted.
9	500-8	Barrier Liner 7U40523	Low density areas in X-ray.	Accepted.
10	500-9	Crossover Ring 7U40516-04	Foreign inclusions (fibers).	Accepted.
11	500-10	Movable Housing Assy, 7U40520	Bond gap in exit oversize.	Accepted.
12	500-11	Throat Overwrap 7U40520-03	OD 0.001 to 0.100 in. undersize.	Accepted. (Gap filled with resin.)
13	500-12	Throat Overwrap 7U40520-03	Test slab shear value low.	Accepted. (Vacuum lost on cure of test slab.)
14	500-13	Throat Overwrap 7U40520-03	Inclusions in overwrap.	Accepted.
15	500-14	Barrier Liner 7U40523	(See discussion in text.)	Reworked and accepted.

SECTION IV

GRAIN DESIGN

A. BALLISTICS DESIGN

(U) The 156-9 motor grain design was based on the use of existing motor hardware and tooling while achieving contractually required motor performance. Major design considerations were maximum expected operating pressure (MEOP), aft grain limitations imposed by the configuration of the submerged nozzle, and chamber pressure vs time neutrality.

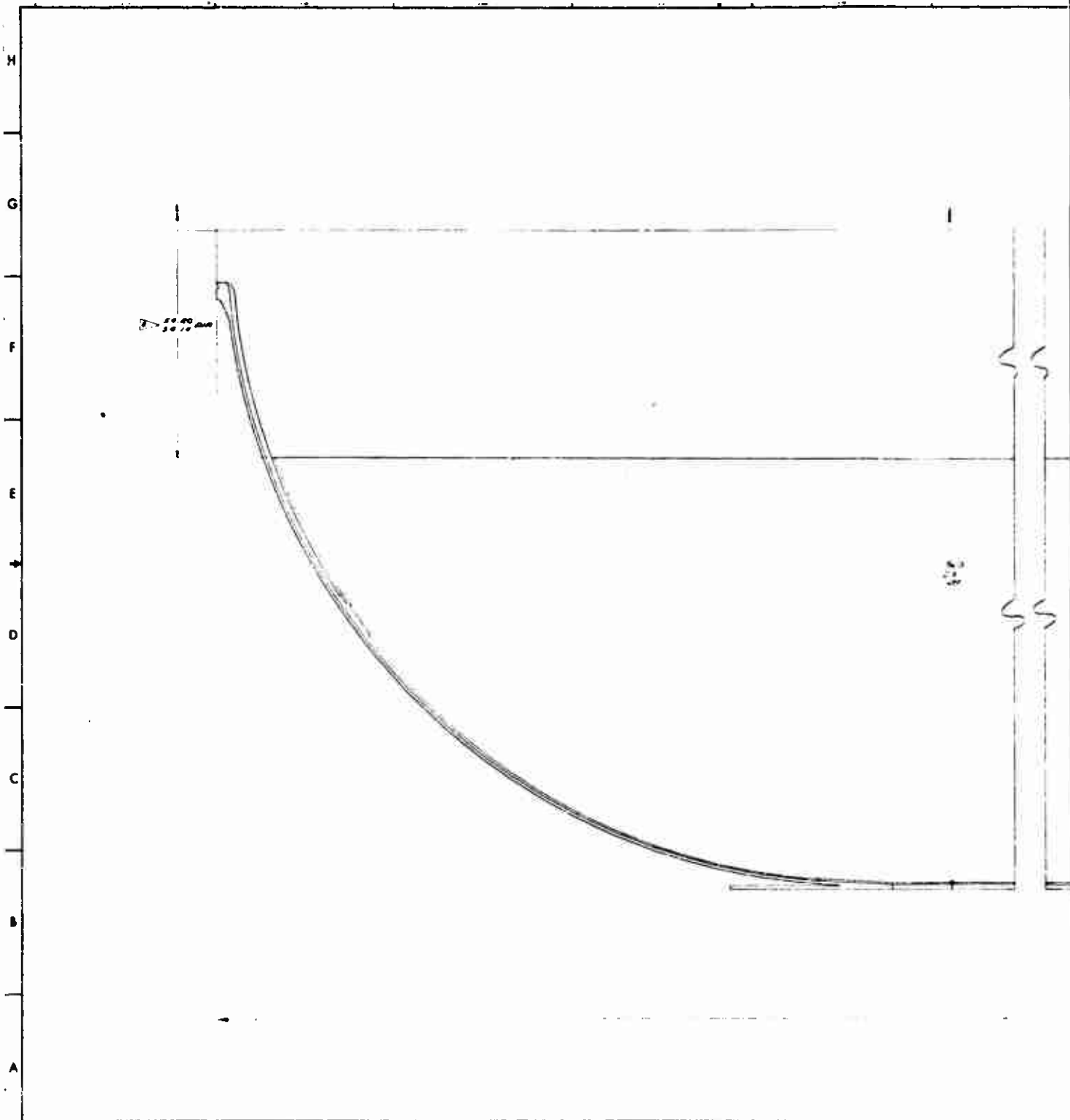
(U) The motor contained a slotted, cylindrically perforated grain having a 64 percent web fraction. The grain was in the monolithic case in two sections separated by a 6.5 in. slot located near the nose of the nozzle (Figure 66). The core diameter was 54.2 in. in the forward end and 77.25 in. in the vicinity of the submerged nozzle (motor aft end).

1. PREDICTED PERFORMANCE

(U) The predicted performance (Table XIII) satisfies the work statement requirements. The prediction was based on actual propellant batch data. These values were modified slightly from the original design when the batch data became available.

2. PRESSURE AND THRUST VS TIME

(U) The predicted chamber pressure and thrust vs time at 80°F are shown in Figure 67. These traces show the neutrality achieved with the 156-9 grain design.



1

2

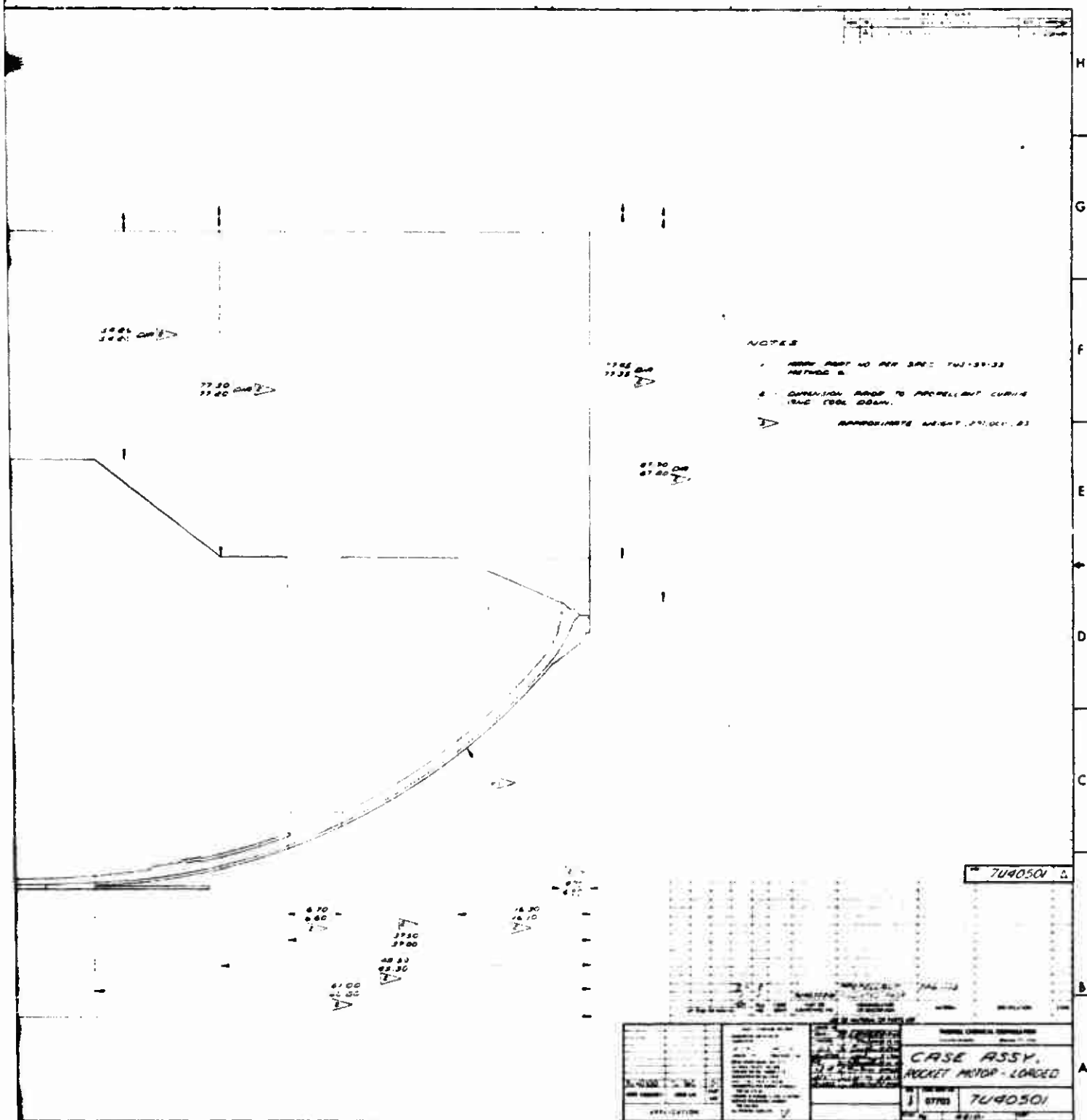


Figure 66. Loaded Rocket Motor Case Assembly

CONFIDENTIAL

TABLE XIII

156-9 ROCKET MOTOR PREDICTED PERFORMANCE AT 80 AND 100 ° F

<u>Web Time Parameters</u>	<u>80° F</u>	<u>100° F</u>
Burning Time (sec)	68.5	67.6
Average Pressure (psia)	654	673
Maximum Pressure (psia)	697	718
MEOP (psia)	753	775
Total Impulse Utah Conditions (lbf-sec)	66,389,800	66,570,550
Average Thrust Utah Conditions (lbf)	969,600	984,480
Maximum Thrust Utah Conditions (lbf)	1,049,900	1,082,000
Propellant Burning Rate at P_{cb} (in. /sec)	0.724	0.733
TU-131 Burning Rate at 700 psia (in. /sec)	0.698	0.710
Burning Rate Scale Factor	1.067	1.067
Propellant Weight Expended (lbm)	273,874	273,874
Maximum to Average Pressure Ratio	1.06	1.06
<u>Action Time Parameters</u>		
Action Time (sec)	70.51	69.64
Average Pressure (psia)	641	660
Total Impulse Utah Conditions (lbf-sec)	67,023,200	67,189,340
Average Thrust Utah Conditions (lbf)	950,550	964,810
Specific Impulse Utah Conditions (lbf-sec/lbm)	242.0	242.6
Thrust Coefficient ($\gamma = 1.18$, $\lambda = 0.977$)	1.5334	1.5378
Motor Coefficient, C_M	0.989	0.989
Reference Specific Impulse ¹ (lbf-sec/lbm)	249.4	249.4
Propellant Weight Expended (lbm)	276,921	276,921

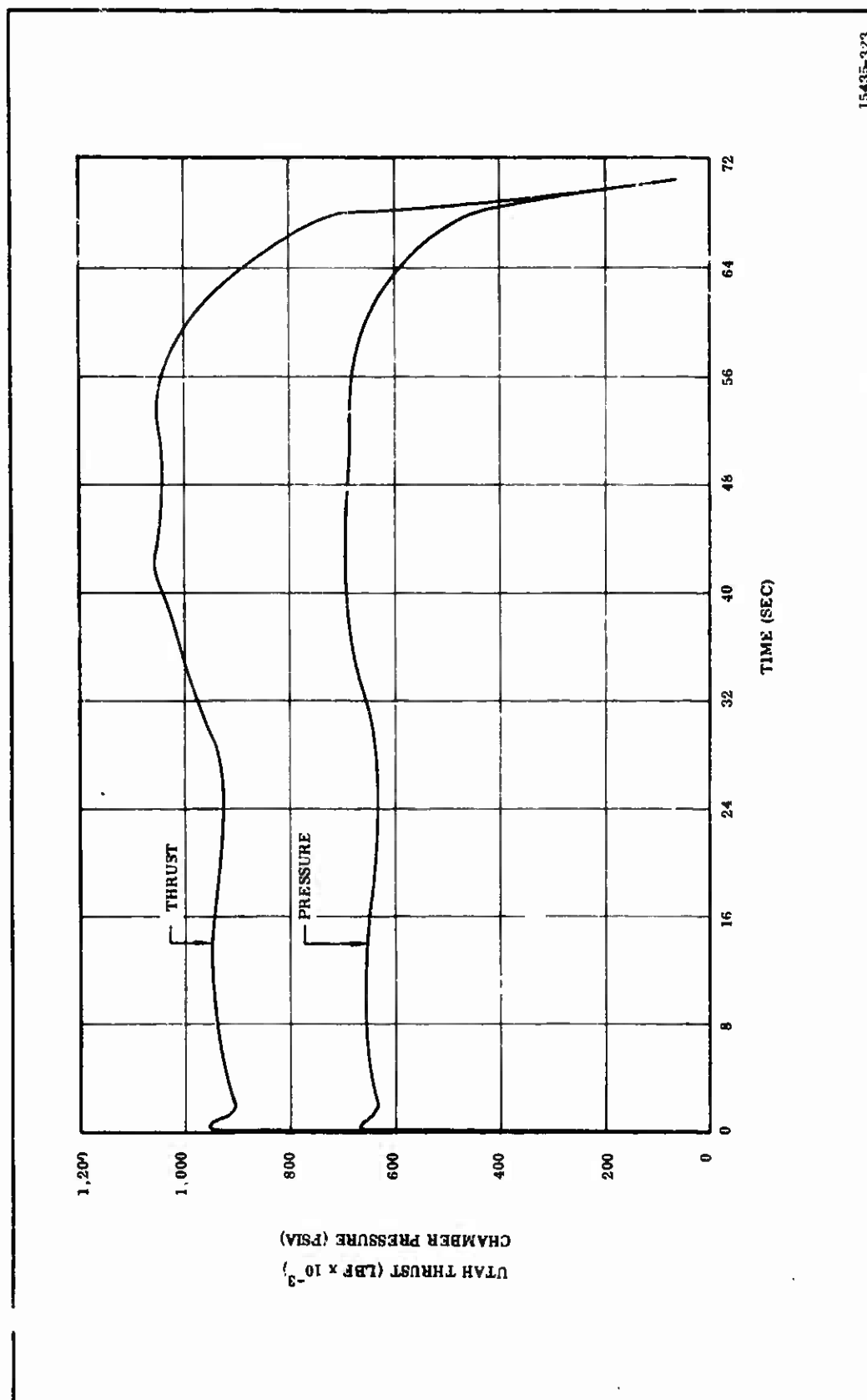


Figure 67. Chamber Pressure and Thrust vs Time at 80°F

(U) 3. GAS FLOW CHARACTERISTICS

The 156-9 motor was designed to use the same basic core to form the internal grain configuration as was used in the 156-6 motor. Use of a submerged nozzle on the 156-9 motor necessitated a change in the nozzle cutout grain geometry. An aerodynamic analysis was conducted. The methods used are discussed in Section III. The mass flow per unit area at several sections have been compared to show that the 156-9 motor grain design results in more conservative gas velocities in the motor aft plenum chamber than was predicted for the successfully tested 156-6 motor.

(U) A sketch of the aft motor configurations of the 156-6 and 156-9 motors is shown in Figure 68. The flow analysis of the 156-9 motor was made with the nozzle in the vectored position (4 deg) resulting in additional conservatism in the analysis. The aft slot location and configuration in both motors are similar, with the design slot width being approximately 6.5 inches. The nozzle in the 156-6 motor extended farther over the aft slot than in the 156-9 motor.

(U) A comparison of pertinent parameters of the two motors at the various locations in the aft plenum identified in Figure 68 is presented in Table XIV. A comparison at Stations 3, 4, and 5 reveals that the one dimensional Mach numbers in the 156-9 motor are less than in the 156-6 motor.

(U) The Lockheed final program report* revealed that after cure shrinkage and grain slumpage, the slot width at the slot exit was approximately 8.77 inches. Other grain dimensions around the nozzle remained essentially the same. This increase in slot width reduced the theoretical Mach number at Station 4 (Figure 68) in the 156-6 motor to 0.05, with a velocity of 173 ft/sec. Grain shrinkage also tends to increase the slot width and reduce the gas velocity at the slot exit below the 311 ft/sec indicated.

* Technical Report No. AFRPL-TR-66-109 156-Inch Diameter Motor Liquid Injection TVC Program, Volume 1, Book 1. Lockheed Propulsion Company, July 1966.

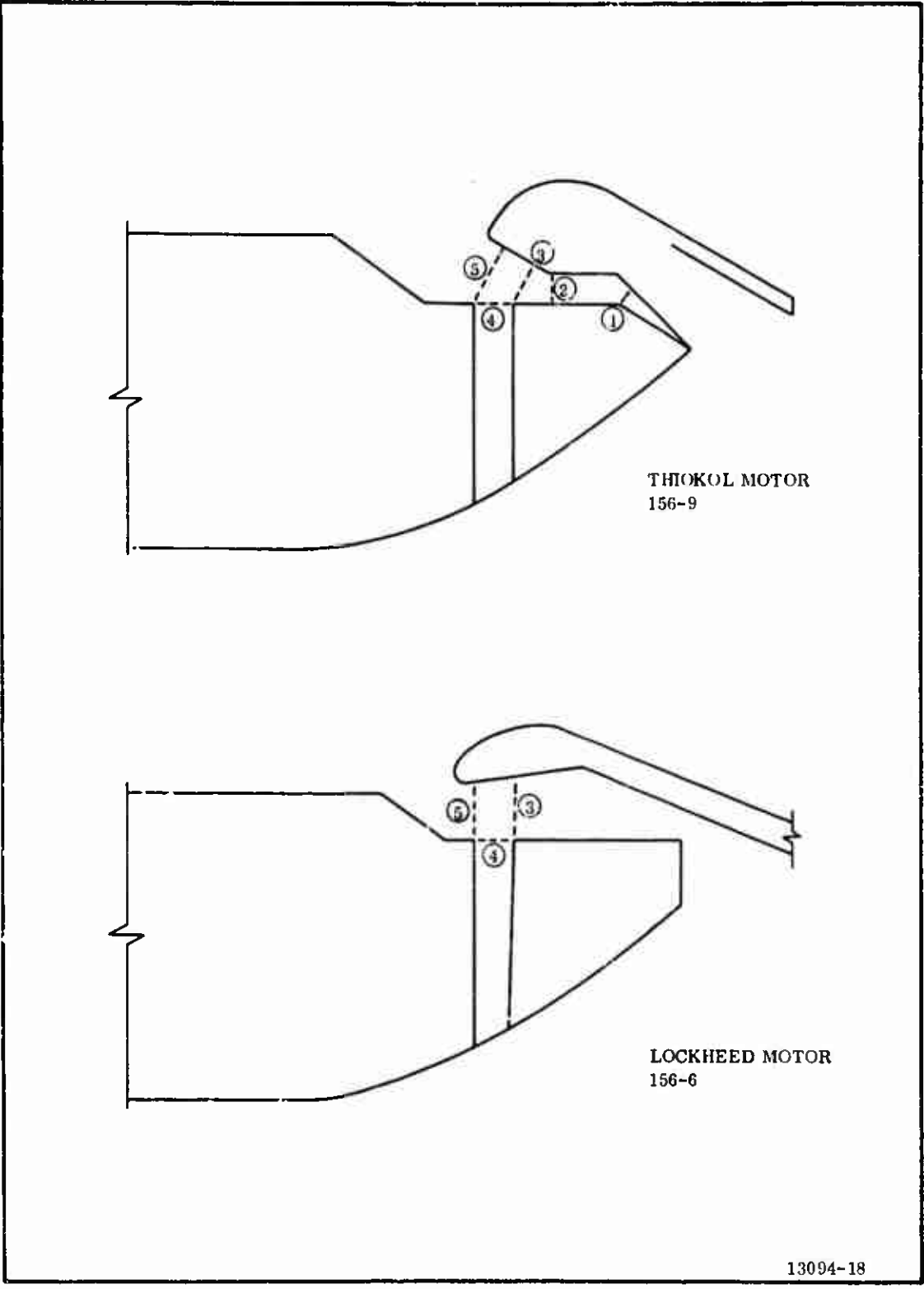


Figure 68. Flow Comparison Points in the 156-6 and 156-9 Plenums

TABLE XIV

AFT PLENUM INITIAL FLOW CHARACTERISTIC COMPARISON

	<u>156-6*</u>	<u>156-9</u>
Surface Area Aft of Station No. (sq in.)		
Station 1	--	3,765
Station 2	--	5,782
Station 3	8,314	7,240
Station 4	22,660	20,526
Station 5	30,974	27,766
Local Flow Areas (sq in.)		
Station 1	--	1,003
Station 2	--	1,004
Station 3	1,663	1,471
Station 4	1,465	1,615
Station 5	1,663	2,113
Local A_s/A_t Ratio		
Station 1	--	3.8
Station 2	--	5.8
Station 3	5.0	4.9
Station 4	15.5	12.7
Station 5	18.6	13.1
Local Mach No.		
Station 1	--	0.026
Station 2	--	0.041
Station 3	0.04	0.036
Station 4	0.11	0.090
Station 5	0.13	0.094
Local Velocity (ft/sec)		
Station 1	--	90
Station 2	--	142
Station 3	138	124
Station 4	380	311
Station 5	449	325

* Technical Report No. AFRPL-TR-65-212 156 Inch Diameter Motor Liquid Injection TVC Program, Lockheed Propulsion Company, October 1965.

(U) It was concluded that the grain configuration in the aft plenum chamber of the 156-9 motor was satisfactory and that the backside of the nozzle would not be subject to velocities significantly greater than already experienced in the 156-6 motor. The predicted one dimensional Mach number at the end of the grain of the 156-9 motor was 0.137 (velocity = 473 ft/sec). Propellant erosive burning would, therefore, not be significant in predicting motor performance.

B. STRUCTURAL DESIGN

(U) A comprehensive stress analysis of the propellant grain of the 156-9 motor was conducted. The analysis was based on an axisymmetric elastic stiffness matrix method that was developed at Redstone Arsenal Research Division of Rohm and Haas Company. The stress and strain patterns for conditions of cure and thermal shrinkage and pressurization have been calculated and compared to the failure criteria. The failure criteria used was the Smith failure boundary derived from uniaxial tests of the propellant. The analysis showed satisfactory margins between the calculated imposed loads and the failure boundary in all cases.

1. GRAIN CONFIGURATION

(U) The 156-9 rocket motor is a 156 in. diameter steel case motor with a slotted cylindrically perforated propellant grain (Figure 66). Although the grain consisted of two separate sections, the stress study considered them as one body. The main grain web fraction was 64.0 percent, and the length to diameter ratio was 1.68. The most significant characteristics are given in Table XV. The loading conditions considered were cure and thermal shrinkage to +60°F and ignition transient pressurization of 682 psia.

CONFIDENTIAL
(THIS PAGE IS UNCLASSIFIED)

TABLE XV
GRAIN DESIGN PARAMETERS

Grain Outside Diameter (in.)	154.5
Grain Inside Diameter (in.)	55.39
Cross-sectional Loading Density (percent)	0.87
Port Area (sq in.)	2,437
Initial Port/Throat Area Ratio ($\frac{1}{J}$)	2.6
Web Thickness (in.)	49.57
Web Fraction (percent)	0.64
Slot Width at Bore (in.)	6.65
Slot Angle to Motor Q_L (deg)	90

2. STRUCTURAL ANALYSIS

- (U) The stress analysis of the 156-9 rocket motor grain was performed using a computer program developed at the Redstone Arsenal Research Division of Rohm and Haas Company. *
- (U) The input data of the program included description of geometry, material properties, and boundary conditions (both displacement and tractions). The program output consisted of displacement of the element corners, and stress and strain over the elements. In addition, an auxiliary program permits the plotting of stress and strain contours, in addition to displacement grids. For long time associated phenomena, the propellant equilibrium modulus as a function of temperature was used. For short time occurrences, the stress relaxation modulus for the appropriate time of the event was used.
- (U) a. Input Parameters--Accurate material properties are essential in conducting useful or dependable stress analyses. The time history of the various loading conditions also must be known. TP-H1115 propellant was not characterized; however, under cognizance of the Poseidon and Large Booster Programs, TP-H1096, TP-H1114, and TP-H8163 propellants have been characterized and their actual properties are considered in this report as experimental data for TP-H1115 propellant. A comparison of the formulation and basic physical properties is shown on Table XVI.

*Becker, E. B. and Brisbane, J. J. Special Report No. S-76, Application of the Finite Element Method of Stress Analysis of Solid Propellant Rocket Grains, Rohm and Haas Company, Redstone Arsenal Research Division, Huntsville, Alabama, November 1965.

CONFIDENTIAL

TABLE XVI
156-9 MOTOR PROPELLANT

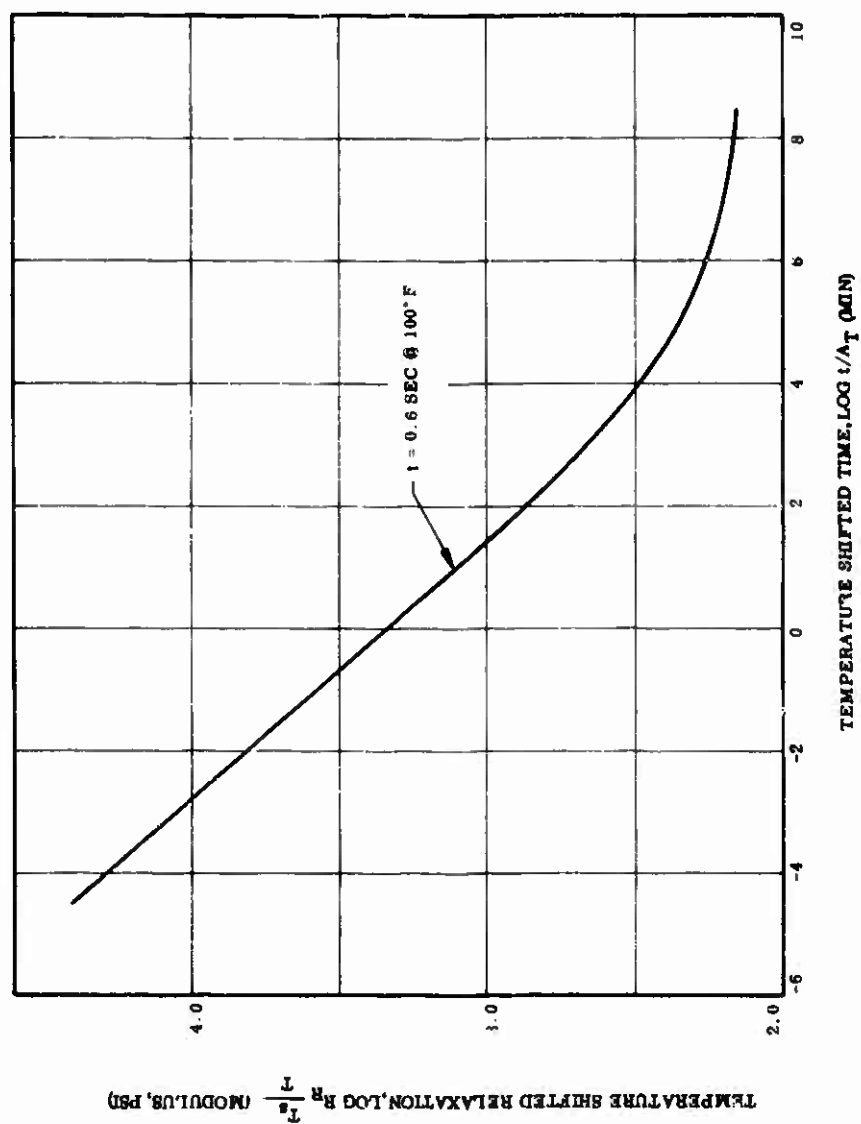
<u>Material</u>	<u>Formulation Composition Comparisons (Percent by Weight)</u>			
	<u>TP-H1096*</u>	<u>TP-H8163*</u>	<u>TP-H1114*</u>	<u>TP-H1115**</u>
HB Polymer Epoxy Resin	12.00	12.00	12.00	13.00
Diethyl Adipate	2.00	2.00	2.00	-0-
Ferric Oxide	1.00	1.00	0.30	1.00
Aluminum Powder	16.00	16.00	16.00	18.00
Ammonium Perchlorate	69.00	69.00	69.70	68.00

<u>Property</u>	<u>Physical Properties Comparisons</u>					
	<u>TP-H1096*</u>		<u>TP-H8163*</u>		<u>TP-H1114*</u>	
	<u>Min</u>	<u>Max</u>	<u>Min</u>	<u>Max</u>	<u>Min</u>	<u>Max</u>
Maximum Stress (psi)	40	--	40	--	40	--
Strain at Cracking (in./in.)	0.25	--	0.30	--	0.25	--
Modulus of Elasticity (psi)	400	600	300	600	400	700
Density of Cured Propellant (lb/cu in.)	0.0637	0.0649	0.0637	0.0649	0.0637	0.0649
						0.0651

*Specification
**Actual

CONFIDENTIAL

- (U) The significant material properties are stress relaxation modulus (E_R) as a function of temperature, thermal coefficient of linear expansion (TCLE) as a function of temperature, coefficient of cure shrinkage (ϕ_R) and Poisson's ratio. The time to soak and the pressure vs time history data were derived from theoretical calculations.
- (U) The propellant stress relaxation curve vs time and temperature that was utilized is shown in Figure 69. This curve was obtained from broad spectrum data reduction techniques. The long time or equilibrium modulus approaches 200 psi.
- (U) The thermal coefficient of linear expansion (TCLE) was taken from propellant experimental data. The TCLE vs temperature has an inflection point at approximately 0°F. Above and below this point, the value is 6.26×10^{-6} and 6.67×10^{-5} in./in./°F. For conservatism, the average of these was used in the analysis.
- (U) Stress inducing cure shrinkage may range as high as 0.8 percent in very small motors and as low as 0.1 percent in very large motors. A conservative value of 0.4 percent was used in this study. The computer program cannot calculate the cure shrinkage factor directly, so this factor is translated to an increment of temperature as a function of the TCLE. An increment of 21°F was used in the analysis.
- (U) All computer runs were based on a Poisson's ratio input of 0.5. For cure and thermal shrinkage conditions (i.e., very low strain rate), as Poisson's ratio decreases from 0.5, the bore strains decrease. Therefore, if the exact value is less than 0.5, this approach is conservative. For pressurization conditions, the elastic relationships between bulk modulus, Young's modulus, and Poisson's ratio perhaps should be used; but for a lightly loaded motor like the 156-9, no significant difference is apparent. Hence, a Poisson's ratio of 0.5 was considered best for end result accuracy.
- (U) Experience suggested the selection of 1,000 psi as an effective modulus for the pressure runs. Figure 69 indicates that for a time of 0.6 sec and a temperature range of 60 to 100°F, the lowest modulus would exceed 1,000 psi by at least 33 percent. Since the previously selected number would result in a higher induced bore strain, the original computer runs were not changed.



t = TIME
 T = TEMPERATURE
 R = RELAXATION MODULUS
 R_0 = EQUILIBRIUM MODULUS
 $T_0 = 250^\circ \text{K}$
 $\log A_T = \frac{-8.88(T-T_0)}{101.6 + T - T_0}$

13094-22

Figure 69. Propellant Stress Relaxation Modulus

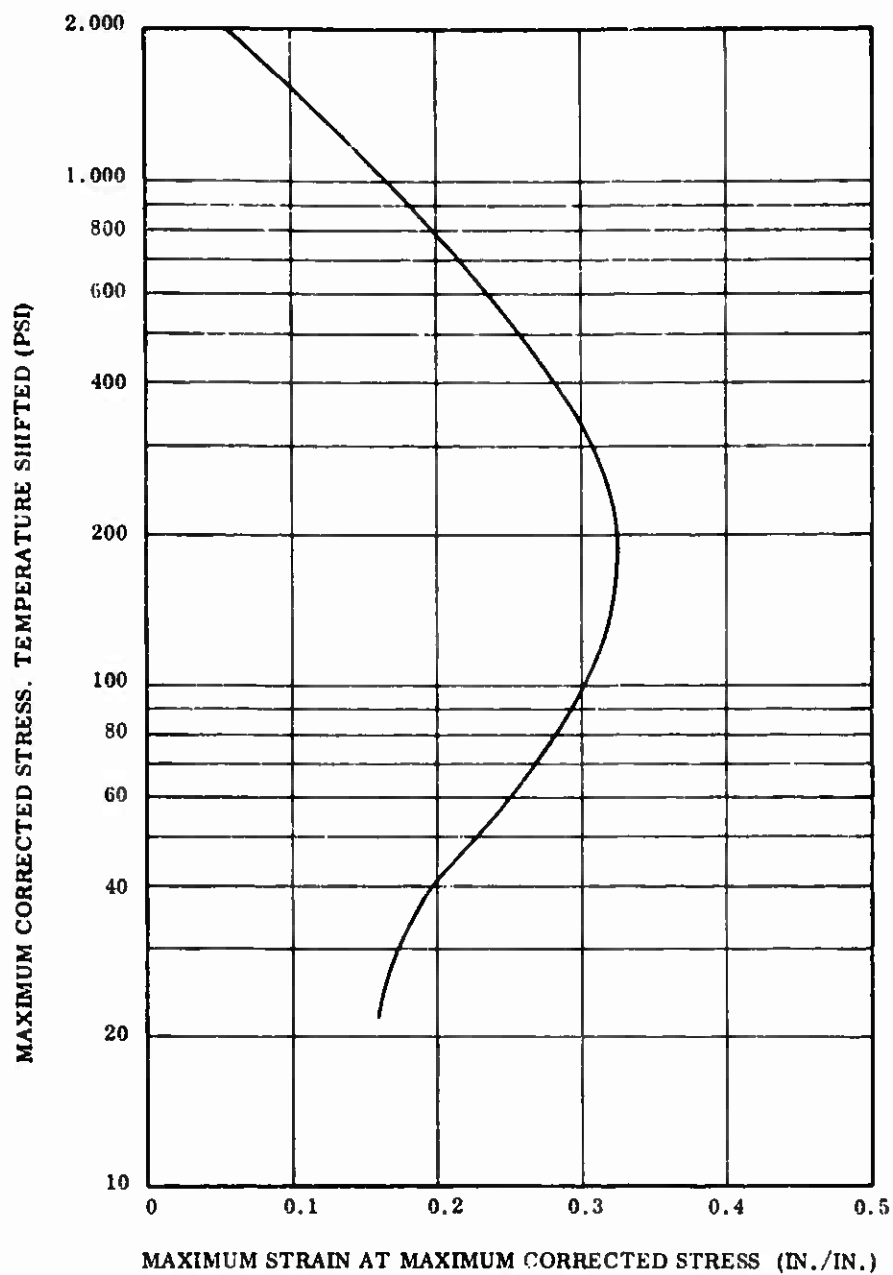
(U) b. Failure Criteria--Many different strain and stress inducing conditions are involved in the 156-9 study and no single failure criterion is adequate for all loads. Also, a wide diversity of opinions are extant within the solid propellant industry about which failure criteria are the most realistic. Thiokol has been using stress-strain boundary failure criteria as shown in Figure 70. The boundary used is determined by whether the failure is dilatational or distortional. For dilatational failure, the boundary used is the sum of the principal stresses vs the maximum principal strain. For distortional failure, the boundary is the maximum deviatoric stress vs the maximum principal strain.

(U) A Castor II motor was successfully fired for which the sum of the inner bore hoop strain due to shrinkage and pressure significantly exceeded the propellant capability in an unpressurized state. If the unpressurized failure boundary is used, it must be concluded that the motor is safe. To date, a satisfactory means of determining a margin of safety has not been developed for the stress-strain boundary. The interpretation of safety for the stress-strain boundary is merely the stipulation that the end point of the condition under consideration be inside the boundary, and in such a position, that stress decay will not result in the trace crossing the boundary. If statistical limits for batch to batch variability and age are used to reduce the boundaries, then determination of a margin should be unnecessary.

(U) c. Stress Analysis and Failure Criteria Results--In general, the 156-9 stress analysis studies have defined for the stress inducing loads considered:

1. Grain deformations,
2. Stress-strain contours throughout the grain,
3. Worst grain stress-strain conditions compared to propellant capability limits.

(U) The first two limits may be illustrated by plots obtained from the original computer output. The grain deformations due to cure and thermal shrinkage to +60°F and ignition transient pressure to 682 psi are presented in Figures 71 and 72, respectively.



13094-45

Figure 70. Failure Boundary Selected for the 156-9 Study

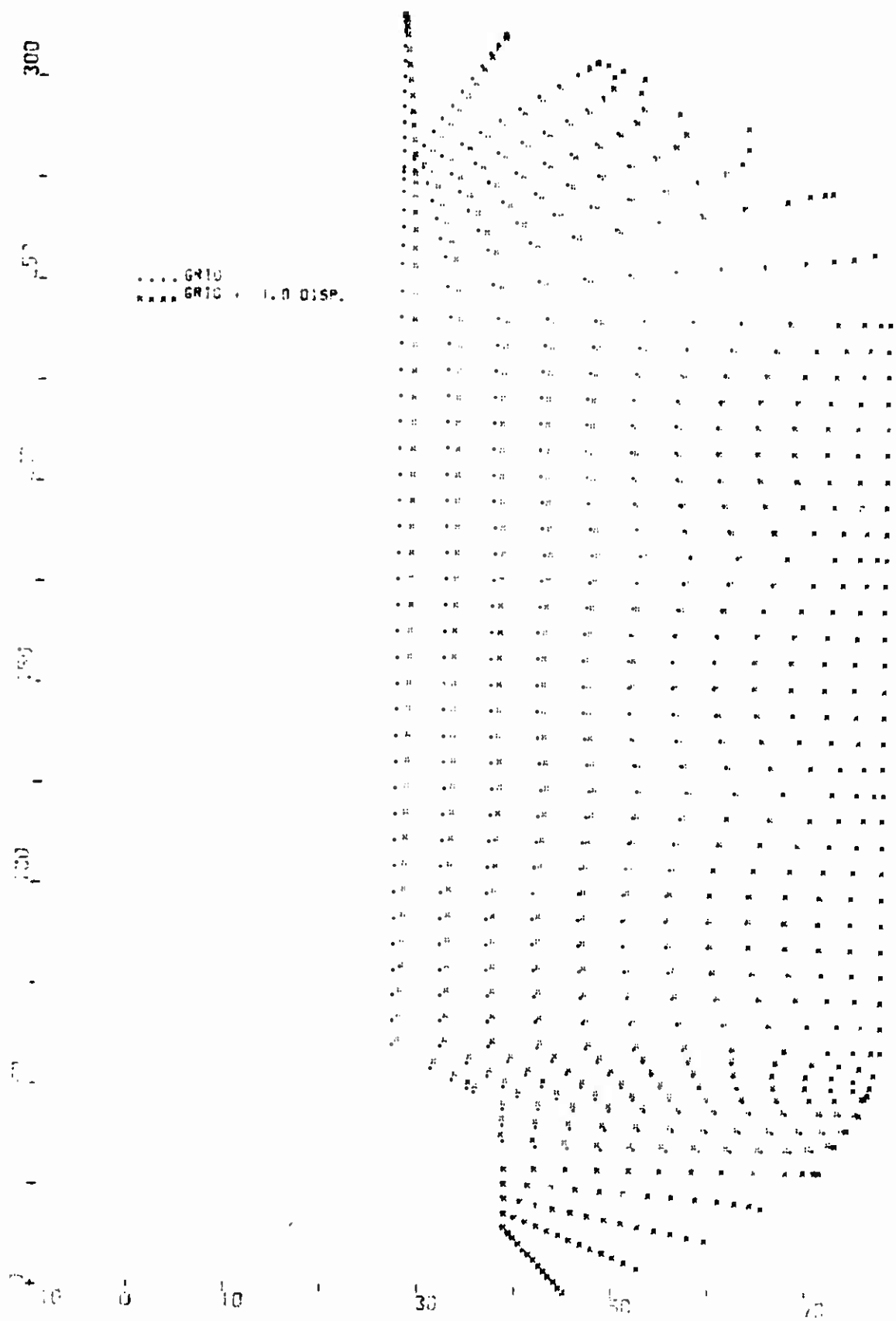


Figure 71. 156-9 Cure-Thermal Shrinkage Stress Analysis Grain Deformation

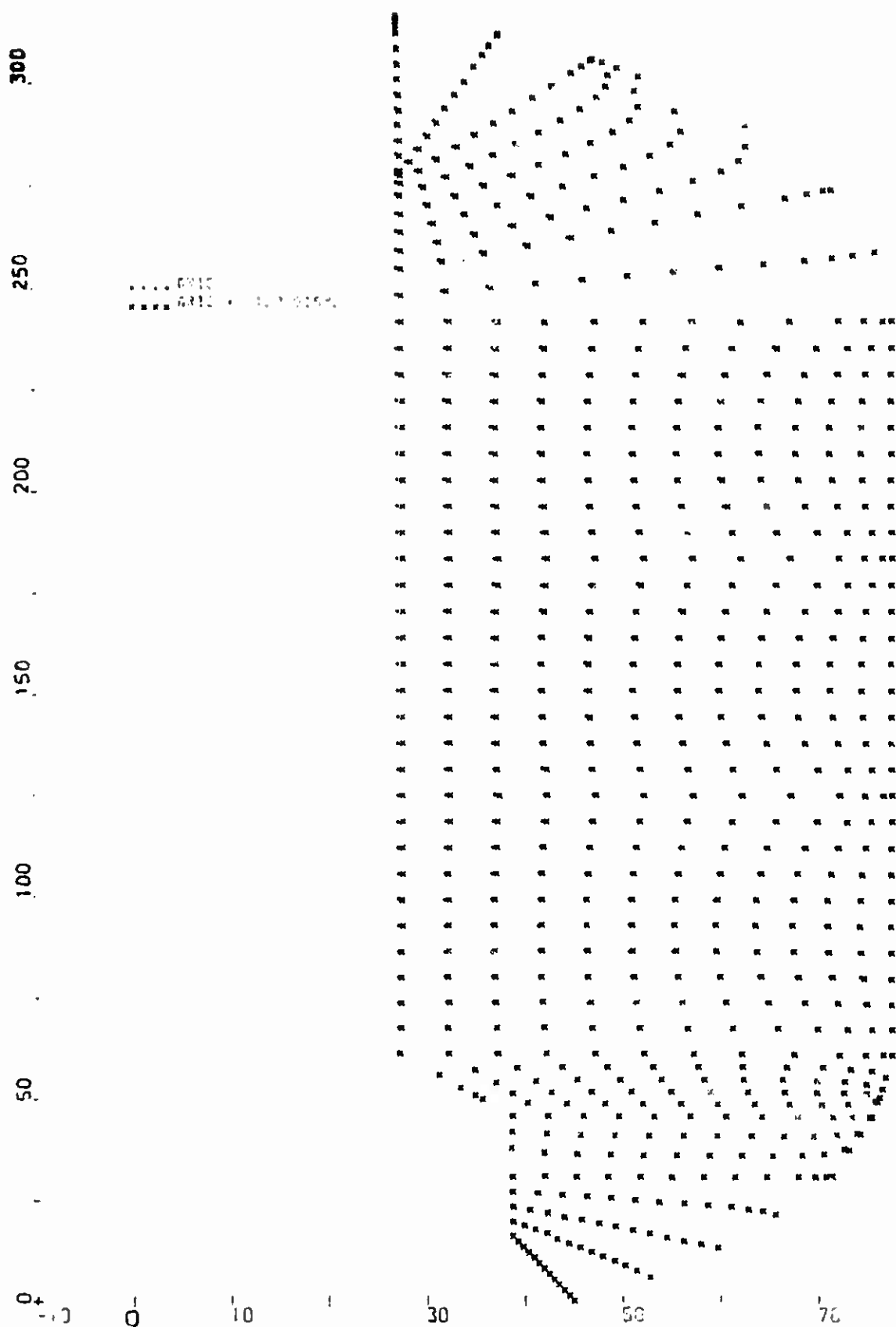


Figure 72. 156-9 Ignition Pressure 682 psi Stress Analysis Grain Deformation

(U) The dilatational and distortional failure boundaries, including the maximum induced grain stress-strain points, are shown in Figures 73 and 74. Figure 74 is the accumulation of cure and thermal shrinkage and pressure effects. These figures indicate that the induced stresses and strains never approach the respective boundaries. Table XVII further illustrates the inherent structural integrity of the 156-9 grain. The worst stress-strain points, the propellant capability, and the resulting margins of safety are shown. Margin of safety is defined as propellant capability divided by induced load, less 1.0. The bases for determining safety margins may be stated as follows.

1. The path to the failure boundary will follow a constant stress line (hence, a maximum principal strain limit).
2. The path to the failure boundary will follow a constant strain line (hence, a maximum principal stress limit).
3. The failure limit lies at a point on the boundary where a constant percentage increase of both stress and strain has been used.

(U) The latter statement attempts to establish a unified margin of safety for the stress-strain failure criteria. Since it results in generally lower margins than the other two, a limited condition is assumed. Prior to calculating the margin of safety (Table XVII) the stress-strain capabilities were reduced by 21.8 percent and 17.6 percent, respectively. Statistically these have been determined to be the three sigma limits on the individual parameter batch to batch variations. Insufficient data precludes preparation of the three sigma limits on the failure boundary. The limited data examined to date indicate that on a unified basis the stress-strain boundary deviations will be smaller than either of those used.

(U) d. Conclusions--From the foregoing, the 156-9 motor obviously has no grain structural behavior problems. With a least margin of safety as shown in Table XVI the grain is predicted to be extremely reliable.

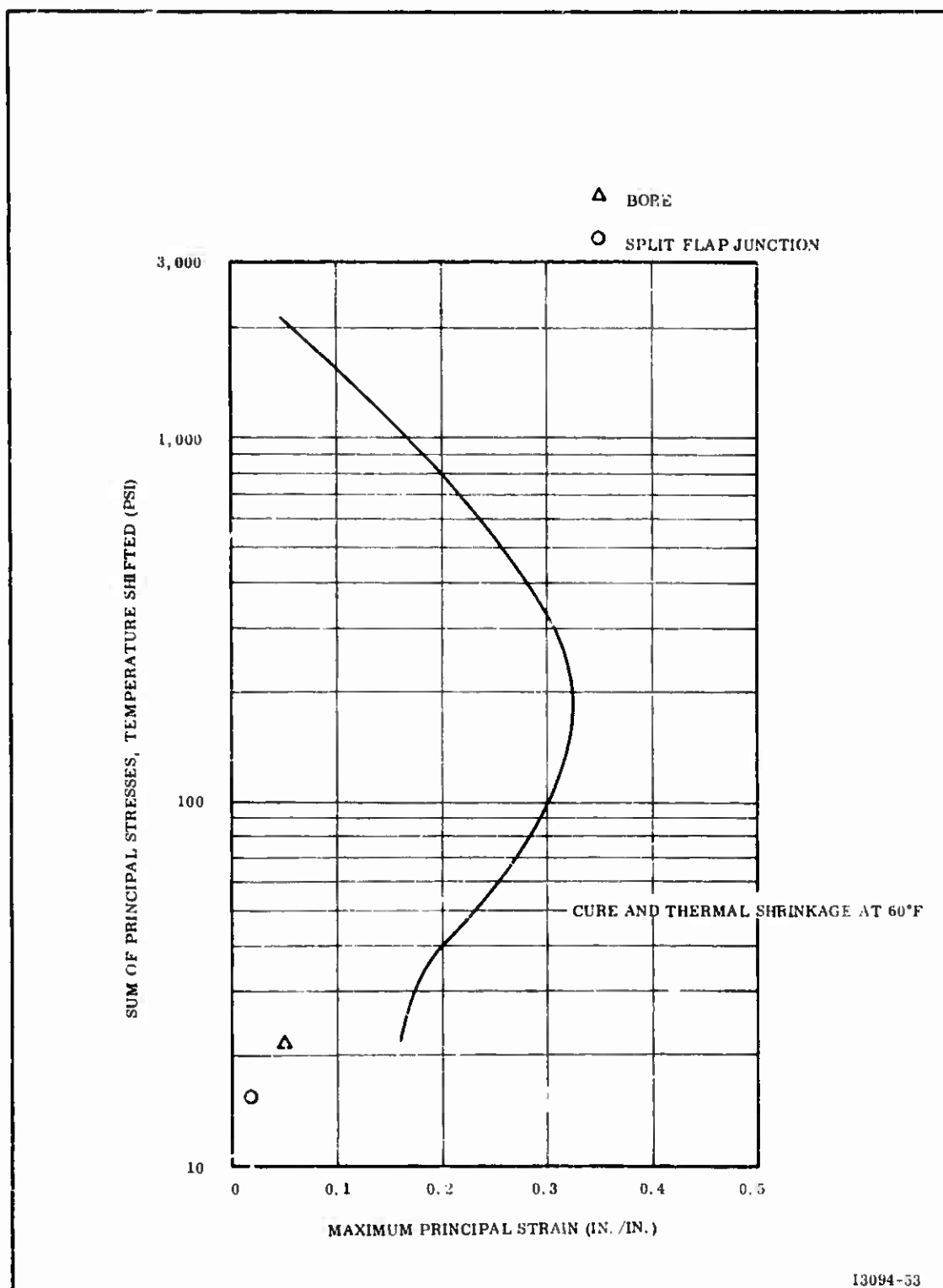


Figure 73. Dilatational Failure Boundary

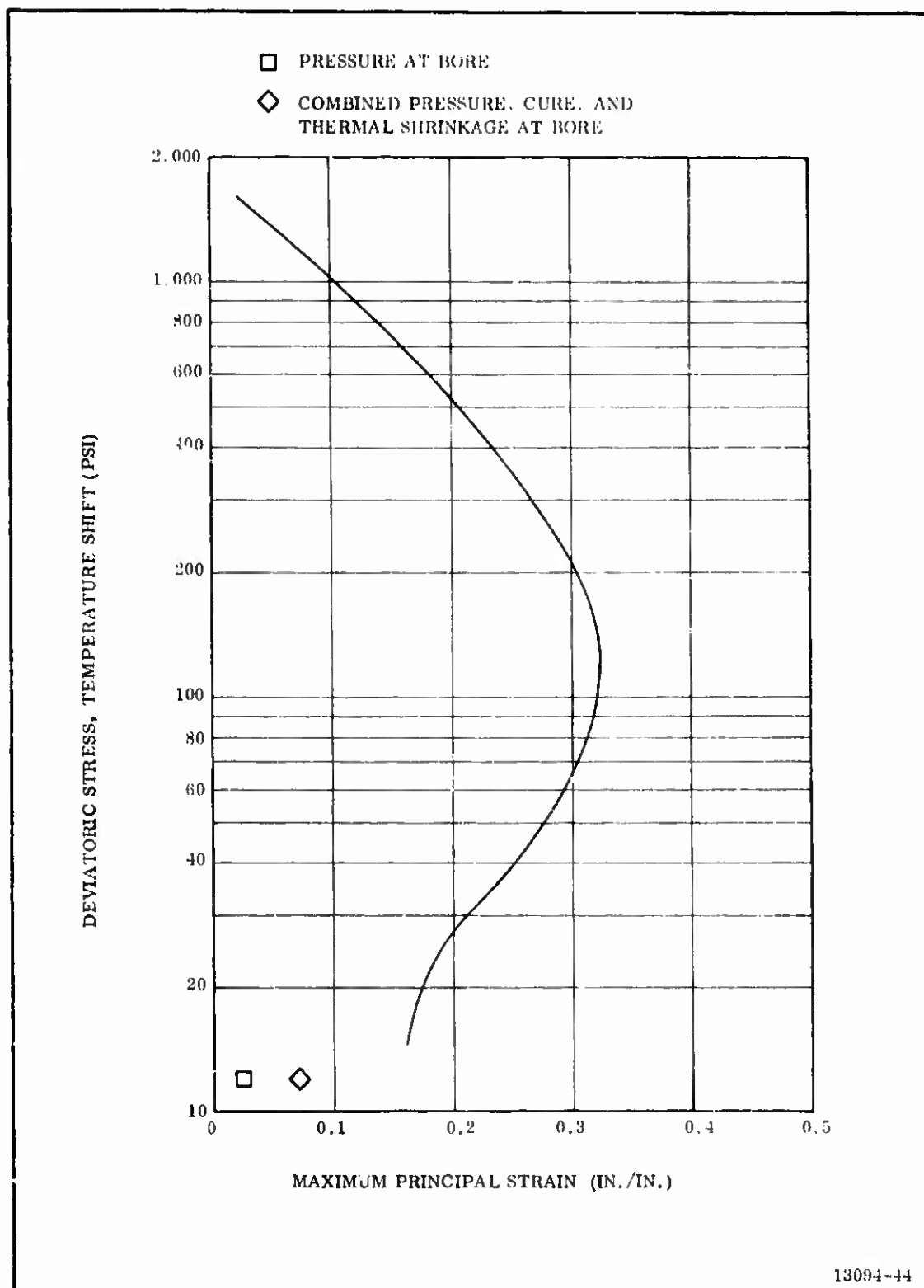


Figure 74. Distortional Failure Boundary

TABLE XVII
WORST STRESS-STRAIN CONDITIONS AND FAILURE CRITERIA COMPARISON

Load	Location	Sum of Maximum Principal or Deviatoric Stress (psi)	Maximum Principal Strain (in./in.)	Propellant Capability			Margin of Safety*		
				1	2	3	1	2	3
1-Cure and Thermal Shrinkage to 60°F	Split Flap Case Junction	15.5	0.019	--	--	--	--	--	--
	Bore	22.0	0.050	0.16	2,100	--	1.72	73.0	--
2-Pressure, 682 psi	Split Flap Case Junction	8	0.012	--	--	--	--	--	--
	Bore	12	0.021	0.16	1,700	--	5.48	109.0	--
3-Combined Shrinkage and Pressure	Split Flap Case Junction	8	0.031	--	--	--	--	--	--
		12	0.07	0.16	1,200	0.175 30	0.87	77.0	1.00

* Propellant capability has been reduced 17.6 and 21.8 percent for strain and stress respectively before calculating margins. 1 is strain, 2 is stress, and 3 is combined stress-strain.

SECTION V

CASE

A. ACCEPTANCE INSPECTION

- (U) The GFP case arrived at the Wasatch Division of Thiokol Chemical Corporation on 11 Nov 1966 where it was inspected for shipping damage.
- (U) After the residual insulation was removed from the inside of the case, the paint was removed from welds and die penetrant inspection was performed. The die penetrant inspection revealed a defect 0.050 in. long at 90 deg in the aft gore weld (Figure 75). The area was radiographically inspected but the defect could not be detected using cobalt source. Further visual examination revealed the defect was not a crack, but two very small inclusions. The thickness of material was measured in the area around the defect ultrasonically and with micrometer calipers. These measurements are presented in the grid in Figure 75. The ultrasonic measurements are indicated by an asterisk. The defect was polished out leaving the minimum case wall thickness 0.342 inch.
- (U) The basic membrane stress in the area of the crack was calculated as 195.19 ksi, this was based on a wall thickness of 0.342 in., and results in a Margin of Safety of 0.23 ($M.S. = \frac{f_{tu}}{\sigma_T} - 1$). The area was adjacent to a weld area where some mismatch was observed, but no attempt was made to adjust the stress calculations to compensate for this discontinuity.
- (U) Visual inspection of the welds in the aft dome revealed numerous discontinuities. The discontinuities were generally departures from the contour of the case straight sections at the edge of the formed gores resulting from either a sucking in or out due to heat differential during welding. These areas caused unknown localized

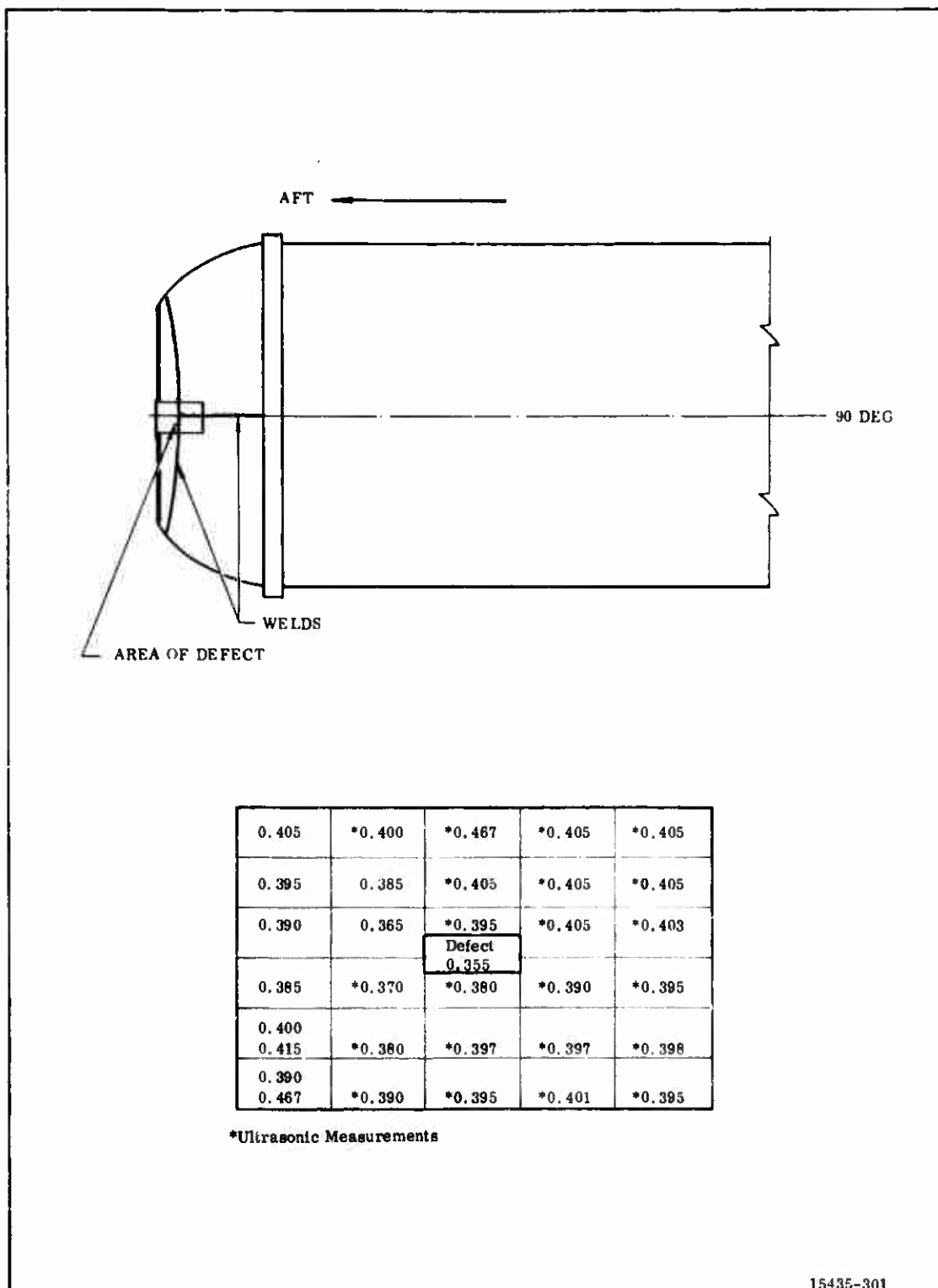


Figure 75. Aft Dome Thickness Measurements in Area of Defect

concentrations of high stress in the yield range during pressurization cycles and may eventually limit the number of pressure cycles the case can withstand.

- (U) The drill jig fabricated for drilling the mating bolt circle of the nozzle was obtained and dryfitted to the case. The first attempt was made on the empty case in the horizontal position with only the GFP handling rings installed. This attempt was not successful due to an out of round condition, however, a later attempt in the vertical position, with the Thiokol harness installed, was successful. It should be noted that no problem was encountered in achieving nozzle fit.

B. CASE REFURBISHMENT

- (U) When received at the Wasatch Division, the motor case contained insulation and char from the previous firing. The major part of this material was removed at the Case Preparation Facility using air hammers with chisel attachments. Complete removal was accomplished by grit blasting the case interior with zirconium grit. At the same time the external weld areas were grit blasted to permit dye penetrant inspection of these areas.
- (U) Following grit blasting operations, the case interior was hand degreased with trichloroethylene. Koropon was then sprayed on the case interior to protect against rusting. Two coats of Koropon were applied; each 0.002-0.003 in. thick. The first coat was cured at ambient temperature for 18 hours and the second for 168 hours, also at ambient temperature.

SECTION VI

INSULATION AND LINER DESIGNS

A. INSULATION DESIGN

1. DESIGN CRITERIA

- (U) The internal case insulation must insure that the original structural integrity of the pressure vessel is not degraded by thermal effects throughout the duration of the motor operation. A conservative insulation design performs its function by providing thermal protection to the case so that the case material is not heated above ambient temperature during motor operation.

2. INSULATION DESIGN, FORMULATION, AND PREDICTED PERFORMANCE

- (U) The purpose of the 156-9 motor was to test the flexible seal movable nozzle; therefore, the insulation was designed to minimize risk to the test vehicle. No attempt was made to optimize material thickness and conservative safety factors were applied. The insulation selection was based on proven materials and manufacturing techniques.
- (U) The internal case insulation was TI-H704B (asbestos filled HC polymer). The insulation materials composition is shown on Table XVIII.
- (U) The insulation design included stress relief flaps at each end of the large forward portion of the propellant grain. The stress relief flaps were fiberglass fabric reinforced TI-H704B insulation. By using TI-H704B flaps, compatibility between insulation and flap material was assured. This concept has been proven during the programs listed in Table XIX.

TABLE XVIII
TI-H704B INSULATION

Composition (percent)

HC Binder and Curing Agents	45
XL-434 Polymeric (HC)	
HX-760	
HX-740	
Asbestos	30
Carbon Black	15
Dibasic Ammonium Phosphate	10

Physical Properties

Density (lb/cu ft)	75
Ultimate Stress Minimum Allowable (psi)	175
Ultimate Strain (in./in.)	150
Hardness (Shore A)	70
Tensile Adhesion to Steel Case (psi)	80

Thermal Properties

Specific Heat (cal/gm-°C)	0.325
Thermal Conductivity (cal/cm-sec-°C)	9.15×10^{-4}
Thermal Diffusivity (sq cm/sec)	2.35×10^{-3}

Processing Properties

Pot Life at 135°F (hr)	1.5 - 2.0
Cure at 135°F (day)	5

TABLE XIX

PREVIOUS USAGE OF TI-H704B AND TL-H714A INSULATION LINER SYSTEM

<u>Motor</u>	<u>Case Size (in.)</u>	<u>Propellant</u>	<u>Average Chamber Pressure During Web Time (psia)</u>	<u>Area of Use</u>
156-2C-1	156	TP-H8163 16% Al/85% Solids HB Polymer	668	Case forward dome, cylinder and aft dome
TU-455.01	65	TP-H1096 16% Al/85% Solids HB Polymer	734	Case forward dome and cylinder
TU-455.02	65	TP-H1096 16% Al/85% Solids HB Polymer	714	Case forward dome and cylinder
TU-418.01	65	TP-H8163 16% Al/85% Solids HB Polymer	598	Case forward dome and cylinder
TU-418.02	65	TP-H8163 16% Al/85% Solids HB Polymer	640	Case forward dome and cylinder and nozzle inlet

- (U) The insulation configuration is shown on Figure 76 (Insulated Case Drawing). The predicted material loss and the insulation design criteria are shown in Figure 77. The predicted material loss rate was based primarily on results reported for the 156-6 motor. When the 156-6 case was received at Thiokol, the insulation was removed. Additional thickness measurements were taken and the results compared to those previously reported. As a result of correlating the Lockheed erosion and gas flow studies*, the 156-9 insulation design thickness was increased to insure thermal protection to all areas of the case. The total thickness including this increase is given in Figure 77. No thermal protection to the case is attributed to the liner.

3. PREVIOUS EXPERIENCE

- (U) Past usage of TI-H704B insulation is shown in Table XIX. Results from the test motors shown on this table and insulation performance from the 156-7 motor were used in predicting insulation performance for the 156-9.

4. WEIGHT ANALYSIS

- (U) The insulation weight is calculated to be 4,817 pounds of which 161 pounds are stress relief flaps.

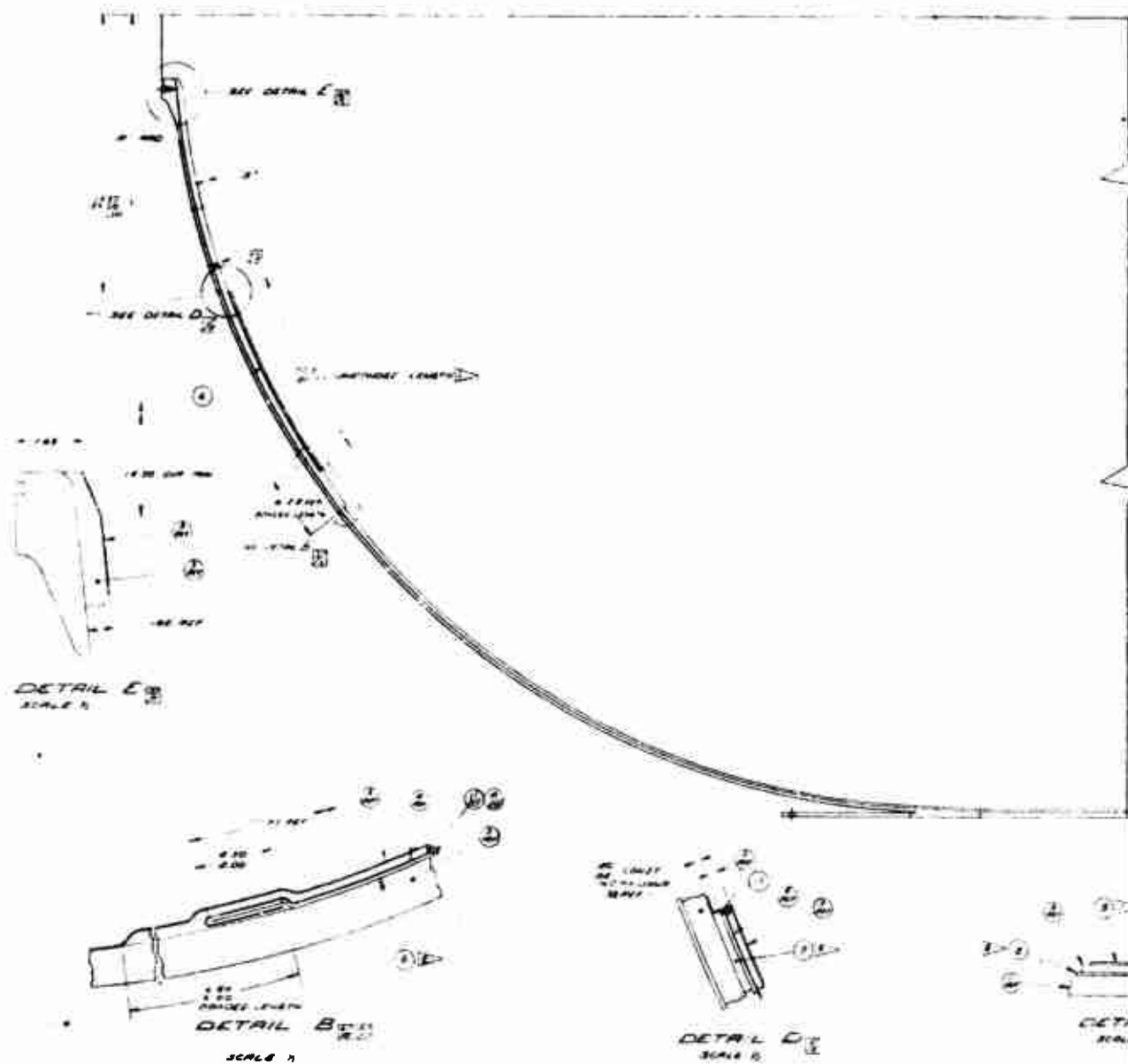
B. LINER DESIGN

1. LINER DESIGN CRITERIA

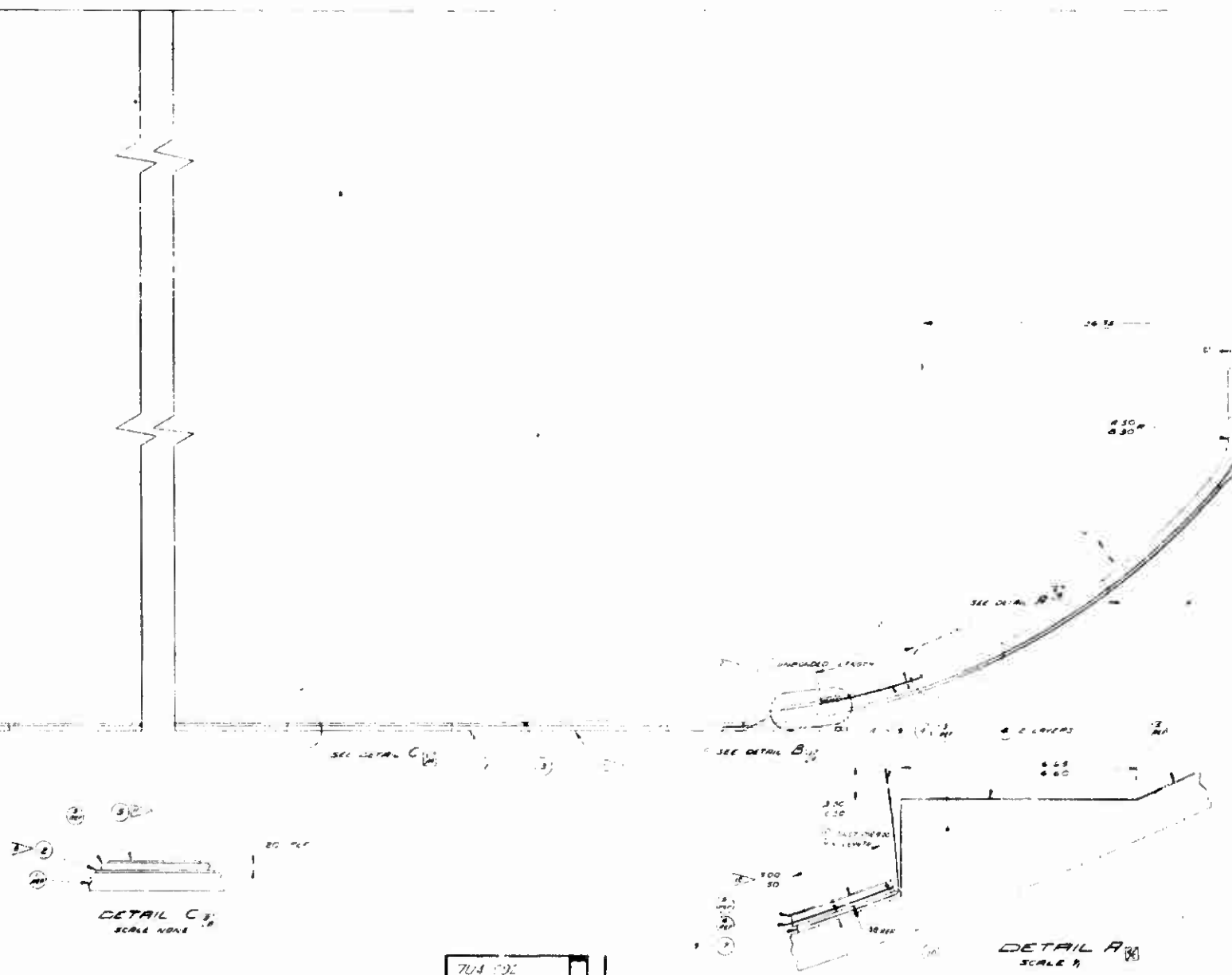
- (U) The liner for the 156-9 had to provide the bond between the TI-H704B insulation and the TP-H1115 propellant. It had to be compatible with long duration high temperature during heat soak and casting (200 hours).

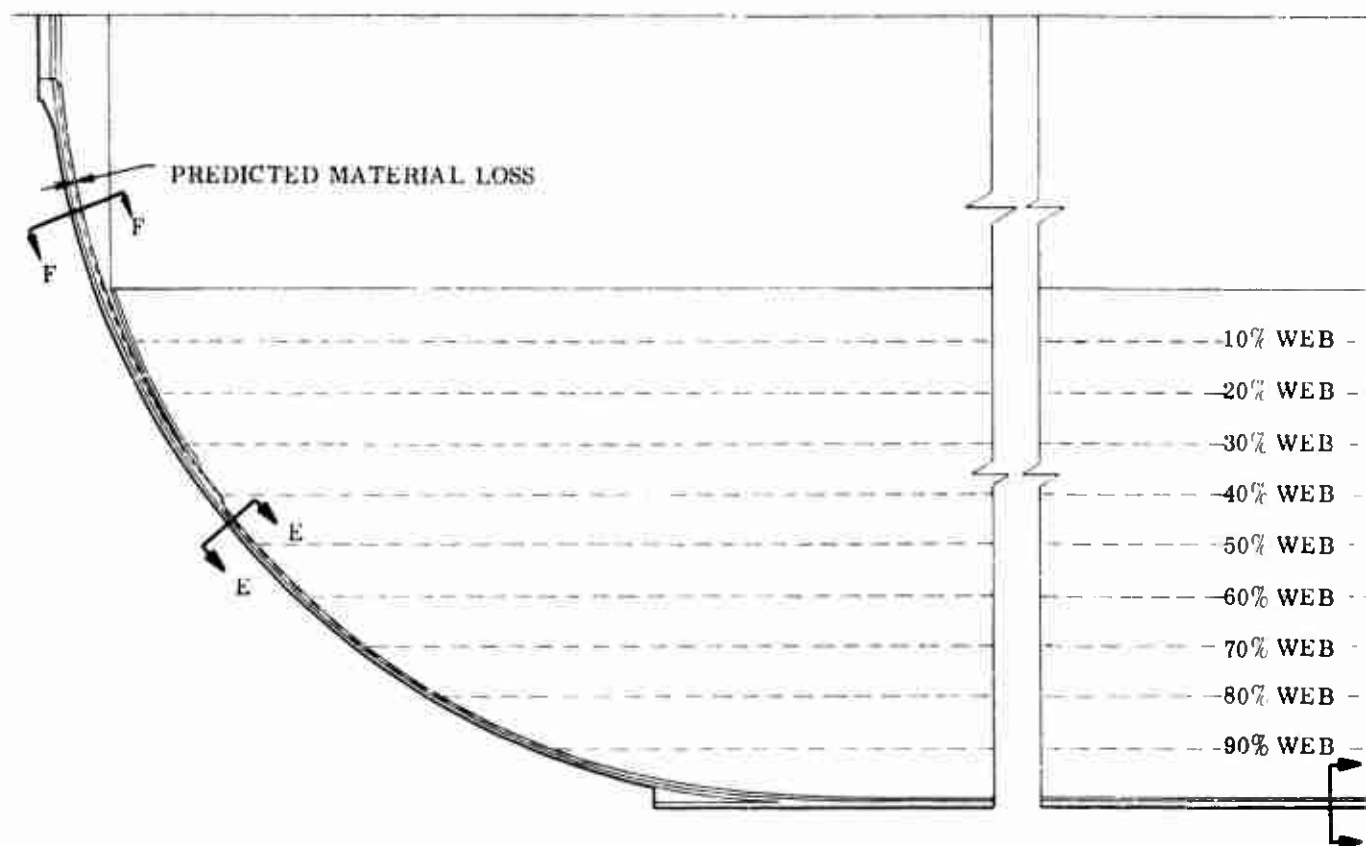
*Technical Report No. AFRPL-TR-66-109 156-Inch Diameter Motor Liquid Injection TVC Program, Volume 1, Book 1. Lockheed Propulsion Company, July 1966.

MEAN	END
STATION	STATION
67.00	0
67.10	10
67.20	20
67.30	30
67.40	40
67.50	50
67.60	60
67.70	70
67.80	80
67.90	90
68.00	100
68.10	110
68.20	120
68.30	130
68.40	140
68.50	150
68.60	160
68.70	170
68.80	180
68.90	190
69.00	200

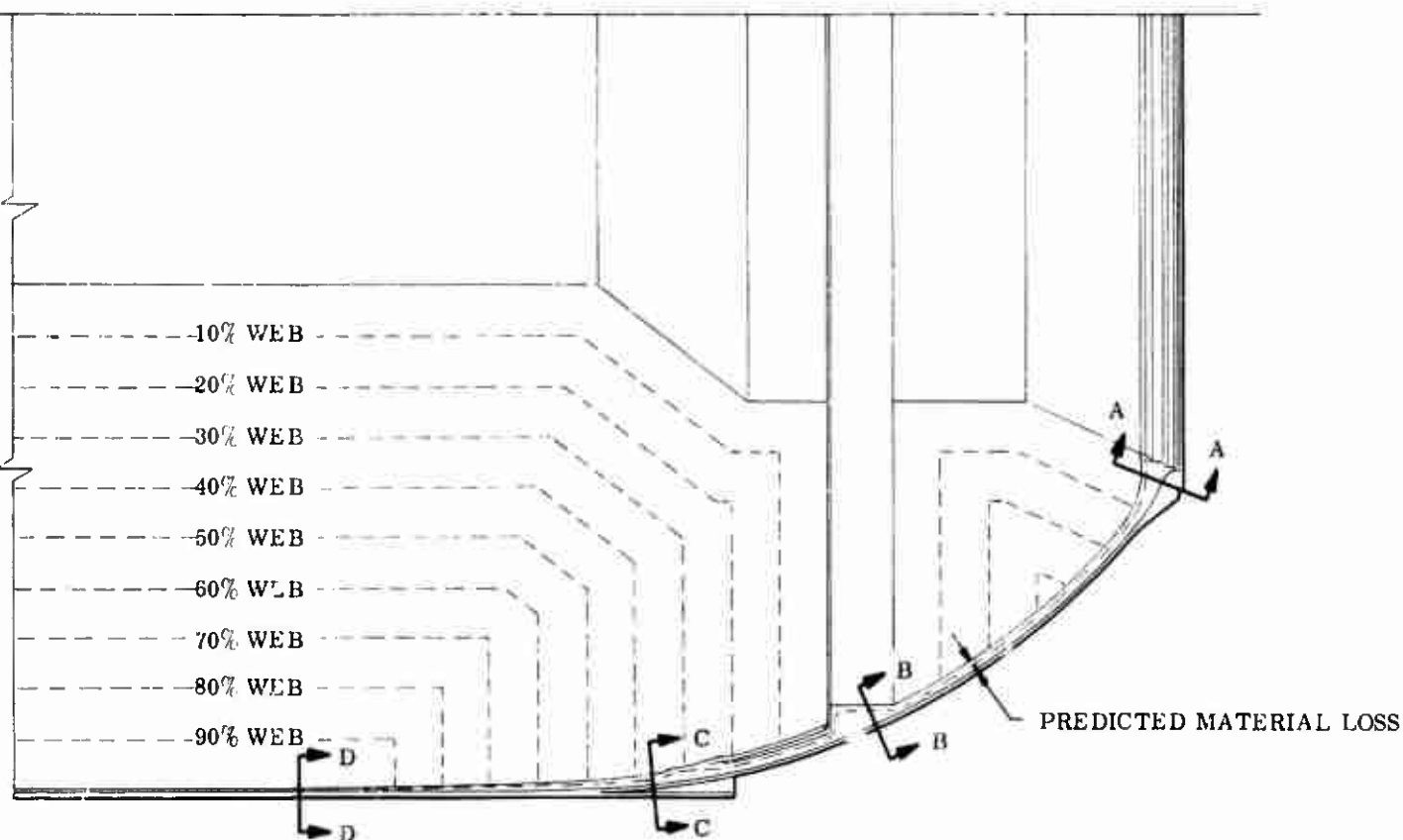


RPT END	
5 00	100
53 40	100
50 40	31
33 40	81
40 40	71
43 40	38
70 10	67
73 50	34
80 40	44
83 30	34
10 30	18
13 40	20





SECTION	PREDICTED EXPOSURE TIME (SEC)	PREDICTED MATERIAL LOSS RATE (MIL/SEC)	PREDICTED THICKNESS FOR EROSION (IN.)	ADD FOR SAFETY FACTOR
A-A	65	10.0	0.520	0.260
B-B	65	10.0	0.520	0.260
C-C	42	10.0	0.420	0.210
D-D	--	--	--	--
E-E	36	4.0	0.144	0.072
F-F	65	4.0	0.260	0.130



THICKNESS FOR PROTECTION (IN.)	ADD FOR SAFETY FACTOR	THERMAL PROTECTION (IN.)	TOTAL THICKNESS REQUIRED (IN.)	DESIGN THICKNESS (IN.)
20	0.260	0.200	0.980	2.40
20	0.260	0.200	0.980	1.19
20	0.210	0.200	0.830	0.99
20	--	0.050	0.050	0.05
44	0.072	0.200	0.416	0.42
60	0.130	0.200	0.590	0.60

13094-5

Figure 77. Insulation Design Information

2. LINER DESIGN AND FORMULATION

- (U) The liner selected was TL-H714. Its formulation is given in Table XX. TL-H714 liner utilizes the same basic binder system as does the insulation. The binder system consists of HC polymer, HX-760 and HX-740 curing agents with carbon black filler. The liner does not contain asbestos floats.
- (U) The design thickness of TL-H714 liner was 0.050 in. to give full coverage. This system resulted in a propellant to insulation bond having a 180 deg peel strength of 7 to 12 pli and a tensile adhesion of 98 to 115 psi.

3. PREVIOUS EXPERIENCE

- (U) TL-H714 liner was developed by Thiokol's Space Booster Division for use in the 260 inch diameter motor program. Since its development, it has been used extensively in development motors listed in Table XIX.

4. WEIGHT ANALYSIS

- (U) The weight of TL-H714A liner applied to the motor case was 310 pounds.

C. VERIFICATION TESTING

1. TYPES OF TESTS

- (U) The compatibility of the TI-H704B insulation, TL-H714A liner and TP-H1115 propellant system was tested to insure that a satisfactory bond between the propellant grain, liner, insulation, and case would exist. The testing verified compatibility of formulations, raw material lots, and processing. The raw material lots and processes planned for use in the motor were used in preparing the test specimens. The tests were divided into four phases as follows.

TABLE XX

TL-H714A LINER

Composition (percent)

HC Binder and Curing Agents	70
XL-434 Polymeric (HC)	
HX-760	
HX-740	

Carbon Black	30
--------------	----

Physical Properties

Density (lb/cu ft)	69
Ultimate Stress Minimum Allowable (psi)	175
Ultimate Strain (in. /in.)	200
Hardness (Shore A)	40
Tensile Adhesion to Insulation (psi)	80
Tensile Adhesion to Propellant (psi)	80

Thermal Properties

Specific Heat (cal/gm-°C)	0.375
Thermal Conductivity (cal/cm-sec-°C)	6.28×10^{-4}
Thermal Diffusivity (sq cm/sec)	1.52×10^{-3}

Processing Properties

Cure Time at 135°F (day)	6
--------------------------	---

1. Phase I was to verify the bond strength of TI-H704B insulation to steel and Koropon coated steel.
2. Phase II was to verify the bond strength of insulation to liner to propellant.
3. Phase III was to verify the effect of liner cure on liner to propellant bond strength.
4. Phase IV was to verify the compatibility of insulation to liner to propellant bond strength as affected by liner cure conditions.

(U) Phase IVA was conducted just prior to casting propellant into the motor when it was learned that casting time would possibly be longer than expected. The purpose of Phase IVA testing was to verify that the liner surface could be satisfactorily activated with fresh liner if propellant casting time became extensive.

(U) Four types of standard physical tests were used in insulation to liner to propellant compatibility verification. They were:

1. Peel, 180 deg;
2. Tensile adhesion, tenshear;
3. Adhesion cup;
4. Lap shear.

(U) a. 180 Degree Peel Test--This test is used to determine the comparative peel or stripping characteristics of adhesives. Results are expressed in average load per unit width of bond required to separate one material from the adhered surface at a separation angle of approximately 180 degrees. Units are pounds per linear inch. The test specimen consists of a piece of flexible material which is bonded to a steel plate or to a slab of insulation or propellant by the formulation under test. Testing is completed in a power driven machine which can apply tension at a uniform rate and can record the applied load. The apparatus and test is detailed in Federal Test Standard No. 175 (Figures 78 and 79).

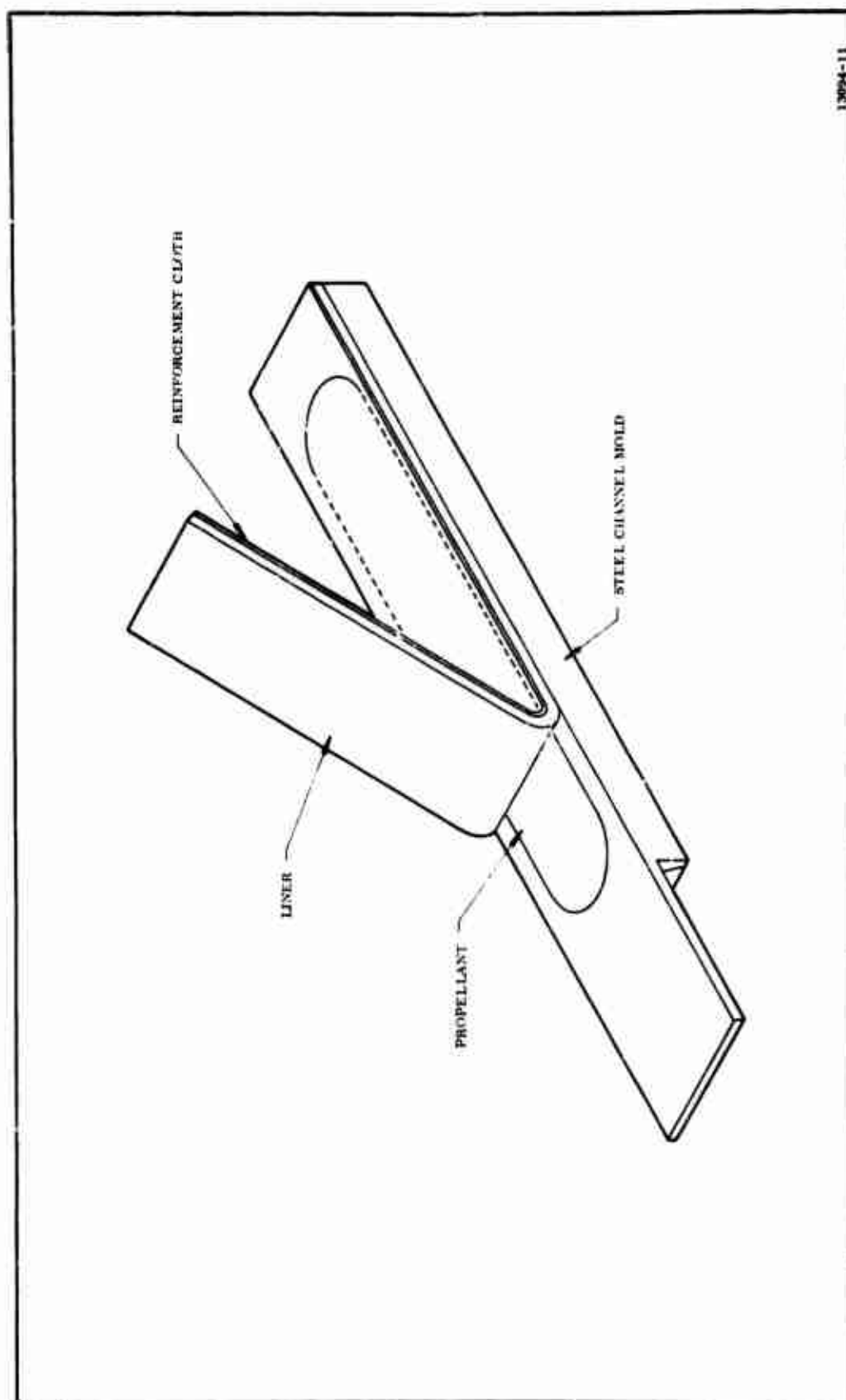


Figure 78. 180 Degree Peel Test Specimen

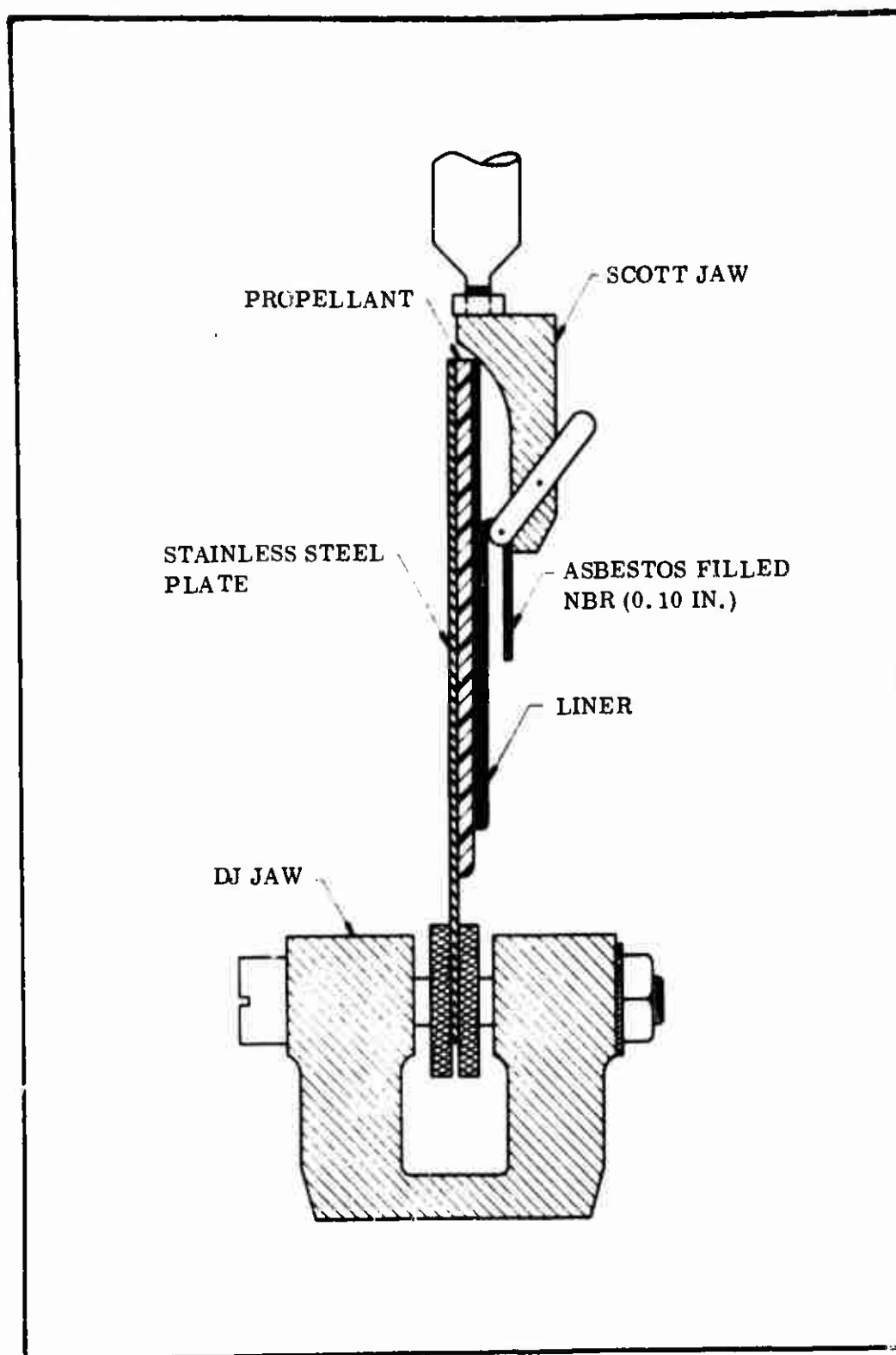
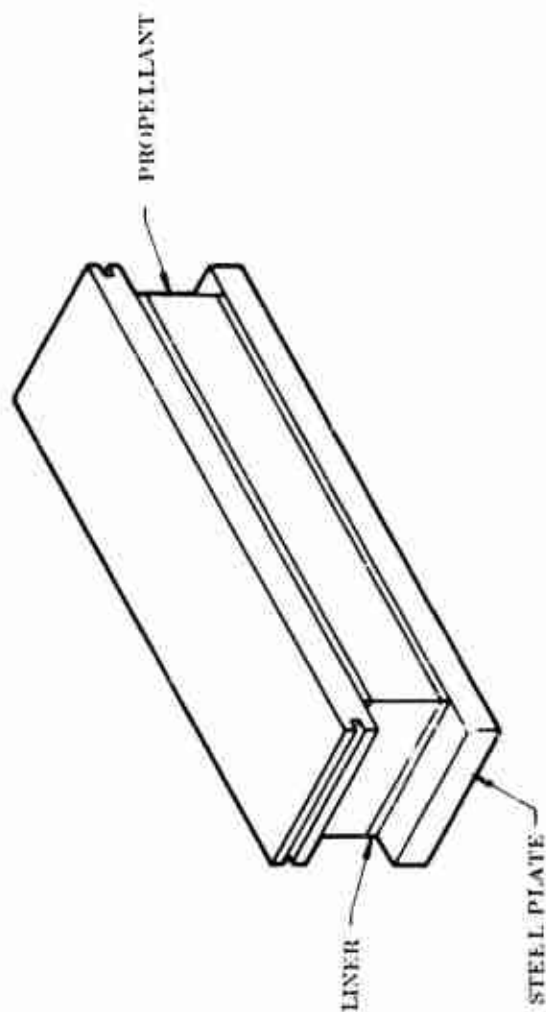


Figure 79. 180 Degree Peel Test Specimen and Arrangement

- (U) b. Tensile Adhesion, Tenshear--In this test, two steel plates (2 by 4 in.) are bonded together with a fixed area and fixed liner, propellant, glueline thickness (Figures 80 and 81). Testing is completed using an Instron tensile tester and the force required to separate the plates is recorded.
- (U) c. Adhesion Cup--This specimen consists of a 2 by 2 in. steel plate to which liner, insulation, or other substrate materials are applied. A Teflon spacer is placed on the plate to circumscribe a definite area of adhesion. A 2 in. diameter steel tube is placed on the Teflon spacer and filled with propellant or other adherent (Figure 82). Force is applied by an Instron tensile tester and the amount required to separate the tube from the plate is recorded.
- (U) d. Lap Shear--This test specimen consists of two 1 by 4 in. steel plates overlapping each other at 180 degrees. The adherent is placed on the last inch of the overlapping plates. The double lap shear consists of a third 1 by 4 in. plate placed above and parallel to the bottom plate (Figure 83). Force is applied by an Instron tensile tester and the amount required to separate the plates is recorded.

2. TEST PROCEDURE

- (U) General specimen process requirements were to simulate predicted processing of the 156-9 motor except where specified otherwise. All samples were coated with Koropon, Lot No. 9505-0008.
- (U) The adhesion cups, shear, and tenshear samples were pulled at 0.5 in./min and the 180 deg peel samples at 12.0 in./min on an Instron tester.
- (U) a. Phase I Tests--The purpose of the Phase I testing was to verify the bond strength of TI-H704B insulation at the steel interface under motor conditions. Two sets of samples were prepared and tested as follows:
1. Adhesion plates and lapshear plates were sandblasted and hand degreased with Trichlorethylene. One set was sprayed with Koropon, and air dried 5 hours at $80 \pm 20^\circ\text{F}$. A second coat of Koropon was applied and cured 303 hours at $80 \pm 20^\circ\text{F}$.



13094-14

Figure 80. Tensile Adhesion, Tenshear

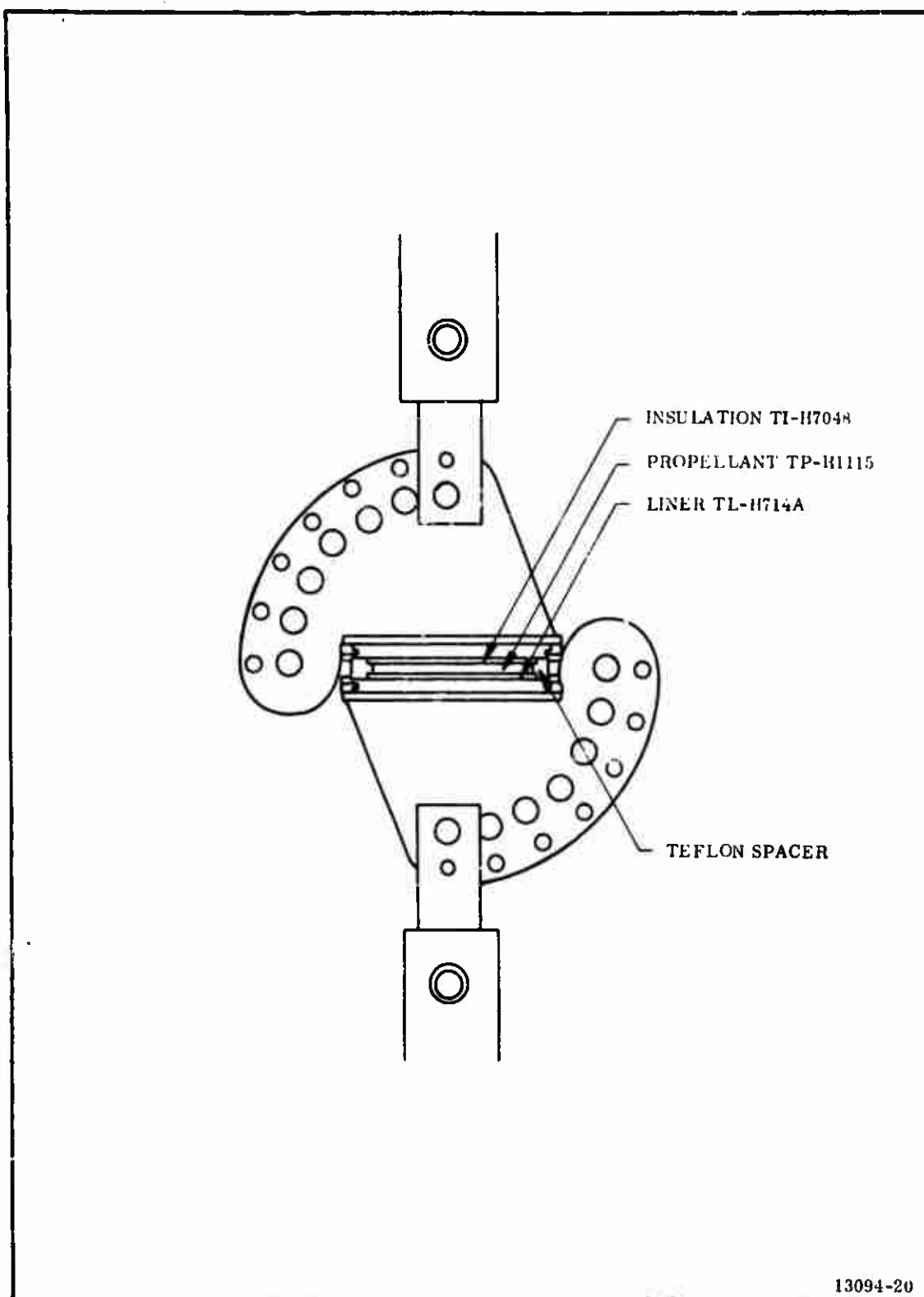


Figure 81. Tenshear Test Apparatus

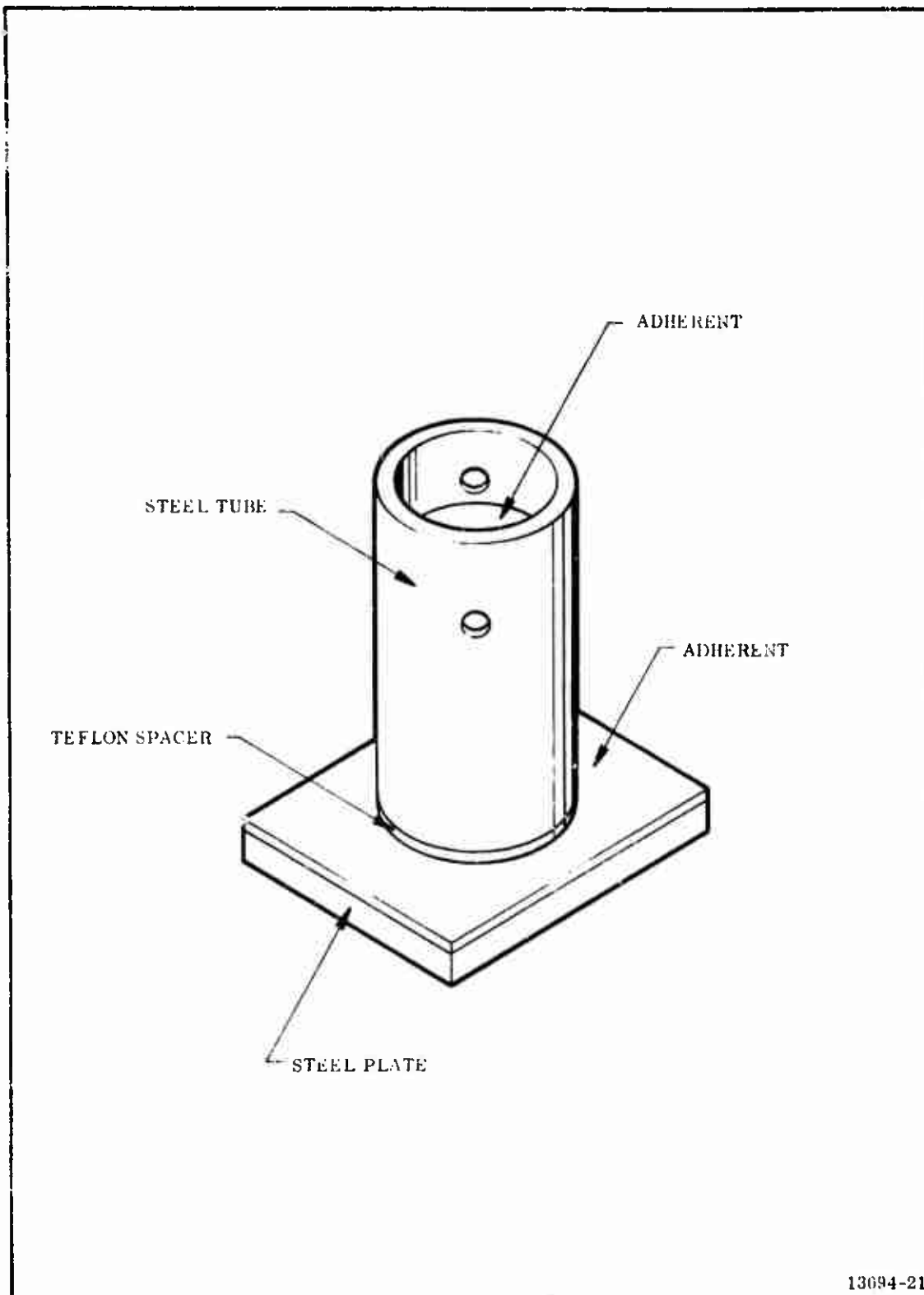


Figure 82. Adhesion Cup Test Specimen

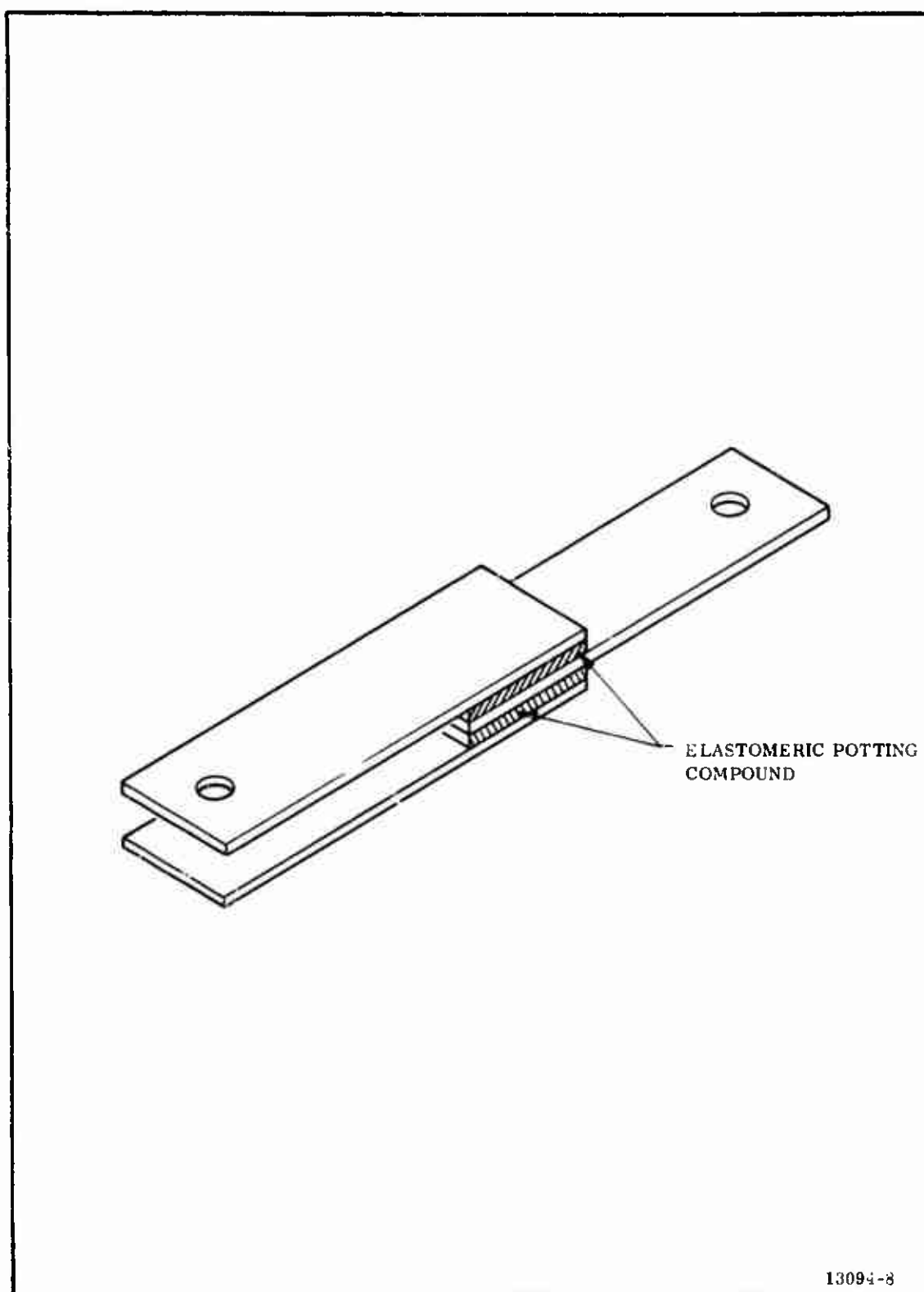


Figure 83. Lap Shear Adhesion Test Specimen

2. TI-H704B insulation 0.15 in. thick was used to assemble the lapshear samples and to fill the adhesion cups on the plates.
3. The samples were cured 148 hours at $80 \pm 20^\circ\text{F}$ plus 228 hours at $135 \pm 5^\circ\text{F}$ to simulate motor conditions.
4. The samples were pulled on an Instron tester at the rates listed above.

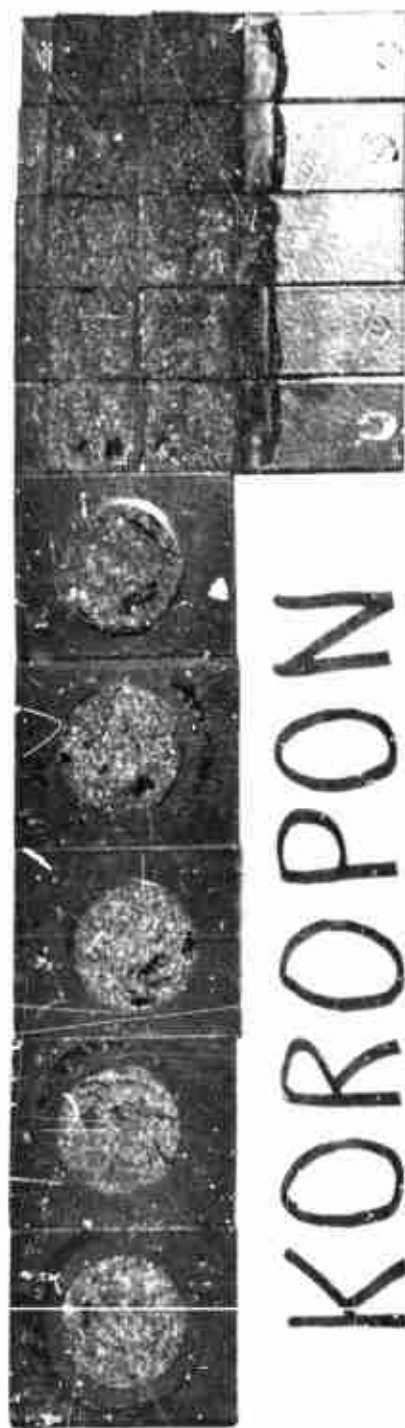
(U) The following is a matrix showing the specimen composite and the results therefrom.

	Sample Test Set	
	<u>No. 1</u>	<u>No. 2</u>
Primer	Koropon	None
Insulation	TI-H704B	TI-H704B
Conditions	Prime steel plate with Koropon; apply 0.15 in. thick layer of TI-H704B insulation and cure.	Apply 0.15 in. thick layer of TI-H704B insulation and cure.
Number Adhesion Cups	5	5
Average value (psi)	377	382
Range (psi)	28	28
Number Lap Shear Tests	5	5
Average value (psi)	287	294
Range (psi)	5	12

(U) There was no difference in the shear strength of TI-H704B insulation to steel (set No. 2) and TI-H704B insulation to Koropon coated steel (set No. 1). There was a small amount of bond failure on the plain steel samples (Figure 84).

(U) b. Phase II Tests--The purpose of the Phase II testing was to determine the bond strength between insulation, liner, and propellant. The specimens were prepared as follows:

1. Adhesion plates and tenshear plates were cleaned and coated with Koropon as in Phase I, Step 1.



KOROPON



STEEL
PHASE I

Figure 84. Phase I Test Specimens

2. TI-H704B insulation was applied 0.15 in. thick to the plates and cured 146 hours at $80 \pm 20^\circ\text{F}$.
3. TL-H714A liner was applied 35 mils (nominal) thick to the plates prepared in Step 1 and 2. A piece of broadcloth was added for 180 deg peel samples. The liner was cured 34 hours at $135 \pm 5^\circ\text{F}$ plus 50 hours at $135 \pm 5^\circ\text{F}$ at 1 ± 0.2 in. Hg absolute pressure. Between the 6th and 16th hour the pressure varied between 1.0 and 2.4 in. Hg because of a leak in the vacuum line.
4. TP-H1115 propellant was cast on the samples within 1 hour after the liner cure and the propellant was cured 143 hours at $135 \pm 5^\circ\text{F}$.
5. The samples were pulled on an Instron tester.

(U) The following matrix shows the Phase II specimen composite and the results therefrom:

Insulation	TI-H704B
Condition	Cured
Liner	TL-H714A
Condition	Cured
Propellant	TP-H1115
180 deg Peel Tests	4
Average value (pli)	11.8
Range (pli)	0.3
Tenshear Tests	4
Average value (psi)	105
Range (psi)	11
Adhesion Cup	5
Average value (psi)	105
Range (psi)	7

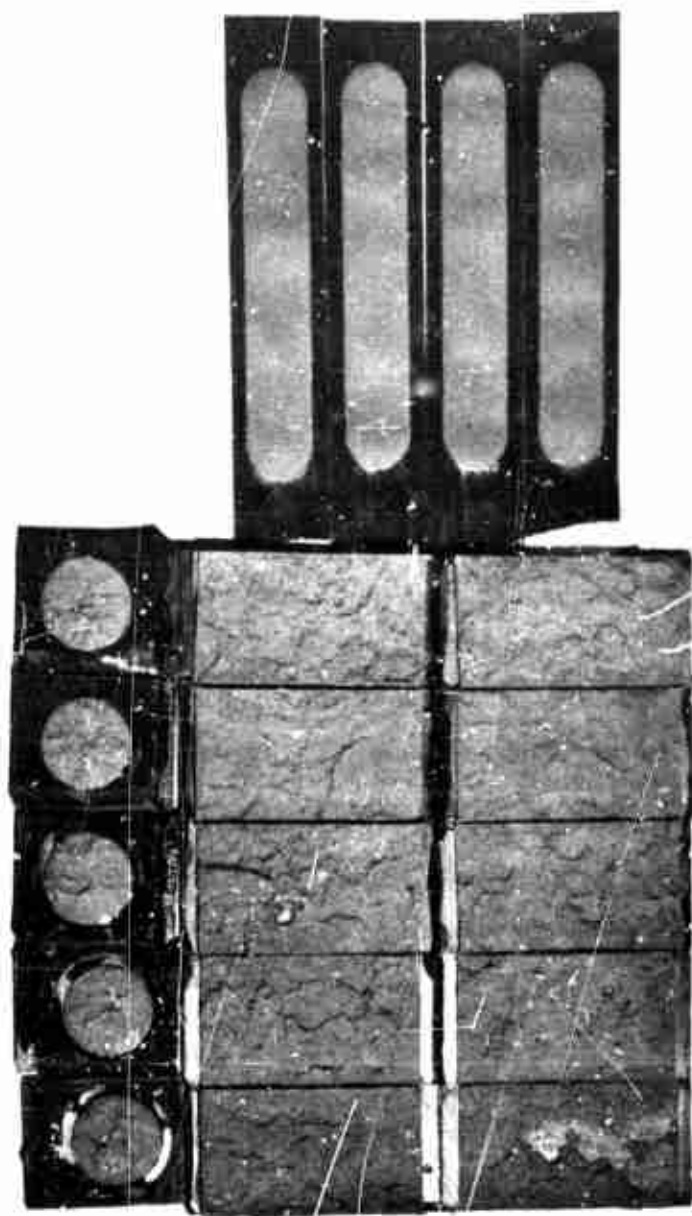
(U) TP-H1115 propellant adhesion to TL-H714A lined TI-H704B insulation resulted in acceptable bond strength with the desirable failure occurring in the propellant (Figure 85).

(U) c. Phase III Tests--The purpose of the Phase III testing was to determine the effects of liner cure upon liner bond strength. Five sets of specimens were prepared in the following manner.

1. Tenshear plates were cleaned and coated with Koropon as in Phase I, Step 1.
2. TI-H704B insulation was applied 0.15 in. thick to the tenshear plates and broadcloth added for the 180 deg peel samples. The samples were cured 146 hours at $80 \pm 20^\circ\text{F}$.
3. TL-H714A liner was applied 35 mils (nominal) thick to the TI-H704B insulation. The samples were cured for 48, 72, 120, 144, and 200 hours at $135 \pm 5^\circ\text{F}$.
4. TP-H1115 propellant was cast on the samples within 1 hour after the liner had cured on the 48, 72, 120, and 144 hour samples and within 12 hours after the liner had cured on the 200 hour samples. The propellant was then cured 144 hours at $135 \pm 5^\circ\text{F}$.
5. The samples were pulled on an Instron tester.

(U) The following matrix shows the specimen composite, their processing and the results therefrom:

	Sample Test Set				
	No. 1	No. 2	No. 3	No. 4	No. 5
Insulation	TI-H704B				
Condition	Cured				
Liner	TL-H714A				
Cure condition at 135°F prior to casting (hr)	48	72	120	144	200



PHASE II

Figure 85. Phase II Test Specimens

	Sample Test Set				
	No. 1	No. 2	No. 3	No. 4	No. 5
Propellant	← TP-H1115 →				
180 deg Peel Tests	4	4	4	4	4
Average value (pli)	11.8	9.9	9.0	9.1	7.4
Range (pli)	0.5	0.5	0.9	0.6	0.6
Tenshear Tests	5	5	5	5	5
Average value (psi)	107	110	107	103	98
Range (psi)	13	7	6	4	4

(U) The Phase III tests indicated there would be a slight decrease in the bond strength of TP-H1115 propellant to TL-H714A lined TI-H704B insulation as the liner cure increases prior to casting propellant. After 48 hours of cure at 135° F, adhesion was 107 psi versus 98 psi at 200 hour cure. Peel strength decreased with increased liner cure (11.8 lb/in. at 48 hour cure to 7.4 lb/in. at 200 hour cure). The amount of propellant on the peel samples also decreased as the liner cure increased.

(U) d. Phase IV Tests--The purpose of the Phase IV testing was to verify the compatibility of liner cure conditions. Three sets of samples were prepared as follows:

1. Adhesion plates were cleaned and coated with Koropon as in Phase I, Step 1.
2. TI-H704B insulation was applied 0.15 in. thick to the plates and broadcloth added for the 180 deg peel samples. The samples were cured 146 hours at $80 \pm 20^\circ \text{F}$.
3. TL-H714A liner was applied 25 mils (nominal) thick to the TI-H704B insulation and cured 34 hours at $135 \pm 5^\circ \text{F}$. The samples in test set No. 1 were cured for an additional 5 hours. The samples in test sets No. 2 and 3 were cured for an additional 50 hours at $135 \pm 5^\circ \text{F}$ at 1 ± 0.2 in. Hg absolute pressure. Between the 6th and 16th hour the pressure varied between 1.0 and 2.4 in. Hg because of

a leak in the vacuum line. Sample test set No. 3 was cured an additional 72 hours at $135 \pm 5^\circ \text{F}$ (no vacuum).

4. TP-H1115 propellant was cast on the samples within 1.5 hours after the liner cure. The propellant was cured 144 ± 1 hour at $135 \pm 5^\circ \text{F}$.
5. The samples were pulled on an Instron tester.

(U) The following matrix shows the specimen composite, processing cycle used, and the results of the tests.

	Sample Test Set		
	No. 1	No. 2	No. 3
Substrate	Steel		
Primer	Koropon		
Insulation	TI-H704B		
Liner	TL-H714A		
Cure Conditions	34 hr at $135 \pm 5^\circ \text{F}$		
	5 hr at 1 in. Hg	50 hr at 1 in. Hg	50 hr at 1 in. Hg
	--	--	72 hr at $135 \pm 5^\circ \text{F}$
Propellant	TP-H1115		
Cure Conditions	144 hr at 135°F		
Number 180 deg Peel Tests	4	4	4
Average value (pli)	12.8	11.6	10.5
Range (pli)	0.4	1.2	0.8
Number Adhesion Cup Tests	5	5	5
Average value (psi)	104	106	99
Range (psi)	1.1	0.8	1.0

(U) TP-H1115 propellant adhesion to TL-H714A liner that was subjected to the additional 5 and 50 hour cure at 1 inch Hg vacuum exhibited equal bond strengths (104 vs 106 psi). Peel strength tests (180 deg) under the same conditions decreased slightly (12.8 vs 11.6 lb/in.) Subjecting the 50 hour, 1 inch Hg

samples to an additional 72 hour cure decreased their adhesion to 99 psi and their 180 deg peel strength to 10.5 lb/in. All samples failed with 100 percent heavy propellant film.

- (U) e. Phase IVA Tests--The purpose of the Phase IVA testing was to assess the effect of applying fresh liner to old liner if propellant casting time became excessive.

The samples were prepared as follows:

1. Adhesion plates and broadcloth were coated with TL-H714A liner and cured 8 days at $135 \pm 5^\circ \text{F}$.
2. Fresh TL-H714A liner was used to brush coat one set of samples prepared in Step 1. An additional set was prepared on plates and broadcloth using fresh liner only.
3. The samples were all cured one day at $135 \pm 5^\circ \text{F}$ and TP-H1115 propellant (from the motor casting) was cast on all samples and cured 6 days at $135 \pm 5^\circ \text{F}$.
4. The 180 deg peel samples were pulled at 12.0 in./min and adhesion samples at 0.5 in./min on an Instron tester.

- (U) The following matrix shows the specimen composite, processing cycle used, and the results of the tests:

	Sample Test Set		
	No. 1	No. 2	No. 3
Substrate	Steel	Steel	Steel
Liner	TL-H714A	TL-H714A	--
Original Cure (Days)	8	8	--
Recoated	--	TL-H714A	TL-H714A
Final Liner Cure (Days)	--	1	1
Propellant Cast	← TP-H1115 →		
Propellant Cure (Days)	6	6	6
180 deg Peel Tests	2	3	3
Average value (pli)	5.7	15.9	15.5
Range (pli)	0.1	2.1	1.4

	Sample Test Set		
	No. 1	No. 2	No. 3
Adhesion Plates	6	6	6
Average value (pli)	107	110	103
Range (pli)	13	5	18

- (U) The tensile adhesion shows no difference in bond strength of the 8-day cured liner compared to the one-day cured liner - 107 versus 103 psi. Failures did show a difference. There were samples in the 8-day group that showed interface failures.
- (U) Peel strength was greatly affected by the liner age. The 8-day cured liner had a propellant to liner peel strength of 5.7 lb/in. compared to 15.5 and 15.9 lb/in. for the one-day cured liner.

D. INSULATION AND LINER INSTALLATION

1. INSULATION APPLICATION

- (U) The application of the TI-H704B insulation was performed in the Case Preparation Facility. The material was mixed in 80-quart capacity Readco and Hobart mixers, deaerated and extruded into logs three inches in diameter. Because uncured insulation is extremely viscous and glutinous, the mix bowls were modified by adding an outlet to the bottom of the bowl to allow direct transfer of the mixed insulation to the vacuum deaeration chamber (Figure 86). After deaeration, the material was extruded (Figure 87) for ease in handling and installed manually in the case. Once in position in the case the material was worked to required thickness by hand and pneumatic hammers.
- (U) a. Propellant Slot Former Fabrication--Using a template which mounted on the nozzle boss and pivoted about the case centerline, the plaster slot former mold was swept into the case. After a 48 hour cure at ambient temperature, excess plaster was removed from the slot former support area between the two mold halves.



Figure 86. Modified TI-H704B Mixing Bowl Mounted on Vacuum Deaeration Chamber

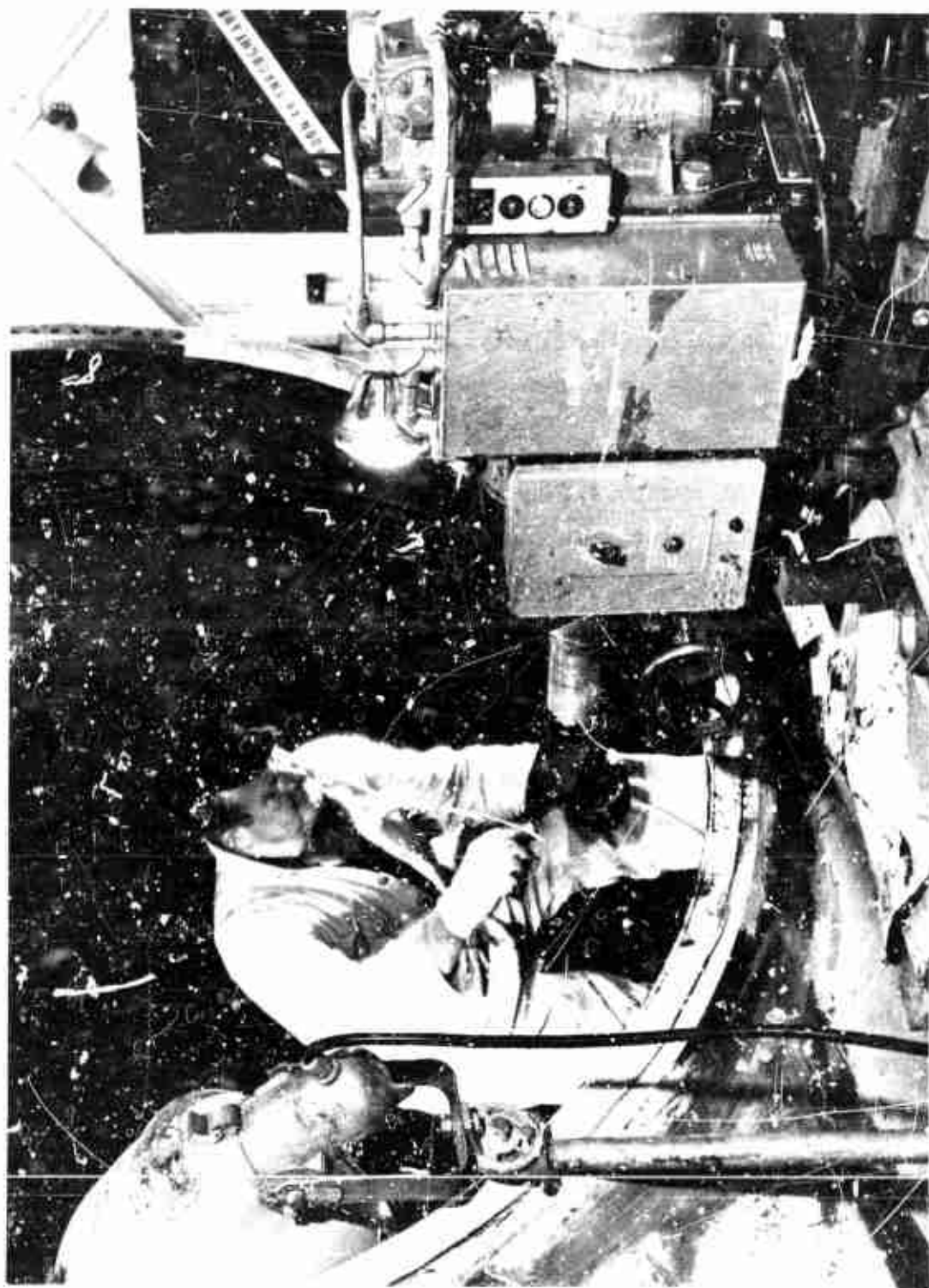


Figure 87 Extruding TI-H704B Insulation for Ease in Handling

The Koropon film was slightly damaged during plaster removal and was subsequently repaired by brushing fresh Koropon on the damaged areas and curing for 133 hours. The mold surfaces were subsequently covered with Teflon tape.

- (U) TI-H704B insulation was then prepared, as described above, applied to the area between the mold halves, compacted using pneumatic hammers, covered with polyethylene and worked with hand rollers until level and flush with the top surface of the plaster mold. Seven mixes were required to fill the mold.
- (U) The insulation was cured for 61 hours at ambient temperature, after which the plaster mold was chipped away leaving the finished slot former support ring (Figure 88).
- (U) The main motor chamber was insulated using 63 mixes of TI-H704B insulation applied by the same process as previously described (Figure 89). After cure at ambient temperature for 96 hours, the igniter and nozzle boss mold rings were installed. Six mixes were required to build the insulation configuration at the ports (Figure 90). The mold rings were removed after 48 hours of cure.
- (U) b. Propellant Relief Flap Fabrication--The propellant relief flaps at the head end and at the slot former support were fabricated of reinforced TI-H704B insulation. Layers of insulation, fiberglass, polyethylene, and broadcloth were installed as required to form the specified configuration. The flaps were fabricated in place, on the motor, and cured for 48 hours at ambient temperature. Thirteen mixes were required.
- (U) The aft relief flap was secured by placing strips of vacuum putty between the flap and the case insulation and by securing the broadcloth, molded into the end of the flap, to the slot former support ring. The forward flap was not secured at this time. Upon completion of these operations the case was shipped to the casting pit complex for lining.



Figure 88. Slot Former Support Ring after Plaster Mold Removal

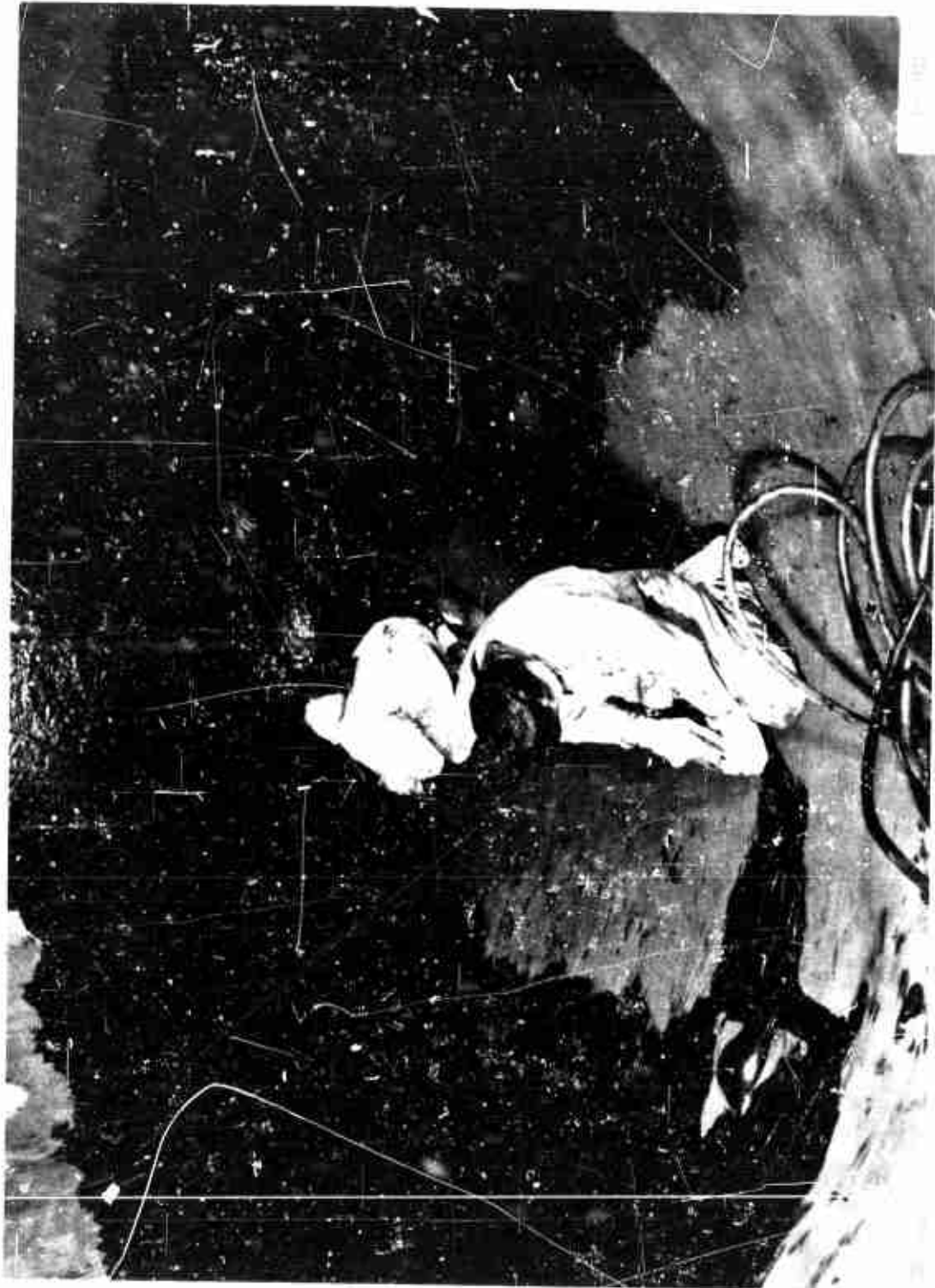


Figure 89. Insulating the 156-9 Motor Case



Figure 90. Applying Insulation at the Nozzle Mold Ring

2. LINER APPLICATION

- (U) The case was installed vertically in Pit M-49 and the forward relief flap was trimmed to the core diameter and packed with vacuum putty. A Model "A" sling liner, with a six slotted, nine inch diameter disc, was positioned over the case (Figure 91). Three mixes of TI-H714A liner were prepared and applied to the case through the sling liner. Upon completion of the sling lining operation, the aft 12 in. of the aft dome was brush lined with a 10 pound batch of liner. A total of 346 pounds of liner was mixed and 303 pounds applied to the case resulting in a liner with a nominal thickness of 0.050 inch.
- (U) The liner was cured for 8 hours at ambient temperature and 24 hours at 135° F. Inspection of the liner after cure revealed no defects. Cured liner, which had bridged between the forward flap and the insulation, was trimmed to assure that the flap would function after propellant cure and cooldown.

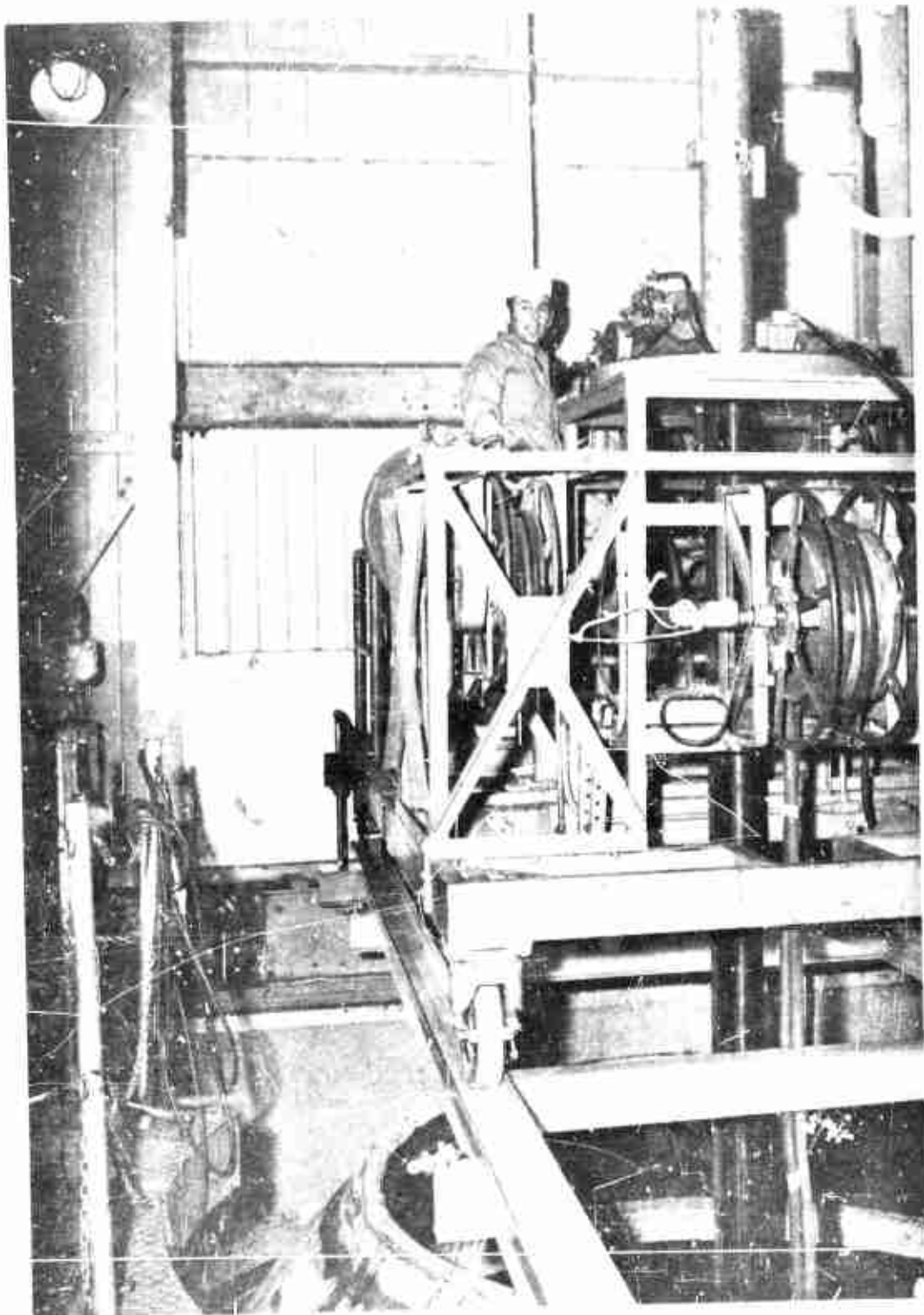


Figure 91. Liner Application Arrangement

CONFIDENTIAL
(THIS PAGE IS UNCLASSIFIED)

SECTION VII

PROPELLANT DESIGN AND PROCESSING

A. PROPELLANT DESIGN

1. PROPELLANT DESIGN CRITERIA

- (U) The propellant design criteria were influenced by the case, nozzle, and casting tooling. A study of these influencing factors dictated a propellant which would produce a maximum action time of 70 sec and an MEOP no greater than 885 psi. The propellant was required to be of the polybutadiene/AP/Al family of propellants, exhibit an acceptable degree of reproducibility of both physical and ballistic properties, and have a class 2 explosive characteristic.

2. FORMULATION AND PROPERTIES

- (U) The propellant for the 156-9 was designated TP-H1115. It contained (polybutadiene, acrylic acid, acrylonitrile) terpolymer binder, ammonium perchlorate oxidizer, and aluminum metal additive. The propellant formulation is given in Table XXI, physical properties are given in Table XXII, and ballistic properties are given in Table XXIII.

CONFIDENTIAL
(THIS PAGE IS UNCLASSIFIED)

CONFIDENTIAL

TABLE XXI

PROPELLANT CHARACTERISTICS TP-H1115

<u>Formulation</u>	<u>Percent</u>
HB/ECA Binder and Curing Agent	13
Aluminum Fuel	18
Ammonium Perchlorate Oxidizer	68
Iron Oxide Burning Rate Catalyst	1

TABLE XXII

PHYSICAL PROPERTIES OF TP-H1115 PROPELLANT

	<u>Percent</u>
Modulus	450
Maximum Stress	100
Strain at Maximum Stress (in. /in.)	0.21
Strain at Cracking (in. /in.)	0.37
Density (lb/in. ³)	0.065

CONFIDENTIAL

TABLE XXIII

TP-H1115 PROPELLANT BALLISTIC PROPERTIES

Characteristic Velocity (ft/sec)	5,161
Ratio of Specific Heats	1.18
Flame Temperature (chamber, °F)	5,944
Flame Temperature (throat, °F)	5,581
Flame Temperature (exit, °F)	3,707

3. PREVIOUS EXPERIENCE

- (U) TP-H1115 propellant was developed specifically for use in the 156-9 motor. It was, however, formulated using the same binder system as the Minuteman propellant. Ferric oxide was added to the formulation to increase burning rate as has been done in past motors. Because of the much higher burning rate requirements (0.717 in. /sec at 700 psia) in a TU-131 motor, a special fine oxidizer (5 micron) fraction was included with an unground fraction. Special fine oxidizer had not previously been ground or handled in large scale at Wasatch Division.

B. PROPELLANT STANDARDIZATION AND VERIFICATION

- (C) Ballistic and physical property requirements for TP-H1115 propellant are as follows:

TU-131 r_b	-----	0.717 in. /sec at 700 psia
$E_{2.6}$	-----	450 psi

- (C) The ballistic and physical properties obtained from all mixes manufactured are summarized in Table XXIV.

CONFIDENTIAL

(THIS PAGE IS UNCLASSIFIED)

TABLE XXIV

SUMMARY OF BALLISTIC AND PHYSICAL PROPERTIES TP-H1115 PROPELLANT EVALUATION 518

Mix Number	Special Fine AP (%)	HB (%)	Strand	T10-131	T10-131	δm (psi)	2,6 ϵ_R (%)	2,6 ϵ_m (%)	E 2,6 (psi)	Density (lb/in. ³)
			r_b (1,500 psia) (in./sec)	r_b (Kn 93.6) (in./sec)	r_b (700 psia) (in./sec)					
Standardization										
5185001	50	88.0	1.066	0.849	0.815	170	35	28	774	0.0653
5185002	40	88.0	0.886	0.564	0.629	160	34	28	754	0.0652
5185003	45	87.5	0.978	0.657	0.688	119	40	31	498	0.0652
5185004	50	87.0	1.061	0.781	0.765	98	42	34	382	0.0656
5185005	40	87.0	0.899	0.577	0.640	98	44	36	366	0.0654
Verification										
5186001	47	87.7	0.979	0.649	0.673	118	38	32	475	0.0651
5186002	47	87.7	1.021	0.708	0.715	130	38	30	567	0.0652
5186003	47	87.7	0.995	0.708	0.719	114	42	32	457	0.0651
Production										
5180001	48	87.7	1.044	0.731	0.722	91	46	35	339	0.0651
5180036	47	87.7	1.029	0.718	0.717	98	34	29	421	0.0651
5180002	48	87.7	1.053	--	--	--	--	--	--	--
5180037	47	87.7	1.038	--	--	89	36	32	550	0.0652
5180003	46	87.7	1.007	--	--	90	36	32	340	0.0651
5180007	47	87.7	1.026	--	--	86	44	34	330	0.0652
5180004	46	87.7	1.020	--	--	88	43	31	324	0.0652
5180009	47	87.7	1.036	--	--	02	48	36	332	0.0652
5180010	46	87.7	1.017	0.677	0.690	106	42	36	374	0.0651
5180041	46	87.7	0.994	--	--	104	46	34	388	0.0652
5180005	46	87.7	1.006	0.672	0.688	107	30	30	430	0.0651
5180042	46	87.7	1.005	--	--	93	44	34	350	0.0651
5180043	46	87.7	1.041	--	--	96	42	34	364	0.0652
5180006	46	87.7	1.040	--	--	105	32	30	420	0.0652
5180044	46	87.7	1.055	0.726	0.719	115	36	31	464	0.0651
5180045	46	87.7	1.026	0.685	0.694	98	44	33	388	0.0652
5180007	46	87.7	1.018	--	--	86	46	36	315	0.0651
5180046	46	87.7	1.009	--	--	102	40	34	384	0.0652
5180047	45	87.7	0.986	--	--	76	55	39	252	0.0650
5180018	45	87.7	1.001	--	--	110	36	33	416	0.0651
5180049	45	87.7	0.987	--	--	94	46	35	348	0.0652
5180050	45	87.7	1.002	0.665	0.683	97	46	35	363	0.0652
5180008	45	87.7	0.977	--	--	86	38	35	307	0.0651
5180051	45	87.7	0.999	0.682	0.693	95	42	33	386	0.0652
5180009	45	87.7	0.989	--	--	90	46	34	350	0.0651
5180052	45	87.7	0.987	--	--	96	44	34	380	0.0652
5180053	45	87.7	0.993	--	--	103	42	32	415	0.0651
5180010	45	87.7	1.012	0.574	0.687	83	42	34	322	0.0651
5180011	46	87.7	1.001	--	--	92	45	36	317	0.0651
5180054	46	87.7	1.011	--	--	104	42	36	408	0.0651
5180055	46	87.7	1.007	0.683	0.693	102	46	36	384	0.0651
5180056	46	87.7	1.018	--	--	118	39	34	496	0.0651
5180012	46	87.7	0.981	--	--	102	44	36	383	0.0651
5180057	46	87.7	1.016	--	--	114	36	30	470	0.0652
5180013	46	87.7	1.010	--	--	95	42	34	351	0.0651
5180058	46	87.7	1.010	--	--	92	36	34	342	0.0652

CONFIDENTIAL

(THIS PAGE IS UNCLASSIFIED)

TABLE XXIV(Cont)

SUMMARY OF BALLISTIC AND PHYSICAL PROPERTIES TP-11115 PROPELLANT EVALUATION 518

Mix Number	Special Fine AP (%)	HB (%)	Strand r_b (1,500 psia) (in./sec)	TU-131 r_b (K _n 93.6) (in./sec)	TU-131 r_b (700 psia) (in./sec)	δm (psi)	2.6 ϵ_R (%)	2.6 ϵ_m (%)	E _{2.6} (psi)	Density (lb/in. ³)
5180059	46	87.7	1.020	--	--	114	36	32	450	0.0651
5180014	46	87.7	0.999	--	--	91	40	34	358	0.0650
5180015	46	87.7	1.019	0.718	0.715	87	42	34	336	0.0651
5180061	46	87.7	1.009	--	--	104	38	32	407	0.0651
5180062	46	87.7	1.020	0.709	0.699	105	42	33	412	0.0650
5180016	46	87.7	1.008	--	--	112	34	30	463	0.0650
5180060	46	87.7	1.019	--	--	117	42	31	482	0.0650
5180063	46	87.7	1.036	--	--	114	40	30	466	0.0651
5180017	46	87.7	1.004	--	--	105	41	32	415	0.0650
5180064	46	87.7	1.016	--	--	109	43	32	434	0.0651
5180065	46	87.7	1.024	0.686	0.695	104	41	33	394	0.0651
5180018	46	87.7	1.013	--	--	111	40	33	431	0.0650
5180066	46	87.7	1.009	--	--	114	40	33	452	0.0651
5180067	46	87.7	1.006	--	--	98	43	34	368	0.0650
5100019	46	87.7	1.000	--	--	114	36	32	466	0.0651
5100068	46	87.7	1.004	--	--	94	41	36	349	0.0651
5100069	46	87.7	1.008	--	--	116	40	32	473	0.0651
5100020	46	87.7	0.995	0.676	0.693	114	36	32	450	0.0650
5100070	46	87.7	1.028	0.692	0.699	115	34	30	496	0.0651
5100021	46	87.7	1.009	--	--	87	46	36	313	0.0651
5100071	46	87.7	1.006	--	--	90	46	36	328	0.0651
5100072	46	87.7	1.017	--	--	85	50	37	302	0.0651
5100022	46	87.7	1.003	--	--	106	33	29	430	0.0651
5100073	46	87.7	0.996	--	--	91	44	36	340	0.0651
5100023	46	87.7	1.003	--	--	84	42	35	314	0.0651
5100074	46	87.7	1.001	--	--	96	43	35	356	0.0651
5100075	46	87.7	0.997	0.666	0.683	90	48	36	326	0.0651
5100076	46	87.7	1.012	--	--	92	46	36	342	0.0651
5100024	46	87.7	1.002	--	--	--	--	--	--	--
5100025	46	87.7	0.995	0.709	0.703	106	30	27	471	0.0651
5100026	46	87.7	1.016	--	--	108	36	31	462	0.0651
5100027	46	87.7	1.012	--	--	80	40	34	297	0.0651
5100028	46	87.7	1.025	--	--	108	32	29	446	0.0651

CODE:

Mix Number	Mixer Type
5185001 thru 5185005	5 gal. vertical
5186001	430 gal. vertical
5186002 thru 5186003	5 gal. vertical
5180001 thru 5180028	430 gal. vertical
5180036 thru 5180076	200 gal. horizontal

(THIS PAGE IS UNCLASSIFIED)

CONFIDENTIAL

1. STANDARDIZATION

- (U) Five standardization mixes were prepared in the 5 gal. vertical mixer according to the following formulation matrix:

	50	X		X
Percent Spec Fine AP	45		X	
	40	X		X
	87.0	87.5	88.0	
	Percent HB (Liquids)			

- (C) The ballistic and physical property data obtained from these mixes are presented in Figures 92 and 93. Analysis of these data indicated that a special fine/unground oxidizer ratio of 47/53 and an HB/ECA ratio of 87.7/12.3 would produce a propellant with the required ballistic and physical properties.

2. VERIFICATION

- (U) Three verification mixes were prepared with the above formulation. One mix was processed in the 430 gal. vertical mixer. The five gal. vertical mixer was used for the other two verification mixes. * Ballistic and physical property data from these verification mixes are presented in Figures 92 and 93. Figure 94 presents the curve developed from a pressure exponent (K_n) study conducted in conjunction with the 430 gal. verification mix.
- (U) Analysis of these data indicated a significant burn rate and scaleup factor between the five gal. and 430 gal. vertical mixers. Raw material availability, however, prohibited manufacture of a second 430 gal. mix to verify this scale factor.
- (U) In order to increase mixing capacity during motor production, the 300 gal. horizontal mixers were to be used to supplement the 430 gal. vertical mixer. Past experience with these type mixers and a common propellant formulation was limited

* The first of these five gal. mixes was prepared to evaluate a second lot of unground oxidizer assigned to the program, while the second was to evaluate an unexpected low burn rate in the 430 gal. mix.

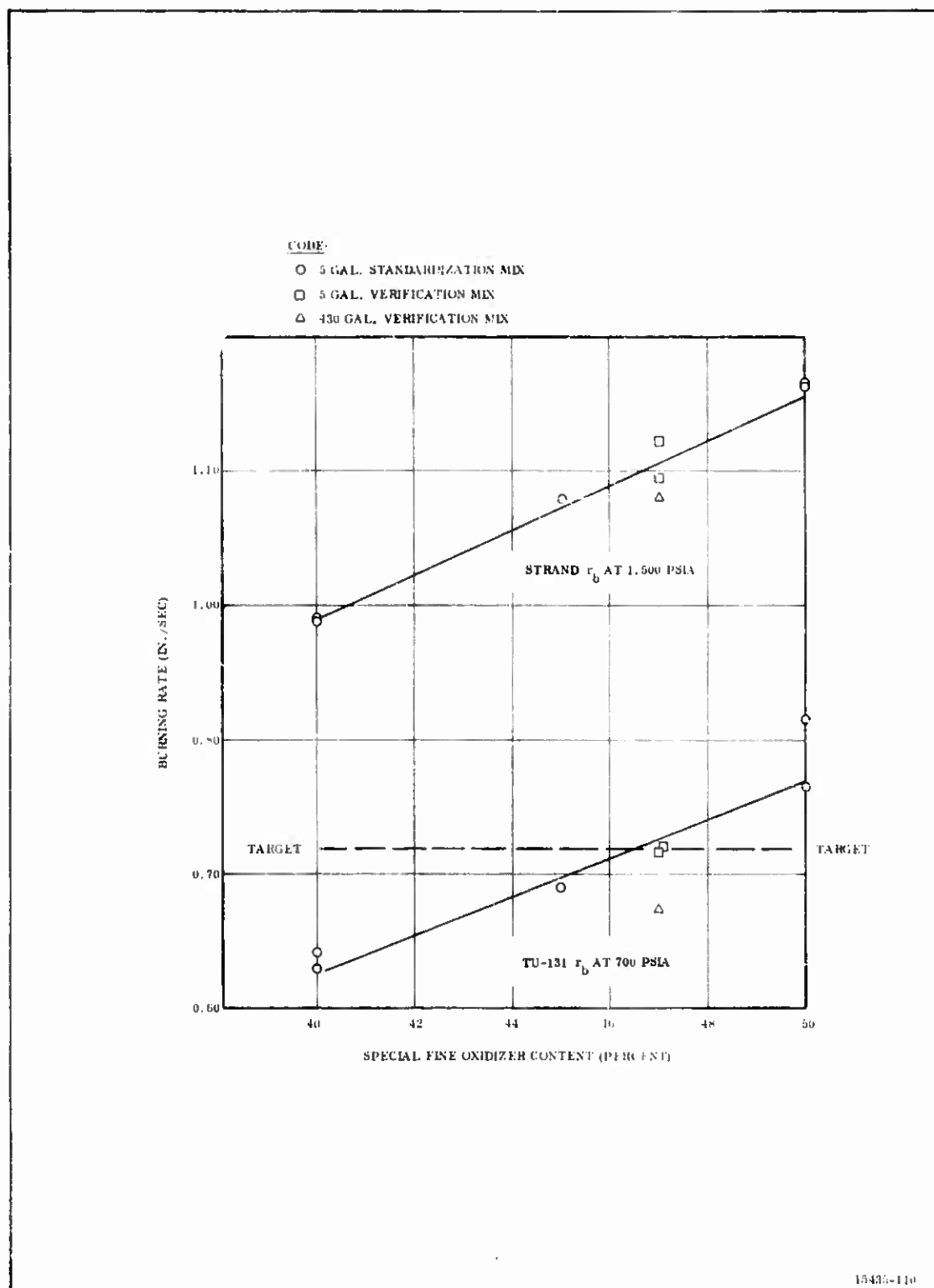


Figure 92. Burning Rate vs Special Fine Oxidizer.
TP-H1115 Propellant Standardization

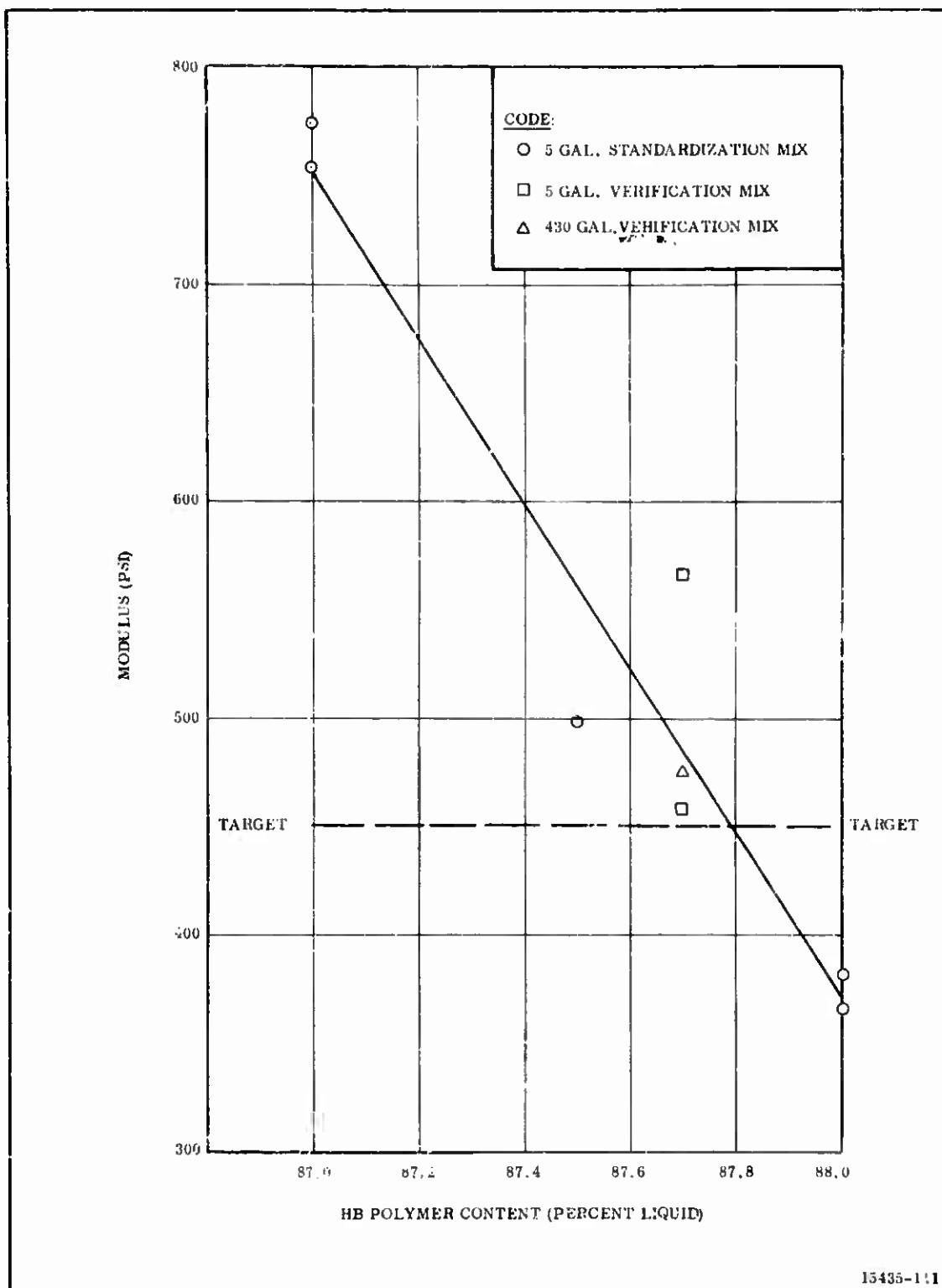
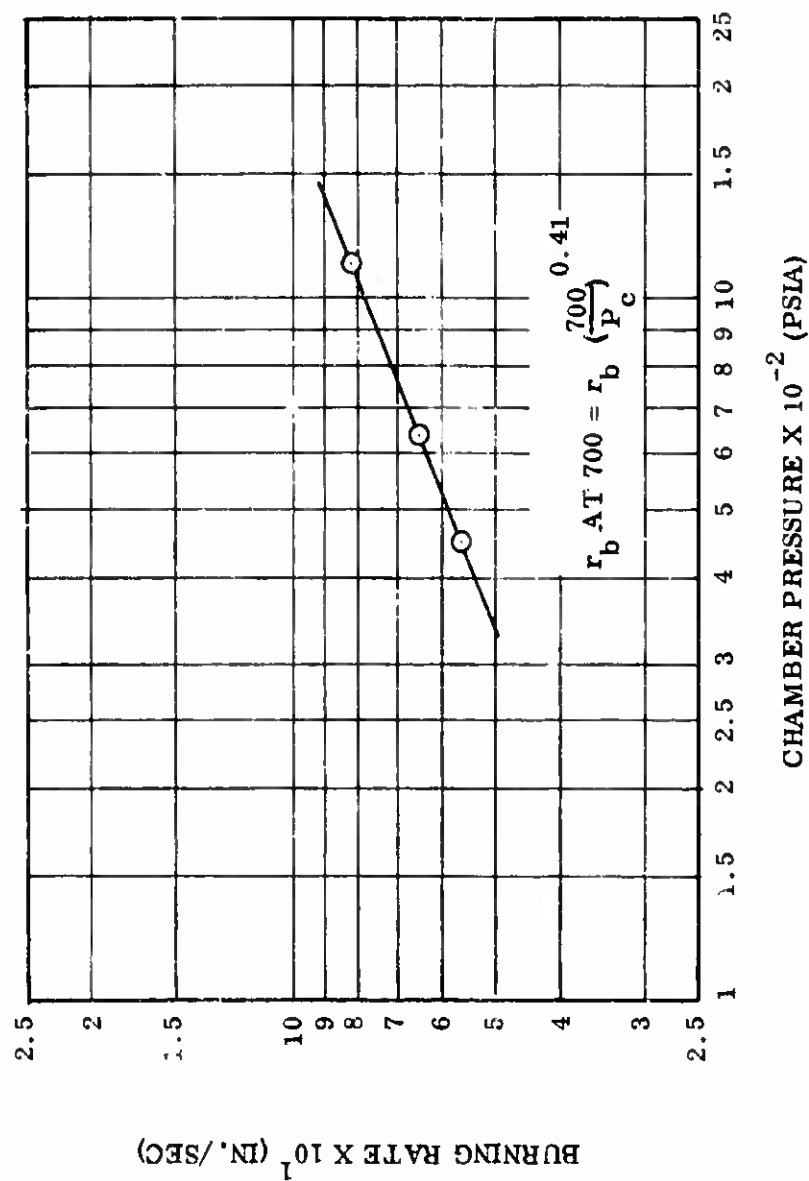


Figure 93. Modulus vs HB Polymer,
TP-H1115 Propellant Standardization



15435-112

Figure 94. Pressure Exponent (K_n) Curve (Burning Rate vs Chamber Pressure, TP-H1115 Propellant, 430 Gallon Verification Mix)

to TP-H1011 propellant used in the TU-312 motor program. Data from this program indicated a TU-131 motor burn rate scale factor of approximately 0.018 in./sec with the higher burn rate being characteristic of the horizontal mixers. A scale factor for TP-H1115 propellant containing a higher percentage of special fine (5 micron) oxidizer was, however, unpredictable.

- (U) The formulation recommended for use in production is tabulated below by mixer type:

<u>Mixer Type</u>	<u>Special Fine (5 micron)/ Unground AP</u>	<u>HB/ECA</u>
430 gal. vertical	48/52	87.7/12.3
300 gal. horizontal	47/53	87.7/12.3

- (U) These data represent adjustments in the special fine oxidizer content to compensate for anticipated mixer scaleup between the five gal. vertical, 430 gal. vertical, and 300 gal. horizontal mixers.

- (U) An uncured strand burn rate target was determined from TU-131 motors and strand burn rate data obtained in the standardization and verification mixes. These data were assumed to be independent of mixer type. A strand target of 1.005 in./sec at 1,500 psia and 100° F was selected.

3. PRODUCTION

- (U) Strand burn rate and modulus data obtained from production mixes are presented in Figures 95 and 96, respectively. Because of the uncertainties in the estimates of mixer scale factors and a variation in the oxidizer grinding process,* adjustments were made in the special fine oxidizer content based on strand burn rate data as the casting progressed. The following data show the adjustments made during casting.

*Special fine oxidizer used in the standardization and verification mixes was ground at a rate of 900 lb/hr. It was found, however, that this rate could not be sustained over a long period of time and was therefore reduced to 800 lb/hr.

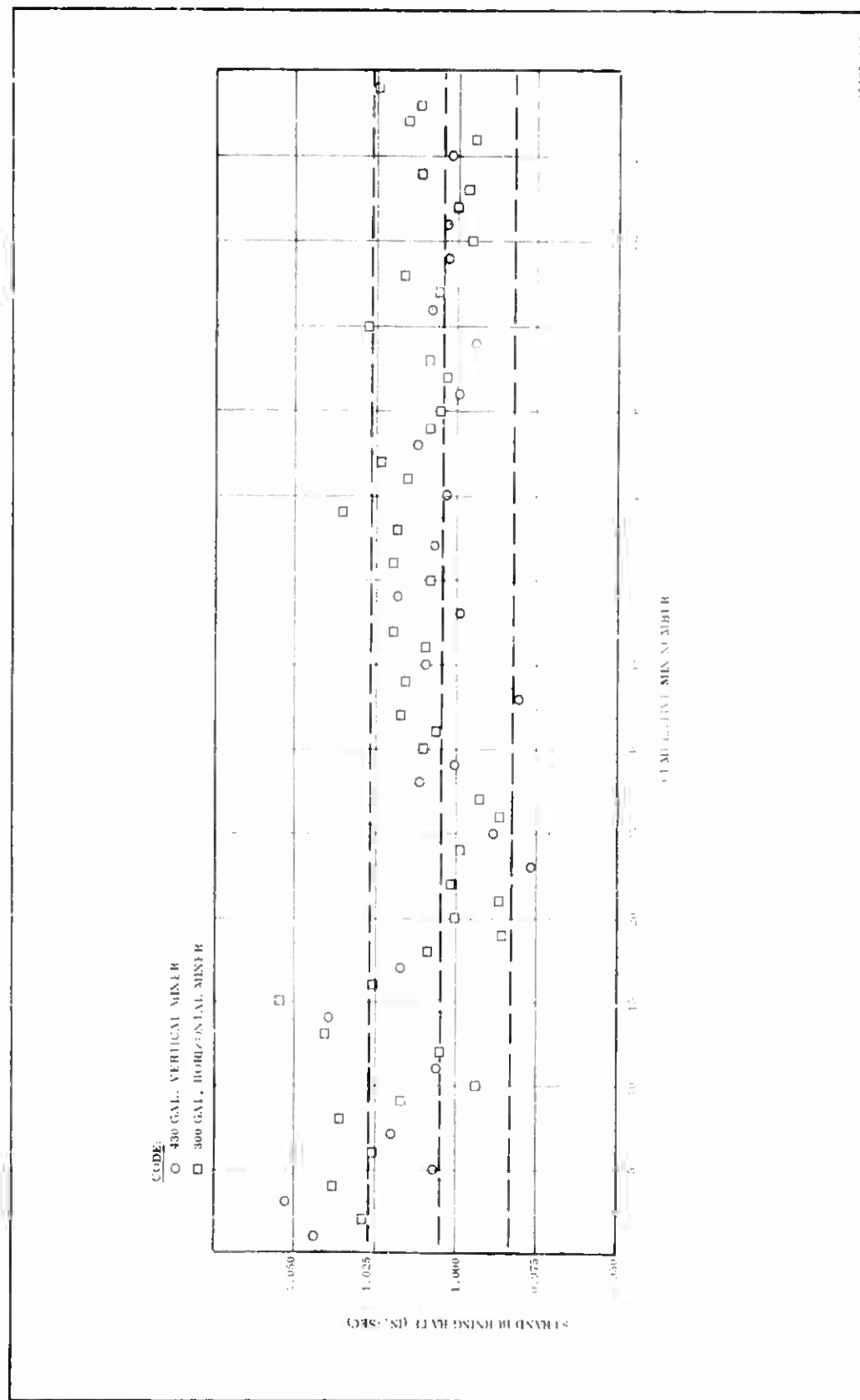


Figure 95. Strand Burning Rate vs Cumulative Mix Number, TP-H111 Propellant Production

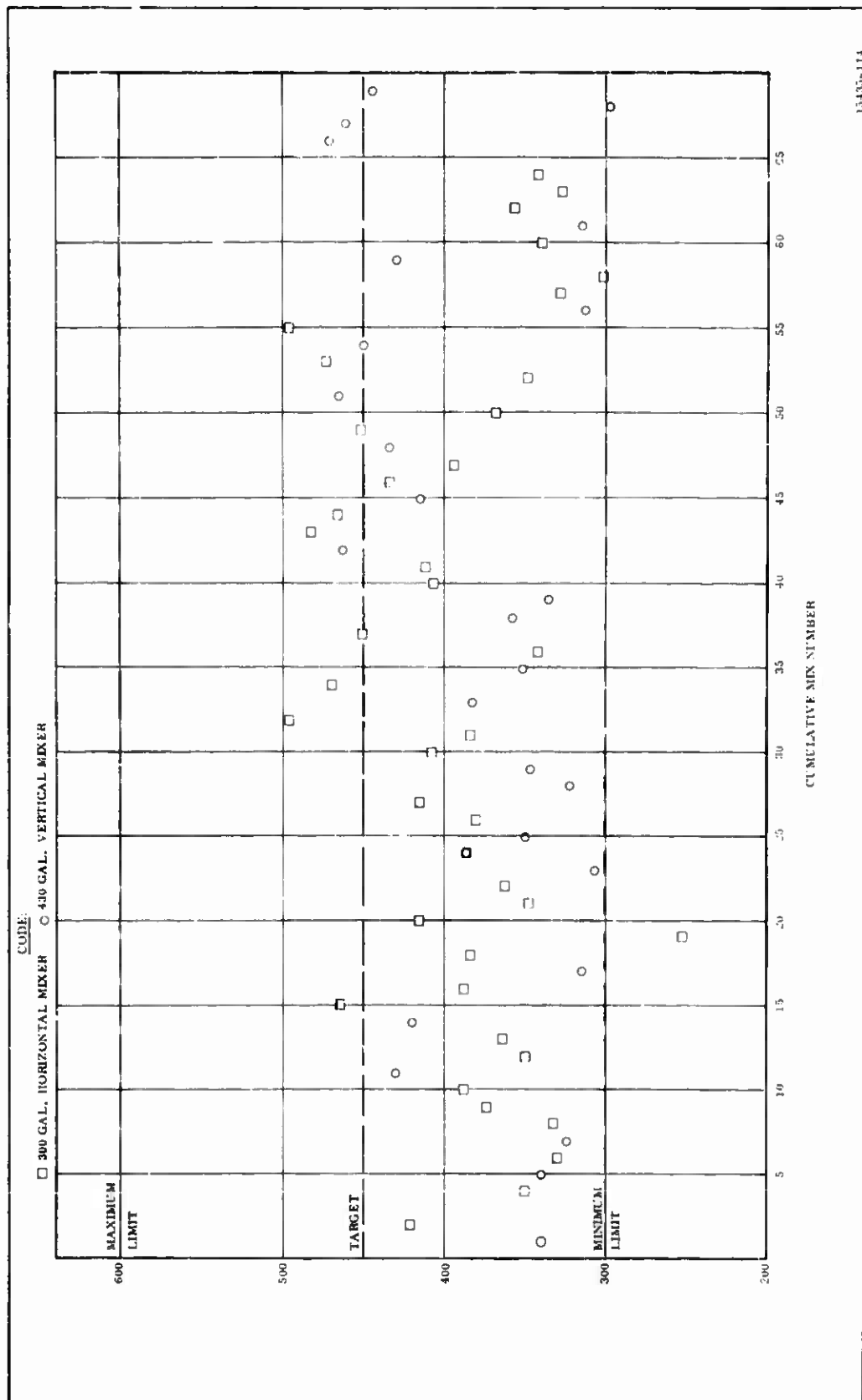


Figure 96. Modulus vs Cumulative Mix Number, TP-H1115 Propellant Production

Vertical Mixer		Horizontal Mixer	
<u>Mix Number</u>	<u>Percent Special Fine AP</u>	<u>Mix Number</u>	<u>Percent Special Fine AP</u>
5180001 thru 2	48	5180036 thru 39	47
5180003 thru 7	46	5180040 thru 46	46
5180008 thru 10	45	5180047 thru 53	45
5180011 and subsequent	46	5180054 and subsequent	46

4. DISCUSSION

- (U) TU-131 motors were cast and tested from 17 random production mixes. For purposes of the following analysis, these mixes were assumed to be representative.
- (U) a. Mixer Scale Factor--A comparison of the TU-131 motor burn rate of mixes prepared in the 430 gal. vertical mixer and the 300 gal. horizontal mixer with 46 percent special fine oxidizer content is shown as follows.

Vertical Mixer		Horizontal Mixer	
<u>Mix No.</u>	<u>TU-131 r_b at 700 psia (in./sec)</u>	<u>Mix No.</u>	<u>TU-131 r_b at 700 psia (in./sec)</u>
5180005	0.688	5180040	0.690
5180015	0.715	5180044	0.719
<u>5180020</u>	<u>0.693</u>	5180045	0.694
Avg	0.6987	5180055	0.693
		5180062	0.699
		5180065	0.695
		5180070	0.699
		<u>5180075</u>	<u>0.683</u>
		Avg	0.6965

- (U) It is concluded from this data that a burn rate scale factor between the 300 gal. horizontal and 430 gal. vertical mixers with TP-H1115 propellant is insignificant. This is presumably due to the fact that the increase in oxidizer

surface area due to mixer attrition is very small in comparison to the initial surface area because of the special fine fraction.

- (U) b. Optimum Special Fine Oxidizer Content--TU-131 motor burn rate data obtained from the production mixes are presented in Figure 97. Analysis of the standardization, verification, and production data results in the following relationship:

$$\text{TU-131 motor } r_b \text{ at 700 psia} = 0.05689 + 0.01402 (\text{percent special fine AP})$$
$$r^2 = 0.76$$

This equation indicates that in order to obtain a TU-131 motor burn rate of 0.717 in. /sec at 700 psia, a special fine oxidizer content of 47.08 percent would be required.

- (U) c. Uncured Strand Target--Uncured strand burn data obtained from the 17 representative production mixes are presented also in Figure 97. Analysis of the standardization, verification, and the above representative production mixes results in the following relationship:

$$\text{Strand } r_b \text{ at 1,500 psia} = 0.2344 + 0.0168 (\text{percent special fine AP})$$
$$r^2 = 0.79$$

This equation indicates that use of the optimum special fine oxidizer content (47.08 percent) would produce a nominal strand burn rate of 1.025 in. /sec, based on the present level of experience with TP-H1115 propellant tested in Minuteman strands.

- (U) It should be noted, however, that range of strand burning rates within each batch consistently decrease as mixing sequences progressed. This was evident at the 1,500 psi test condition for batches mixed in both the vertical and horizontal mixer, and for batches grouped and not grouped for a uniform percent special fine oxidizer.

- (U) The strand burning rate range was approximately 0.030 in. /sec during the first ten batches, it decreased to 0.018 in. /sec by the 30th batch, and to 0.014 in. /sec by the 50th batch.

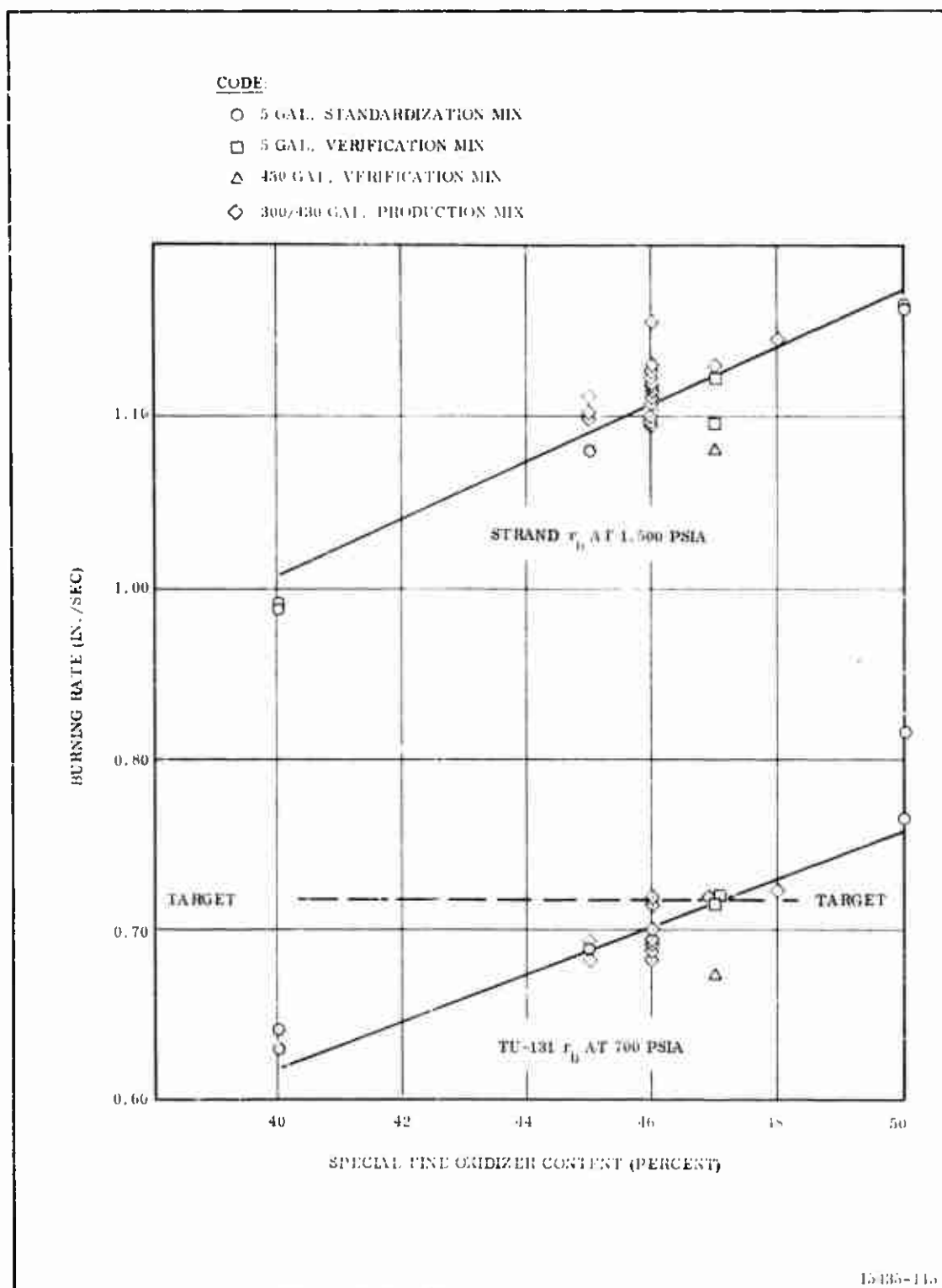


Figure 97. Burning Rate vs Special Fine Oxidizer,
TP-H1115 Propellant Production

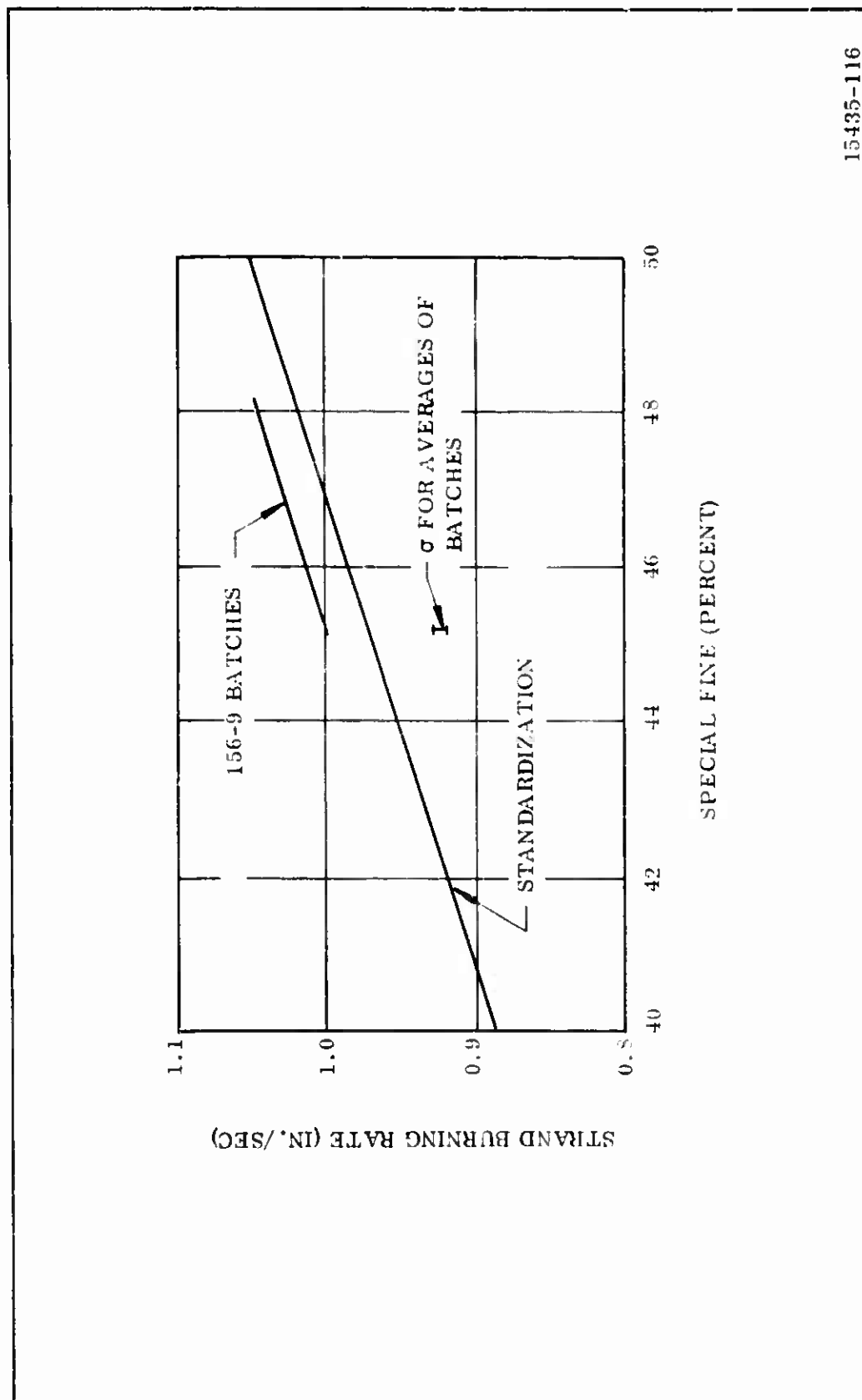
(U) The above analyses indicate that the decrease in variation with sequence of batches was real, however, this change in variation did not indicate a change in nominal value other than due to grind ratio change. For example, the highest and lowest strand burning rates observed for batches having 46 percent special fine and cast into the 156-9 were within five batches in sequential order.

(U) A bias did exist between nominal value of strand burning rate for 156-9 batches and the respective standardization batches and is represented graphically in Figure 98. The bias is equivalent to a change of two percent of special fine oxidizer and three times as large as the length of the vertical line representing the standard deviation among batches cast in the 156-9 (Figure 98). Had this bias been recognized the percent fine oxidizer would have not been reduced during production. In retrospect it is unwise to use strands as control unless sufficient experience has been gained with the particular propellant being used. The strains and techniques being used were developed for Minuteman (TP-H1011) propellant possessing a burn rate of approximately one-half of that of the 156-9 (TP-H1115) propellant. Also, different propellant formulations respond differently in strands relative to motor firings. Without this experience, the propellant process becomes more dependable than the control, except for infrequent gross errors in weighup, etc. For this reason, during the loading of the 156-9, acceptance was changed to be based on total solids content.

(U) d. Optimum HB/ECA Ratio--Modulus data obtained from the 17 representative production mixes are presented in Figure 99. Analysis of the standardization, verification, and representative production mix data results in the following relationship:

$$\begin{aligned}\text{Modulus} &= 38,500.50 - 434.17 (\text{percent HB}) \\ r^2 &= 0.69\end{aligned}$$

This equation indicates that an HB/ECA ratio of 87.64/12.36 would produce a nominal propellant modulus of 150 psi.



15435-116

Figure 98. Comparison of Regression Lines for Strand Burning Rate vs Percent Special Fine Oxidizer

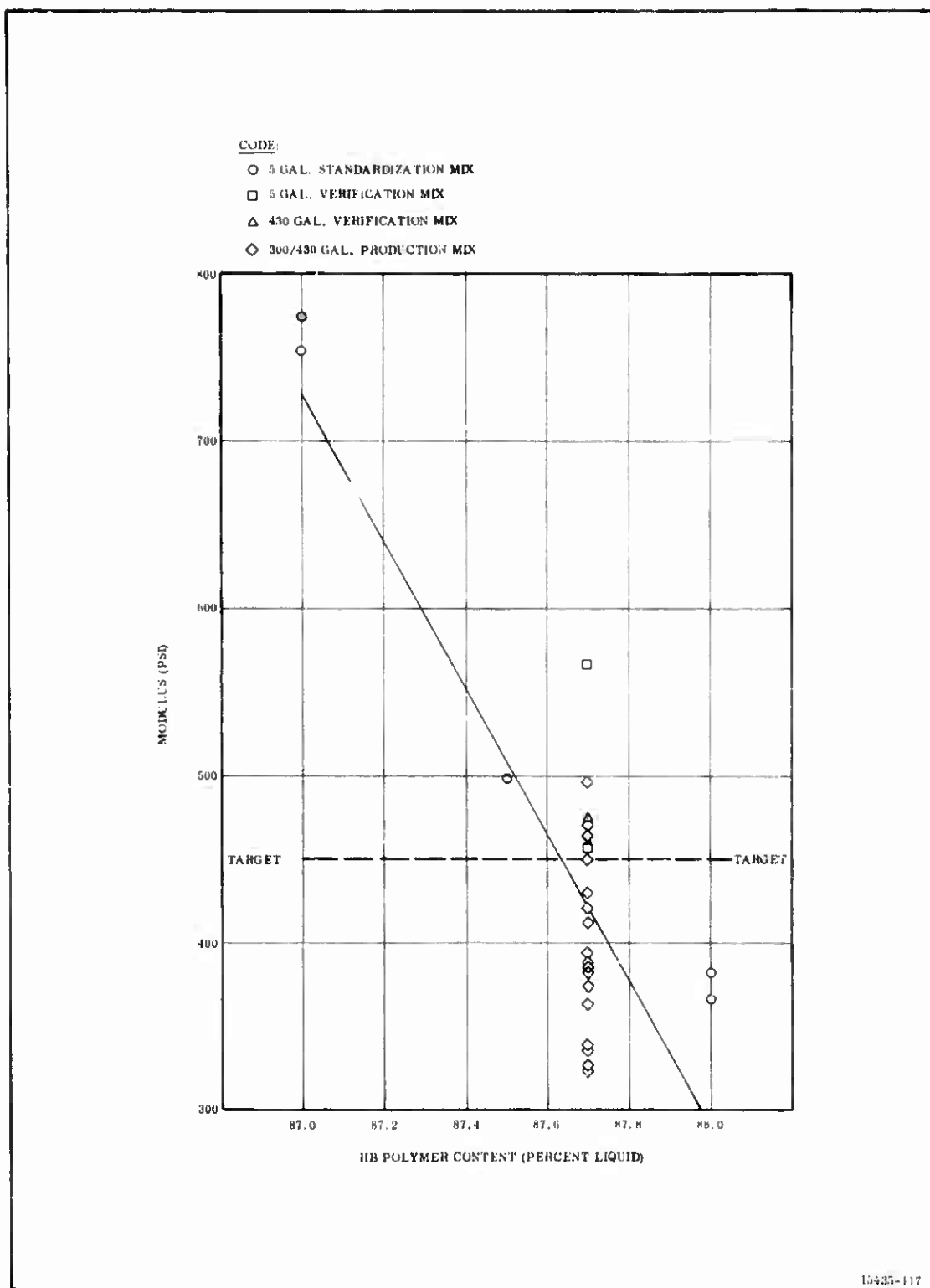


Figure 99. Modulus vs HB Polymer, TP-H1115 Production Mix

5. SUMMARY

- (U) Post analysis of available data indicates that the optimum propellant formulation to produce target ballistic and physical properties is as follows:

Special Fine (5 micron)/Unground AP	47.08/52.92
HB/ECA	87.64/12.36

- (U) This formulation would be applicable to the 430 gal. vertical and 300 gal. horizontal mixers. An uncured strand burning rate target of 1.025 in. /sec at 1,500 psia would be compatible with the above formulation.

C. PROPELLANT PROCESSING

1. MIXING PROCEDURE

- (U) The ground oxidizer fraction was prepared in a fluid energy mill from special coarse feed stock. A feed rate of 900 ± 25 lb/hr was originally specified, but could not be maintained even with frequent stops to clean the mill. Consequently, the feed rate was reduced to 800 ± 50 lb/hr and grinding proceeded with normal cleanup frequency.
- (U) Laboratory tests have established the relationship between mill feed rates and propellant burn rates. The data obtained from these tests have been selected as the best and most reproducible basis for controlling the oxidizer grinding. The burn rate difference resulting from a change from 900 to 800 lb/hr is negligible.
- (U) For informational purposes only, particle size is analyzed on each mill run.
- (U) The original operating procedure also required the attainment of $210 \pm 10^\circ\text{F}$ prior to the start of a grinding sequence. s requirement was subsequently changed to $200 \pm 10^\circ\text{F}$ to reduce cycle time when it was observed that 190°F could be obtained in 2-3 minutes, whereas approximately 15 minutes were required to obtain 200°F .

- (U) A total of 97,900 lb of material was ground during a 13 day period prior to and during the casting of the main grain. The mill output reached a maximum of 10,000 lb per day during the grinding operations. The ground oxidizer was stored in desiccated oxidizer tote bins prior to being combined with the unground fraction for addition to the mixers.
- (U) The special fine oxidizer for this program was stored in sealed containers with moisture-free air. Fresh molecular sieve desiccant in quantities sufficient to maintain the required dryness was placed in each container prior to sealing. Storage was for a period of less than 30 days. Cycling of ambient temperature in the storage area was restricted to a maximum of 20° F in 24 hrs.
- (U) No unusual problems were experienced during the storage period.
- (U) Oxidizer feeding problems were encountered in both the vertical and horizontal mixers. In the vertical mixer, oxidizer bridging was experienced in the feed system on two mixes. Bridging problems were anticipated in the horizontal mixers since the screen mesh size is half that of the vertical mixer screen. Therefore, the oxidizer feed rate was cut back to the minimum prior to attempting any propellant processing in these mixers. Nevertheless, bridging problems were experienced on the majority of horizontal mixes. Oxidizer feeding in these mixers required one hour nominally versus 20 minutes in the vertical mixer. Feeding problems were more severe if the oxidizer was held in the tote bin and hopper with the bin discharge door open and not fed immediately into the mixer. All oxidizer feeding problems were attributed to moisture absorption by the special fine oxidizer fraction.
- (U) Seven tail-end lots of aluminum powder were assigned to the program. These lots were apportioned into each Econ-O-Bin to provide for an even distribution of each lot into the motor.
- (U) Premixes, containing aluminum, HB polymer, and iron oxide, were prepared in a vertical change can type mixer for all propellant batches manufactured in the horizontal mixers. Premixes for the vertical mixer were prepared in its mixer bowl. Prior to mixing, the materials were stirred sufficiently to wet the solids. The epoxy curing agent was included in the premixes for the vertical mixer.

(U) The propellant was mixed in both horizontal and vertical mixers. Original planning required the use of only the vertical mixer to provide a minimum casting rate of 4 in. /hr. When the special fine oxidizer density was found to be much lower than expected, it was necessary to process the oxidizer in two tote bins per mix. This additional handling extended the mix cycle to the point where the vertical mixer could support a casting rate of only 2.6 in. /hr. The use of three horizontal mixers increased the theoretical casting rate to 4.9 in. /hr.

(U) Twenty-four vertical and forty-one horizontal mixes were prepared for the main grain and four vertical mixes for the aft grain. One vertical mix was rejected due to indication of high burn rate based on strand burning rate and a second vertical mix was discarded at the end of the main grain casting. Several burning rate adjustments were accomplished during the mixing sequence by changing the ground oxidizer ratio.

(U) The initial mixes gave indication of a high burn rate based on strand limits of 1.005 ± 0.022 . The strand burn rates for these mixes are as follows.

First	1.044	(from vertical mixer)
Second	1.029	(from horizontal mixer)
Third	1.053	(from vertical mixer)
Fourth	1.038	(from horizontal mixer)

(U) The third mix was scrapped. This decision was partially due to the high burn rate and partially due to expiration of process life.

(U) The above mixes were based on a 48 percent special fine grind for the vertical mixer and a 47 percent special fine grind for the horizontal mixer. As a result of the above high strand burn rates, the formulation was changed to include only 46 percent special fine for both the vertical and horizontal mixers. This change was effected on the fifth mix for the vertical mixer and the ninth mix for the horizontal mixer. From this point on, mixes were within tolerance limits until the 14th and 15th mixes which resulted in 1.040 and 1.055 in. /sec respective strand burn rate. In order to offset these and the previously indicated high burn rate mixes, the special fine grind ammonium perchlorate was reduced to 45 percent for the 19th

through 28th mixes and then adjusted back to 46 percent for the remainder of the motor. The specification also was changed to accept mixes on total solids.

2. CASTING AND CURING PROCEDURE

- (U) The motor was cast in the vertical position with the forward end down. The vacuum casting was accomplished in two phases, with the cast and cure of the main grain completed prior to casting of the aft end grain. In preparation for casting the main grain, all casting fixtures were dry fitted to insure that the components would fit and function as intended. No major problems were encountered during the dry fit operation.
- (U) The core was preheated in a 150°F environment for 44 hours, then moved to casting pit M-49 and installed in the case. The casting fixtures were installed and the case, core, and fixtures preheated in a 135°F environment for approximately 94 hours, at which time the main grain casting was started.
- (U) The initial casting arrangement required that propellant arriving from the mixers be dumped, from the vertical mix bowl or propellant transfer hoppers, into a large (14,000 lb capacity), hot water jacketed hopper. The propellant flowed from this hopper, through a deaeration assembly and into the motor (Figure 100). To eliminate the possibility of propellant buildup on the dispersion cone between mixes, which would result in having to tear down the casting arrangement, it was decided to maintain a continual flow of propellant into the motor. This was accomplished by initially restricting the propellant flow and thereby allowing the propellant to build up in the hopper.
- (U) After casting approximately 16 mixes, a propellant buildup was observed on the sides of the hopper. Mixing operations were suspended in an attempt to allow the hopper to empty. However, the buildup rate exceeded the casting rate and finally cut off propellant flow into the motor with approximately 8,600 lb of propellant still in the hopper. The hopper arrangement was removed from the casting house and the propellant discarded.

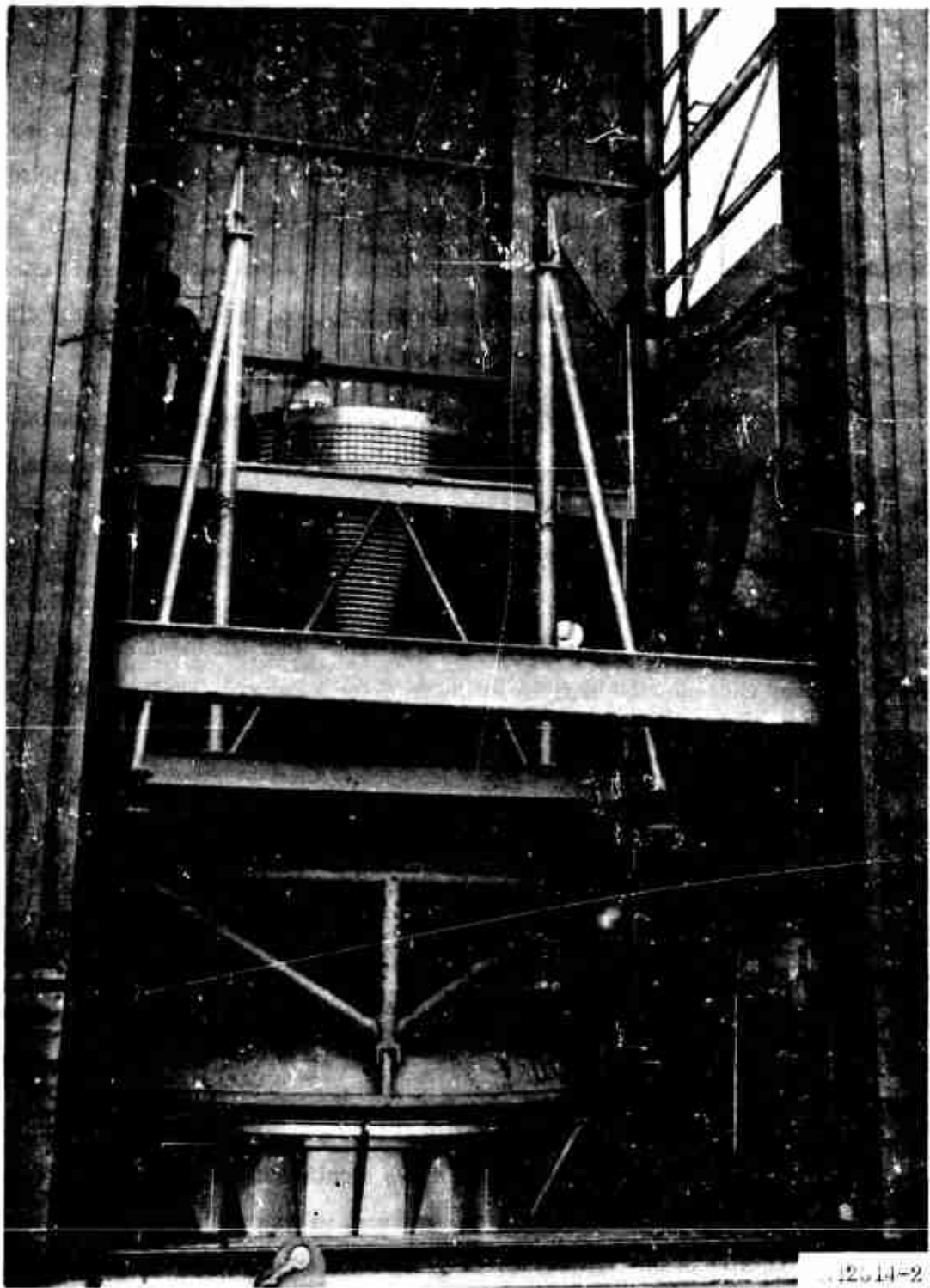


Figure 100. Initial 156-9 Motor Propellant Casting and Deaeration Arrangement

- (U) Since the propellant in the hopper had set up and could not be immediately removed, the casting arrangement was changed to that currently employed on the Minuteman program. This arrangement required that the propellant be shipped to the casting site in transfer hoppers which are attached directly to the flexible tube and valve assembly above the deaeration assembly (Figure 101). Use of this arrangement resulted in an interrupted propellant flow since each hopper is emptied and removed before the next propellant batch is received, but the anticipated dispersion conc buildup problem did not materialize.
- (U) Casting in this manner required no change in the processing cycle at the horizontal mixers, since propellant from these mixers was shipped to the casting site in transfer hoppers under the initial casting arrangement. Propellant from the vertical mixer, however, had previously been shipped in the mixer bowl. Therefore, it was necessary to set up a dumping station in Building M-16 to transfer the propellant from the mixer bowl to transfer hoppers. Since the batch size of the vertical mixes exceeded the capacity of the transfer hopper, it was necessary to split each mix between two hoppers.
- (U) The change over to the transfer hopper system was accomplished and casting resumed in approximately seven hours. Vacuum was released during the down time. Casting of the main grain continued with no major problems; however, the propellant flow rate was not as high as desired. Therefore, after casting the 13th mix, vacuum was again released and a 3/16 in. slit plate was installed in the deaeration assembly in place of the 1/8 in. plate. This change resulted in a down time of only 1 1/4 hours.
- (U) At the same time, it was concluded that the flow rate of propellant from the second transfer hopper of each vertical mix was significantly lower than the first hopper and the hoppers from the horizontal mixers. This problem was eliminated by reducing the size of the vertical mixes to that of the horizontal mixes effective on the 35th mix (13th mix from the vertical mixer). This change also aided mixer scheduling operations.

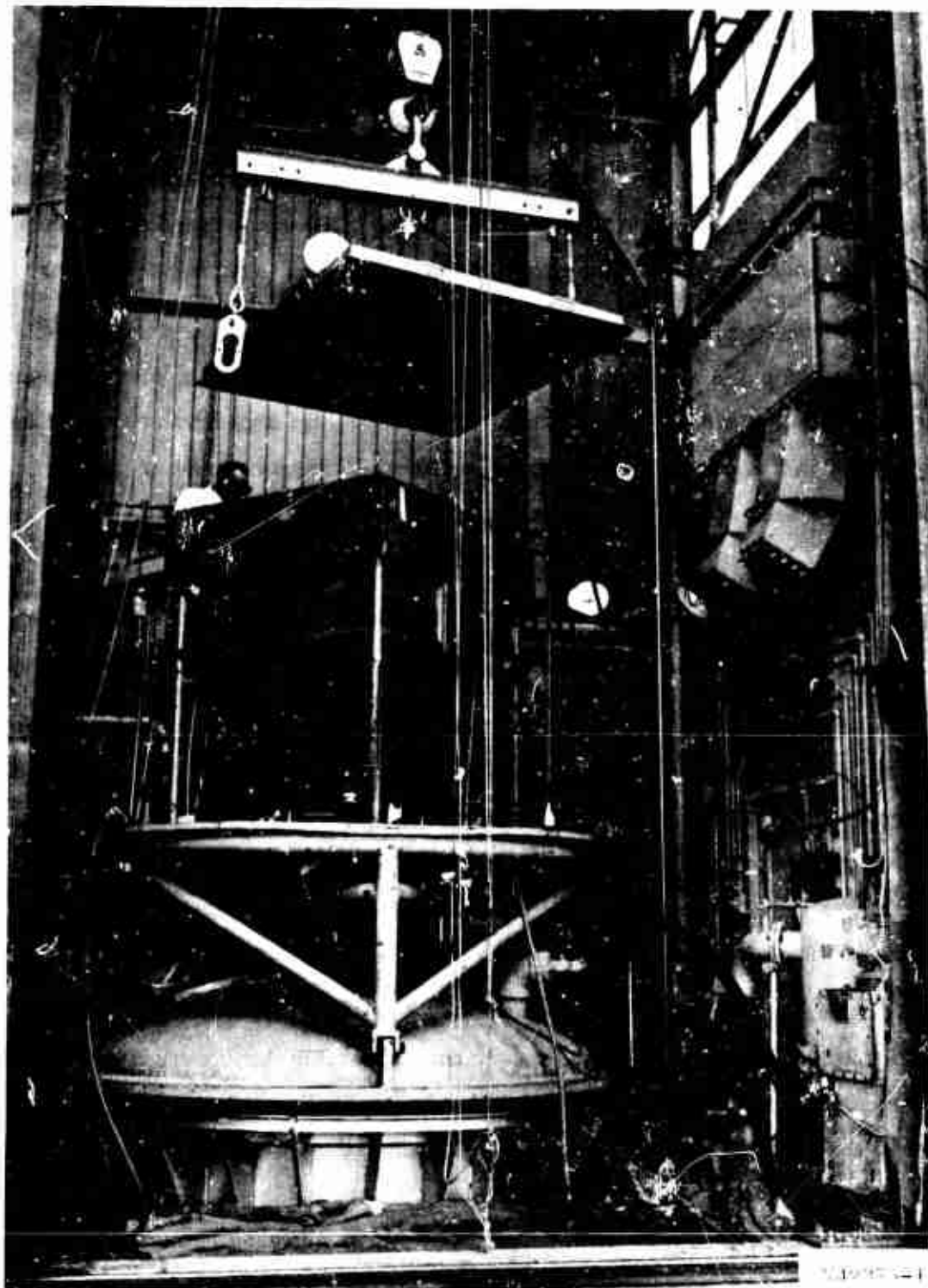


Figure 101. Minuteman Program Propellant Casting and Deaeration Arrangement

- (U) Thereafter, casting of the main grain proceeded without problems. The propellant was cast to the level of the slot former support. Vacuum was reduced from 0.5 to 3.0 in. of mercury and the propellant was observed to settle approximately 0.5 inch. Casting was resumed, at 3.0 in. of mercury, and the propellant level raised to 0.5 in. above the lower edge of the slot former support. Vacuum was completely released and the propellant settled an additional 0.5 inch.
- (U) The casting pit was maintained at 135°F during casting operations. The propellant was cured at 135°F for 95 hours. After propellant cure, the dispersion cone and dispersion cone extension were removed and the broadcloth securing the aft relief flap was cut and removed (Figure 102). A sheet of 0.006 in. thick polyethylene was placed on the propellant surface.
- (U) Sixteen slot former segments were installed, sealed with vacuum putty, and covered with a sheet of polyethylene. The core cap, dispersion cone, casting dam, and vacuum dome were installed and the motor preheated at 135°F for 31 hours.
- (U) The aft grain was cast using the vertical mixer and the original (14,000 lb propellant hopper) casting arrangement. This time, however, the temperature in the water jacket on the hopper was reduced from 150 to 140°F and no attempt was made to maintain propellant flow. The hopper was emptied between each mix. Four mixes were required to complete the casting of the aft grain. No casting problems were encountered and no mixes were rejected.
- (U) After casting approximately three inches up onto the casting dam, casting was terminated and the dumping arrangement and vacuum dome were removed. The casting dam was seated remotely with a hydraulically actuated seating assembly. Seating involved lowering the dam until it contacted the core cap. Teflon dividers were placed in the excess propellant between the dam and the dispersion cone and core cap so that, when cured, the propellant could be removed in blocks. Discs, with ropes attached, were embedded in this propellant to provide a means of lifting the cured propellant blocks from the motor (Figure 103).

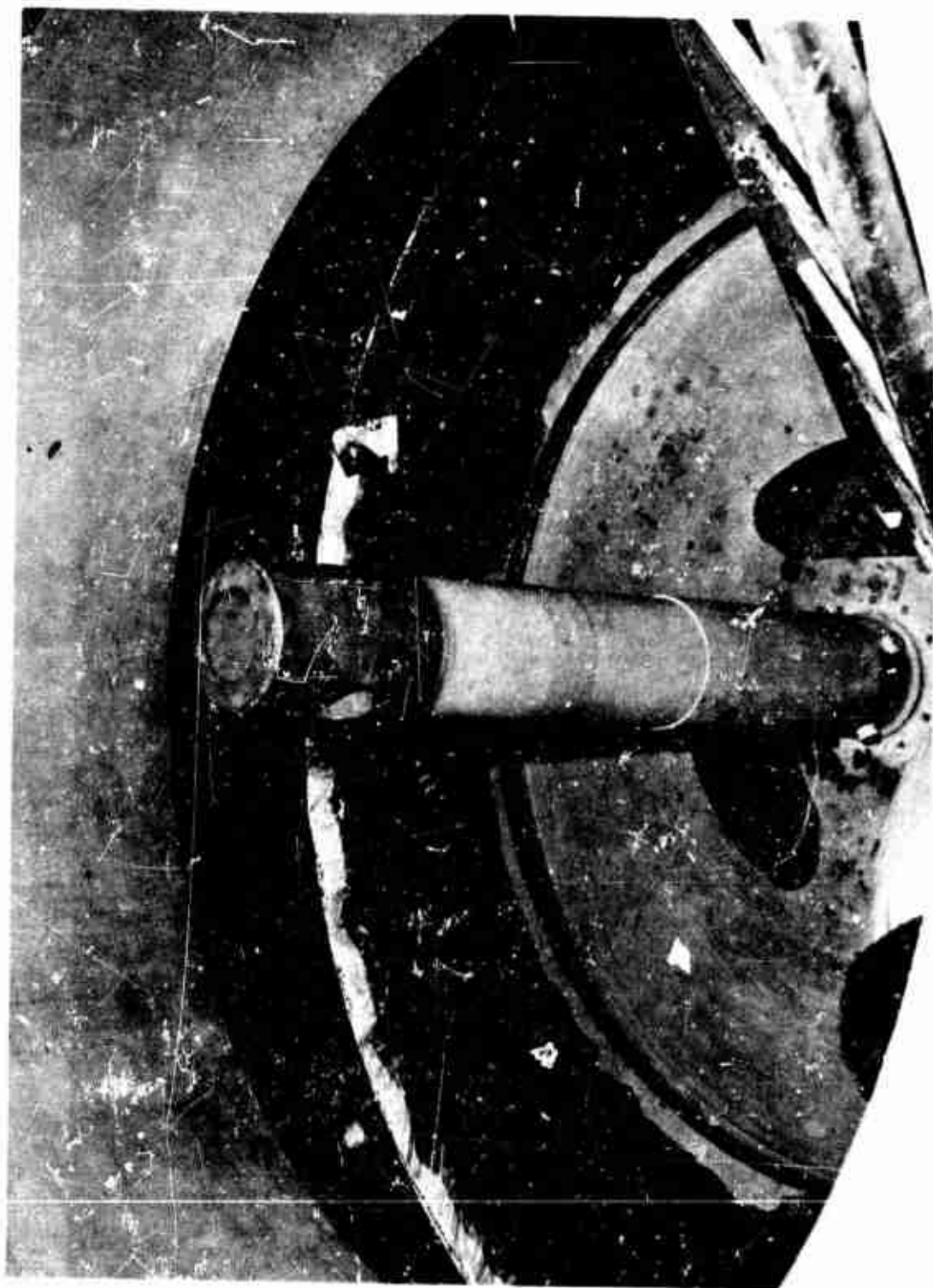


Figure 102. Removing Broadcloth Which Secures the Aft Relief Flap

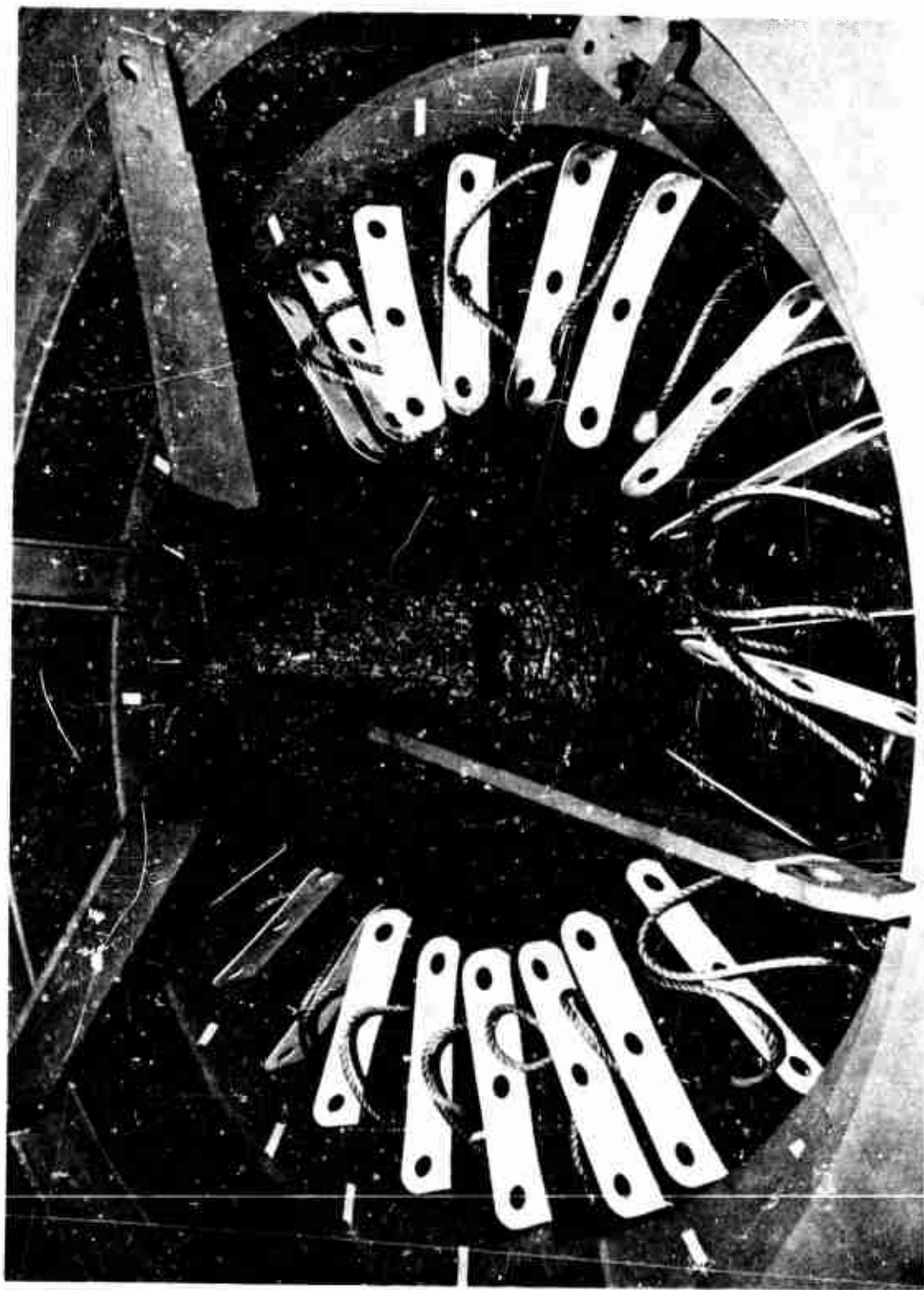
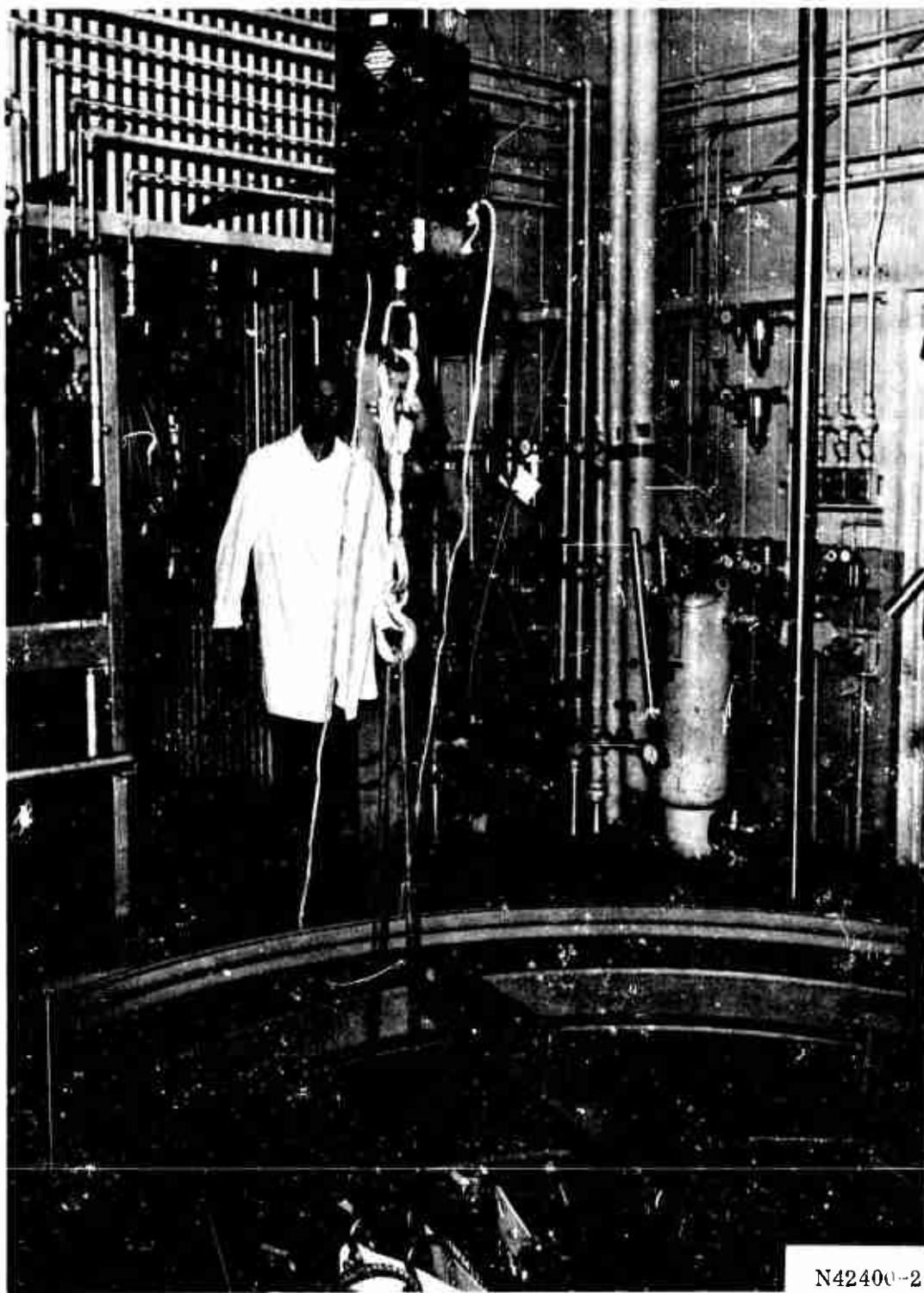


Figure 103. Discs Used to Remove Cured Propellant Blocks from the Motor

- (U) The casting pit temperature was again maintained at 135°F during casting. The propellant was cured at 135°F for 144 hours and then cooled for 5 hours.

3. FINISHING

- (U) After propellant cooldown, the Teflon dividers were removed (Figure 104). Attempts to remove the propellant blocks were unsuccessful because the ropes on the propellant slings broke. Therefore, the casting dam was unseated to release one side of the blocks (Figure 105). A force of 20,000 lb was required to pop the dam. Removal of the propellant blocks was then accomplished with no further problems (Figure 106).
- (U) The dispersion cone and core cap were removed. A force of 36,000 lb was required to pop the core cap. Removal of this tooling exposed the slot formers. To aid slot former removal, the motor was allowed to cool down for an additional 12 hours.
- (U) Slot formers at the Wasatch Division have traditionally been tape wound with removal accomplished by fragmentation. The 156-9 motor design presented a favorable relationship between slot ID and OD, permitting consideration of removal without fragmentation. Each slot former segment, therefore, incorporated a metal superstructure and was designed to be removed in one piece (Figure 107).
- (U) As conceived, the slot former removal process required the use of a cable, a Hydraset, and an overhead hoist to pull the segments from between the main and aft propellant grains. In practice, however, the segments, once started, moved so easily that removal was accomplished by hand in almost every case. After removal of the segments, the polyethylene sheets were removed.



N42400-2

Figure 104. Removing Teflon Dividers

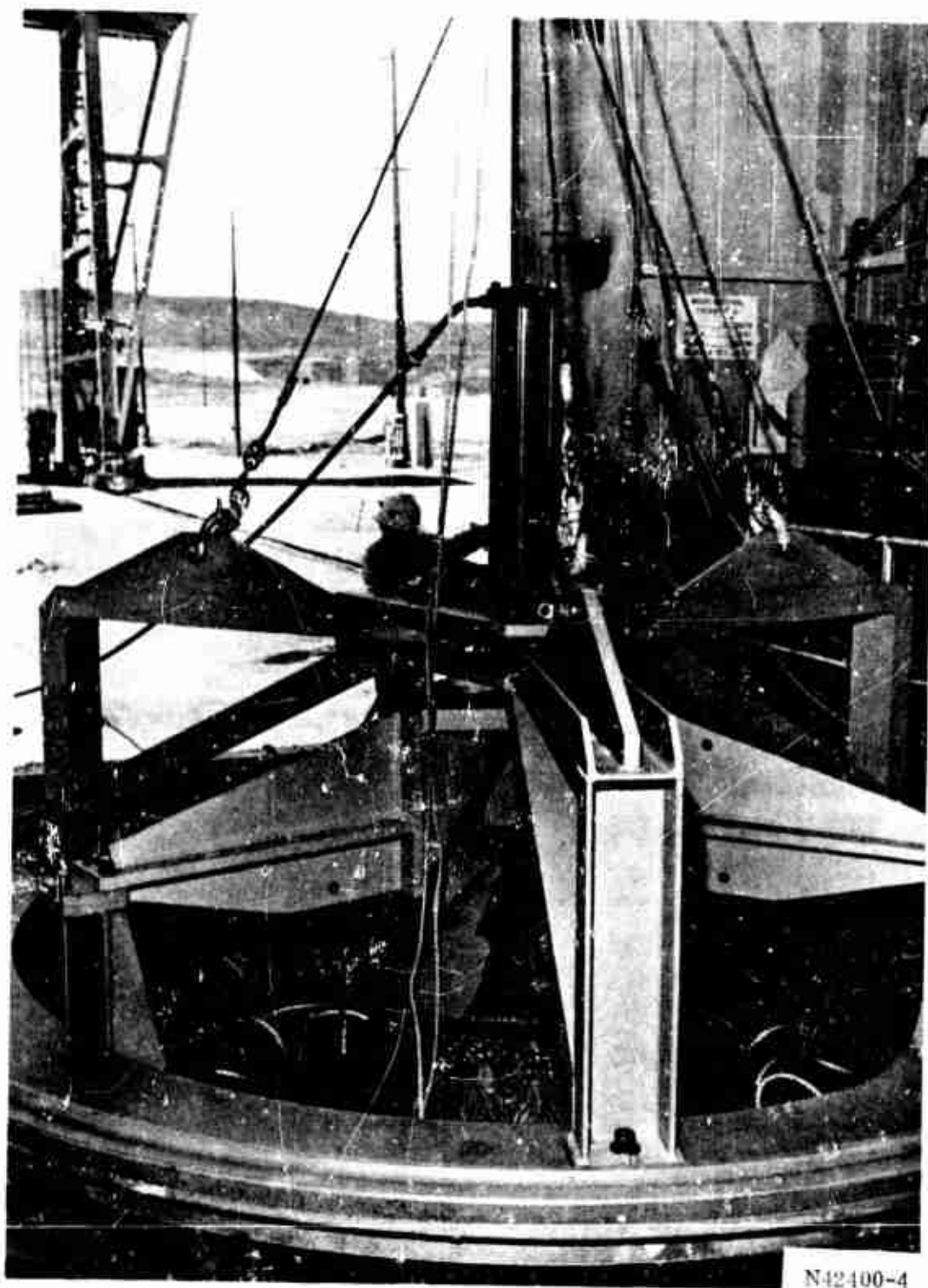


Figure 105. Unseating the Casting Dam

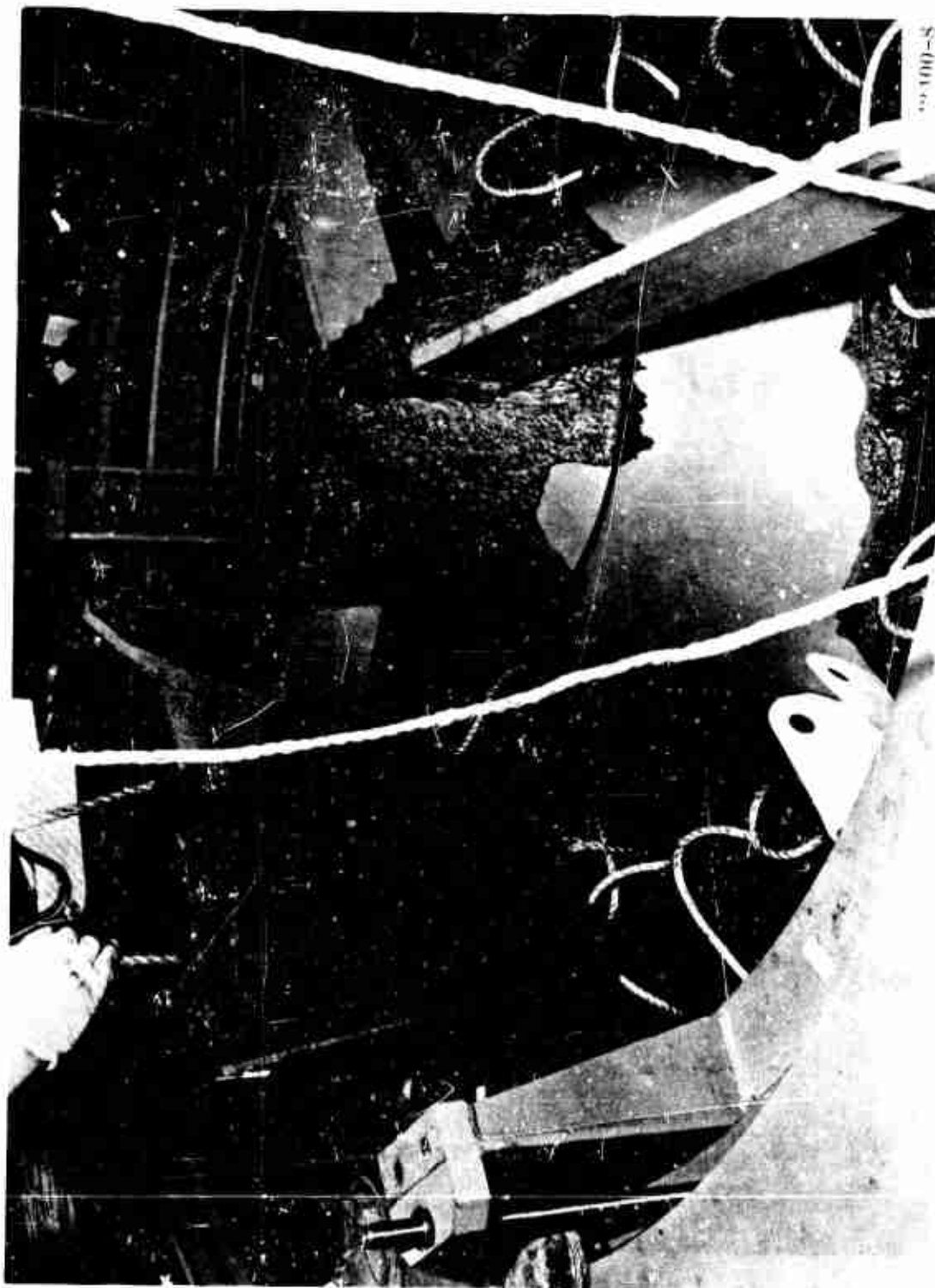


Figure 106. Removing Cured Propellant Blocks

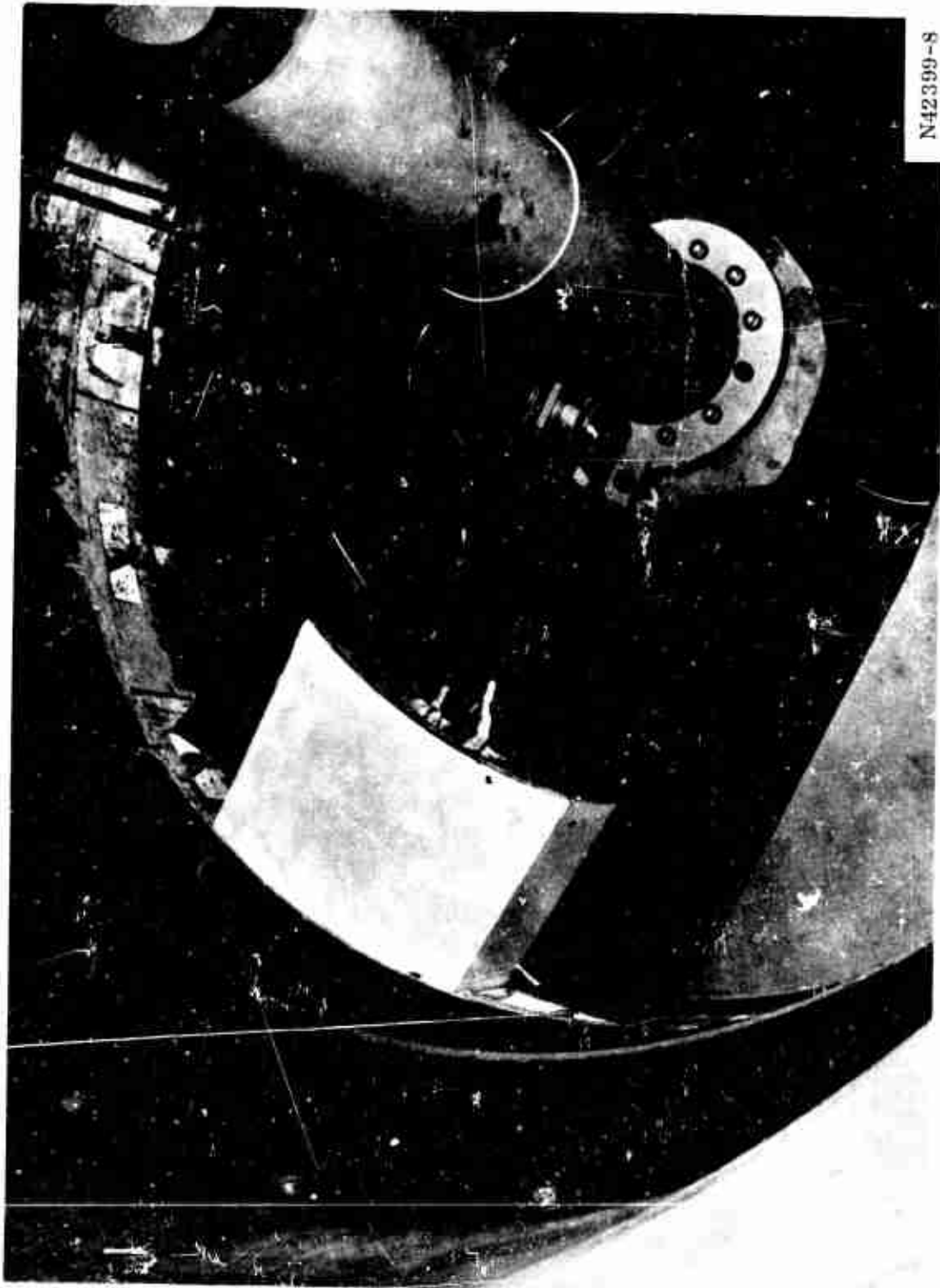
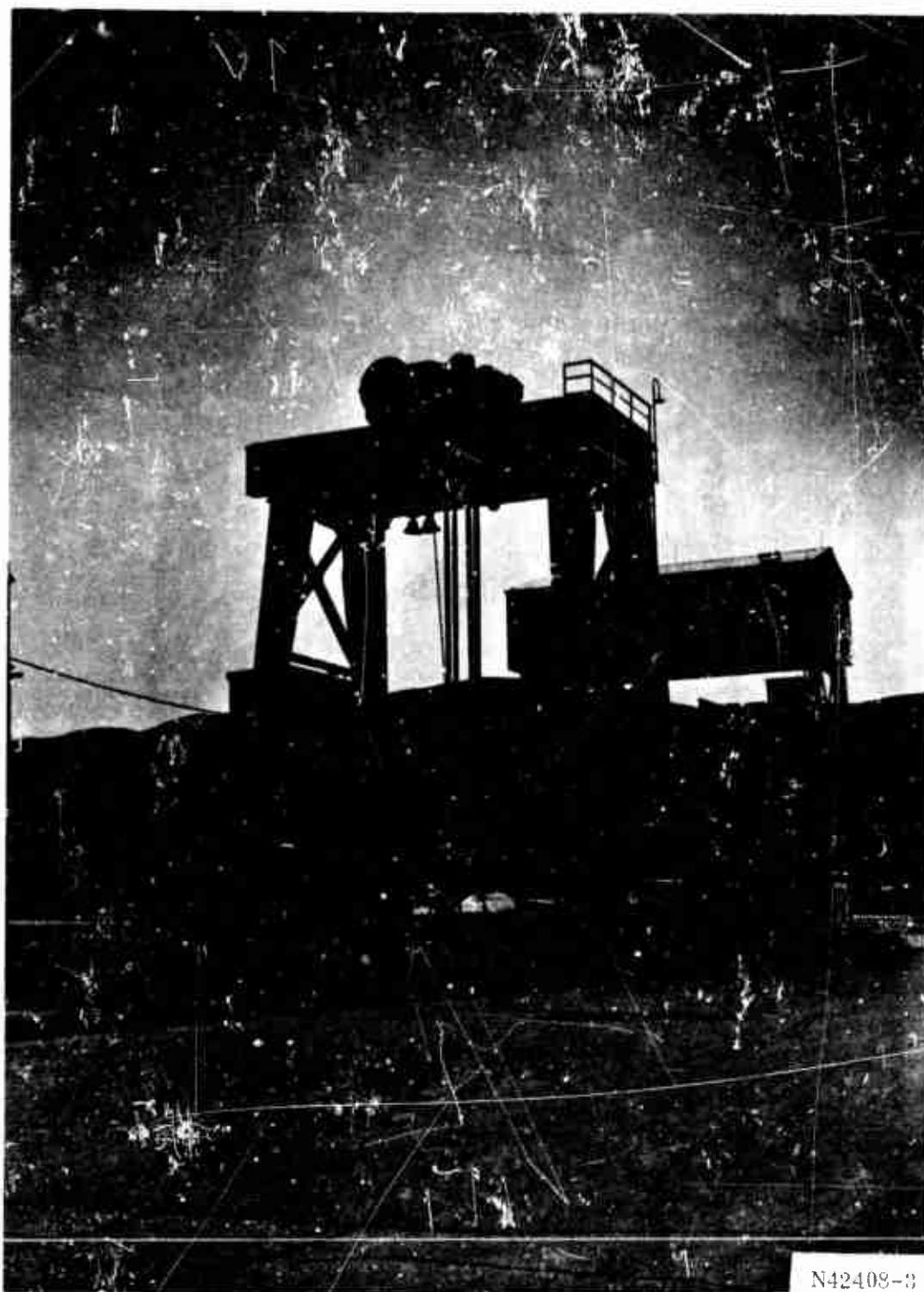


Figure 107. Removing Slot Former Segment

(U) Core removal was initiated immediately after slot former removal and approximately 37 hours after termination of the cure of the aft grain. The core popped after the application of 86 tons of force for 10 minutes. The force required to move the core decreased rapidly to 14.5 tons after popping. The core was then removed with a gantry crane.

(U) After installation of the igniter assembly, the loaded motor was removed from the casting pit (Figure 108) and broken over to the horizontal position (Figure 109). The motor was loaded on a 200-ton transporter (Figure 110), the igniter was installed, and the motor was shipped to the test bay (Figure 111) for nozzle and instrumentation installation and static test.

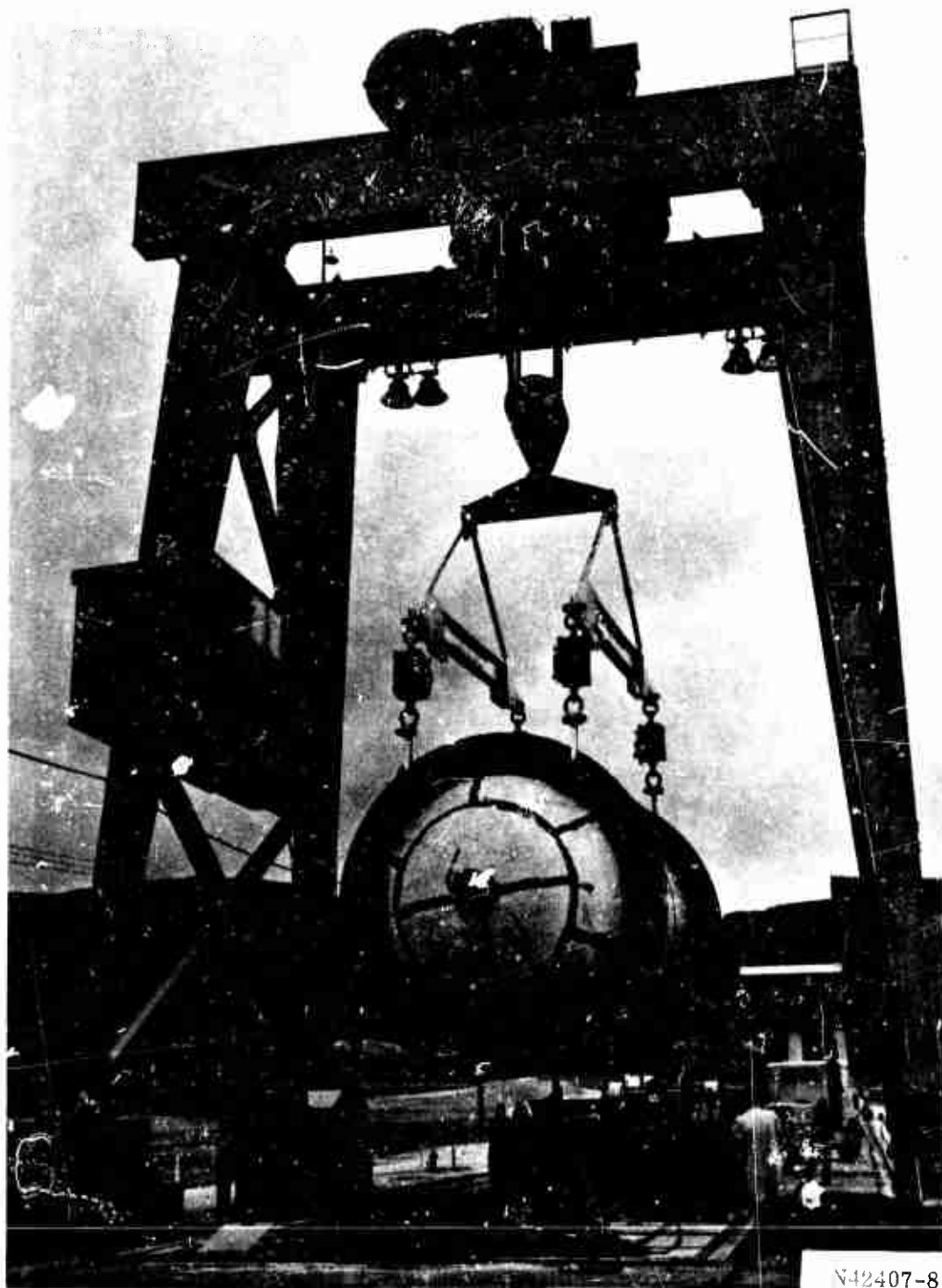


N42408-3

Figure 108. Removing the Loaded Motor from the Casting Pit



Figure 109. Breaking the Loaded Motor Over to the Horizontal Position



N42407-8

Figure 110. Loading the 156-9 Motor on the Transporter

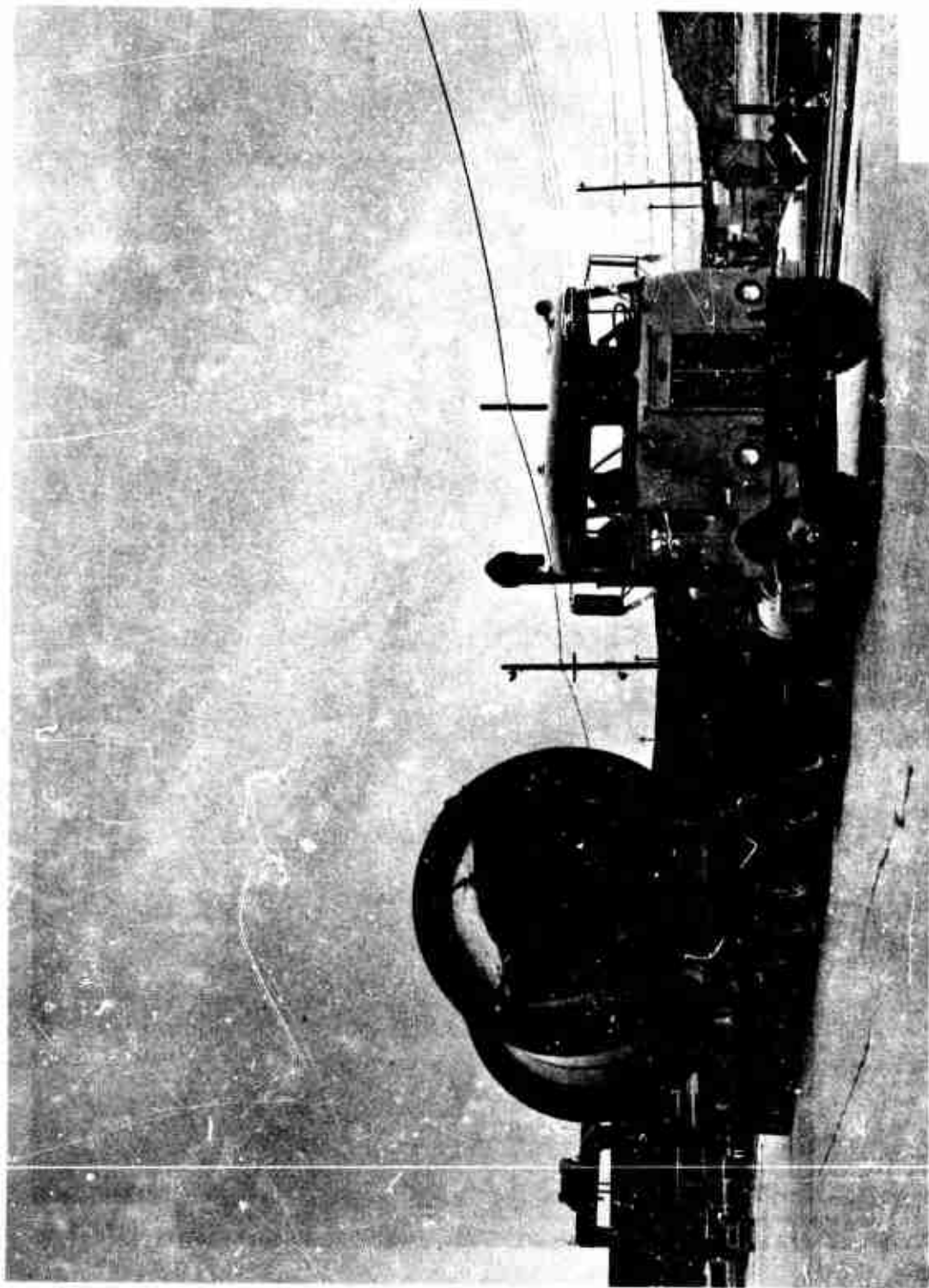


Figure 1i1. Transporting the 156-9 Motor to the Test Bay

SECTION VIII

IGNITION SYSTEM DESIGN AND FABRICATION

A. IGNITION SYSTEM DESIGN

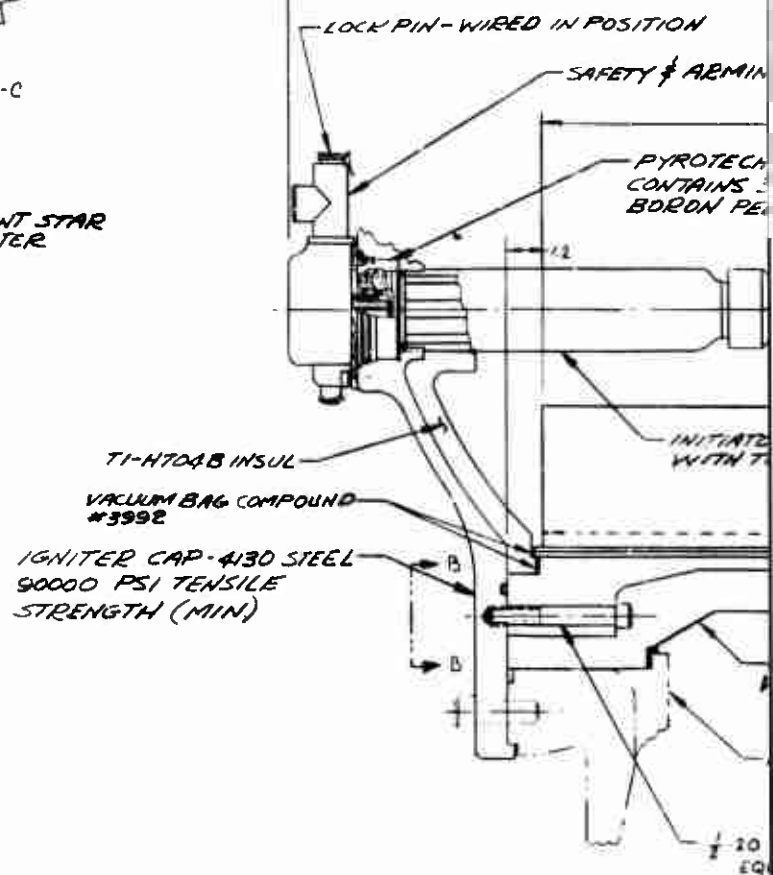
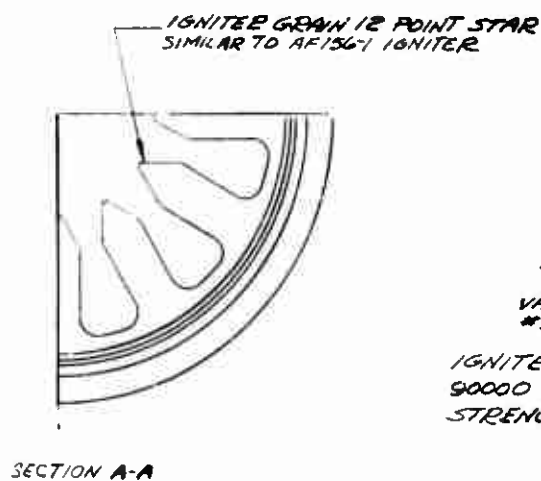
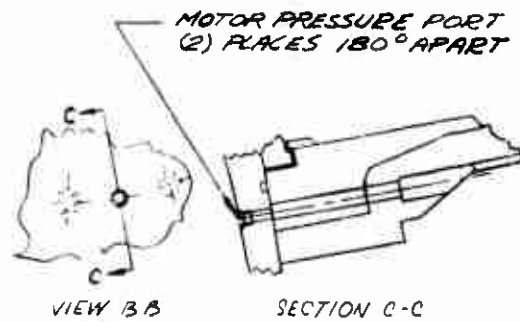
(U) The ignition system for the 156-9 motor was designed as a head end ignition system (Figure 112) in accordance with the contract work statement. The design criteria were: (1) the igniter mate with the GFP case, (2) existing hardware and tooling be used to the greatest extent possible, (3) the design of the loaded case assembly be such that one design could be used for the 156-8 motor ignition as well as the 156-9 motor ignition and, therefore, use common verification testing, common tooling, and (4) be a proven design requiring no development.

(U) The system was composed of the following four main subassemblies.

1. Safety and arming device.
2. Initiating system.
3. Booster PYROGEN igniter.
4. Adapters, booster igniter to motor and ignition system to motor.

1. SAFETY AND ARMING (S & A) DEVICE

(U) The S & A device selected for the 156-9 ignition system is currently being used on the Stage I, II, and III Minuteman motors. Thiokol developed this device for the Stage I motor ignition system and later it was standardized for all three stages. The S & A has been qualified to the latest Air Force requirements and over 2,500 have been produced for various development, qualification, flight test, and production programs.



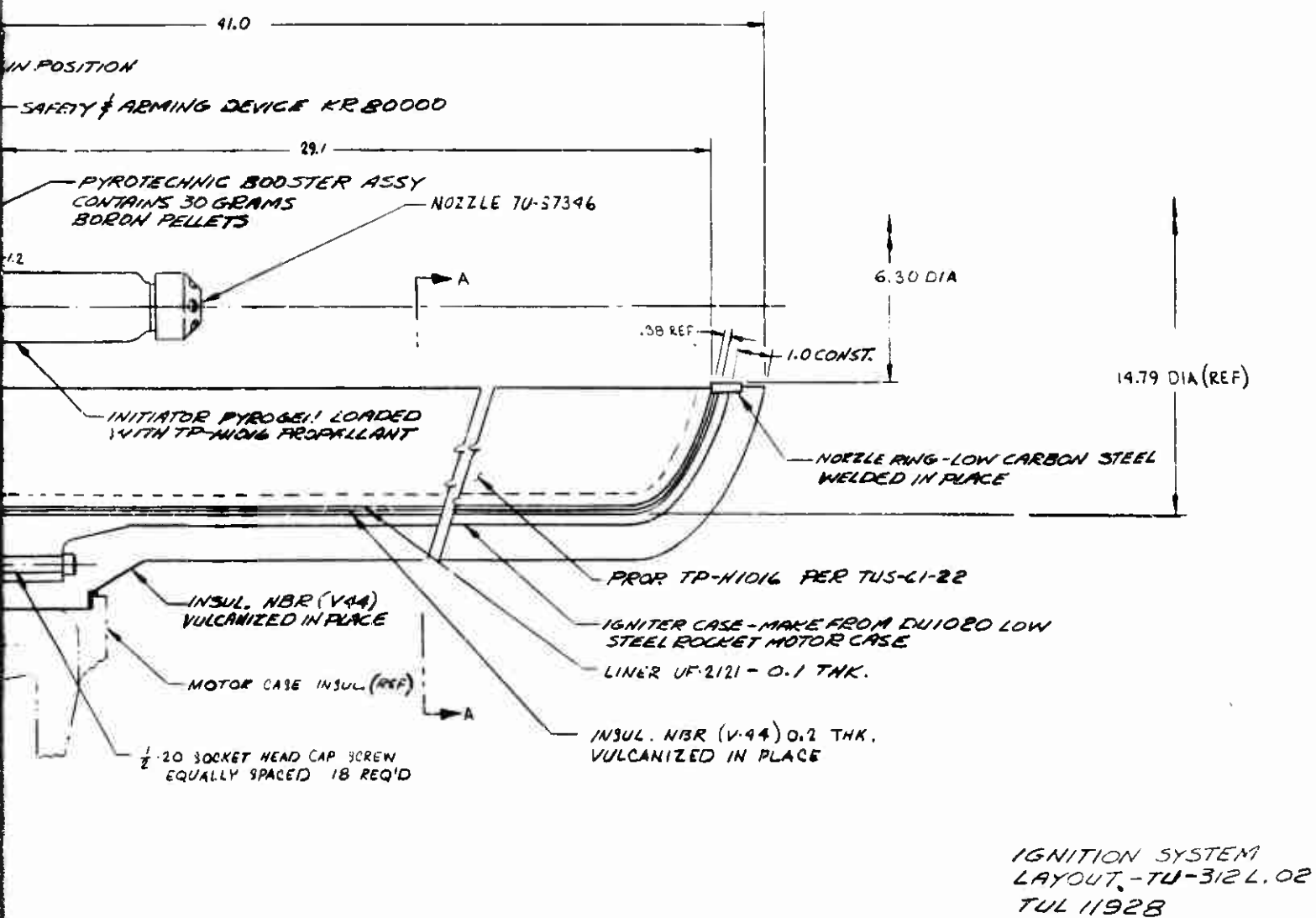


Figure 112. 156-9 Rocket Motor Ignition System

1

2

- (U) Upon initiation, two ES-003 electrical squibs start the ignition train for the motor ignition sequence. In the safe position, the squibs are electrically shorted and mechanically isolated from the ignition train. The S & A device has a visual indicator, mechanical lockpin, separate connectors for the control and firing circuits, hermetic seals, and other safety features which minimize the possibility of inadvertent firing. A lockwire secures the lockpin in place to insure assembly of the S & A device to the PYROGEN igniter in the unarmed (safe) condition. The lockwire and lockpin must be removed manually before the device can be armed electrically. This feature satisfies the requirement that the S & A device cannot be installed in the motor while in the armed condition.

2. INITIATING SYSTEM

- (U) The initiating system consists of an adapter, pyrotechnic booster assembly, and an initiating PYROGEN igniter.
- (U) a. Adapter--The adapter, made from low carbon steel, adapts the PYROGEN igniter, pyrotechnic booster, and the S & A device into one integral assembly. This assembly is installed in the motor adapter and held in place with a beveled retaining ring.
- (U) b. Pyrotechnic Booster--The pyrotechnic booster is the link in the ignition train between the S & A device and the initiating PYROGEN igniter. It contains 30 gm of 2A boron-potassium nitrate pellets, and the container is identical to the design used on the Stage I Minuteman.
- (U) c. PYROGEN Igniter--The initiating PYROGEN igniter, loaded with TP-H1016 propellant (Stage I Minuteman igniter propellant), ignites the booster PYROGEN igniter. It produces a mass discharge rate for booster PYROGEN ignition of 3.5 lb/sec for approximately 0.3 second. A multiple port nozzle diffuses the flame for a fast smooth ignition of the booster PYROGEN igniter. The case and grain designs have been demonstrated in the 156-1 motor static test and the Mace program for which this design was originally developed.

3. BOOSTER PYROGEN

- (U) The booster PYROGEN igniter assembly consisted of a mild steel case, NBR external and internal insulation, UF-2121 liner, and TP-H1016 propellant. The grain was the same 12 point star configuration used in the booster PYROGEN for the 156-1 motor. The igniter will operate at an average pressure of 840 psia, have a maximum pressure of 1,005 psia, and provide a mass discharge rate of 170 lb/sec for approximately 0.6 second. Pressure and mass flow then drop. The total burning time is approximately 1.1 seconds (Figure 113).
- (U) At 1,005 psi the booster PYROGEN igniter case has a design structural safety factor of 1.7. The low carbon steel igniter case is 30 in. long and 15.5 in. in diameter. A 6.3 in. ID steel ring is welded in the aft end to serve as the nozzle throat. The selection of a steel case for the 156-9 igniter was based upon economic considerations rather than weight performance.
- (U) The steel case was insulated internally and externally to prevent melting during the motor firing. Thermodynamic calculations indicated that 0.03 in. of insulation would prevent melting from the inside; however, to protect the bond of the external case insulation to the steel case, additional internal insulation was necessary. The final design used 0.20 in. of NBR layup, vulcanized in place, and 0.10 in. of UF-2121 liner. The thickness of the internal insulation controlled the propellant web thickness and provided more than enough insulation on the internal surfaces to prevent bond failure of the external insulation.

4. ADAPTERS

- (U) a. Booster Igniter to Motor--The booster igniter adapter facilitates installation of the igniter loaded case assembly to the motor igniter adapter. Made from low carbon steel, this adapter permits installation of the booster igniter from the aft

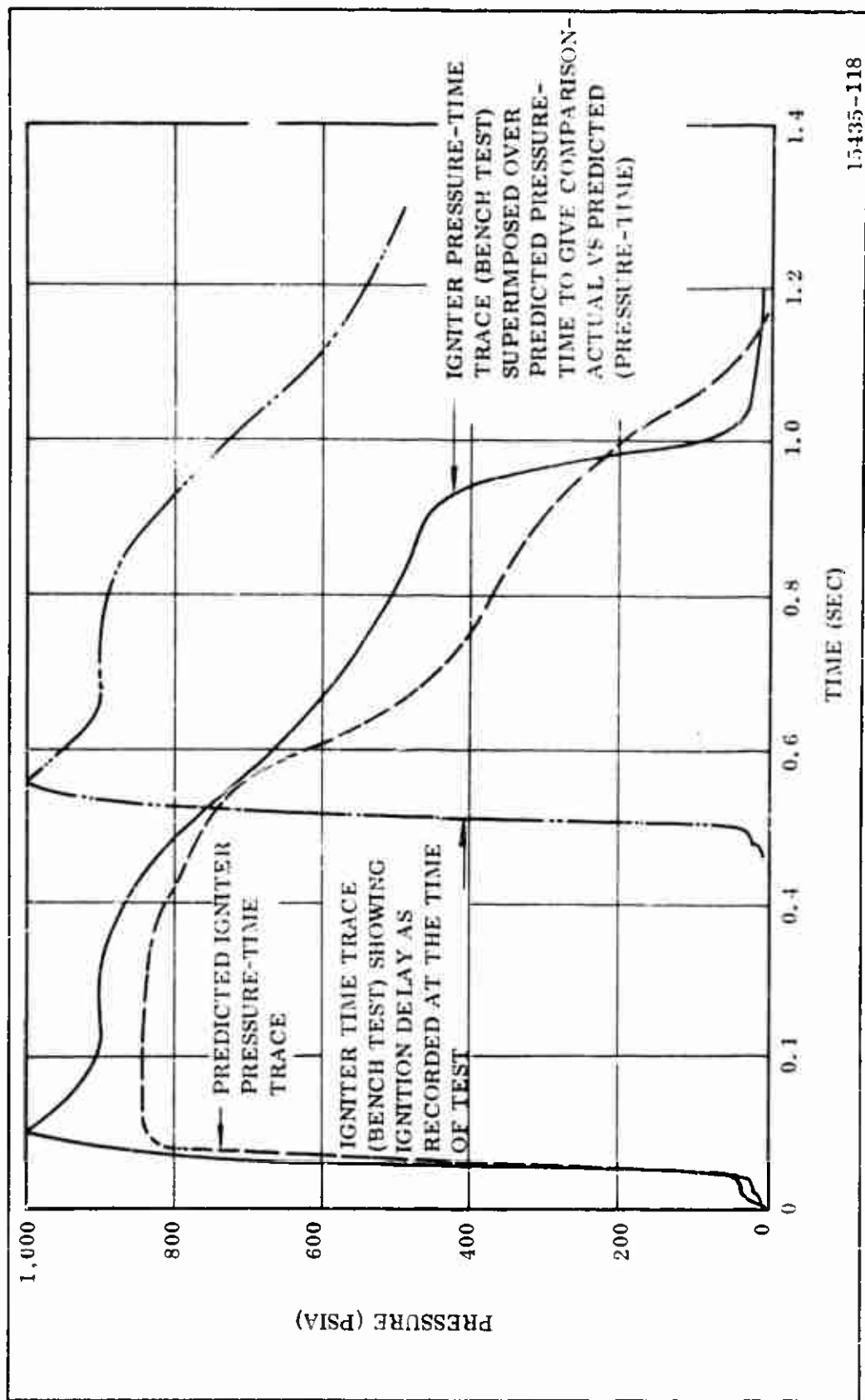


Figure 113. Igniter Pressure Time Trace

end of motor, down the propellant port, and through the motor polar boss where it interfaces with the motor adapter. The booster igniter adapter has ports that mate with the motor adapter and are used to monitor igniter pressure, motor pressure, and provide passage for the carbon dioxide quench system.

- (U) b. Ignition System to Motor--The adapter connecting the ignition system to the motor is made from 4130 steel in the annealed condition. The booster assembly is attached to this motor adapter. The initiating system is attached to the motor adapter with a beveled retaining ring.

B. IGNITER BALLISTIC DESIGN AND MOTOR IGNITION TRANSIENT

- (U) The empirical PYROGEN igniter coefficient is the primary parameter used for determining the required size of a booster PYROGEN igniter. When the ratio of igniter mass flow rate (lb/sec) to the motor throat area (sq in.) is in the range of 0.15 to 0.25, satisfactory ignition will result. Thus, an approximate PYROGEN igniter motor mass flow rate can be established for a motor having specified nozzle dimensions. Usually, the values selected for the PYROGEN igniter coefficient have been in the range of 0.17 to 0.20. The igniter has a mass flow rate of 1.70 lb/sec, which results in a coefficient of 0.182.

- (U) Motor ignition occurs sequentially through the action of a pyrotechnic charge and two PYROGEN igniters. The S & A device is electrically armed and two electrical squibs are initiated; the flame and pressure created by the squibs ruptures two diaphragms and ignites the pyrotechnic booster charge; the flame from the booster charge ignites the initiating PYROGEN igniter; and the initiating PYROGEN igniter exhaust gases ignite the booster PYROGEN igniter.

(U) The ignition transient for the motor is made up of four relatively distinct time periods identified as follows.

1. Igniter response time.
2. Time to achieve motor pressure-igniter output equilibrium prior to motor propellant ignition.
3. Lag time or time between equilibrium pressure achievement and first ignition of motor propellant.
4. Flame spreading time or time from end of lag time until all surfaces of the motor grain have been ignited.

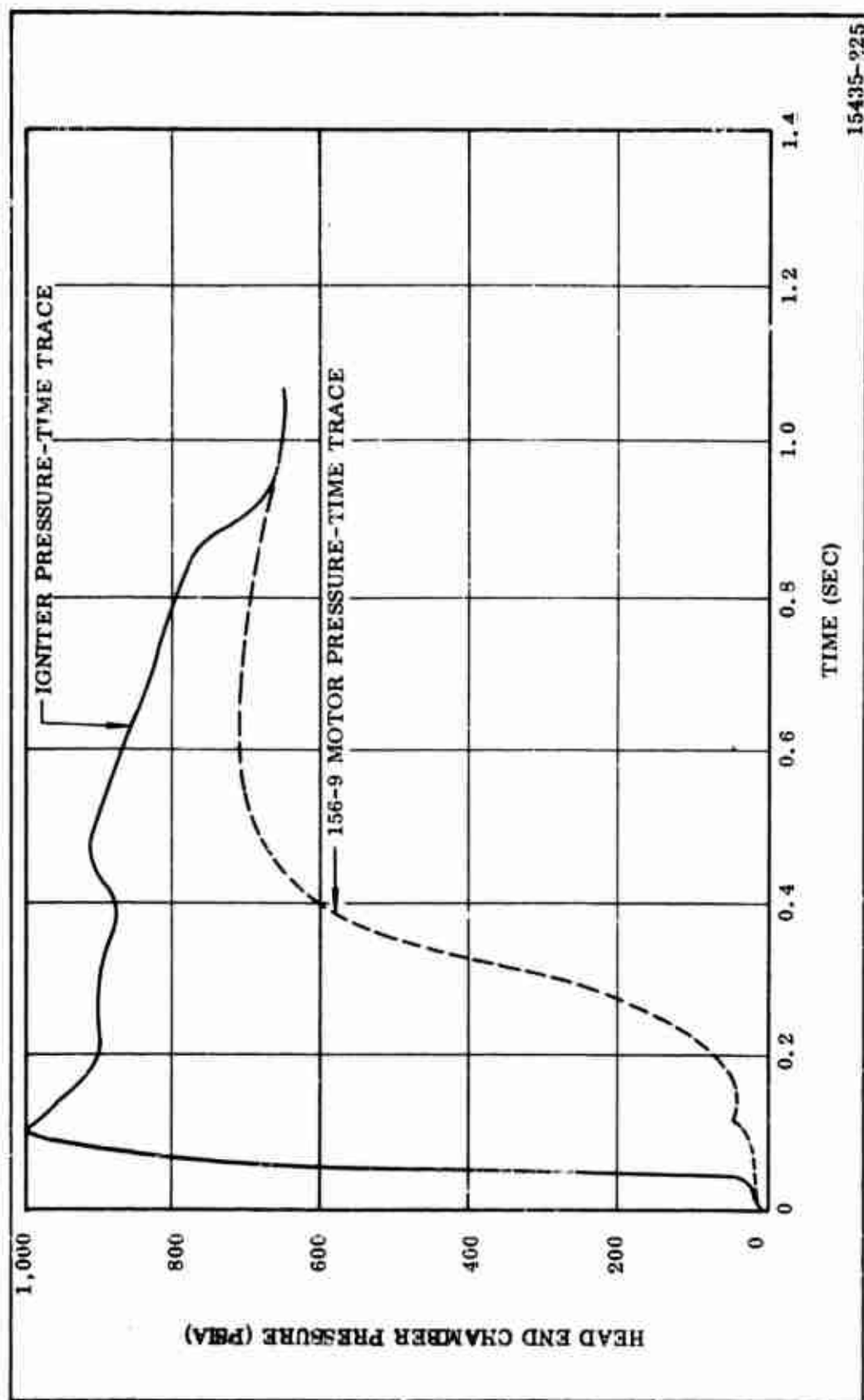
(U) Thiokol predicted the ignition transients expected for the 156-9 motor. The prediction included an equilibrium calculation which begins at the end of lag time and ends upon achievement of motor equilibrium pressure. The prediction was based on the ballistic and physical characteristics of the 156-9 motor grain, the ignition data of the bench test igniter, estimated time of first ignition, and flame spreading rates over all propellant surfaces in the motor. Motor pressure, thrust, mass flow rate, and surface area ignited, plus igniter pressure and mass flow rate were computed as functions of time.

(U) The predicted chamber pressure transients for the 156-9 motor and igniter are illustrated in Figure 114.

C. IGNITER INSULATION DESIGN

1. CASE INTERNAL INSULATION

(U) The case internal insulation provides thermal protection and controls the web thickness of the propellant grain. The internal insulation consisted of two 0.1 in. thick plies of asbestos filled NBR laid up and vulcanized in place. The insulation was sealed with Koropon prior to the application of a 0.1 in. coating



15435-225

Figure 114. Predicted Igniter and Motor Pressure vs Time During Ignition Transient (Utah Conditions)

of UF-2121 liner. The UF-2121 liner provided a high strength bond to the TP-H1016 propellant. This insulation-liner-propellant bond system has historically resulted in propellant bonds of 120 psi tensile adhesion and 6.8 pli for the 180 deg peel test.

2. CASE EXTERNAL INSULATION

- (U) The igniter case external insulation prevents the steel case from melting during the motor firing, precluding the ejection of igniter case fragments. The external insulation consisted of 1.0 in. of asbestos filled NBR laid up and vulcanized in place. The insulation thickness was calculated for the 156-8 motor which has an action time of 122 sec, compared to 70.51 sec for the 156-9 motor. To facilitate use of the same design without excessive engineering and manufacturing changes, the same external igniter insulation thickness was used for the 156-9 as for the 156-8. The insulation thickness was calculated for the 156-8 based on a char rate of 5.5 mil/sec with a 1.5 safety factor. By comparison, the external insulation thickness for the 156-9 igniter is more than adequate.

3. IGNITER CAP INSULATION

- (U) The insulation applied to the adapter (Figure 112) was TI-H704B (the same as the 156-9 motor case insulation). The insulation was a mastic material containing primarily HC binder, asbestos, and carbon black (see Section VIA2 for physical and thermal properties). It is most effective in areas of low gas velocity, and was selected as the PYROGEN igniter insulation because of its relatively low cost, ease of application to any configuration, and ability to cure at ambient temperature.

D. IGNITER WEIGHT ANALYSIS

(U) The component weights for the PYROGEN igniter are listed below.

	<u>Weight (lb)</u>
Loaded Case Booster PYROGEN Igniter	
Case	260.8
External Insulation	87.6
Internal Insulation	13.306
UF-2121 Liner	4.1
TP-H1016 Propellant	131.9
Initiating PYROGEN Igniter	
Case	3.9
TP-H1016 Propellant	1.2
Nozzle	0.6
Booster Assembly	0.481
S & A Device	4.800
Adapter (7U40511)	51.425
Adapter (7U40512)	6.687
Insulated Adapter (7U40514)	113.153
Miscellaneous	<u>11.23</u>
TOTAL	691.176

CONFIDENTIAL

E. IGNITION SYSTEM PROPELLANT

- (U) The propellant selected for use in the ignition system is designated TP-H1016. The composition, ballistic and physical properties of this propellant are shown in the following tabulations.

(C) TP-H1016 Propellant Composition

<u>Constituent</u>	<u>Composition by Weight (Percent)</u>
Ammonium Perchlorate	77
Aluminum Powder	2
HB and ERL*	18
Ferric Oxide	3

(C) Ballistic Properties

Characteristic Velocity, C^* (ft/sec)	4,945
Density (lb/in. ³)	0.0605
Exponent Burn Rate, n	0.35
Burn Rate at 1,000 psi (in./sec)	0.84
Flame Temperature (°F)	4,770
Ratio of Specific Heats (γ)	1.23

(U) Physical Properties

	<u>Minimum</u>	<u>Maximum</u>
Density (lb/in. ³)	0.0599	0.0611
Maximum Strain (psi)	140	227
Strain at Maximum Stress (in./in.)	0.20	0.33
Modulus of Elasticity (psi)	600	1,200

*The ratio of HB to ERL is determined from raw material standardization to achieve the desired physical properties.

CONFIDENTIAL

(THIS PAGE IS UNCLASSIFIED)

F. IGNITION SYSTEM STRUCTURAL ANALYSIS

(U) The ignition system booster igniter case, the adapters that integrate ignition system and adapt the igniter to the motor, the motor case polar boss, and the forward portion of the motor case were analyzed to determine structural integrity and compatibility. The following conditions were investigated to determine the most severe loading.

1. Booster igniter case pressurized to an ignition pressure of 1,100 psi (1.35 times average pressure) with motor unpressurized.
2. 156-9 motor pressurized to MEOP (885) psi with booster igniter case at equilibrium pressure.

(U) The analytical results are summarized in Figures 115 and 116. Margins of safety shown were calculated from the greatest stresses existing at the critical points of the structure and ultimate material strengths. A negative margin of safety is shown in condition 2 at the center of the adapter ring.

(U) The stress is almost entirely due to bending moment. The computer program used was not programmed to use an applicable 1.5 bending factor. Hand calculating a 1.5 bending factor, the following margin of safety exists.

$$1 - \frac{101,101}{(1.5)(90,000)} = 0.25$$

G. IGNITER FABRICATION, ASSEMBLY AND INSTALLATION

(U) The igniter case was fabricated from a TU-121 motor case. The lifting lugs, PYROGEN igniter boss and head end skirt were removed, the PYROGEN igniter hole was opened to 7 in. and a nozzle ring welded in place. The weld area was stress relieved and the nozzle ring finish machined. Each igniter case was hydrotested

CONFIDENTIAL

(THIS PAGE IS UNCLASSIFIED)

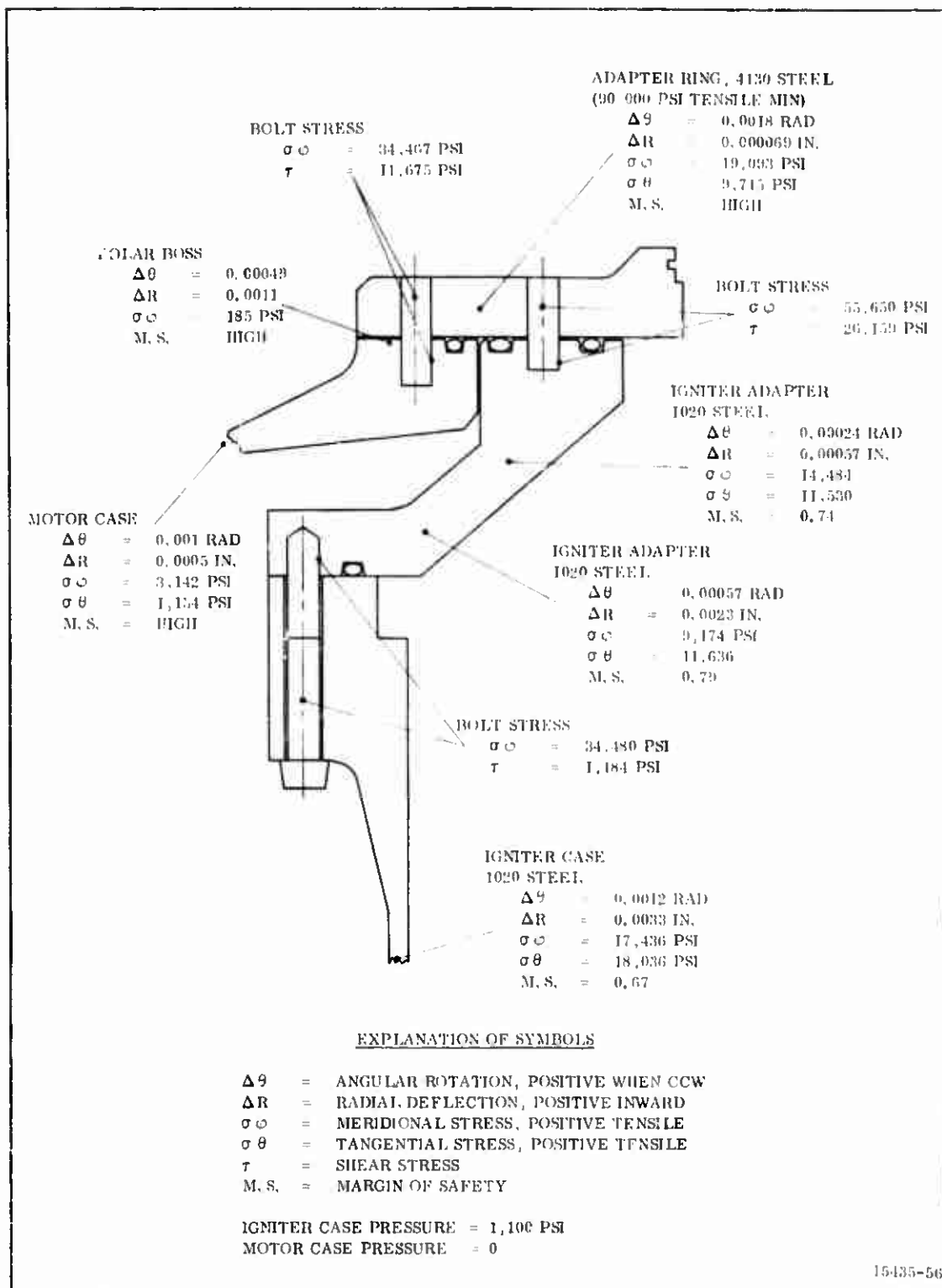


Figure 115. Summary of Structural Analysis, Condition 1

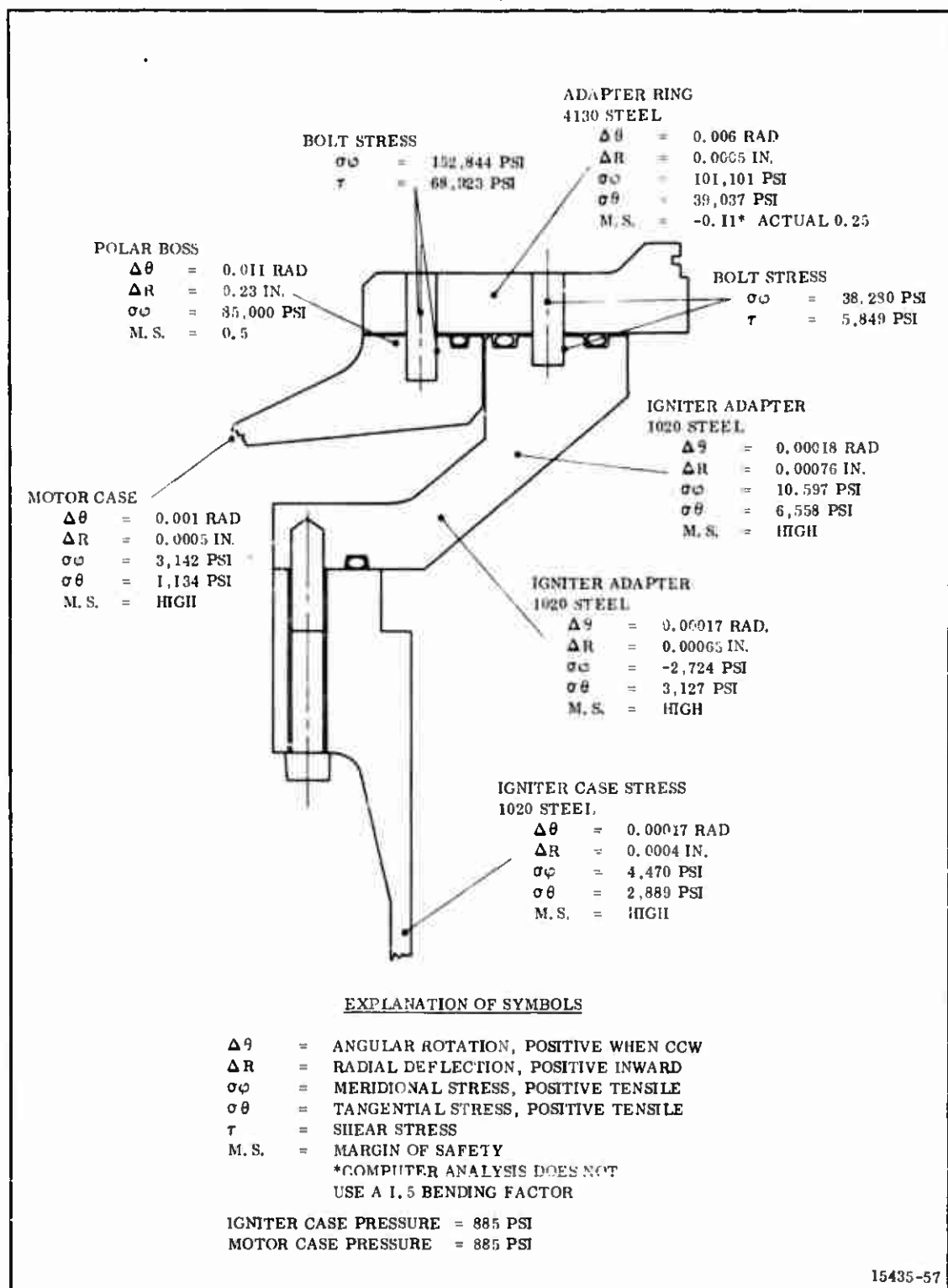


Figure 116. Summary of Structural Analysis, Condition 2

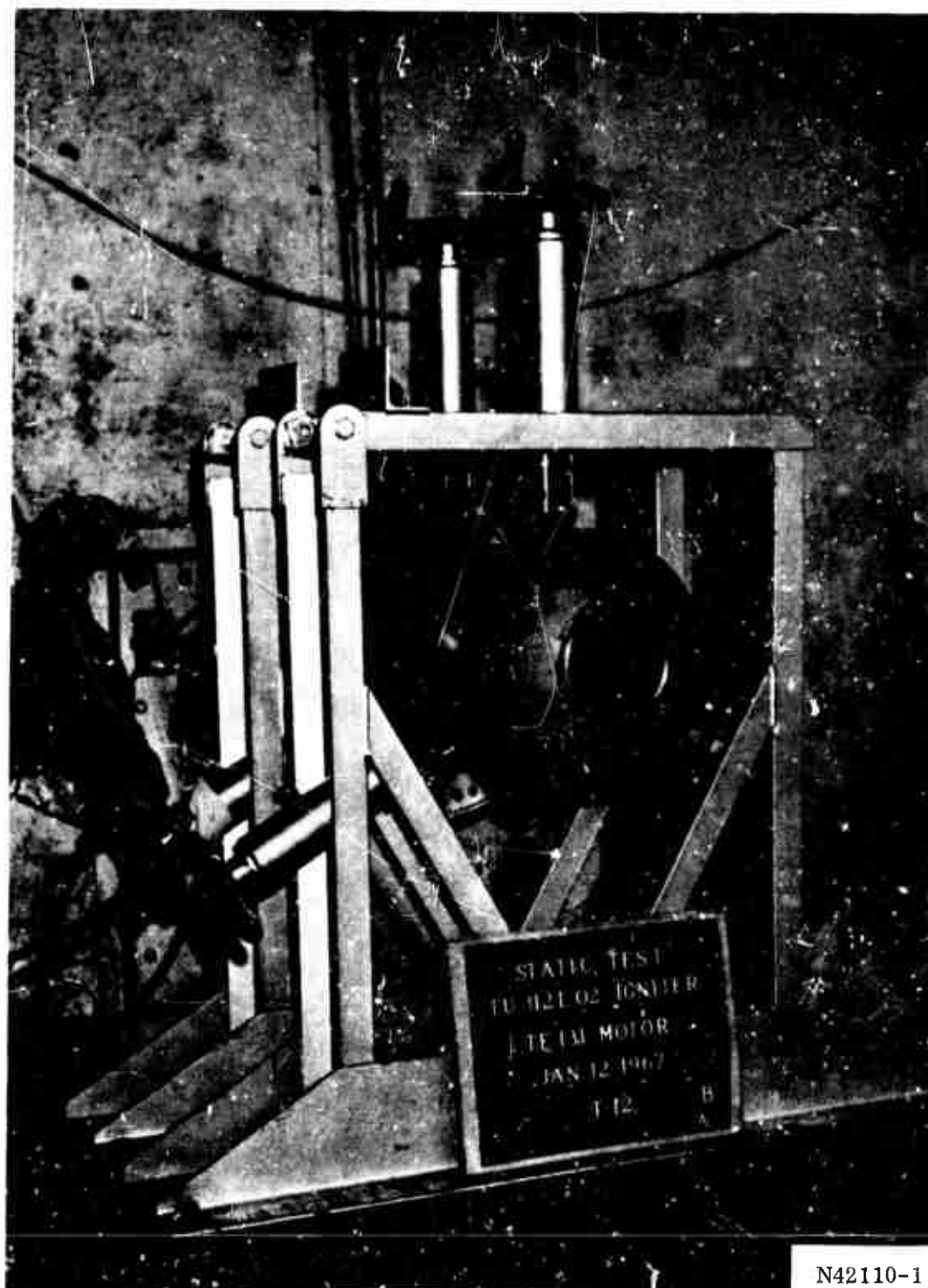
to 1,100 psig. Four cases were fabricated; two for the 156-8 program and two for the 156-9 program. One of the 156-8 cases was used as the bench test igniter for both the 156-8 and 156-9 programs.

- (U) After machining, the interior and exterior surfaces were grit blasted and vapor degreased. V-44 NBR insulation was applied to both the interior and exterior surfaces of the case, using a Chemlok 203 and 220 bonding system, and vulcanized in an autoclave at 100 psig and 250° F for 3 hours, 310° F for 3 hours, then cooled for 6 hours. The external surface and nozzle area insulation were then final machined.
- (U) The internal insulation was abraded, and cleaned with MEK. Koropon was applied to the internal insulation and cured for 5 hours at ambient temperature. UF-2121 liner was then applied and cured for 3 hours at ambient temperature and 40 hours at 135° F.
- (U) Casting fixtures were assembled in the case and the igniter was vacuum cast with TP-H1016 propellant. After a propellant cure of 96 hours at 135° F and a 24 hour cooldown at ambient, the core was removed and the propellant cut back to print configuration.
- (U) Final assembly of the igniter was accomplished by bolting the insulated adapter to the igniter and filling over the bolts, which were countersunk in the NBR, with UF-1155 insulation. The UF-1155 insulation was cured for 2 hours at ambient temperature.
- (U) The initiator assembly, a modified TU-P140 (MACE) PYROGEN igniter, was also cast with TP-H1016 propellant after degreasing and lining with UF-2109 liner. The liner was cured for 18 hours and the propellant for 96 hours at 135° F. After propellant cure and casting fixture removal, the nozzle and adapter were installed on the loaded initiator case using UF-3131 sealant. The booster was installed and the assembly painted.

- (U) The igniter was installed in the motor by lowering it through the nozzle port with the motor in the vertical position. Attachment to the motor case was accomplished by means of a metal adapter through which bolts attached to both the igniter and the case boss. After installation, all bolts were lock wired.
- (U) The initiator was manually installed after the motor was positioned horizontally. Vacuum tape was applied to the initiator to seal between it and the igniter's insulated adapter. A snap ring was used to secure the initiator in the igniter adapter.

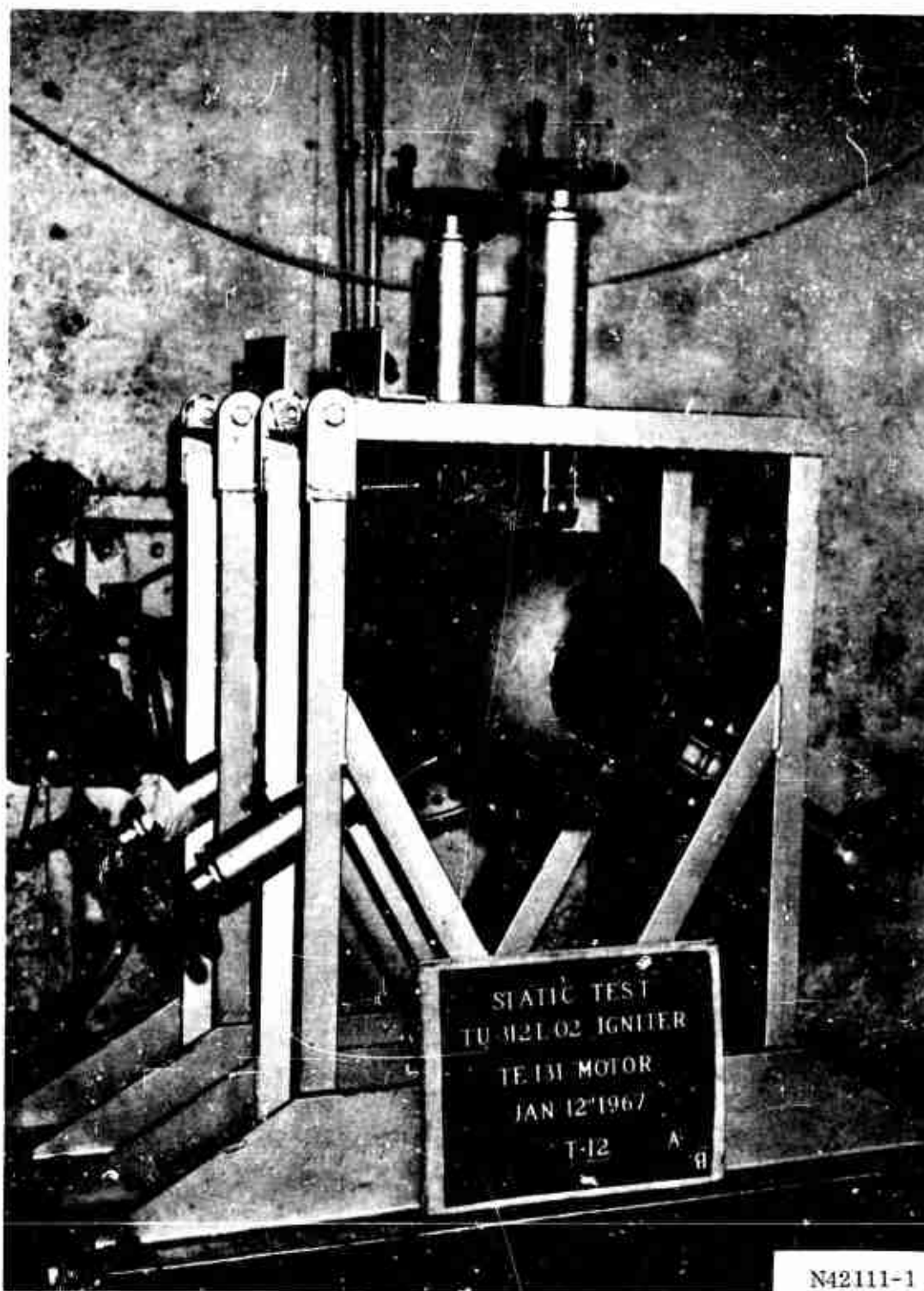
H. IGNITION SYSTEM FUNCTIONAL VERIFICATION (BENCH TEST)

- (U) The ignition system consisted of components previously demonstrated in the AF 156-1 motor test. The only modification to the AF 156-1 igniter is that the booster PYROGEN igniter is somewhat shorter. Consequently, only minimal bench testing was required to verify components and performance. This testing included the static firing of one complete igniter assembly with a rebuilt S & A device and without external insulation. This test was conducted under the AF 156-8 program since 156-8 and 156-9 ignition systems are identical except for adapting to their respective motors. The primary objective of this test was to evaluate performance parameters such as igniter response time, igniter ignition delay, and booster PYROGEN lag time, and pressures. Instrumentation consisted of pressure gages on the booster PYROGEN igniter.
- (U) The 156-9 ignition system was successfully tested during the week ending 13 Jan 1967 in the TU-121 delta test stand (Figure 117 before test and Figure 118 after test) and fired when the igniter grain temperature was at 74°F. The igniter had been temperature conditioned for a minimum of 12 hr at a temperature of 85 ± 5°F. The igniter ballistic characteristics (Table XXV) and the pressure time trace (Figure 113) verified that satisfactory ignition of the 156-9 motor would occur, resulting in a smooth transient through ignition without an excessive pressure spike.



N42110-1

Figure 117. 156-9 Igniter in Test Stand (Before Firing)



N42111-1

Figure 118. 156-9 Igniter in Test Stand (After Firing)

CONFIDENTIAL

TABLE XXV

BALLISTIC CHARACTERISTICS - 156-9 (TU-562) IGNITER

<u>Characteristics</u>	<u>Predicted</u>	<u>Bench Test</u>
Mass flow rate, first level 0.56 sec (lb/sec)	158	170
Burning time, 10 percent P_{\max} to 10 percent P_{\max} (sec)	1.1	0.95
Maximum operating pressure (psia)	850	1,005
Average operating pressure, first level (psia)	820	840
Average operating pressure, second level (psia)	350	529
Ignition delay T_0 to 10 percent P_{\max} for booster PYROGEN igniter (sec)	0.050	0.040*
Ignition interval booster PYROGEN igniter T_0 to 90 percent P_{\max} (sec)	0.076	0.069*
156-9 ignition delay time T_0 to 75 percent P_{\max} (sec)	--	0.39**
156-9 maximum motor pressure at ignition (psia)	--	717**
156-9 igniter coefficient (lb/sec/in. ²)	0.168	0.182**
Total Impulse (lb-sec)	24,208	
Specific Impulse (lb-sec/lb)	184.5	

*Based on first pressure indication being T_0 . The time T_0 as recorded at time of test appears to be erroneous.

**Based on bench test data.

SECTION IX

ACTUATION SYSTEM

A. ACTUATION SYSTEM DESIGN

- (U) The thrust vector control system used on the 156-9 motor consisted of two actuators, each controlled by a servovalve. The servovalves in turn were controlled by an external electronic system and a program magnetic tape. Hydraulic power was supplied to the system from a ground hydraulic power source located near the test bay. An accumulator was installed in the system just ahead of the servovalves.

1. ACTUATOR DESIGN

- (U) The actuator cylinder (Figure 119) was a standard industrial unit manufactured by Parker-Hannifin as their model KD-2HLST13. This basic double acting cylinder had a 6 in. bore, a 7 in. stroke and a 2-1/2 in. rod diameter. It was rated at 3,000 psig operating pressure.

- (U) The basic cylinder was modified slightly to better tailor it to this particular application. The principal changes are outlined below.

1. A linear variable differential transformer (LVDT) type position feedback transducer was mounted inside one rod. The LVDT was used to assure compatibility with a similar unit which is standard equipment on the servovalve selected. Internal mounting gives maximum protection.

PRECEDING PAGE BLANK-NOT FILMED

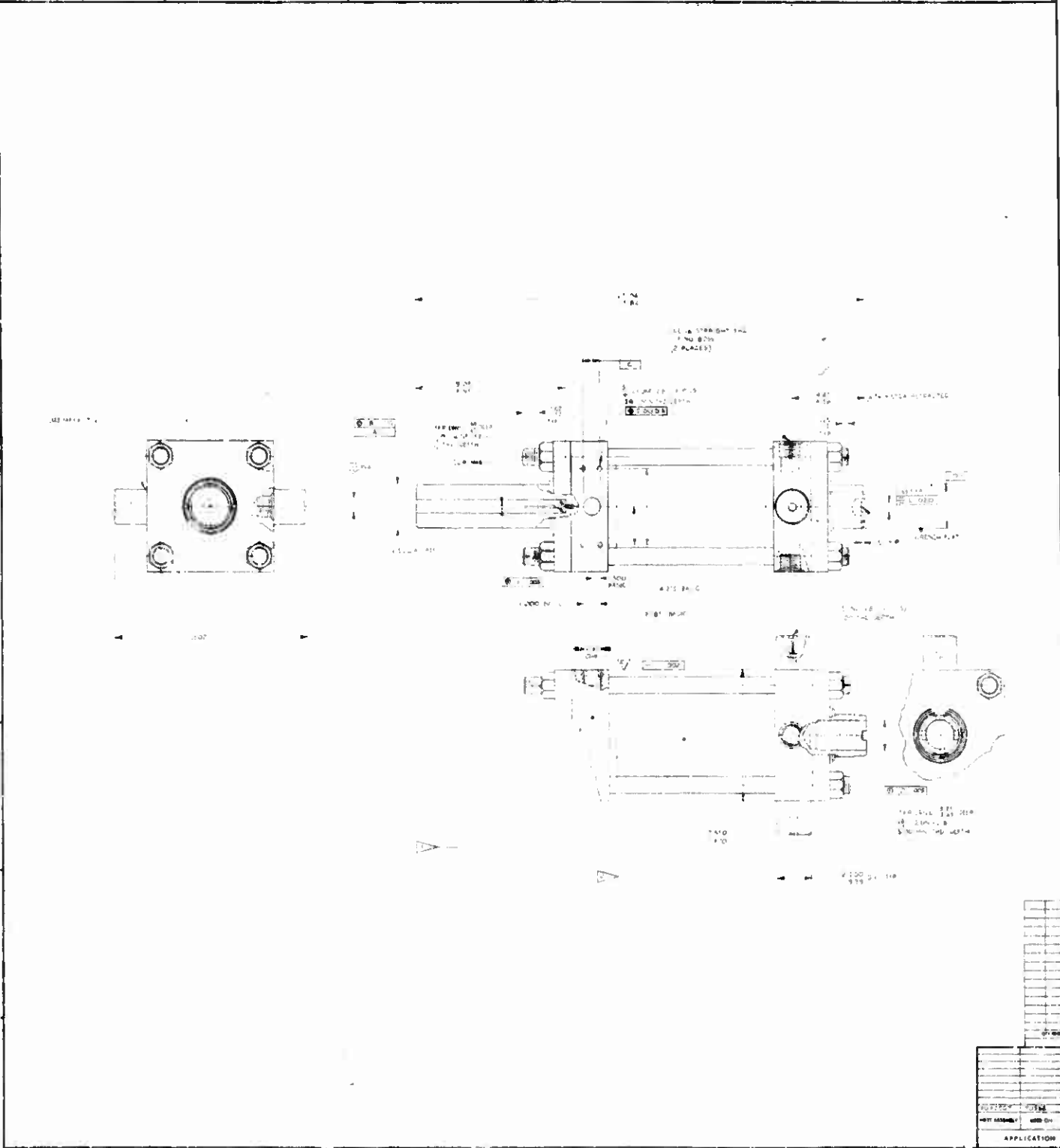


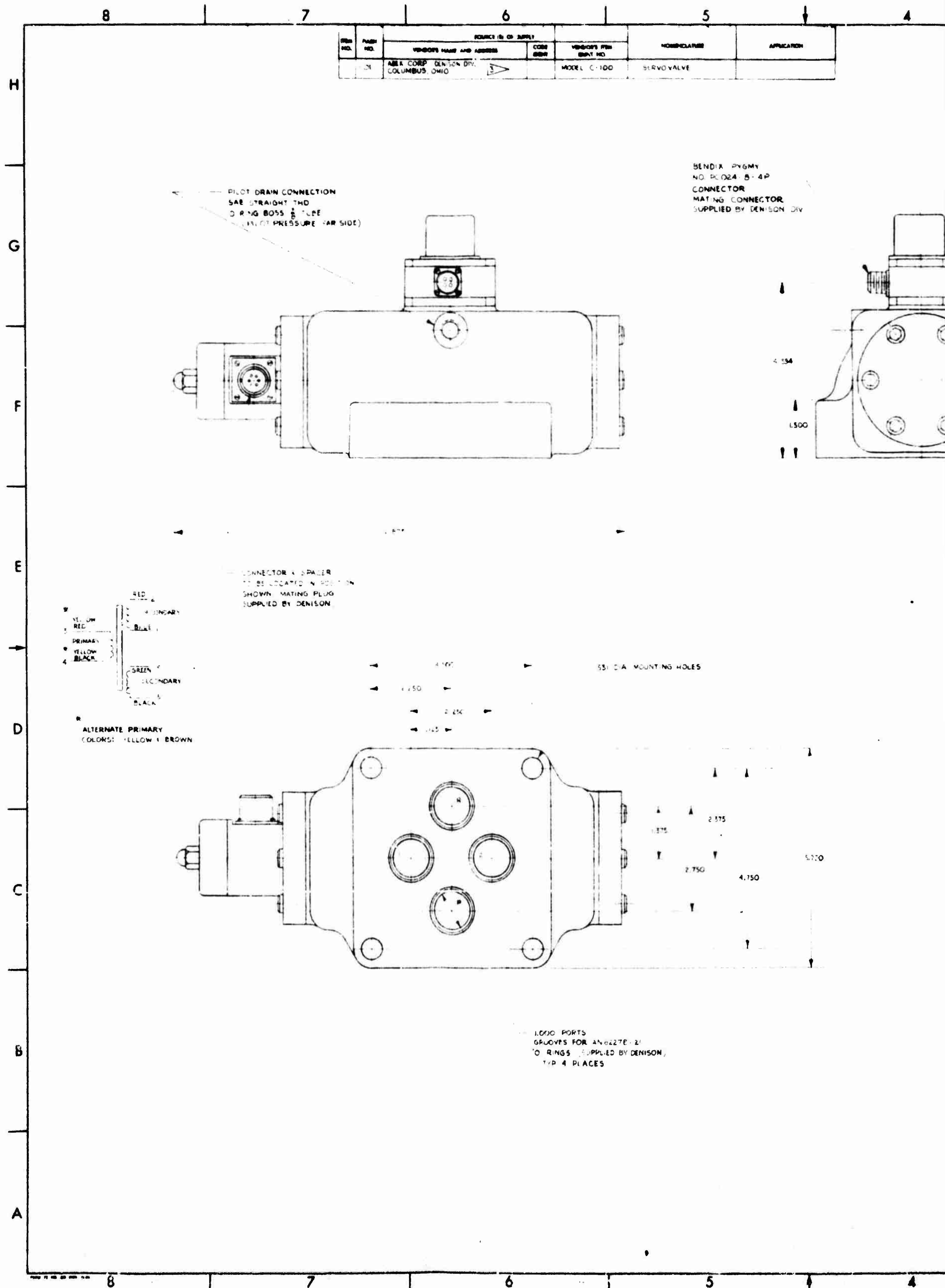
Figure 1

2. Internal threads in the other rod were changed to accept a spherical rod end bearing selected for its high strength.
3. Tapped holes were provided in one of the cylinder head blocks to mount the servovalve and manifold assembly as well as the position feedback transducer housing.
4. Straight through porting to match that in the manifold was also provided on one head block. Two threaded port holes were provided on the other head block to receive two hydraulic lines direct from the manifold. These changes were made to increase the cylinder porting capacity and thus enable them to handle the higher flow requirements.

(U) The actuators were mounted in a universal trunnion assembly to allow for actuation in the opposite plane. Trunnions were located on the actuator head block to minimize structural design requirements in the actuator mounting brackets as well as to eliminate the tendency toward buckling when the rod is extended.

2. SERVOVALVE DESIGN

(U) The servovalves shown in Figure 120 are three stage units marketed commercially as Model C-100 by the Denison Division of Abex Company. They employ Atchley Model 410 servovalves as the first two (pilot) stages. Pilot valve flow controls a third stage spool which is equipped with a LVDT position feedback. (It was this LVDT feature that prompted Thiokol to use a LVDT feedback on actuator position.) The servovalves are capable of operating throughout a -65 to +275° F temperature range with a null shift per 100° F of less than 2 percent. The rate of flow at 1,000 psi drop is 100 gpm with a null leakage at 3,000 psi of less than 3 gpm. Flow linearity from 0 to 100 gpm is at least 5 percent.



(U) • A manifold is mounted between the servovalve and the actuator to direct the hydraulic oil flow.

(U) The above defined actuator, servovalve and manifold together with the associated rod end bearing, fittings and hydraulic lines make up the servoactuator assembly P/N 7U40505-01. This unit is shown in Figure 121.

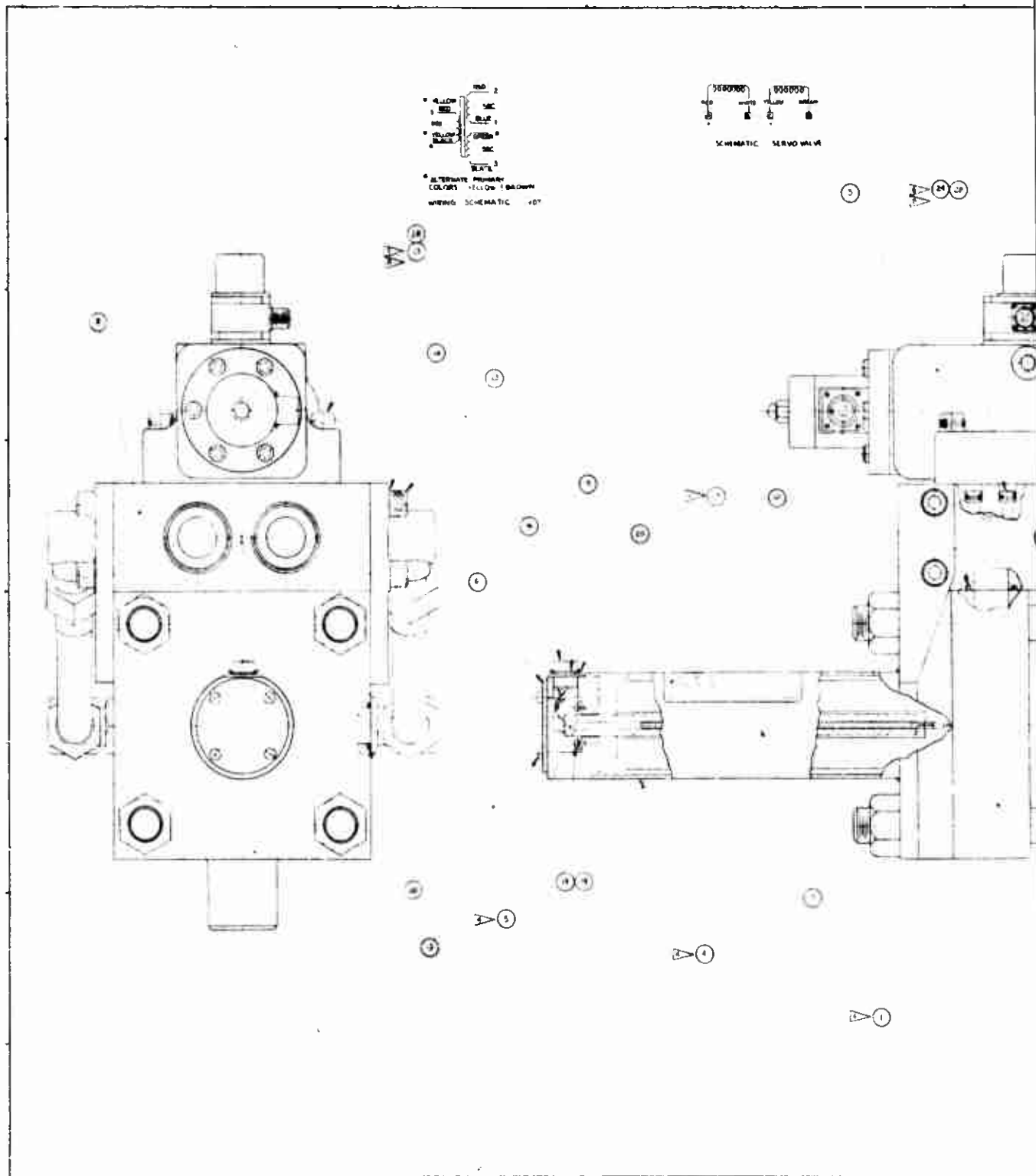
3. TORQUE ANALYSIS

(U) Complete torque analyses are presented in Section III of this report. Actuation design torque is established by considering all torque factors and adding those the actuator must overcome. Preliminary torque values used in the actuation system design were:

Dynamic spring	1,356,000 in.-lb
Viscous seal	250,000 in.-lb
Offset	171,000 in.-lb
Gravitational	<u>186,000 in.-lb</u>
	1,963,000 in.-lb

(U) Early in the firing the aerodynamic torque is opposite in direction to spring torque due to the location of the nozzle pivot point. It later goes to zero. Inertial torque is always opposite in direction to spring torque when deflections are large enough to make total torque an important design consideration. Therefore, these two torques have been neglected in arriving at a total actuation design torque of 1,963,000 in.-lb.

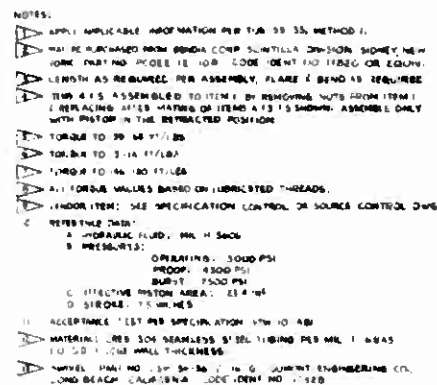
PRECEDING PAGE BLANK-NOT FILMED





1

2



1	10/10/50	10:00	1000	1000
2	10/10/50	10:00	1000	1000
3	10/10/50	10:00	1000	1000
4	10/10/50	10:00	1000	1000
5	10/10/50	10:00	1000	1000
6	10/10/50	10:00	1000	1000
7	10/10/50	10:00	1000	1000
8	10/10/50	10:00	1000	1000
9	10/10/50	10:00	1000	1000
10	10/10/50	10:00	1000	1000
11	10/10/50	10:00	1000	1000
12	10/10/50	10:00	1000	1000
13	10/10/50	10:00	1000	1000
14	10/10/50	10:00	1000	1000
15	10/10/50	10:00	1000	1000
16	10/10/50	10:00	1000	1000
17	10/10/50	10:00	1000	1000
18	10/10/50	10:00	1000	1000
19	10/10/50	10:00	1000	1000
20	10/10/50	10:00	1000	1000
21	10/10/50	10:00	1000	1000
22	10/10/50	10:00	1000	1000
23	10/10/50	10:00	1000	1000
24	10/10/50	10:00	1000	1000
25	10/10/50	10:00	1000	1000
26	10/10/50	10:00	1000	1000
27	10/10/50	10:00	1000	1000
28	10/10/50	10:00	1000	1000
29	10/10/50	10:00	1000	1000
30	10/10/50	10:00	1000	1000
31	10/10/50	10:00	1000	1000
32	10/10/50	10:00	1000	1000
33	10/10/50	10:00	1000	1000
34	10/10/50	10:00	1000	1000
35	10/10/50	10:00	1000	1000
36	10/10/50	10:00	1000	1000
37	10/10/50	10:00	1000	1000
38	10/10/50	10:00	1000	1000
39	10/10/50	10:00	1000	1000
40	10/10/50	10:00	1000	1000
41	10/10/50	10:00	1000	1000
42	10/10/50	10:00	1000	1000
43	10/10/50	10:00	1000	1000
44	10/10/50	10:00	1000	1000
45	10/10/50	10:00	1000	1000
46	10/10/50	10:00	1000	1000
47	10/10/50	10:00	1000	1000
48	10/10/50	10:00	1000	1000
49	10/10/50	10:00	1000	1000
50	10/10/50	10:00	1000	1000
51	10/10/50	10:00	1000	1000
52	10/10/50	10:00	1000	1000
53	10/10/50	10:00	1000	1000
54	10/10/50	10:00	1000	1000
55	10/10/50	10:00	1000	1000
56	10/10/50	10:00	1000	1000
57	10/10/50	10:00	1000	1000
58	10/10/50	10:00	1000	1000
59	10/10/50	10:00	1000	1000
60	10/10/50	10:00	1000	1000
61	10/10/50	10:00	1000	1000
62	10/10/50	10:00	1000	1000
63	10/10/50	10:00	1000	1000
64	10/10/50	10:00	1000	1000
65	10/10/50	10:00	1000	1000
66	10/10/50	10:00	1000	1000
67	10/10/50	10:00	1000	1000
68	10/10/50	10:00	1000	1000
69	10/10/50	10:00	1000	1000
70	10/10/50	10:00	1000	1000
71	10/10/50	10:00	1000	1000
72	10/10/50	10:00	1000	1000
73	10/10/50	10:00	1000	1000
74	10/10/50	10:00	1000	1000
75	10/10/50	10:00	1000	1000
76	10/10/50	10:00	1000	1000
77	10/10/50	10:00	1000	1000
78	10/10/50	10:00	1000	1000
79	10/10/50	10:00	1000	1000
80	10/10/50	10:00	1000	1000
81	10/10/50	10:00	1000	1000
82	10/10/50	10:00	1000	1000
83	10/10/50	10:00	1000	1000
84	10/10/50	10:00	1000	1000
85	10/10/50	10:00	1000	1000
86	10/10/50	10:00	1000	1000
87	10/10/50	10:00	1000	1000
88	10/10/50	10:00	1000	1000
89	10/10/50	10:00	1000	1000
90	10/10/50	10:00	1000	1000
91	10/10/50	10:00	1000	1000
92	10/10/50	10:00	1000	1000
93	10/10/50	10:00	1000	1000
94	10/10/50	10:00	1000	1000
95	10/10/50	10:00	1000	1000
96	10/10/50	10:00	1000	1000
97	10/10/50	10:00	1000	1000
98	10/10/50	10:00	1000	1000
99	10/10/50	10:00	1000	1000
100	10/10/50	10:00	1000	1000

1. NAME OF THE COMPANY OR PERSON 2. ADDRESS 3. CITY 4. STATE 5. ZIP CODE 6. PHONE NUMBER 7. FAX NUMBER 8. E-MAIL ADDRESS 9. NAME OF THE PERSON TO WHOM THE ORDER SHOULD BE SENT 10. TITLE OF THE PERSON 11. COMPANY OR PERSON'S PHONE NUMBER 12. COMPANY OR PERSON'S FAX NUMBER 13. COMPANY OR PERSON'S E-MAIL ADDRESS 14. NAME OF THE PERSON TO WHOM THE ORDER SHOULD BE SENT 15. TITLE OF THE PERSON 16. COMPANY OR PERSON'S PHONE NUMBER 17. COMPANY OR PERSON'S FAX NUMBER 18. COMPANY OR PERSON'S E-MAIL ADDRESS		USE OF MATERIAL ON PARTS LIST 19. NAME OF THE COMPANY OR PERSON 20. ADDRESS 21. CITY 22. STATE 23. ZIP CODE 24. PHONE NUMBER 25. FAX NUMBER 26. E-MAIL ADDRESS 27. NAME OF THE PERSON TO WHOM THE ORDER SHOULD BE SENT 28. TITLE OF THE PERSON 29. COMPANY OR PERSON'S PHONE NUMBER 30. COMPANY OR PERSON'S FAX NUMBER 31. COMPANY OR PERSON'S E-MAIL ADDRESS	THORNDYKE CHEMICAL CORPORATION 1000 N. 10TH AVE. MINNEAPOLIS, MN 55412-1000
32. NAME OF THE COMPANY OR PERSON 33. ADDRESS 34. CITY 35. STATE 36. ZIP CODE 37. PHONE NUMBER 38. FAX NUMBER 39. E-MAIL ADDRESS 40. NAME OF THE PERSON TO WHOM THE ORDER SHOULD BE SENT 41. TITLE OF THE PERSON 42. COMPANY OR PERSON'S PHONE NUMBER 43. COMPANY OR PERSON'S FAX NUMBER 44. COMPANY OR PERSON'S E-MAIL ADDRESS		45. NAME OF THE COMPANY OR PERSON 46. ADDRESS 47. CITY 48. STATE 49. ZIP CODE 50. PHONE NUMBER 51. FAX NUMBER 52. E-MAIL ADDRESS 53. NAME OF THE PERSON TO WHOM THE ORDER SHOULD BE SENT 54. TITLE OF THE PERSON 55. COMPANY OR PERSON'S PHONE NUMBER 56. COMPANY OR PERSON'S FAX NUMBER 57. COMPANY OR PERSON'S E-MAIL ADDRESS	SERVO ACTUATOR ASSEMBLY
58. NAME OF THE COMPANY OR PERSON 59. ADDRESS 60. CITY 61. STATE 62. ZIP CODE 63. PHONE NUMBER 64. FAX NUMBER 65. E-MAIL ADDRESS 66. NAME OF THE PERSON TO WHOM THE ORDER SHOULD BE SENT 67. TITLE OF THE PERSON 68. COMPANY OR PERSON'S PHONE NUMBER 69. COMPANY OR PERSON'S FAX NUMBER 70. COMPANY OR PERSON'S E-MAIL ADDRESS		71. NAME OF THE COMPANY OR PERSON 72. ADDRESS 73. CITY 74. STATE 75. ZIP CODE 76. PHONE NUMBER 77. FAX NUMBER 78. E-MAIL ADDRESS 79. NAME OF THE PERSON TO WHOM THE ORDER SHOULD BE SENT 80. TITLE OF THE PERSON 81. COMPANY OR PERSON'S PHONE NUMBER 82. COMPANY OR PERSON'S FAX NUMBER 83. COMPANY OR PERSON'S E-MAIL ADDRESS	84. NAME OF THE COMPANY OR PERSON 85. ADDRESS 86. CITY 87. STATE 88. ZIP CODE 89. PHONE NUMBER 90. FAX NUMBER 91. E-MAIL ADDRESS 92. NAME OF THE PERSON TO WHOM THE ORDER SHOULD BE SENT 93. TITLE OF THE PERSON 94. COMPANY OR PERSON'S PHONE NUMBER 95. COMPANY OR PERSON'S FAX NUMBER 96. COMPANY OR PERSON'S E-MAIL ADDRESS

Figure 121. Servoactuator Assembly

B. ACTUATOR SIZE AND FORCE OUTPUT

1. ACTUATOR SIZE

(U) Using design criteria established by the work statement and/or nozzle and flexible seal designs, the actuator size was determined as follows.

(U) The actuator must maintain a vector velocity of 20 deg/sec under the maximum possible torque 1,963,000 in.-lb. Using a minimum lever arm of 48.2 in., the minimum required actuator effective piston area A_E becomes

$$A_E = \frac{1,963,000 \text{ in.-lb}}{(48.2 \text{ in.}) (2,000 \text{ psi})} = 20.3 \text{ sq in.}$$

(U) An industrial cylinder was available with a 6 in. bore, a 2.5 in. rod, and having an effective area of 23.4 sq inch.

(U) With this piston area and the geometric relationship of 0.86 in. of stroke per degree of travel, a flow rate of 105 gpm was required to achieve a vector velocity of 20 deg/sec. At this flow rate, the pressure drop across the selected servovalve would be 1,100 psi, leaving 1,900 psi load pressure. Torque capabilities are:

$$\text{Actuator Dynamic Torque} = (23.4) (1,900) (48.2) = 2,140,000 \text{ in.-lb}$$

$$\text{Actuator Stall Torque} = (23.4) (3,000) (48.2) = 3,380,000 \text{ in.-lb}$$

(U) The above actuator provides a dynamic torque safety factor of 1.09 over the maximum expected torque of 1,963,000 in.-lb, and a safety factor of 1.60 over the nominal expected torque of 1,338,100 in.-lb.

2. ACTUATION GEOMETRY

(U) Due to the degree of nozzle submergence, it was impossible to employ a completely linear actuation system. However, the nonlinearity is relatively minor as evidenced by the following table.

<u>Angular Position</u>	<u>Lever Arm</u>	<u>Stroke</u>
0 deg	49.2 in.	--
4 deg Extend	49.5 in.	3.446
4 deg Retract	48.2 in.	3.407

- (U) These values are applicable to the pressurized condition. Compression of the bearing under pressure results in a 0.07 deg change in alignment. This was compensated for by offsetting the nozzle 0.07 deg cold so that it came into alignment with motor centerline when pressurized.
- (U) It requires 6.853 in. of usable stroke to obtain a total travel of 8 degrees. The actuators were originally designed with a total stroke of 7.00 in., leaving ± 0.073 in. for the combined requirements of overtravel, compliance and mechanical stop.
- (U) Later this was considered too marginal and an Engineering Change Order (ECO) changing the actuator stroke from 7.00 to 7.56 in. was processed. Unfortunately, the first tier vendor who built and tested the actuator assembly misinterpreted the Change Order and procured cylinders having a 7 in. stroke (Figure 121). The fact that cylinder stroke had not been increased was discovered by Thiokol during actuator assembly acceptance tests. At this point there was insufficient time to procure additional cylinders without serious schedule impact and the decision to use the marginal 7 in. stroke cylinders was made. Layouts at the time indicated that even with a maximum lever arm of 49.5 in. the vector angle on the motor would reach 4 deg if nozzle/actuator system compliance was low.
- (U) It should be noted that a vector angle of only 3.75 deg was reached during flexible seal tests. This, however, was due to the fact that the test fixture had a lever arm of 51.4 inches.
- (U) Interaction of pitch and yaw actuation, commonly referred to as crosstalk, was minimized because of the relatively small difference in longitudinal station from the nozzle pivot to the fixed actuator pivot. A full four deg deflection in one plane resulted in only 0.05 deg deflection in the other plane. This was not considered large enough to warrant correction in the duty cycle program tape.

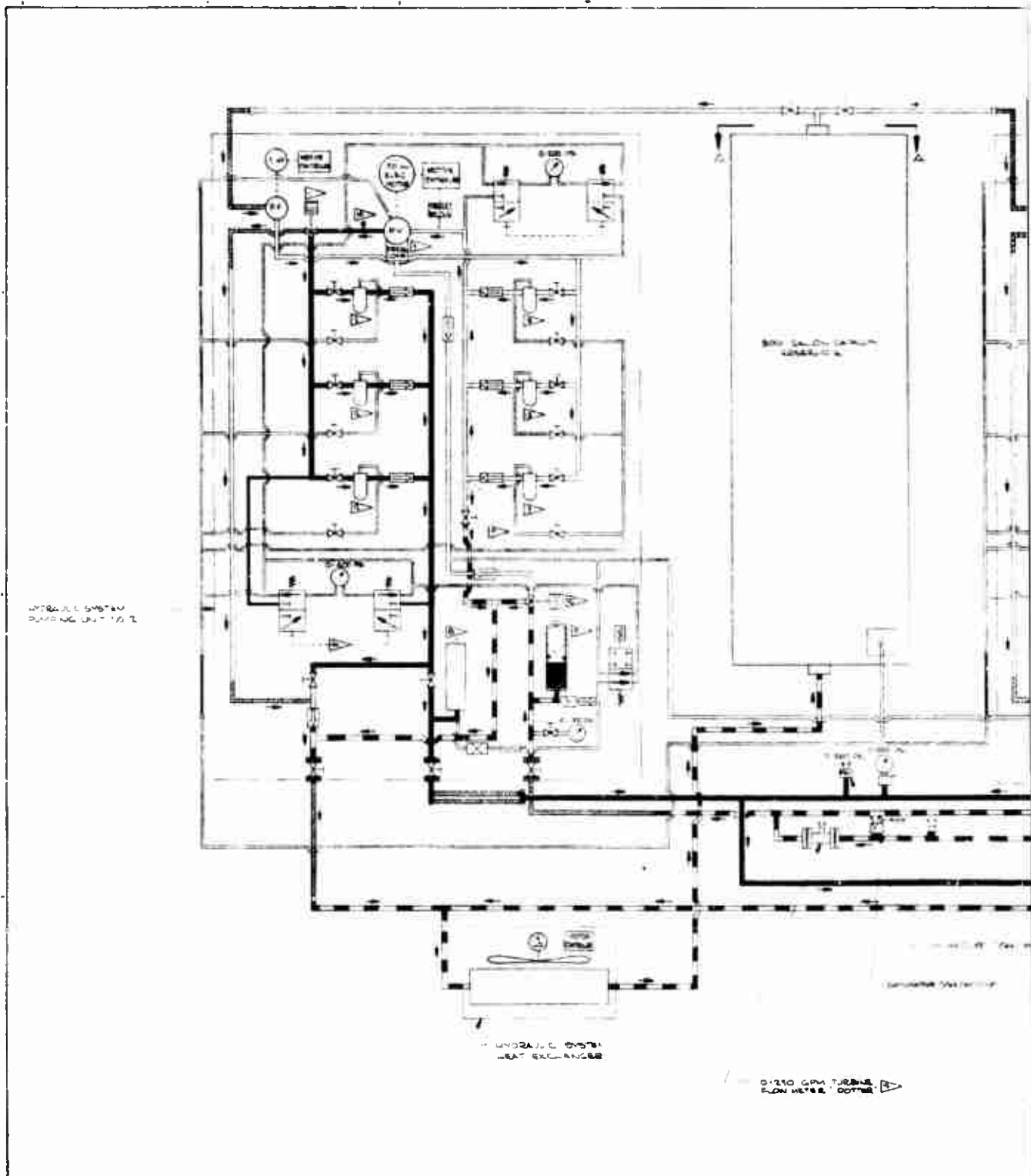
C. WEIGHT ANALYSIS

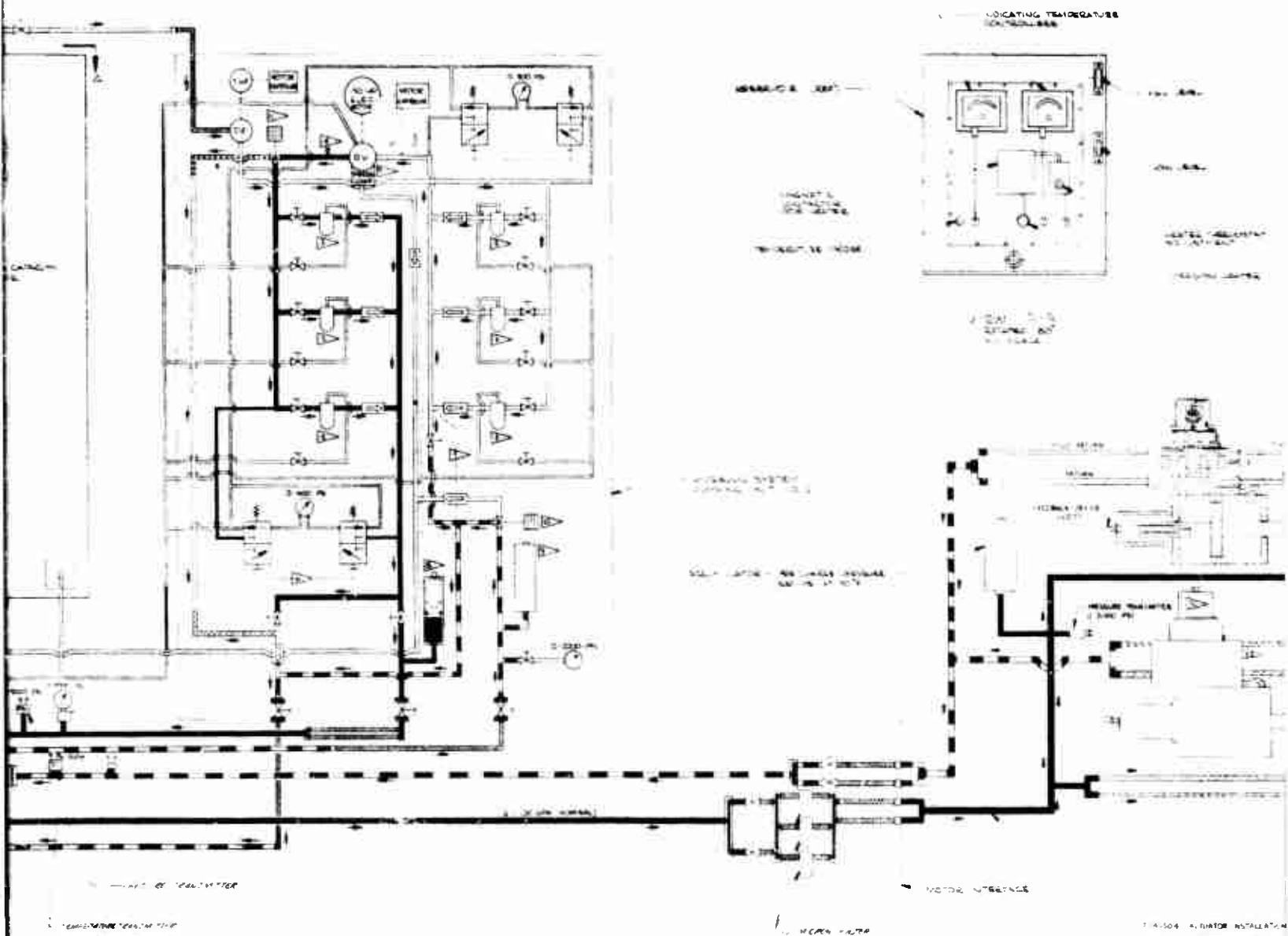
- (U) No attempt was made to optimize actuation system weight and all components were heavyweight. The dry weight of one complete servoactuator assembly, for example, is 288 pounds. It is felt that this weight could be reduced by as much as 30 percent if a lightweight system were employed.

D. HYDRAULIC SYSTEM

- (U) Hydraulic power is supplied by two electric motor driven variable displacement pumps operating in parallel. These same pumps provided hydraulic power for the 156-1 motor. Each pump is capable of delivering 95 gpm at 3,500 psi. The actual output is limited, however, to 60 gpm each in order to preclude any possibility of overloading the electrical circuits. Either pump alone could support the firing at a reduced vectoring rate.
- (U) A prepressurized piston type accumulator is mounted on the motor to dampen line surges and to provide the necessary flow during the period of time required for the pumps to respond to a step demand. Since the peak flow of 105 gpm remains constant for 1.6 seconds, no attempt was made to provide a significant portion of peak flow from the accumulator.
- (U) Line losses at maximum flow were calculated to be approximately 750 psi. The major portion of this loss was contributed by the existing facility supply line. A pressure transducer records system pressure at the motor mounted manifold. If this transducer should show a greater than allowable line loss, no-flow system pressure will be increased. Since the entire system has been proof tested to 4,500 psi, the supply pressure could safely be raised to at least 3,300 psi if required.
- (U) A hydraulic system schematic is shown in Figure 122.

PRECEDING PAGE BLANK-NOT FILMED





7J40587

1

2

E. ELECTRICAL SYSTEM

- (U) A block diagram of the actuation electrical control system is shown in Figure 123. The servocontrol unit, procured for the 156-7 motor firing, provided all electronic components of the system to include LVDT excitation demodulators and servoamplifiers. It was modified for use in a double feedback system required by the three stage servovalve. Modifications include bypassing the phase splitters, tying two demodulator outputs to one servoamplifier input, and changing feedback gain resistors. The unit was rack mounted and all adjustment potentiometers brought to the front panel.
- (U) The operating characteristics of the servovalve transducer were verified using a 5 Kc square wave transducer with the servocontrol unit electronics. Operation was entirely satisfactory and the scale factor under these conditions was determined.
- (U) The nominal open loop gain settings are 150 and 50 sec^{-1} for the valve loop and the total loop respectively. Analog performance analysis showed this to provide a stable system which was later verified by actual test data run under these settings (Figures 124 and 125). The entire system has been successfully demonstrated on the flexible seal tests.

F. 156-9 DUTY CYCLE

- (U) The actuation duty cycle for the 156-9 nozzle (Figure 126 and Table XXVI) meets the requirements of the program work statement. The side impulse produced by nozzle deflection is predicted to be 1.37 percent of the axial impulse as compared to the requirement of 1.10 percent. The nozzle will be in motion or at a position other than null for 33.6 seconds of motor operation. The duty cycle requires a full deflection of 4 degrees during two events: two triangular cycles at 1.25 cps and two

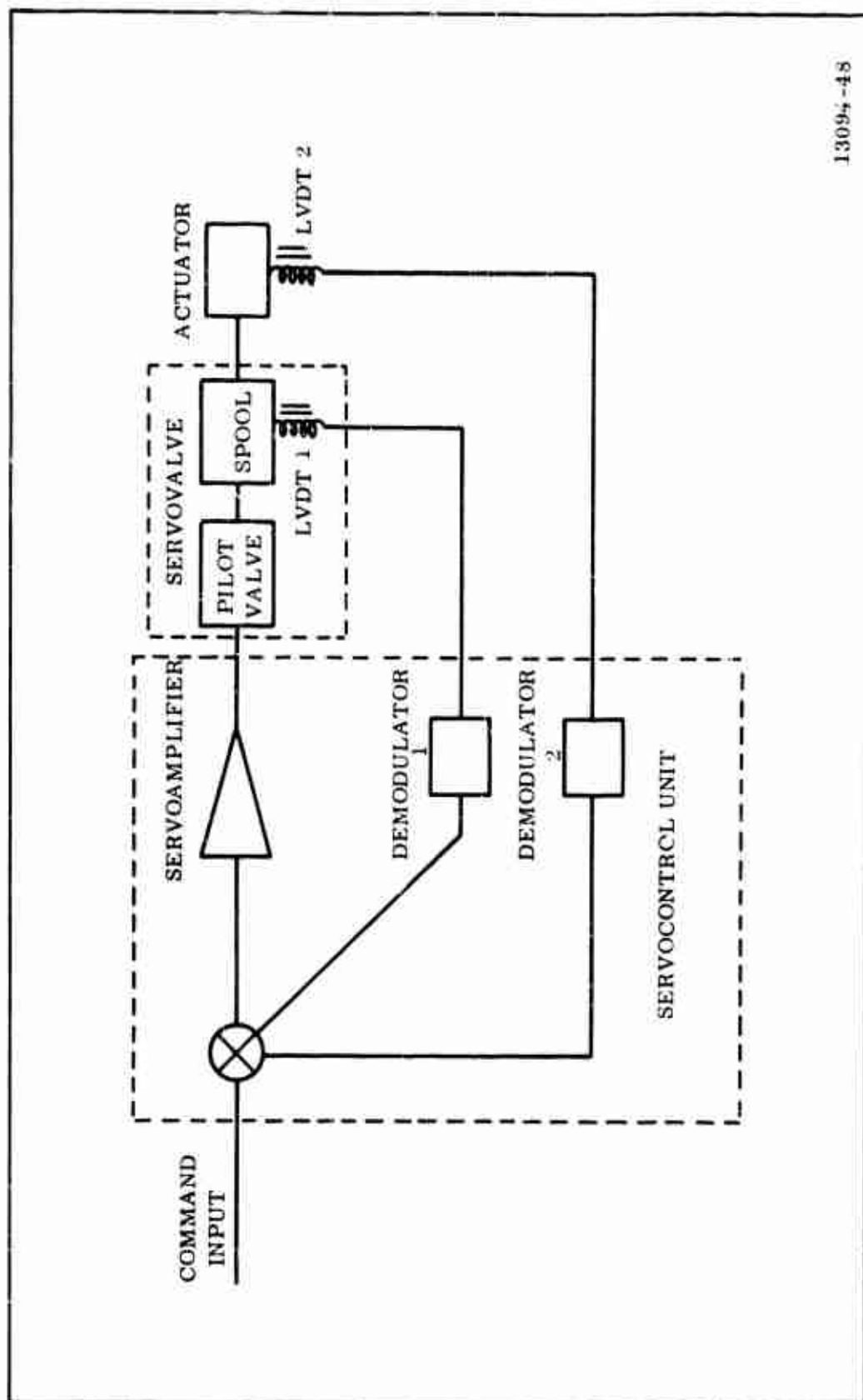
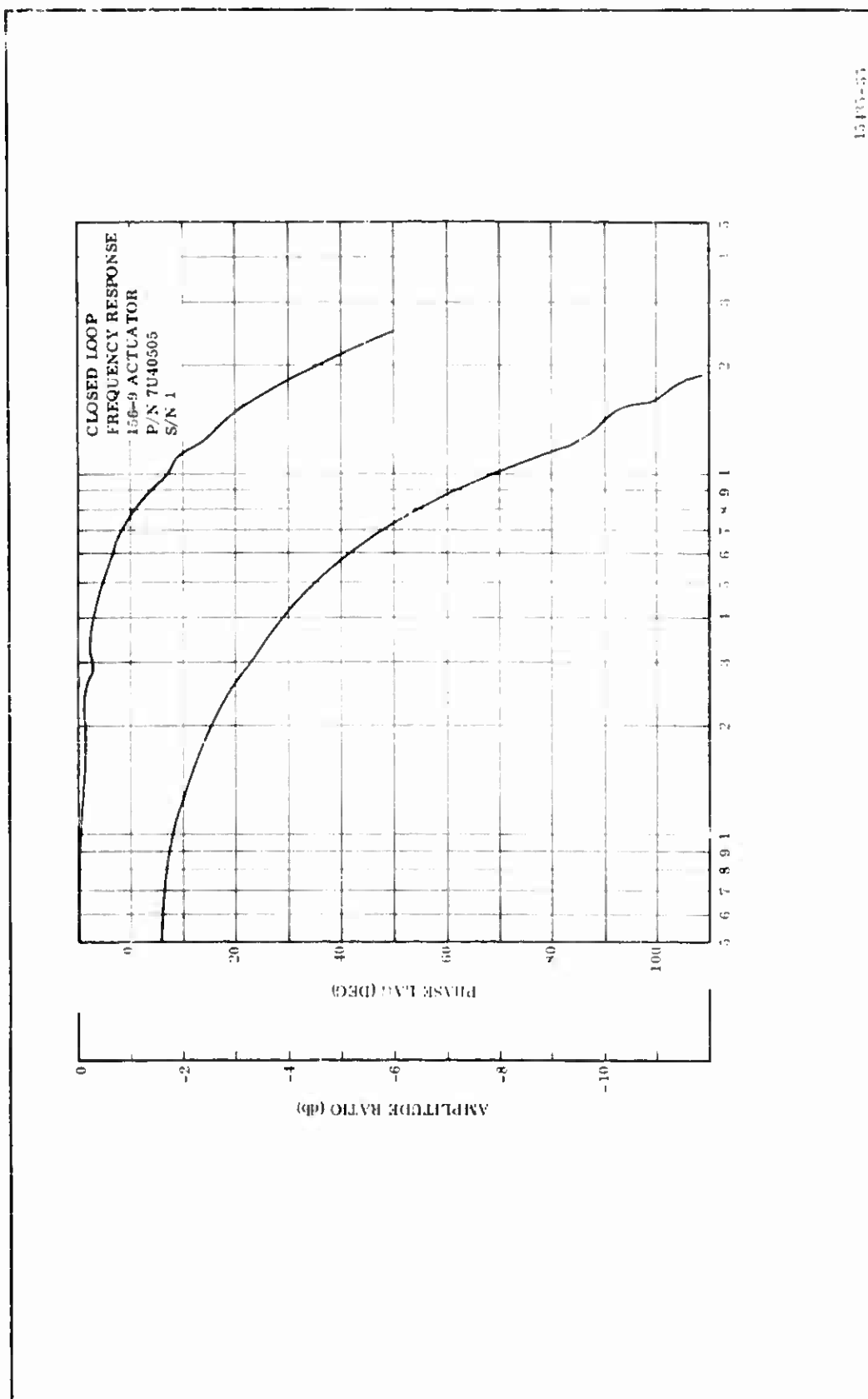


Figure 123. Block Diagram of Actuation Control System



15435-55

Figure 124. Frequency Response Actuator S/N 1

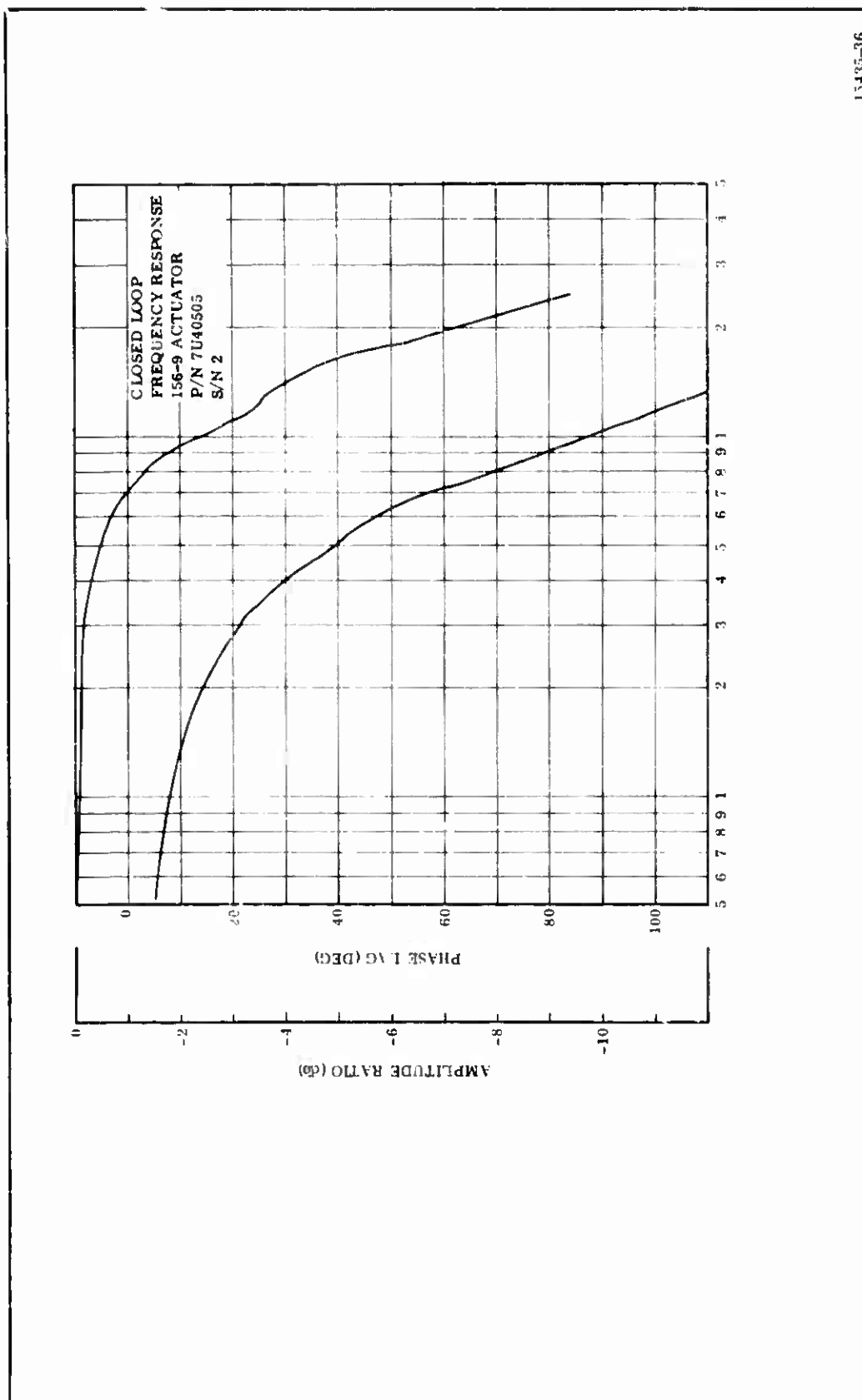


Figure 125. Frequency Response Actuator S/N 2

15435-36

CONFIDENTIAL

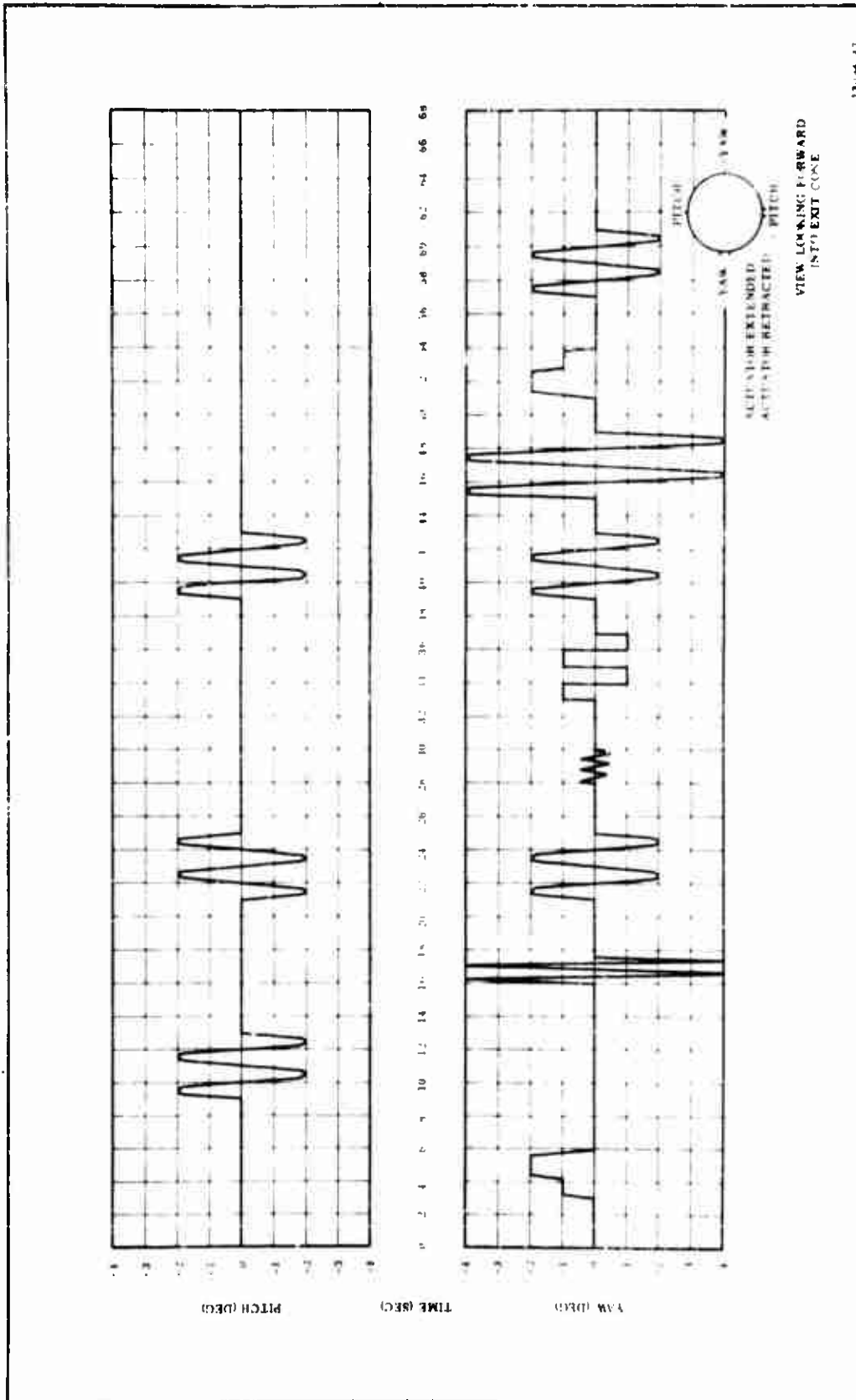


Figure 126. 156 Motor Duty Cycle

CONFIDENTIAL

CONFIDENTIAL

TABLE XXVI
156-9 NOZZLE ACTUATION DUTY CYCLE

Event	Time (sec)	Duration (sec)	Function	Amplitude (deg)	Rate (deg/sec)	Axis	Position (deg)
1	0-3.0	3.0	Hold	--	--	--	0
2	3.0-3.2	0.2	Ramp	--	5.0	Yaw	Ramp from 0 to +1
3	3.2-4.2	1.0	Hold	--	--	Yaw	+1 Yaw
4	4.2-4.4	0.2	Ramp	--	5.0	Yaw	Ramp from +1 to +2
5	4.4-5.6	1.2	Hold	--	--	Yaw	+2 Yaw
6	5.6-6.0	0.4	Ramp	--	5.0	Yaw	Ramp from +2 to 0
7	6.0-9.0	3.0	Hold	--	--	--	0
8	9.0-13.0	4.0	Sine	+2	(0.5 cps)	Pitch	--
9	13.0-16.0	3.0	Hold	--	--	--	0
10	16.0-17.6	1.6	Triangular	+4	(1.25 cps)	Yaw	--
11	17.6-21.0	3.4	Hold	--	--	--	0
12	21.0-25.0	4.0	Sine	+2	(0.5 cps)	Yaw and Pitch	--
13	25.0-28.0	3.0	Hold	--	--	--	0
14	28.0-30.0	2.0	Triangular	+0.5	(1.5 cps)	Yaw	--
15	30.0-33.0	3.0	Hold	--	--	--	0
16	33.0-37.0	4.0	Square	+1	(0.5 cps)	Yaw	--
17	37.0-39.0	2.0	Hold	--	--	--	0
18	39.0-43.0	4.0	Sine	+2	(0.5 cps)	Yaw and Pitch	--
19	43.0-45.0	2.0	Hold	--	--	--	0
20	45.0-49.0	4.0	Sine	+4	(0.5 cps)	Yaw	--
21	49.0-51.0	2.0	Hold	--	--	--	0
22	51.0-51.4	0.4	Ramp	--	5.0	Yaw	Ramp from 0 to +2
23	51.4-52.6	1.2	Hold	--	--	Yaw	+2
24	52.6-52.9	0.2	Ramp	--	5.0	Yaw	Ramp from +2 to +1
25	52.8-53.8	1.0	Hold	--	--	Yaw	+1
26	53.8-54.0	0.2	Ramp	--	5.0	Yaw	Ramp from +1 to 0
27	54.0-57.0	3.0	Hold	--	--	--	0
28	57.0-61.0	4.0	Sine	+2	(0.5 cps)	Yaw	--
29	61.0-70.0	9.0	Hold	--	--	--	0

sinusoidal cycles at 0.5 cps. During the former event the maximum required slow rate of 20 deg per second is achieved. The maximum required cyclic rate of 1.5 cps is achieved during an event that consists of three triangular cycles to 0.5 degrees vector angle.

- (U) A variety of functions has been included in the duty cycle to enable the characterization of the behavior of a flexible seal nozzle in response to these signals. Sinusoidal events, ramps, triangular events, square waves, and holds at vector have all been included.
- (U) The events are concentrated in the yaw plane as shown in Figure 126. Since the firing will be horizontal, events in the pitch plane will be affected by gravity.
- (U) Two events are included in the oblique planes--one at +45 deg. and one at -45 degrees. Both are sinusoidal to 2 deg in each the yaw and pitch planes resulting in 2.828 deg in the 45 deg plane.

G. TVC ACTUATION SYSTEM FABRICATION

- (U) Two servoactuator assemblies were fabricated by LTV Electrosystems Inc. in Garland, Texas, under subcontract to Thiokol. The remainder of the actuation system was assembled by Thiokol from purchased components, i. e., fittings, tubing, accumulator hoses, etc. Hydraulic power was supplied by an existing pump facility.
- (U) The servoactuator assemblies were designed by Thiokol. LTV Electrosystems was contracted to fabricate the valve manifold, transducer housings and the test manifold, and to assemble and test the actuator assemblies. The cylinders, servovalves, and common hardware were purchased by LTV.

1. BENCH TEST

- (U) Bench testing or "acceptance testing" was performed by LTV Electrosystems to Thiokol specifications. Basically these specifications controlled acceptance testing in the following areas:
1. Proof pressure test,
 2. Dynamic response tests,
 3. Internal leakage,
 4. Operational checkout.
- (U) S/N 1 actuator was bench tested on 21 Feb 1967. Internal leakage of 2.7 gpm exceeded the 1 gpm specified by Thiokol and the phase lag at 8 cps of 56 degrees exceeded the specified 45 degrees. In all other respects, the actuator performed satisfactorily.
- (U) S/N 2 actuator was bench tested on 28 Feb 1967. Internal leakage of 2.35 gpm and phase lag at 8 cps of 58 degrees exceeded Thiokol specifications. In all other respects the actuator performed satisfactorily.

- (U) With regard to the above discrepancies, the following comments are in order.
- (U) Thiokol's original drawing of the servovalve 7U100137 (Figure 120) allowed internal leakage up to 3 gpm. This was reduced to 1 gpm in our procurement requirement based on claims of various servovalve suppliers. Actual leakage was nearer the 3 gpm allowed on the original drawing and our requirement was revised to reflect this fact. Internal leakage of 3 gpm of the overall actuation system is acceptable.
- (U) The specified phase lag of 45 degrees at 8 cps was based on the use of pilot stage valves of 5 gpm capacity. Unfortunately, these were not available and the servovalves were equipped with 1 gpm pilot stage valves. This 4 gpm difference in capacity caused the excessive phase lag. Since the actuation system would perform satisfactorily with 1 gpm pilot stage valves and the corresponding increase in phase lag, the procurement requirement was revised to accept performance with 1 gpm pilot stage valves.
- (U) Thiokol specifications also controlled certain procedures and settings to be used during bench tests. These were adhered to by LTV ElectroSystems with but three exceptions.
1. Servoamplifier gain settings were increased above that specified in order to raise the overall loop gain to the specified 50 sec^{-1} . This was due to the use of a 1 gpm rather than the 5 gpm pilot stage valve.
 2. The piston rod amplitude used for frequency response tests was reduced to ± 0.10 in. rather than the specified 10 and 50 percent of full stroke because the LTV ElectroSystems hydraulic power supply capacity was limited to 55 gpm, which is not sufficient to achieve 10 and 50 percent of full stroke.

3. Thiokol specifications erroneously required internal leakage plotted as a function of valve input signal which normally controls spool position. In this particular three stage system spool position is not controlled by valve input signal. LTV ElectroSystems plotted internal leakage as a function of spool position output voltage which is proper.

(U) Visual examination, proof pressure testing and operational checkout was accomplished without incident. All testing was done with a Thiokol design engineer present.

2. COMPATIBILITY TESTS

(U) The complete actuation system was assembled and checked out prior to installation on the motor. This work was accomplished in conjunction with the flexible seal tests. On these tests, the 7U40505 actuators were assembled on a test fixture. They were connected to the existing facility hydraulic power source through the same piping and hoses that were later used during motor firing. This included the same accumulator, porting blocks and all fittings. The entire system was controlled through the same electronic circuitry to be used during motor firing. During one phase of the testing, the program tape, cut for motor firing, was used to command the system in the yaw plane. Yaw was selected as it was the more severe duty cycle. Once the system was adjusted and balanced, the flexible seal followed the programmed duty cycle with almost perfect response.

SECTION X

MASS PROPERTIES

- (U) The mass properties data shown in Table XXVII were calculated based on available motor "as-built" dimensions and theoretical densities. A detail data breakdown of the nozzle assembly, igniter assembly, and motor internal insulation data may be found in their respective design sections. The center of gravity reference system is shown in Figure 127. Moment of inertia data is taken about an axis through the part or assembly center of gravity and is in slug feet squared.

TABLE XXVII
MASS PROPERTIES DATA 156-9 MOTOR SUMMARY

Item	Weight (lb)	Center of Gravity		Moment of Inertia			
		Longitudinal	Lateral	Vertical	Pitch	Roll	Yaw
Case	22,193.015	207.731	100.000	100.000	51,635.872	25,909.800	51,636.872
Insulation	4,817.477	242.715	100.000	100.000	14,832.650	4,781.438	14,832.650
Liner	312.000	196.318	100.000	100.001	705.588	358.514	705.588
Koropon Primer	44.960	196.879	100.000	100.000	106.176	51.557	106.176
Ignition System	691.175	50.951	99.998	99.999	23.988	7.696	23.983
Nozzle	18,247.000	371.027	99.007	99.007	6,627.119	5,455.427	6,627.057
Nozzle Attachment Provisions	152.160	359.525	100.000	100.000	53.253	66.505	33.258
Total Inert Parts	46,457.786	273.573	99.610	99.610	141,222.900	36,634.650	141,223.832
Propellant	271,832.934	198.307	100.000	100.000	447,093.953	190,983.514	447,093.953
Total Motor	321,290.719	209.190	99.944	99.944	636,909.461	227,620.773	636,910.398
Mass Fraction	0.855						

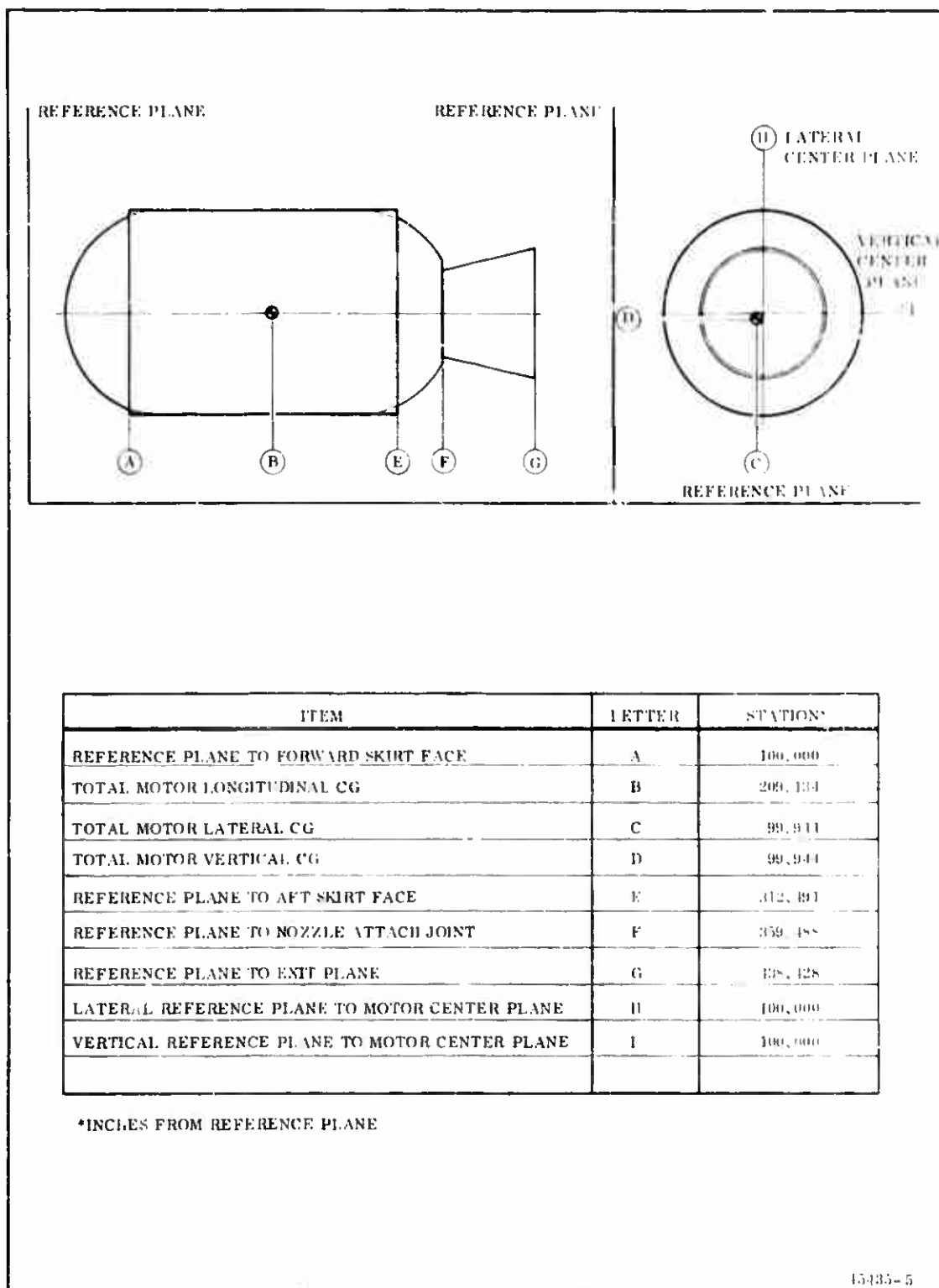


Figure 127. 156-9 Motor Center of Gravity Reference Sketch

SECTION XI

TOOLING

A. PROCESS TOOLING

- (U) Existing tooling was used where possible to keep tooling cost at a minimum. The majority of the new and modified tooling was required for propellant casting. Minor modifications to the handling equipment consisted mainly of drilling and tapping holes in existing tooling and relocating brackets to accommodate a different case length. The vacuum casting fixtures arrangement (Figure 128) shows the propellant casting tooling assembled for casting. The major modifications or new tools are described below.

1. PROCESS HANDLING HARNESS

- (U) The decision to load and test the 156-9 motor prior to the static test of the 156-8 motor made it necessary to use joint harness rings on the 156-9 motor rather than skirt harness rings as originally planned. The joint harness rings were re-worked to make them compatible with the skirt harness brackets and the static test arrangement.

2. SLOT FORMER

- (U) The slot former was fabricated of urethane foam with a metal structure inside. It was sectioned in pie shaped wedges allowing force to be selectively

PRECEDING PAGE BLANK-NOT FILMED



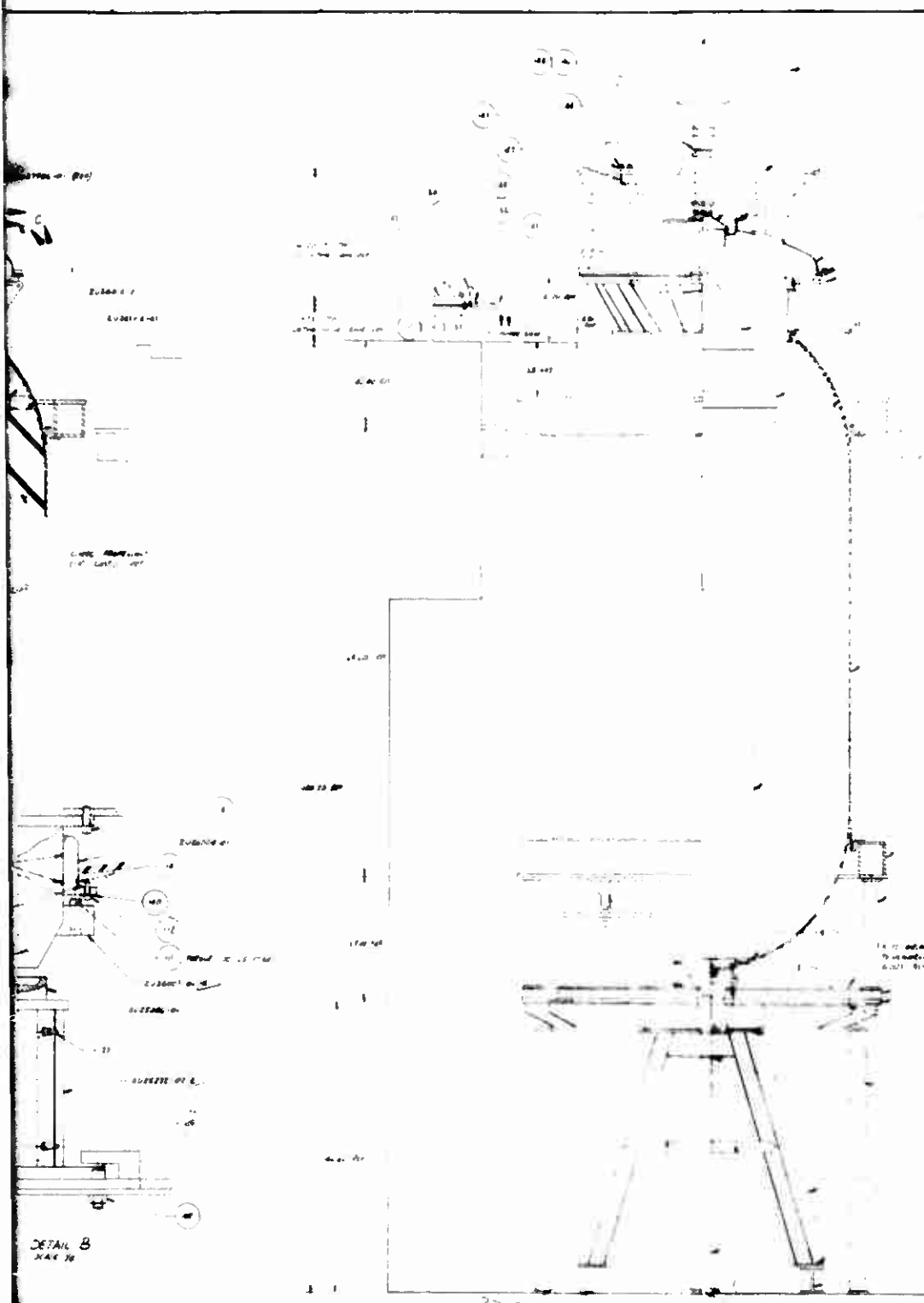


FIGURE 1
PUMP AND MOTOR
1-10-54

FIGURE 2
PUMP AND MOTOR
1-10-54

FIGURE 3
PUMP AND MOTOR
1-10-54

FIGURE 4
PUMP AND MOTOR
1-10-54

FIGURE 5
PUMP AND MOTOR
1-10-54

FIGURE 6
PUMP AND MOTOR
1-10-54

FIGURE 7
PUMP AND MOTOR
1-10-54

FIGURE 8
PUMP AND MOTOR
1-10-54

FIGURE 9
PUMP AND MOTOR
1-10-54

FIGURE 10
PUMP AND MOTOR
1-10-54

FIGURE 11
PUMP AND MOTOR
1-10-54

FIGURE 12
PUMP AND MOTOR
1-10-54

- NOTES**
1. PUMP AND MOTOR TO BE USED IN THE FOLLOWING MANNER:
 2. PUMP AND MOTOR TO BE USED IN THE FOLLOWING MANNER:
 3. PUMP AND MOTOR TO BE USED IN THE FOLLOWING MANNER:
 4. PUMP AND MOTOR TO BE USED IN THE FOLLOWING MANNER:
 5. PUMP AND MOTOR TO BE USED IN THE FOLLOWING MANNER:
 6. PUMP AND MOTOR TO BE USED IN THE FOLLOWING MANNER:
 7. PUMP AND MOTOR TO BE USED IN THE FOLLOWING MANNER:
 8. PUMP AND MOTOR TO BE USED IN THE FOLLOWING MANNER:
 9. PUMP AND MOTOR TO BE USED IN THE FOLLOWING MANNER:
 10. PUMP AND MOTOR TO BE USED IN THE FOLLOWING MANNER:
 11. PUMP AND MOTOR TO BE USED IN THE FOLLOWING MANNER:
 12. PUMP AND MOTOR TO BE USED IN THE FOLLOWING MANNER:

1

2

Handwritten notes on lined paper, including a date "10-10-10" and a signature "J. H. H."

28

1. $\frac{1}{2} \times \frac{1}{2} = \frac{1}{4}$ (Probability of getting two heads in two tosses)
2. $\frac{1}{2} \times \frac{1}{2} = \frac{1}{4}$ (Probability of getting two tails in two tosses)
3. $\frac{1}{2} \times \frac{1}{2} = \frac{1}{4}$ (Probability of getting one head and one tail in two tosses)
4. $\frac{1}{2} \times \frac{1}{2} = \frac{1}{4}$ (Probability of getting one tail and one head in two tosses)
5. $\frac{1}{2} \times \frac{1}{2} = \frac{1}{4}$ (Probability of getting one head and one tail in two tosses)
6. $\frac{1}{2} \times \frac{1}{2} = \frac{1}{4}$ (Probability of getting one tail and one head in two tosses)
7. $\frac{1}{2} \times \frac{1}{2} = \frac{1}{4}$ (Probability of getting one head and one tail in two tosses)
8. $\frac{1}{2} \times \frac{1}{2} = \frac{1}{4}$ (Probability of getting one tail and one head in two tosses)
9. $\frac{1}{2} \times \frac{1}{2} = \frac{1}{4}$ (Probability of getting one head and one tail in two tosses)
10. $\frac{1}{2} \times \frac{1}{2} = \frac{1}{4}$ (Probability of getting one tail and one head in two tosses)

© 2000 Blackwell Science Ltd

5748

100

[illegible]

114

2000 年 4 月

Results

00000000

13. 10: 45

for name in:

FEDERAL BUREAU OF INVESTIGATION		U. S. DEPARTMENT OF JUSTICE	
<p>REPORT MADE AT: NEW YORK</p> <p>DATE OF REPORT: 10/10/54</p> <p>REPORT MADE BY: SA [redacted]</p> <p>CHARACTER OF CASE: SECURITY - R</p>		<p>FILE NO.: 100-354611</p> <p>NEW YORK FILE NO.: 100-101081</p>	
<p>TITLE: INTERNAL SECURITY - R</p> <p>SYNOPSIS: [redacted]</p>		<p>DETAILS: [redacted]</p>	
<p>REFERENCE: [redacted]</p>		<p>REMARKS: [redacted]</p>	
<p>APPROVED: [redacted]</p>		<p>COPIES: [redacted]</p>	

Figure 128. Propeller Vacuum Cast - Fixture

2

3

applied on the inner metal structure to remove the wedges after the propellant was cured. Molds were designed and fabricated to form the segments during foaming operations.

3. DISPERSION CONE EXTENSION

- (U) The dispersion cone extension attached to the core and directed the propellant flow from the dispersion cone to the motor chamber. It was utilized during the casting of the main grain and was configured to provide maximum flow area and visibility between itself and the vacuum dome adapter.

4. CORE CAP

- (U) The core cap bolted to the aft end cover of the modified core and extended the core up to the aft end of the case. It molded the major portion of the large diameter propellant bore.

5. CASTING DAM SEATING AND REMOVAL TOOL

- (U) Remote operation of the casting dam seating and removal tool was required because of the potential hazards involved. The tool consisted of a framework and hydraulic ram. When actuated in the down direction, it forced the casting dam downward in the aft propellant and seated the dam against the core cap. A reverse actuation, after propellant cure, served to pop the casting dam free of the propellant grain. The tool was also used to pop the core cap.

6. CASTING HOPPER ADAPTER BASE

- (U) Original plans were to use only horizontal 300 gal. mixers for propellant casting. With the installation of a 430 gal. vertical mixer, however, a savings in

propellant mixing and casting operations was possible. To use the 430 gal. vertical mixer on this program, an adapter to the 430 gal. casting hopper was designed and fabricated. This adapter mated to the 300 gal. hopper stand on the vacuum dome and to the stand supporting the 430 gal. casting hopper.

7. HOPPER FUNNEL ADAPTER

- (U) The hopper funnel adapter mated the 430 gal. casting hopper to the Minuteman deaeration assembly. The design incorporated a slip joint to compensate for tolerance buildup in the casting arrangement and to aid in installation.

8. PLASTER SWEEP TEMPLATE

- (U) The plaster sweep template was designed to form the plaster mold used to install the slot former support on the case wall. The tool attached to the case nozzle boss, and by rotating about the case centerline, assured the concentricity of the slot former support.

9. VACUUM DOME ADAPTER

- (U) To utilize existing vacuum casting equipment, which included the vacuum dome used on the Minuteman casting bells, an adapter was designed to mate the nozzle port flange to the vacuum casting bell dome. This adapter also served as a nozzle port insulation mold during insulation installation and as a guide for the casting dam.

10. CASTING DAM

- (U) A casting dam was designed to net mold the propellant grain and eliminate machining of the propellant in the aft nozzle port. During propellant casting the dam was in a raised position allowing propellant to flow between the core cap and the casting dam. After the motor was filled with propellant, the casting dam was remotely seated forming the final contour of the aft grain.

11. DISPERSION CONE

- (U) The dispersion cone was installed on the dispersion cone extension or core cap and served to initially direct the propellant flow around the core and into the motor chamber. Three arms welded to the top of the cone contacted the vacuum dome adapter and thereby served to center the aft end of the core.

12. CORE MODIFICATION

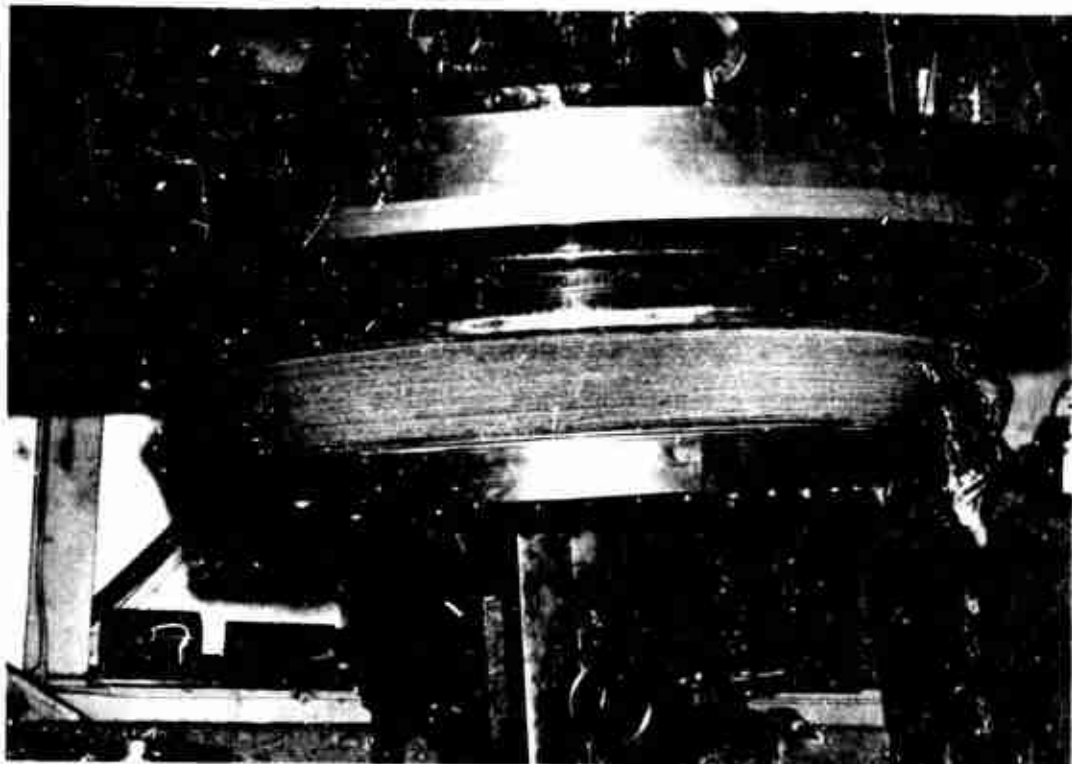
- (U) To adapt the GFP core, for casting propellant in the 156-9 motor, an aft end cover, a ring, and a cone section were welded to the aft end. These items formed a portion of the coned section of the propellant grain and provided a means of positioning the slot formers. A locator ring and neoprene pad were placed on the forward end of the core to provide a vacuum seal against the insulation. The forward end was also drilled and tapped to accept a forward end core alignment stud.

B. TEST TOOLING

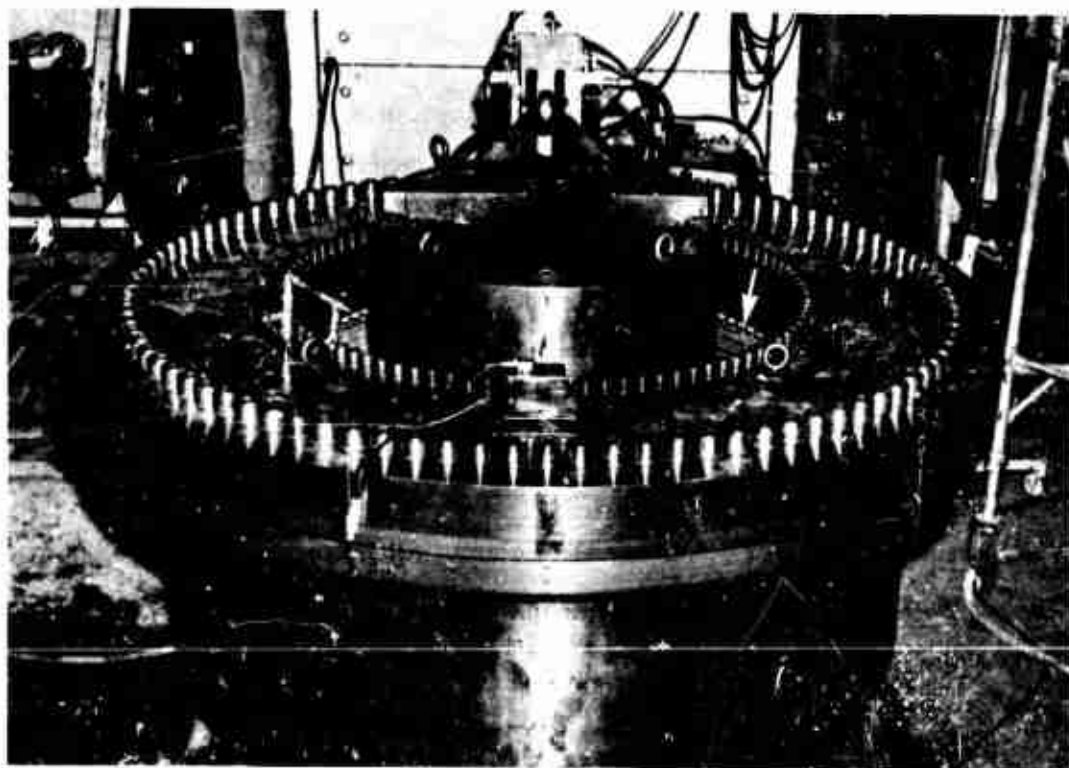
- (U) The majority of the tooling required for static testing was in existence. Minimum modification of the test stand was required. Holes for brackets were relocated and the side thrust load train adapters were adjusted.
- (U) Two major pieces of equipment were required in support of the static test and are described below.

1. FLEXIBLE SEAL TEST FIXTURE

- (U) The fixture used to test all flexible seals associated with this program was designed by Thiokol and fabricated by Lasker Boiler and Engineering Corp. , Chicago, Illinois. Basically, it is a large pressure vessel (2,500 psi) using the flexible seal as one ID ring (Figure 129). The kettle like fixture is opened by removing 96 large through bolts and then lifting off the cover. In use, a flexible seal is first bolted to the cover, the seal and cover are then lowered into place on the column assembly and the pivoted column assembly installed. This assembly is then lowered onto the fixture body and the 96 cover bolts installed and torqued.
- (U) A unique feature of this fixture was the column assembly which acted as a reaction piston (not shown) that pinned to a clevis below the seal. This reaction piston provided a fixed point for the bearing to pivot around and a means of reacting out some of the nozzle compression and blowout load on the flexible seal. Thus the walls of the seal could be exposed to MEOP (830 psi) and the seal compressive load would be the same as the nozzle blowout load expected during static firing. Leaving the piston unpinned and operating at a lower pressure (400 psi) duplicated the nozzle blowout load and allowed the pivot point to be established by the seal being tested.
- (U) The fixture worked well and all planned seal testing was completed without incident.



FLEXIBLE SEAL ASSEMBLY INTO TEST FIXTURE



FLEXIBLE SEAL TEST FIXTURE, SEAL INSTALLED (ARROW)

Figure 129. Flexible Seal Test Fixture

2. NOZZLE HANDLING ARRANGEMENT

- (U) New equipment for handling the nozzle was kept to a minimum by adapting existing lifting beams, trunnions, breakover stands, and other hardware where possible. The only three new items required for this handling arrangement were (1) trunnion brackets, (2) extension bracket, and (3) a 3 point lifting beam. The trunnion brackets were required to adjust the cg of the nozzle and attached directly to the circumferential stiffening ring as shown in Figure 130. The function of the nozzle handling tooling and sequence of operations is also shown in Figure 130.

C. FLEXIBLE SEAL AND PROTECTIVE BOOT FABRICATION TOOLING

1. FLEXIBLE SEAL TOOLING

- (U) The flexible seal assembly fixture is shown in Figure 131. The tool is essentially an open mold with all seal dimensions controlled from the inside. The six dash 102 Support Assemblies control the precise distance between the base and cover plates and thus control flexible seal length. Radial indexing of the forward and aft end rings was accomplished by use of suitable dowel pins and holes in two of the six support assemblies and the base and cover plates. The concentric location of shims was also controlled by the ramps on each of the support assemblies.
- (U) The dash 108, 107, and 106 rams were used to debulk at 20, 40, and 50 shims, respectively. For debulking at 20 shims, all three rams were bolted to the upper platen of the debulk press. Debulking at 40 shims was accomplished by removing the dash 108 ram. The dash 108 and 107 rams were removed for debulking at 60 shims. Final debulking and pressing to net at 82 shims was accomplished by use of the aft end ring.

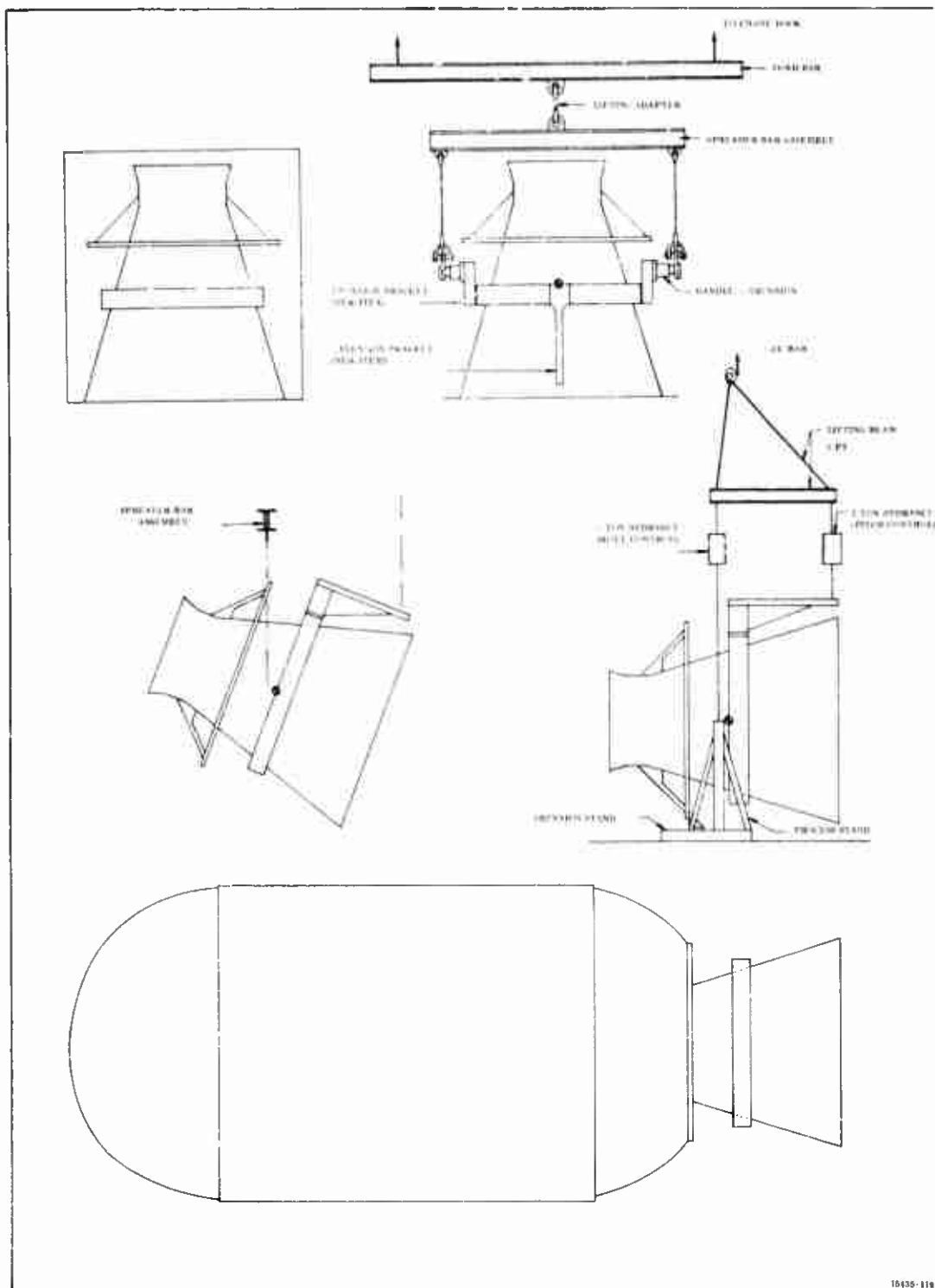
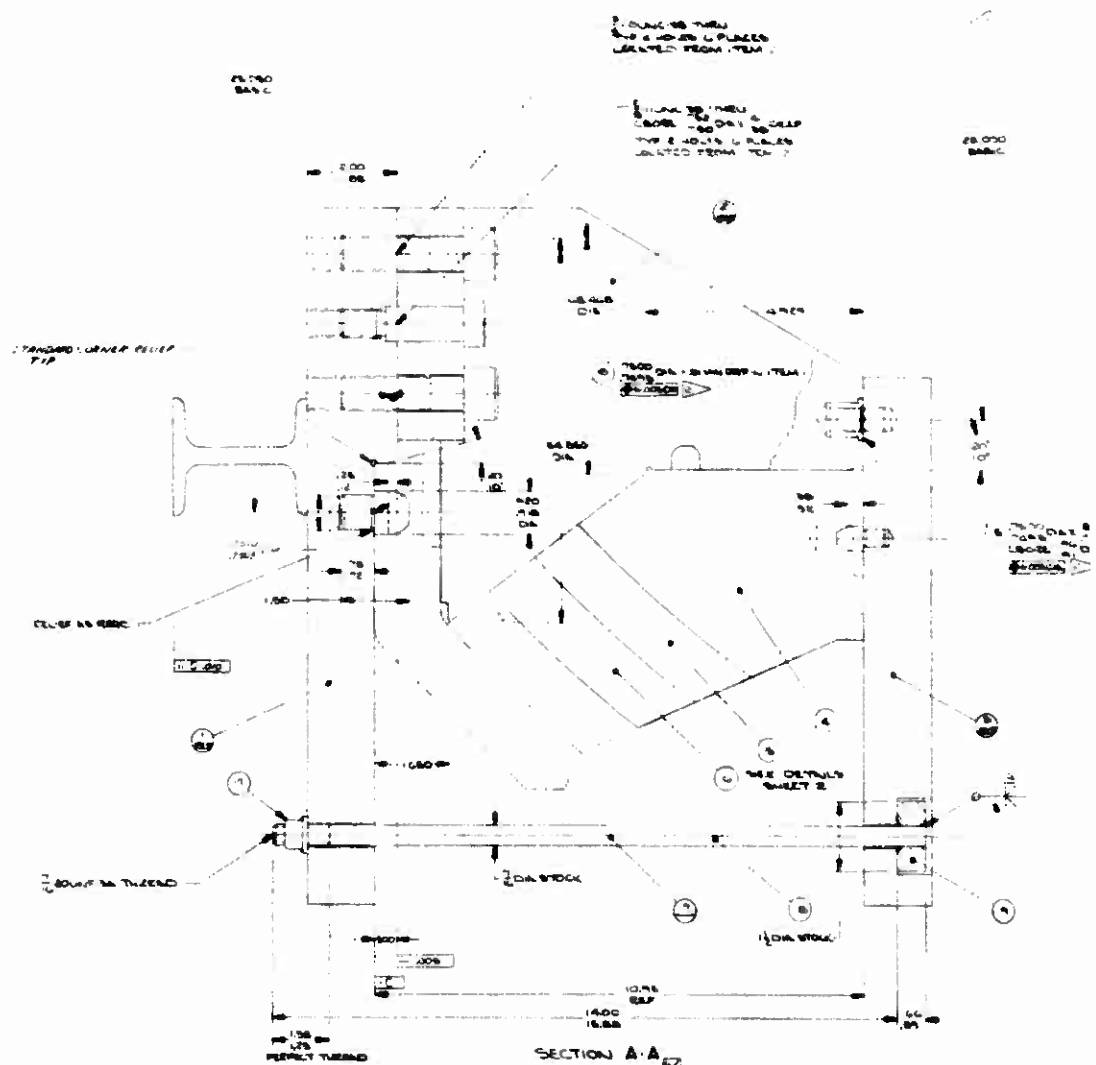


Figure 130. Nozzle Handling Operation Sequence

PUNCHING PAGE BLANK-NOT FILLED



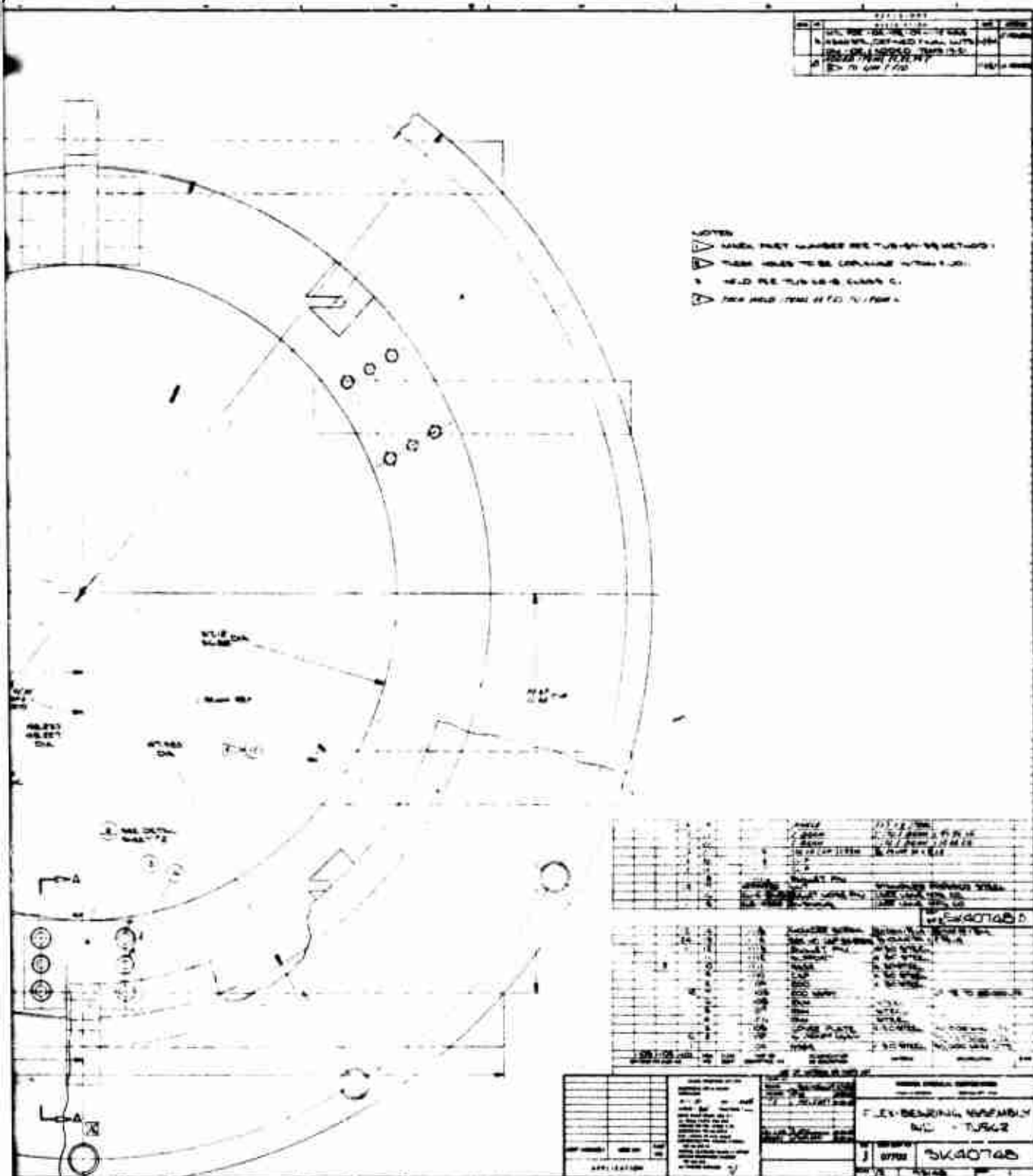
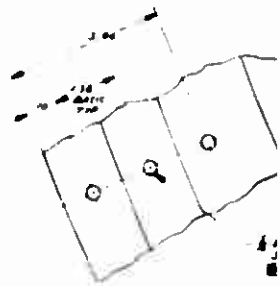

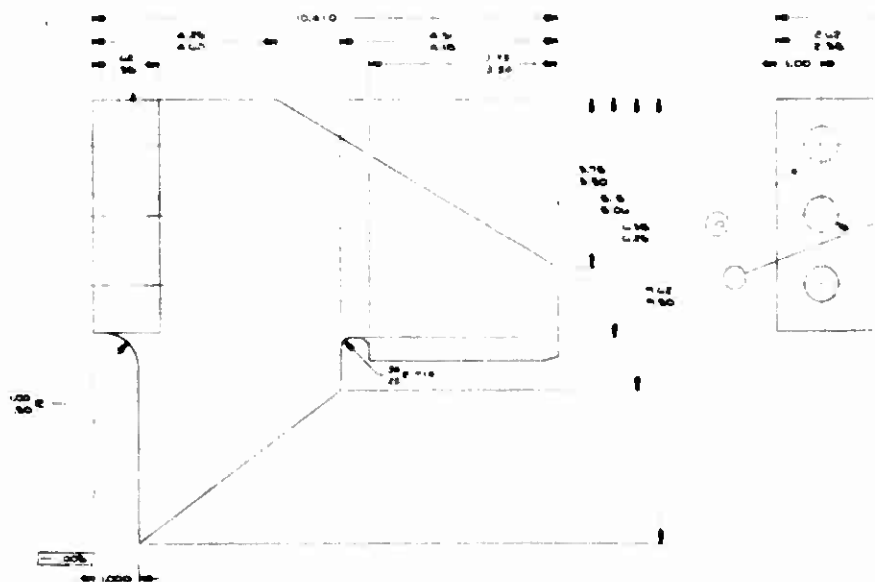


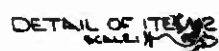
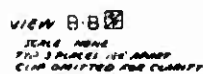
Figure 131. Flexible Seal Assembly Fixture (sheet 1 of 2)



VIEW B-B 
 SCALE NONE
 3/4" = 1'-0" (AS SHOWN)
 CIP CONCRETE AND G.



DETAIL OF ITEM 2
SCALE: X



SK 40740

3

Fig.

(U) In general, the tool worked satisfactorily. The tie bolt failure associated with the cure of AF serial number 1 seal (Section II) was due to faulty repair of tie bolts broken when the fixture containing an IR & D flexible seal was water cooled. The fixture has been redesigned to eliminate welding of any sort on the tie bolts.

(U) Another undesirable feature, discovered by use of the tool, was that the support assembly ramps did not push an improperly placed shim into a concentric position during debulking. Rather, the shim curled or buckled locally under the seating pressure. It was concluded that the support assembly ramps should be used to guide shims during placement and should be moved inward to avoid contacting shims during debulk. A single design change to provide movable ramps on the support assemblies would improve the tool by allowing the support assembly ramps to guide the shims during placement.

2. BOOT TOOLING

(U) The protective boot was made by hand laying strips of V-45 rubber over a forming fixture. This fixture is essentially a male mold with sectioned OD rings at each end. The rings form a closed mold for each end (interface area) of the boot in order to hold the tighter tolerances required. The forming fixture was also used as a holding fixture for machining the OD of the boot between ends. No difficulties were encountered in the use of the fixture.

SECTION XII

STATIC TEST RESULTS

A. INTRODUCTION

(U) The 156-9 rocket motor was successfully static tested on 26 May 1967 at the Wasatch Division of Thiokol Chemical Corp under Contract AF 04(611)-11643. The scope of this program included the design and development of an omniaxial flexible seal movable nozzle (OFSMN). The effort is described in four tasks as follows:

- Task A. Motor Demonstration. The design and fabrication of all motor components and assemblies.
- Task B. Special Tooling. The design, procurement, fabrication and/or modification, checkout, and maintenance of special tooling required for the program.
- Task C. System Support. Implementation of a Quality Assurance plan that would assure successful accomplishment of tasks A and B.
- Task D. Program Administration and Reporting. The effort required for management, control, and direction of the program and also includes all reporting and documentation effort.

1. TEST OBJECTIVES

(U) The primary objectives of the 156-9 motor static test demonstration were:

1. To demonstrate the performance and functional capabilities of the submerged omniaxial flexible seal movable nozzle.
2. To obtain data that can be used for future nozzle designs including nozzle actuation torque.
3. Evaluate the performance of the barrier seal protective gap, cavity, and projecting insulation.
4. Evaluate the nozzle and plastic materials performance during static firing conditions.
5. Evaluate performance of the nozzle actuation system.

(U) The secondary test objectives were:

1. Demonstrate motor performance.
2. Evaluate and verify design of case insulation.
3. Demonstrate large motor handling and assembly procedures.

2. TEST ARTICLE DESCRIPTION

(U) The 156-9 rocket motor shown in Figure 1 was a 156-in. diameter solid propellant rocket motor of the one-million pound thrust class. It was designed and fabricated to demonstrate an omniaxial flexible seal movable nozzle. The motor included a case, a nozzle incorporating the OFSMN, an actuation system, and a head end ignition system. The case was insulated internally with a mastic compound and loaded with an 87 percent solids polybutadiene acrylonitrile propellant (Figure 1).

(U) a. Nozzle--The 156-9 nozzle (Figure 32) was a submerged movable nozzle with ± 4 degree omnialaxial vectoring capability provided by a flexible seal that joined the fixed and movable sections of the nozzle. The throat and exit diameters of the nozzle were 34.54 and 98.64 in., respectively, corresponding to an initial expansion ratio of 8.15. The overall length of the nozzle assembly was 116.1 in., 47 percent of which was submerged. The aerodynamic design of the internal nozzle surface from the nose tip to the exit plane was identical to the 156-6 nozzle. The nose tip was defined by a radius of 1.62 inches. An 8.00 in. radius joined the tip radius to a 15.00 in. radius into the throat. The throat and the 17.5 deg exit cone were joined at a radius of 13.859 inches.

(U) Structural integrity and maintenance of the aerodynamic contour was provided by a mechanical design consisting of steel structural components, reinforced plastic erosion liners and thermal insulators. Nozzle structural and insulation subassemblies were fabricated independently, and bolted or bonded to form the complete nozzle assembly.

(U) The nozzle fixed housing assembly consisted of a steel structure protected by silica cloth phenolic insulation. The steel structure consisted of two forged flanges welded to a conical section fabricated by the roll and weld construction method. The small end of the silica had an outer surface spherical about the flexible seal pivot point. This surface formed the fixed part of the barrier gap which protected the flexible seal from direct radiant heating and sharply reduced convective flow. Ply orientation of the silica tape was parallel to the nozzle centerline in order to provide a more direct vent path between plies.

(U) Two actuator support brackets were bolted to clips on the fixed housing.

(U) The movable part of the secondary barrier consisted of two bonded silica cloth phenolic insulating rings. Both of the silica components were tape wrapped parallel to the centerline.

- (U) The nose assembly consisted of an entrance housing, two carbon cloth phenolic liners, a graphite cloth crossover ring, and two silica cloth phenolic insulators. The steel entrance housing was of roll and weld construction. The nose liner (back-side or chamber side of the nose) was carbon cloth phenolic tape wrapped parallel to the centerline. The crossover ring was graphite cloth rosette with ply orientation 90 deg to the centerline. The silica cloth insulator behind the nose liner was a rosette layup with ply orientation parallel to the aft surface. The insulator behind the entrance liner was also a rosette layup.
- (U) The exit assembly consisted of a steel shell, three liners, and two insulators. The forward ring of the shell was a ring forging; the remainder was of roll and weld fabrication. A reinforcing I-beam type structure girdled the aft exit cone to limit distortion during vectoring and distribute the actuator loads. The throat liner was a single piece graphite cloth tape wrap with ply orientation 70 deg to the centerline. This is similar to the throats successfully tested on the 156-5, 156-7 and Thiokol TU-455.02 as well as the 260-in. diameter motor nozzles. An overwrap of silica phenolic tape insulated behind the throat liner.
- (U) The upper exit cone liner was carbon cloth phenolic tape wrapped parallel to centerline. This extended to an expansion ratio of 2.44 as in the 156-6 design. From this point to the exit the liner was silica phenolic tape, also wrapped parallel to centerline. Both liners were overwrapped with glass phenolic tape prior to final cure of the three components as an assembly. A row of retaining pins through the shell into the insulation was provided at an expansion ratio of 2.5 as a backup against bond failure.
- (U) The nozzle was actuated by two linear servoactuators, 90 deg apart, mounted between the nozzle fixed housing and the exit housing. One servoactuator controlled pitch motion, and the other controlled yaw motion. Intermediate angles of vector were accomplished by simultaneous combination motions.
- (U) The two specially adapted linear electrohydraulic servoactuators were operated by a ground hydraulic power supply in a closed loop control system.

The actuators were standard heavy-duty industrial type, modified to permit mounting of the servovalve and position feedback device.

- (U) The servovalves were three-stage industrial units which employ linear variable displacement transducer (LVDT) feedback on the third stage spool. A manifold provided straight-through porting to one side of the cylinder and two external lines to the other side.
- (U) A standard LVDT position transducer was mounted inside the piston rod to insure minimum exposure hazard and to minimize the length of the unit.
- (U) The actuators were trunnion mounted at the head end of the unit. The rod ends included self-aligning bearings to accommodate misalignment caused by oblique vectoring.
- (U) The actuators had a 6-in. bore, 2 1/2 in. rod, and 7-in. stroke. At the 3,000 psi operating pressure, this results in a stall torque capability of 3.32 million in.-lb and a dynamic torque capability of 2.12 million in.-lb at the maximum vectoring rate of 20 deg per second.
- (U) b. Flexible Seal--The flexible seal consisted of alternate spherical laminations of thin rubber and thin metal reinforcements vulcanized into a composite structure. The seal had a mean spherical radius of 36.757 in., a radial thickness of 5.355 in., and a mean width of 6.34 inches. The mean radius about the nozzle axis is 27.47 inches. The radial thickness of 5.355 in. was comprised of 83 layers of polyisoprene rubber, each 0.025 in. thick; 82 layers of stainless steel shim reinforcements, each 0.040 in. thick. Total rubber thickness was 2.075 in., and total metal thickness was 3.28 inches.
- (U) c. Case--The government furnished case for the 156-9 motor was the same 250 ksi grade, 18 percent nickel, maraging steel with an ultimate uniaxial tensile strength of 240,000 psi and a yield strength of 230,000 psi that was used for the 156-6 motor.
- (U) d. Insulation and Liner--The case was insulated using Thiokol TI-H704B insulation, an asbestos filled carboxyl terminated polybutadiene polymer. The aft dome insulation tapered from 1.19 in. minimum at the aft polar opening to 0.05 in. minimum in the cylindrical section. The forward dome insulation thickness tapered from

0.60 in. minimum at the forward polar opening to 0.05 in. minimum in the cylindrical section. Prior to insulation installation the interior of the case was covered with a 0.005 in. minimum layer of Koropon (epoxy) primer.

(U) Unbonded relief flaps were provided in the forward and aft domes. The entire inner surfaces of the case insulation that was in contact with propellant was coated with a 0.025 in. thickness of TL-H714/ liner to provide for propellant bonding and case insulation at tailoff.

(U) e. Propellant--The propellant used in the 156-9 motor was designated TP-H1115, and was a member of the polybutadiene AP/Al family of propellants. This propellant contained 87 percent solids and incorporated extra fine ammonium perchlorate and iron oxide to produce the required burn rate. The composition of the propellant is shown in Table XXI. The propellant was cast into a cylindrically perforated grain having a 6 in. slot near the nose of the nozzle. The core diameter was 54.2 in. increasing to 77.25 in. in the aft end to provide for nozzle clearance.

(U) f. Ignition System--The ignition system was composed of four main subassemblies: (1) Safety and Arming (S & A) Device; (2) Initiating System; (3) Booster PYROGEN Device; (4) Adapters, booster igniter to motor and ignition system to motor. A description of each main subassembly is as follows:

1. The S & A device contained two ES-003 electrical squibs, which, upon initiation, start the ignition train for the motor ignition sequence. In the safe position, the squibs were electrically shorted and mechanically isolated from the ignition train. The device also had a visual indicator, a mechanical lock-pin, separate connectors for the control and firing circuits, hermetic seals, and other safety features that minimize the possibility of inadvertent firing.
2. The initiating system consisted of an adapter, pyrotechnic booster assembly, and an initiating PYROGEN igniter. The initiating system adapter, made of low carbon steel, adapted the initiating PYROGEN igniter,

pyrotechnic booster, and the S & A device into one integral assembly. This assembly was installed in the motor adapter and held in place with a beveled retaining ring. The pyrotechnic booster provided the ignition train between the S & A device and the initiating PYROGEN igniter. It contained 30 gm of 2A boron-potassium nitrate pellets, and the container was identical to the design used on the Stage I Minuteman and AF 156-1 motors. The initiating PYROGEN igniter ignited the booster PYROGEN igniter. It was loaded with TP-H1016 propellant and produced a mass discharge rate for booster igniter ignition of 3.5 lb/sec for approximately 0.3 second. The case length was 11.5 inches.

3. The booster PYROGEN igniter assembly consisted of a mild steel case, NBR external and internal insulation, UF-2121 liner, and TP-H1016 propellant. The grain was cast in a 12 point star configuration. The igniter was designed to operate at a pressure of 820 psia and provide a mass discharge rate of 156 lb/sec for approximately 0.6 sec after which pressure and mass flow drop off for a total burning time of approximately 1.1 seconds.
4. A booster igniter adapter facilitates installation of the igniter loaded case assembly to the motor igniter adapter. This adapter permits installation of the booster igniter from the aft end of motor, down the propellant port, and through the motor polar boss where it interfaces with the motor ignition system adapter. The booster igniter adapter had ports that mate with the motor adapter and were used to monitor igniter pressure and motor pressure and for the carbon dioxide quench system.

B. MOTOR HANDLING AND ASSEMBLY

1. MOTOR INSTALLATION IN TEST BAY

- (U) Motor installation in test bay T-24 followed the standard Thiokol procedure briefly outlined below (Figure 132).
- (U) The motor centerline distance of 118 in. above the bay floor was established from motor and test fixture drawings. A hole was drilled and tapped in the center of the test block 118 in. above the floor. To this lone connection the thrust measuring load cell was affixed and optically aligned perpendicular to the thrust block face. Using the gantry crane, the thrust adapter was then attached to the load cell and optically aligned perpendicular to thrust block face. Suitable jacks were placed under the thrust adapter to hold it in position and free the gantry crane.
- (U) In order to minimize the time that the motor was exposed to ambient temperature conditions, the above work was accomplished prior to motor arrival.
- (U) At a predetermined time the motor transporter arrived at the test bay and was positioned under the gantry crane. The environmental control house was moved back out of the way. Suitable lifting beams and cables were arranged to provide a 4 point lift with hydrasets in each of the 4 legs. The hydrasets provided a means of weighing the motor and harness as well as providing pitch and roll control for alignment. With this lifting arrangement the motor was lifted off the transporter, leveled to within 0.100 in. in both lateral and longitudinal planes and hydraset load readings taken. While hanging from the gantry crane 4 jack pads were installed on the harness rings. Using suitable alignment pins and bushings the motor was carefully attached to the thrust adapter. Care was taken not to disturb the thrust adapter alignment. While being held in this totally aligned position, four jacks were placed under the jack pads and adjusted to take the motor weight but not disturb

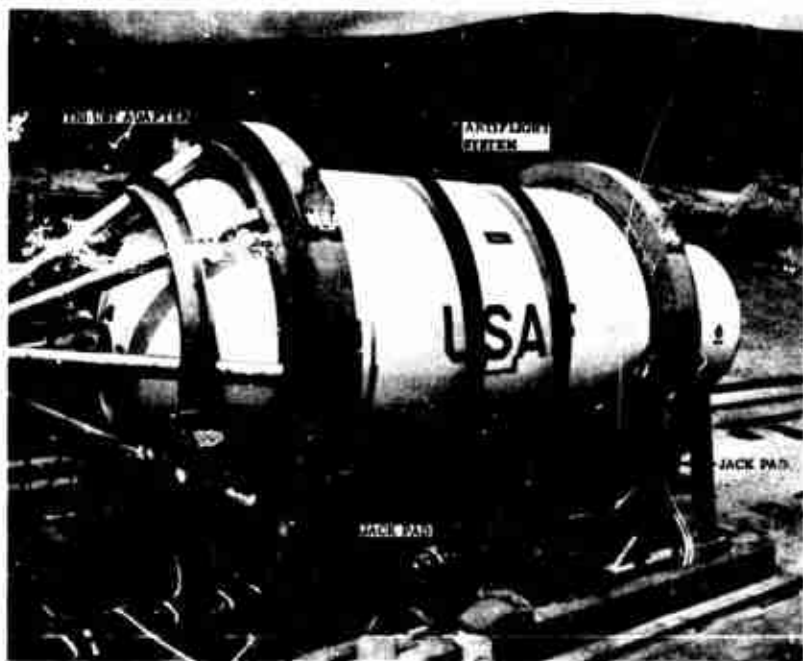
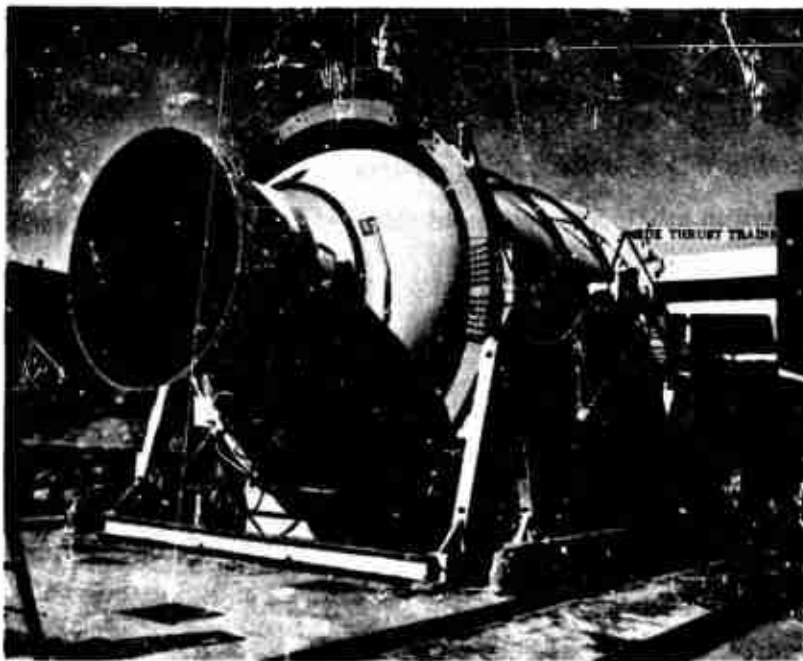


Figure 132. 156-9 Motor Installed in the Test Bay

the alignment. The gantry crane was then moved back out of the way, and the environmental conditioning house moved up to cover the motor.

(U) The motor remained in this position (under environmental control) while the following work, described in other paragraphs of this report, was accomplished.

1. Nozzle installation and checkout
2. Leak test
3. Quench system installation
4. Antiflight system installation

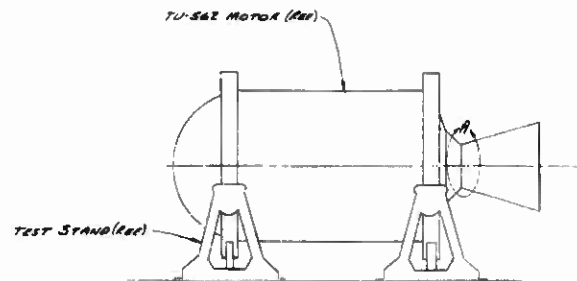
The house was moved back and the four straight line support brackets were installed over the trunnions provided on the harness. The gantry crane was used to lift these brackets: the brackets were leveled, shimmed underneath to take the motor weight and then bolted and grouted in place. Using a mobile crane, the side thrust reaction structure was positioned on the side thrust reaction piers. Two side thrust trains, complete with load cells, were then positioned on the side thrust reaction structure at a horizontal centerline of 118 in. and vertical centerlines of 79.90 in. forward and 417.07 aft. Vertical centerlines for the forward and aft trains were established from drawings (in this instance the forward was 79.90 in. aft of the main thrust block face and the aft was 417.07 in. aft of the main thrust block face). With the side thrust trains properly attached to the motor harness and properly aligned to the reaction structure, bolt holes were match drilled in the reaction structure. The thrust trains were then removed to provide clearance for the environmental conditioning house which was again brought over the motor assembly. When installed, the forward and aft side thrust load trains prevent the use of the environmental conditioning house. Therefore, the load trains were finally installed on the day of the firing.

2. NOZZLE INSTALLATION AND CHECKOUT

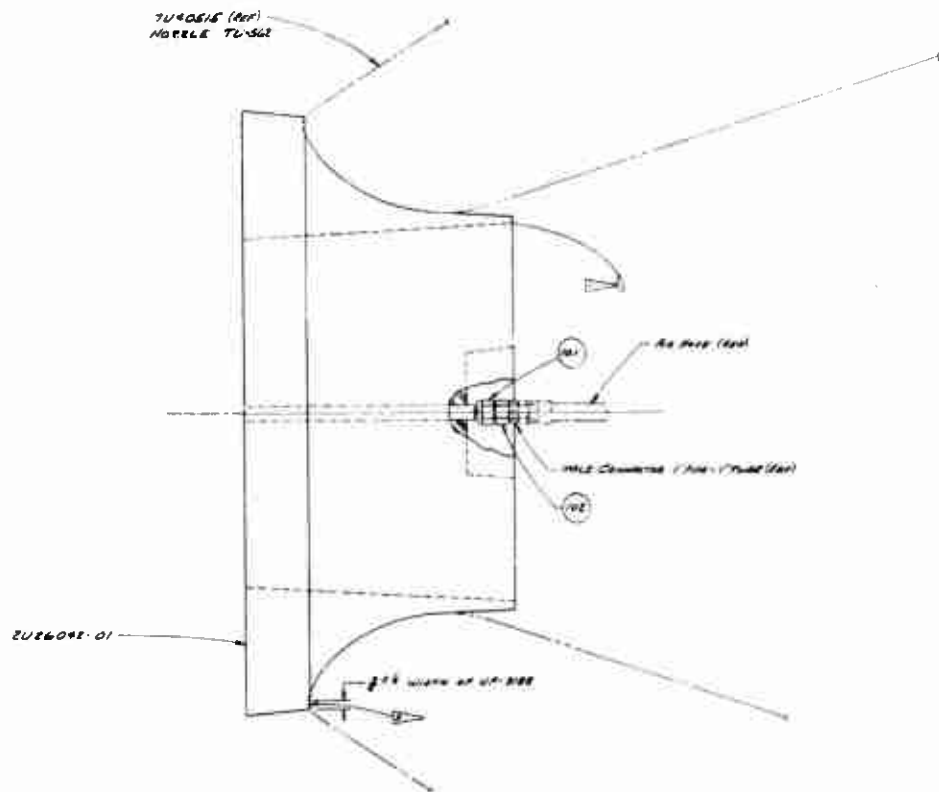
(U) Nozzle installation and checkout, including receiving inspection, were performed in test bay T-24.

- (U) The nozzle arrived via motor truck. It was securely attached, aft end down, to a large pallet which in turn was anchored to the truck bed. Protective covering during transit was afforded by a large box (4 walls and a top) attached to the pallet. After positioning the truck under the gantry crane the walls and top were removed as a unit. The nozzle and pallet were then lifted as a unit and placed on the apron by conventional sling and eye bolts attached to the fixed housing bolt circle. While resting thus on the apron a nozzle plug (Figure 133) was installed in the throat.
- (U) Breakover to the horizontal position was accomplished using the tooling and procedures shown in Figure 130 Nozzle Handling Arrangement. The large adapter brackets (P/N 2U26124-01) were needed to locate trunnions near the nozzle cg and thus minimize breakover loads. After breakover the nozzle was placed in a trunnion stand and the breakover sling arrangement was replaced with a three point handling sling. Hydrasets were used in the three point cable hookup to provide the pitch and roll control needed for nozzle alignment and mating to the case. It should be noted that during all nozzle handling and breakover the four shipping links were left installed. These links rigidly held the fixed and movable nozzle portions such that the flexible seal was always under compression.
- (U) The nozzle was dry fitted to the case in the following manner. Three alignment pins were installed in the case at 0, 120, and 240 degrees. The O-ring was lubricated and installed and the 168 attach bolts readied by applying Molycote Lubricant to the threads. Four impression samples made from vacuum putty were installed over the aft case insulation at 0, 90, 180, and 270 degrees. The nozzle was then carefully brought to the case, aligned by differential use of the Hydrasets, and 24 of the 168 attach bolts were installed and torqued. One bolt was tested in the remaining holes prior to removing the nozzle.
- (U) After removing the nozzle and again installing it in the trunnion stand the impression samples were measured. The amount of vacuum putty required to create an effective seal between case and nozzle insulation was determined from the samples.

PRECEDING PAGE BLANK-NOT FILMED



-01 CONFIGURATION
SCALE $\frac{1}{32}$



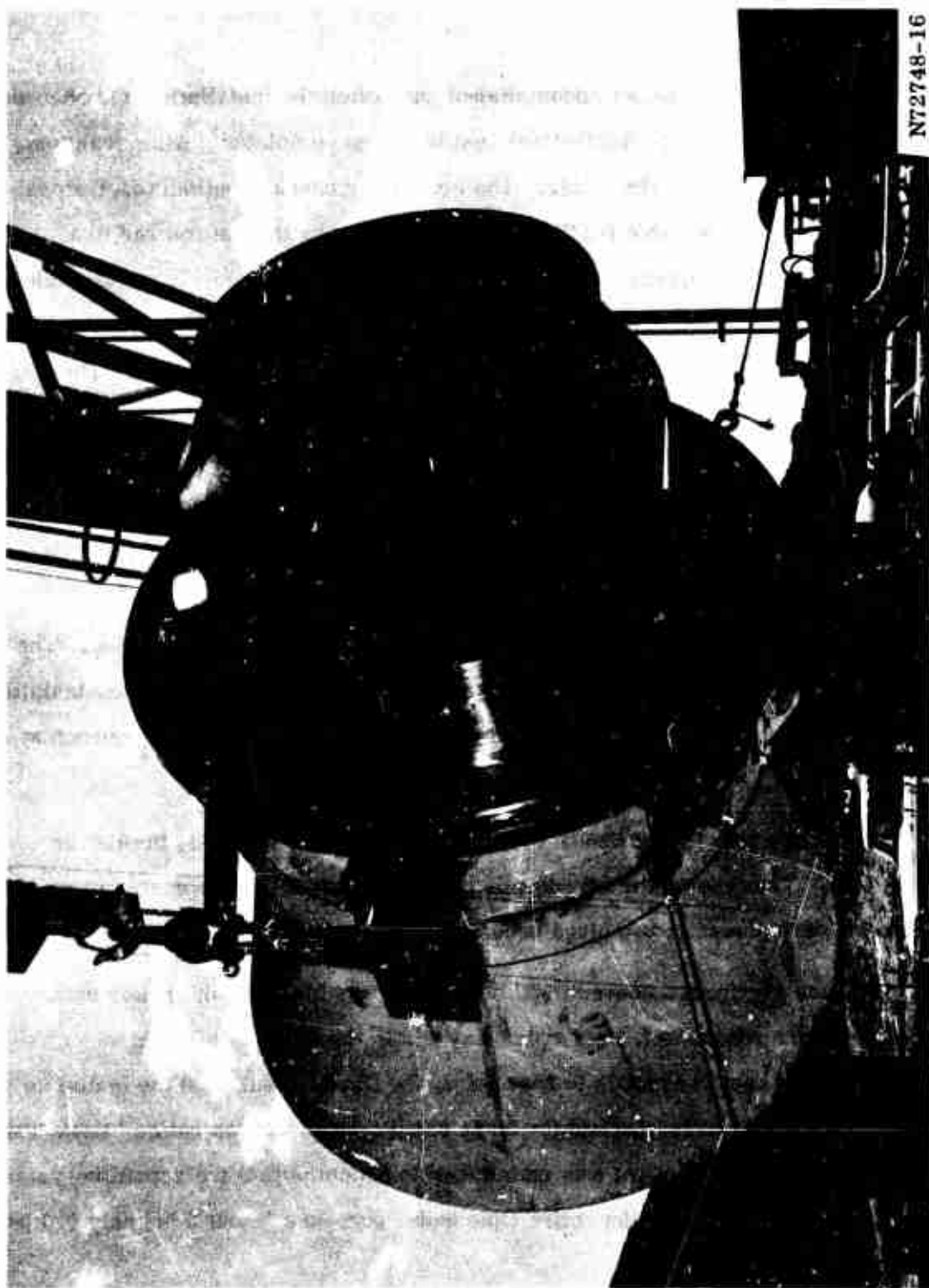
DETAIL A
SCALE $\frac{1}{16}$

This amount was then laid up in the aft case. Mating surfaces were cleaned, the O-ring reinstalled, and the nozzle installed as before. All bolts were torqued and sealed.

- (U) Nozzle checkout was not accomplished until after the installation and checkout of the TVC actuation system and the leak test had been completed. After leak test, the 50 psig was retained in the motor. The previously checked out servoactuators were connected to the movable portion of the nozzle by pinning the rod end to a clevis provided. The shipping links were then removed and the nozzle put through the entire duty cycle to be used during static test (Figure 126). All control and data acquisition systems used on this test were the same as the static test. The installation and checkout of the nozzle was conducted as planned and no significant problems were encountered.

3. LEAK TEST

- (U) A leak test of the motor case and nozzle was conducted prior to firing. The motor was sealed by the installation of a plug in the nozzle. The igniter was installed prior to shipping the motor to the test bay and required only that the CO₂ quench system ports be plugged.
- (U) The nozzle plug (P/N 2U2604-01) was installed prior to nozzle breakover (Figure 134). Thus the motor aft end was properly sealed. Appropriate pressure transducers were placed in two plugs provided in the igniter cap.
- (U) Nitrogen gas from a conventional bottle cart was bled into the motor until the case pressure reached 47.5 psi which was within the 50 ± 10 psi requirement. While under pressure, the nozzle to case joint, the flexible seal, and the igniter to adapter to case joints were checked for leaks using a soap solution called "Leak-Tec." No leaks were found. Pressure was maintained to accommodate the actuation system and nozzle checkout. During the entire time under pressure (about 3 hr) only 0.5 psi drop in pressure was noted.



N72748-16

Figure 134. Nozzle Plug Installed

4. QUENCH SYSTEM

(U) A quench system was used to extinguish insulation burning and reduce the heat flow to metal parts after motor tailoff. The system simply injected carbon dioxide (CO_2) into the motor case on command of the Test Conductor. Thiokol calculations showed that 2,030 lb of CO_2 would be required to cool the nozzle to ambient temperature and 1,950 lb of CO_2 would be required to cool the case insulation.

(U) Eight holes were drilled through the PYROGEN adapter and fitted with 1/8 in. stainless steel nipples 2-1/2 in. long. These nipples discharged the CO_2 directly inside the PYROGEN case and were sized to act as orifices in the system. Thus the vaporization cooling took place within the case making maximum use of CO_2 as a refrigerant. This design also eliminated the possibility of ice plugging the ports. Sixteen 1/2 in. ball check valves (2 per port in series) were attached to the eight pipe nipples to prevent the back flow of combustion gases. These in turn were connected by 1/2 in. stainless steel tubing to a manifold made from a series of 3/4 in. stainless steel pipe tees. The tees centered on a common 1 in. solenoid operated poppet valve. This valve in turn was connected to a 1-1/2 in. Jamesbury manual controlled ball valve which was fed by the main supply line from an 8,000 lb CO_2 receiver. The CO_2 receiver was placed adjacent to the test bay behind hydraulic pump house bunker.

(U) Prior to installation, the system was tested by discharging to the atmosphere for three minutes. No icing occurred and the flow rate was measured at 400 lb per minute. From this it was determined that the required 3,980 lb of CO_2 could be ejected in about 10 minutes.

5. ANTIFLIGHT

(U) The antiflight system was simply a system of heavy cables attached such as to prevent the motor from moving up, side or rear any appreciable distance.

The system shown in Figure 132 was comprised of eight 1/2 in. wire ropes looped over the motor case. These were held off the motor by a channel iron tray. Four 1-1/2 in. cables, two on each side, were attached from the aft harness ring to the test bay floor. All twelve cables were anchored to two large brackets which in turn were lagged to the test bay floor by fourteen 1-1/2 in. bolts. In addition to the above, lateral displacement was limited by two large fixtures placed under the forward and aft harness rings and securely lagged to the test bay floor.

C. INSTRUMENTATION

- (U) The 156-9 motor was instrumented to measure and record all parameters necessary to completely evaluate the test objectives. Additional instrumentation (strain gages) was installed to evaluate any possible unpredicted failure of the case.
- (U) There were 103 instrumentation channels as follows; 8 event, 6 force, 9 pressure, 49 strains, 30 thermocouple, and 1 flow monitor.
- (U) All instrumentation is listed in Table XXVIII with the appropriate coding. The instrumentation is described in detail on Figure 135.
- (U) All instruments (except strain gages and thermocouples) used to obtain physical measurements of system parameters were calibrated in accordance with MIL-C-45662A.
- (U) Due to the nature of strain gages and thermocouples, no calibration was performed. However, the following steps were taken to insure adequacy of recorded data.
1. Strain gages were checked for continuity. An electrical bridge calibration was performed within the period of T minus one minute and T minus zero.
 2. Thermocouples were checked for continuity. Electrical bridge calibration was performed at the same time as strain.
- (U) Four thermocouples, identified as T215, T216, T217, and T218, located on the steel behind the nozzle throat, were installed by Thiokol engineers at HITCO just prior to nozzle assembly. Eight thermocouples were installed on the flexible seal after qualification testing and prior to shipment to HITCO for installation in the nozzle. All other instrumentation was installed by Thiokol personnel at the Wasatch Division.

TABLE XXVIII
INSTRUMENTATION CODING SYSTEM

<u>Pickup Code</u>	<u>Priority</u>	<u>Expected Range</u>	<u>Required Accuracy (%)</u>	<u>Remarks and Location</u>
E601	R	<u>+20 vdc</u>	<u>+5.0</u>	Pitch SV Amplifier Input
E602	R	<u>+20 vdc</u>	<u>+5.0</u>	Yaw SV Amplifier Input
E603	R	<u>+1 vdc</u>	<u>+5.0</u>	Pitch Inner Loop Position Feedback
E604	R	<u>+5 vdc</u>	<u>+5.0</u>	Pitch Outer Loop Position Feedback
E605	R	<u>+1 vdc</u>	<u>+5.0</u>	Yaw Inner Loop Position Feedback
E606	R	<u>+5 vdc</u>	<u>+5.0</u>	Yaw Outer Loop Position Feedback
E607	R	<u>+6 vdc</u>	<u>+5.0</u>	Pitch SV Feedback Voltage
E608	R	<u>+6 vdc</u>	<u>+5.0</u>	Yaw SV Feedback Voltage
F001	M	0 to 1,200,000 lb	<u>+3.0</u>	Longitudinal Thrust
F002	R	0 to 1,200,000 lb	<u>+5.0</u>	Longitudinal Thrust
F003	M	<u>+50,000 lb</u>	<u>+5.0</u>	Forward Lateral Thrust
F004	R	<u>+50,000 lb</u>	<u>+5.0</u>	Forward Lateral Thrust
F005	M	<u>+100,000 lb</u>	<u>+5.0</u>	Aft Lateral Thrust
F006	R	<u>+100,000 lb</u>	<u>+5.0</u>	Aft Lateral Thrust
P001	M	0 to 1,000 psia	<u>+0.5</u>	Pressure Chamber
P002	R	0 to 1,000 psia	<u>+0.5</u>	Pressure Chamber
P003	M	0 to 2,000 psia	<u>+0.7</u>	Pressure Ignition
P004	R	0 to 2,000 psia	<u>+5.0</u>	Pressure Ignition

TABLE XXVIII (Cont)
INSTRUMENTATION CODING SYSTEM

<u>Pickup Code</u>	<u>Priority</u>	<u>Expected Range</u>	<u>Required Accuracy (%)</u>	<u>Remarks and Location</u>
P201	M	0 to 3,000 psia	± 5.0	Pressure Hydraulic Supply
P202	R	0 to 3,000 psia	± 5.0	Pressure Hydraulic System
P203	R	0 to 1,000 psia	± 5.0	Pressure Hydraulic Return
P204	M	$\pm 3,000$ psid	± 5.0	Pressure Differential Pitch Actuator
P205	M	$\pm 3,000$ psid	± 5.0	Pressure Differential Yaw Actuator
S001	R	0 to 0.004 in./in.	± 5.0	Strain Forward Dome at 40 deg
S002	R	0 to 0.004 in./in.	± 5.0	Strain Forward Dome at 40 deg
S003	R	0 to 0.004 in./in.	± 5.0	Strain Forward Dome at 160 deg
S004	R	0 to 0.004 in./in.	± 5.0	Strain Forward Dome at 160 deg
S005	R	0 to 0.004 in./in.	± 5.0	Strain Forward Dome at 280 deg
S006	R	0 to 0.004 in./in.	± 5.0	Strain forward Dome at 280 deg
S007	R	0 to 0.004 in./in.	± 5.0	Strain Case at 90 deg
S008	R	0 to 0.004 in./in.	± 5.0	Strain Case as 90 deg
S009	R	0 to 0.004 in./in.	± 5.0	Strain Case at 180 deg
S010	R	0 to 0.004 in./in.	± 5.0	Strain Case at 180 deg
S011	R	0 to 0.004 in./in.	± 5.0	Strain Aft Dome at 0 deg
S012	R	0 to 0.004 in./in.	± 5.0	Strain Aft Dome at 0 deg

TABLE XXVIII (Cont)
INSTRUMENTATION CODING SYSTEM

<u>Pickup Code</u>	<u>Priority</u>	<u>Expected Range</u>	<u>Required Accuracy (%)</u>	<u>Remarks and Location</u>
S013	R	0 to 0.004 in./in.	± 5.0	Strain Aft Dome at 60 deg
S014	R	↑ ↓	↑ ↓	Strain Aft Dome at 60 deg
S015	R			Strain Aft Dome at 120 deg
S016	R			Strain Aft Dome at 120 deg
S017	R			Strain Aft Dome at 180 deg
S018	R			Strain Aft Dome at 180 deg
S019	R			Strain Aft Dome at 240 deg
S020	R			Strain Aft Dome at 240 deg
S021	R			Strain Aft Dome at 300 deg
S022	R			Strain Aft Dome at 300 deg
S023	R			Strain Aft Dome at 180 deg
S024	R			Strain Aft Dome at 180 deg
S025	R	0 to 0.004 in./in.	± 5.0	Strain Aft Dome at 180 deg
S201	R	± 0.004 in./in.	± 5.0	Strain Nozzle Actuation Bracket
S202	R	± 0.004 in./in.	± 5.0	Strain Nozzle Actuation Bracket
S203	R	± 0.004 in./in.	± 5.0	Strain Nozzle Actuation Bracket
S204	R	± 0.004 in./in.	± 5.0	Strain Nozzle Actuation Bracket
S205	R	± 0.004 in./in.	± 5.0	Strain Nozzle Housing

TABLE XXVIII (Cont)
INSTRUMENTATION CODING SYSTEM

Pickup Code	Priority	Expected Range	Required Accuracy (%)	Remarks and Location
S206	R	± 0.004 in./in.	± 5.0	
S207	R			
S208	R			
S209	R			
S210	R			Strain Nozzle Housing
S211	R			Strain Nozzle Actuation Clevis
S212	R			Strain Nozzle Actuation Clevis
S213	R			Strain Nozzle Actuation Bracket
S214	R			
S215	R			
S216	R			Strain Nozzle Actuation Bracket
S217	R			Strain Housing Exit
S218	R			Strain Housing Exit
S219	R			Strain Housing Exit
S220	R			
S221	R			
S222	R			
S223	R			
S224	R	± 0.004 in./in.	± 5.0	Strain Housing Exit

TABLE XXVIII (Co' ,
INSTRUMENTATION CODING SYSTEM

<u>Pickup Code</u>	<u>Priority</u>	<u>Expected Range</u>	<u>Required Accuracy (%)</u>	<u>Remarks and Location</u>
T001	R	0 to 500°F ↑ ↓	+5.0 ↑ ↓	Temperature Forward Dome
T002	R			↑
T003	R			↓
T004	R			Temperature Forward Dome
T005	R			Temperature Case
T006	R			↑
T007	R			↓
T008	R			Temperature Case
T009	R			Temperature Aft Dome
T010	R			↑
T011	R			↓
T012	R			Temperature Aft Dome
T201	R			Temperature Nozzle Housing
T202	R			Temperature Nozzle Housing
T203	P			Temperature Nozzle Forward End Ring
T204	R	0 to 500°F ↑ ↓	+5.0 ↑ ↓	↑
T205	R			↓
T206	R			Temperature Nozzle Forward End Ring
T207	R			Temperature Nozzle Housing
T208	R			↑
T209	R			↓
T210	R			Temperature Nozzle Housing

TABLE XXVIII (Cont)

INSTRUMENTATION CODING SYSTEM

Pickup Code	Priority	Expected Range	Required Accuracy (%)	Remarks and Location
T211	R	0 to 500°F	+5.0	Temperature Nozzle Aft End Ring
T212	R			
T213	R			
T214	R			Temperature Nozzle Aft End Ring
T215	R			Temperature Nozzle Housing
T216	R			
T217	R			
T218	R	0 to 500°F		Temperature Nozzle Housing
W601	R	0 to 200 GPM	+5.0	Flowmeter Hydraulic System

PRECEDING PAGE BLANK-NOT FILLED

INSTRUMENTATION (REF)		
INSTRUMENT CODE	PARAMETER	LOCATION
S001	STRAIN - RADIAL	FWD DOME @ 40° (SEE DETAIL A)
S002	STRAIN - CIRCUM	FWD DOME @ 40° (SEE DETAIL A)
S003	STRAIN - RADIAL	FWD DOME @ 170° (SEE DETAIL A)
S004	STRAIN - CIRCUM	FWD DOME @ 170° (SEE DETAIL A)
S005	STRAIN - RADIAL	FWD DOME @ 280° (SEE DETAIL A)
S006	STRAIN - CIRCUM	FWD DOME @ 280° (SEE DETAIL A)
S007	STRAIN - LONG.	CASE @ 90° (SEE DETAIL E)
S008	STRAIN - HOOP	CASE @ 90° (SEE DETAIL E)
S009	STRAIN - LONG.	CASE @ 180° (SEE DETAIL E)
S010	STRAIN - HOOP	CASE @ 180° (SEE DETAIL E)
S011	STRAIN - RADIAL	AFT DOME @ 0° (SEE DETAIL F)
S012	STRAIN - CIRCUM	AFT DOME @ 0° (SEE DETAIL F)
S013	STRAIN - RADIAL	AFT DOME @ 60° (SEE DETAIL F)
S014	STRAIN - CIRCUM	AFT DOME @ 60° (SEE DETAIL F)
S015	STRAIN - RADIAL	AFT DOME @ 120° (SEE DETAIL F)
S016	STRAIN - CIRCUM	AFT DOME @ 120° (SEE DETAIL F)
S017	STRAIN - RADIAL	AFT DOME @ 180° (SEE DETAIL F)
S018	STRAIN - CIRCUM	AFT DOME @ 180° (SEE DETAIL F)
S019	STRAIN - RADIAL	AFT DOME @ 240° (SEE DETAIL F)
S020	STRAIN - CIRCUM	AFT DOME @ 240° (SEE DETAIL F)
S021	STRAIN - RADIAL	AFT DOME @ 300° (SEE DETAIL F)
S022	STRAIN - CIRCUM	AFT DOME @ 300° (SEE DETAIL F)
S023	STRAIN - RADIAL	AFT DOME @ 180° (SEE DETAIL F)
S024	STRAIN - CIRCUM	AFT DOME @ 180° (SEE DETAIL F)
S025	STRAIN - TRANSVERSE	AFT DOME @ 180° (SEE DETAIL F)
S201	STRAIN - LONG.	NOZZLE @ 0° (SEE VIEW G-G)
S202	STRAIN - CIRCUM	NOZZLE @ 0° (SEE VIEW G-G)
S203	STRAIN - LONG.	NOZZLE @ 0° (SEE VIEW G-G)
S204	STRAIN - CIRCUM	NOZZLE @ 0° (SEE VIEW G-G)
S205	STRAIN - LONG.	NOZZLE @ 0° (SEE VIEW B-B)
S206	STRAIN - CIRCUM	NOZZLE @ 0° (SEE VIEW B-B)
S207	STRAIN - LONG.	NOZZLE @ 90° (SEE VIEW H-H)
S208	STRAIN - CIRCUM	NOZZLE @ 90° (SEE VIEW H-H)
S209	STRAIN - LONG.	NOZZLE @ 0° (SEE VIEW B-B)
S210	STRAIN - CIRCUM	NOZZLE @ 0° (SEE VIEW B-B)
S211	STRAIN - RADIAL	NOZZLE @ 0° (SEE VIEW C-C)
S212	STRAIN - CIRCUM	NOZZLE @ 0° (SEE VIEW C-C)
S213	STRAIN - LONG.	NOZZLE @ 0° (SEE VIEW B-B)
S214	STRAIN - CIRCUM	NOZZLE @ 0° (SEE VIEW B-B)
S215	STRAIN - LONG.	NOZZLE @ 0° (SEE VIEW A-A)
S216	STRAIN - CIRCUM	NOZZLE @ 0° (SEE VIEW B-B)
S217	STRAIN - LONG.	NOZZLE @ 0° (SEE VIEW D-D)
S218	STRAIN - CIRCUM	NOZZLE @ 0° (SEE VIEW D-D)
S219	STRAIN - LONG.	NOZZLE @ 90° (SEE VIEW D-D)
S220	STRAIN - CIRCUM	NOZZLE @ 90° (SEE VIEW D-D)
S221	STRAIN - LONG.	NOZZLE @ 0° (SEE VIEW D-D)
S222	STRAIN - CIRCUM	NOZZLE @ 0° (SEE VIEW D-D)
S223	STRAIN - LONG.	NOZZLE @ 90° (SEE VIEW D-D)
S224	STRAIN - CIRCUM	NOZZLE @ 90° (SEE VIEW D-D)
T001	TEMPERATURE	FWD DOME @ 0°
T002	TEMPERATURE	FWD DOME @ 90°
T003	TEMPERATURE	FWD DOME @ 0°
T004	TEMPERATURE	FWD DOME @ 90°
T005	TEMPERATURE	CASE @ 0°
T006	TEMPERATURE	CASE @ 90°
T007	TEMPERATURE	CASE @ 0°
T008	TEMPERATURE	CASE @ 90°
T009	TEMPERATURE	AFT DOME @ 0°
T010	TEMPERATURE	AFT DOME @ 90°

INSTRUMENTATION (REF)		
INSTRUMENT CODE	PARAMETER	
T011	TEMPERATURE	AFT
T012	TEMPERATURE	AFT
T201	TEMPERATURE	NOZ
T202	TEMPERATURE	NOZ
T203	TEMPERATURE	FLE
T204	TEMPERATURE	FLE
T205	TEMPERATURE	FLE
T206	TEMPERATURE	FLE
T207	TEMPERATURE	NOZ
T208	TEMPERATURE	NOZ
T209	TEMPERATURE	NOZ
T210	TEMPERATURE	NOZ
T211	TEMPERATURE	FLE
T212	TEMPERATURE	FLE
T213	TEMPERATURE	FLE
T214	TEMPERATURE	FLE
T215	TEMPERATURE	MOA
T216	TEMPERATURE	MOA
T217	TEMPERATURE	MOA
T218	TEMPERATURE	MOA

INSTRUMENTATION (NEF)		REVISIONS				
PARAMETER	LOCATION	ZONE	REV	DESCRIPTION	DATE	APPROVED
TEMPERATURE	AFT DOME @ 0°					
TEMPERATURE	AFT DOME @ 90°					
TEMPERATURE	NOZZLE @ 0° (SEE VIEW K)					
TEMPERATURE	NOZZLE @ 270° (SEE VIEW K)					
TEMPERATURE	FLEX BEARING ASSY @ 0°					
TEMPERATURE	FLEX BEARING ASSY @ 90°					
TEMPERATURE	FLEX BEARING ASSY @ 180°					
TEMPERATURE	FLEX BEARING ASSY @ 270°					
TEMPERATURE	NOZZLE FIXED HOUSING ASSY @ 0°					
TEMPERATURE	NOZZLE FIXED HOUSING ASSY @ 90°					
TEMPERATURE	NOZZLE FIXED HOUSING ASSY @ 180°					
TEMPERATURE	NOZZLE FIXED HOUSING ASSY @ 270°					
TEMPERATURE	FLEX BEARING ASSY @ 0°					
TEMPERATURE	FLEX BEARING ASSY @ 90°					
TEMPERATURE	FLEX BEARING ASSY @ 180°					
TEMPERATURE	FLEX BEARING ASSY @ 270°					
TEMPERATURE	MOVABLE HOUSING ASSY @ 0°					
TEMPERATURE	MOVABLE HOUSING ASSY @ 90°					
TEMPERATURE	MOVABLE HOUSING ASSY @ 180°					
TEMPERATURE	MOVABLE HOUSING ASSY @ 270°					

NOTES:

1. TOLERANCES FOR LOCATING INSTRUMENTS SHALL BE ± 0.25 AND ± 5 DEGREES UNLESS OTHERWISE SPECIFIED.
2. INSTALL THERMOCOUPLES PER DOCUMENT INSTRUCTION DOCUMENT NO. 01-1-44.
3. INSTALL STRAIN GAGES PER DOCUMENT INSTRUCTION DOCUMENT NO. 01-1-47.
4. ITEM 2, PART NO. C6-141, ITEM 3, PART NO. C6-121-N3V; INSTRUMENTS DIVISION, BUDG COMPANY, PHOENIXVILLE, PA. CODE IDENT NO. 07995 (ON EQUIV)
5. THERMOCOUPLES T203-T206 AND T211-T218 SHALL BE INSTALLED PRIOR TO ASSY OF FLEXIBLE BEARING ASSY TO FIXED HOUSING ASSY.

LIST OF MATERIAL ON PARTS LIST		SHEET 1 OF 2
QTY REQD PER DASH NO.	ITEM NO. CODE IDENT. PART OR IDENTIFYING NO.	NOMENCLATURE OR DESCRIPTION MATERIAL SPECIFICATION ZONE
	1 3	DOCUMENT 01-1-47
	46 2	DOCUMENT 01-1-44
	30 1	STRAIN GAGE 3 4
	-01	STRAIN GAGE 3 4
		THERMOCOUPLE 2 5
		UIE 1905-03

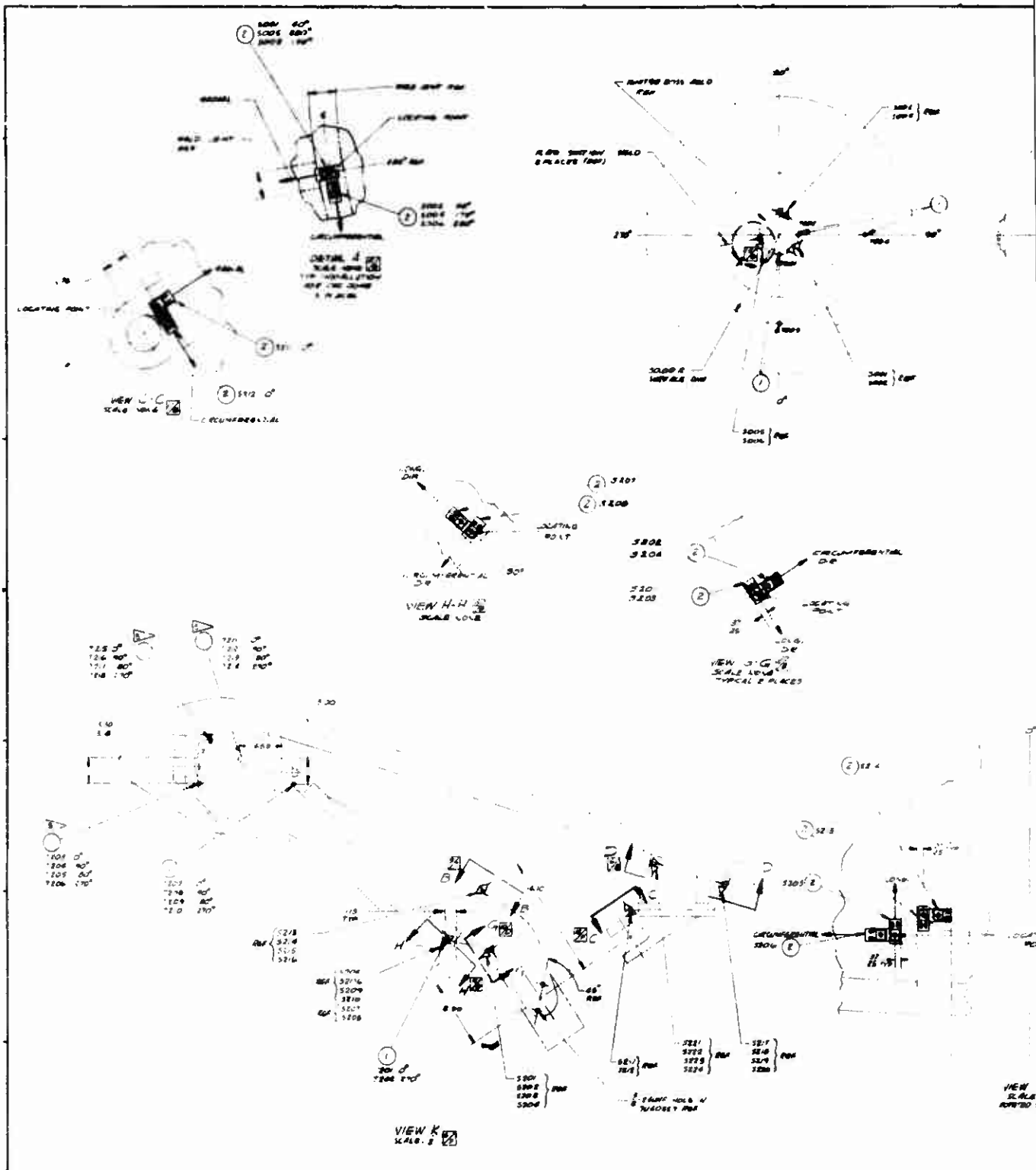
UNLESS OTHERWISE SPECIFIED		THOROL CHEMICAL CORPORATION	
DRAWINGS ARE IN INCHES	TOLERANCES	DRAWN BY <u>R. ZEIGLER</u> 3-1-67	CHECKED BY <u>C. J. WILSON</u> 3-1-67
ANGLES: 0° 180° 90° 270°	FRACCTIONS: 1/2 1/4 3/8 1/8 1/16 1/32 1/64	DESIGNED BY <u>J. M. KELLER</u> 1-25-67	TESTED BY <u>J. M. KELLER</u> 1-25-67
BREAK SHARP EDGES 0.015	ALL SHAFT PROFILES 0.005-0.010	REWORK BY <u>J. M. KELLER</u> 1-25-67	REWORK BY <u>J. M. KELLER</u> 1-25-67
THREADS PER STD. 19-1	THREADS PER STD. 19-1	REWORK BY <u>J. M. KELLER</u> 1-25-67	REWORK BY <u>J. M. KELLER</u> 1-25-67
DIMENSIONS PER STD. 19-1	ALL DIMENSIONS PER STD. 19-1	REWORK BY <u>J. M. KELLER</u> 1-25-67	REWORK BY <u>J. M. KELLER</u> 1-25-67
NONDESTRUCTIVE TESTING SYMBOLS	PER STD. 19-1	REWORK BY <u>J. M. KELLER</u> 1-25-67	REWORK BY <u>J. M. KELLER</u> 1-25-67
FINISHES: STANDARD TO 125-14 APPLICABLE	SURFACE ROUGHNESS SYMBOLS	REWORK BY <u>J. M. KELLER</u> 1-25-67	REWORK BY <u>J. M. KELLER</u> 1-25-67
PER ASA 19-1	ALL FINISHED SURFACES	REWORK BY <u>J. M. KELLER</u> 1-25-67	REWORK BY <u>J. M. KELLER</u> 1-25-67

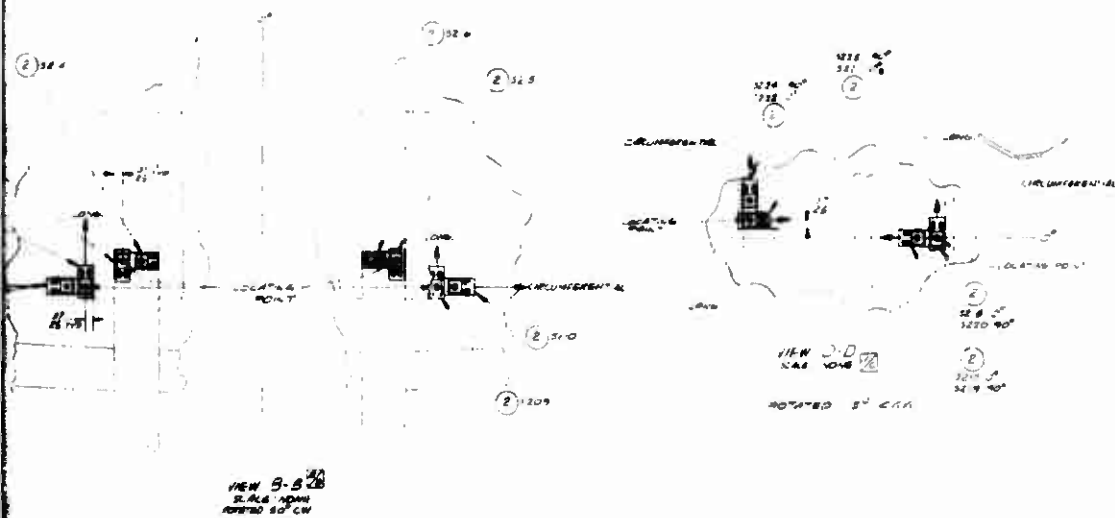
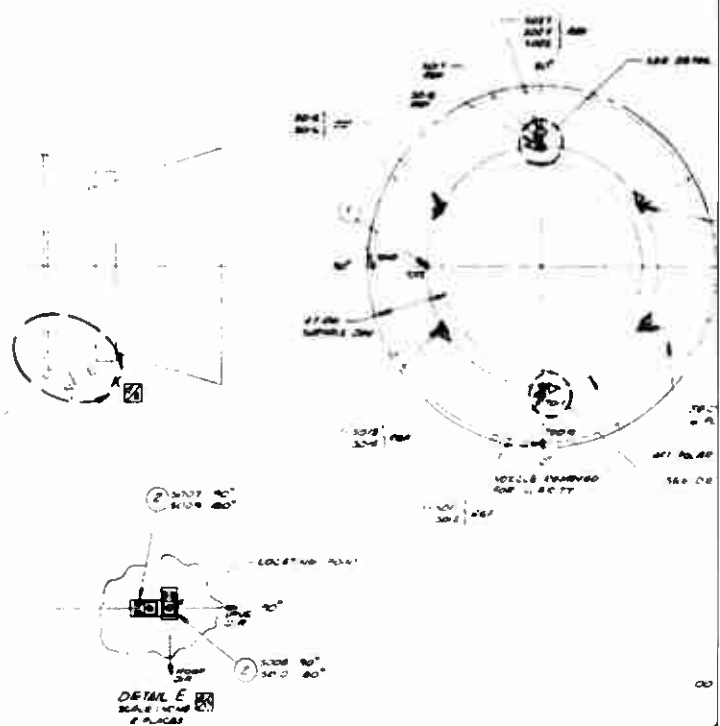
APPLICATION	NEXT ASSEMBLY	UMD ON	PART NO.	DATE	BY

SIZE	CODE IDENT NO.	TITLE
D	07703	INSTRUMENTATION INSTALLATION-TU-562
SCALE 1/20	35103	SHEET 1 OF 2

Figure 135. Instrumentation Drawing (Sheet 1 of 2)

PRECEDING PAGE BLANK-NOT FILMED





7U40586

2

1

2

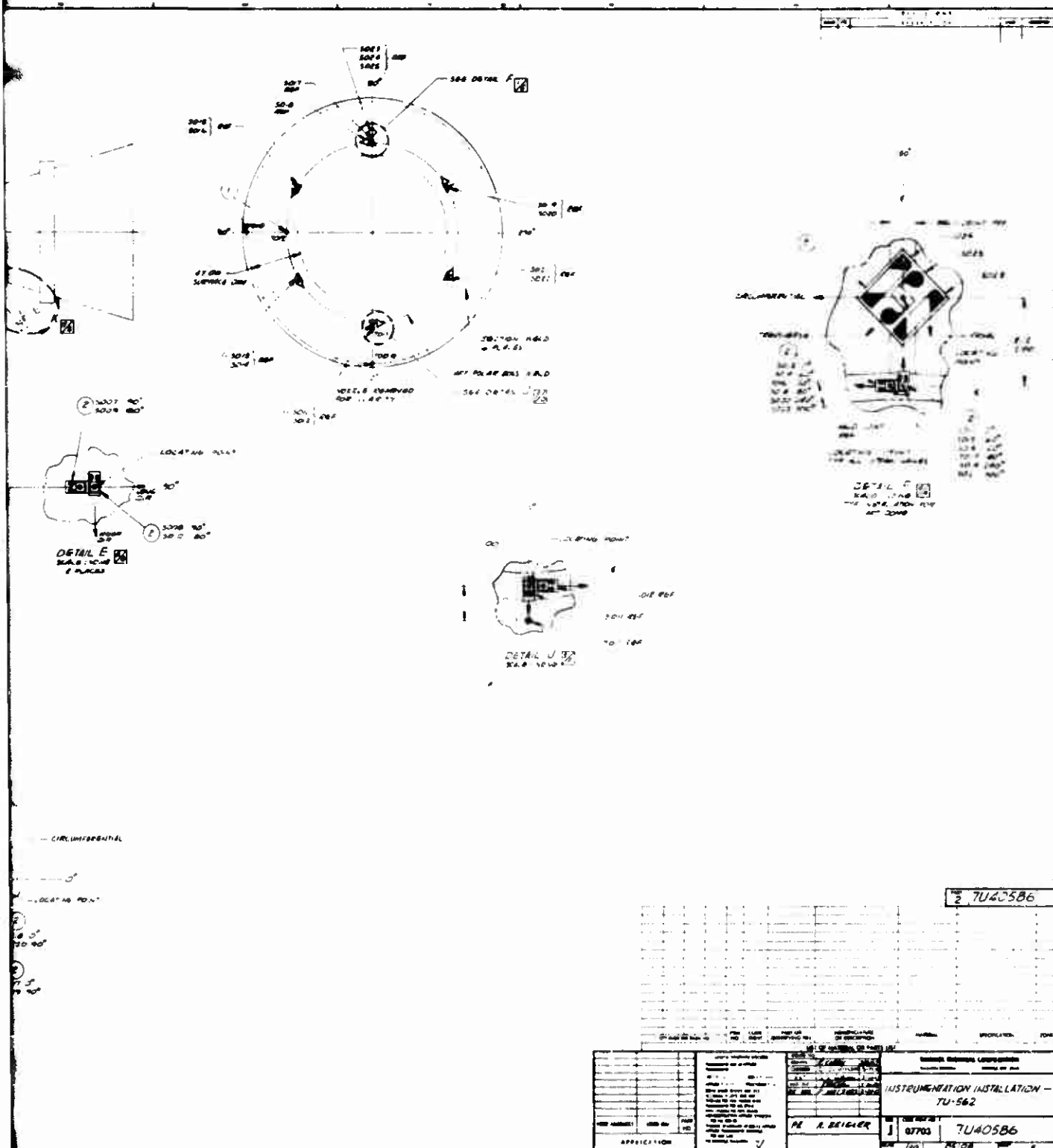


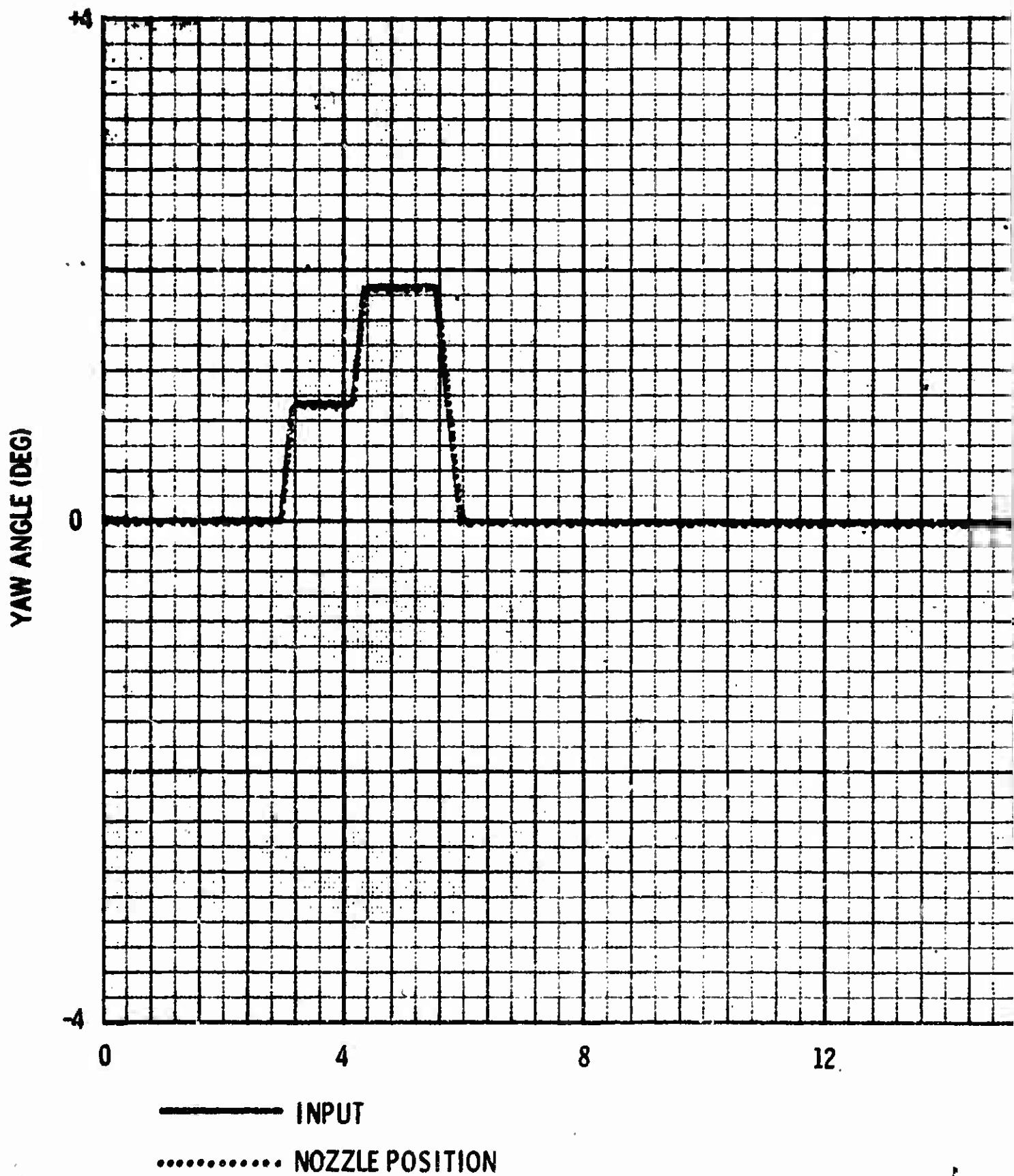
Figure 107. Instrumentation Drawing (Sheet 2)

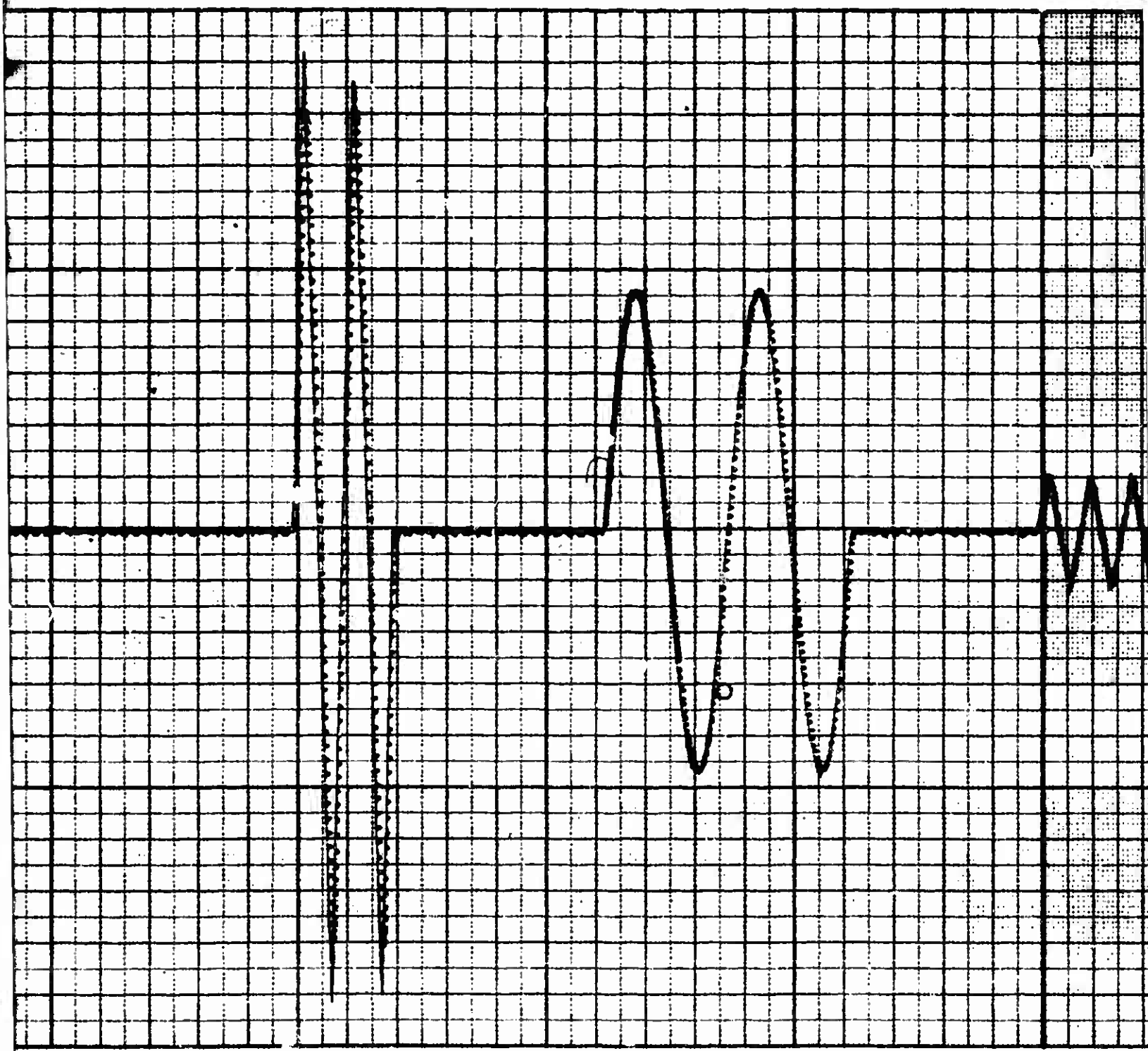
D. TEST RESULTS SUMMARY

1. GENERAL RESULTS

- (U) The 156-9 motor was successfully static fired at Thiokol's Wasatch Division on 26 May 1967. Motor performance was entirely satisfactory and the overall objective of successfully static testing a one million pound thrust class 156 inch diameter monolithic solid propellant rocket motor with an OFSMN thrust vector control system was satisfied. The actuation system, nozzle and flexible seal, and motor case and insulation were in excellent condition after the test. The extended motor burn time did not cause significant degradation of components.
- (U) a. Results of Primary Objectives--A successful demonstration of the performance and functional capabilities of the submerged omniaxial flexible seal movable nozzle was achieved. The nozzle followed the programmed duty cycle as evidenced in Figure 136.
- (U) Data that can be used for future nozzle designs were obtained, including the effective location of nozzle pivot point and nozzle actuation torque. Torques were slightly less than predicted, but the nozzle pivot point did not vary.
- (U) The successful demonstration made it possible to accurately evaluate the performance of the nozzle barrier seal protective gap, cavity and projecting insulation. All nozzle and aft case insulation materials were in excellent condition. There was evidence of very minor heat and erosion exposure on the boot protecting the flexible seal indicating exceptional performance of the barrier assembly.
- (U) Good strain gage and thermocouple data allowed accurate evaluation of nozzle and plastic material performance during static firing conditions. Erosion and char of nozzle plastic parts were as predicted. It was evident that the nozzle metal parts received little, if any, heat and were not highly stressed.

PRECEDING PAGE BLANK-NOT FILMED





12

16

20

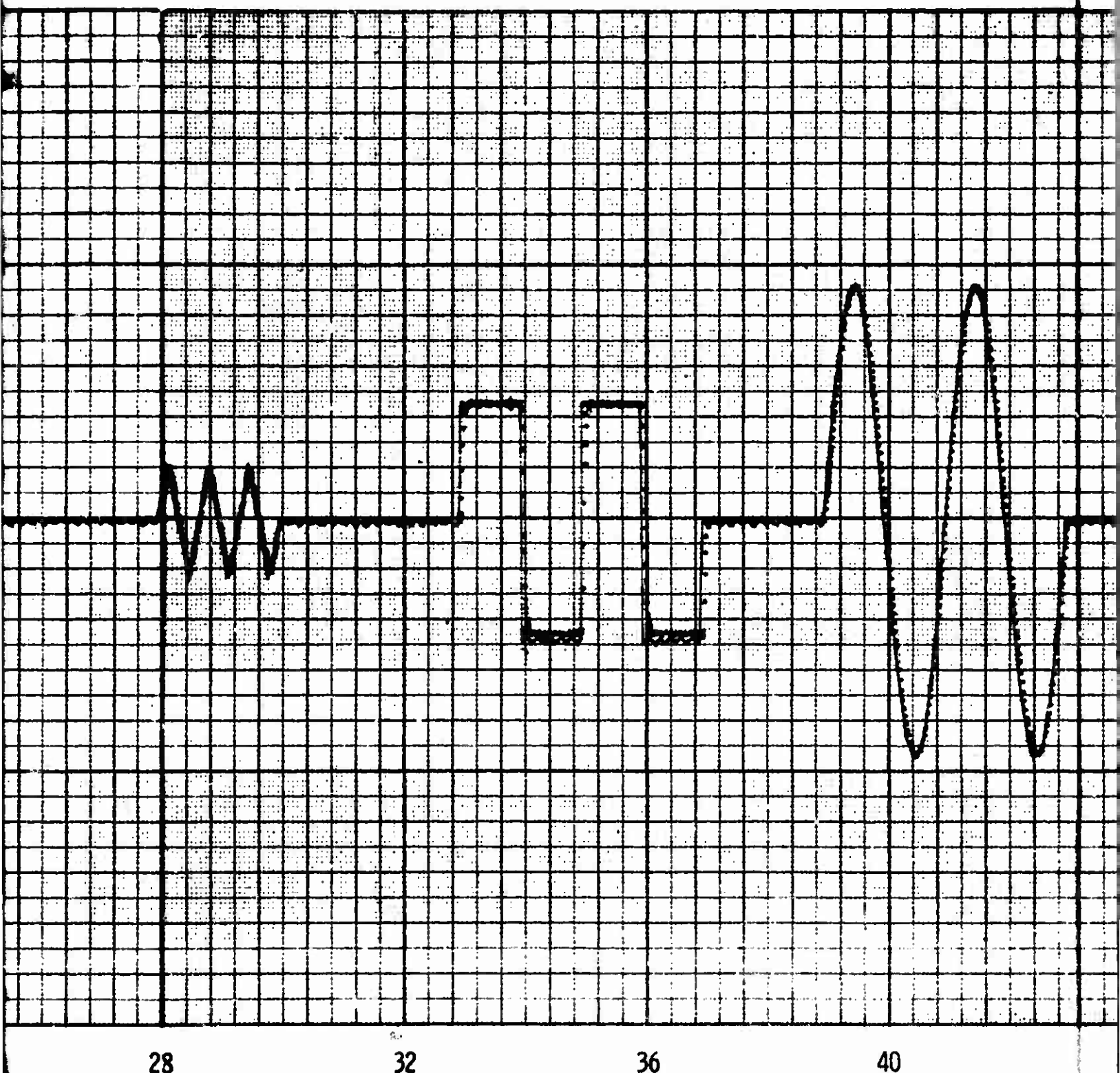
24

28

1

2

CONFIDENTIAL



28

32

36

40

TIME (SEC)

CONFIDENTIAL

2

3

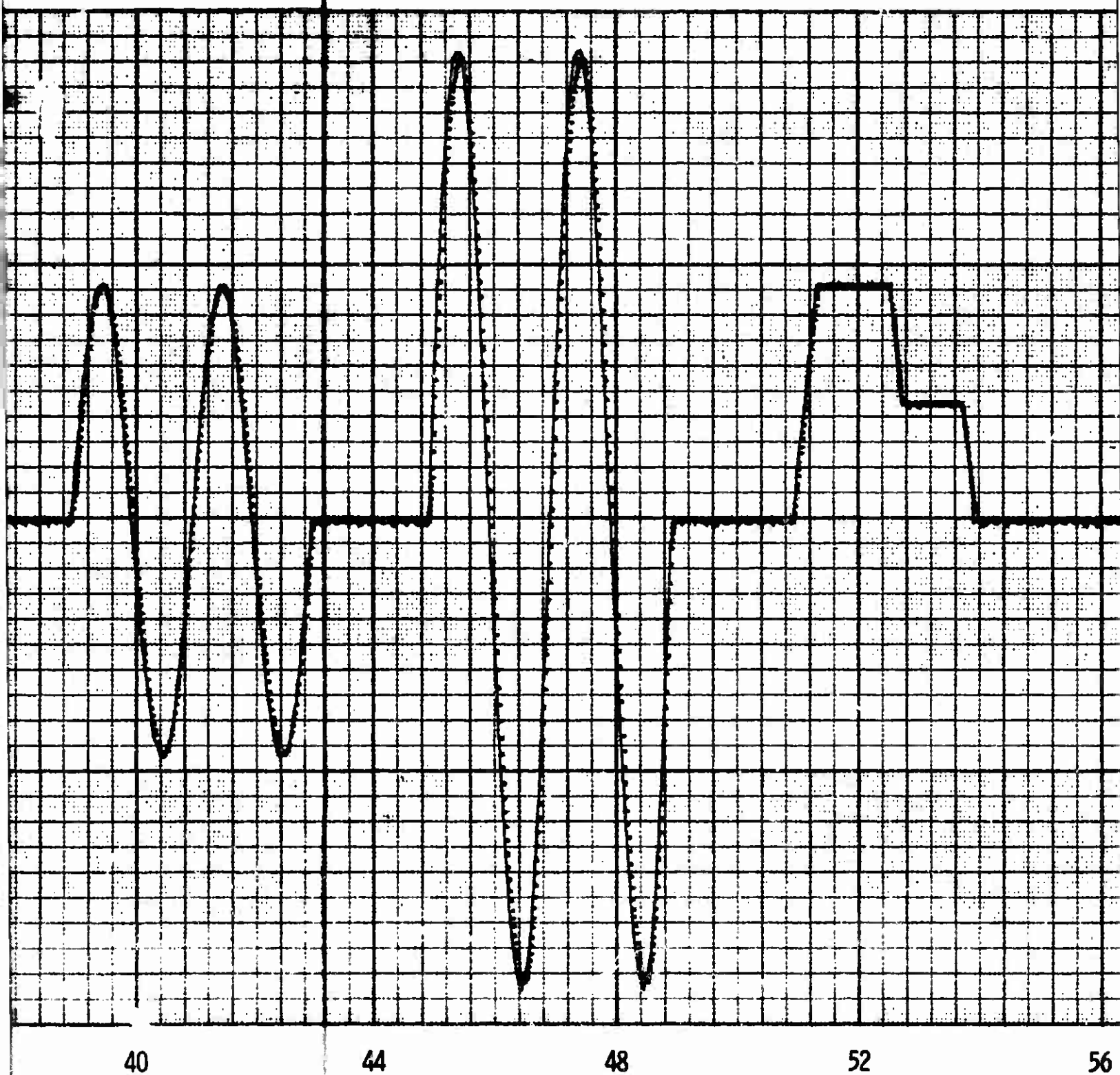


Figure 136. 156-9 Duty Cycle Actual N

3

4

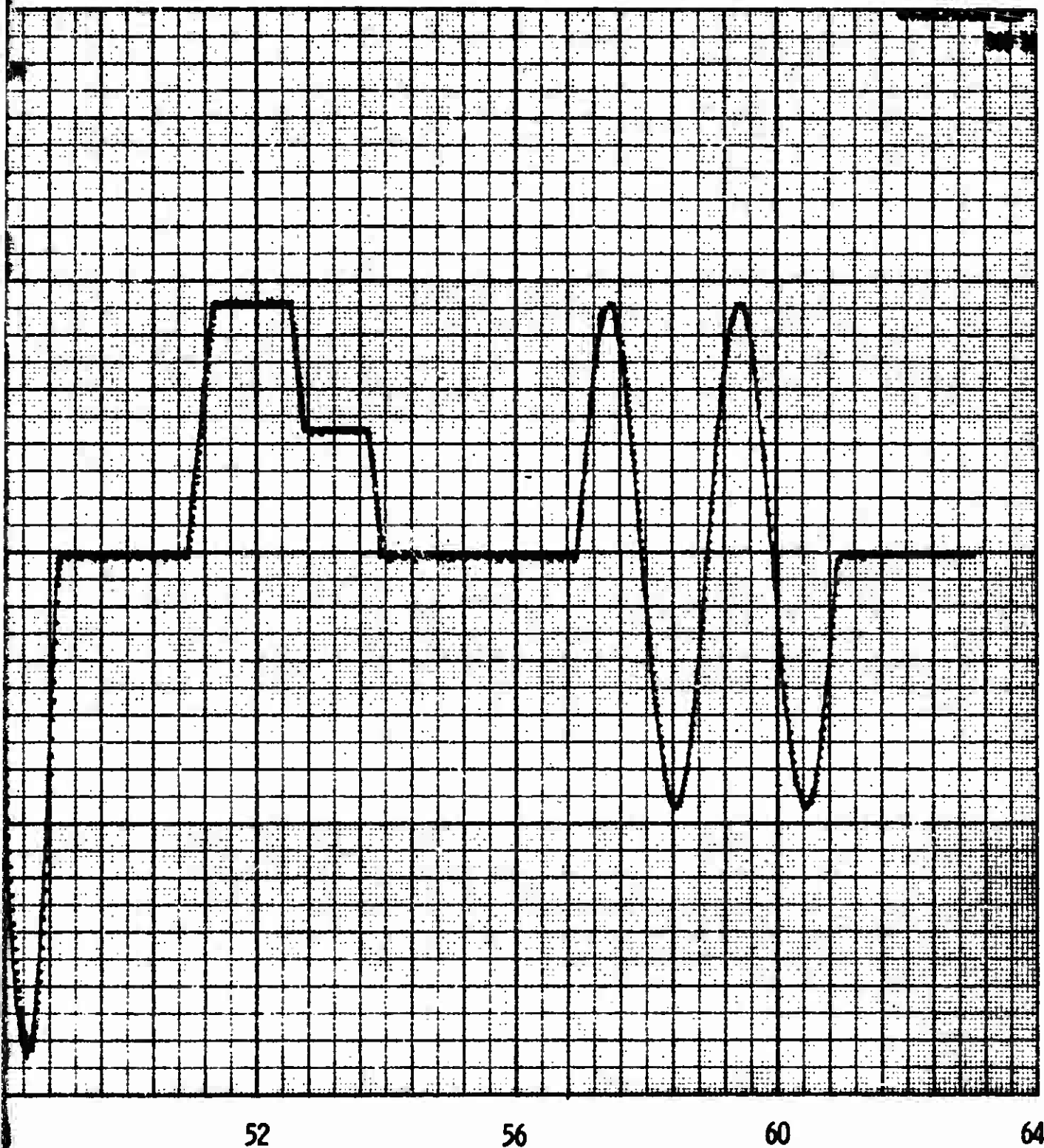


Figure 136. 156-9 Duty Cycle Actual Nozzle Position Superimposed on Programmed Input

4

25

CONFIDENTIAL

- (C) Complete acquisition of data associated with nozzle actuation permitted a detailed evaluation of the performance of the nozzle actuation system. The system performed exactly as predicted. The maximum nozzle vector angle of 3.66 deg was approximately 10 per cent less than the design criteria of 4 degrees. However, this was predicted because the hydraulic actuators which were procured had a stroke of 7 in. instead of 7-1/2 in. required by the design.
- (U) b. Results of Secondary Objectives--The static test demonstrated 156 inch motor performance as being quite satisfactory. The motor ignited and produced good pressure and thrust traces. The motor burned longer than predicted, but this did not adversely affect the test results.
- (U) Case insulation was in excellent condition after the firing. A thorough evaluation of insulation design and material performance was achieved.
- (U) Large motor handling and assembly procedures were demonstrated effectively. No difficulties were encountered during motor transportation, off loading, installation and alignment in bay, and installation of thrust adapters and measuring devices. Nozzle transportation, off loading, breakover, and installation on the motor also were accomplished without incident.

CONFIDENTIAL
(THIS PAGE IS UNCLASSIFIED)

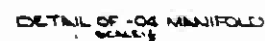
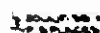
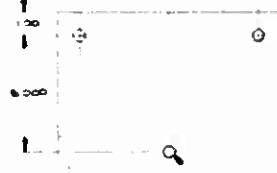
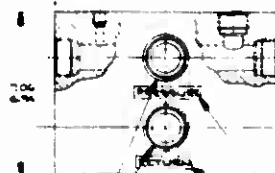
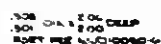
2. FLEXIBLE SEAL PERFORMANCE

(U) a. Nozzle Actuation--The TVC actuation system performance was checked out and evaluated in the yaw plane during flexible seal component tests and in the pitch and yaw plane both during the nozzle checks. Acceptable performance was thus verified prior to installation on the motor.

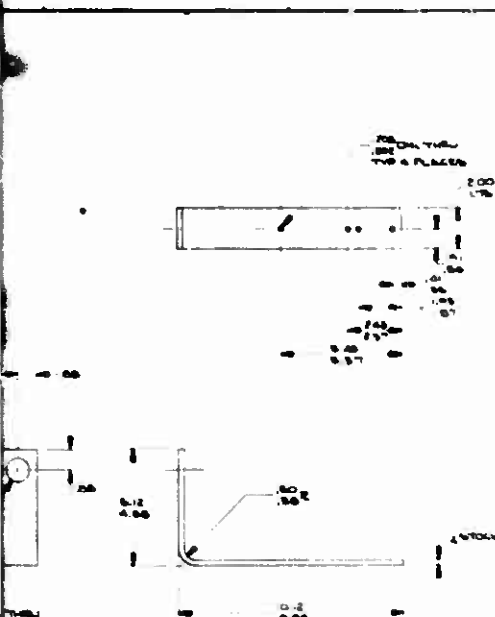
(U) Actuation bracket assemblies, trunnion assemblies, actuator clevis brackets and servoactuators were assembled as shown in Figure 32. The remainder of the actuation system was installed in accordance with Figure 137. System flushing and filtering was accomplished by first connecting the actuator supply and return lines together. Next the accumulator was pressurized to 100 psig and the system pressure raised and lowered around this point several times to completely flush the accumulator. The entire system was then flushed for 8 hours. Supply and return hoses were then individually wrapped with heat protective foil tape. Those on the floor were covered with sand bags. Supply and system pressure transducers were then installed and connected. Servocontrol electronics were calibrated and connected. The servoactuators (rod end disconnected) were operated through the duty cycle using the program tape.

Performance of the TVC actuation system was as expected throughout the static test. This is evidenced by the command and position vs time traces of Figures 138 and 139. Performance requirements were met in all areas except for the maximum thrust vector angle of 4 degrees. The maximum nozzle vector angle obtained was 3.658 degrees. This was the direct result of two factors acting in combination.

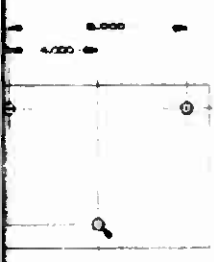
1. The servoactuators were built with a 7.0 in. stroke instead of 7.5 in. stroke.
2. The fixed housing actuator brackets had a much higher than expected compliance. A total of approximately 0.4 deg of otherwise usable stroke was absorbed by bracket deflection.



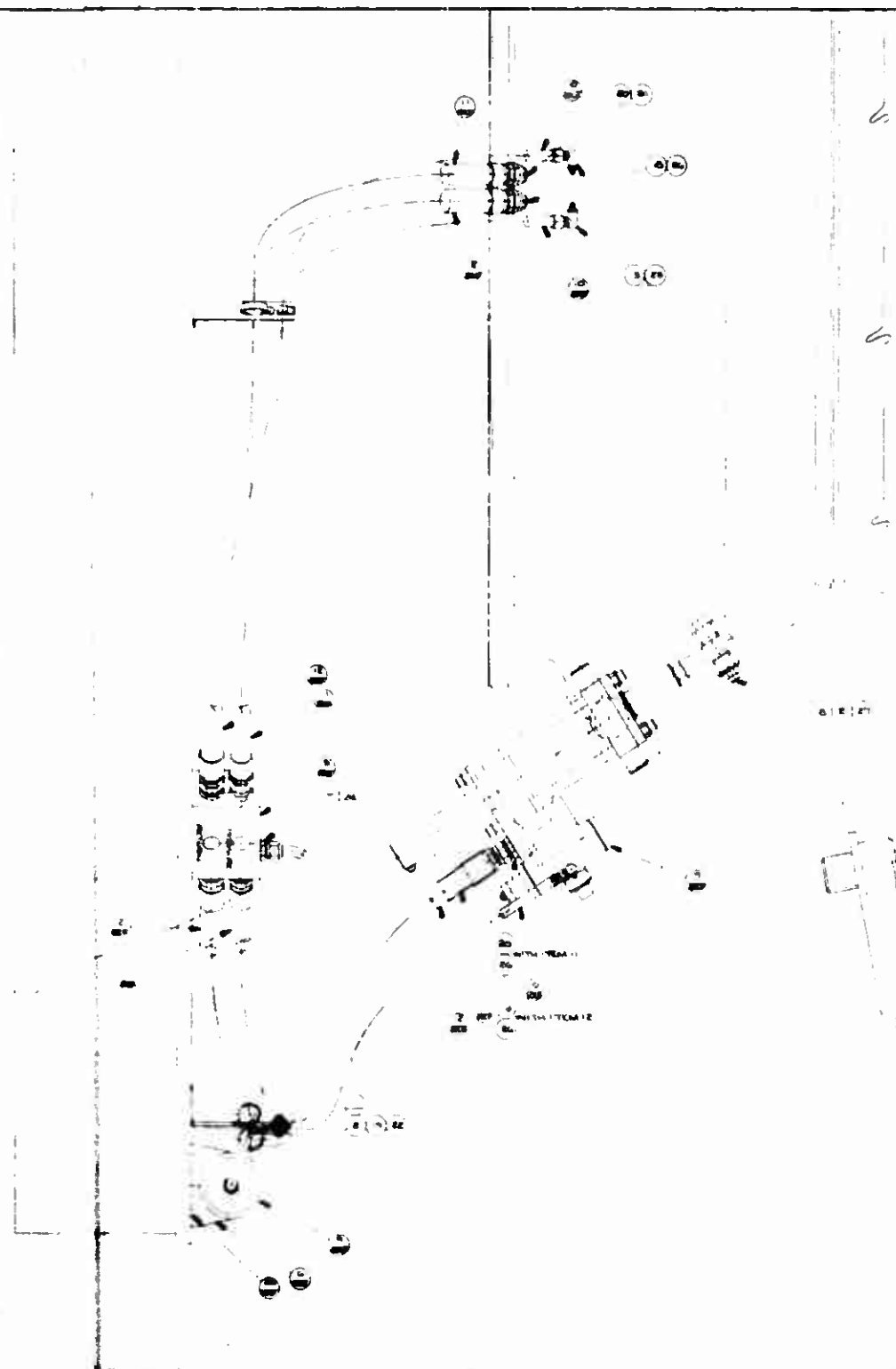
7U40588



DETAIL OF LOG BRACKET

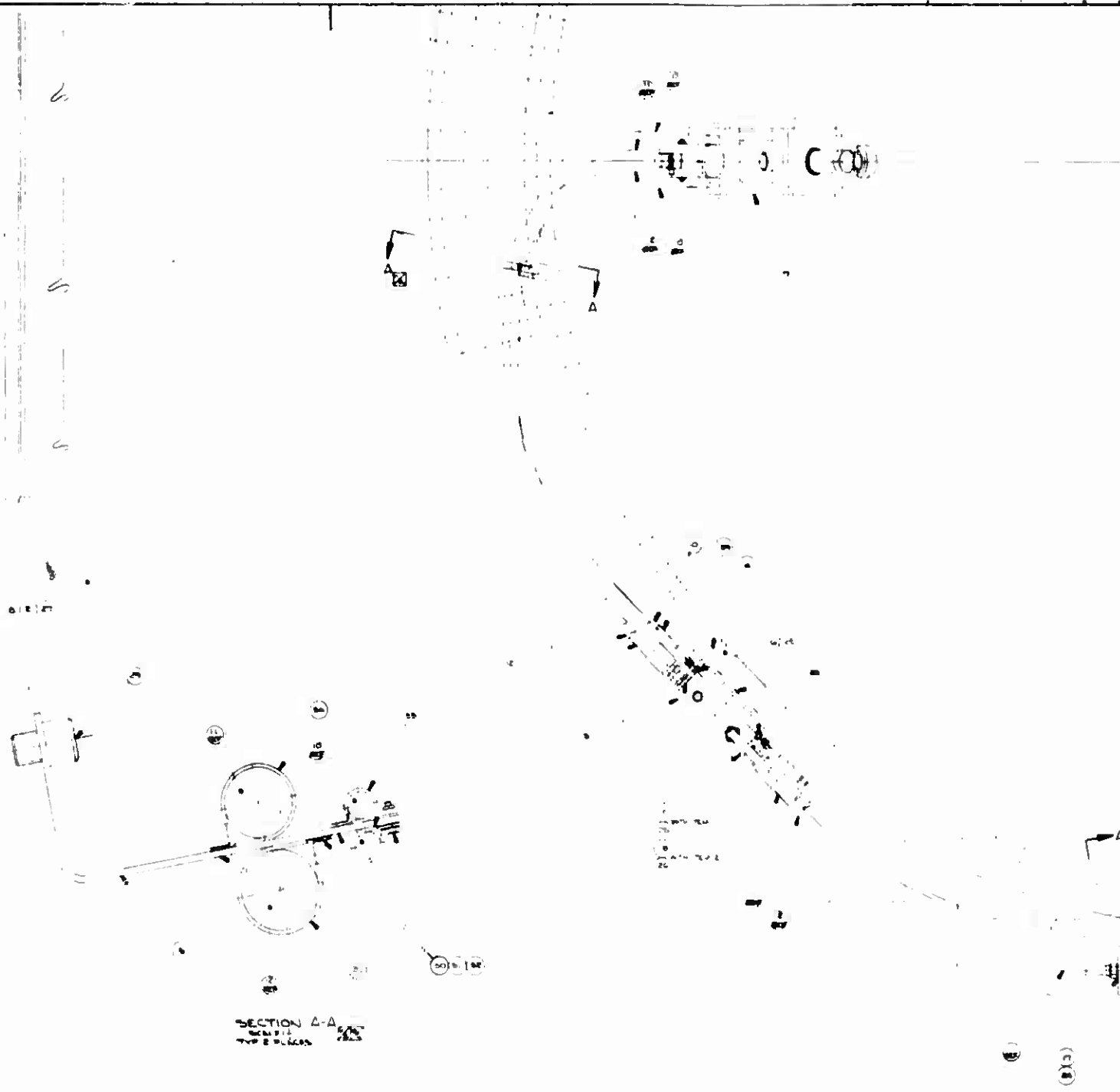


DETAIL OF LOG BRACKET



1

2



SECTION A-A
TYPE B PULLEY

7U40588

2

3



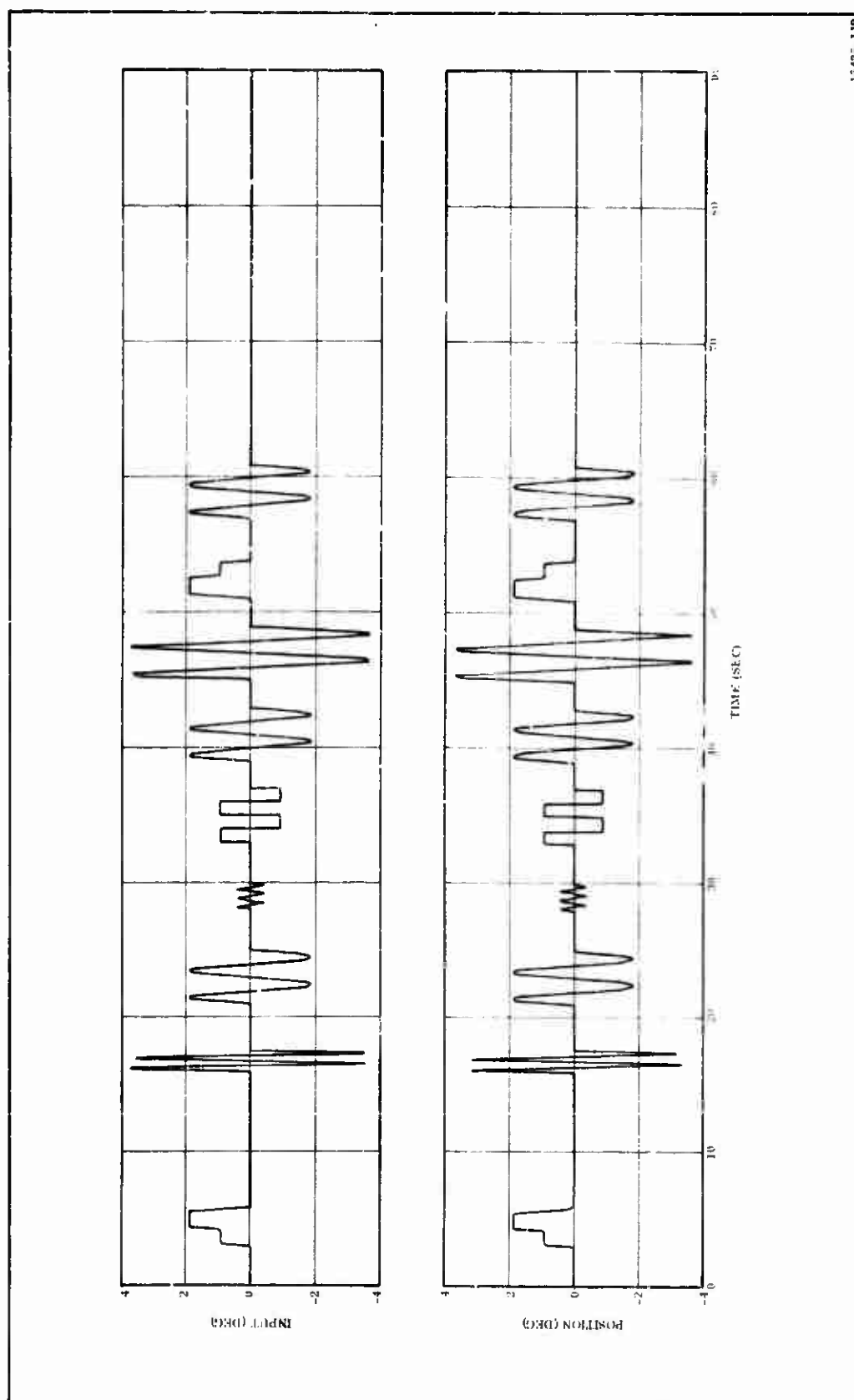
- [illegible]

7U40583

373

4

CONFIDENTIAL



1343-119

Figure 138. Yaw Servoamplifier Input and Position Feedback

CONFIDENTIAL

CONFIDENTIAL

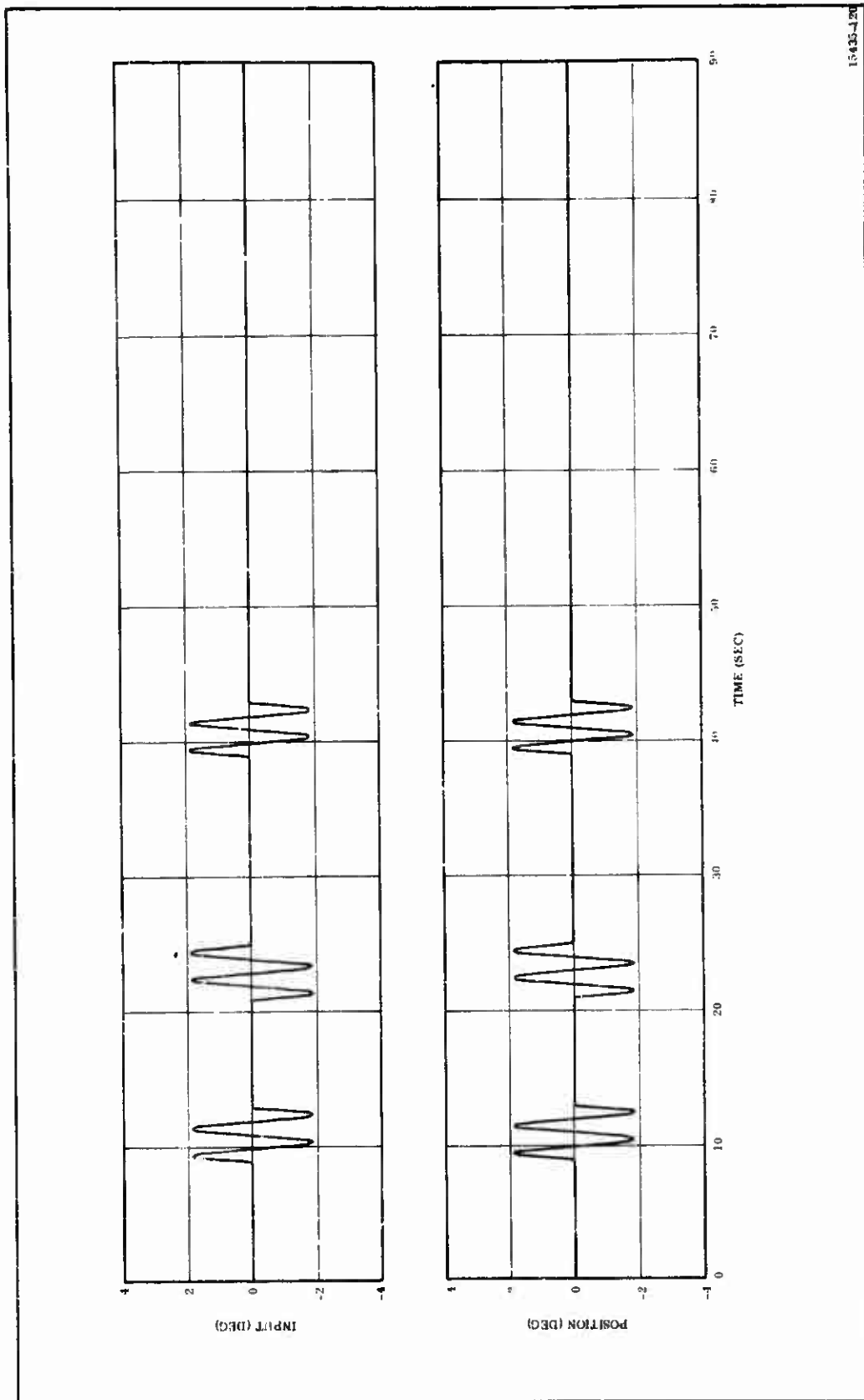


Figure 139. Pitch Servoamplifier Input Position Feedback

CONFIDENTIAL

CONFIDENTIAL

(THIS PAGE IS UNCLASSIFIED)

- (U) The maximum deflection obtainable under static conditions was 3.72 deg (measured with a clinometer in the pitch plane). Therefore, to allow the use of the existing program tape, the programmer gain was adjusted for full scale of 3.72 instead of 4.00 degrees. The program input for all events was correspondingly lower than planned by the same percentage; i. e., 1.86 and 0.93 deg instead of 2.00 and 1.00 deg, respectively. These amplitudes however, were sufficient to meet all side impulse requirements based on the predicted ballistic performance.
- (U) Expanded scale plots of command and position for sine, triangular, and square wave inputs are presented in Figures 140, 141, and 142, respectively. The 0.5 cps sine wave shows an amplitude attenuation of less than 2 percent and a phase lag of 7 deg (0.039 sec). The 1.25 cps triangular wave response of Figure 141 again shows a time lag of about 0.04 second. The amplitude was attenuated 0.5 deg, primarily due to rounding of the peaks, which is inherent to triangular wave programming. The average velocity between plus and minus 3 deg is 16.6 deg per second. However, the square wave response of Figure 142 demonstrates a maximum slew rate exceeding 26 deg per second.
- (U) Figure 143 shows hydraulic system pressure vs time, as measured at the pump and at the motor mounted manifold. Nominal supply pressure was approximately 3,130 psi, dropping to about 2,750 psi during the triangular wave high flow event. Return pressure and hydraulic flow vs time are presented in Figure 144. Hydraulic flow corresponded to known actuator displacement rates within the accuracy limitations imposed by line surges.
- (U) b. Actuation Torque--The 156-9 rocket motor nozzle actuation torque data are presented in Figures 145 thru 152. Figures 145 and 146 show total torque vs firing time in the yaw and pitch planes, respectively. Also shown on Figure 145 are peak torque values recorded during the dry run actuation. A summary of the torques experienced during the various events of the static test duty cycle is shown on Table XXIX.

CONFIDENTIAL

(THIS PAGE IS UNCLASSIFIED)

CONFIDENTIAL

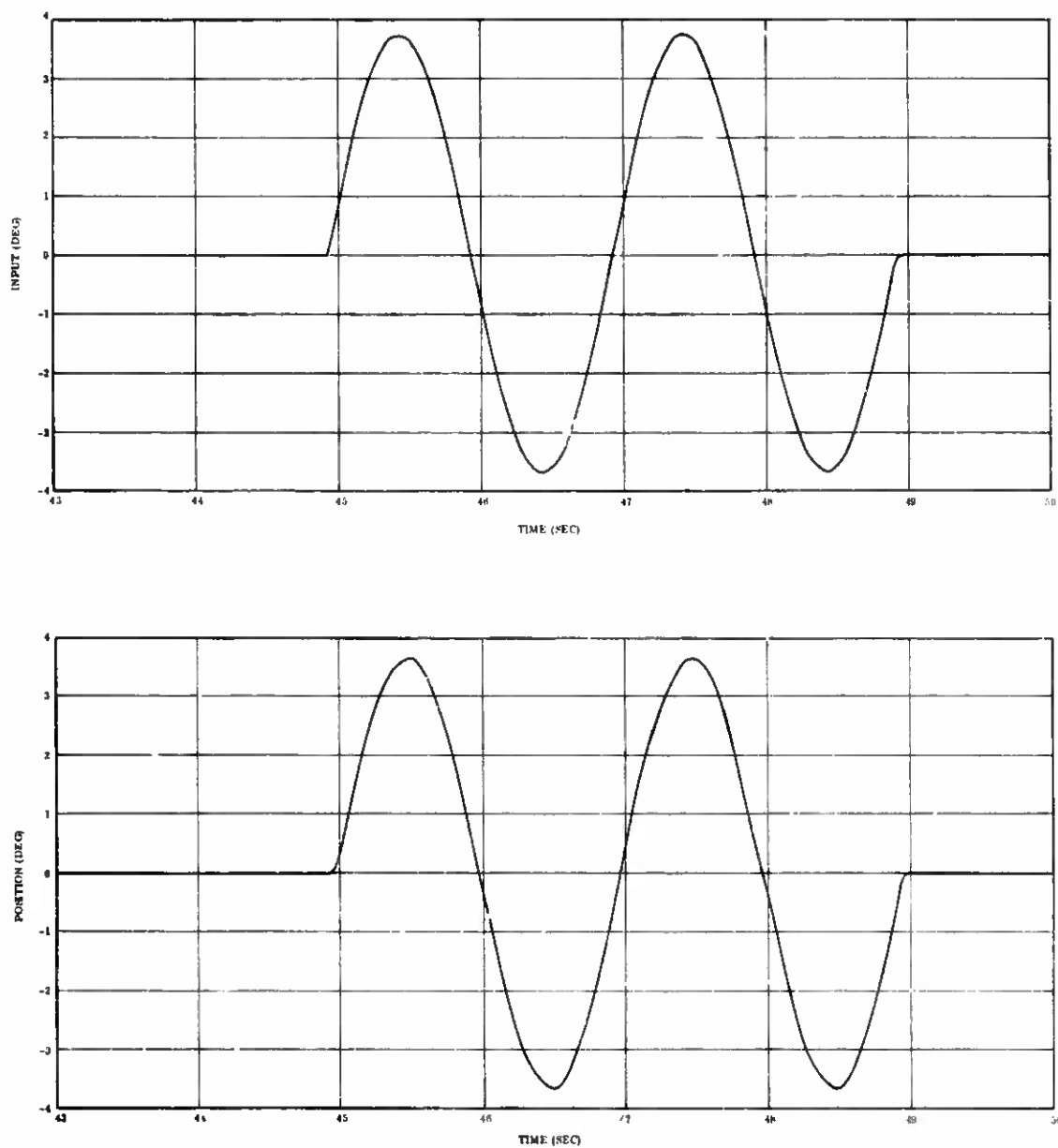


Figure 140. Yaw Servoamplifier Input and Outer Loop Position Feedback, T + 43 to 50 Seconds

CONFIDENTIAL

CONFIDENTIAL

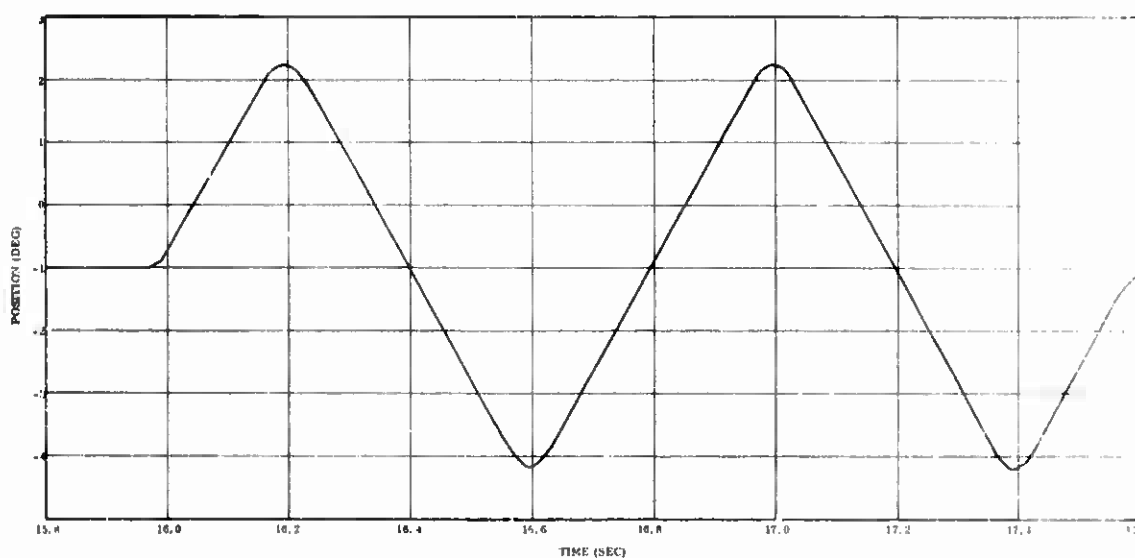
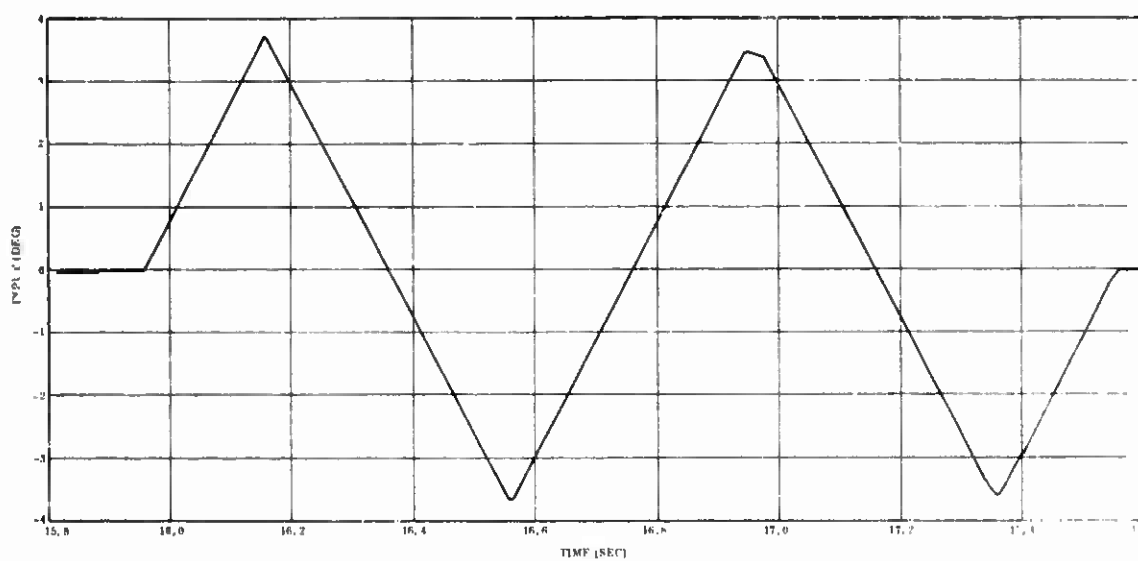


Figure 141. Yaw Servoamplifier Input and Outer Loop Position Feedback, T + 15.8 to 17.6 Seconds

CONFIDENTIAL

CONFIDENTIAL

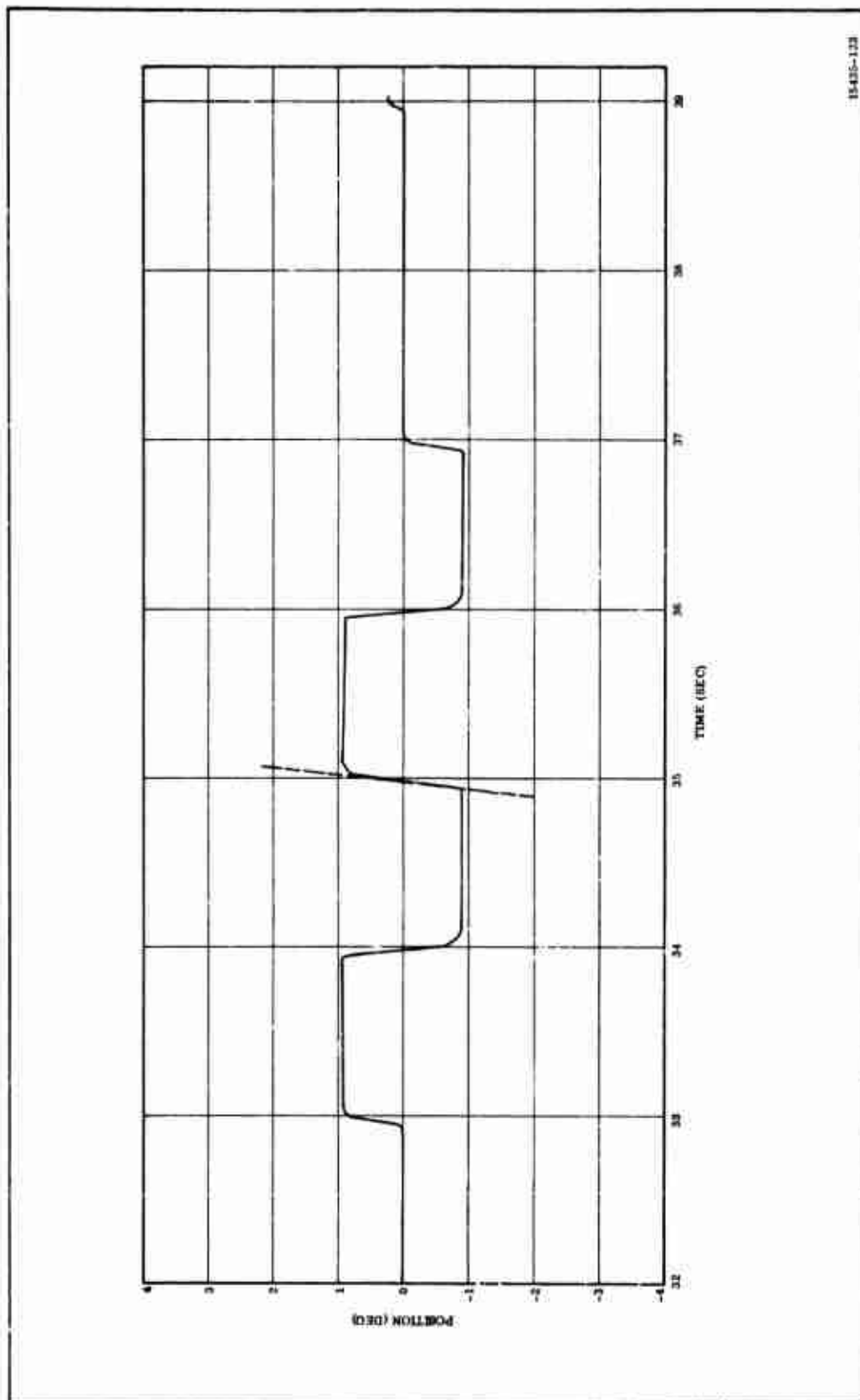
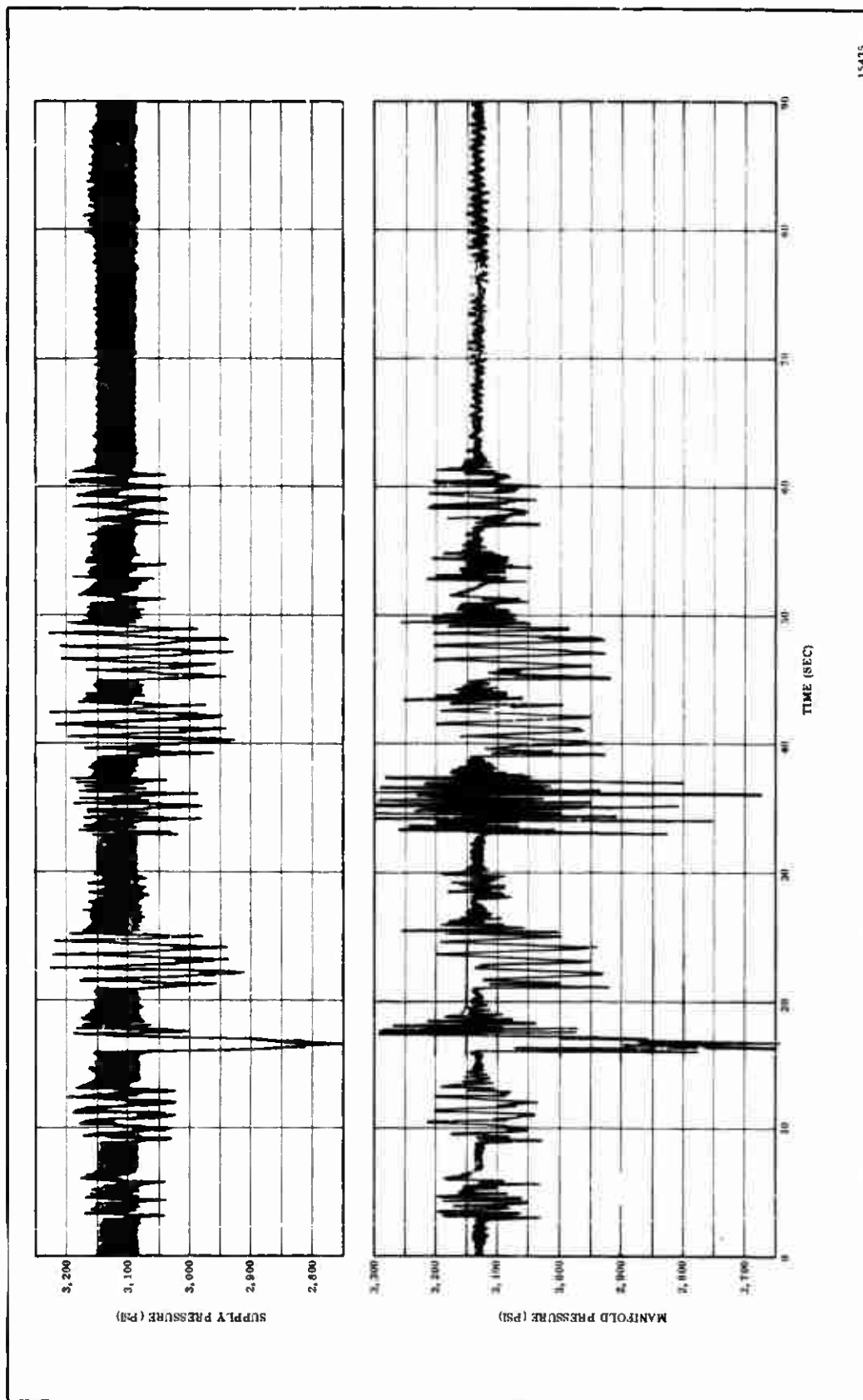


Figure 142. Yaw Outer Loop Position Feedback T+32 to 39 Seconds

CONFIDENTIAL



15435

Figure 143. Hydraulic Supply and Manifold Pressure

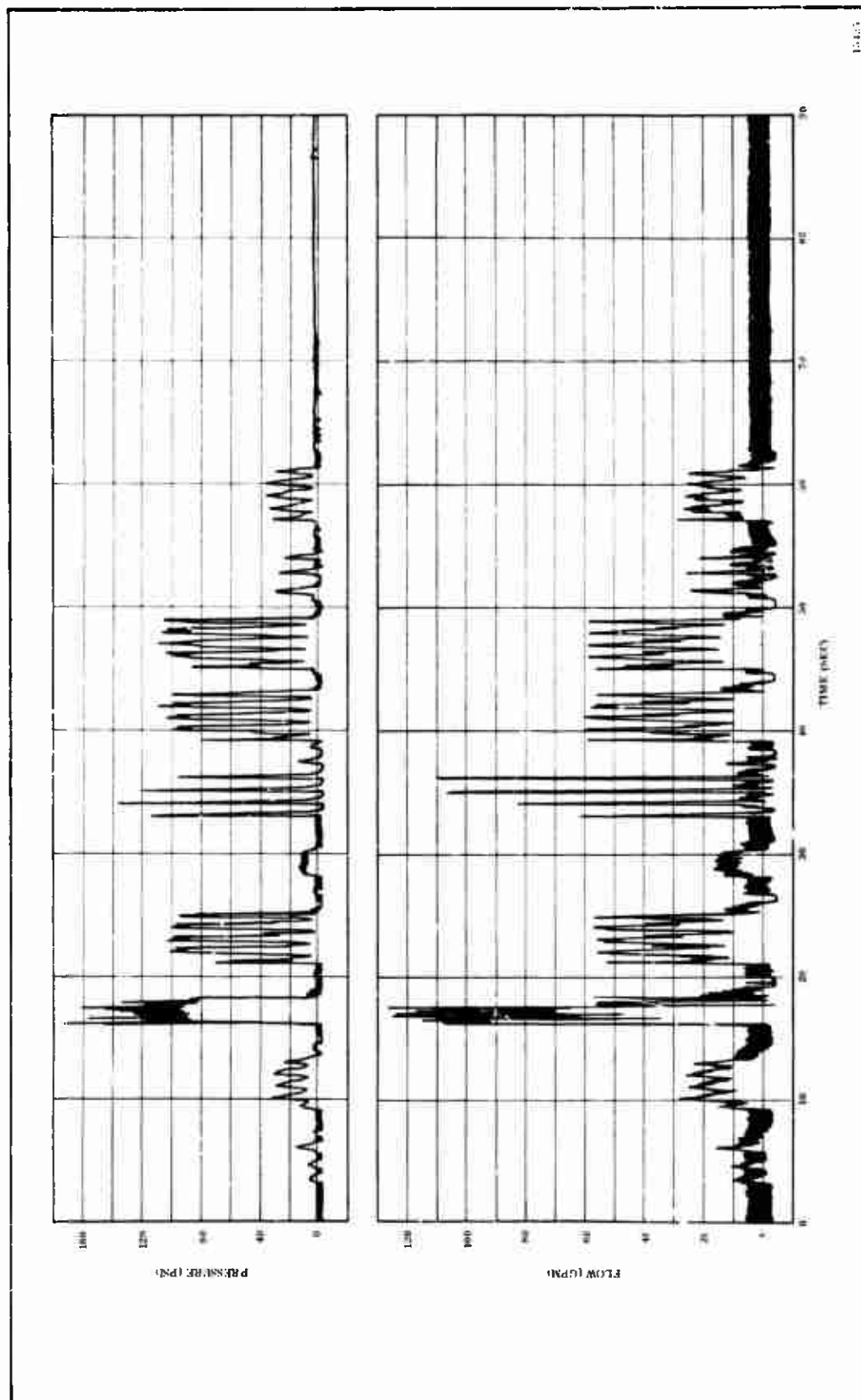


Figure 144. Hydraulic Return Pressure and System Flow

CONFIDENTIAL

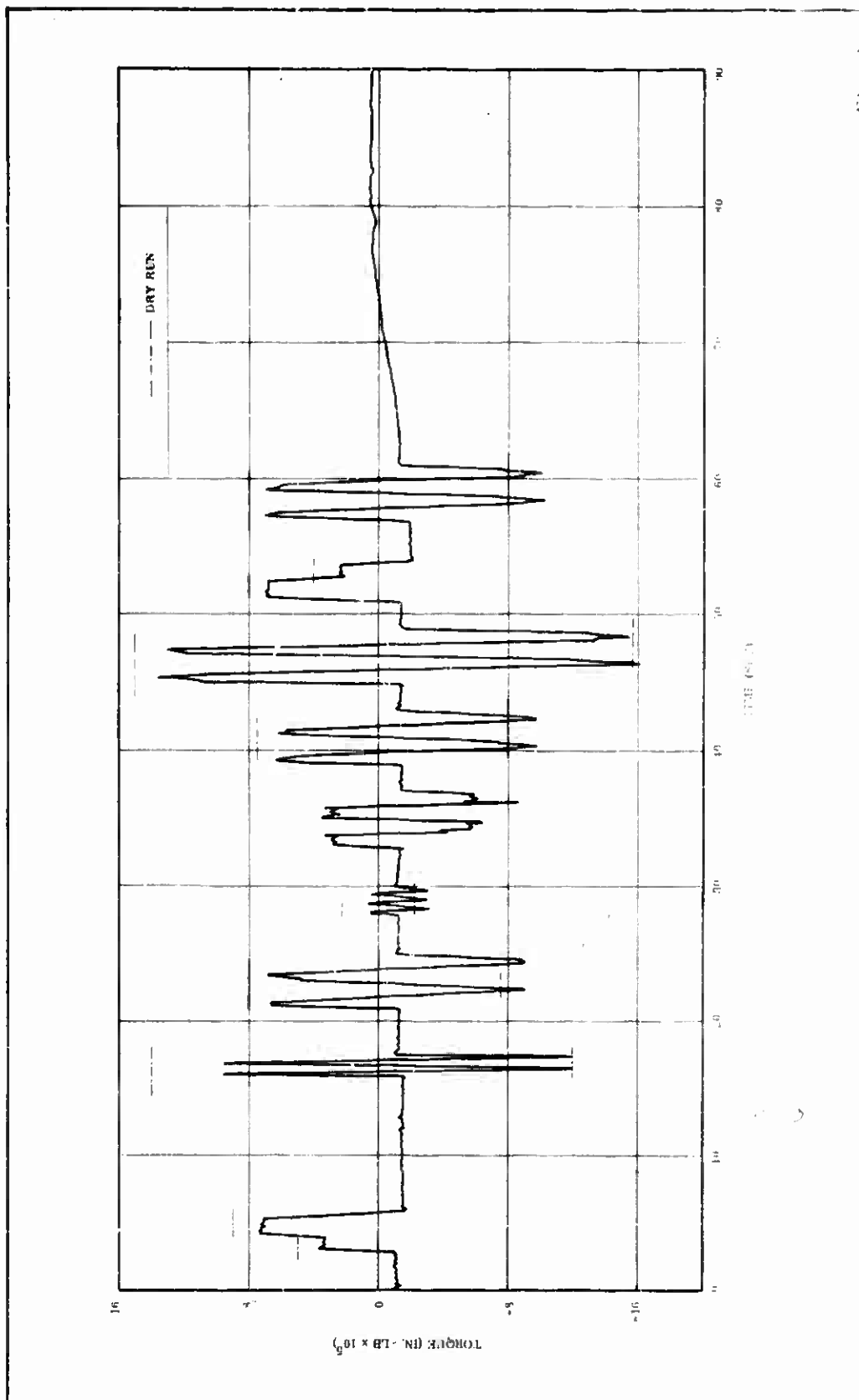


Figure 145. Yaw Actuator Differential Torque

CONFIDENTIAL

CONFIDENTIAL

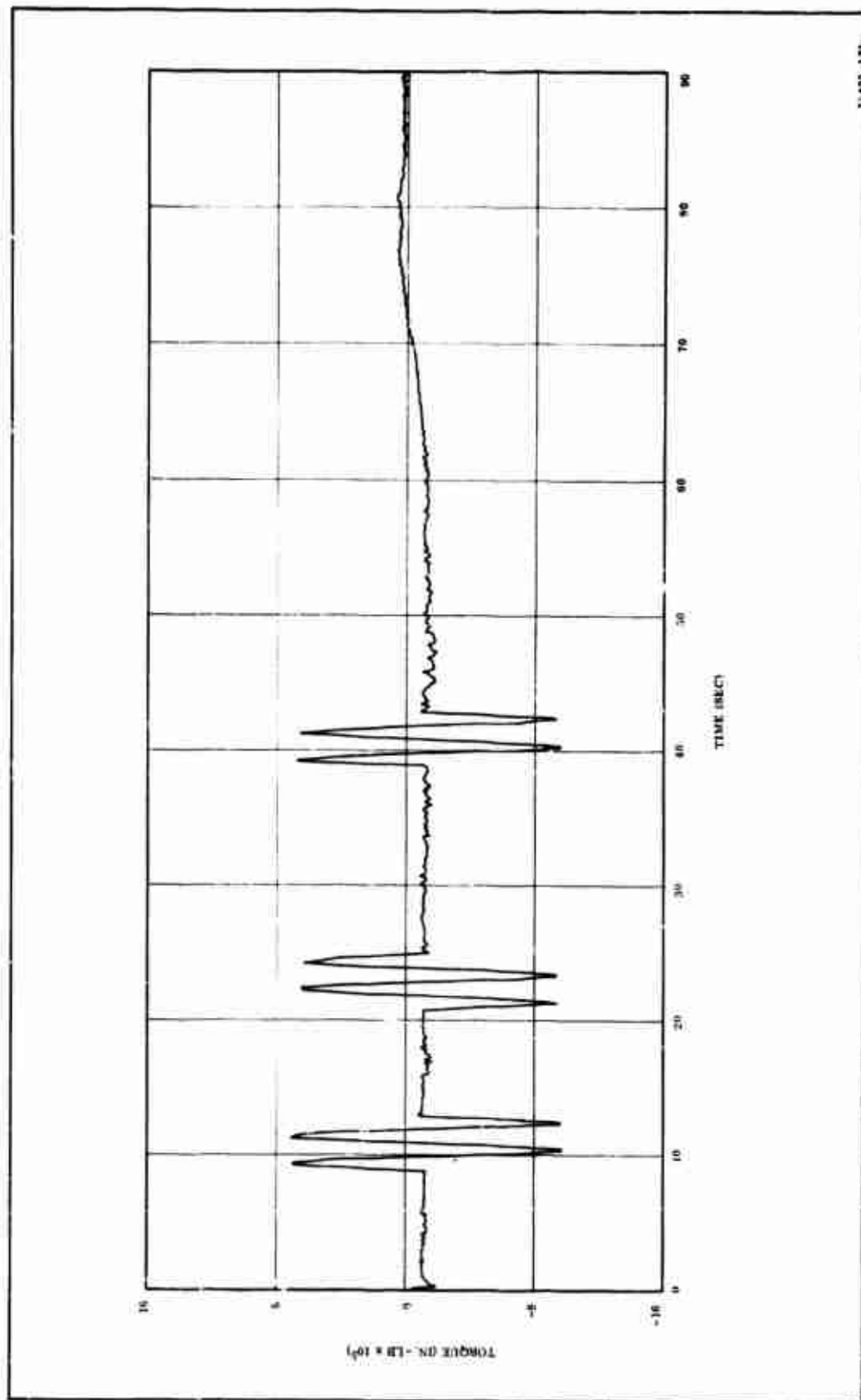


Figure 146. Pitch Actuator Differential Torque

CONFIDENTIAL

CONFIDENTIAL

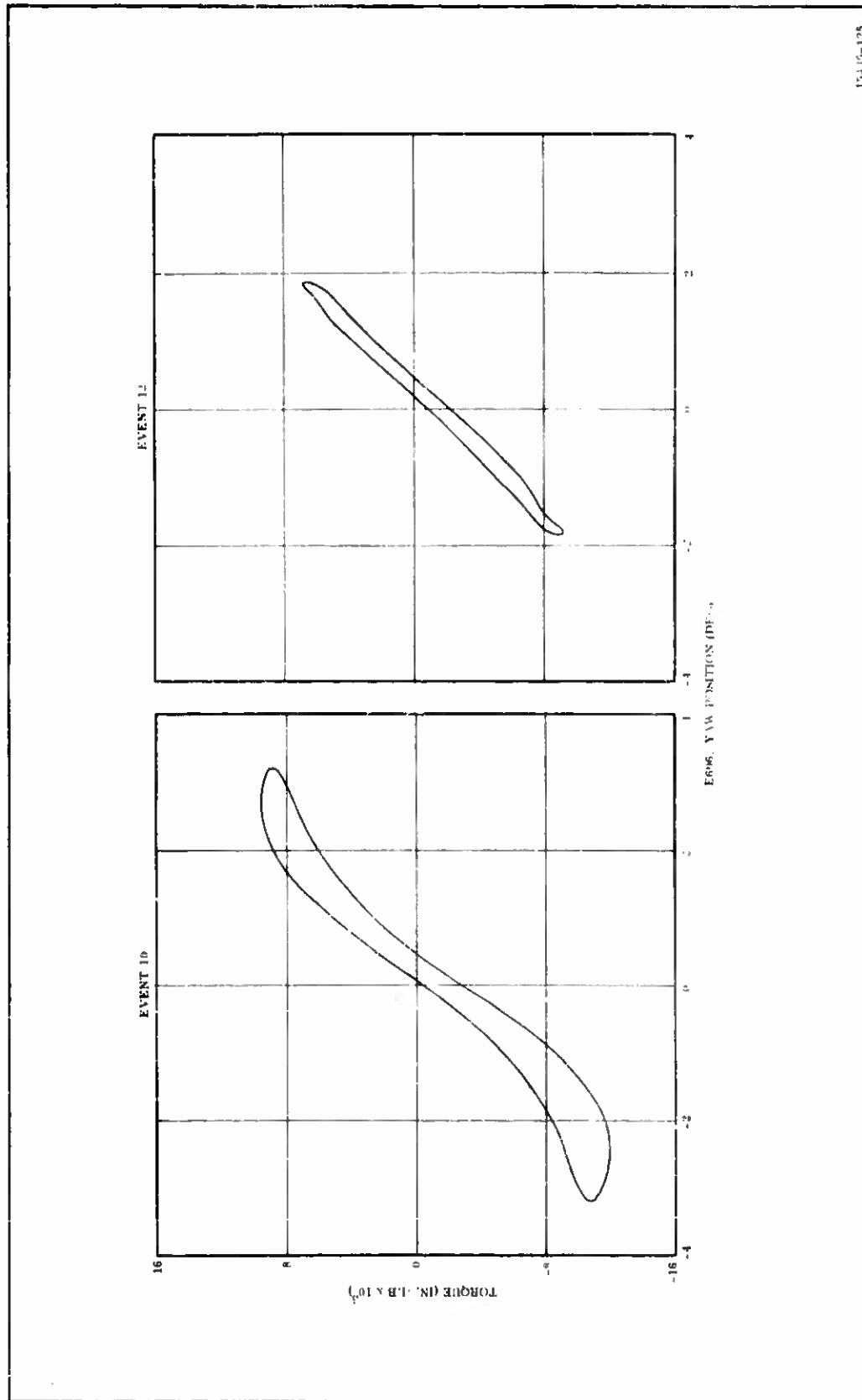


Figure 147. Yaw Actuator Differential Torque, Events 10 and 12

CONFIDENTIAL

CONFIDENTIAL

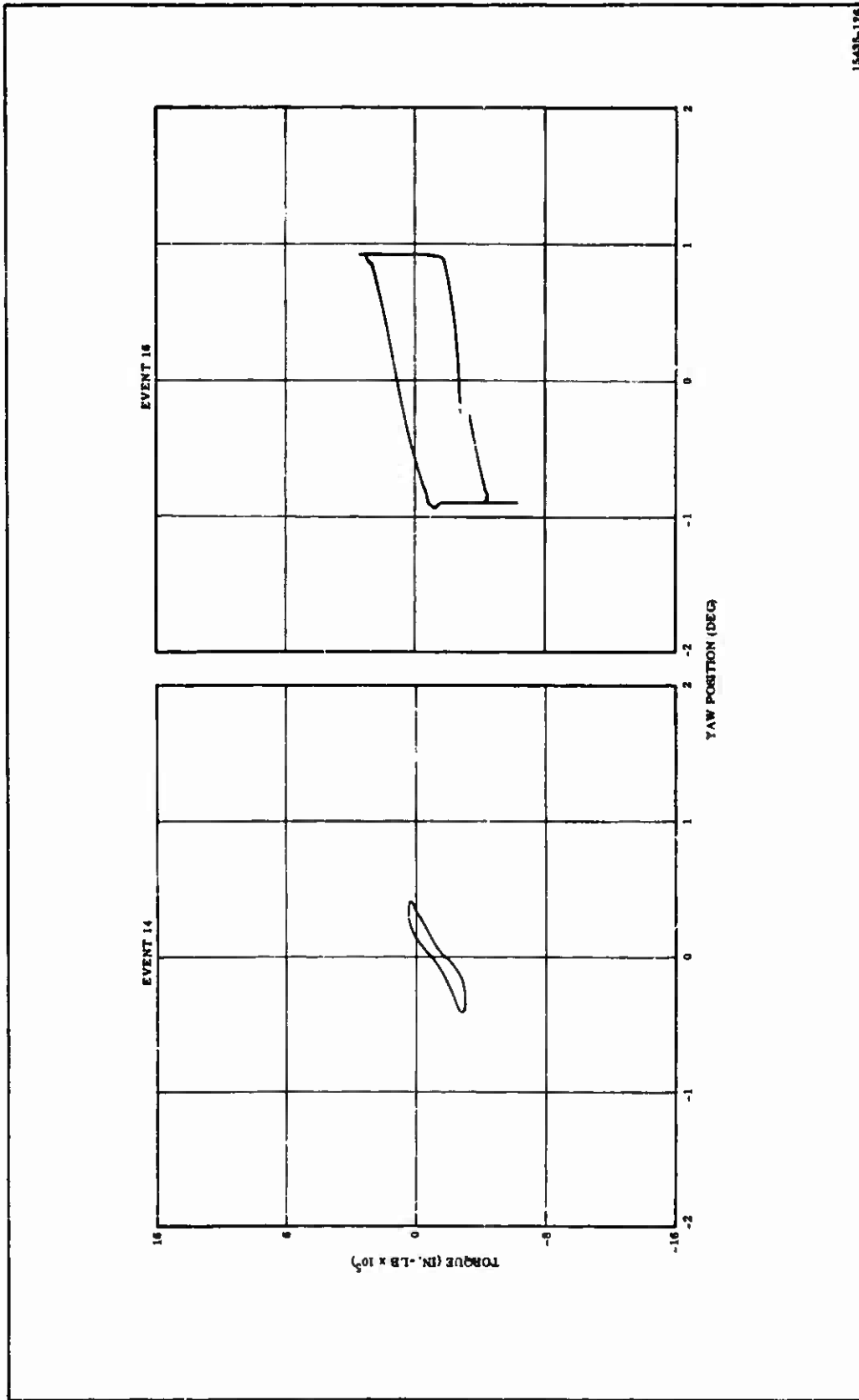


Figure 148. Yaw Actuator Differential Torque, Events 14 and 16

CONFIDENTIAL

CONFIDENTIAL

(THIS PAGE IS UNCLASSIFIED)

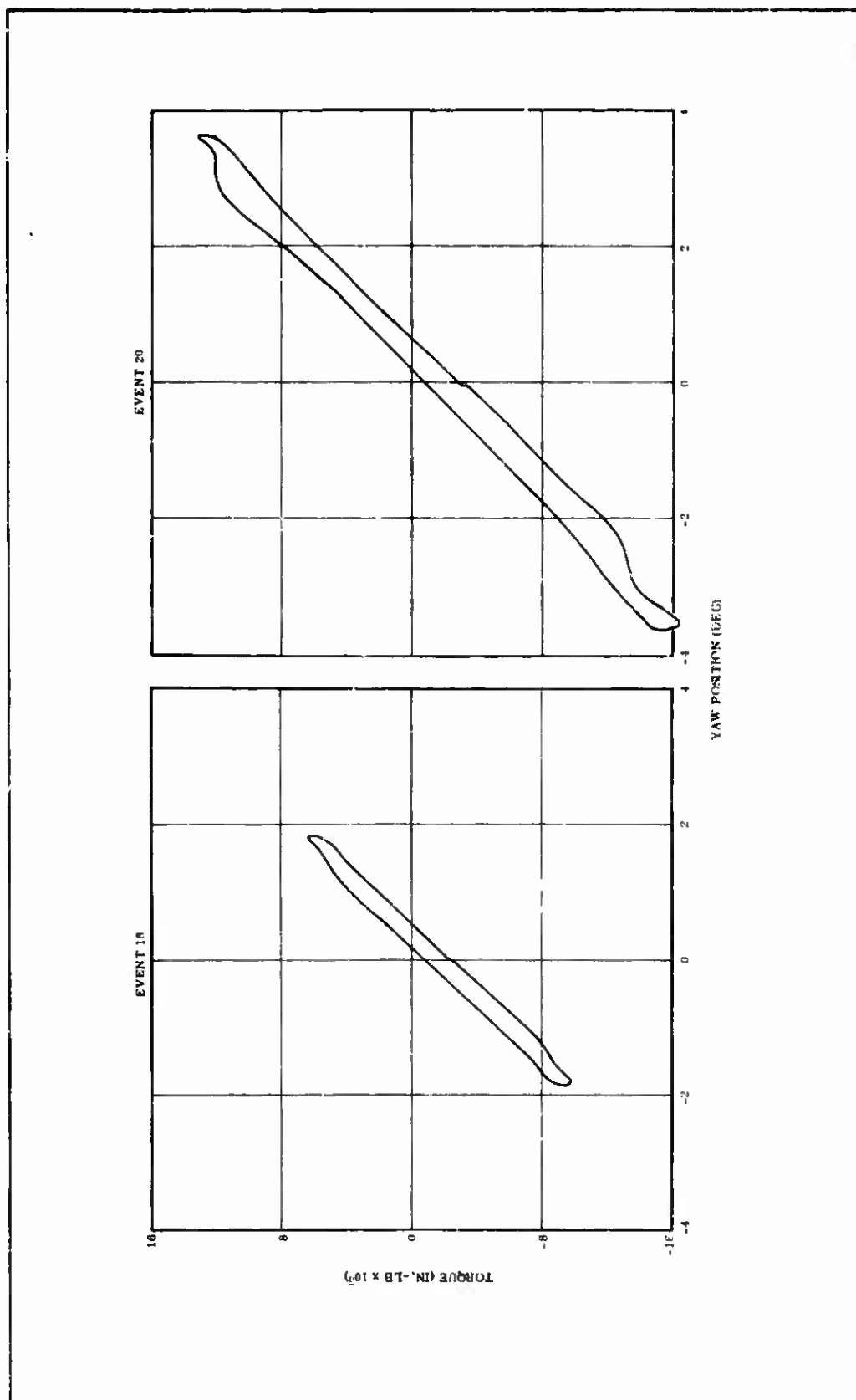


Figure 149. Yaw Actuator Differential Torque, Events 18 and 20

CONFIDENTIAL

(THIS PAGE IS UNCLASSIFIED)

CONFIDENTIAL

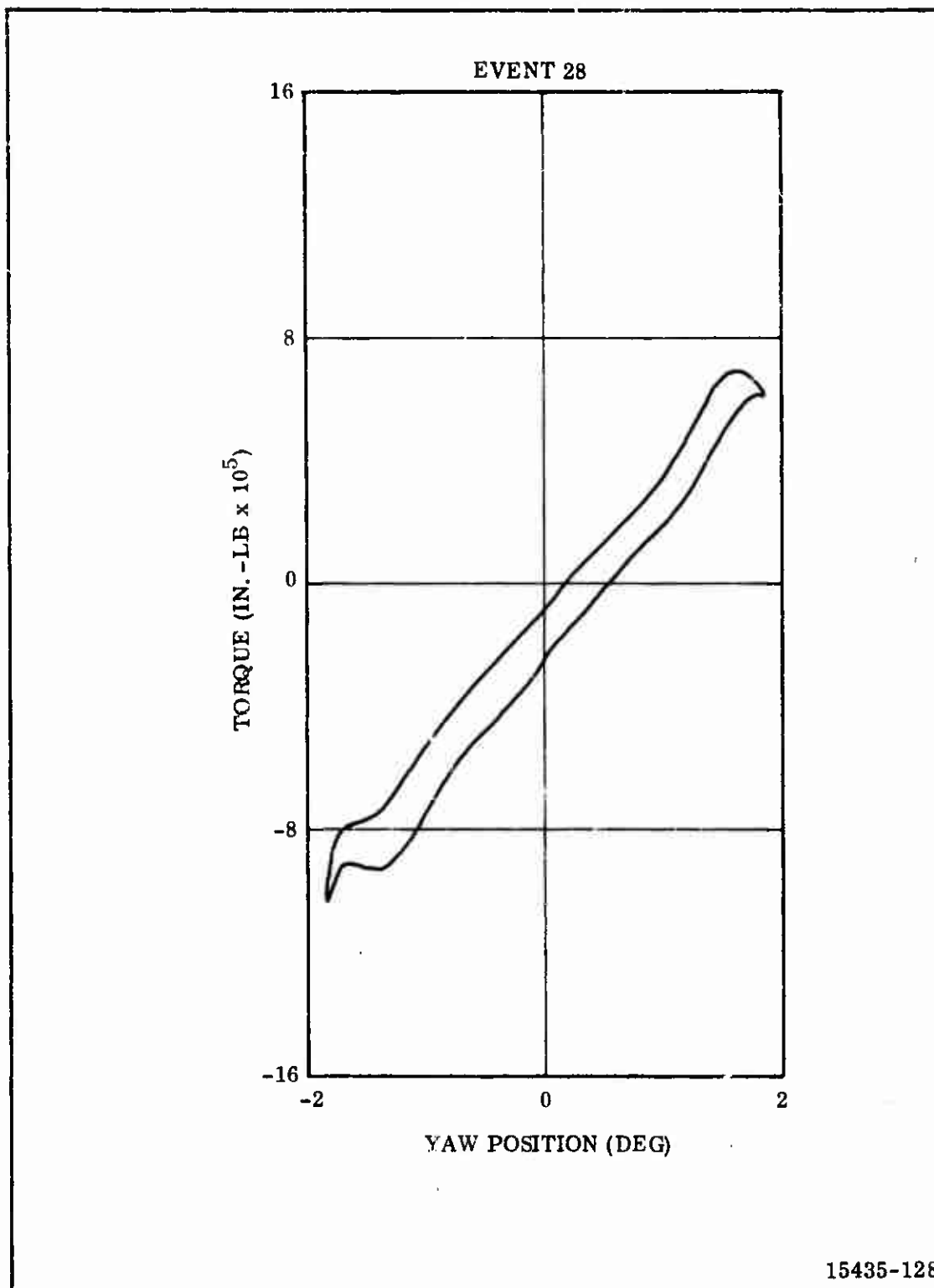


Figure 150. Yaw Actuator Differential Torque, Event 28

CONFIDENTIAL

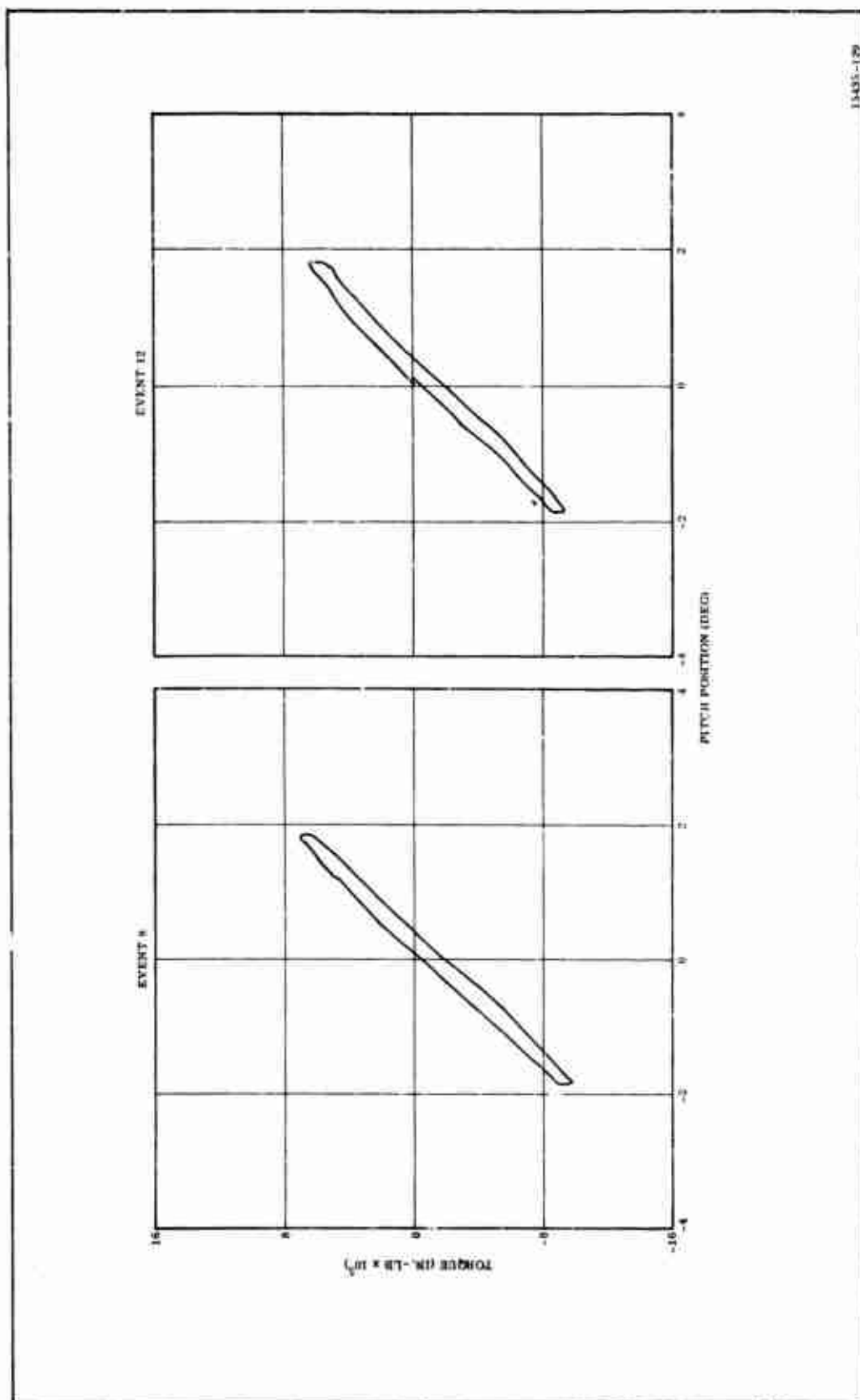


Figure 151. Pitch Actuator Differential Torque, Events 8 and 12

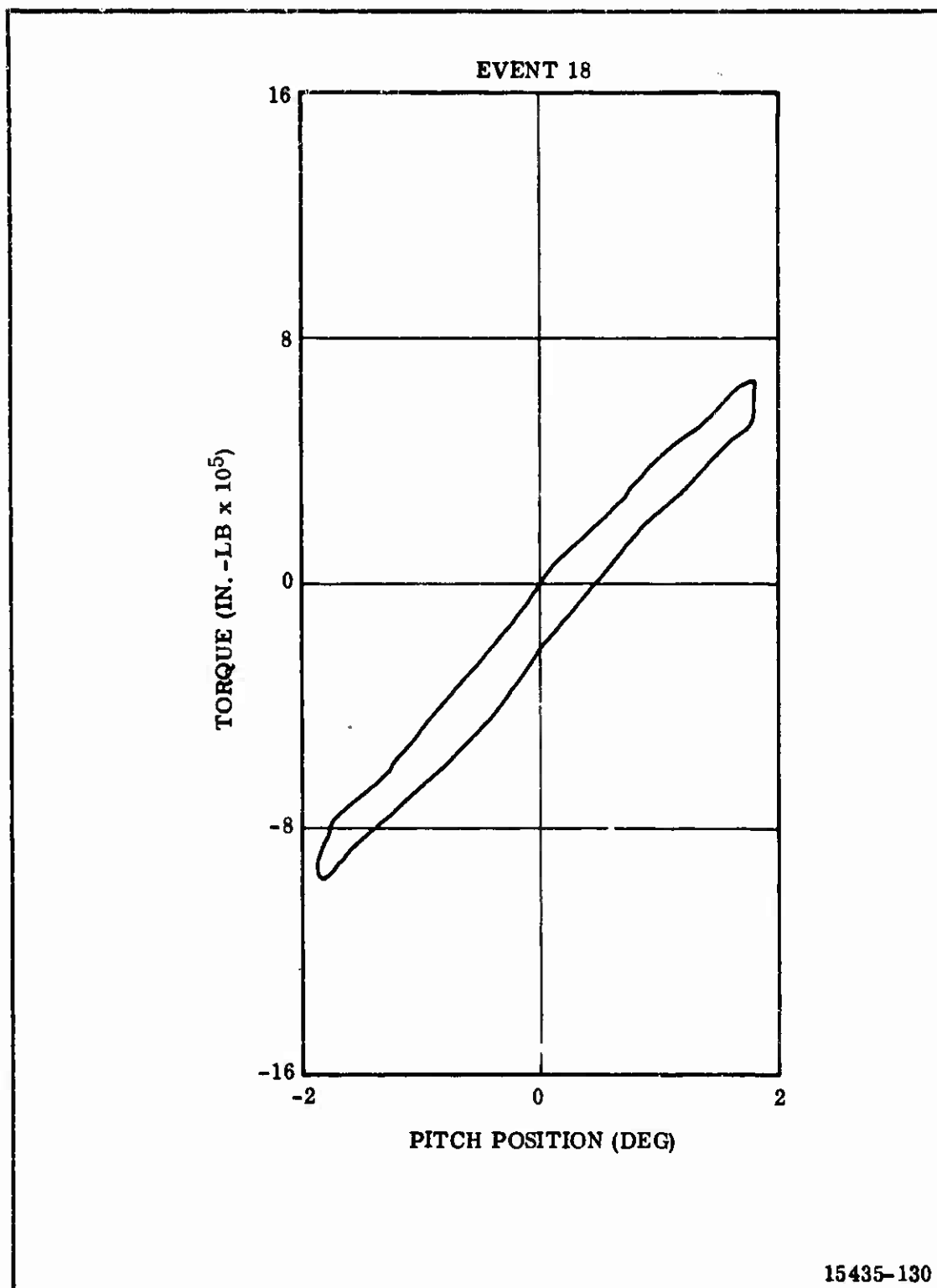


Figure 152. Pitch Actuator Differential Torque, Event 18

CONFIDENTIAL

(THIS PAGE IS UNCLASSIFIED)

TABLE XXIX

TORQUE AT VARIOUS EVENTS OF DUTY CYCLE

<u>Event</u>	<u>Maximum Torque (in. -lb)</u>
Yaw Actuation	
+ 0.94 Deg Hold	+ 360,000
+ 1.85 Deg Hold	+ 720,000
<u>±</u> 3.2 Deg Triangle	+ 960,000 - 1,200,000
<u>±</u> 1.85 Deg Sine	+ 680,000 - 920,000
<u>±</u> 0.4 Deg Triangle	+ 60,000 - 320,000
<u>±</u> 0.9 Deg Square	+ 350,000 - 860,000
<u>±</u> 1.85 Deg Sine	+ 640,000 - 990,000
<u>±</u> 3.6 Deg Sine	+ 1,370,000 - 1,640,000
+ 1.85 Deg Hold	+ 690,000
+ 0.95 Deg Hold	+ 230,000
<u>±</u> 1.85 Deg Sine	+ 700,000 - 1,040,000
Pitch Actuation	
<u>±</u> 1.85 Deg Sine	+ 710,000 - 980,000
<u>±</u> 1.85 Deg Sine	+ 650,000 - 940,000
<u>±</u> 1.85 Deg Sine	+ 680,000 - 970,000

CONFIDENTIAL

- (C) This comparison shows good agreement between dry run and firing torque values indicating that the internal aerodynamic torque contribution is minor. The aerodynamic torque predicted for the 156-9 nozzle was -138,000 in.-lb/deg. This component should be acting opposite to the bearing load thus reducing the total torque. Aerodynamic torque normally reduces with firing time due to grain burnout such that agreement between firing and dry run data should improve with firing time. This was generally true; however, it appears that the aerodynamic torque component was considerably less than predicted. Comparison of the spring rate measured in Event 12 with that measured from pressurized bench testing at the same actuation rate shows the firing spring rate to be 45,000 in.-lb less than for the bench test. This difference is assumed to be the aerodynamic spring rate.
- (U) Loop plots (torque vs position) are presented in Figures 147 thru 152. These plots are used to determine the various torque components. However, since the aerodynamic torque and the seal torque vary linearly with nozzle position, these components cannot be determined individually. Therefore, a combined spring rate is presented. The spring rates for various actuation events are shown in Table XXX. Values obtained from pressurized bench testing of the seal are also presented for comparison purposes.
- (U) Loop plots from Events 10 and 14 are for a triangular wave actuation and do not provide a typical loop pattern. Therefore, the spring rate listed for these events is questionable.
- (C) An investigation of the dynamics of the nozzle during Event 10 revealed that the inertial load produced by rapid deceleration of the nozzle near the fully extended position was partially responsible for the rounding of the loop plots. A variation in the shear modulus of the rubber shims could produce a nonlinear spring rate.
- (U) Strain rate testing of materials similar to that used in the 156-9 seal indicated that shear modulus increases approximately 40 percent above the static modulus for strain rate of approximately 200 in./in./min. This strain rate is nearly the same as that experienced by the outer shims during the 4 deg triangular wave actuation (Event 10). Also, the stress strain curve for most rubbers is nonlinear

CONFIDENTIAL

TABLE XXX

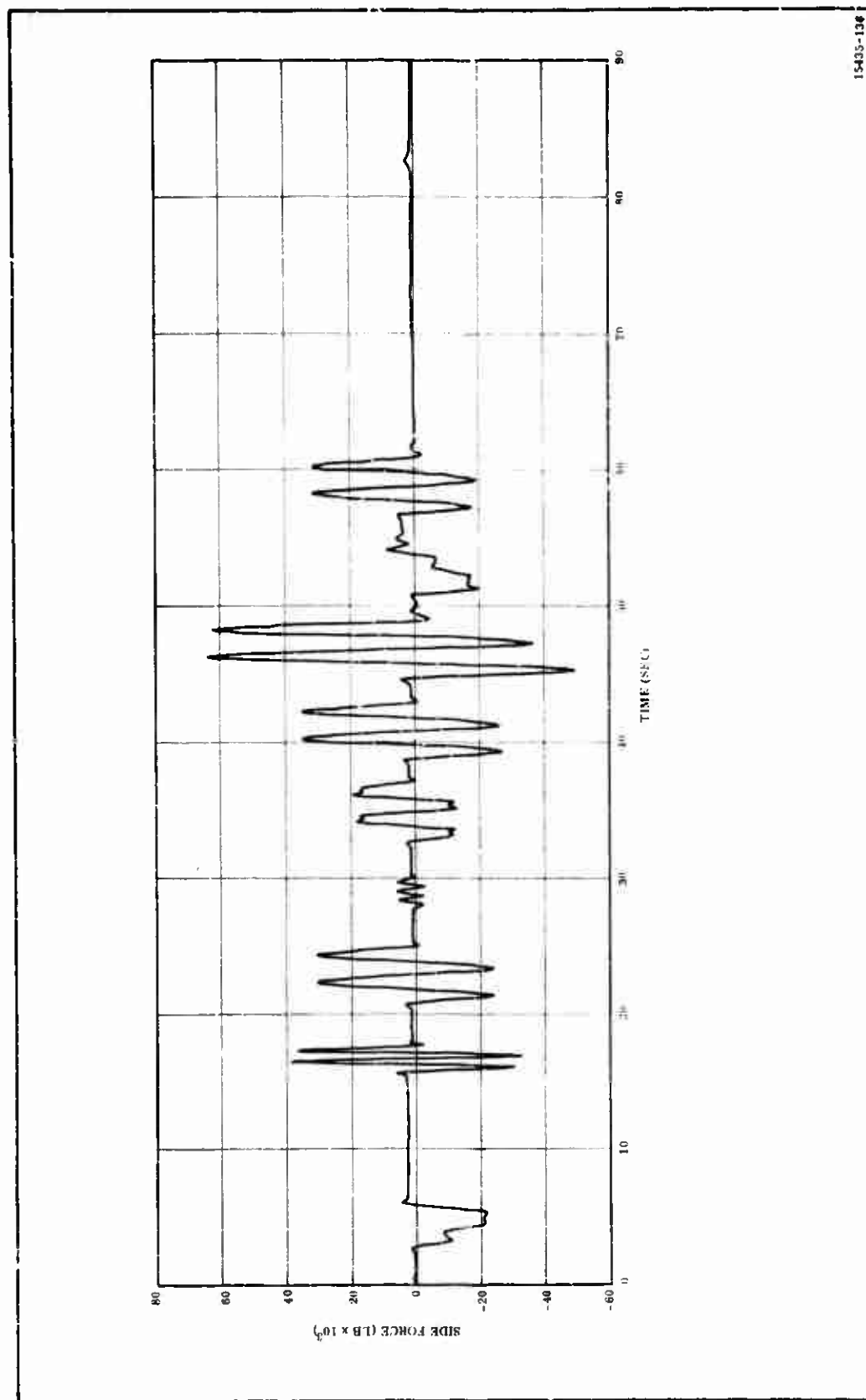
SPRING RATES FOR VARIOUS ACTUATION EVENTS

<u>Event</u>		<u>Maximum Vector Angle (deg)</u>	<u>Spring Rate</u>	
			<u>Bench Test (in. -lb/deg)</u>	<u>Static Firing (in. -lb/deg)</u>
10	Yaw	4	--	420,000
12	Yaw	2	465,000	420,000
14	Yaw	5	--	500,000
16	Yaw	1	--	500,000
18	Yaw	2	--	450,000
20	Yaw	4	400,000	400,000
28	Yaw	2	--	470,000
8	Pitch	2	--	450,000
12	Pitch	2	--	430,000
18	Pitch	2	--	440,000

CONFIDENTIAL

for large deflections. Therefore, a combination of these two phenomena as well as the high inertial loads on the nozzle are responsible for the abnormal shape associated with the triangular wave loop plots.

- (C) Spring rates measured from loop plots for sinusoidal actuations vary from 40⁰, 000 to 470, 000 in. -lb. The predicted maximum spring rate was 389, 800 in. -lb.
- (C) Offset torque due primarily to unsymmetrical flow in the unvectored nozzle varied from -120, 000 to -140, 000 in. -lb over most of the firing. At approximately T + 53 sec the offset torque shifted to approximately -200, 000 in. -lb until T + 60 seconds. The offset then decreased gradually reaching zero at T + 73 seconds.
- (C) A nominal offset torque value of + 144, 000 in. -lb and a maximum value of + 171, 000 in. -lb were predicted.
- (U) The torque data from the 156-9 motor firing are of good quality and measured data agree quite well with predicted values.
- (U) Actuation Events 12 and 18 provide actuation in both the pitch and yaw planes simultaneously. Torque data from these events do not show evidence of one actuator affecting the loading on the other actuator. It is therefore assumed that "cross-talk" between the pitch and yaw actuators is minimal on the 156-9 actuation system.
- (C) The net side force is presented as a function of firing time in Figure 153. A maximum side force of 64, 000 lb was recorded during Event 20 at T + 46. 488 seconds. This was a 4 deg, 1/2 cps sinusoidal actuation. The nozzle position at the time of maximum side force was + 3. 649 degrees. Figure 154 is a plot of thrust vector angle vs time. The thrust vector angle at the time of maximum side force was calculated to be approximately 3. 75 degrees.
- (C) Thrust vector angle is plotted vs nozzle position in Figures 155 thru 158. Theoretical curves are also shown in these figures. Comparison of the zero position thrust vector angle with the theoretical value shows the thrust misalignment to vary from 0. 1 to 0. 35 degree. This was probably the result of a slight motor misalignment on the thrust stand and/or nozzle to case misalignment.



15435-136

Figure 153. Total Side Force vs Time

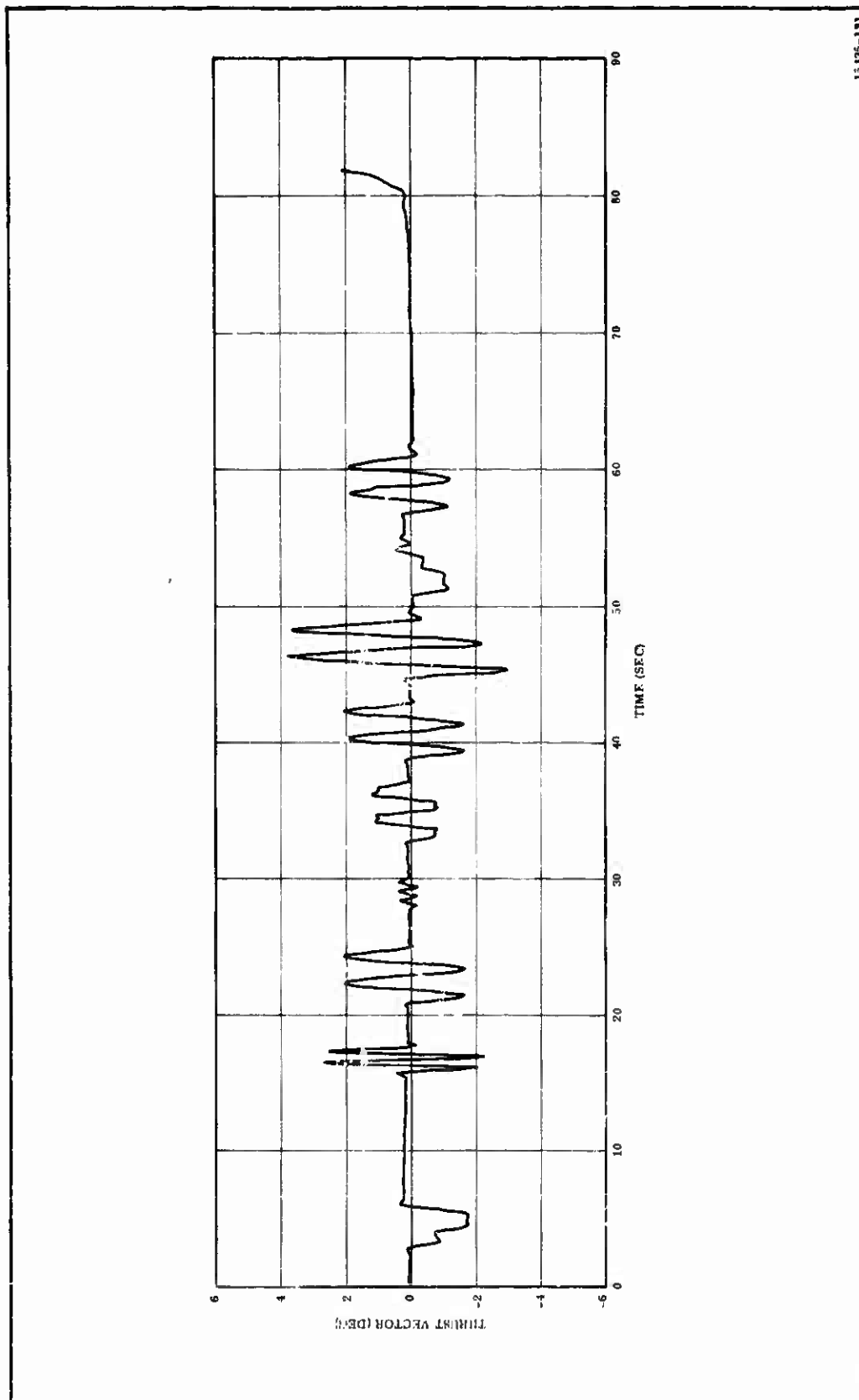
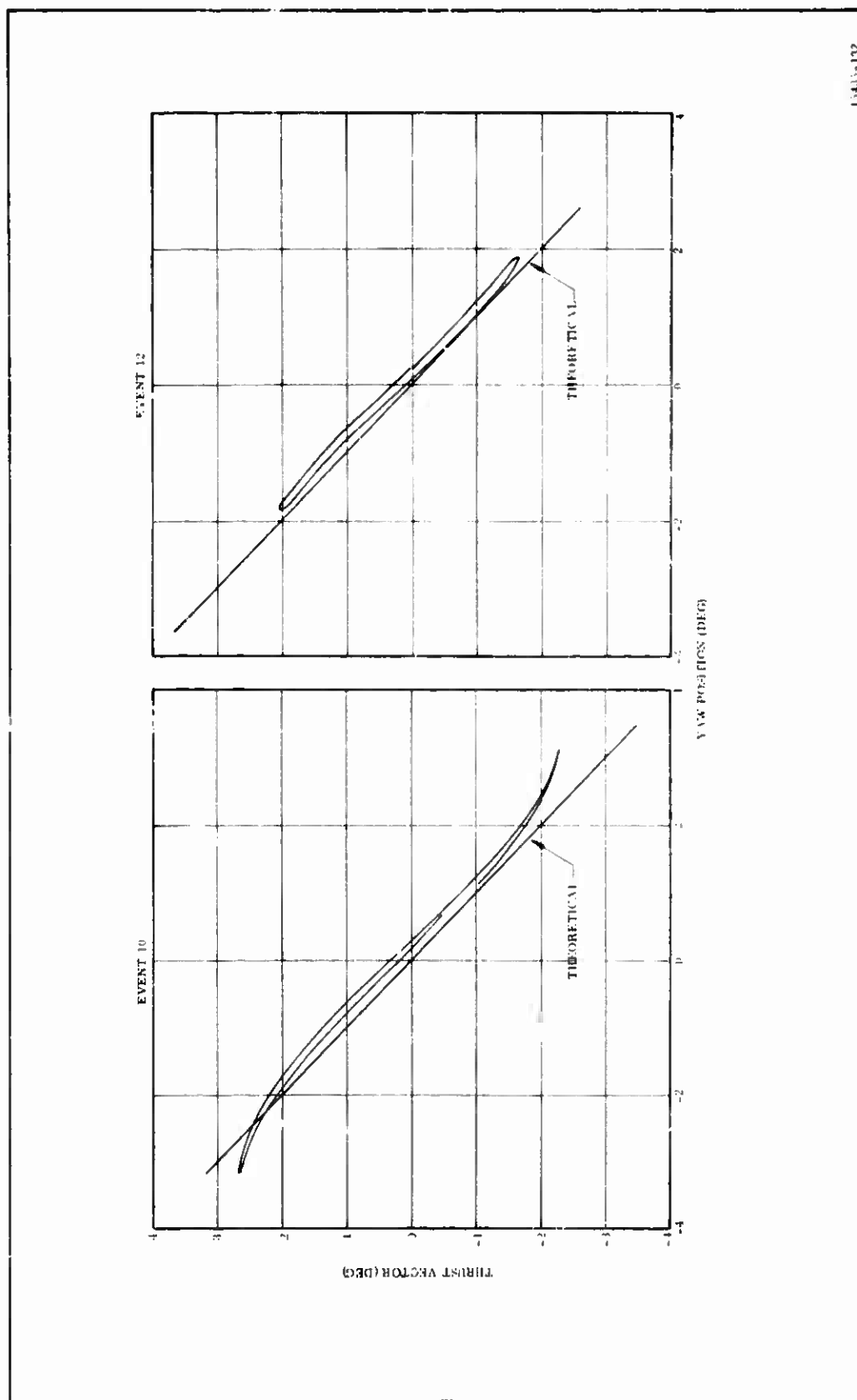
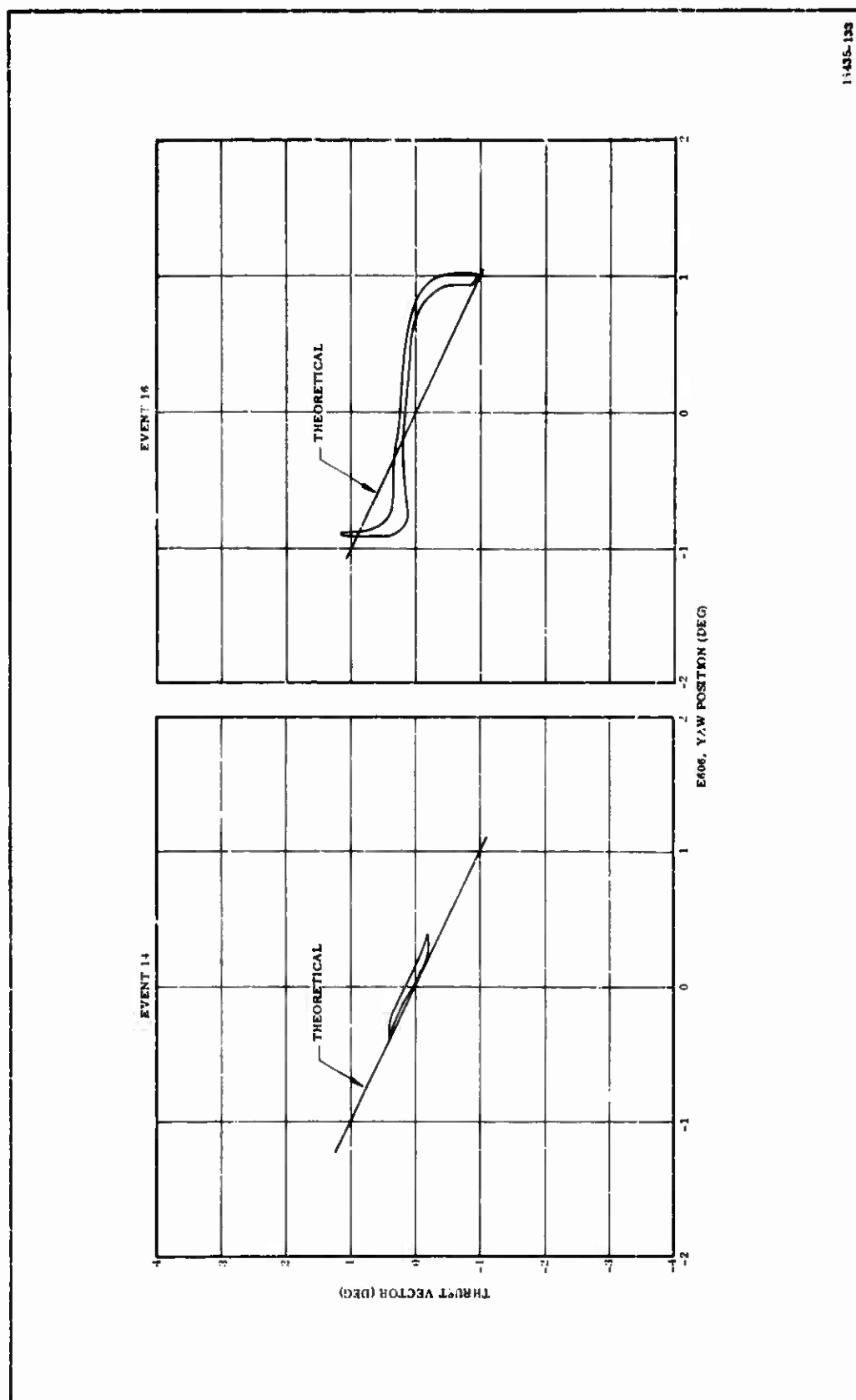


Figure 154. Thrust Vector Angle vs Time



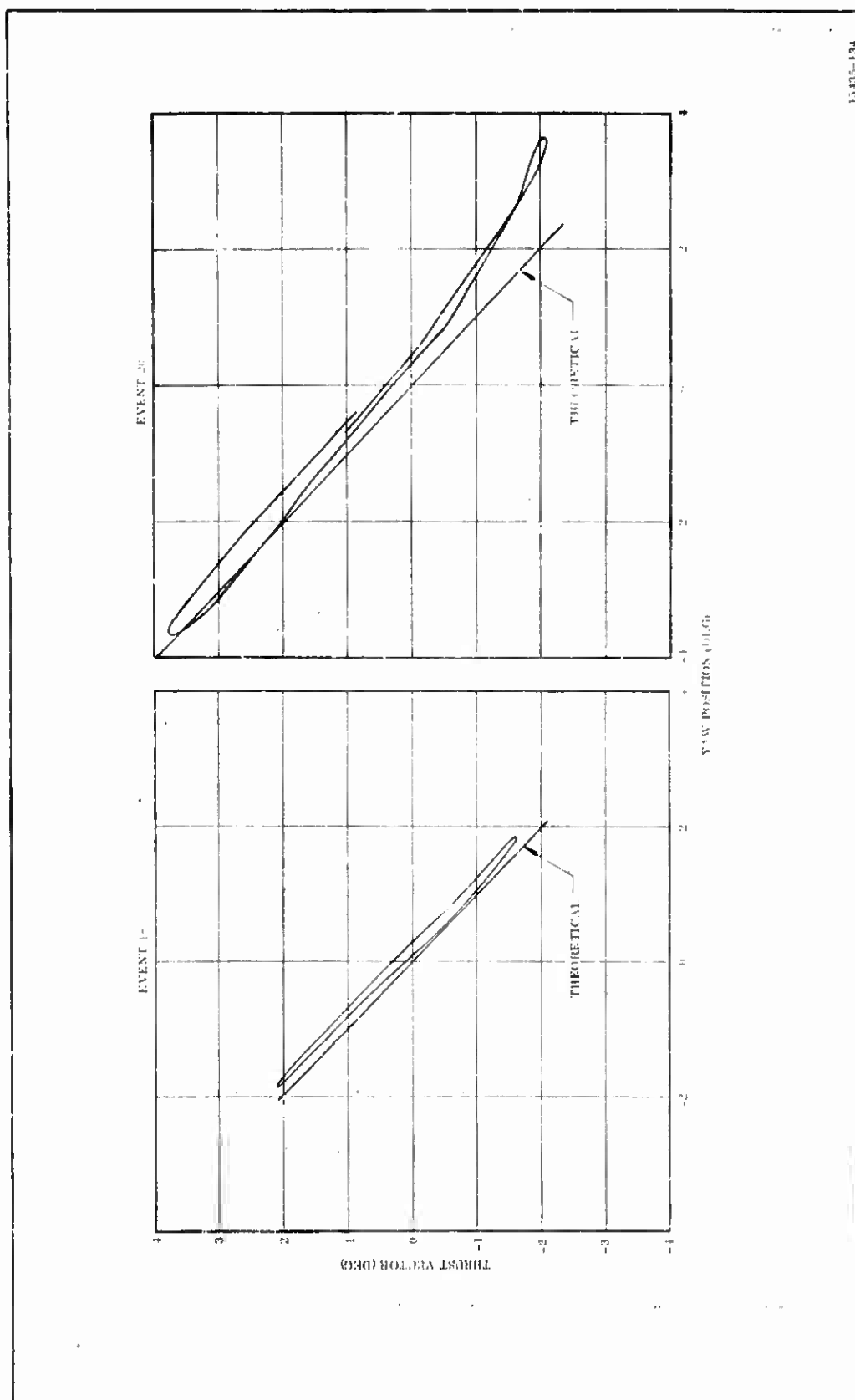
1343-132

Figure 155. Thrust Vector Angle vs Nozzle Position. Events 10 and 12



11435-133

Figure 156. Thrust Vector Angle vs Nozzle Position, Events 14 and 16



15435-134

Figure 157. Thrust Vector Angle vs Nozzle Position, Events 18 and 20

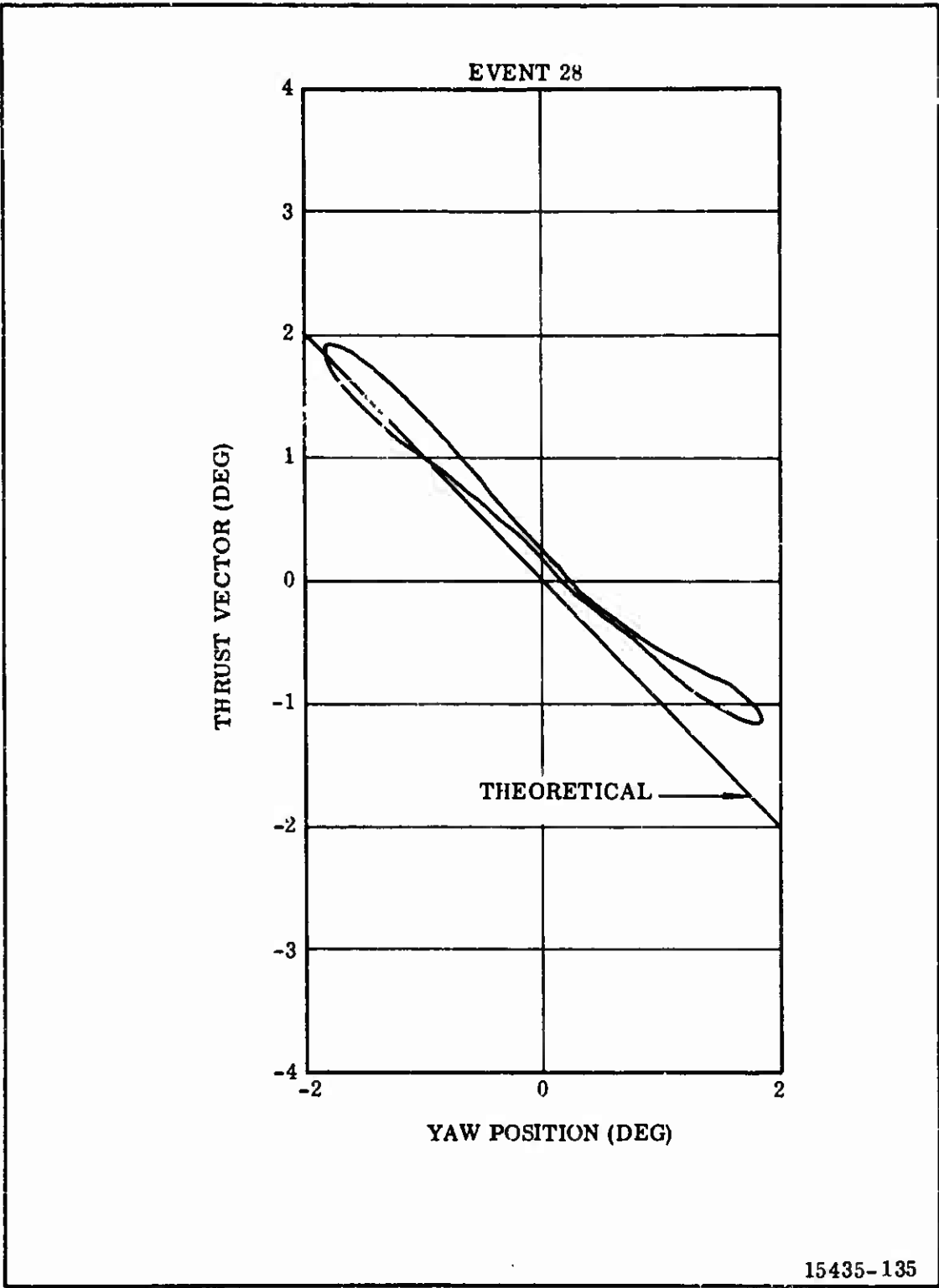


Figure 158. Thrust Vector Angle vs Nozzle Position, Event 28

- (U) Reasonable agreement between thrust vector angle and nozzle position was demonstrated throughout the firing.
- (U) c. Analysis of Flexible Seal Instrumentation--The only instrumentation located directly on the flexible seal was eight thermocouples. These were placed on the outside of the forward and aft end rings at 0, 90, 180, and 270 degrees. They were installed as close to the rubber/shim laminate as possible (Figure 135). A detailed review of the test data indicated that the temperature of the flexible seal remained the same throughout the firing.
- (U) Other indirect instrumentation such as nozzle position and the delta pressure across the actuator pistons was used to evaluate seal performance. All data acquired indicated that the flexible seal performed as predicted.
- (U) d. Flexible Seal Postfire Condition--Postfire examination revealed that the flexible seal was in like new condition. The RTV rubber coating on the motor chamber side of the seal revealed no discoloration. Most of the DC-4 grease between the protective boot and the RTV rubber was not discolored indicating no flow and near ambient temperatures in this region. The protective boot was intact and completely flexible. The small holes drilled through the boot to equalize pressure during firing (and through which the DC-4 grease was injected) were enlarged somewhat. These holes were drilled with a conventional metal drill which did leave ragged edges. It is believed the enlarged holes were simply these ragged edges being blown into the cavity between seal and boot prior to pressure equalization. There was no evidence of continued gas flow through these holes.
- (U) A photograph of a cross section of the flexible seal is shown in Figure 159. A detailed examination proved that the seal, after firing, would have been entirely satisfactory for reuse.



Figure 159. Cross Section of Flexible Seal

3. NOZZLE PERFORMANCE

(U) a. Plastic Parts Performance--All plastic components of the 156-9 nozzle performed extremely well. The measured erosion rates were uniform, and equal to or less than predicted.

(U) The postfired exit cone is shown in Figure 160. Carbon dioxide from the quench system is seen flowing from the nozzle.

(U) Figure 161 presents a postfired view of the nose, throat, and upper exit cone. The boundaries between the nose, crossover ring, throat, upper exit liner (brick-like appearance), and the lower exit liner are clearly visible. The two quadrants of the nose which were drilled and the two quadrants not drilled are apparent.

(U) Figure 162 presents three views of the submerged portion of the nozzle. This photo clearly shows that the gap between the fixed and movable sections of the nozzle remained open. Aluminum oxide deposits formed on both the fixed and movable surfaces near the gap, but the gap was not bridged or filled.

(U) Close-ups of the nose cap are shown in Figures 163 and 164. The four interfaces between the quadrants drilled with vent holes and those quadrants not drilled are presented. It is evident that the holes were detrimental at the forward-most point of the nose in that gouges were produced by the forward two rows of holes. Furthermore, there was no improvement in surface condition or erosion depth on the remaining surface drilled with vent holes. It is therefore concluded that vent holes are not advisable within two in. of the nose tip, or on surfaces with a ply angle to the surface which is large, such as with the 156-9 nozzle. (The ply-to-surface angle on the 156-9 was 32 degrees. Vent holes have been proven helpful on the 156-7 nozzle and on the Thiokol TU-455.02 and TU-465 nozzles where the ply-to-surface angles were between 0 and 15 degrees).

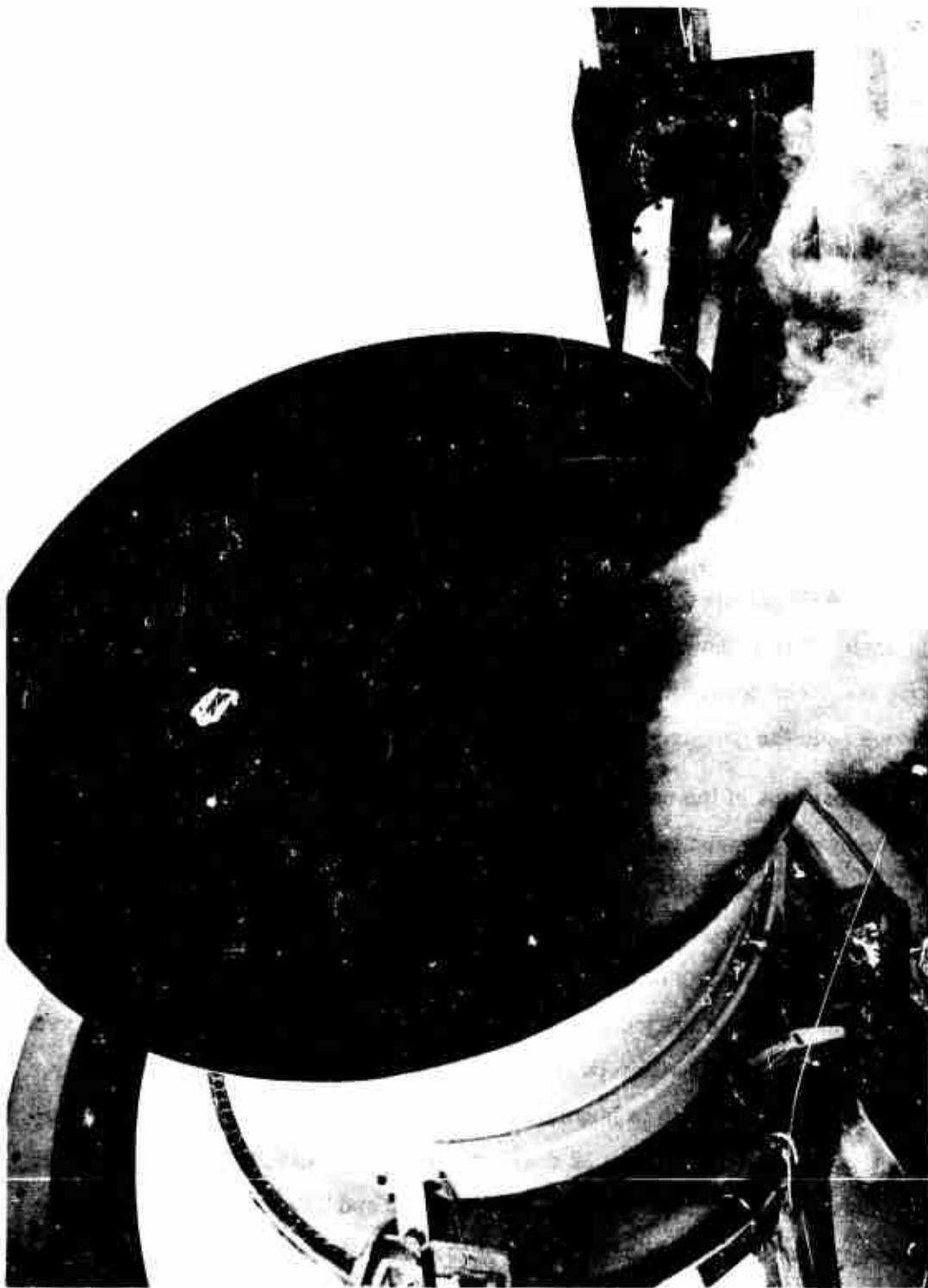


Figure 160. Postfired Nozzle Exit Cone



Figure 161. Postfired Nozzle Submerged Section

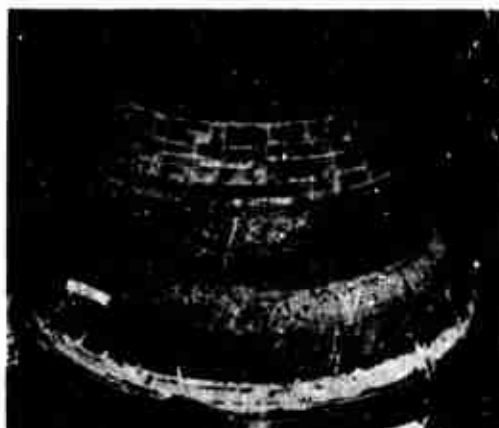


Figure 162. Nozzle Submerged Section

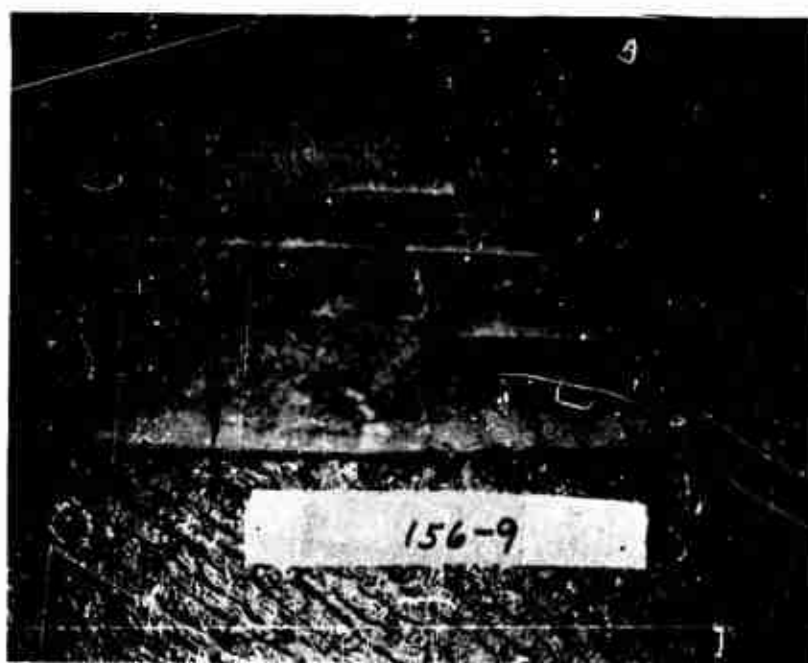


Figure 163. Nose Cap, Drilled and Non-Drilled Surfaces

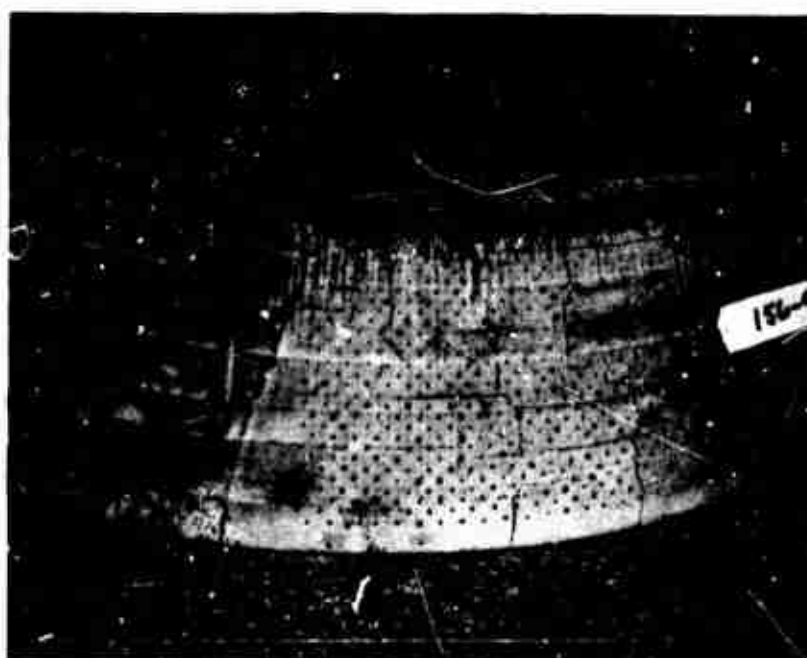
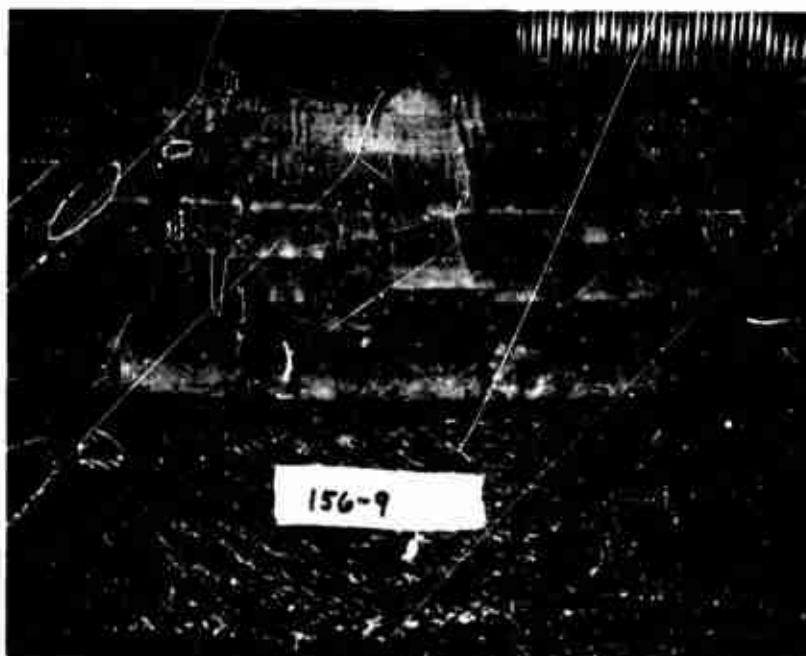


Figure 164. Nose Cap, Drilled and Non-Drilled Surfaces

- (U) The excellent condition of the post-fired crossover ring is demonstrated by Figure 165. The ring, which is the transition of the ply orientation between the nose section and the throat section, is still integral and structurally sound after loss of over 50 percent of the original material through ablation.
- (U) The postfired condition of the movable surface of the gap between the fixed and movable sections is shown in Figure 166. Some ply separation is visible on the rosette surface, but this is confined to the char layer. The boot protecting the flexible seal is also shown to be in excellent condition. Dark spots can be seen on the boot where small amounts of silicone grease from the cavity have melted and flowed through the pressurization holes in the boot and seeped into the charred surface. Virgin grease can be seen in the middle photo where the top of the boot has been cut away. The maximum depth of heat penetration in this region was into this grease near the pressurization holes. The flexible seal itself and the RTV rubber coating on the outside of the flexible seal received no increased heat during firing.
- (U) The fixed surface of the gap is seen in Figure 167. Some deposits are evident, but comparison of the torque during firing to dry run torque indicates the surfaces did not contact each other.
- (U) Figure 168 presents a cross-sectioned piece of the reworked barrier assembly which was discussed in Volume I. It is seen that the rework was fully successful.
- (U) Nose sections from the two quadrants with vent holes are compared to a typical section from one of the other quadrants in Figure 169. The added erosion resulting from the gouges emanating from the forward two rows of vent holes is evident. Two different hole patterns, 3/4 in. and 1/2 in. spacing, were used. No difference in either erosion or gouging was apparent between the two patterns.
- (U) The perfectly uniform erosion of the throat is shown in Figure 170 in which sections from 0, 90, 180, and 270 deg have been placed together with the back surfaces aligned.

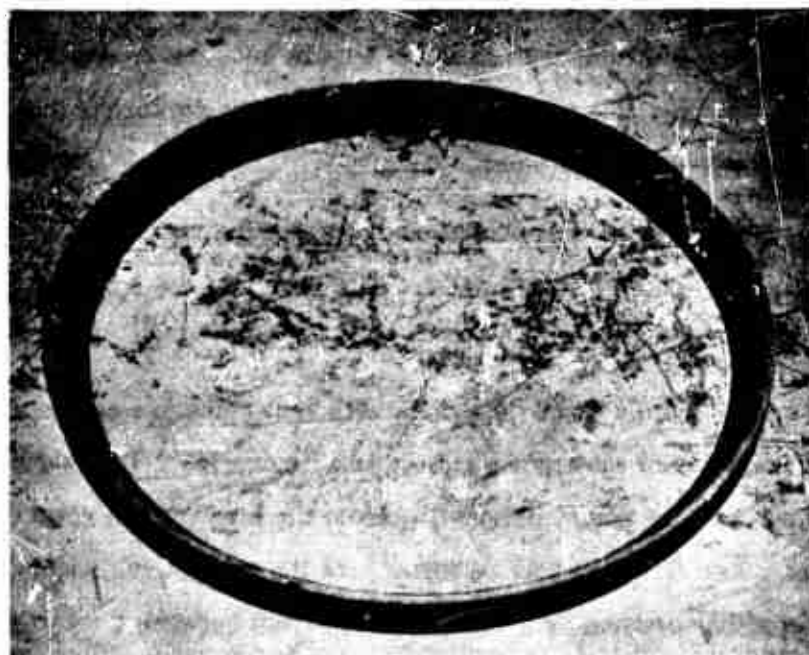
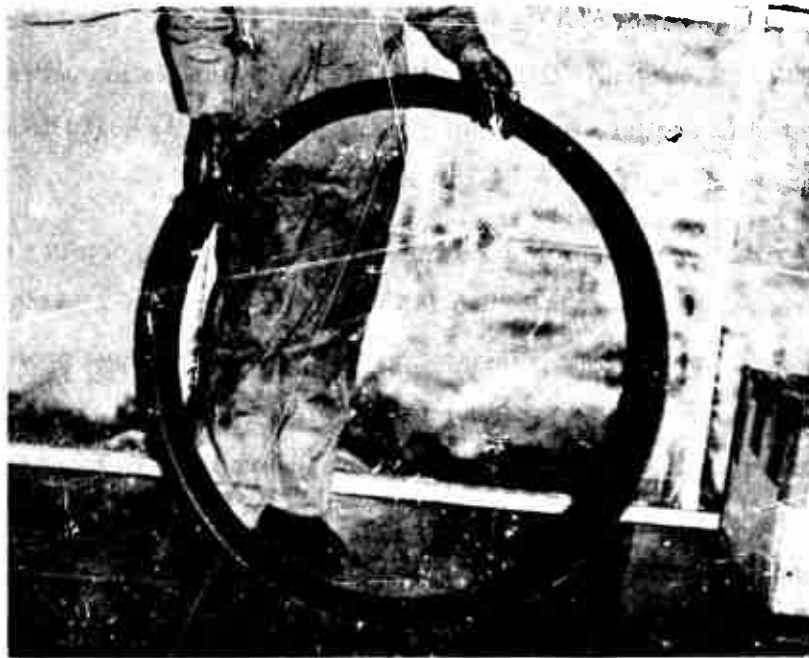


Figure 165. Crossover Ring

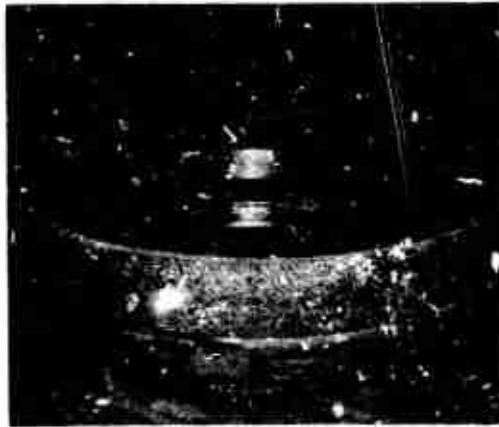


Figure 166. Movable Surface of Gap

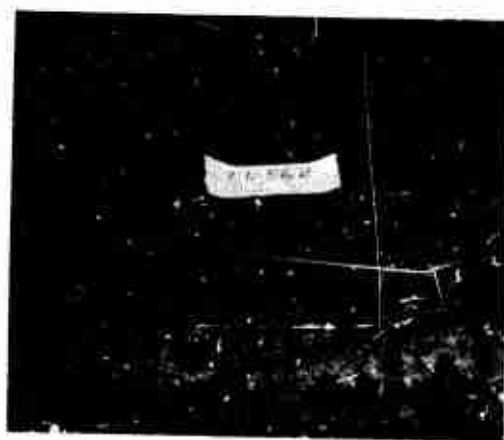


Figure 167. Fixed Surface of Ga_2



SILICA CLOTH PHENOLIC

MX-2646

ROSETTE

Figure 168. Cross-Section of Repaired Barrier Assembly



Figure 169. Comparison of Nose Cross-Sections

CONFIDENTIAL
(THIS PAGE IS UNCLASSIFIED)

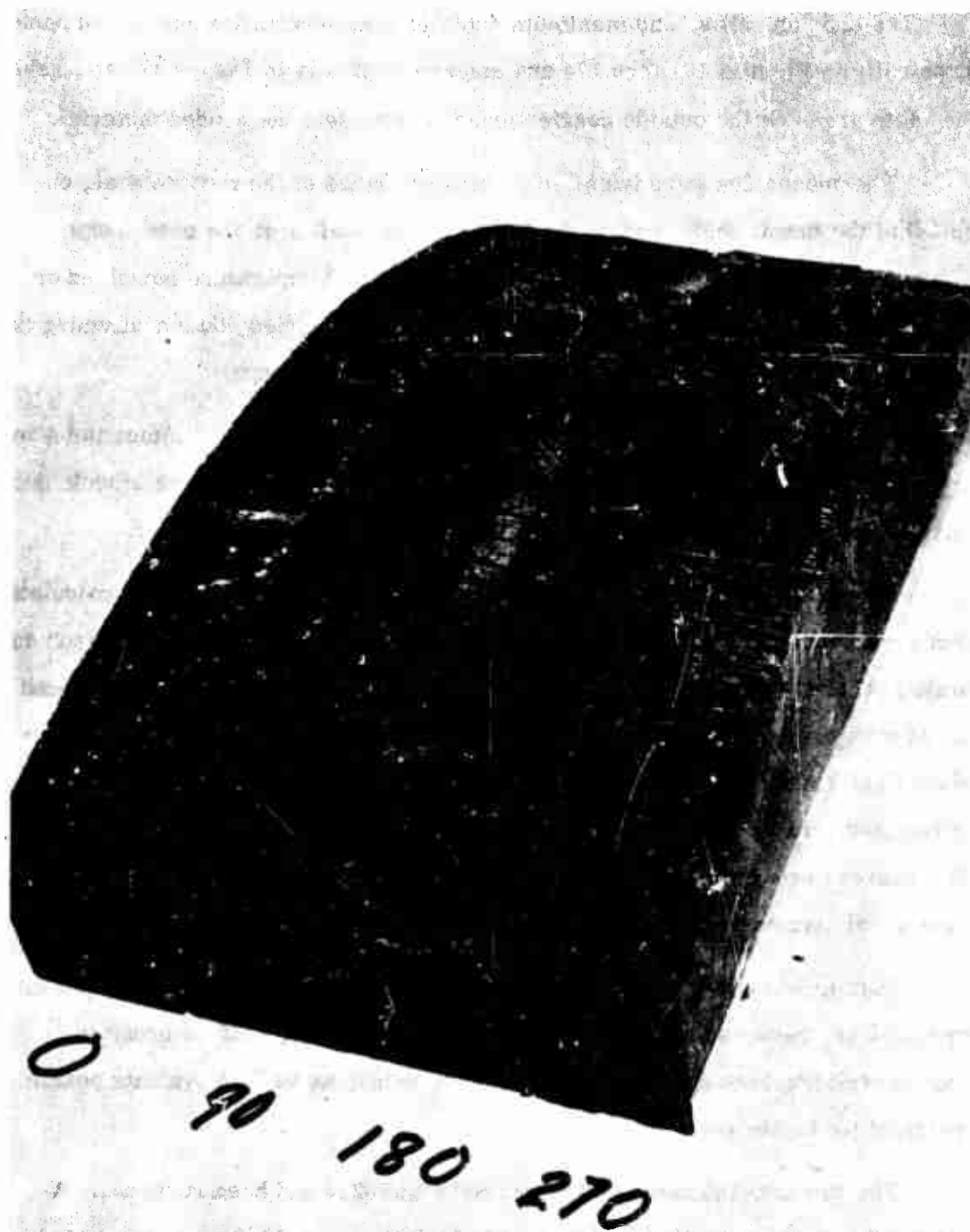


Figure 170. Comparison of Throat Erosion Sections

415

CONFIDENTIAL
(THIS PAGE IS UNCLASSIFIED)

CONFIDENTIAL

- (U) The erosion, char, and maximum depth of heat penetration are shown photographically in Figures 171 thru 174 and diagrammatically in Figure 175 and Table XXXI. The white areas on the outside nozzle surfaces represent the eroded material.
- (U) Thermocouples were installed on both end rings of the flexible seal, on the OD of the throat shell, and on the fixed housing shell near the case flange (Figure 135). All thermocouples indicated that the temperature remained at ambient throughout firing and the subsequent heat soak period, thus confirming the integrity of plastic components and the value of postfire quench.
- (U) b. Metal Parts Performance--All metal parts of the nozzle were intact and showed no deterioration whatsoever. In fact, they were all reusable. Thermocouple data indicated that all metal parts remained at ambient throughout the firing.
- (C) Deflection of the actuator brackets at the trunnion centerline was calculated from strain gage data to be 0.070 inch. This compares to 0.320 in. measured during nozzle prefiring checkout. It was expected since prefiring calculations indicated the bulk of measured compliance to be due to deflection of the membrane area of the nozzle fixed housing. This membrane stiffens considerably when the motor is pressurized. The compliance analysis does point out that the inability to vector a full 4 degrees was primarily caused by a short stroke actuator and not by deflections in the metal structure.
- (U) Data from strain gages located on the nozzle and the actuator attachment brackets were reviewed and converted to stresses (Table XXXII) in order to check correlation between actual and predicted values as well as evaluate nozzle structural performance.
- (U) The raw data indicated that Gages S213 and S214 had been reversed. A check on the instrumentation hookup verified this fact and the figures presented in Table XXXII have been switched to their proper relationship.
- (U) Review of the data indicates that the predicted stresses in most areas were above the actual stresses experienced during the firing. This, in part, was due to

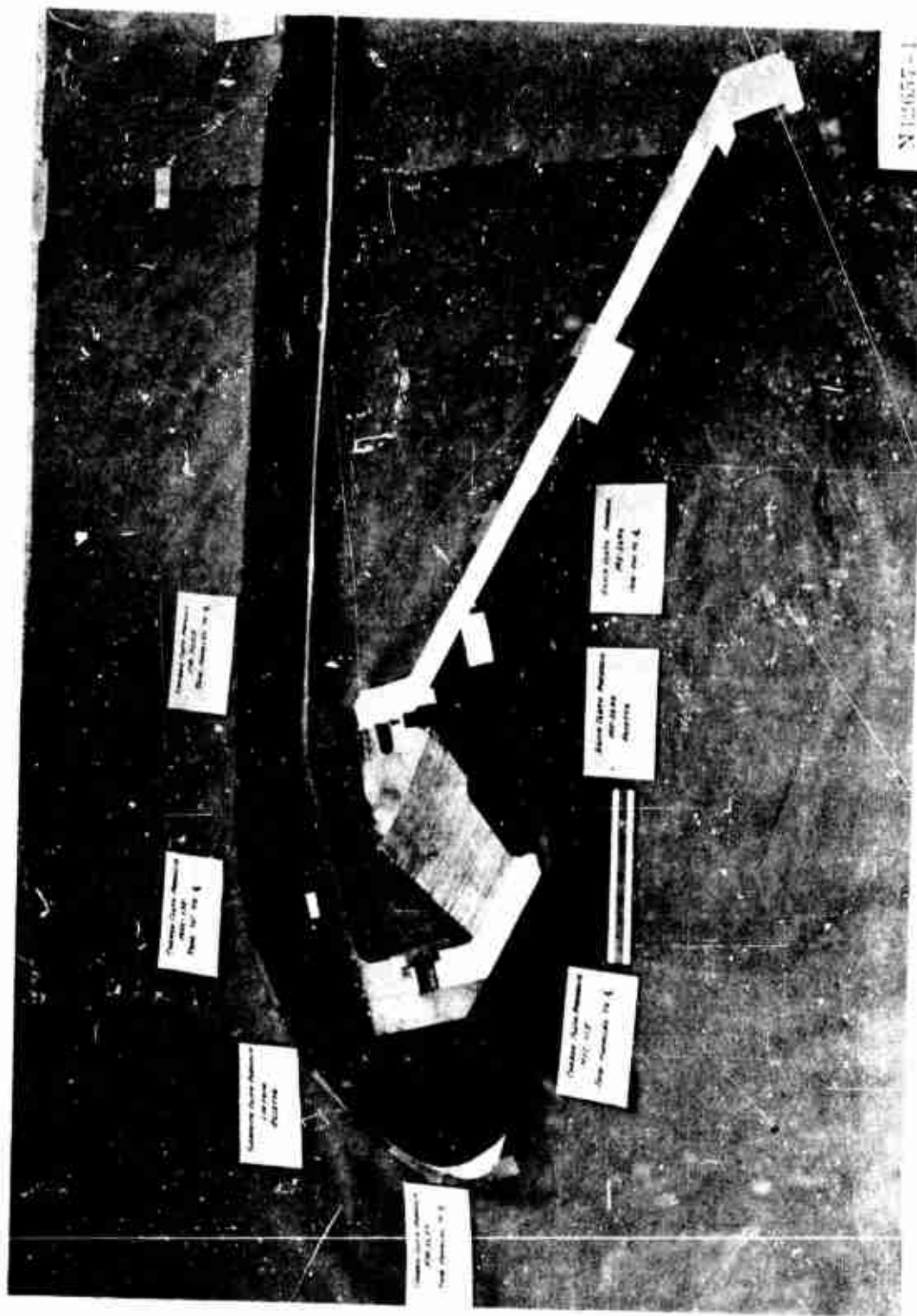


Figure 171. Submerged Section Erosion



Figure 172. Nose Erosion

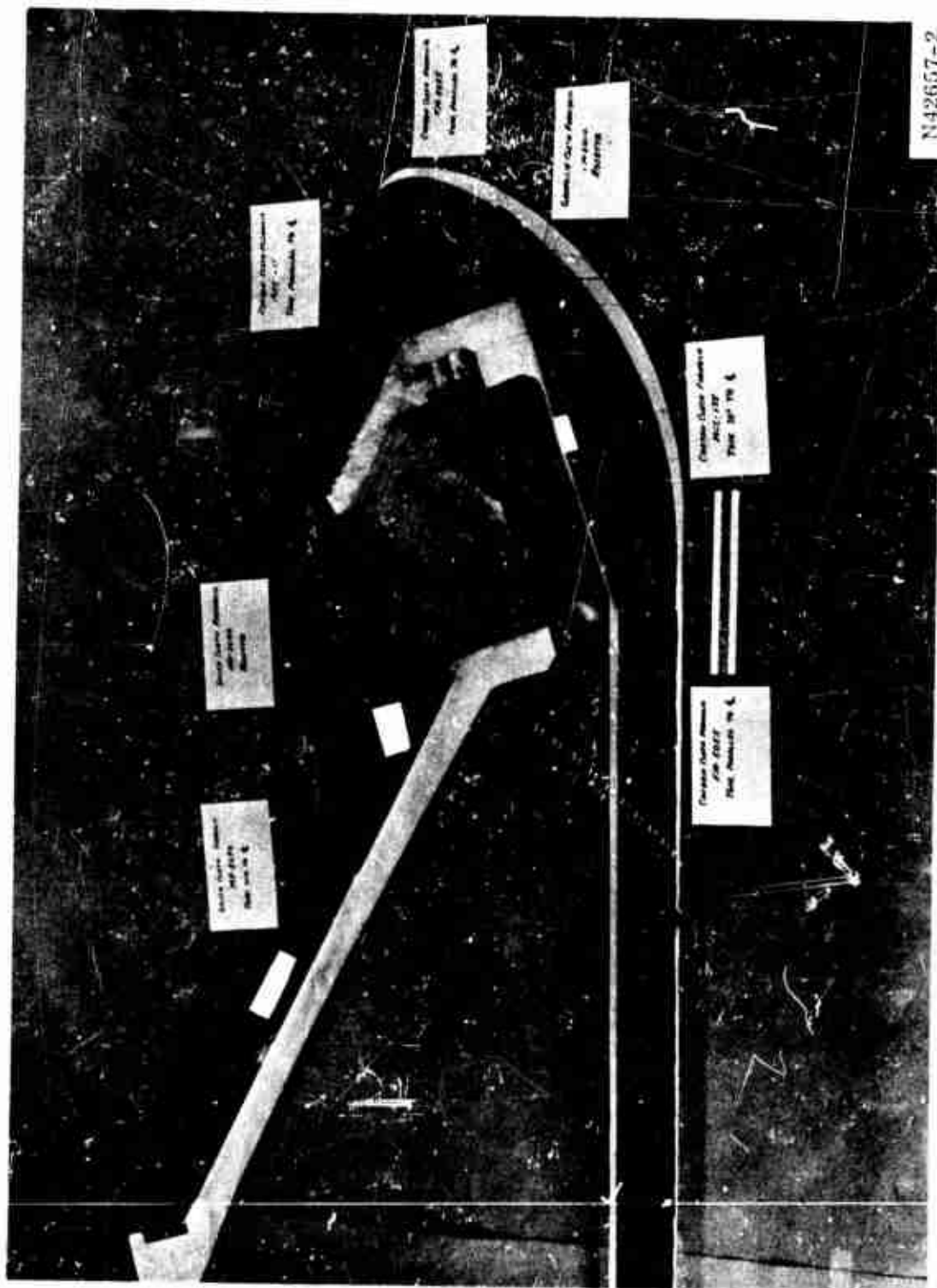


Figure 1/3. Throat Erosion

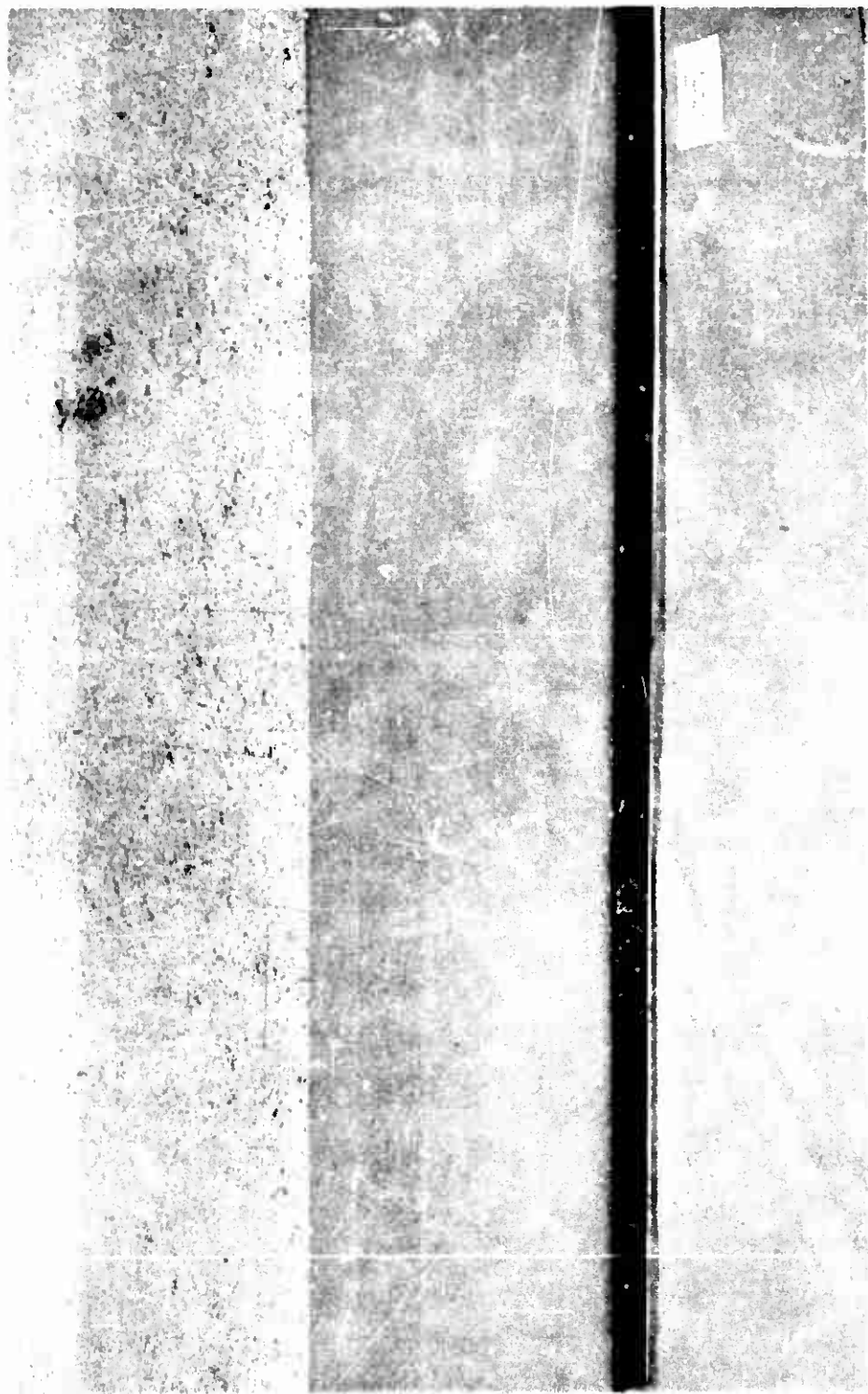
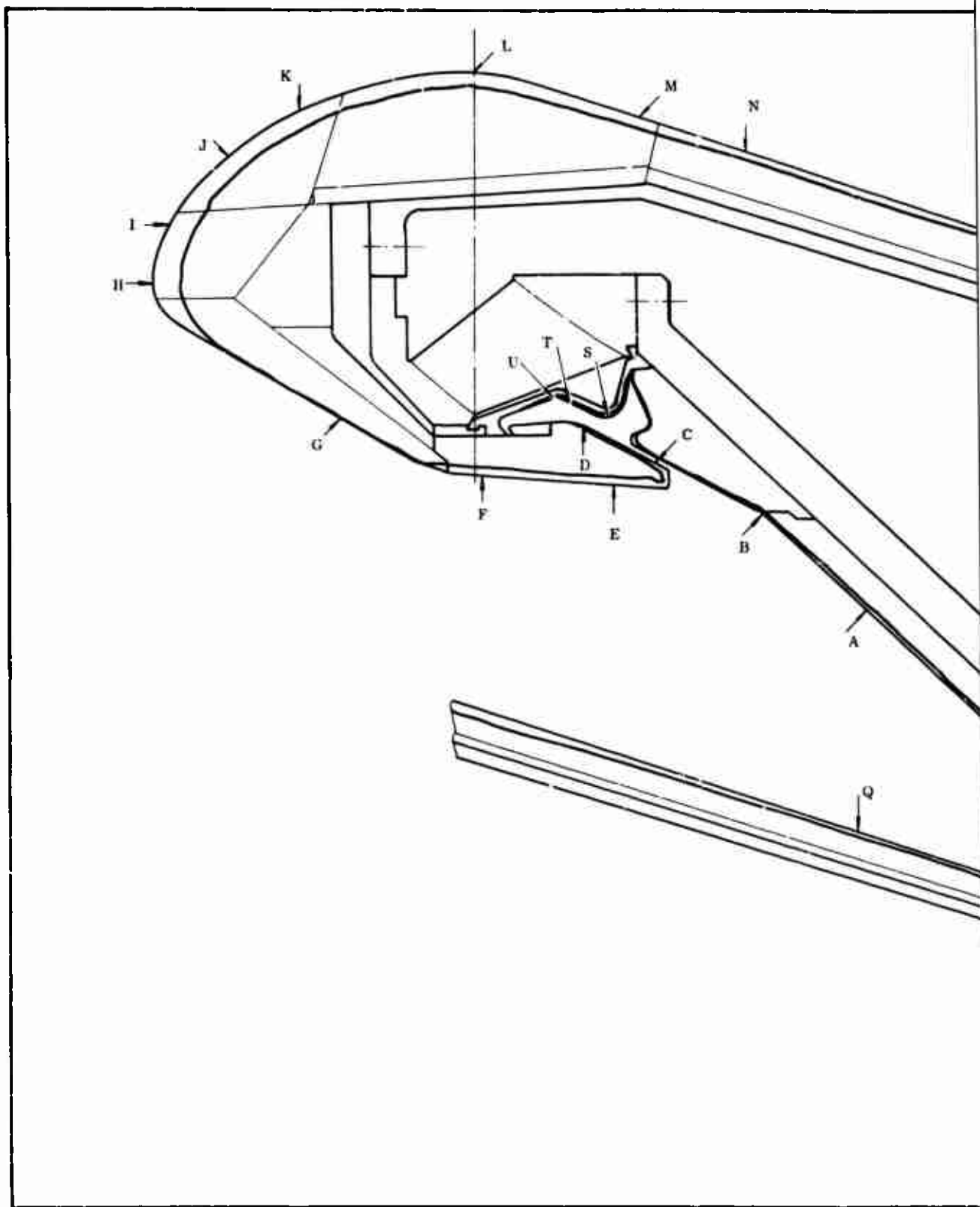


Figure 174. Exit Cone Erosion



CONFIDENTIAL

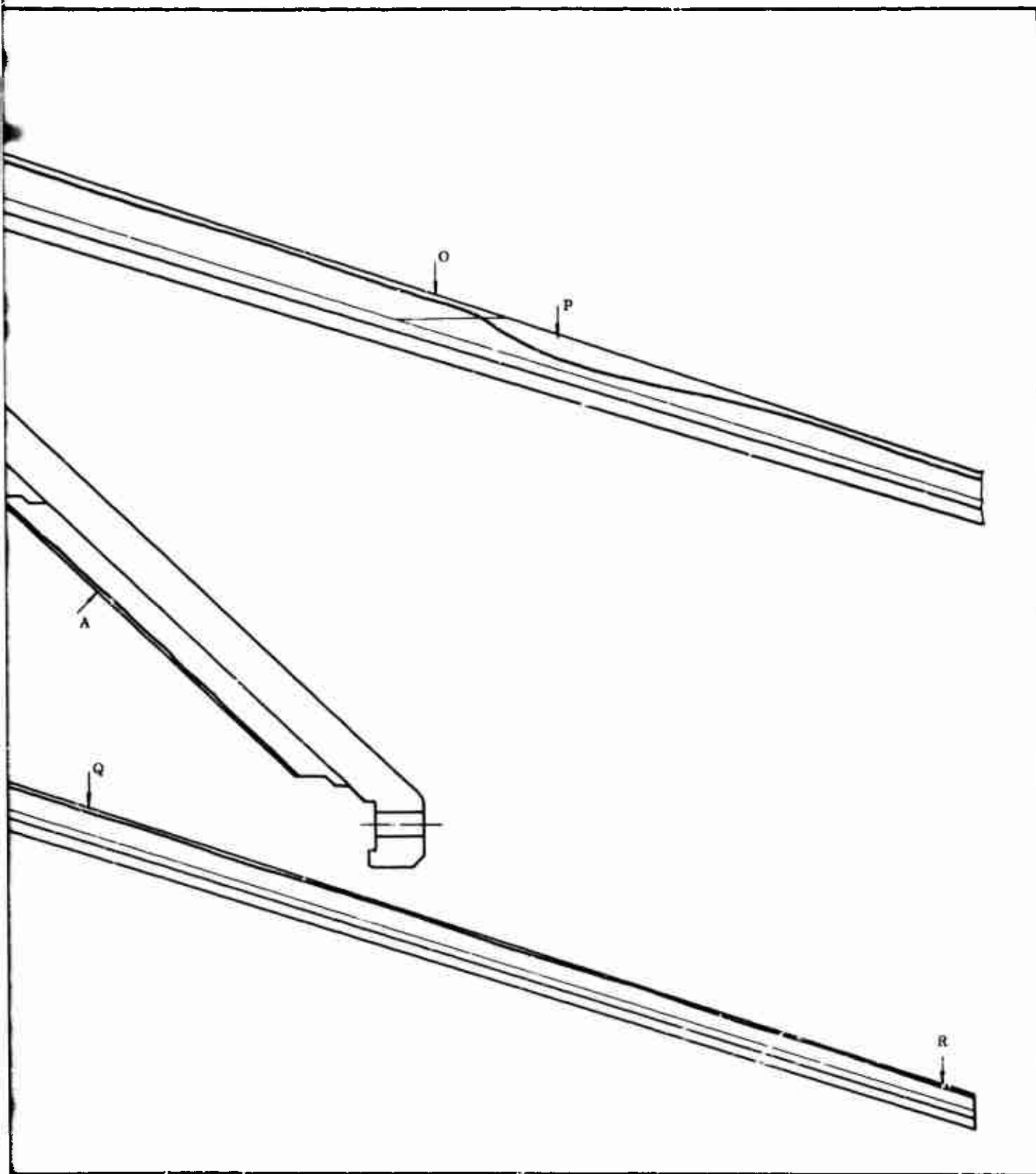


Figure 175. Erosion and Char Measurements (Sheet 1 of 2)

421

CONFIDENTIAL

2

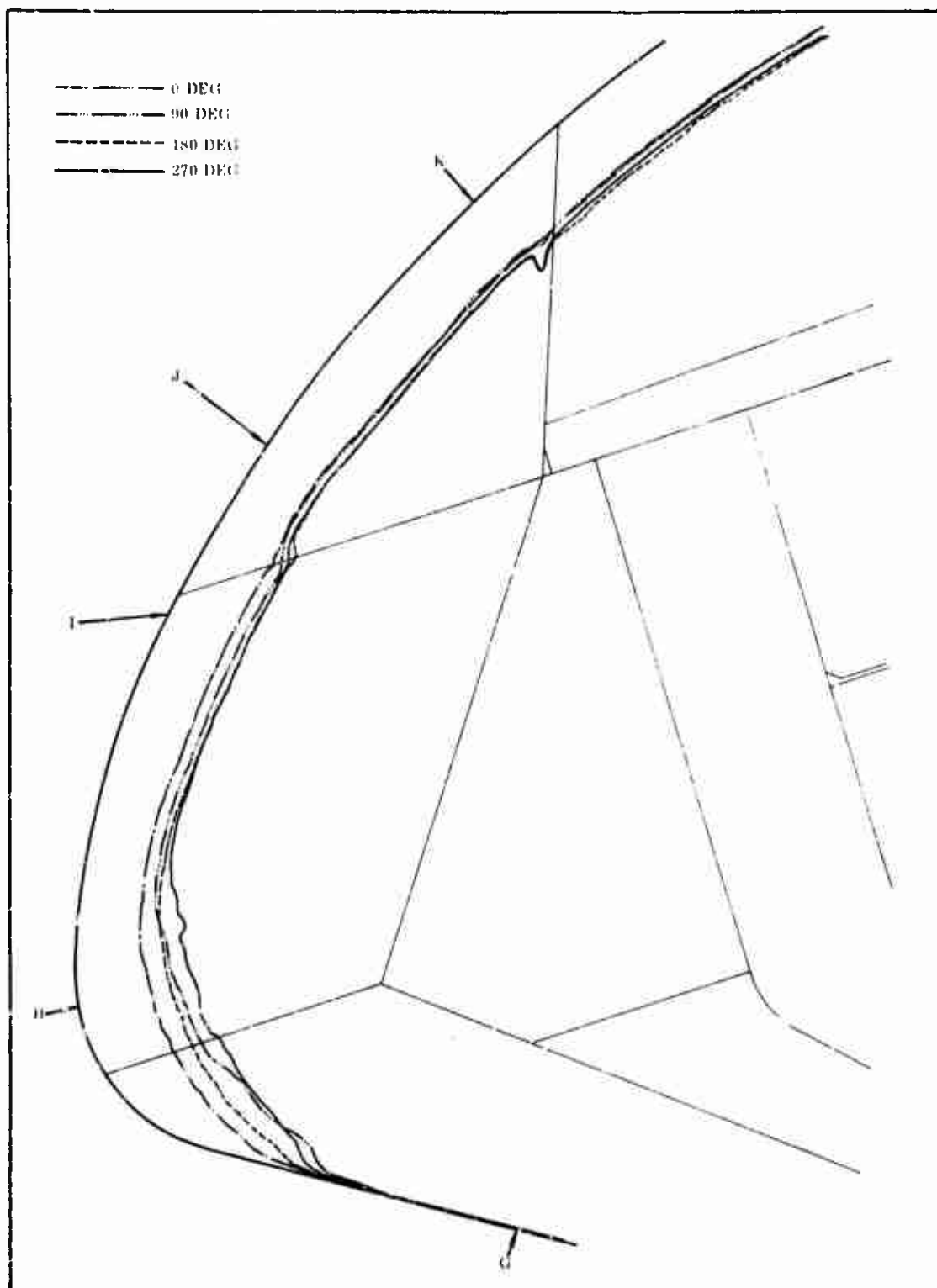


Figure 175. Erosion and Char Measurements (Sheet 2)

PRECEDING PAGE BLANK-NOT FILLED

TABLE XXXI

EROSION AND CHAR ME

Station	Expansion Ratio	Material	Erosion Depth (in.)					Erosion Rate (
			Average	0 Deg	90 Deg	180 Deg	270 Deg	Average	0 Deg	90 Deg	
A	4.55	Silica Cloth Phenolic MX2646	0.160	0.15	0.15	0.16	0.18	2.078	1.95	1.95	
B	3.84	Silica Cloth Phenolic MX2646	0.145	0.11	0.13	0.12	0.22	1.883	1.429	1.688	
C	3.59	Silica Cloth Phenolic MX2646	0.090	0.09	0.12	0.05	0.10	1.169	1.169	1.558	
D	3.34	Silica Cloth Phenolic MX2646	0.045	0.04	0.07	0.03	0.04	0.5845	0.5195	0.909	
E	3.77	Silica Cloth Phenolic MX2646	0.285	0.27	0.30	0.34	0.23	3.70	3.506	3.896	
F	3.593	Silica Cloth Phenolic MX2646	0.390	0.36	0.36	0.38	0.46	5.06	4.675	4.675	
G	3.18	Carbon Cloth Phenolic MXC175	0.025	0.03	NO HOLES		0.02	--	0.32465	0.3896	--
G'	3.18	Carbon Cloth Phenolic MCX175	0.025	--	0.04	HOLES		0.01	0.3247	--	0.519
H	2.07	Carbon Cloth Phenolic FM5055	0.795	0.68	--	0.91	--	10.325	8.831	--	
H'	2.07	Carbon Cloth Phenolic FM5055	0.99	--	0.90	--	1.08	12.857	--	11.688	
I	1.62	Carbon Cloth Phenolic FM5055	0.725	0.63	--	0.82	--	9.416	8.182	--	
I'	1.62	Carbon Cloth Phenolic FM5055	0.74	--	0.70	--	0.78	9.610	--	9.091	
J	1.32	Graphite Cloth Phenolic FM5014 Rosette	0.6975	0.60	0.68	0.76	0.75	9.059	7.79	8.831	
K	0.892	Carbon Cloth Phenolic MXC175	0.7525	0.68	0.73	0.84	0.76	9.773	8.831	9.481	
L	1.006	Carbon Cloth Phenolic MXC175	0.585	0.55	0.58	0.62	0.59	7.539	7.143	7.532	
M	1.18	Carbon Cloth Phenolic MXC175	0.2775	0.28	0.28	0.28	0.27	3.604	3.636	3.636	
N	1.25	Carbon Cloth Phenolic FM5055	0.240	0.21	0.27	0.26	0.22	3.117	2.727	3.507	
O	2.21	Carbon Cloth Phenolic FM5055	0.09	0.10	0.11	0.07	0.08	1.169	1.299	1.429	
P	2.77	Silica Cloth Phenolic MX2646	0.8175	0.78	0.84	0.85	0.80	10.617	10.129	10.909	
Q	5.41	Silica Cloth Phenolic MX2646	0.2325	0.23	0.22	0.25	0.23	3.019	2.985	2.857	
R	8.15	Silica Cloth Phenolic MX2646	0.925	0.08	0.09	0.08	0.12	1.201	1.039	1.169	
			Average	Boot 1		Boot 2		Average	Boot 1		
S	3.15	V-45 Rubber	0.105	0.12		0.09		1.3535	1.558		
T	3.10	V-45 Rubber	0.095	0.11		0.08		1.134	1.429		
U	3.06	V-45 Rubber	0.125	0.13		0.12		1.623	1.688		

CONFIDENTIAL

TABLE XXXI

ION AND CHAR MEASUREMENTS

Erosion Rate (mil/sec)					Char Depth (in.)				Maximum Depth of Heat Penetration (in.)					Comments
0 Deg	90 Deg	180 Deg	270 Deg	Average	0 Deg	90 Deg	180 Deg	270 Deg	Average	0 Deg	90 Deg	180 Deg	270 Deg	
1.95	1.95	2.078	2.34	0.320	0.30	0.35	0.32	0.31	0.590	0.56	0.60	0.60	0.60	
1.429	1.688	1.558	2.857	0.2725	0.28	0.26	0.27	0.28	0.538	0.60	0.50	0.50	0.53	
1.169	1.558	0.649	1.298	0.1375	0.10	0.15	0.12	0.18	0.4875	0.50	0.55	0.50	0.40	
0.5195	0.9091	0.3896	0.5195	0.0575	0.06	0.08	0.08	0.01	0.250	0.20	0.25	0.28	0.27	
3.506	3.896	4.416	2.987	0.1625	0.15	0.14	0.18	0.18	0.2875	0.25	0.30	0.35	0.25	
4.675	4.675	4.935	5.974	0.12	0.10	0.10	0.10	0.18	0.2575	0.20	0.28	0.25	0.30	
0.3896	--	0.2597	--	0.63	0.58	--	0.68	--	0.70	0.70	--	0.70	--	No Holes
--	0.5195	--	0.1299	0.63	--	0.60	--	0.66	0.725	--	0.70	--	0.75	Holes
8.831	--	11.818	--	0.44	0.48	--	0.40	--	0.55	0.60	--	0.50	--	No Holes
--	11.688	--	14.026	0.435	--	0.39	--	0.48	0.47	--	0.49	--	0.45	Holes
8.182	--	10.65	--	0.35	0.38	--	0.32	--	0.425	0.40	--	0.45	--	
--	9.091	--	10.129	0.36	--	0.39	--	0.33	0.60	--	0.60	--	0.60	
7.79	8.831	9.870	9.740	0.4675	0.50	0.47	0.48	0.42	0.50125	0.50	0.50	0.50	0.55	
8.831	9.481	10.91	9.87	0.3475	0.39	0.29	0.33	0.38	0.475	0.60	0.50	0.45	0.35	
7.143	7.532	7.818	7.662	0.5350	0.58	0.48	0.53	0.55	0.76	0.80	0.68	0.80	0.76	Throat
3.636	3.636	3.636	3.507	0.6225	0.70	0.63	0.58	0.58	0.8375	0.90	0.78	0.89	0.78	
2.727	3.507	3.377	2.857	0.5375	0.38	0.38	0.40	0.39	0.578	0.60	0.62	0.59	0.50	
1.299	1.429	0.909	1.039	0.4225	0.40	0.40	0.44	0.45	0.58	0.64	0.68	0.50	0.50	
10.129	10.909	11.04	10.39	0.10	0.10	0.10	0.10	0.10	0.305	0.30	0.32	0.30	0.30	
2.985	2.857	3.247	2.985	1.325	0.12	0.13	0.15	0.13	0.35	0.35	0.35	0.30	0.40	
1.039	1.169	1.039	1.558	1.925	0.19	0.20	0.20	0.18	0.42	0.40	0.46	0.40	0.42	
Boot 1		Boot 2		Average	Boot 1		Boot 2		Average	Boot 1		Boot 2		Two Specimens
1.558		1.149							0.025	0.03		0.02		
1.429		1.039							0.0325	0.02		0.045		
1.688		1.558							0.020	0.015		0.025		

CONFIDENTIAL

2

CONFIDENTIAL

TABLE XXXII
SUMMARY OF NOZZLE STRESSES

Gage No.	Stress (psi)			
	Predicted		Actual	
	Long.	Circumferential	Long.	Circumferential
S201 and S202	63,295	N/P*	32,800	14,340
S203 and S204	63,295	N/P	32,240	17,470
S205 and S206	-46,628	78,599	-25,880	62,736
S207 and S208	-46,628	78,599	-20,400	76,978
S209 and S210	-46,628	78,599	-20,275	67,418
S211 and S212	-1,731	-8,750	-1,319	-1,896
S213 and S214	-84,517	N/P	-22,391	363
S215 and S216	-84,517	N/P	-23,110	-33
S217 and S218	N/P	N/P	3,692	329
S219 and S220	N/P	N/P	429	2,571
S221 and S222	N/P	N/P	-742	1,127
S223 and S224	N/P	N/P	-99	2,970

*N/P = Not predicted.

CONFIDENTIAL

(THIS PAGE IS UNCLASSIFIED)

the use of actuator stall load in the original analysis. Actuator stall load was 70,000 lb while the maximum load experienced during firing was only 34,000 pounds.

(U) Strain data were reduced by the utilization of Hooke's Law.

$$\sigma = \frac{E (\epsilon_1 + \mu \epsilon_2)}{1 - \mu^2}$$

CONFIDENTIAL

(THIS PAGE IS UNCLASSIFIED)

4. CASE PERFORMANCE

- (U) The general performance of the case was as expected. There was no change in physical appearance as a result of the static firing. Thermocouple data show that the case remained near ambient temperature throughout the firing and the soak period that followed. This is attributed to the excellent insulation and quench system performance. Strain gage data indicate extremely low stresses throughout the case which leads to an opinion that the case is reusable.
- (U) Case strain data were reviewed and converted to stresses to check the correlation between actual and predicted values as well as assess the case performance. These data are shown in Table XXXIII.
- (U) It should be noted that the raw data indicated that gages S013 and S014 were reversed. A check on the instrumentation hookup has verified this fact so the figures presented in Table XXXIII are switched back to their proper relationship.
- (U) Review of the reduced data indicated that the predicted stresses, in most areas, were well above the actual stresses experienced during the firing. This, in part, was due to the fact that predicted stresses were based on an MEOP of 830 psi which was predicted before actual propellant properties were known. The actual case pressure was 656 psi.
- (U) Strain gages S011 thru S025 reflect stresses well below the predicted values for the areas monitored. This variation was probably due to the location of the strain gage. The area involved had a rapidly changing stress field due to the increased cross-section as it blends into the aft attachment boss.
- (U) The predicted values for gages S011 thru S025 did not include the stresses caused by membrane bending inasmuch as the gages average the bending stresses over the area of the gage and reflect a lower and more realistic value.

(U)

Strain data was reduced by the utilization of Hooke's Law.

$$\sigma = \frac{E (\epsilon_1 + \mu \epsilon_2)}{1 - \mu^2}$$

CONFIDENTIAL

TABLE XXXIII
SUMMARY OF CASE STRESSES

Gage No.	Stress (psi)					
	Predicted			Actual		
	Longitudinal	Circumferential	Radial	Longitudinal	Circumferential	Radial
S001 and S002	N/A**	N/P*	N/P	--	104,176	127,253
S003 and S004	N/A	N/P	N/P	--	104,350	152,811
S005 and S006	N/A	N/P	N/P	--	101,538	138,461
S007 and S008	N/P	N/P	N/A	1,087	106,286	--
S009 and S010	N/P	N/P	N/A	129,560	71,868	--
S011 and S012	N/A	-30,000	-70,000	--	-13,747	-14,176
S013 and S014	N/A	-30,000	-70,000	--	-29,835	-4,451
S015 and S016	N/A	-30,000	-70,000	--	-10,582	-6,725
S017 and S018	N/A	-30,000	-70,000	--	-20,110	-2,967
S019 and S020	N/A	-30,000	-70,000	--	-3,956	-16,813
S021 and S022	N/A	-30,000	-70,000	--	-11,238	-17,637
S023, S024, and S025	N/A	-30,000	-70,000	--	-13,187	-11,040

*N/P = Not predicted.

**N/A = Not applicable.

CONFIDENTIAL

CONFIDENTIAL

(THIS PAGE IS UNCLASSIFIED)

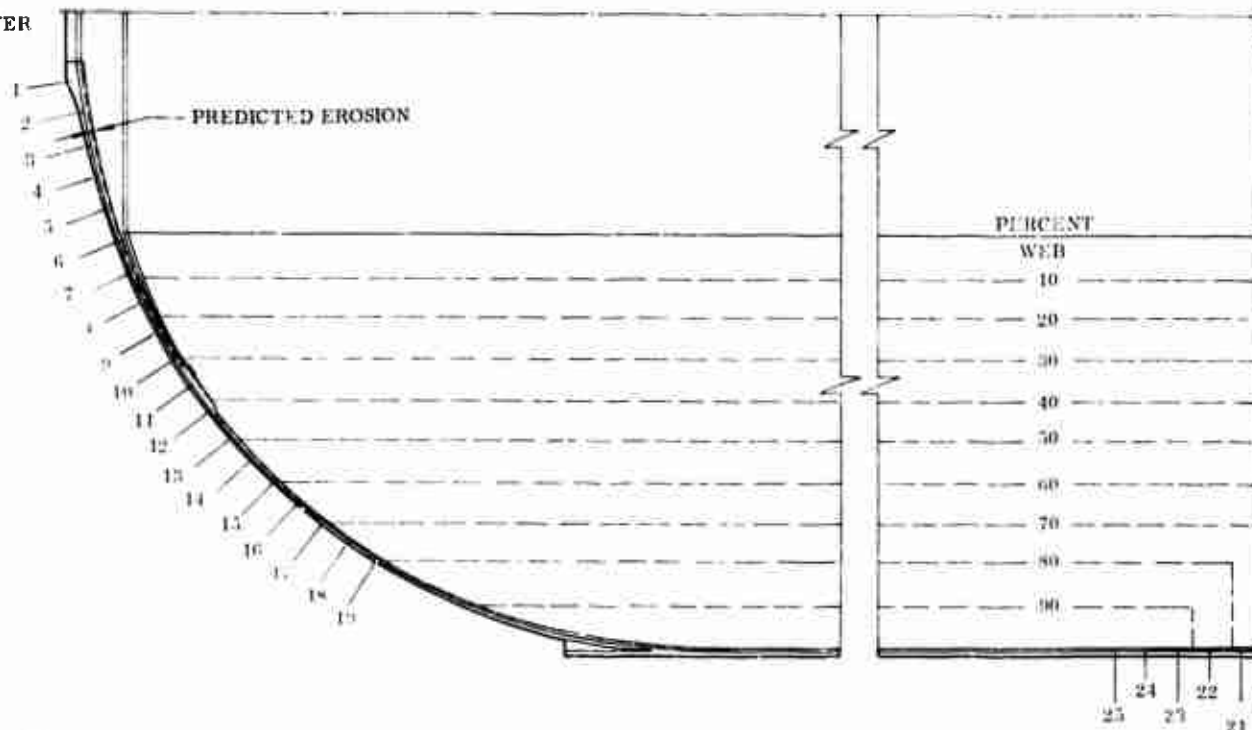
5. INSULATION PERFORMANCE

(U) The case insulation performed as predicted. In general, erosion in the aft case insulation was less than expected. In fact, it matched the head end loss fairly closely which would indicate that the head and aft end environments were approximately the same. Loss rates are shown in Figure 176. The case insulation erosion was measured by measuring the depth of holes drilled through the insulation to the case wall prior to loading of the motor. The depth measurements and location were recorded and the holes filled. Following static test, holes were again drilled in the approximate same location, their depths measured, and compared with the prefire measurements. The TI-H704B insulation increases in volume somewhat as it becomes heat affected. The loss rates measured in the aft case were those associated with an average Mach number of approximately 0.025. The erosion on the nozzle fixed housing near the case-nozzle joint was also about what would be expected at the same flow conditions. Since the comparative performance of the TI-H704B insulation and the silica cloth phenolic on the fixed housing is consistent, exceptional performance of the TI-H704B insulation may be ruled out.

(U) The loss rates shown in Figure 176 are not corrected for this volume increase and are therefore somewhat less than actual. An additional inaccuracy in these measurements is due to the irregularity of the insulation surface. This irregularity is characteristic of a mastic insulation installed in a hand operation. Because of this surface irregularity, any slight misalignment between the pre and postfire measurements causes an error in the calculation of the amount of material lost.

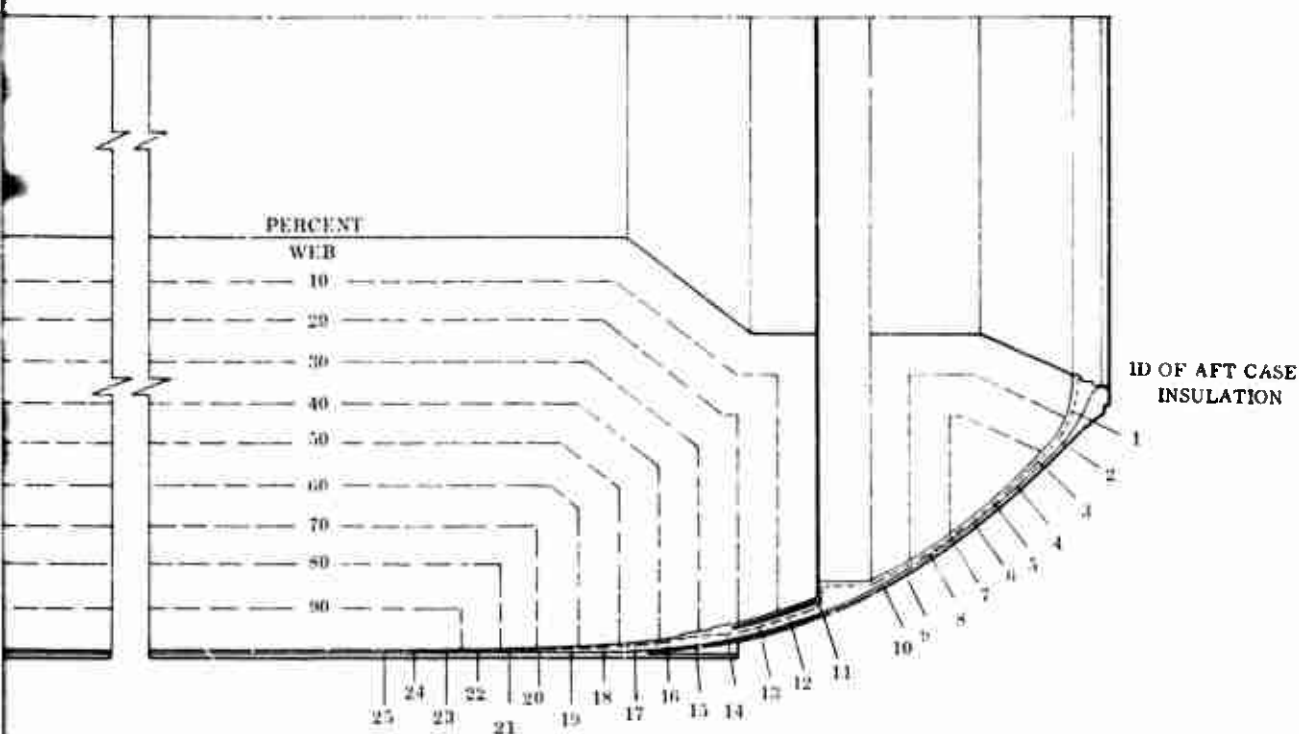
(U) Assuming an arbitrary 30 percent increase in loss rates to compensate for the above defined inaccuracies, the amount of material lost was still generally below that predicted in the aft section of the motor and approximately as predicted on the forward dome. Thus the aft end environment was not as severe as predicted.

IGNITER
BOSS



Distance from the 1D of the Igniter Boss Insulation		Exposure Time	Prefire Thickness	Postfire Thickness	Material Lost	Actual Loss Rate	Predicted Loss Rate	Distance from the 1D of the Aft Case Insulation		Exposure Time
(station)	(in.)	(sec)	(in.)	(in.)	(in.)	(mil/sec)	(mil/sec)	(station)	(in.)	(sec)
1	2	80.8	1.02	*	*	*	*	1	4.0	74.2
2	6	80.8	0.77	*	*	*	*	2	7.8	68.0
3	10	80.8	0.80	0.64	0.16	2.0	*	3	11.6	62.1
4	14	80.8	0.80	0.58	0.22	2.7	*	4	15.3	56.6
5	18	80.8	0.90	0.60	0.30	3.7	4.0	5	18.8	55.9
6	22	80.8	0.90	0.65	0.25	3.1	*	6	22.6	60.8
7	26	Flap	0.65	0.74	+0.10	*	*	7	25.9	65.1
8	30	Flap	0.70	Flap	*	*	*	8	29.5	70.2
9	34	Flap	0.60	Flap	*	*	*	9	32.5	74.3
10	38	Flap	0.50	Flap	*	*	*	10	31.6	70.5
11	42	51.9	0.50	Flap	*	*	*	11	52.1	56.4
12	46	46.9	0.58	*	"	*	4.0	12	56.1	48.6
13	50	41.7	0.52	0.39	0.13	3.1	*	13	60.1	43.5
14	54	37.2	0.50	0.41	0.09	2.4	*	14	64.1	36.9
15	58	32.7	0.48	0.40	0.08	2.4	*	15	68.1	30.7
16	62	28.3	0.42	0.35	0.07	2.5	*	16	72.1	24.2
17	66	26.5	0.50	0.30	0.20	7.6	*	17	76.1	17.6
18	70	20.8	0.32	0.39	+0.07	*	*	18	80.1	11.2
19	74	17.4	0.40	0.35	0.05	2.9	*	19	84.1	4.8
								20	88.1	3.00
								21	92.1	0.90
								22	96.1	0.00
								23	100.1	0.00
								24	104.1	0.00
								25	108.1	0.00

*Not Measurable.



Actual Loss Rate (mil/sec)	Predicted Loss Rate (mil/sec)	Distance from the ID of the Aft Case Insulation (station)	Exposure Time (sec)	Prefire Thickness (in.)	Postfire Thickness (in.)	Material Lost (in.)	Actual Loss Rate (mil/sec)	Predicted Loss Rate (mil/sec)
*	*	1	4.0	74.2	1.30	1.12	0.18	2.4
*	*	2	7.8	65.0	1.45	1.22	0.23	3.4
2.0	*	3	11.6	62.1	1.40	1.34	0.06	1.0
2.7	*	4	15.3	56.6	1.54	1.54	0.00	0.0
3.7	4.0	5	18.8	55.9	1.54	1.45	0.09	1.6
5.1	*	6	22.6	60.8	1.60	1.40	0.20	3.3
*	*	7	25.9	65.1	1.57	1.27	0.30	4.6
*	*	8	29.5	70.2	1.72	1.41	0.31	4.4
*	*	9	32.5	74.3	1.72	1.51	0.21	2.8
*	*	10	31.6	70.5	1.44	1.41	0.03	0.4
*	*	11	52.1	56.4	1.32	1.56	+0.24	*
*	4.0	12	56.1	48.6	1.22	1.16	0.06	1.2
5.1	*	13	60.1	43.5	0.92	0.98	+0.06	*
2.4	*	14	64.1	36.9	1.02	0.90	0.12	3.3
2.4	*	15	68.1	30.7	0.82	0.96	+0.14	*
2.5	*	16	72.1	24.2	0.92	0.89	0.03	1.2
7.6	*	17	76.1	17.6	0.82	0.79	0.03	1.7
*	*	18	80.1	11.2	0.74	0.81	+0.07	*
2.9	*	19	84.1	4.8	0.64	0.68	+0.04	*
		20	88.1	0.00	0.67	0.73	+0.06	*
		21	92.1	0.00	0.42	0.56	+0.12	*
		22	96.1	0.00	0.12	Liner	*	*
		23	100.1	0.00	0.27	Liner	*	*
		24	104.1	0.00	0.12	Liner	*	*
		25	108.1	0.00	0.14	Liner	*	*

Figure 176. Insulation Material Loss

CONFIDENTIAL

6. BALLISTIC PERFORMANCE

- (C) A tabulation of the ballistic performance data obtained from the 156-9 static test is presented in Table XXXIV. The actual and predicted pressure and thrust traces for the 156-9 motor are presented in Figures 177 and 178, respectively. Examination of Figure 177 indicates that the actual performance of the 156-9 motor deviated significantly from that predicted. The pressure during the first 30 seconds of motor operation was considerably below that predicted. The tailoff portion of motor operation was also considerably longer than predicted and obviously indicates some deviation from the normal or predicted burnout pattern.
- (C) The in-process evaluation of the propellant batches used in casting the 156-9 motor was based on uncured strand burning rates. The evaluation led to a change in the special fine ammonium perchlorate oxidizer distribution in the propellant over a range of 4 percent during the casting sequence. A sketch of the motor grain showing the location of the various grind ratios is presented in Figure 179. An analysis of the standardization, verification, and production TU-131 (7 lb batch check motor) data indicated a sensitivity of the burning rate of approximately 14 mils per percent change in special fine ammonium perchlorate oxidizer. The changes made in the oxidizer grind ratio during the casting of the 156-9 motor, based on uncured strand burning rates, therefore, led to a potential maximum variation in burning rate between various batches within the motor of approximately 56 mils. The burning rate deviations undoubtedly were a major contribution to the long tailoff exhibited by the 156-9 motor static test. Propellant burning rate data obtained from TU-131 batch check motors subsequent to cast and cure of the 156-9 indicated the mean propellant burning rate was 0.698 in./sec at 700 psi compared to the target burning rate of 0.717 in./sec.

CONFIDENTIAL

TABLE XXXIV
156-9 MOTOR PERFORMANCE

<u>Web Time Parameters</u>	<u>Work Statement Requirements</u>	<u>Predicted at 30° F</u>	<u>Measured</u>
Burning Time (sec)	--	68.5	77.0
Average Pressure (psia)	--	654	574
Maximum Pressure (psia)	--	697	656
MEOP (psia)	885	753	--
Total Impulse, Utah Conditions (lb-sec)	--	66,180,000	64,288,000
Average Thrust, Sea Level (lbf)	1,000,000	--	916,400
Utah Conditions (lbf)	--	969,600	834,700
Maximum Thrust, Sea Level (lbf)	--	--	964,900
Utah Conditions (lbf)	--	1,049,900	982,700
Propellant Burning Rate P_{cb} (in./sec)	--	0.724	0.644
Burning Rate Scale Factor	--	1.067	1.00
Propellant Weight Expended (lbm)	95 reg	273,874	270,783
Maximum to Average Pressure Ratio	--	1.06	1.14
<u>Action Time Parameters</u>			
Action Time (sec)	70 (max)	70.51	60.81
Average Pressure (psia)	--	641	556
Total Impulse, Sea Level (lbf-sec)	65,000,000	--	63,714,000
Utah Conditions (lbf-sec)	--	67,023,200	65,116,000
Average Thrust, Sea Level (lbf)	--	--	788,440
Utah Conditions (lbf)	--	930,500	805,800
Specific Impulse, Sea Level (lbf-sec/lbm)	--	--	231.8
Utah Conditions (lbf-sec/lbm)	--	247.0	236.9
Thrust Coefficient ($\gamma = 1.18, \lambda = 0.997$)	--	1.5334	1.497
Motor Coefficient (C_M)	--	0.980	0.991
Reference Specific Impulse (lbf-sec/lbm)	--	249.4	247.8
Propellant Weight Expended (lbm)	--	276,921	274,833
PARAMETERS USED IN PERFORMANCE CALCULATIONS			
<u>Nozzle Parameters</u>			
Average Throat Area (in. ²)	--	--	969
Average Throat Diameter (in.)	--	--	35.1
Average Exit Area (in. ²)	--	--	7,040
Average Exit Diameter (in.)	--	--	98.6
Initial Throat Diameter (in.)	--	--	34.5
Average Expansion Ratio	--	--	7.89
dr/dt (in./sec)	--	--	0.0075
Effective Half Angle	--	--	17.5
Effective λ	--	--	0.9769
<u>Grain Design Parameters</u>			
Grain Outside Diameter (in.)	--	--	154.53
Grain Inside Diameter (in.)	--	--	55.39
Grain-Sectional Loading Density (percent)	--	--	0.87
Port Area (in. ²)	--	--	2,437
Initial Port/Throat Area Ratio ($\frac{1}{J}$)	--	--	2.6
Web Thickness (in.)	--	--	49.57
Web Fraction (percent)	--	--	0.64
Slot Width at Bore (in.)	--	--	6.63
Slot Angle to Motor Centerline (deg)	--	--	90

CONFIDENTIAL

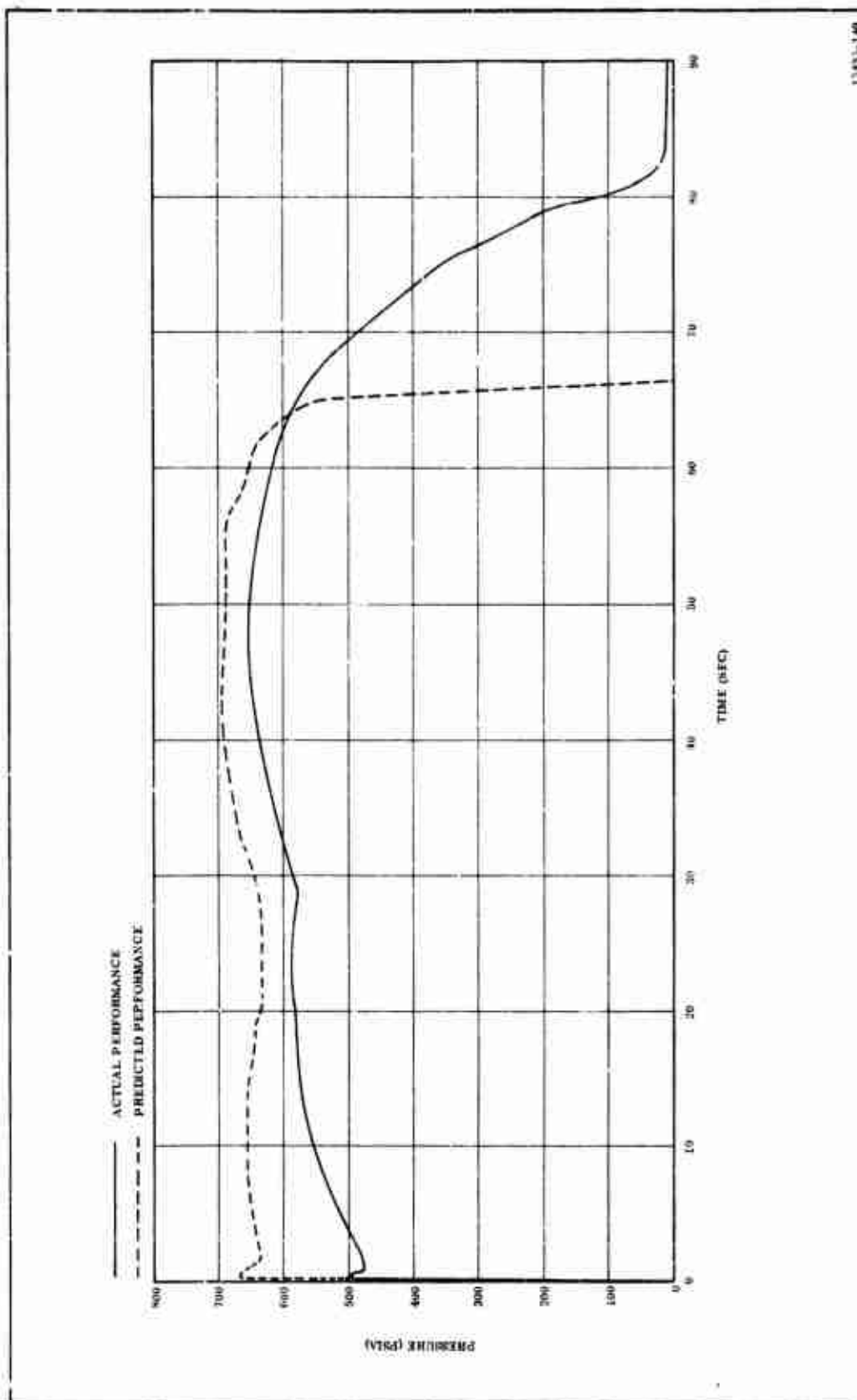


Figure 177. Chamber Pressure vs Time , Predicted and Actual

CONFIDENTIAL

CONFIDENTIAL

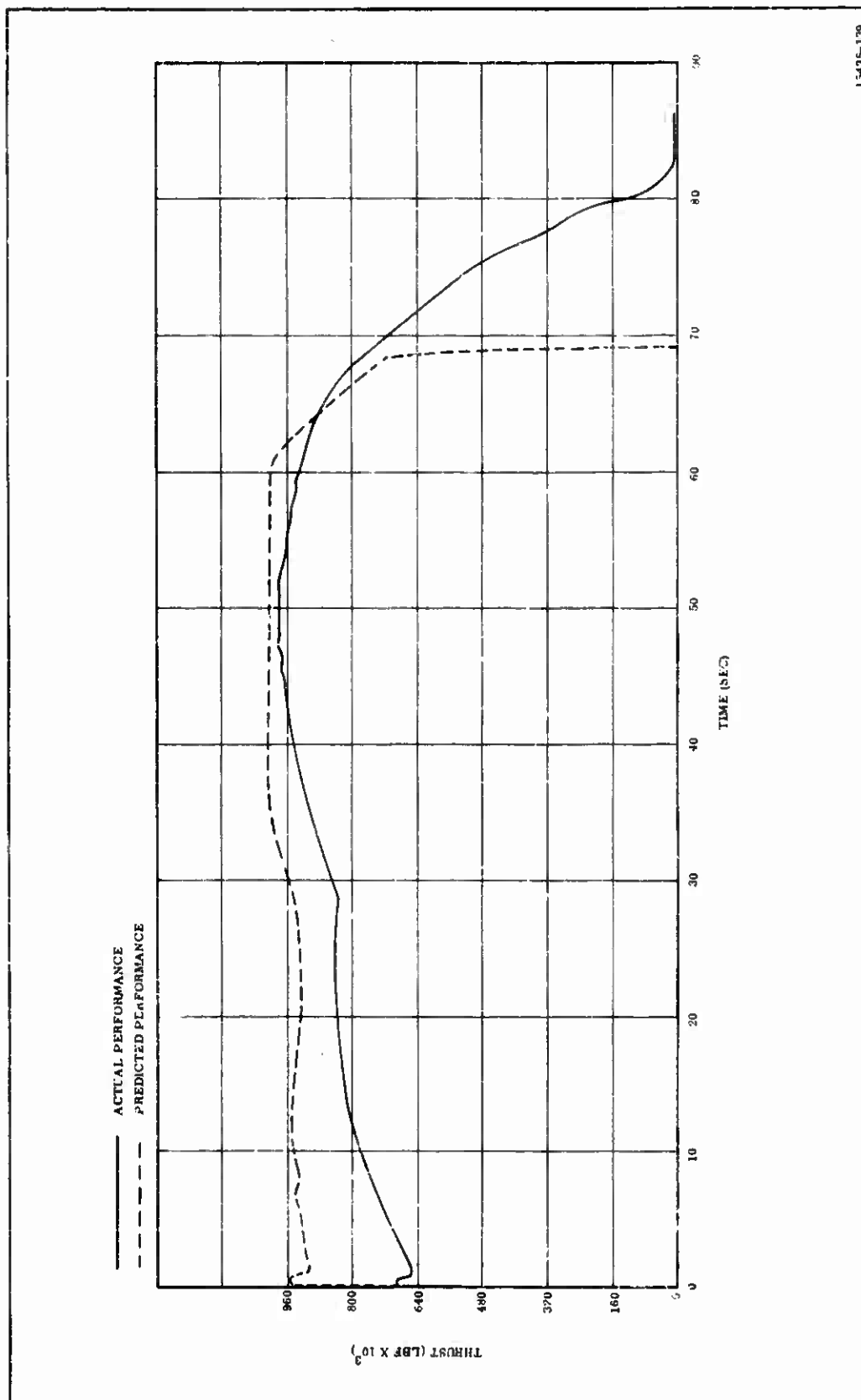


Figure 178. Axial Thrust vs Time, Predicted and Actual

CONFIDENTIAL

CONFIDENTIAL

(THIS PAGE IS UNCLASSIFIED)

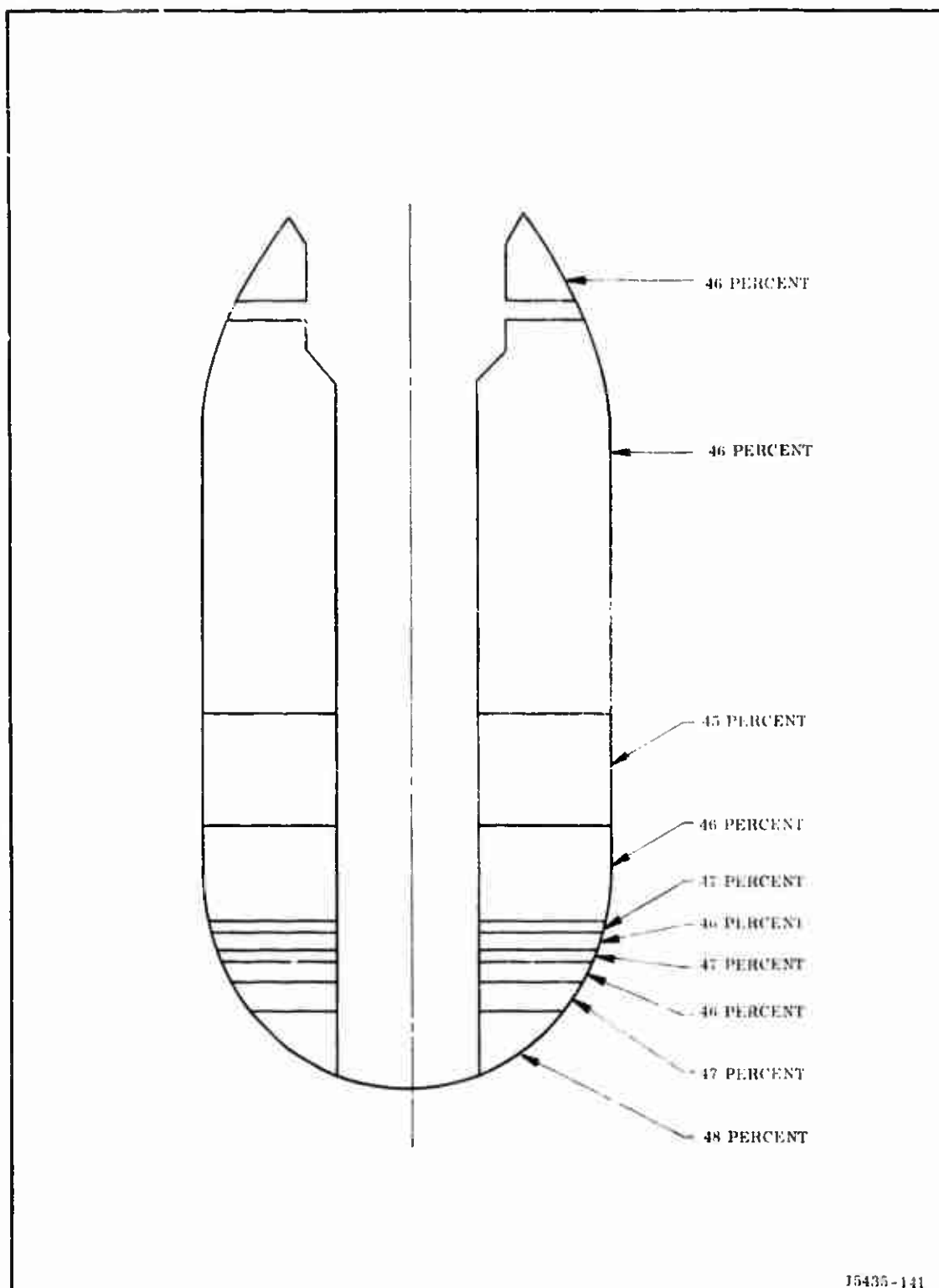


Figure 179. Special Fine Oxidizer Distribution

CONFIDENTIAL

(THIS PAGE IS UNCLASSIFIED)

CONFIDENTIAL

Due to the characteristics of the tailoff portion of the pressure time trace of the 156-9 motor, determination of the web burning time is very difficult using conventional techniques. Figure 180 illustrates a plot of the depressurization rate as a function of time (dp/dt) during the tailoff portion of motor operation. Web time (77 sec) was chosen as the first inflection point on the tailoff dp/dt curve. This figure agrees reasonably well with that which would be determined from the usual method of tangents.

- (C) In addition to the propellant burning rate being below target, there was no apparent burning rate scaleup indicated from the batch check to the 156-9 motor. The apparent lack of a burning rate scaleup may have been a contributor to the deviation between predicted and measured performance. A 7 percent scaleup factor was used in predicting 156-9 motor performance. The normal scaleup (batch check to large motor) in propellant burning rate experienced with large motors is of the order of 5 to 7 percent. The absence of an apparent scaleup is unusual and may be due to the rounded tailoff and the way in which web burning time was determined, or it may be characteristic of the propellant.
- (C) The TP-H1115 propellant utilized in the 156-9 motor did contain iron oxide and a large portion of special fine oxidizer in order to achieve the required propellant burning rate. It is possible, that high burning rate propellant formulations of this type will not exhibit a burning rate scaleup of the magnitude indicated by lower burning rate propellants. It has been shown that fast burning propellants are less sensitive to erosive burning than slow burning propellants.
- (C) The delivered performance of the motor was considerably lower than that predicted primarily because of the lower motor operating pressure. The specific impulse data indicated for the motor are based on calculated propellant weights. Past experience has indicated that theoretically predicted propellant

CONFIDENTIAL

(THIS PAGE IS UNCLASSIFIED)

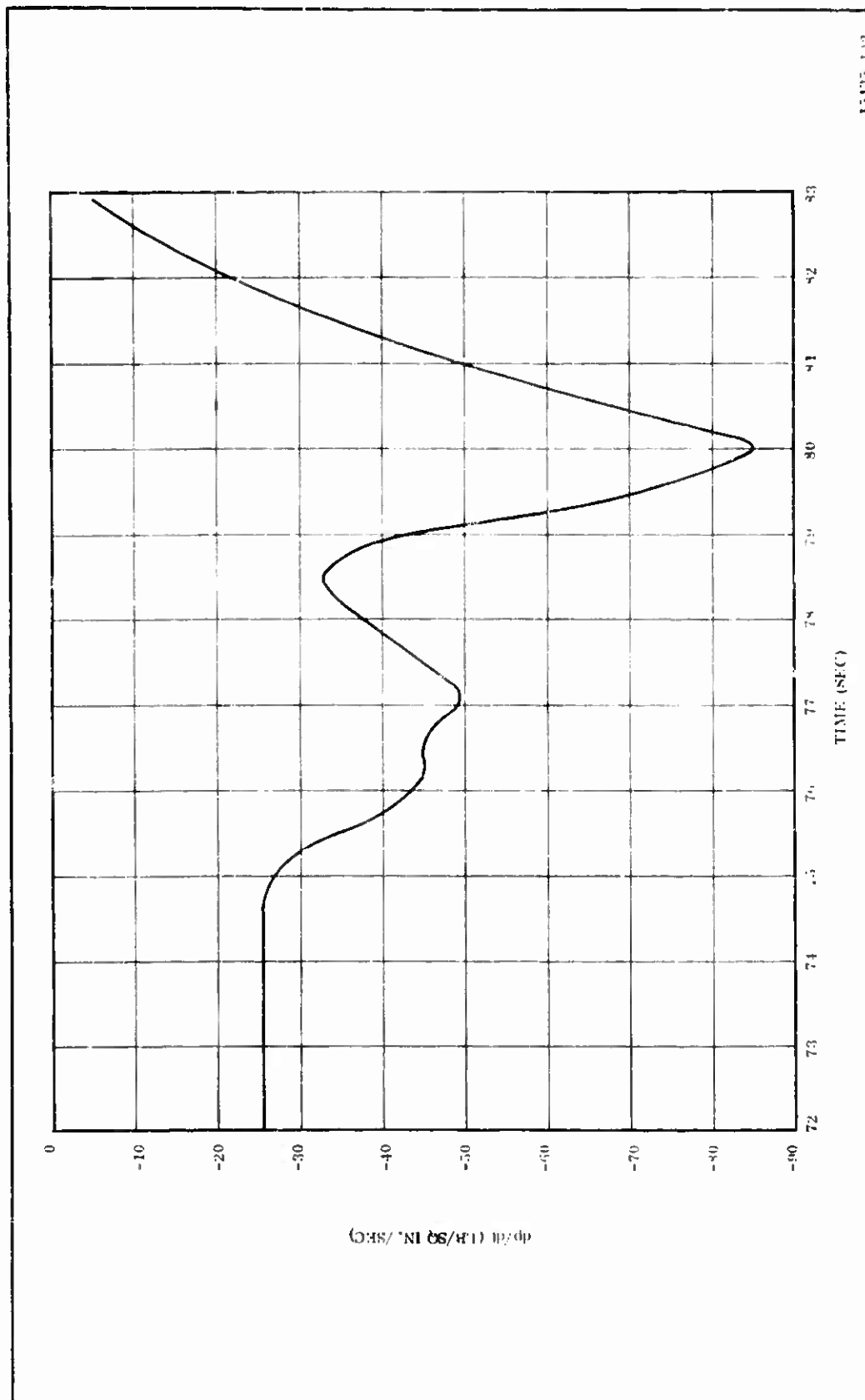


Figure 180. Depressurization Rate as a Function of Time (dp/dt, During Tailoff

CONFIDENTIAL

(THIS PAGE IS UNCLASSIFIED)

CONFIDENTIAL

weights are accurate within a range of ± 0.4 percent. The delivered specific impulse of the motor corrected to reference conditions was 247.8 lb-sec/lbm which compared reasonably well to the predicted value of 249.4 lb-sec/lbm.

- (C) A requirement for the test of the 156-9 motor was the development of side impulse equal to 1.1 percent of axial impulse. Analysis of actual performance data indicated that side impulse was equal to 1.06 percent of axial impulse. Failure to achieve the target side impulse of 1.1 percent was due to the low operating conditions (pressure and thrust) with the thrust vector duty cycle programed for the predicted higher thrust and shorter duration performance. A significant portion of the axial motor impulse was delivered after completion of the TVC duty cycle.

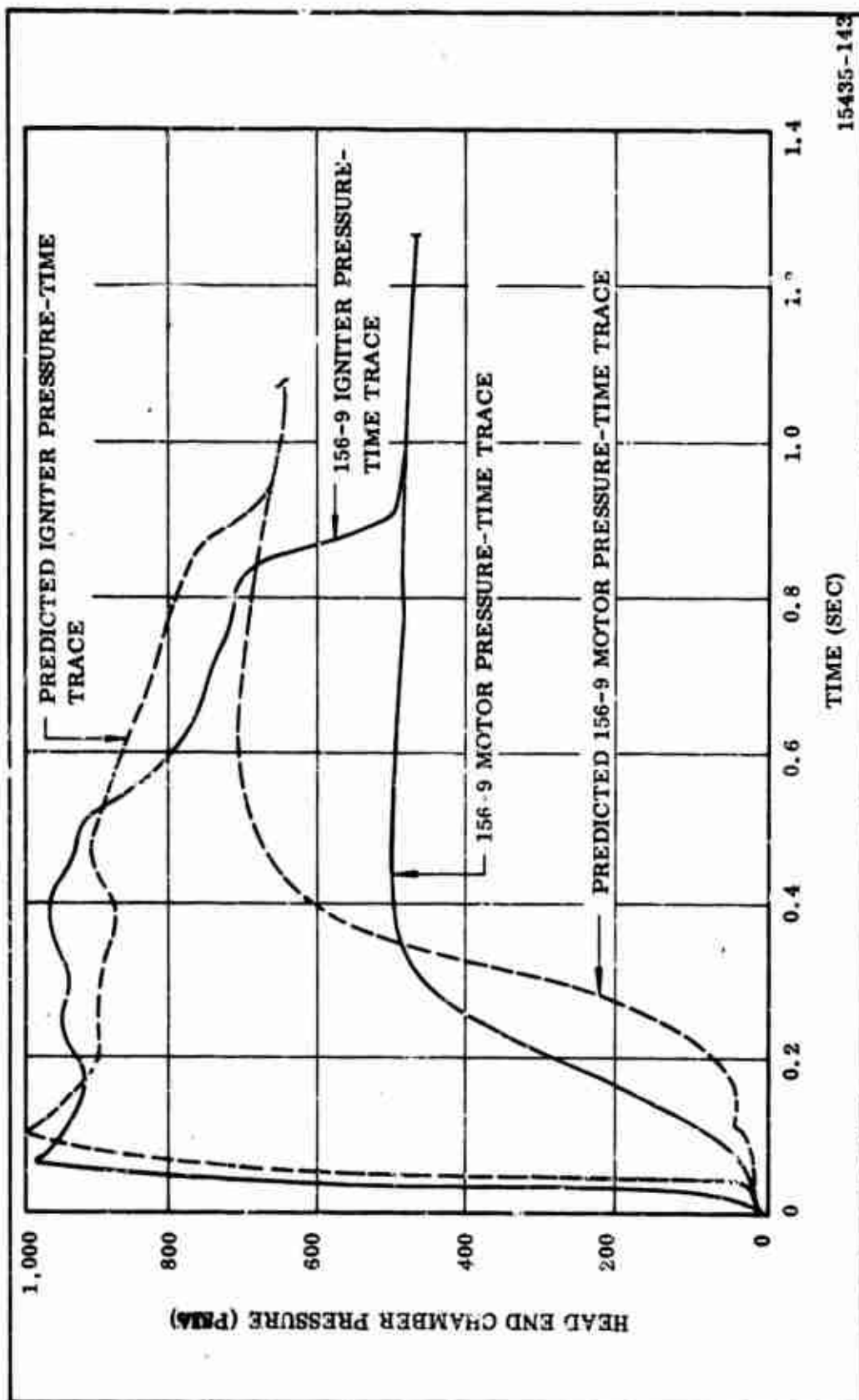
CONFIDENTIAL

7. IGNITION SYSTEM PERFORMANCE

- (U) The ignition system satisfactorily ignited the 156-9 motor and all components performed as predicted. The motor pressure vs time trace and the igniter pressure vs time traces are shown in Figure 181, for comparison with the predicted traces. The igniter performance in general was almost identical to the bench test igniter performance (Table XXXV) except that igniter ignition delay was approximately 14 milliseconds less.
- (U) a. Motor Ignition Transient--The motor pressure vs time trace during ignition transient, rate of rise, and ignition delay were within the predicted variable tolerance that can be expected for an R & D motor of this nature. The maximum pressure during ignition was lower than predicted because of the lower burn rate characteristic of the propellant.
- (U) b. Ignition System Post-Test Analysis--The ignition system post-test analysis shows no areas of malfunction or deviation from normal (Figure 182). All of the hardware, O-ring seals, and insulation were in good condition.
- (U) The insulation thickness was sized for the 156-8 motor (the 156-9 and the 156-8 igniter having identical loaded case assemblies), since it had the longer action time (120 seconds). To facilitate measuring and evaluation of the internal and external insulation, the igniter case was cut longitudinally (Figure 183) in four equal parts. The measurements taken will provide data for future motor head end and igniter insulation design.
- (C) (1) External Insulation Measurement--The igniter case external insulation thickness, virgin material, was measured in the areas having the maximum erosion (minimum insulation remaining). The minimum thickness (0.485 in.) occurred 29 in. from the flange face of the igniter case (Figure 184). The average thickness measurement between the 19.5 in. station and the 27 in. station was 0.6 inch. The external insulation remained bonded to the case in all areas exposed for examination.

CONFIDENTIAL

(THIS PAGE IS UNCLASSIFIED)



15435-143

Figure 181. Igniter and Motor Pressure vs Time Curves during Ignition Transient

CONFIDENTIAL

(THIS PAGE IS UNCLASSIFIED)

CONFIDENTIAL

TABLE XXXV
IGNITER PERFORMANCE

<u>Characteristics</u>	<u>Predicted*</u>	<u>156-9 Motor Test</u>
Mass Flow Rate, First Level 0.56 sec (lb/sec)	170	170
Burning Time, 10 percent P_{max} to 10 percent P_{max} (sec)	0.95	0.95
Maximum Operating Pressure (psia)	1,005	985 4
Average Operating Pressure, First Level (psia)	840	840
Average Operating Pressure, Second Level (psia)	529	--
Ignition Delay, 10 percent P_{max} for Booster PYROGEN (sec)	0.040	0.026
Ignition Interval Booster PYROGEN T_o to 90 percent P_{max} (sec)	0.069	0.044
156-9 Ignition Delay Time T_o to 75 percent P_{max} (sec)	0.39	0.40
156-9 Maximum Motor Pressure at Ignition (psia)	717	456
156-9 Igniter Coefficient (lb/sec/sq in.)	0.182	0.182

*Based on bench test data.

CONFIDENTIAL
(THIS PAGE IS UNCLASSIFIED)



Figure 182. Postfired Ignition System

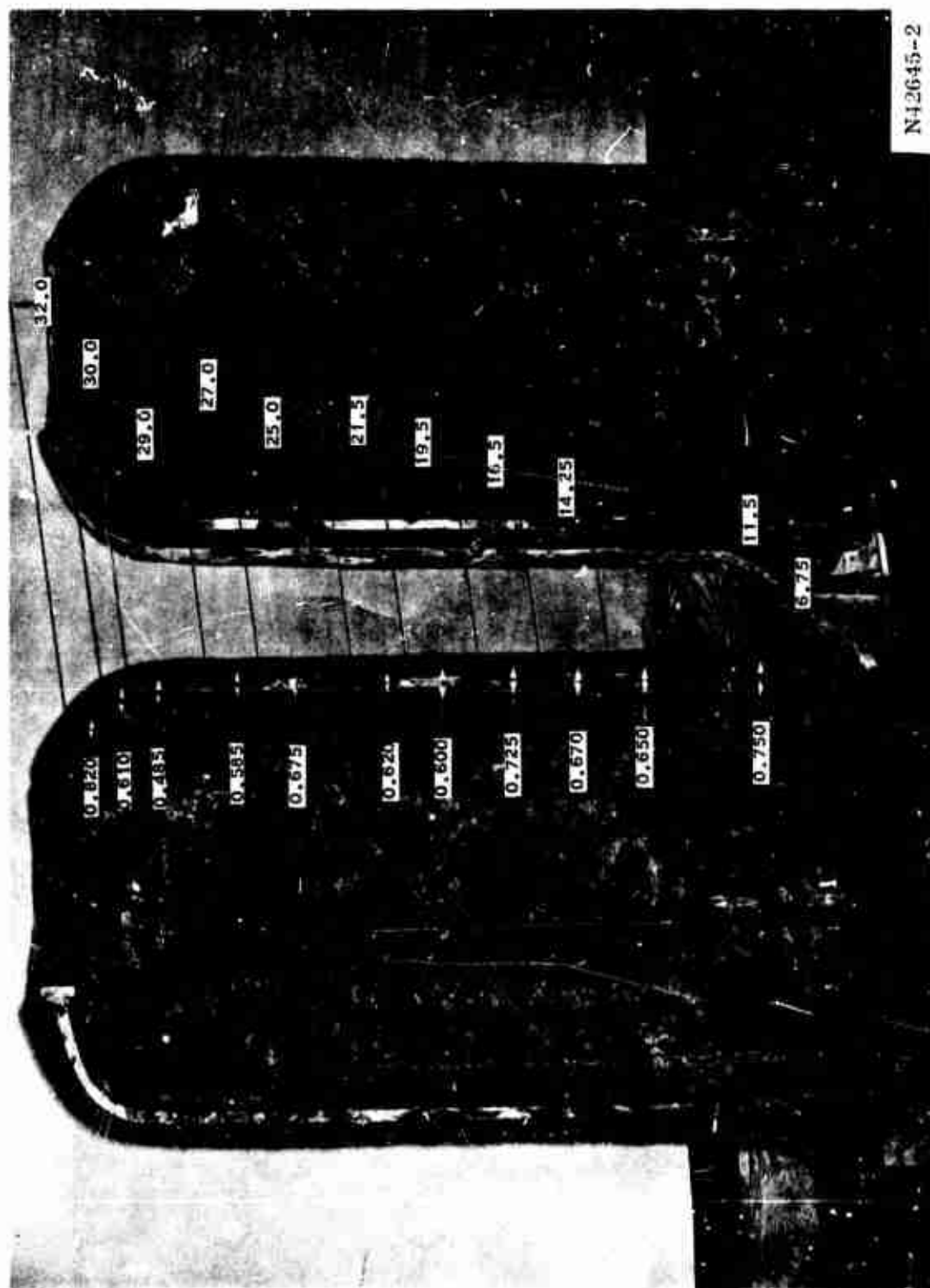


Figure 183. Sectioned Igniter Case Showing Insulation Thickness

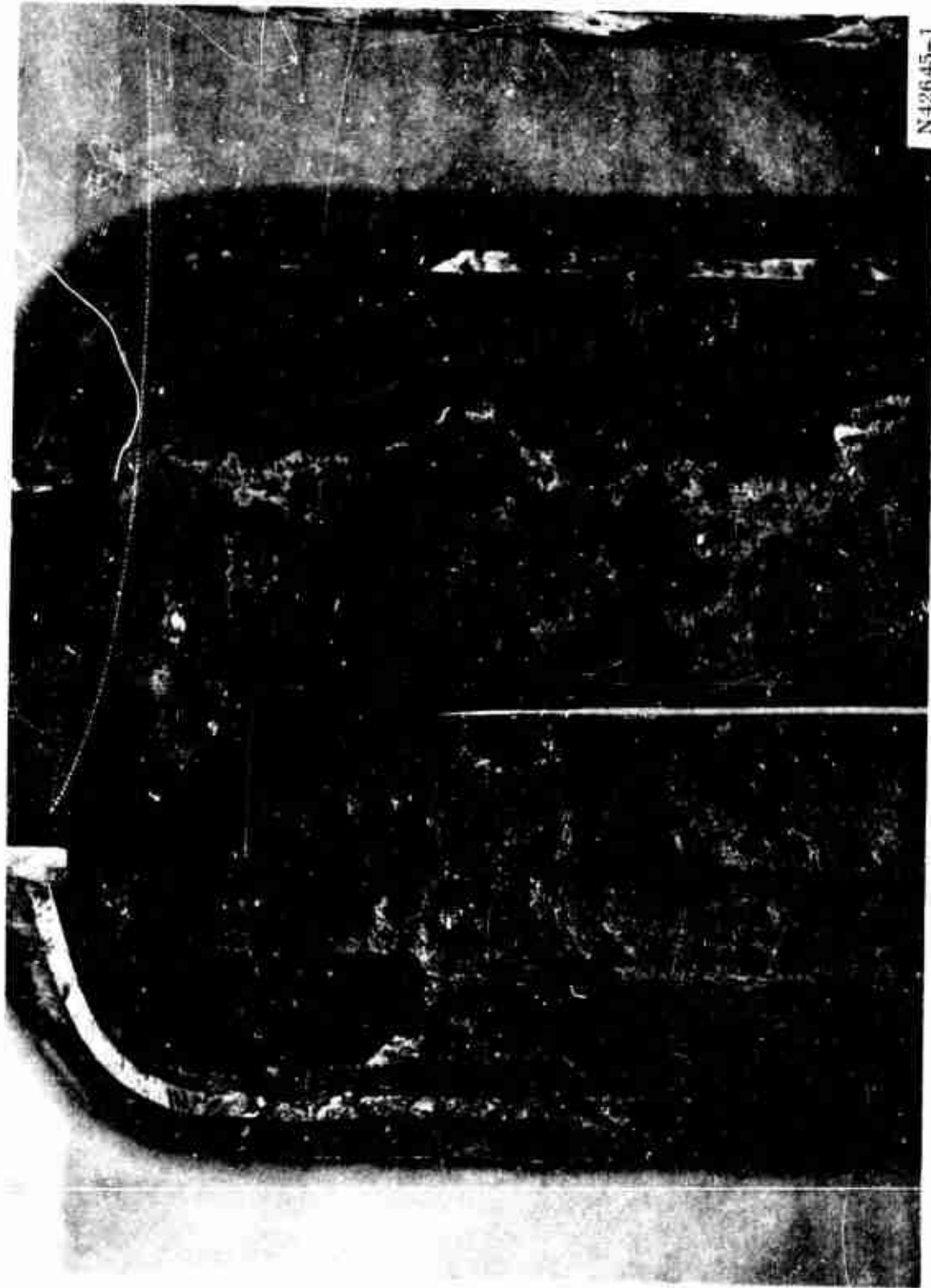


Figure 184. Sectioned Igniter Case Showing Minimum Insulation Thickness

CONFIDENTIAL

- (C) (2) Internal Insulation Post-Test Analysis--The internal insulation consisted of 0.20 in. of NBR layup, vulcanized in place and 0.10 in. of UF-2121 liner. Approximately 0.150 in. of NBR rubber remained after test and the 0.1 in. of UF-2121 liner was charred through or eroded away. A small section, adjacent to the 0.485 in. external insulation measurement, was separated from the case (Figure 184). This was of no consequence as the insulation remained in an integral section, providing thermal protection for the case material.

8. MOTOR QUENCH

- (U) The motor quench system was remotely activated immediately after tailoff. At $T + 5$ minutes, the case and external nozzle shell were at near ambient temperature. Cold gases were visibly escaping from the nozzle (Figure 185) and the temperature of the case and external nozzle shell was not increasing. At $T + 20$ minutes, after 5,000 lb of CO_2 had been discharged, the quench system was shut down for an average rate of about 250 lb per minute. This rate was 150 lb per minute lower than during the test because of a back pressure within the PYROGEN case and the lower flow rate associated with decreasing receiver pressure as the receiver discharges.
- (U) The motor quench system performed its function of keeping metal parts cool and extinguishing insulation burning. More CO_2 was used than calculations warranted but operation of the system verified that the calculated amount would have been adequate.

CONFIDENTIAL
(THIS PAGE IS UNCLASSIFIED)



Figure 185. Motor Quench

450

CONFIDENTIAL
(THIS PAGE IS UNCLASSIFIED)

9. INSTRUMENTATION PERFORMANCE

- (U) In general, the performance of the instrumentation and data acquisition system was extremely good. Of the 104 instrument channels, 100 checked out satisfactorily just prior to static test. One chamber pressure channel (P002) was lost due to an internally plugged port. This measurement was redundant to P001 and not mandatory. Three of the 30 thermocouples installed were open at the time of firing. These three (T203, T204, and T205) were located on the forward end ring of the flexible seal. Their loss is attributed to the handling associated with shipping and installing the seal after thermocouples had been installed. The lost thermocouples were not mandatory. The remaining one thermocouple provided adequate indication of the end ring temperature which did not go above ambient.
- (U) During the static test firing all of the 100 remaining instrumentation channels performed perfectly and data were obtained from each channel.

CONFIDENTIAL

(THIS PAGE IS UNCLASSIFIED)

SECTION XIII

CONCLUSIONS AND RECOMMENDATIONS

A. CONCLUSIONS

- (U) A flexible seal, to be used for omniaxial thrust vector control (TVC) on large solid propellant rocket motors, has been demonstrated to be within the industry state-of-the-art. The 156-9 flexible seal performed perfectly. Demonstrated torques are reasonable with respect to actuation system power requirements, although at present, facility power sources are used for nozzle actuation. Torque can be reduced by simply changing the rubber modulus and accepting a lower (but more realistic for missile systems) factor of safety. This program demonstrated that flexible seals are dependable, simpler than any other type of TVC device, and can be manufactured at low cost.
- (U) For all practical purposes, the 156-9 flexible seal was subjected to no combustion heat or erosion; the seal was designed so it could have withstood a considerable amount of both. The splitline gap apparently was smaller than required, but can be increased. Increasing this gap would allow nozzle and flexible seal manufacturing tolerances to be relaxed considerably, resulting in significant cost savings. Furthermore, the barrier may not be needed. The flexible seal can perhaps be exposed to the aft case environment with only a rubber boot for protection, obviating the need for some expensive machined plastics. Elimination of these plastics would provide both weight and cost savings.

(THIS PAGE IS UNCLASSIFIED)

CONFIDENTIAL

- (U) Nozzle metal parts were designed conservatively, as evidenced by the low stresses recorded. Nozzle plastic parts also were designed conservatively, as evidenced by the erosion profiles. This conservative approach was the result of a deliberate attempt to insure durability in a one motor program. Nozzle weight and cost can be reduced significantly for any multi-unit program.
- (U) The vent holes in the nozzle nose cap did not improve performance and are, therefore, not warranted in this particular area.
- (C) The nozzle vector angle obtained during firing was 3.658 deg, rather than 4.00 degrees. The smaller angle is attributed to the TVC actuation system rather than the flexible seal. The actuators procured had a 7.0 rather than 7.5 in. stroke. Previous bench testing on the flexible seal has proven the seals capable of vectoring a full 4.00 deg when pressurized to MEOP.
- (U) The motor design was conservative as evidenced by the amount of insulation remaining in the case after firing. This conservatism was deliberate to insure motor durability where only one firing was scheduled. Motor mass fraction can be increased readily.
- (U) The motor operated at a lower than expected chamber pressure and a longer than expected burn time. Thus, the nozzle and flexible seal were exposed to a slightly less than expected pressure and gas flow environment for a considerably longer than expected time. The total environment was more severe with respect to nozzle and flexible seal erosion and thermal environment.

B. RECOMMENDATIONS

- (U) The overall test results from the 156-9 motor demonstration were excellent; however, the following recommendations are made to improve the design and performance for system application.

- (U) A design study is warranted to refine the design parameters and techniques applicable to flexible seal technology. The feasibility of flexible seal TVC has been well demonstrated by this program; however, available data on optimum design for various size motors are in conflict. Scaleup data are required in the form of design curves, and a computer program is required for optimizing shim thickness for large seals. Also, various elastomers and different materials for the shims should be investigated. The only material used to date for shims has been steel. The possibility of fiberglass or aluminum for weight and cost savings should be considered.
- (U) To complement the flexible seal TVC for system application, a program to develop a high horsepower, lightweight, TVC actuation system should be initiated. Torque requirements for flexible seal systems are relatively high. Although they can be reduced significantly by using different elastomeric materials, the requirements still exceed the capability of demonstrated lightweight power systems for large motors with severe duty cycle requirements.

UNCLASSIFIED

Security Classification

DOCUMENT CONTROL DATA - R&D		
(Security classification of title, body of abstract and indexing annotation must be entered when the overall report is classified)		
1 ORIGINATING ACTIVITY (Corporate author) Thiokol Chemical Corporation Wasatch Division Brigham City, Utah 84302		2a REPORT SECURITY CLASSIFICATION CONFIDENTIAL
		2b GROUP IV
3 REPORT TITLE Development and Demonstration of an Omniaxial Flexible Seal Movable Nozzle for Thrust Vector Control (U)		
4 DESCRIPTIVE NOTES (Type of report and inclusive dates) Final Technical Report - July 1966 thru June 1967		
5 AUTHOR(S) (Last name, first name, initial) T. Walker		
6 REPORT DATE October 1967	7a TOTAL NO. OF PAGES 488	7b NO. OF REFS 9
8a CONTRACT OR GRANT NO. AF 04(611)-11643 b. PROJECT NO	9a. ORIGINATOR'S REPORT NUMBER(S) 1067-15435	
c d	9b OTHER REPORT NO(S) (Any other numbers that may be assigned this report) AFRPL-TR-67-196	
10 AVAILABILITY/LIMITATION NOTICES In addition to security requirements which must be met, this document is subject to special export controls and each transmittal to foreign governments or foreign nationals may be made only with prior approval of AFRPL (RPPR/STINFO), Edwards, California 93523.		
11 SUPPLEMENTARY NOTES N/A	12. SPONSORING MILITARY ACTIVITY Air Force Rocket Propulsion Laboratory, Research and Technology Division, Air Force Systems Command, Edwards, California	
13 ABSTRACT The 156-9 Motor Program, Development and Demonstration of an Omniaxial Flexible Seal for Thrust Vector Control, was conducted by Wasatch Division, Thiokol Chemical Corporation for the Air Force Space Systems Division. The program was under the technical direction of the Air Force Rocket Propulsion Laboratory. Primary objective of the program was to develop and successfully demonstrate an omniaxial flexible seal movable nozzle on a one million pound thrust class, 156 in. diameter motor. This objective was attained. The 156-9 motor was static test fired on 26 May 1967 and successfully demonstrated the flexible seal design and fabrication concept for movable nozzles. All motor and nozzle components were intact and in good condition at the completion of the test. The motor operated longer and at a lower chamber pressure than predicted, but with no adverse effect on the overall objective. Post-test inspection of the motor and components disclosed that the internal insulation, nozzle design, and flexible seal design were satisfactory and the nozzle performed as predicted. The torque required for thrust vector control was demonstrated to be reasonable with respect to actuation system power requirements.		

DD FORM 1473
1 JAN 64

UNCLASSIFIED

Security Classification

UNCLASSIFIED

Security Classification

14 KEY WORDS	LINK A		LINK B		LINK C	
	ROLE	WT	ROLE	WT	ROLE	WT

INSTRUCTIONS

1. **ORIGINATING ACTIVITY:** Enter the name and address of the contractor, subcontractor, grantee, Department of Defense activity or other organization (corporate author) issuing the report.

2a. **REPORT SECURITY CLASSIFICATION:** Enter the overall security classification of the report. Indicate whether "Restricted Data" is included. Marking is to be in accordance with appropriate security regulations.

2b. **GROUP:** Automatic downgrading is specified in DoD Directive 5200.10 and Armed Forces Industrial Manual. Enter the group number. Also, when applicable, show that optional markings have been used for Group 3 and Group 4 as authorized.

3. **REPORT TITLE:** Enter the complete report title in all capital letters. Titles in all cases should be unclassified. If a meaningful title cannot be selected without classification, show title classification in all capitals in parenthesis immediately following the title.

4. **DESCRIPTIVE NOTES:** If appropriate, enter the type of report, e.g., interim, progress, summary, annual, or final. Give the inclusive dates when a specific reporting period is covered.

5. **AUTHOR(S):** Enter the name(s) of author(s) as shown on or in the report. Enter last name, first name, middle initial. If military, show rank and branch of service. The name of the principal author is an absolute minimum requirement.

6. **REPORT DATE:** Enter the date of the report as day, month, year; or month, year. If more than one date appears on the report, use date of publication.

7a. **TOTAL NUMBER OF PAGES:** The total page count should follow normal pagination procedures, i.e., enter the number of pages containing information.

7b. **NUMBER OF REFERENCES:** Enter the total number of references cited in the report.

8a. **CONTRACT OR GRANT NUMBER:** If appropriate, enter the applicable number of the contract or grant under which the report was written.

8b, &c, & 8d. **PROJECT NUMBER:** Enter the appropriate military department identification, such as project number, subproject number, system numbers, task number, etc.

9a. **ORIGINATOR'S REPORT NUMBER(S):** Enter the official report number by which the document will be identified and controlled by the originating activity. This number must be unique to this report.

9b. **OTHER REPORT NUMBER(S):** If the report has been assigned any other report numbers (either by the originator or by the sponsor), also enter this number(s).

10. **AVAILABILITY/LIMITATION NOTICES:** Enter any limitations on further dissemination of the report, other than those

imposed by security classification, using standard statements such as:

- (1) "Qualified requesters may obtain copies of this report from DDC."
- (2) "Foreign announcement and dissemination of this report by DDC is not authorized."
- (3) "U. S. Government agencies may obtain copies of this report directly from DDC. Other qualified DDC users shall request through _____."
- (4) "U. S. military agencies may obtain copies of this report directly from DDC. Other qualified users shall request through _____."
- (5) "All distribution of this report is controlled. Qualified DDC users shall request through _____."

If the report has been furnished to the Office of Technical Services, Department of Commerce, for sale to the public, indicate this fact and enter the price, if known.

11. **SUPPLEMENTARY NOTES:** Use for additional explanatory notes.

12. **SPONSORING MILITARY ACTIVITY:** Enter the name of the departmental project office or laboratory sponsoring (paying for) the research and development. Include address.

13. **ABSTRACT:** Enter an abstract giving a brief and factual summary of the document indicative of the report, even though it may also appear elsewhere in the body of the technical report. If additional space is required, a continuation sheet shall be attached.

It is highly desirable that the abstract of classified reports be unclassified. Each paragraph of the abstract shall end with an indication of the military security classification of the information in the paragraph, represented as (TS), (S), (C), or (U).

There is no limitation on the length of the abstract. However, the suggested length is from 150 to 225 words.

14. **KEY WORDS:** Key words are technically meaningful terms or short phrases that characterize a report and may be used as index entries for cataloging the report. Key words must be selected so that no security classification is required. Identifiers, such as equipment model designation, trade name, military project code name, geographic location, may be used as key words but will be followed by an indication of technical content. The assignment of links, rules, and weights is optional.

UNCLASSIFIED

Security Classification